frontiers | Research Topics

Delivering nucleic acids to immune and non-immune cells

Edited by
Francesca Re, Kirill Afonin and Diana Boraschi

Published in
Frontiers in Immunology

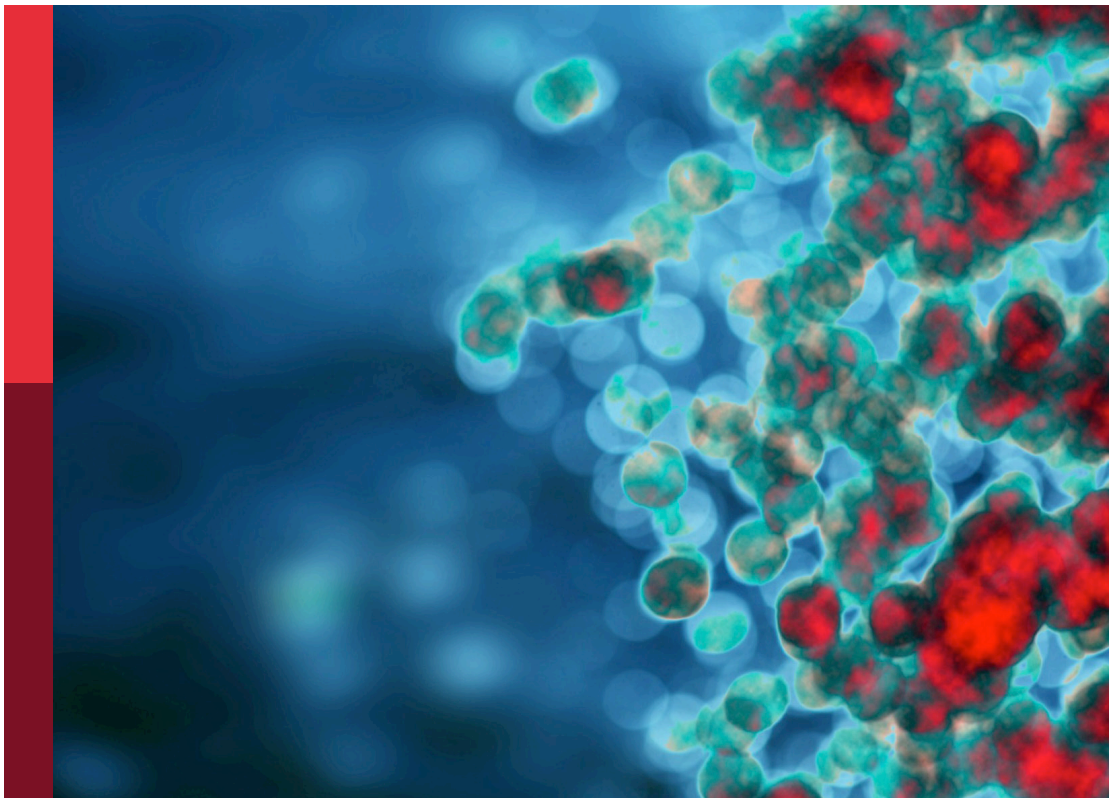

ISSN 1664-8714
ISBN 978-2-8325-4476-1
DOI 10.3389/978-2-8325-4476-1

About Frontiers

Frontiers is more than just an open access publisher of scholarly articles: it is a pioneering approach to the world of academia, radically improving the way scholarly research is managed. The grand vision of Frontiers is a world where all people have an equal opportunity to seek, share and generate knowledge. Frontiers provides immediate and permanent online open access to all its publications, but this alone is not enough to realize our grand goals.

Frontiers journal series

The Frontiers journal series is a multi-tier and interdisciplinary set of open-access, online journals, promising a paradigm shift from the current review, selection and dissemination processes in academic publishing. All Frontiers journals are driven by researchers for researchers; therefore, they constitute a service to the scholarly community. At the same time, the *Frontiers journal series* operates on a revolutionary invention, the tiered publishing system, initially addressing specific communities of scholars, and gradually climbing up to broader public understanding, thus serving the interests of the lay society, too.

Dedication to quality

Each Frontiers article is a landmark of the highest quality, thanks to genuinely collaborative interactions between authors and review editors, who include some of the world's best academicians. Research must be certified by peers before entering a stream of knowledge that may eventually reach the public - and shape society; therefore, Frontiers only applies the most rigorous and unbiased reviews. Frontiers revolutionizes research publishing by freely delivering the most outstanding research, evaluated with no bias from both the academic and social point of view. By applying the most advanced information technologies, Frontiers is catapulting scholarly publishing into a new generation.

What are Frontiers Research Topics?

Frontiers Research Topics are very popular trademarks of the *Frontiers journals series*: they are collections of at least ten articles, all centered on a particular subject. With their unique mix of varied contributions from Original Research to Review Articles, Frontiers Research Topics unify the most influential researchers, the latest key findings and historical advances in a hot research area.

Find out more on how to host your own Frontiers Research Topic or contribute to one as an author by contacting the Frontiers editorial office: frontiersin.org/about/contact

Delivering nucleic acids to immune and non-immune cells

Topic editors

Francesca Re – University of Milano Bicocca, Italy

Kirill Afonin – University of North Carolina at Charlotte, United States

Diana Boraschi – Shenzhen Institute of Advanced Technology, Chinese Academy of Sciences (CAS), China

Citation

Re, F., Afonin, K., Boraschi, D., eds. (2024). *Delivering nucleic acids to immune and non-immune cells*. Lausanne: Frontiers Media SA. doi: 10.3389/978-2-8325-4476-1

Table of contents

frontiers | Frontiers in Immunology

TYPE Editorial
PUBLISHED 08 August 2023
DOI 10.3389/fimmu.2023.1237506

OPEN ACCESS

EDITED AND REVIEWED BY
Bernd Lepenies,
University of Veterinary Medicine
Hannover,Germany

*CORRESPONDENCE
Kirill A. Afonin
kafonin@uncc.edu
Francesca Re
francesca.re1@unimib.it
Diana Boraschi
diana.boraschi@itb.cnr.it

RECEIVED 09 June 2023
ACCEPTED 28 July 2023
PUBLISHED 08 August 2023

CITATION
Afonin KA, Re F and Boraschi D (2023) Editorial: Delivering nucleic acids to immune and non-immune cells.
Front. Immunol. 14:1237506.
doi: 10.3389/fimmu.2023.1237506

Editorial: Delivering nucleic acids to immune and non-immune cells

Kirill A. Afonin[1]*, Francesca Re[2]* and Diana Boraschi[3,4,5]*

[1]Nanoscale Science Program, Department of Chemistry, University of North Carolina Charlotte, Charlotte, NC, United States, [2]Department of Medicine and Surgery, University of Milano Bicocca, Milano, Italy, [3]Shenzhen Institute of Advanced Technology (SIAT) of the Chinese Academy of Science (CAS), and China-Italy Joint Laboratory of Pharmacobiotechnology for Medical Immunomodulation, Shenzhen, China, [4]Institute of Biochemistry and Cell Biology, Consiglio Nazionale delle Ricerche, Napoli, Italy, [5]Stazione Zoologica Anton Dohrn, Napoli, Italy

KEYWORDS

delivery, nucleic acids, vaccination, antigen presentation, nanoparticles, NANPs

Editorial on the Research Topic
Delivering nucleic acids to immune and non-immune cells

For decades, there has been ongoing research focused on the targeted delivery of therapeutic DNA and/or RNA molecules designed to regulate the expression of specific genes. This field of study aims to advance new clinical approaches for therapies that target the genetic components of various diseases in a personalized manner. The technology had an impressively rapid advancement and gained global recognition, particularly in the new vaccination strategies adopted during the COVID-19 pandemic (1, 2). However, a major obstacle that still hinders the broader success of nucleic acid-based therapies and vaccines lies in the inefficient delivery of these biopolymers to human cells, as well as in ensuring their subsequent intracellular release and optimal performance. The challenges arise from the inherent limitations of naked, non-modified oligonucleotides, among which are their susceptibility to rapid degradation by nucleases and renal clearance, the inefficient crossing of biological membranes, and the potential to induce uncontrolled immunological responses (3, 4). To optimize the efficacy while minimizing the harmful side effects of nucleic acid cargos, recent research has focused on improving the design of delivery systems suitable for rationally designed DNA and RNA molecules (5). A special emphasis on targeting immune cells is warranted in the case of vaccination. The strategy aims to shuttle the antigen-coding nucleic acids to cells that will be able to synthesize, process, and present the antigens. By doing so, optimally protective immune responses will lead to the development of long-term protective immunological memory.

The current Research Topic features a collection of fifteen review and research articles curated by international leaders in the fields of nucleic acid therapies, immunology, and drug delivery. The manuscripts present a range of innovative technologies encompassing the design of various nucleic acid-based therapeutics, assessment of their biological activities, and optimization of administration conditions.

Antigen-encoding nucleic acids can be optimized for a particular application through several strategies. The review by Vishweshwaraiah and Dokholyan provides a comprehensive assessment of rational design and optimization strategies for mRNA vaccines, highlights different platforms available for vaccine delivery, and discusses the limitations and future challenges associated with this emerging technology.

By encoding appropriate target proteins, such as the Spike protein of SARS-CoV-2, and selecting between the B- and T-cell epitopes, it becomes possible to elicit either antibody or cellular responses. Also, the specification of CD4 and CD8 epitopes can assist in the stimulation of helper and cytotoxic responses, respectively. The research by Del Riego et al. provides an analysis of the levels of SARS-CoV-2 specific antibodies and T cells in intensive care unit workers. The aim is to gain additional insights into their immune protection following vaccination. Additionally, Becker et al. share longitudinal vaccination response data in dialysis patients and control subjects, as part of a mixed mRNA vaccination scheme, and Raptis et al. report differences in immune responses for patients with inflammatory rheumatic diseases, which depended on the type of administered mRNA vaccine. Garcia-Dominguez et al. discover that the dosing intervals in mRNA vaccination could improve the durability of immune responses, with longer intervals being preferable.

The inclusion of chemical modifications and sequence optimization plays a crucial role in defining the stability, cellular localization, and therapeutic efficacy of delivered mRNA (6, 7). These strategies enable fine-tuning mRNA physicochemical properties, enhancing its lifetime, and optimizing its performance as a therapeutic agent. In their research article, Bai et al. present a nucleoside-modified Rabies mRNA-lipid nanoparticle vaccine able to induce prolonged immune responses in animal models, while Rice at al. employ heterologous vaccination to elicit robust cellular immunogenicity with increased protection against the emerging variants of SARS-CoV-2 infection.

Nucleic acid technologies, combined with the innate capacity of the human immune system to detect nucleic acids and initiate efficient immune/inflammatory responses, have paved the way for their potential use as adjuvants and immunostimulants (8). These applications are crucial for enhancing vaccine efficacy. The review by Gu et al. provides a good overview on the relationship between circular RNA and immunity, highlighting the current applications and future directions of these technologies. Consequently, it is imperative to focus research efforts on the design of nucleic acids that can induce controlled inflammation in a limited manner, both temporally and anatomically. For instance, this can be achieved by targeting Toll-like receptors (TLRs) or NOD-like receptors (NLRs). A clinical trial reported by Daniel et al. reveals the first-in-human Phase 1 study of immunostimulatory spherical nucleic acids designed to target TLR9. The results make this compound promising as an immunotherapy agent.

Recent advancements in nucleic acid bioengineering have led to the emergence of nucleic nanoparticles (NANPs), multistranded nanoassemblies composed exclusively of RNA, DNA, and their chemical analogs, which offer an innovative approach for regulated personalized immunostimulation and drug delivery (9, 10). By changing the composition and architectural features of NANPs, it becomes possible to target the activation of specific pattern recognition receptors (e.g., TLR7 or RIG-I) and promote the delivery of scaffolded antigens and therapeutics to the diseased cells (11, 12). Panigaj et al. review recent developments and applications of NANPs, rationally designed for therapeutic immunomodulation, and identified current limitations and future directions of this innovative platform.

Efficient intracellular delivery of nucleic acid therapeutics relies on the use of various carriers, among which are viral vectors, highly efficient but with problems of immunogenicity and specificity of targeting, lipid nanoparticles (LNPs), currently the lead delivery systems for nucleic acid-based vaccines and therapeutics, exosomes, extracellular vesicles, a recent promising delivery and diagnostic technology that is still at early stages of its development, as well as various inorganic nanoparticles and polymers (13, 14). In their review, González-Rioja et al. revise the synthetic methods, physicochemical characterization, and pharmacokinetics of surfactant ionizable lipid nanoparticles loaded with RNA therapeutics. The review articles by Gao et al. and Zhang et al. discuss the application of extracellular vesicles and exosomes as new diagnostic tool and drug delivery carriers for cancer immunotherapies, respectively. Finally, Gusta et al. develop a panel of cationic gold nanoparticle-based nanovectors used for the safe and sustained internalization of mRNAs via endocytosis. The obtained results with cell culture experiments show promise for this technology to be used as a delivery platform for nucleic acids.

With further developments of nucleic acid-based technologies, it is essential to address the potential risks associated not only with therapeutic cargos but also with other formulation components that can lead to excessive inflammation, cytokine storms, and the development of autoimmune and inflammatory diseases (15, 16). The review by Dobrovolskaia shares the valuable insights obtained from the extensive experience of the Nanotechnology Characterization Laboratory regarding the interactions between different nanoparticles and the immune system, which significantly impact the safety and effectiveness of formulations.

In summary, while nucleic acid therapies hold immense promise and have achieved significant advancements, their broader applications still necessitate further improvements, among which are increasing delivery efficiencies, providing storage and handling of all formulations at ambient temperatures, design-driven regulation of immunorecognition and toxicities, and lowering production costs by addressing technological hurdles and logistical challenges (17).

Author contributions

KA, DB, and FR contributed to writing and revision of the manuscript. All authors contributed to the article and approved the submitted version.

Funding

Research reported in this publication was supported by the National Institute of General Medical Sciences of the National Institutes of Health under Award Number R35GM139587 (to KA). The content is solely the responsibility of the authors and does not necessarily represent the official views of the National Institutes of Health. DB was supported by the EU H2020 project PANDORA (GA 671881) and by the Key Collaborative Research Program of the Alliance of International Science Organizations (ANSO-CR-KP-2022-01). FR was supported by the Centro Nazionale per lo

sviluppo di terapia genica e farmaci con tecnologia a RNA, PNRR Ministero dell'Università e della Ricerca of Italy.

Conflict of interest

The authors declare that the research was conducted in the absence of any commercial or financial relationships that could be construed as a potential conflict of interest.

Publisher's note

References

1. Tseng HF, Ackerson BK, Luo Y, Sy LS, Talarico CA, Tian Y, et al. Effectiveness of mRNA-1273 against SARS-CoV-2 Omicron and Delta variants. *Nat Med* (2022) 28 (5):1063–71. doi: 10.1038/s41591-022-01753-y

2. Jackson LA, Anderson EJ, Rouphael NG, Roberts PC, Makhene M, Coler RN, et al. An mRNA Vaccine against SARS-CoV-2 - Preliminary Report. *N Engl J Med* (2020) 383(20):1920–31. doi: 10.1056/NEJMoa2022483

3. Kulkarni JA, Witzigmann D, Thomson SB, Chen S, Leavitt BR, Cullis PR, et al. The current landscape of nucleic acid therapeutics. *Nat Nanotechnol* (2021) 16(6):630–43. doi: 10.1038/s41565-021-00898-0

4. Johnson MB, Chandler M, Afonin KA. Nucleic acid nanoparticles (NANPs) as molecular tools to direct desirable and avoid undesirable immunological effects. *Adv Drug Deliver Rev* (2021) 173:427–38. doi: 10.1016/j.addr.2021.04.011

5. Afonin KA, Dobrovolskaia MA, Church G, Bathe M. Opportunities, barriers, and a strategy for overcoming translational challenges to therapeutic nucleic acid nanotechnology. *ACS Nano* (2020) 14(8):9221–7. doi: 10.1021/acsnano.0c04753

6. Leppek K, Byeon GW, Kladwang W, Wayment-Steele HK, Kerr CH, Xu AF, et al. Combinatorial optimization of mRNA structure, stability, and translation for RNA-based therapeutics. *Nat Commun* (2022) 13(1):1536. doi: 10.1038/s41467-022-28776-w

7. Zhang H, Zhang L, Lin A, Xu C, Li Z, Liu K, et al. Algorithm for optimized mRNA design improves stability and immunogenicity. *Nature* (2023). doi: 10.1038/s41586-023-06127-z

8. Pulendran B, SA P, O'Hagan DT. Emerging concepts in the science of vaccine adjuvants. *Nat Rev Drug Discovery* (2021) 20(6):454–75. doi: 10.1038/s41573-021-00163-y

9. Chandler M, Jain S, Halman J, Hong E, Dobrovolskaia MA, Zakharov AV, et al. Artificial immune cell, AI-cell, a new tool to predict interferon production by peripheral blood monocytes in response to nucleic acid nanoparticles. *Small* (2022) 18(46):e2204941. doi: 10.1002/smll.202204941

10. Hong E, Halman JR, Shah AB, Khisamutdinov EF, Dobrovolskaia MA, Afonin KA. Structure and composition define immunorecognition of nucleic acid nanoparticles. *Nano Lett* (2018) 18(7):4309–21. doi: 10.1021/acs.nanolett.8b01283

11. Chandler M, Rolband L, Johnson MB, Shi D, Avila YI, Cedrone E, et al. Expanding structural space for immunomodulatory nucleic acid nanoparticles (Nanps) via spatial arrangement of their therapeutic moieties. *Adv Funct Mater* (2022) 32 (43):2205581. doi: 10.1002/adfm.202205581

12. Johnson MB, Halman JR, Miller DK, Cooper JS, Khisamutdinov EF, Marriott I, et al. The immunorecognition, subcellular compartmentalization, and physicochemical properties of nucleic acid nanoparticles can be controlled by composition modification. *Nucleic Acids Res* (2020) 48(20):11785–98. doi: 10.1093/nar/gkaa908

13. Ke WN, Afonin KA. Exosomes as natural delivery carriers for programmable therapeutic nucleic acid nanoparticles (NANPs). *Adv Drug Deliver Rev* (2021) 176:113835. doi: 10.1016/j.addr.2021.113835

14. Mendes BB, Conniot J, Avital A, Yao D, Jiang X, Zhou X, et al. Nanodelivery of nucleic acids. *Nat Rev Methods Primers* (2022) 2:24. doi: 10.1038/s43586-022-00104-y

15. Dobrovolskaia MA, Afonin KA. Use of human peripheral blood mononuclear cells to define immunological properties of nucleic acid nanoparticles. *Nat Protoc* (2020) 15(11):3678–98. doi: 10.1038/s41596-020-0393-6

16. Dobrovolskaia MA, McNeil SE. Strategy for selecting nanotechnology carriers to overcome immunological and hematological toxicities challenging clinical translation of nucleic acid-based therapeutics. *Expert Opin Drug Delivery* (2015) 12(7):1163–75. doi: 10.1517/17425247.2015.1042857

17. Afonin KA, Dobrovolskaia MA, Ke WN, Grodzinski P, Bathe M. Critical review of nucleic acid nanotechnology to identify gaps and inform a strategy for accelerated clinical translation. *Adv Drug Deliver Rev* (2022) 181:114081. doi: 10.1016/j.addr.2021.114081

frontiers | Frontiers in Immunology

REVIEW
published: 25 May 2022
doi: 10.3389/fimmu.2022.894707

Past, Present and Future: The Relationship Between Circular RNA and Immunity

Junjie Gu[1†], Chongying Su[1†], Fei Huang[1†], Yuwei Zhao[2] and Jing Li[1*]*

[1] State Key Laboratory of Oral Diseases, National Clinical Research Center for Oral Diseases, Chinese Academy of Medical Sciences Research Unit of Oral Carcinogenesis and Management, West China Hospital of Stomatology, Sichuan University, Chengdu, China, [2] Chengdu Blood Center, Blood Research Laboratory, Chengdu, China

The immune system has evolved since the birth of humans. However, immune-related diseases have not yet been overcome due to the lack of expected indicators and targeting specificity of current medical technology, subjecting patients to very uncomfortable physical and mental experiences and high medical costs. Therefore, the requirements for treatments with higher specificity and indicative ability are raised. Fortunately, the discovery of and continuous research investigating circular RNAs (circRNAs) represent a promising method among numerous methods. Although circRNAs wear regarded as metabolic wastes when discovered, as a type of noncoding RNA (ncRNA) with a ring structure and wide distribution range in the human body, circRNAs shine brilliantly in medical research by virtue of their special nature and structure-determined functions, such as high stability, wide distribution, high detection sensitivity, acceptable reproducibility and individual differences. Based on research investigating the role of circRNAs in immunity, we systematically discuss the hotspots of the roles of circRNAs in immune-related diseases, including expression profile analyses, potential biomarker research, ncRNA axis/network construction, impacts on phenotypes, therapeutic target seeking, maintenance of nucleic acid stability and protein binding research. In addition, we summarize the current situation of and problems associated with circRNAs in immune research, highlight the applications and prospects of circRNAs in the treatment of immune-related diseases, and provide new insight into future directions and new strategies for laboratory research and clinical applications.

Keywords: circRNAs, immunity, immune-related diseases, autoimmune diseases, tumor, infectious diseases

OPEN ACCESS

Edited by:
Damjan Glavač,
University of Ljubljana, Slovenia

Reviewed by:
Manish Muhuri,
Biogen Idec, United States
Yin Tailang,
Wuhan University, China

****Correspondence:***
Jing Li
lijing1984@scu.edu.cn
Yuwei Zhao
cdbczyw@163.com

[†]These authors have contributed equally to this work

Specialty section:
This article was submitted to Cancer Immunity and Immunotherapy, a section of the journal Frontiers in Immunology

Received: *12 March 2022*
Accepted: *28 April 2022*
Published: *25 May 2022*

Citation:
Gu J, Su C, Huang F, Zhao Y and Li J (2022) Past, Present and Future: The Relationship Between Circular RNA and Immunity. Front. Immunol. 13:894707. doi: 10.3389/fimmu.2022.894707

1 INTRODUCTION

CircRNAs are molecules belonging to the noncoding RNA family that form ring-like structures with covalent bonds without 5' caps and 3' poly (A) tails (1). CircRNAs were first found in pathogens but were regarded as meaningless or even incorrect expression products for decades. In recent years, researchers have begun to realize the importance of circRNAs with the rapid development of specific biochemical and computational methods, such as high-throughput sequencing technology and microarray techniques (2, 3). CircRNAs are generally stable and thought to have unique structural

conformations that differ from their linear RNA homology (4). As confirmed, circRNAs are principally formed *via* the junction of a downstream 3' site with an upstream 5' site, generated *via* back-splicing or exon skipping of premRNAs in general (5, 6). Over years of research, circRNAs have been found to feature four main characteristics (**Figure 1**). First, circRNAs are connected from end to end to form ring structures, enhancing their stability and resistance to most ribonucleases. Studies have shown that the half-life of circRNAs is longer than that of corresponding linear transcripts, which is beneficial for the transportation, preservation, and analysis of samples. Second, circRNAs are conserved, tissue- and spatiotemporal specific, resulting in acceptable reproducibility and individual differences (7). Third, circRNAs are abundant and almost endogenous (8, 9). The expression level of circRNAs changes accordingly under physiological or pathological conditions. Therefore, the change in the amount of circRNAs can reflect the stage of disease to some extent. Fourth, circRNAs are widely distributed and have high detection sensitivity (8). Currently, circRNAs are commonly divided into the following four categories according to their constituent sequences: exonic circRNAs (ecircRNAs), circular intronic RNAs (ciRNAs), exon–intron circRNAs (EIciRNAs) and tRNA intronic circular RNAs (tricRNAs). However, the circRNAs currently found are mainly derived from exons (5, 9).

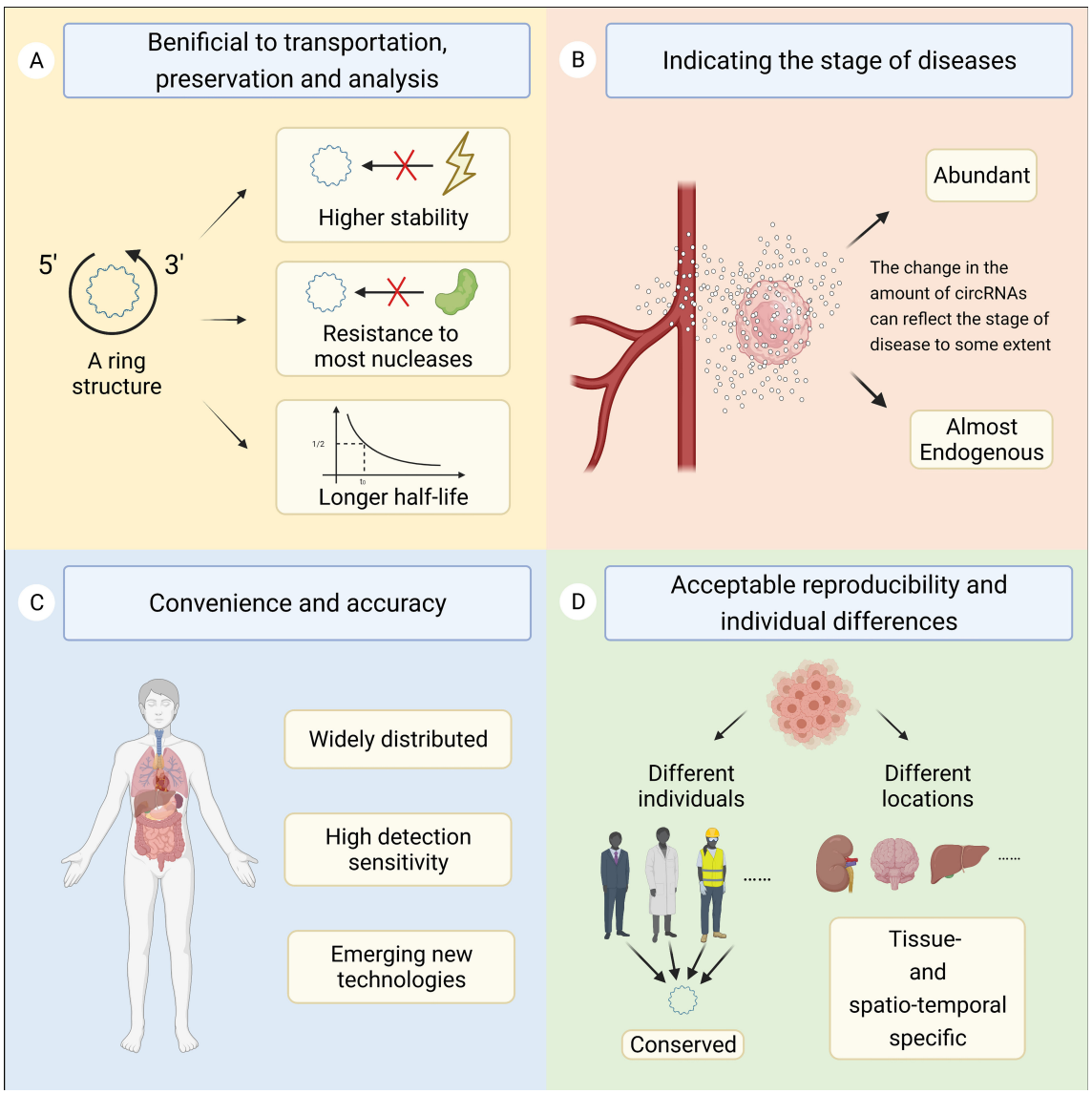

FIGURE 1 | This figure shows the four main characteristics of circRNAs. **(A)** The ring structure is beneficial for the transportation, preservation, and analysis of samples. **(B)** The change in the amount of circRNAs can reflect the stage of disease to some extent. **(C)** CircRNAs are widely distributed and have high detection sensitivity. **(D)** CircRNAs are conserved, tissue- and spatiotemporal specific, resulting in acceptable reproducibility and individual differences.

Since the advent of empirical immunology, research investigating immunity has lasted for a long time. The immune system plays a dual role in the fight against diseases. On the one hand, the body's immune barrier acts as a defense against intruders, and a functioning immune system can quickly detect and address abnormal conditions in the body. On the other hand, a dysregulated response of the human immune system may lead to the deterioration of the disease or the emergence of autoimmune diseases. With the development of research, scientists have noticed that circRNAs are of vital importance in human immunity and have potential clinical significance in the diagnosis and treatment of autoimmune diseases, tumor immunity, infectious diseases and other immune-related diseases (9–12).

This review expounds upon the progress and existing problems in this field and provides potential development directions for the future to improve the environment for clinical treatment.

2 BIOLOGICAL FUNCTIONS OF CIRCRNAS

According to current studies, circRNAs participate in different physiological processes of human diseases and perform a wide range of functions as miRNA sponges, transcription templates, special protein binding sites and regulators of host genes. Many current studies have focused on circRNAs in the cytoplasm, and some of those circRNA were reported to act as competing endogenous RNAs (ceRNAs) and usually function as sponges for miRNAs, thereby regulating miRNAs targeting gene expression (13, 14). A typical example is CDR1as, namely, ciRS-7, which contains more than 70 miRNA response elements (MREs) for miR-7 and can combine with miR-7 to downregulate its miRNA actions (15–17). In addition, circRNAs can use their specific regions to interact with proteins (18), function as protein scaffolds (19) and recruit specific proteins to certain locations in cells (20); thus, circRNAs with internal ribosome entry sites (IRESs) and infinite open reading frames (ORFs) can be translated under specific circumstances (21, 22). Moreover, circRNAs correlated with RNA polymerase II (Pol II) in human cells, localizing in the nucleus, could modulate the expression of their host genes (23, 24). However, unfortunately, research concerning the function of circRNAs only focuses on a small fraction of circRNAs that have been found, thereby requiring more specificity. Therefore, there is still more development space for other types of circRNAs that are less studied, rending the future of this field full of uncertainty and promises.

3 ROLES OF CIRCRNAS IN IMMUNE-RELATED DISEASES

Many studies have been performed to uncover the mechanism of immunity with the purpose to solve the problems of immunological diseases. With continuous research development, increasing evidence has emerged showing that circRNAs are able to intervene in the biological processes of assorted immune-related diseases by acting as miRNA sponges, protein interactors, mRNA stability maintainers, potential biomarkers and therapeutic targets *via* diverse axes and intricate signaling pathways (**Table 1**). In this section (**Figure 2**), we describe new experimental progress in circRNAs that participate in organ-specific autoimmune diseases (OSADs), systemic autoimmune diseases (SADs), tumor immunology, and infectious diseases and summarize the roles of circRNAs in other studies.

3.1 CircRNAs in Organ-Specific Autoimmune Diseases

In OSADs, autoantigens are a specific component of an organ, and the pathological damage and dysfunction of tissue are limited to the organ targeted by antibodies or lymphocytes. Multiple sclerosis (MS) is an autoimmune disease that demyelinates the white matter of the central nervous system. Although the specific pathogenesis remains unclear, circRNAs have been found to participate in the progression of MS (55). Cardamone et al. indicated that the abnormal metabolism of circRNAs is a potential characteristic of MS (26). Moreover, Iparraguirre et al. found two downregulated circRNAs and considered them potential biomarkers of MS (25). Among ncRNAs, miRNAs and lncRNAs are currently popular issues in MS, while circRNAs are relatively less studied; thus, more research is needed to supplement the regulatory network of ncRNAs in MS (56).

In addition to MS, circRNAs play an important role in many other OSDAs. For example, circRNAs showed promise as candidate biomarkers of primary biliary cholangitis (27), and plasma circRNA_002453 could be used as a novel biomarker of lupus nephritis (28). Researchers also found that circSnx5 control the immunogenicity of dendritic cells as a miRNA sponge, thereby alleviating experimental autoimmune myocarditis (29). Although the participation of circRNAs has further increased the complexity of the mechanism of OSAD, current research is still very simple, and it is difficult to promote the understanding of this type of disease and the therapeutic application of circRNAs.

3.2 CircRNAs in Systemic Autoimmune Diseases

Systemic autoimmune disease is a type of systemic multiple organ damage caused by the extensive deposition of antigen and antibody complexes on the vascular wall, and systemic lupus erythematosus (SLE) is a common disease. The exact cause of SLE is still unclear, but circRNAs have recently been regarded as vital molecules in SLE. Li et al. compared the different circRNA profiles in T cells from healthy and ailing patients and then revealed the biofunction of hsa_circ_0045272 (30). Currently, many circRNAs have been identified as biomarkers of SLE (31–34). Recently, Zhang et al. retrieved the GEO database and obtained a regulatory network, providing novel insight into the role of circRNAs in SLE (57).

TABLE 1 | Roles of circRNAs in four main immune-related diseases.

Diseases	circRNAs	Functions	Related molecules	Related pathways	Ref
			Organ-specific autoimmune diseases		
Multiple sclerosis	circ_0005402 circ_0035560	Potential biomarker	——	——	(25)
	hsa_circ_0106803	Potential biomarker	——	——	(26)
Primary biliary cholangitis	hsa_circ_402458	Potential biomarker	——	——	(27)
Lupus nephritis	circ_002453	Potential biomarker	——	——	(28)
Autoimmune myocarditis	circSnx5	miRNA sponge	miR-544, SOCS1, PU.1	JAK/STAT signaling pathway, MAPK signaling pathway	(29)
			Systemic autoimmune diseases		
Systemic lupus erythematosus	hsa_circ_0045272	miRNA sponge	IL-2, hsa-miR-6127	Apoptosis signaling pathway	(30)
	hsa_circ_0000479	Potential biomarker	——	——	(31)
	hsa_circ_0044235 hsa_circ_0068367	Potential biomarker	——	——	(32)
	circPTPN22	Potential activity indicator	——	——	(33)
	hsa_circ_407176 hsa_circ_001308	Potential biomarker	——	——	(34)
Rheumatoid arthritis	hsa_circ_0001200 hsa_circ_0001566 hsa_circ_0003972 hsa_circ_0008360	Potential biomarker	——	——	(35)
	hsa_circ_0000396 hsa_circ_0130438	Potential biomarker	——	——	(36)
	hsa_circ_0088036	miRNA sponge	miR-140-3p, SIRT1	AMPK signaling pathway, mTOR signaling pathway	(37)
Primary Sjögren's syndrome	hsa_circ_001264 hsa_circ_104121 hsa_circ_045355	Potential biomarker	——	——	(38)
			Tumor immunology		
Laryngeal squamous cell carcinoma	hsa_circ_001569 hsa_circ_001859	miRNA sponge	CD274, IL-10, FOXP3	Th17 cell differentiation	(39)
Pancreatic adenocarcinoma	circUBAP2	miRNA sponge	CXCR4, ZEB1	Wnt signaling pathway, MAPK signaling pathway	(40)
Melanoma	circ_0020710	miRNA sponge	miR-370-3p, CXCL12	mTOR signaling pathway	(41)
Non-small cell lung cancer	circMET	miRNA sponge	miR-145-5p, CXCL3	TNF signaling pathway	(42)
	circFGFR1	miRNA sponge	miR-381-3p, CXCR4	HIF-1 signaling pathway, Wnt signaling pathway	(43)
Hepatocellular carcinoma	circUHRF1	miRNA sponge, potential biomarker	miR-449c-5p, IFN-γ, TNF-α, TIM-3	TNF signaling pathway, MAPK signaling pathway	(44)
Colorectal cancer	circSPARC	miRNA sponge, protein binder, potential biomarker and therapeutic target	miR-485-3p, JAK2, STAT3, FUS	JAK/STAT signaling pathway	(45)
			Infectious diseases		
Pulmonary tuberculosis	hsa_circ_14623 hsa_circ_09585 hsa_circ_005538 hsa_circ_09993 hsa_circ_00074 hsa_circ_13478	miRNA sponge, potential biomarker	——	Endocytosis pathways in cancer, MAPK signaling pathway, HTLV-1 infection, and ubiquitin- mediated proteolysis signaling pathway	(46)
	hsa_circ_0005836	potential biomarker and therapeutic target	——	——	(47)

(Continued)

TABLE 1 | Continued

Diseases	circRNAs	Functions	Related molecules	Related pathways	Ref
Active tuberculosis	hsa_circ_001937	potential biomarker	— —	— —	(48)
Bacterial meningitis	hg38_circ_0002276	miRNA sponge	hsa-miR-548o-3p	— —	(49)
	hg38_circ_0031043		hsa-miR-548o-3p		
	hg38_circ_0027134		hsa-miR- 148a-3p		
	hg38_circ_0032477		hsa-miR- 148a-3p		
	hg38_circ_0008980		hsa-miR-660-5p		
	hg38_circ_0001582		hsa-miR-194-5p		
	hg38_circ_0017427		hsa-miR-107		
Viral infection	circRNAs	interacting with proteins	K63, RIG-I, IRF3, NF90/110	Innate immunity	(50, 51)
COVID-19	Ppp1r10	miRNA sponge	mmu-miR-124-3p,	Antiviral mechanism by IFN-stimulated genes	(52)
	C330019G07RiK		Ddx58, Gm26917		
Microbial infection	circRasGEF1B	maintaining the stability of the mature mRNA	ICAM-1, LPS, NF-κB	LPS pathway, NF-κB pathway, cell cycle, macrophage polarization	(53)
Chlamydia infection	hsa_circ_001226	miRNA sponge	— —	Endocytosis, MAPK and PI3P-Akt signaling pathway	(54)
	hsa_circ_007046				
	hsa_circ_400027				

Another common type of systemic autoimmune disease is rheumatoid arthritis (RA), whose pathogenesis has not been fully elucidated thus far. Currently, in the research field of circRNAs in RA, research mainly focuses on expression profile analyses, biomarker research and the proliferation and migration of fibroblast-like synovial cells. Wen et al. constructed a network of differentially expressed circRNAs and miRNAs and eventually revealed the expression profile of peripheral blood mononuclear cells (PBMCs) in patients with RA (35). Yang et al. used RNA sequencing technology to uncover the circRNA expression profiles of PBMCs in experimental and control groups and found that circRNAs are novel diagnostic markers of RA (36). Regarding the proliferation and migration of fibroblast-like synovial cells, Zhong et al. found that hsa_circ_0088036 promoted the proliferation and migration of fibroblast-like synovial cells *via* the miR-140-3p/SIRT1 axis in RA (37). In addition to SLE and RA, circRNAs are of great concern in some SADs. For example, Su et al. reported that hsa_circ_001264 might be a biomarker of primary Sjögren's syndrome (pSS) (38). Although circRNAs are closely connected to SADs such as SLE, RA and pSS, research concerning SADs, such as scleroderma, dermatomyositis and polymyositis, currently mainly focuses on miRNAs. Consequently, there is substantial untapped potential in research investigating the mechanisms of circRNAs and SADs.

3.3 CircRNAs in Tumor Immunology

Currently, the study of tumor immunology focuses on the body's immune response to tumors, the mechanism of tumor immune escape tumor immune diagnosis and immune prevention. Over years of research, scientists have discovered that circRNAs are very important molecules in various tumors, playing a variety of immunological functions. The hottest research area is the competing endogenous RNA (ceRNA) network and its regulatory molecules. Sun et al. constructed ceRNA networks based on 133 laryngeal squamous cell carcinoma (LSCC) patients and found that hsa_circ_001569 and hsa_circ_001859 might regulate the expression of CD274, IL-10 and FOXP3, thus intervening in the immune escape of LSCC (39). In another study on ceRNA networks in pancreatic adenocarcinoma (PAAD), Zhao et al. reported that CXCR4 and ZEB1 were regulated by the circUBAP2-mediated ceRNA network, inhibiting antigen presentation and promoting tumor immune escape (40). Among studies investigating ceRNA networks, research focusing on the circRNA/miRNA/mRNA axis is especially plentiful. The effects on cell phenotypes are mainly reflected in the ability to drive tumor immune escape and promote proliferation and metastasis *via* different axes (41, 42). In addition, studies related to anti-PD-1 therapy are included in these reports (43, 44).

With the deepening of understanding, researchers have discovered the potential of circRNAs as therapeutic targets and biomarkers with abilities to assist with diagnosis and prognosis and their function in the immune regulation of exosomes. Wang et al. showed that circSPARC might conceivably act as a possible biomarker for diagnosis and prognosis and a target for therapy in colorectal cancer (CRC) (45). In another study concerning

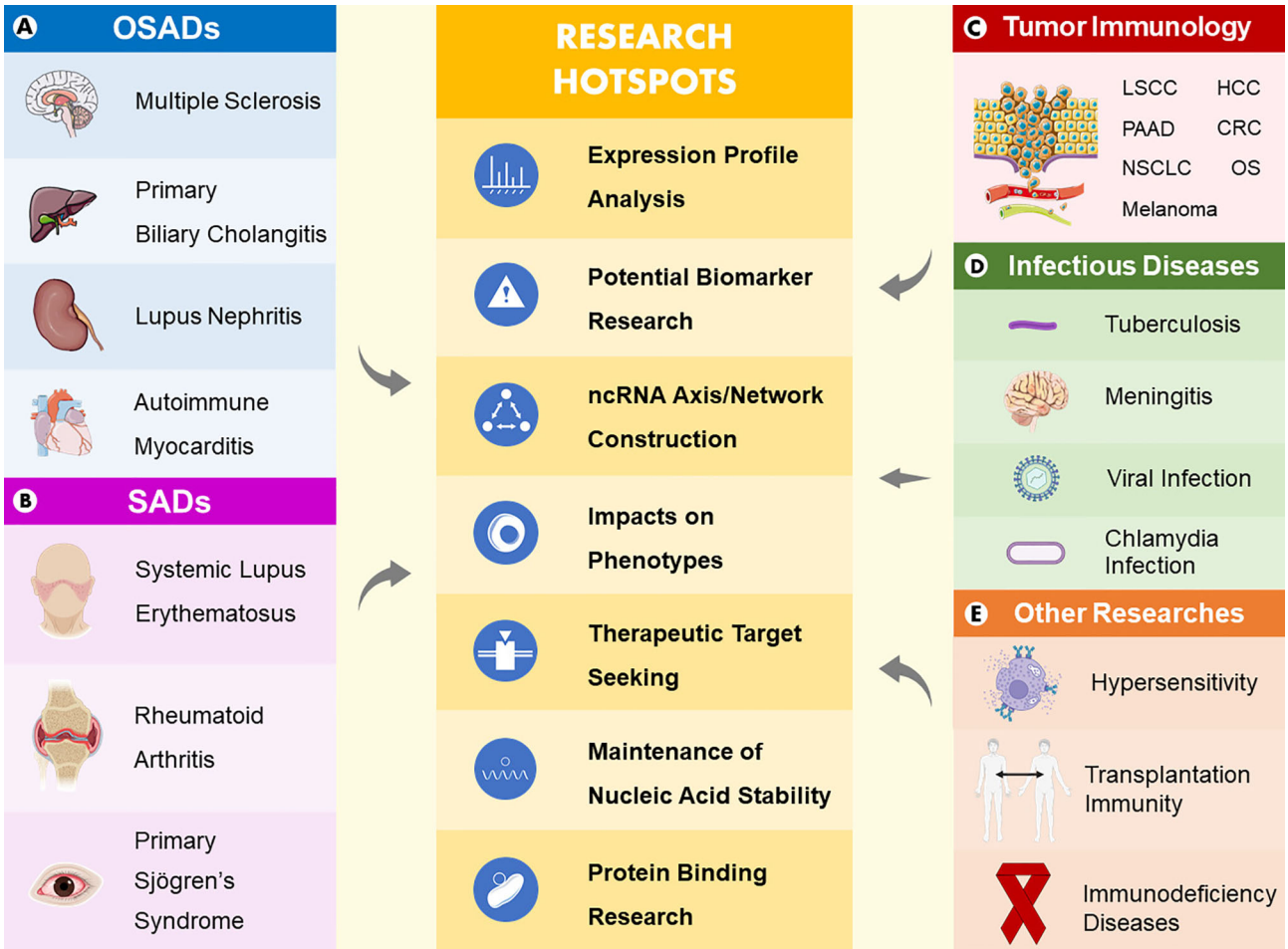

FIGURE 2 | Main areas and research hotspots of the roles of circRNAs in immune-related diseases. Five main areas consist of organ-specific autoimmune diseases **(A)**, systemic autoimmune diseases **(B)**, tumor immunology **(C)**, infectious diseases **(D)**, and other studies **(E)**. In summary, research hotspots of the roles of circRNAs in immune-related diseases include expression profile analyses, potential biomarker research, ncRNA axis/network construction, impacts on phenotypes, therapeutic target seeking, maintenance of nucleic acid stability and protein binding research.

hepatocellular carcinoma (HCC), scientists reported that the upregulated level of plasma exosomal circUHRF1 decreased NK-cell tumor infiltration, curbing the function of NK cells (44).

Generally, from the laboratory to the clinical level, current research focusing on circRNAs in tumor immunology is proceeding in an orderly manner. Therefore, the application of circRNAs in the future may have a very positive impact on many aspects of tumor immunotherapy, such as diagnosis, treatment, and prognosis.

3.4 CircRNAs in Infectious Diseases

Infectious diseases refer to diseases in which bacteria, viruses, fungi, parasites, and other infectious agents, invade, grow, and reproduce in the body, causing damage to the normal metabolic functions of the tissue structure. Thus far, circRNAs have been found to be used as biomarkers of many infectious diseases in most cases, while emergent corroboration indicates that a small number of circRNAs are verified to directly impact the regulatory network of infectious diseases (58). By regulating the NF-κB pathway, the potential miRNA targets of hsa_circ_001937 exert effectiveness in antibacterial immune responses in patients with tuberculosis (46, 48). In a bioinformatics analysis experiment, Zhuang et al. found that hsa_circ_0005836 could be a novel biomarker for diagnosis and prognosis and a target for therapy of active pulmonary tuberculosis (47). In a similar experiment, Yang et al. performed a circRNA transcription analysis of primary human brain microvascular endothelial cells infected with meningeal Escherichia coli and preliminarily constructed a potential regulatory network that enhanced our understanding of the mechanisms of bacterial meningitis (49). Additionally, in Marinov et al.'s study focusing on an LPS-inducible circRNA called circRasGEF1B, the authors assumed that inducible RasGEF1B circular RNA may play an essential role in protecting cells against microbial infection by preserving the constancy of the mature mRNA of ICAM-1 in LPS-activated

cells (53), providing a new idea for antimicrobial infection therapies. CircRNAs are of vital importance to the infection of viruses because the abnormal expression of circRNAs may promote or suppress the infection progress of viruses, and vice versa. Studies have shown that when infected with viruses, circRNAs are rapidly degraded by RNase L, releasing PKR (dsRNA-activated protein kinase) linked to circRNAs and participating in innate cellular immune responses (35, 59). Notably, circRNAs initiate innate immunity by combining with K63, which links ubiquitin chains, and RIG-I (retinoic acid-inducible gene I). Exogenous circRNAs without m6A modification can attach to K63 and RIG-I. This complex can promote the polymerization and activation of RIG-I, affect the aggregation of downstream mitochondrial antiviral signals, guide the dimerization and activation of interaction regulating factor 3 (IRF3), and finally induce the expression of autoimmune-related pathway genes (50, 60, 61). The antiviral dsRNA-binding protein NF90/110 can stabilize the secondary structure of intronic RNA, thereby promoting the biogenesis of circRNAs. NF90/110 can also act as global regulators of circRNA biogenesis by reducing their nuclear levels during viral infection (51, 62).

Since the end of 2019, the world has experienced several rounds of outbreaks caused by variants of severe acute respiratory syndrome coronavirus 2 (SARS-CoV-2) and improper anti-epidemic measures. Omicron, a newly discovered SARS-COV-2 variant with high transmission, is causing unease and uncertainty. Therefore, whether focusing on the present or the future, it is particularly important to develop new treatment technologies on the basis of existing epidemic prevention measures such as drug development and vaccination (63). CircRNAs, molecules closely associated with viral infection, is one option. A differential host circRNA expression profile analysis in human lung epithelial cells infected with SARS-CoV-2 was completed (64), and two circRNA profile analyses revealed abundant and diverse information regarding the identification and characterization of the circRNAs encoded by SARS-CoV-1, SARS-CoV-2 and MERS-CoV (65, 66), facilitating future studies concerning on COVID-19 infection and pathogenesis. Arora et al. identified a circRNA/lncRNA-miRNA–mRNA ceRNA network involving two circRNAs in SARS-CoV-2-infected cells, enhancing the current understanding of the mechanisms associated with coronavirus disease 2019 (COVID-19) (52). Specific segments of the SARS-CoV-2 5'-untranslated region can be expeditiously accessed by particular antisense circRNAs, resulting in bringing an approximately 90% cutback in virus proliferation in cell culture with a minimal duration of 2 days, which is attractive and promising (67). Briefly, relevant research focused on expression profile analyses, ceRNA construction and therapeutic target seeking. Although circRNAs are in the initial stage in the prevention and treatment of novel coronavirus, with the development of cross-discipline and the emergence of more advanced technology, it is believed that there will be opportunities for circRNAs to display their clinical talents in the future.

In addition to bacteria and viruses, circRNAs function in many other infectious diseases, such as chlamydia infection (54). In addition to modulating the human body, circRNAs can play a regulatory role in other organisms during infectious diseases, such as parasite infection. Broadbent et al. identified developmentally regulated lncRNAs and circRNAs by strand-specific RNA sequencing in Plasmodium falciparum malaria (68), but currently, there is no clinical significance.

Overall, current research concerning circRNAs in infectious diseases mostly focuses on viral and bacterial infections, but in addition to research as biomarkers, these results are still a long way from clinical application.

3.5 CircRNAs in Other Immunological Research

Thus far, we mentioned that circRNAs are of great significance in autoimmune diseases, tumors, and bacterial and viral infections. In addition, expanding the perspective to the whole area, circRNAs perform effectively in hypersensitivity, immunodeficiency diseases and transplantation immunity, namely, the pathological changes caused by immune defense function. However, because the contents and categories of current related studies are relatively similar, there are only a few examples, which are no longer explained in detail here. For instance, circHIPK3 was proven to modulate the proliferation of airway smooth muscle cells by the miR-326/STIM1 axis in asthma (69), a group of ample circRNAs and ceRNA networks were found to likely contribute to acquired immune deficiency syndrome (AIDS) (70), and a two-circular RNA signature of donors was thought to be a biomarker of early allograft dysfunction after liver transplantation (71). In addition to the above diseases, circRNAs play vital roles in a variety of immunological diseases and immune cells. Under stimulation by different pathological factors, the way that circRNAs are involved in the activation of macrophages is a large subject (53, 72–74). In addition, a variety of circRNAs have been identified to influence various immune cells, such as intestinal immune cells (75), lung immune cells poisoned by Nd2O3 (76), CD4+ T cells in asthma (77) and immune cells in periodontitis (78). In addition to these effects on different immune cells, there are also some studies focusing on innovative technologies. Recently, Wesselhoeft et al. showed that unmodified exogenous circRNA can bypass cellular RNA sensors, thereby avoiding immune responses in RIG-1- and Toll-like receptor (TLR)-competent cells and mice, suggesting that RNA circularization reduces immunogenicity and can prolong the translation time *in vivo* (61).

Studies concerning circRNAs in immune-related diseases are miscellaneous, but the core functions and mechanisms are constant. The discovery of circRNAs has further deepened researchers' understanding of the intricate immune regulatory network. Generally, the immune system has three major functions, namely, immune defense, immune surveillance and immune homeostasis, and circRNAs realize immune-related mechanisms as follows: 1) during immune defense functions, circRNAs can assist the body in removing pathogenic microorganisms and other antigens in various ways; however, hypersensitivity or immune deficiency occurs when the immune response is too high or too low; 2) when immune surveillance operates regularly, circRNAs can help the body remove mutant

cells and virus-infected cells through various pathways; if this function is abnormal, it could lead to tumor occurrence and persistent virus infection; and 3) when immune homeostasis occurs naturally, circRNAs can aid the body in removing damaged or senescent cells in various ways, but imbalance could lead to autoimmune diseases. Therefore, the balance between the immune system and circRNAs plays a key role in whether the body is in a healthy or pathological state.

3.6 Regulatory Mechanisms of circRNAs in Immune-Related Diseases

The regulatory mechanism of circRNAs in immune-related diseases can be summarized into the following two aspects: the regulatory effects of circRNAs on immune-related signaling pathways (**Figure 3**), such as the MAPK signaling pathway, endocytosis signaling pathway, JAK-STAT signaling pathway, mTOR signaling pathway, and Wnt signaling pathway, and the regulatory effects of circRNAs on immune cells, such as the regulation of macrophages, etc.

3.7 Important Signaling Pathways of circRNAs Involved in the Regulation of Immune-Related Diseases

3.7.1 MAPK Signaling Pathway

The MAPK signaling pathway is a signal transduction system important for eukaryotic cells to mediate extracellular signals in the intracellular response. This pathway transduces extracellular signals in the form of a triple kinase cascade, namely, MAP kinase kinase kinase (MKKK), MAP kinase kinase (MKK) and MAP kinase (MAPK), which regulates a variety of physiological processes, such as cell growth, differentiation, apoptosis and death. There are four main branches of the MAPK pathway as follows: extracellular-signal regulated protein kinase (ERK), c-Jun N-terminal kinase (JNK), p38 mitogen-activated protein kinase (p38 MAPK) and ERK5. Among them, JNK and p38 have similar functions, which are related to inflammation, apoptosis and cell growth; ERK is mainly responsible for cell growth and differentiation, and its upstream signals are the famous Ras and Raf proteins (79, 80). According to current studies, circRNAs mainly play roles as miRNA sponges in the MAPK signaling pathway in immune-related research. For example, Chen et al. found that circSnx5 acted as a sponge of miR-544 to upregulate suppressor of cytokine signaling 1 (SOCS1) (81). Zhang et al. revealed the circUHRF1/miR-449c-5p/TIM-3 axis in HCC (44). Zhao et al. constructed a ceRNA network consisting of 4 DEcircRNAs, 3 DEmiRNAs and 149 DEmRNAs in PAAD (40), which also showed the sponge function of circRNAs. Among the regulated proteins, SOCS1 (82–84), TIM-3 (85–87), ZEB1 (88–90), etc., serve as important regulators in the MAPK signaling pathway.

3.7.2 Endocytosis Signaling Pathway

Endocytosis is the process of transporting extracellular substances into cells through the deformed movement of the plasma membrane. Endocytosis can be divided into phagocytosis, pinocytosis and receptor-mediated endocytosis according to the size and mechanism. According to clathrin dependence, endocytosis can be divided into clathrin-dependent endocytosis (CDE) and clathrin-independent endocytosis (CIE). In terms of trends, the mechanism of the relationship between signal transduction and endocytosis has received increasing attention in studies investigating of the occurrence and development of many diseases. Endocytosis has been proven to be closely related to lipid metabolism, intracellular iron homeostasis, metabolism, immunity and other functions (91–93). On the basis of existing research, circRNAs mainly participate in the endocytosis pathway as miRNA sponges in immune-related research. Abnormally expressed circRNAs were identified in pulmonary tuberculosis (46) and chlamydia infection (54), and all were predicted to be miRNA sponges. Through bioinformatics analyses, these circRNAs were found to be related to the endocytosis signaling pathway. A special study focused on the protein translation function of circRNAs, and verified that circ-EGFR attenuates EGFR endocytosis and degradation (94).

3.7.3 JAK-STAT Signaling Pathway

The JAK-STAT signaling pathway has been revealed to consist of the following four parts: extracellular signaling factors, tyrosine kinase-related receptors, tyrosine kinase called Janus kinase (JAK) that transmits signals, and transducer and activator of transcription (STAT) that exerts effects. When a variety of cytokines and growth factors bind receptors, JAK is activated, and then the activated JAK phosphorylates the receptor and itself. These phosphorylated sites become the binding sites of STAT with an SH2 structure, thus recruiting and phosphorylating STAT and allowing it to enter the nucleus in the form of a dimer to bind to target genes, regulating the transcription of downstream genes and modulating the process of cell proliferation, differentiation and apoptosis (95, 96). In light of research conducted thus far, circRNAs mainly act as miRNA sponges in the JAK-STAT signaling pathway in immune-related research. For instance, Wang et al. uncovered the circSPARC/miR-485-3p/JAK2 axis in CRC (45). In type 1 diabetes mellitus, Yang et al. identified the hsa_circ_0060450/miR-199a-5p/mRNAs axis, which suppressed the JAK-STAT signaling pathway triggered by IFN-I (97).

3.7.4 mTOR Signaling Pathway

Mammalian target of rapamycin (mTOR) is an evolutionarily conserved serine/threonine protein kinase that can regulate a variety of cell functions by phosphorylating its downstream target protein. There are two key complexes in the mTOR signaling pathway called mTOR complex 1 (mTORC1, including mTOR, Raptor, mLST8, etc.) and mTOR complex 2 (mTORC2, including mTOR, Rictor, mLST8, etc.). mTORC1 is activated in the presence of lysosome levels, ER stress, sterols, hypoxia and energy stress to regulate several biological processes, including lipid metabolism, autophagy, protein synthesis and ribosomal biogenesis, while mTORC2 responds to growth factors and controls cytoskeletal organization, metabolism and cell survival (98–100). According to studies, circRNAs mainly exert an influence as miRNA sponges in the mTOR signaling pathway in immune-related research. For example, Zhong et al. revealed

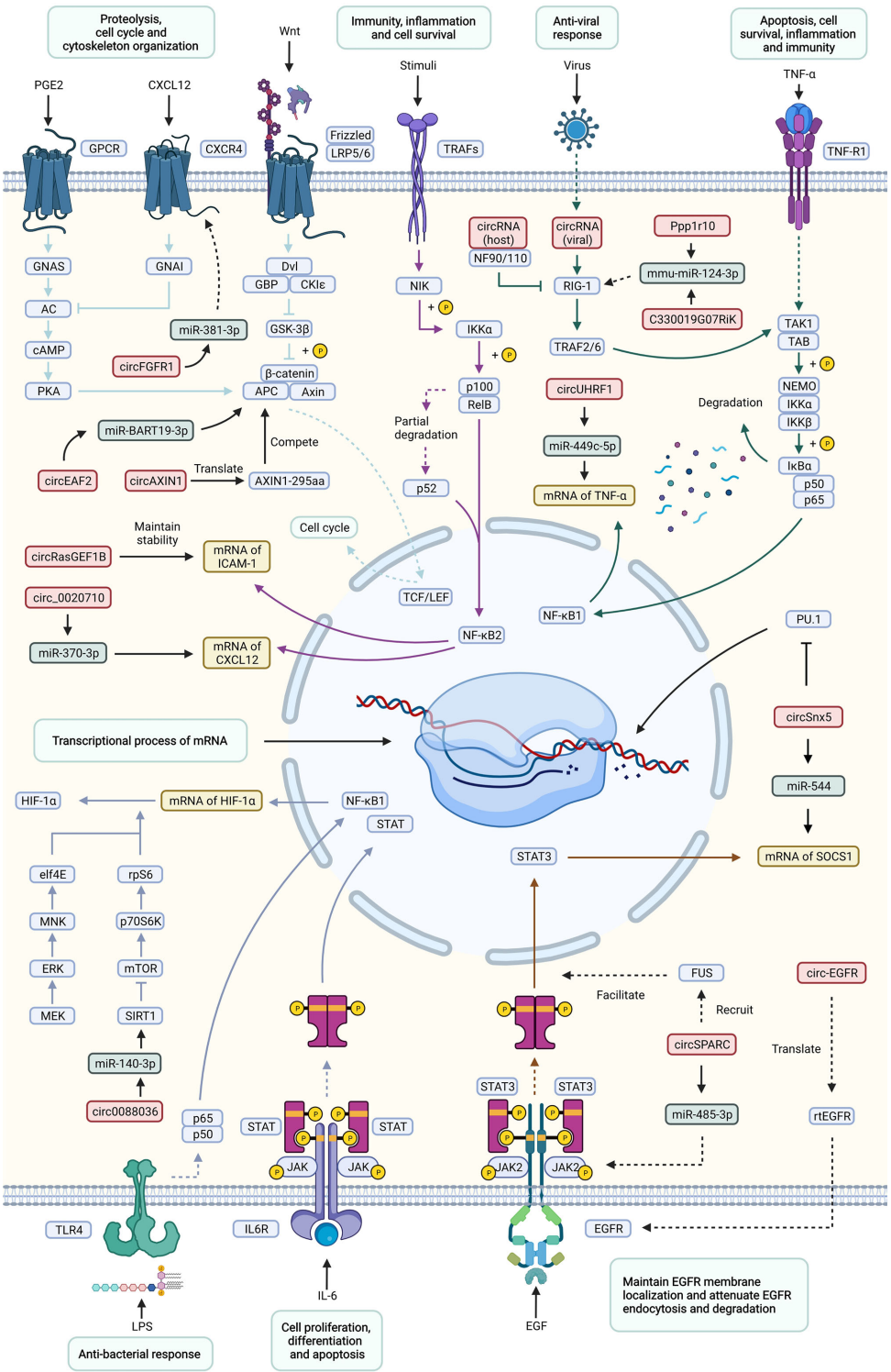

FIGURE 3 | Important signaling pathways of circRNAs involved in the regulation of immune-related diseases. This figure shows how circRNAs influence immune-related diseases *via* a variety of signaling pathways, including the Wnt, TNF, NF-κB, JAK-STAT, mTOR, antiviral and antibacterial pathways. and the corresponding responses. Effects and processes are shown in light green rectangles, circRNAs are shown in red rectangles, miRNAs are shown in dark green rectangles, mRNAs are shown in yellow rectangles, and proteins are shown in blue rectangles. Different signaling pathways are distinguished by arrows and inhibitors of different colors. Solid lines represent direct interactions between molecules, while dotted lines represent indirect interactions.

the circ0088036/miR-140-3p/silent information regulator 1 (SIRT1) axis in the promotion of RA (37). Wei et al. indicated the importance of the circ_0020710/miR-370-3p/CXCL12 axis in melanoma (41). Regarding the regulated proteins, SIRT1 (101–103), CXCL12 (104–106), etc., served as important regulators in the mTOR signaling pathway.

3.7.5 Wnt Signaling Pathway

The Wnt signaling pathway is a complex regulatory network that has been verified to include at least the following three branches: the classical Wnt signaling pathway, namely, the Wnt/β-catenin signaling pathway, Wnt/planar cell polarity (PCP) pathway and Wnt/Ca2+ pathway activated by Wnt5a and Wnt11. Wnt mainly transmits signals through 7 transmembrane receptors of the Frizzled family and LRP5/6 coreceptors and plays a regulatory role in cells through key molecules such as CK1, Deshevelled, GSK3, APC, Axin, and β-Catenin (107–109). Currently, circRNAs mainly produce marked effects as miRNA sponges in the Wnt signaling pathway in immune-related research. For instance, Zhang et al. stated that the circFGFR1/miR-381-3p/CXCR4 axis promoted NSCLC progression and resistance to anti-programmed cell death 1 (PD-1)-based therapy (43). Zhao et al. proposed that circEAF2 counteracts Epstein–Barr virus-positive diffuse large B-cell lymphoma progression *via* the miR-BART19-3p/APC/β-catenin axis (110). Regarding the regulated proteins, CXCR4 (111–113), APC (114–116), etc., served as important regulators in the Wnt signaling pathway. Specifically, a study revealed that a novel protein AXIN1-295aa encoded by circAXIN1 activated the Wnt/β-catenin signaling pathway to promote gastric cancer progression (117).

In addition to the pathways highlighted above, circRNAs participate in the regulation of the TNF, AMPK, HIF-1 and NF-κB. signaling pathways, but generally, the mechanisms are similar; thus, circRNAs exert effects on immune function and immune-related diseases mainly by translating proteins and acting as miRNA sponges.

3.7.6 Regulation of circRNAs in Immune Cells

CircRNAs have various regulatory functions and have been detected in different types of immune cells, such as macrophages, dendritic cells (DCs), natural killer cells (NK cells), CD4+ T cells and CD8+ T cells. By inhibiting or promoting the activation or exhaustion of these cells, circRNAs participate in the development of various diseases.

3.7.7 Regulation of circRNAs in Macrophages

CircRNAs affect the activation of macrophages. For instance, mouse macrophages specifically express circ-RasGEF1B in the form of NF-κB after being stimulated by lipopolysaccharide (LPS), which can activate macrophages by positively regulating the expression of intercellular adhesion molecule-1 (ICAM-1) (53, 72). Zhang et al. found that circPPM1F participates in the activation of MI macrophages in diabetic patients (118), while another study showed that hsa_circ_0110102 inhibits macrophage activation *via* the miR-580-5p/PPARα/CCL2 pathway (119). In addition, SiO_2 induces macrophage activation through the circHECTD1/HECTD1 pathway and circZC3H4 RNA and ZC3H4 protein in the process of pulmonary fibrosis (120, 121). In addition, circRNA HIPK3 and circUbe3a can activate macrophages, while the latter participates in the process of myocardial fibrosis (122, 123).

Furthermore, circRNAs can lead to the polarization of tumor-associated macrophages to M1 or M2 macrophages. One study showed that circN4 bp1 could act as a miR-138-5p sponge for the modulation of macrophage polarization through the regulation of the expression of EZH2 (a histone methyltransferase) (124). Moreover, circRNA Cdyl, circPrkcsh and circPPM1F were found to play a role in inducing M1 macrophage polarization (118, 125, 126). Many studies have highlighted the importance of circRNAs in the occurrence and development of tumors, and one effect is the mediation of the polarization of M2 macrophages. For example, tumor-derived extracellular circFARSA was discovered to mediate the polarization of M2 macrophages (127). Additionally, cyclic RNA PLCE1, circITGB6, circ_0001142 and hsa_circ_0074854 were also found to play such a role (128–131).

CircRNAs also play a role in regulating the macrophage-related inflammatory response; for example, hsa_circ_0005567 can promote M2 macrophage polarization *via* the mir-492/SOCS2 axis (132). Moreover, hsa_circ_0004287 inhibits macrophage-mediated inflammation in an N-methyladenosine-dependent manner in atopic dermatitis and psoriasis (133). Furthermore, circRNAs can also advance the inflammatory response. In gouty arthritis, circHIPK3 was found to be able to activate the macrophage inflammasome (134), as did hsa_circ_0087352, circ_1639 and circ_0001490 (135–137).Significantly, in Mycobacterium tuberculosis infection, circRNAs TRAPPC6B and hsa_circ_0045474 can induce autophagy in macrophages (138, 139). Other studies have found that the circRNA calcitonin gene-related peptide (CGRP) can induce macrophages to express IL-6 (140).

3.7.8 The Regulation of circRNAs on Other Immune Cells

Current research investigating the correlation between circRNAs and immune cells mainly focuses on macrophages, and there are relatively few studies of other cells. Here, we briefly review the regulation of circRNAs in NK cells, DCs, CD4+ T cells and CD8+ T cells.

CircRNAs can promote NK-cell depletion and regulate cytotoxicity. A study found that hsa_circ_0048674 and cancer cell-derived exosome circUHRF1 can induce NK-cell dysfunction (44, 141). Hsa_circ_0007456 regulates NK-cell-mediated hepatocellular carcinoma cytotoxicity through the mir-6852-3p/ICAM-1 axis (131). Moreover, circARSP91 can enhance innate immune surveillance by strengthening the cytotoxicity of NK cells (142). In addition, circrHT1 knockout can aggravate the sensitivity of bladder cancer cells to NK cells, and another study showed that circ_0000977 knockout can enhance the killing effect of NK cells on pancreatic cancer cells through HIF1A and ADAM1 (143, 144). A GO analysis showed that circRNAs were involved in regulating DC differentiation and other biological functions (145). Chen et al. found that circSnx5 controls the immunogenicity of DCs through the miR-

544/SOCS1 axis (29). Furthermore, Wang et al. discovered that the knockdown of circFSCN1 could affect the ability of DCs to activate T cells and enhance Treg generation (146). Another study showed that growth differentiation factor 15 induces tolerant DCs (Tol DCs) by inhibiting the circ_malat-1 and NF-κB signaling pathways and upregulating IDO (147).

Research investigating the connection between circRNAs and CD4+ T cells mainly concentrates on systemic lupus erythematosus (SLE) and asthma. Studies have shown that the DNA methylation of CD11a and CD70 in CD4 T cells form patients with SLE is associated with the downregulation of hsa_circ0012919 (148). In addition, the regulatory network among circHIPK3, LncGAS5 and miR-495 can promote Th2 differentiation in allergic rhinitis (149), and hsa_circ_0002594 and hsa_circ_0005519 can affect asthma by regulating CD4+ T cells (77, 150). Moreover, N-methyladenosine-modified circIGF2BP3 was found to inhibit CD8+ T-cell responses and promote tumor immune evasion (151), while exogenous circTRPS1 was proven to be related to CD8+ T-cell exhaustion (152). In addition, Chen et al. noted that the expression of circRNA100783 is affected by time- and CD28-related CD8(+) T-cell aging during antigen exposure (153). Clinically, cancer cell-derived exosomal circUSP7 was proven to induce CD8+ T cell dysfunction and anti-PD1 resistance by regulating the miR-934/SHP2 axis in NSCLC (154).

3.8 Applications and Prospects of circRNAs in the Treatment of Immune-Related Diseases

Immunotherapy refers to a treatment technique that artificially heightens or represses the immune function of the body to treat immune-related diseases in accordance with the low or hyperactive immune state of the body. Because of their unique structure and various functions, circRNAs have broad application prospects in the treatment of immune-related diseases.

At the current stage, most studies investigating the functions of circRNAs are still in the laboratory stage, and only a few theories have been developed for technical applications in clinical treatment, such as gene therapy. Tens of thousands of studies have proven circRNAs to be substantially considerable in the advancement of many immune-related diseases, suggesting the roles of circRNAs as therapeutic agents and targets (50, 62, 147, 155–157). To date, there are four main approaches to realizing gene therapy as follows: inducing or inhibiting the expression of the target circRNA upstream, chemically modifying key molecules, designing analogs of the target circRNA and designing downstream molecular analogs of the circRNA, i.e., miRNA.

In addition to gene therapy, with the discovery of the function of encoding proteins, circRNAs are speculated to have the potential to be novel drug delivery carriers. Wesselhoeft et al. produced a protein with high quality and stable expression in eukaryotic cells after the circularization of mRNA *in vitro* and indicated that RNA circularization can reduce immunogenicity and extend translational duration in vivo (61, 158, 159), providing insight into the treatment of immune-related diseases. In addition, circRNAs have the potential to function as appropriate biomarkers of immune-related diseases. In case of immune-related diseases, it is usually difficult for patients to determine whether they fell ill by the clinical symptoms in the early stage so that they will not go to the hospital until their symptoms worsen (9). Therefore, circRNAs can function as ideal biomarkers due owing to the four main characteristics mentioned above. Thus far, numerous circRNAs have been found in exosomes, and changes in the content of circRNAs in exosomes can reflect the process of diseases (159). However, the current problem that has blocked the application of circRNAs as biomarkers in the clinic is that with the continuous improvement of the circRNA database in immune-related diseases, the expression of the same circRNA in different diseases may have the same trend, which may interfere with the judgment. Therefore, a more refined database needs to be established.

Unparalleled strides have been made in cancer treatment with the use of immune checkpoint blockade (ICB), but ICB resistance hinders the efficacy of cancer immunotherapies (160). Based on existing research, regulating gene expression at the transcriptional level, acting as miRNA sponges, binding functional proteins and encoding proteins are the four major biological functions of circRNAs, and these functions can play a vital role in regulating immune diseases, such as immune escape, immune tolerance, and antitumor and anti-infection effects, either independently or in combination (7, 12, 161–167). Moreover, circRNAs can achieve cross-cellular regulation *via* exosomes. Recent studies have certified the potential role of exosomes in tumor immunity and resistance to ICB (160). For instance, Lu et al. suggested that immuno-repression and anti-PD1 resistance were caused by exosomal circTMEM181 by increasing the expression of CD39, and suppressing the ATP-adenosine signaling pathway by targeting CD39 on macrophages could rescue anti-PD1 therapy resistance in HCC (168). Therefore, *via* exosomes, circRNAs may yield unusually brilliant clinical results in ICB.

Considering that specially designed antisense circRNAs can effectively access the SARS-CoV-2 5'-untranslated region and inhibit the proliferation of most viruses for a time, circRNAs also an option for the clinical treatment of COVID-19, which is a major achievement that uses of the unique structure of circRNAs and artificial assistance for modification, showing many advantages. The best advantage is that the antisense sequence of circRNAs is better than the corresponding linear configuration and modified antisense oligonucleotides, and antisense circRNAs have strong activity against point mutations in the target sequence. This approach manifests the function of circRNAs as nucleic acid binders, starting novel applications for designing circRNAs and hopeful therapeutic strategies for COVID-19 (67). Fortunately, Qu et al. designed a circular RNA vaccine encoding the receptor domain (RBD) of the spike protein of SARS-CoV-2 for the very virus and its mutants and found that the circRNARBD-Delta vaccine designed for the SARS-CoV-2 Delta mutant was a candidate vaccine for COVID-19 with broad-spectrum protection in rhesus monkeys. A series of comparative evaluations showed that compared with mRNA vaccines, circRNA vaccines have higher

stability and a higher proportion of neutralizing antibodies, which can effectively reduce the potential side effects of vaccine-associated respiratory diseases (VAERD) (169).

Despite numerous studies, research focusing on circRNAs is still limited, and many problems remain to be solved. Although the structure of circRNAs can help attenuate off-target effects, this problem cannot be avoided. Moreover, a specific circRNA may have different functions in different cells and may cause uncontrollable side effects. In addition, if an exogenous circRNA is synthesized without protein-binding partners, it may be recognized by RIG-I as a virus-derived circRNA and thus induce innate immunity (7–9, 62).

3.9 Discussion and Perspectives

CircRNAs perform the functions of sponging miRNAs, binding specific proteins and regulating gene transcription, and some can even encode proteins. Meanwhile, circRNAs are widely distributed in cells, the internal environment and exosomes, coupled with stable ring structures; thus, they have application potential in the diagnosis, treatment and prognosis of immune-related diseases. However, current research investigating related diseases mainly focuses on tumor immunity, bacterial and viral infections, and some autoimmune diseases, while relatively uncommon diseases are rarely studied. The hotspots of the roles of circRNAs in immune-related diseases include expression profile analyses, potential biomarker research, ncRNA axis/network construction, impacts on phenotypes, therapeutic target seeking, maintenance of nucleic acid stability and protein binding research. In addition, the study of the mechanism of circRNAs in immune regulation only occupies the tip of the iceberg in immunology. Currently, few studies on the regulation of circRNAs in the establishment of the immune system and the regulation of the immune system in the normal physiological state. A representative study showed that the structure and decomposition of circRNAs modulate PKR activation in innate immunity (4). At present, this field also faces some unsolved problems, such as off-target effects and unpredictable side effects. Therefore, continuing to supplement the regulatory network of circRNAs, attempting to explore new mechanisms, and developing new functions will be crucial for the entire field in the future, and the birth of new technologies will further contribute to the complete unveiling of the roles of circRNAs in immunity and immune-related diseases.

AUTHOR CONTRIBUTIONS

JG, CS and FH wrote the manuscript, designed the figures, collected the related references and edited the manuscript, and JL and ZY provided guidance and revised this manuscript. All authors approved the final manuscript.

FUNDING

This work was supported by grants from the National Natural Science Foundation of China (81872211 and 82072999), the Sichuan Science and Technology Program (2020YJ0102), the Innovation Research Project of Sichuan University (2022SCUH0029), and the CAMS Innovation Fund for Medical Sciences (2020-I2M-C&T-A-023).

ACKNOWLEDGMENTS

The figures were created with Biorender (https://biorender.com) and Servier Medical Art (https://smart.servier.com).

REFERENCES

1. Zhou Z, Sun B, Huang S, Zhao L. Roles of Circular RNAs in Immune Regulation and Autoimmune Diseases. *Cell Death Dis* (2019) 10:503. doi: 10.1038/s41419-019-1744-5
2. Patop I, Wüst S, Kadener S. Past, Present, and Future of circRNAs. *EMBO J* (2019) 38:e100836. doi: 10.15252/embj.2018100836
3. Xie R, Zhang Y, Zhang J, Li J, Zhou X. The Role of Circular RNAs in Immune-Related Diseases. *Front Immunol* (2020) 11:545. doi: 10.3389/fimmu.2020.00545
4. Liu C, Li X, Nan F, Jiang S, Gao X, Guo S, et al. Structure and Degradation of Circular RNAs Regulate PKR Activation in Innate Immunity. *Cell* (2019) 177:865–80.e21. doi: 10.1016/j.cell.2019.03.046
5. Geng X, Jia Y, Zhang Y, Shi L, Li Q, Zang A, et al. Circular RNA: Biogenesis, Degradation, Functions and Potential Roles in Mediating Resistance to Anticarcinogens. *Epigenomics* (2020) 12:267–83. doi: 10.2217/epi-2019-0295
6. Eger N, Schoppe L, Schuster S, Laufs U, Boeckel J. Circular RNA Splicing. *Adv Exp Med Biol* (2018) 1087:41–52. doi: 10.1007/978-981-13-1426-1_4
7. Li X, Yang L, Chen L. The Biogenesis, Functions, and Challenges of Circular RNAs. *Mol Cell* (2018) 71:428–42. doi: 10.1016/j.molcel.2018.06.034
8. Holdt L, Kohlmaier A, Teupser D. Circular RNAs as Therapeutic Agents and Targets. *Front Physiol* (2018) 9:1262. doi: 10.3389/fphys.2018.01262
9. Chen X, Yang T, Wang W, Xi W, Zhang T, Li Q, et al. Circular RNAs in Immune Responses and Immune Diseases. *Theranostics* (2019) 9:588–607. doi: 10.7150/thno.29678
10. Yang L, Fu J, Zhou Y. Circular RNAs and Their Emerging Roles in Immune Regulation. *Front Immunol* (2018) 9:2977. doi: 10.3389/fimmu.2018.02977
11. Wang M, Yu F, Wu W, Zhang Y, Chang W, Ponnusamy M, et al. Circular RNAs: A Novel Type of Non-Coding RNA and Their Potential Implications in Antiviral Immunity. *Int J Biol Sci* (2017) 13:1497–506. doi: 10.7150/ijbs.22531
12. Meng L, Ding P, Liu S, Li Z, Sang M, Shan B. The Emerging Prospects of Circular RNA in Tumor Immunity. *Ann Trans Med* (2020) 8:1091. doi: 10.21037/atm-19-4751
13. Salmena L, Poliseno L, Tay Y, Kats L, Pandolfi P. A ceRNA Hypothesis: The Rosetta Stone of a Hidden RNA Language? *Cell* (2011) 146:353–8. doi: 10.1016/j.cell.2011.07.014
14. Thomson D, Dinger M. Endogenous microRNA Sponges: Evidence and Controversy. *Nat Rev Genet* (2016) 17:272–83. doi: 10.1038/nrg.2016.20
15. Hansen T, Jensen T, Clausen B, Bramsen J, Finsen B, Damgaard C, et al. Natural RNA Circles Function as Efficient microRNA Sponges. *Nature* (2013) 495:384–8. doi: 10.1038/nature11993
16. Bossi L, Figueroa-Bossi N. Competing Endogenous RNAs: A Target-Centric View of Small RNA Regulation in Bacteria. *Nat Rev Microbiol* (2016) 14:775–84. doi: 10.1038/nrmicro.2016.129
17. Memczak S, Jens M, Elefsinioti A, Torti F, Krueger J, Rybak A, et al. Circular RNAs Are a Large Class of Animal RNAs With Regulatory Potency. *Nature* (2013) 495:333–8. doi: 10.1038/nature11928

18. Abdelmohsen K, Panda A, Munk R, Grammatikakis I, Dudekula D, De S, et al. Identification of HuR Target Circular RNAs Uncovers Suppression of PABPN1 Translation by Circpabpn1. *RNA Biol* (2017) 14:361–9. doi: 10.1080/15476286.2017.1279788
19. Du W, Yang W, Liu E, Yang Z, Dhaliwal P, Yang B. Foxo3 Circular RNA Retards Cell Cycle Progression *via* Forming Ternary Complexes With P21 and CDK2. *Nucleic Acids Res* (2016) 44:2846–58. doi: 10.1093/nar/gkw027
20. Chen N, Zhao G, Yan X, Lv Z, Yin H, Zhang S, et al. A Novel FLI1 Exonic Circular RNA Promotes Metastasis in Breast Cancer by Coordinately Regulating TET1 and DNMT1. *Genome Biol* (2018) 19:218. doi: 10.1186/s13059-018-1594-y
21. Godet A, David F, Hantelys F, Tatin F, Lacazette E, Garmy-Susini B, et al. IRES Trans-Acting Factors, Key Actors of the Stress Response. *Neurosci Lett* (2019) 20:134952. doi: 10.20944/preprints201901.0081.v1
22. Abe N, Matsumoto K, Nishihara M, Nakano Y, Shibata A, Maruyama H, et al. Rolling Circle Translation of Circular RNA in Living Human Cells. *Sci Rep* (2015) 5:16435. doi: 10.1038/srep16435
23. Zhang Y, Zhang X, Chen T, Xiang J, Yin Q, Xing Y, et al. Circular Intronic Long Noncoding RNAs. *Mol Cell* (2013) 51:792–806. doi: 10.1016/j.molcel.2013.08.017
24. Bose R, Ain R. Regulation of Transcription by Circular RNAs. *Adv Exp Med Biol* (2018) 1087:81–94. doi: 10.1007/978-981-13-1426-1_7
25. Iparraguirre L, Muñoz-Culla M, Prada-Luengo I, Castillo-Triviño T, Olascoaga J, Otaegui D. Circular RNA Profiling Reveals That Circular RNAs From ANXA2 can be Used as New Biomarkers for Multiple Sclerosis. *Hum Mol Genet* (2017) 26:3564–72. doi: 10.1093/hmg/ddx243
26. Cardamone G, Paraboschi E, Rimoldi V, Duga S, Soldà G, Asselta R. The Characterization of GSDMB Splicing and Backsplicing Profiles Identifies Novel Isoforms and a Circular RNA That Are Dysregulated in Multiple Sclerosis. *Int J Mol Sci* (2017) 18:576. doi: 10.3390/ijms18030576
27. Jiajia Z, Zhenrong L, Tiancheng W, Yang Z, Yongfeng W. Microarray Expression Profile of Circular RNAs in Plasma From Primary Biliary Cholangitis Patients. *Cell Physiol Biochem* (2017) 44:1271–81. doi: 10.1159/000485487
28. Ouyang Q, Huang Q, Jiang Z, Zhao J, Shi G-P, Yang M. Using Plasma circRNA_002453 as a Novel Biomarker in the Diagnosis of Lupus Nephritis. *Mol Immunol* (2018) 101:531–8. doi: 10.1016/j.molimm.2018.07.029
29. Chen Q, Mang G, Wu J, Sun P, Li T, Zhang H, et al. Circular RNA Circsnx5 Controls Immunogenicity of Dendritic Cells Through the miR-544/SOCS1 Axis and PU.1 Activity Regulation. *Mol Ther* (2020) 28:2503–18. doi: 10.1016/j.ymthe.2020.07.001
30. Li L, Zhu Z, Zhao W, Tao S, Li B, Xu S, et al. Circular RNA Expression Profile and Potential Function of Hsa_Circ_0045272 in Systemic Lupus Erythematosus. *Immunology* (2018) 155:137–49. doi: 10.1111/imm.12940
31. Guo G, Wang H, Ye L, Shi X, Yan K, Lin K, et al. Hsa_circ_0000479 as a Novel Diagnostic Biomarker of Systemic Lupus Erythematosus. *Front Immunol* (2019) 10:2281. doi: 10.3389/fimmu.2019.02281
32. Luo Q, Zhang L, Li X, Fu B, Guo Y, Huang Z, et al. Identification of Circular RNAs Hsa_Circ_0044235 and Hsa_Circ_0068367 as Novel Biomarkers for Systemic Lupus Erythematosus. *Int J Mol Med* (2019) 44:1462–72. doi: 10.3892/ijmm.2019.4302
33. Miao Q, Zhong Z, Jiang Z, Lin Y, Ni B, Yang W, et al. RNA-Seq of Circular RNAs Identified Circptpn22 as a Potential New Activity Indicator in Systemic Lupus Erythematosus. *Lupus* (2019) 28:520–8. doi: 10.1177/0961203319830493
34. Zhang M, Wang J, Zhu Z, Li L, Liu R, Yang X, et al. Differentially Expressed Circular RNAs in Systemic Lupus Erythematosus and Their Clinical Significance. *Biomed Pharmacother = Biomed Pharmacother* (2018) 107:1720–7. doi: 10.1016/j.biopha.2018.08.161
35. Wen J, Liu J, Zhang P, Jiang H, Xin L, Wan L, et al. RNA-Seq Reveals the Circular RNA and miRNA Expression Profile of Peripheral Blood Mononuclear Cells in Patients With Rheumatoid Arthritis. *Biosci Rep* (2020) 40:BSR20193160. doi: 10.1042/BSR20193160
36. Yang X, Li J, Wu Y, Ni B, Zhang B. Aberrant Dysregulated Circular RNAs in the Peripheral Blood Mononuclear Cells of Patients With Rheumatoid Arthritis Revealed by RNA Sequencing: Novel Diagnostic Markers for RA. *Scand J Clin Lab Invest* (2019) 79:551–9. doi: 10.1080/00365513.2019.1674004
37. Zhong S, Ouyang Q, Zhu D, Huang Q, Zhao J, Fan M, et al. Hsa_circ_0088036 Promotes the Proliferation and Migration of Fibroblast-Like Synoviocytes by Sponging miR-140-3p and Upregulating SIRT 1 Expression in Rheumatoid Arthritis. *Mol Immunol* (2020) 125:131–9. doi: 10.1016/j.molimm.2020.07.004
38. Su L, Xu W, Liu X, Fu L, Huang A. Altered Expression of Circular RNA in Primary Sjögren's Syndrome. *Clin Rheumatol* (2019) 38:3425–33. doi: 10.1007/s10067-019-04728-6
39. Sun J, Lian M, Ma H, Wang R, Ma Z, Wang H, et al. Competing Endogenous RNA Network Analysis of CD274, IL−10 and FOXP3 Co−Expression in Laryngeal Squamous Cell Carcinoma. *Mol Med Rep* (2018) 17:3859–69. doi: 10.3892/mmr.2017.8307
40. Zhao R, Ni J, Lu S, Jiang S, You L, Liu H, et al. CircUBAP2-Mediated Competing Endogenous RNA Network Modulates Tumorigenesis in Pancreatic Adenocarcinoma. *Aging* (2019) 11:8484–501. doi: 10.18632/aging.102334
41. Wei C, Zhu M, Lu N, Liu J, Yang Y, Zhang Y, et al. Circular RNA Circ_0020710 Drives Tumor Progression and Immune Evasion by Regulating the miR-370-3p/CXCL12 Axis in Melanoma. *Mol Cancer* (2020) 19:84. doi: 10.1186/s12943-020-01191-9
42. Pei X, Chen S, Long X, Zhu S, Qiu B, Lin K, et al. circMET Promotes NSCLC Cell Proliferation, Metastasis, and Immune Evasion by Regulating the miR-145-5p/CXCL3 Axis. *Aging* (2020) 12:13038–58. doi: 10.18632/aging.103392
43. Zhang P, Pei X, Li K, Jin L, Wang F, Wu J, et al. Circular RNA Circfgfr1 Promotes Progression and Anti-PD-1 Resistance by Sponging miR-381-3p in Non-Small Cell Lung Cancer Cells. *Mol Cancer* (2019) 18:179. doi: 10.1186/s12943-019-1111-2
44. Zhang P, Gao C, Huang X, Lu J, Guo X, Shi G, et al. Cancer Cell-Derived Exosomal Circuhrf1 Induces Natural Killer Cell Exhaustion and may Cause Resistance to Anti-PD1 Therapy in Hepatocellular Carcinoma. *Mol Cancer* (2020) 19:110. doi: 10.1186/s12943-020-01222-5
45. Wang J, Zhang Y, Song H, Yin H, Jiang T, Xu Y, et al. The Circular RNA circSPARC Enhances the Migration and Proliferation of Colorectal Cancer by Regulating the JAK/STAT Pathway. *Mol Cancer* (2021) 20:81. doi: 10.1186/s12943-021-01375-x
46. Zhang X, Zhu M, Yang R, Zhao W, Hu X, Gan J. Identification and Comparison of Novel Circular RNAs With Associated Co-Expression and Competing Endogenous RNA Networks in Pulmonary Tuberculosis. *Oncotarget* (2017) 8:113571–82. doi: 10.18632/oncotarget.22710
47. Zhuang Z, Zhang J, Luo H, Liu G, Lu Y, Ge N, et al. The Circular RNA of Peripheral Blood Mononuclear Cells: Hsa_circ_0005836 as a New Diagnostic Biomarker and Therapeutic Target of Active Pulmonary Tuberculosis. *Mol Immunol* (2017) 90:264–72. doi: 10.1016/j.molimm.2017.08.008
48. Huang Z, Yao F, Xu J, Deng Z, Su R, Peng Y, et al. Microarray Expression Profile of Circular RNAs in Peripheral Blood Mononuclear Cells From Active Tuberculosis Patients. *Cell Physiol Biochem* (2018) 45:1230–40. doi: 10.1159/000487454
49. Yang R, Xu B, Yang B, Fu J, Liu L, Amjad N, et al. Circular RNA Transcriptomic Analysis of Primary Human Brain Microvascular Endothelial Cells Infected With Meningitic Escherichia Coli. *Mol Ther Nucleic Acids* (2018) 13:651–64. doi: 10.1016/j.omtn.2018.10.013
50. Chen Y, Chen R, Ahmad S, Verma R, Kasturi S, Amaya L, et al. N6-Methyladenosine Modification Controls Circular RNA Immunity. *Mol Cell* (2019) 76:96–109.e9. doi: 10.1016/j.molcel.2019.07.016
51. Li X, Liu C, Xue W, Zhang Y, Jiang S, Yin Q, et al. Coordinated circRNA Biogenesis and Function With NF90/NF110 in Viral Infection. *Mol Cell* (2017) 67:214–27.e7. doi: 10.1016/j.molcel.2017.05.023
52. Arora S, Singh P, Dohare R, Jha R, Ali Syed M. Unravelling Host-Pathogen Interactions: ceRNA Network in SARS-CoV-2 Infection (COVID-19). *Gene* (2020) 762:145057. doi: 10.1016/j.gene.2020.145057
53. Ng W, Marinov G, Liau E, Lam Y, Lim Y, Ea C. Inducible RasGEF1B Circular RNA Is a Positive Regulator of ICAM-1 in the TLR4/LPS Pathway. *RNA Biol* (2016) 13:861–71. doi: 10.1080/15476286.2016.1207036
54. Liu Y, Hu C, Sun Y, Wu H, Chen X, Liu Q. Identification of Differentially Expressed Circular RNAs in HeLa Cells Infected With Chlamydia Trachomatis. *Pathog Dis* (2019) 77:ftz062. doi: 10.1093/femspd/ftz062

55. Zurawska A, Mycko M, Selmaj K. Circular RNAs as a Novel Layer of Regulatory Mechanism in Multiple Sclerosis. *J Neuroimmunol* (2019) 334:576971. doi: 10.1016/j.jneuroim.2019.576971
56. Ghafouri-Fard S, Taheri M. A Comprehensive Review of Non-Coding RNAs Functions in Multiple Sclerosis. *Eur J Pharmacol* (2020) 879:173127. doi: 10.1016/j.ejphar.2020.173127
57. Zhang J, Liu Y, Shi G. The circRNA-miRNA-mRNA Regulatory Network in Systemic Lupus Erythematosus. *Clin Rheumatol* (2020) 40(1):331–9. doi: 10.1007/s10067-020-05212-2
58. Xi WD CHEN. Research Progress on circRNA and Infectious Diseases. *Surg Res N Tech* (2020) 9:110–3.
59. Gal-Ben-Ari S, Barrera I, Ehrlich M, Rosenblum K. PKR: A Kinase to Remember. *Front Mol Neurosci* (2018) 11:480. doi: 10.3389/fnmol.2018.00480
60. Chen Y, Kim M, Chen X, Batista P, Aoyama S, Wilusz J, et al. Sensing Self and Foreign Circular RNAs by Intron Identity. *Mol Cell* (2017) 67:228–38.e5. doi: 10.1016/j.molcel.2017.05.022
61. Wesselhoeft R, Kowalski P, Parker-Hale F, Huang Y, Bisaria N, Anderson D. RNA Circularization Diminishes Immunogenicity and Can Extend Translation Duration In Vivo. *Mol Cell* (2019) 74:508–20.e4. doi: 10.1016/j.molcel.2019.02.015
62. Cadena C, Hur S. Antiviral Immunity and Circular RNA: No End in Sight. *Mol Cell* (2017) 67:163–4. doi: 10.1016/j.molcel.2017.07.005
63. Omicron is Bad But the Global Response Is Worse. *Nature* (2021) 600:190. doi: 10.1038/d41586-021-03616-x
64. Yang M, Qi M, Xu L, Huang P, Wang X, Sun J, et al. Differential Host circRNA Expression Profiles in Human Lung Epithelial Cells Infected With SARS-CoV-2. *Infect Genet Evol* (2021) 93:104923. doi: 10.1016/j.meegid.2021.104923
65. Yang S, Zhou H, Cruz-Cosme R, Liu M, Xu J, Niu X, et al. Circular RNA Profiling Reveals Abundant and Diverse circRNAs of SARS-CoV-2, SARS-CoV and MERS-CoV Origin. *BioRxiv Preprint Server Biol* (2020). doi: 10.1101/2020.12.07.415422
66. Cai Z, Lu C, He J, Liu L, Zou Y, Zhang Z, et al. Identification and Characterization of circRNAs Encoded by MERS-CoV, SARS-CoV-1 and SARS-CoV-2. *Briefings Bioinf* (2021) 22:1297–308. doi: 10.1093/bib/bbaa334
67. Pfafenrot C, Schneider T, Müller C, Hung L, Schreiner S, Ziebuhr J, et al. Inhibition of SARS-CoV-2 Coronavirus Proliferation by Designer antisense-circRNAs. *Nucleic Acids Res* (2021) 49(21):12502–16. doi: 10.1093/nar/gkab1096
68. Broadbent K, Broadbent J, Ribacke U, Wirth D, Rinn J, Sabeti P. Strand-Specific RNA Sequencing in Plasmodium Falciparum Malaria Identifies Developmentally Regulated Long Non-Coding RNA and Circular RNA. *BMC Genomics* (2015) 16:454. doi: 10.1186/s12864-015-1603-4
69. Lin J, Feng X, Zhang J. Circular RNA Circhipk3 Modulates the Proliferation of Airway Smooth Muscle Cells by miR-326/STIM1 Axis. *Life Sci* (2020) 255:117835. doi: 10.1016/j.lfs.2020.117835
70. Zhang Y, Zhang H, An M, Zhao B, Ding H, Zhang Z, et al. Crosstalk in Competing Endogenous RNA Networks Reveals New Circular RNAs Involved in the Pathogenesis of Early HIV Infection. *J Trans Med* (2018) 16:332. doi: 10.1186/s12967-018-1706-1
71. Wang K, Wei X, Wei Q, Lu D, Li W, Pan B, et al. A Two-Circular RNA Signature of Donor Circfoxn2 and Circnectin3 Predicts Early Allograft Dysfunction After Liver Transplantation. *Ann Trans Med* (2020) 8:94. doi: 10.21037/atm.2019.12.132
72. Ng W, Marinov G, Chin Y, Lim Y, Ea C. Transcriptomic Analysis of the Role of RasGEF1B Circular RNA in the TLR4/LPS Pathway. *Sci Rep* (2017) 7:12227. doi: 10.1038/s41598-017-12550-w
73. Xu M, Xie F, Tang X, Wang T, Wang S. Insights Into the Role of Circular RNA in Macrophage Activation and Fibrosis Disease. *Pharmacol Res* (2020) 156:104777. doi: 10.1016/j.phrs.2020.104777
74. Holdt L, Stahringer A, Sass K, Pichler G, Kulak N, Wilfert W, et al. Circular Non-Coding RNA ANRIL Modulates Ribosomal RNA Maturation and Atherosclerosis in Humans. *Nat Commun* (2016) 7:12429. doi: 10.1038/ncomms12429
75. Zhu P, Zhu X, Wu J, He L, Lu T, Wang Y, et al. IL-13 Secreted by ILC2s Promotes the Self-Renewal of Intestinal Stem Cells Through Circular RNA Circpan3. *Nat Immunol* (2019) 20:183–94. doi: 10.1038/s41590-018-0297-6
76. Hua Q, Chen Y, Liu Y, Li M, Diao Q, Xue H, et al. Circular RNA 0039411 Is Involved in Neodymium Oxide-Induced Inflammation and Antiproliferation in a Human Bronchial Epithelial Cell Line *via* Sponging miR-93-5p. *Toxicol Sci* (2019) 170:69–81. doi: 10.1093/toxsci/kfz074
77. Huang Z, Cao Y, Zhou M, Qi X, Fu B, Mou Y, et al. Hsa_circ_0005519 Increases IL-13/IL-6 by Regulating Hsa-Let-7a-5p in CD4 T Cells to Affect Asthma. *Clin Exp Allergy* (2019) 49:1116–27. doi: 10.1111/cea.13445
78. Li J, Xie R. Circular RNA Expression Profile in Gingival Tissues Identifies Circ_0062491 and Circ_0095812 as Potential Treatment Targets. *J Cell Biochem* (2019) 120:14867–74. doi: 10.1002/jcb.28748
79. Fang J, Richardson B. The MAPK Signalling Pathways and Colorectal Cancer. *Lancet Oncol* (2005) 6:322–7. doi: 10.1016/S1470-2045(05)70168-6
80. Yaeger R, Corcoran R. Targeting Alterations in the RAF-MEK Pathway. *Cancer Discov* (2019) 9:329–41. doi: 10.1158/2159-8290.CD-18-1321
81. Chen Q, Mang G, Wu J, Sun P, Li T, Zhang H, et al. Circular RNA Circsnx5 Controls Immunogenicity of Dendritic Cells Through the miR-544/SOCS1 Axis and PU.1 Activity Regulation. *Mol Ther* (2020) 28:2503–18. doi: 10.1016/j.ymthe.2020.07.001
82. Souma Y, Nishida T, Serada S, Iwahori K, Takahashi T, Fujimoto M, et al. Antiproliferative Effect of SOCS-1 Through the Suppression of STAT3 and P38 MAPK Activation in Gastric Cancer Cells. *Int J Cancer* (2012) 131:1287–96. doi: 10.1002/ijc.27350
83. Zhou H, Miki R, Eeva M, Fike F, Seligson D, Yang L, et al. Reciprocal Regulation of SOCS 1 and SOCS3 Enhances Resistance to Ionizing Radiation in Glioblastoma Multiforme. *Clin Cancer Res* (2007) 13:2344–53. doi: 10.1158/1078-0432.CCR-06-2303
84. Khalaf H, Demirel I, Bengtsson T. Suppression of Inflammatory Gene Expression in T Cells by Porphyromonas Gingivalis Is Mediated by Targeting MAPK Signaling. *Cell Mol Immunol* (2013) 10:413–22. doi: 10.1038/cmi.2013.23
85. Yoon S, Lee M, Shin D, Kim J, Chwae Y, Kwon M, et al. Activation of Mitogen Activated Protein Kinase-Erk Kinase (MEK) Increases T Cell Immunoglobulin Mucin Domain-3 (TIM-3) Transcription in Human T Lymphocytes and a Human Mast Cell Line. *Mol Immunol* (2011) 48:1778–83. doi: 10.1016/j.molimm.2011.05.004
86. Liu Y, Cai P, Wang N, Zhang Q, Chen F, Shi L, et al. Combined Blockade of Tim-3 and MEK Inhibitor Enhances the Efficacy Against Melanoma. *Biochem Biophys Res Commun* (2017) 484:378–84. doi: 10.1016/j.bbrc.2017.01.128
87. Kataoka S, Manandhar P, Lee J, Workman C, Banerjee H, Szymczak-Workman A, et al. The Costimulatory Activity of Tim-3 Requires Akt and MAPK Signaling and its Recruitment to the Immune Synapse. *Sci Signal* (2021) 14:eaba0717. doi: 10.1126/scisignal.aba0717
88. Lim E, Kim S, Oh Y, Suh Y, Kaushik N, Lee J, et al. Crosstalk Between GBM Cells and Mesenchymal Stemlike Cells Promotes the Invasiveness of GBM Through the C5a/p38/ZEB1 Axis. *Neuro-Oncology* (2020) 22:1452–62. doi: 10.1093/neuonc/noaa064
89. Sheng W, Shi X, Lin Y, Tang J, Jia C, Cao R, et al. Musashi2 Promotes EGF-Induced EMT in Pancreatic Cancer *via* ZEB1-ERK/MAPK Signaling. *J Exp Clin Cancer Res CR* (2020) 39:16. doi: 10.1186/s13046-020-1521-4
90. Richard G, Dalle S, Monet M, Ligier M, Boespflug A, Pommier R, et al. ZEB1-Mediated Melanoma Cell Plasticity Enhances Resistance to MAPK Inhibitors. *EMBO Mol Med* (2016) 8:1143–61. doi: 10.15252/emmm.201505971
91. Sorkin A, von Zastrow M. Endocytosis and Signalling: Intertwining Molecular Networks. *Nat Rev Mol Cell Biol* (2009) 10:609–22. doi: 10.1038/nrm2748
92. Khan I, Steeg P. Endocytosis: A Pivotal Pathway for Regulating Metastasis. *Br J Cancer* (2021) 124:66–75. doi: 10.1038/s41416-020-01179-8
93. Doherty G, McMahon H. Mechanisms of Endocytosis. *Annu Rev Biochem* (2009) 78:857–902. doi: 10.1146/annurev.biochem.78.081307.110540
94. Liu Y, Li Z, Zhang M, Zhou H, Wu X, Zhong J, et al. Rolling-Translated EGFR Variants Sustain EGFR Signaling and Promote Glioblastoma Tumorigenicity. *Neuro-Oncology* (2021) 23:743–56. doi: 10.1093/neuonc/noaa279
95. O'Shea J, Plenge R. JAK and STAT Signaling Molecules in Immunoregulation and Immune-Mediated Disease. *Immunity* (2012) 36:542–50. doi: 10.1016/j.immuni.2012.03.014

96. Villarino A, Kanno Y, O'Shea J. Mechanisms and Consequences of Jak-STAT Signaling in the Immune System. *Nat Immunol* (2017) 18:374–84. doi: 10.1038/ni.3691
97. Yang L, Han X, Zhang C, Sun C, Huang S, Xiao W, et al. Hsa_circ_0060450 Negatively Regulates Type I Interferon-Induced Inflammation by Serving as miR-199a-5p Sponge in Type 1 Diabetes Mellitus. *Front Immunol* (2020) 11:576903. doi: 10.3389/fimmu.2020.576903
98. Shimobayashi M, Hall M. Making New Contacts: The mTOR Network in Metabolism and Signalling Crosstalk. *Nat Rev Mol Cell Biol* (2014) 15:155–62. doi: 10.1038/nrm3757
99. Laplante M, Sabatini D. mTOR Signaling at a Glance. *J Cell Sci* (2009) 122:3589–94. doi: 10.1242/jcs.051011
100. Saxton R, Sabatini D. mTOR Signaling in Growth, Metabolism, and Disease. *Cell* (2017) 168:960–76. doi: 10.1016/j.cell.2017.02.004
101. Zhang H, Wang F, Wang Y, Zhao Z, Qiao P. lncRNA GAS5 Inhibits Malignant Progression by Regulating Macroautophagy and Forms a Negative Feedback Regulatory Loop With the Mir−34a/mTOR/SIRT1 Pathway in Colorectal Cancer. *Oncol Rep* (2021) 45:202–16. doi: 10.3892/or.2020.7825
102. Wang J, Song X, Tan G, Sun P, Guo L, Zhang N, et al. NAD+ Improved Experimental Autoimmune Encephalomyelitis by Regulating SIRT1 to Inhibit PI3K/Akt/mTOR Signaling Pathway. *Aging* (2021) 13:25931–43. doi: 10.18632/aging.203781
103. Yao Q, Wu Q, Xu X, Xing Y, Liang J, Lin Q, et al. Resveratrol Ameliorates Systemic Sclerosis *via* Suppression of Fibrosis and Inflammation Through Activation of SIRT1/mTOR Signaling. *Drug Design Dev Ther* (2020) 14:5337–48. doi: 10.2147/DDDT.S281209
104. Gao D, Tang T, Zhu J, Tang Y, Sun H, Li S. CXCL12 has Therapeutic Value in Facial Nerve Injury and Promotes Schwann Cells Autophagy and Migration *via* PI3K-AKT-mTOR Signal Pathway. *Int J Biol Macromol* (2019) 124:460–8. doi: 10.1016/j.ijbiomac.2018.10.212
105. Li S, Fan Y, Kumagai A, Kawakita E, Kitada M, Kanasaki K, et al. Deficiency in Dipeptidyl Peptidase-4 Promotes Chemoresistance Through the CXCL12/CXCR4/mTOR/Tgfβ Signaling Pathway in Breast Cancer Cells. *Int J Mol Sci* (2020) 21:805. doi: 10.3390/ijms21030805
106. Yang F, Takagaki Y, Yoshitomi Y, Ikeda T, Li J, Kitada M, et al. Inhibition of Dipeptidyl Peptidase-4 Accelerates Epithelial-Mesenchymal Transition and Breast Cancer Metastasis *via* the CXCL12/CXCR4/mTOR Axis. *Cancer Res* (2019) 79:735–46. doi: 10.1158/0008-5472.CAN-18-0620
107. Parsons M, Tammela T, Dow L. WNT as a Driver and Dependency in Cancer. *Cancer Discov* (2021) 11:2413–29. doi: 10.1158/2159-8290.CD-21-0190
108. Rim E, Clevers H, Nusse R. The Wnt Pathway: From Signaling Mechanisms to Synthetic Modulators. *Annu Rev Biochem* (2022). doi: 10.1146/annurev-biochem-040320-103615
109. Zhou Y, Xu J, Luo H, Meng X, Chen M, Zhu D. Wnt Signaling Pathway in Cancer Immunotherapy. *Cancer Lett* (2022) 525:84–96. doi: 10.1016/j.canlet.2021.10.034
110. Zhao C, Yan Z, Wen J, Fu D, Xu P, Wang L, et al. CircEAF2 Counteracts Epstein-Barr Virus-Positive Diffuse Large B-Cell Lymphoma Progression *via* miR-BART19-3p/APC/β-Catenin Axis. *Mol Cancer* (2021) 20:153. doi: 10.1186/s12943-021-01458-9
111. Zhao S, Wang J, Qin C. Blockade of CXCL12/CXCR4 Signaling Inhibits Intrahepatic Cholangiocarcinoma Progression and Metastasis *via* Inactivation of Canonical Wnt Pathway. *J Exp Clin Cancer Res CR* (2014) 33:103. doi: 10.1186/s13046-014-0103-8
112. Yu T, Liu K, Wu Y, Fan J, Chen J, Li C, et al. MicroRNA-9 Inhibits the Proliferation of Oral Squamous Cell Carcinoma Cells by Suppressing Expression of CXCR4 *via* the Wnt/β-Catenin Signaling Pathway. *Oncogene* (2014) 33:5017–27. doi: 10.1038/onc.2013.448
113. Hu T, Yao Y, Yu S, Han L, Wang W, Guo H, et al. SDF-1/CXCR4 Promotes Epithelial-Mesenchymal Transition and Progression of Colorectal Cancer by Activation of the Wnt/β-Catenin Signaling Pathway. *Cancer Lett* (2014) 354:417–26. doi: 10.1016/j.canlet.2014.08.012
114. Hankey W, Frankel W, Groden J. Functions of the APC Tumor Suppressor Protein Dependent and Independent of Canonical WNT Signaling: Implications for Therapeutic Targeting. *Cancer Metastasis Rev* (2018) 37:159–72. doi: 10.1007/s10555-017-9725-6
115. Deng S, Zhang X, Qin Y, Chen W, Fan H, Feng X, et al. miRNA-192 and -215 Activate Wnt/β-Catenin Signaling Pathway in Gastric Cancer *via* APC. *J Cell Physiol* (2020) 235:6218–29. doi: 10.1002/jcp.29550
116. Borowsky J, Dumenil T, Bettington M, Pearson S, Bond C, Fennell L, et al. The Role of APC in WNT Pathway Activation in Serrated Neoplasia. *Mod Pathol* (2018) 31:495–504. doi: 10.1038/modpathol.2017.150
117. Peng Y, Xu Y, Zhang X, Deng S, Yuan Y, Luo X, et al. A Novel Protein AXIN1-295aa Encoded by Circaxin1 Activates the Wnt/β-Catenin Signaling Pathway to Promote Gastric Cancer Progression. *Mol Cancer* (2021) 20:158. doi: 10.1186/s12943-021-01457-w
118. Zhang C, Han X, Yang L, Fu J, Sun C, Huang S, et al. Circppm1fcircular RNA Modulates M1 Macrophage Activation and Pancreatic Islet Inflammation in Type 1 Diabetes Mellitus. *Theranostics* (2020) 10:10908–24. doi: 10.7150/thno.48264
119. Wang X, Sheng W, Xu T, Xu J, Gao R, Zhang ZJA. CircRNA Hsa_Circ_0110102 Inhibited Macrophage Activation and Hepatocellular Carcinoma Progression *via* miR-580-5p/Pparα/CCL2 Pathway. *Aging (Albany NY)* (2021) 13:11969–87. doi: 10.18632/aging.202900
120. Zhou Z, Jiang R, Yang X, Guo H, Fang S, Zhang Y, et al. circRNA Mediates Silica-Induced Macrophage Activation *Via* HECTD1/ZC3H12A-Dependent Ubiquitination. *Theranostics* (2018) 8:575–92. doi: 10.7150/thno.21648
121. Yang X, Wang J, Zhou Z, Jiang R, Huang J, Chen L, et al. Silica-Induced Initiation of Circular ZC3H4 RNA/ZC3H4 Pathway Promotes the Pulmonary Macrophage Activation. *FASEB J* (2018) 32:3264–77. doi: 10.1096/fj.201701118R
122. Lian C, Sun J, Guan W, Zhang L, Zhang X, Yang L, et al. Circular RNA Circhipk3 Activates Macrophage NLRP3 Inflammasome and TLR4 Pathway in Gouty Arthritis via Sponging miR-561 and miR-192. *Inflammation* (2021) 44:2065–77. doi: 10.1007/s10753-021-01483-2
123. Wang Y, Li C, Zhao R, Qiu Z, Shen C, Wang Z, et al. CircUbe3a From M2 Macrophage-Derived Small Extracellular Vesicles Mediates Myocardial Fibrosis After Acute Myocardial Infarction. *Theranostics* (2021) 11:6315–33. doi: 10.7150/thno.52843
124. Zhao D, Wang C, Liu X, Liu N, Zhuang S, Zhang Q, et al. CircN4bp1 Facilitates Sepsis-Induced Acute Respiratory Distress Syndrome Through Mediating Macrophage Polarization via the miR-138-5p/EZH2 Axis. *Mediators Inflamm* (2021) 2021:7858746. doi: 10.1155/2021/7858746
125. Song H, Yang Y, Sun Y, Wei G, Zheng H, Chen Y, et al. Circular RNA Cdyl Promotes Abdominal Aortic Aneurysm Formation by Inducing M1 Macrophage Polarization and M1-Type Inflammation. *Mol Ther* (2022) 30:915–31. doi: 10.1016/j.ymthe.2021.09.017
126. Li X, Kang J, Lv H, Liu R, Chen J, Zhang Y, et al. CircPrkcsh, a Circular RNA, Contributes to the Polarization of Microglia Towards the M1 Phenotype Induced by Spinal Cord Injury and Acts via the JNK/p38 MAPK Pathway. *FASEB J* (2021) 35:. doi: 10.1096/fj.202100993R
127. Chen T, Liu Y, Li C, Xu C, Ding C, Chen J, et al. Tumor-Derived Exosomal circFARSA Mediates M2 Macrophage Polarization via the PTEN/PI3K/AKT Pathway to Promote Non-Small Cell Lung Cancer Metastasis. *Cancer Treat Res Commun* (2021) 28:100412. doi: 10.1016/j.ctarc.2021.100412
128. Yi B, Dai K, Yan Z, Yin ZJB. Circular RNA PLCE1 Promotes Epithelial Mesenchymal Transformation, Glycolysis in Colorectal Cancer and M2 Polarization of Tumor-Associated Macrophages. *Bioengineered* (2022) 13:6243–56. doi: 10.1080/21655979.2021.2003929
129. Li H, Luo F, Jiang X, Zhang W, Xiang T, Pan Q, et al. CircITGB6 Promotes Ovarian Cancer Cisplatin Resistance by Resetting Tumor-Associated Macrophage Polarization Toward the M2 Phenotype. *J Immunother Cancer* (2022) 10:e004029. doi: 10.1136/jitc-2021-004029
130. Lu C, Shi W, Hu W, Zhao Y, Zhao X, Dong F, et al. Endoplasmic Reticulum Stress Promotes Breast Cancer Cells to Release Exosomes Circ_0001142 and Induces M2 Polarization of Macrophages to Regulate Tumor Progression. *Pharmacol Res* (2022) 177:106098. doi: 10.1016/j.phrs.2022.106098
131. Wang Y, Gao R, Li J, Tang S, Li S, Tong Q, et al. Downregulation of Hsa_Circ_0074854 Suppresses the Migration and Invasion in Hepatocellular Carcinoma *via* Interacting With HuR and via Suppressing Exosomes-Mediated Macrophage M2 Polarization. *Int J Nanomed* (2021) 16:2803–18. doi: 10.2147/IJN.S284560
132. Zhang J, Cheng F, Rong G, Tang Z, Gui BJB. Circular RNA Hsa_Circ_0005567 Overexpression Promotes M2 Type Macrophage Polarization Through miR-492/SOCS2 Axis to Inhibit Osteoarthritis Progression. *Bioengineered* (2021) 12:8920–30. doi: 10.1080/21655979.2021.1989999
133. Yang L, Fu J, Han X, Zhang C, Xia L, Zhu R, et al. Hsa_circ_0004287 Inhibits Macrophage-Mediated Inflammation in an N-Methyladenosine-Dependent

Manner in Atopic Dermatitis and Psoriasis. *J Allergy Clin Immunol* (2021) S0091-6749(21)02685-3. doi: 10.1016/j.jaci.2021.11.024
134. Katopodi T, Petanidis S, Domvri K, Zarogoulidis P, Anestakis D, Charalampidis C, et al. Kras-Driven Intratumoral Heterogeneity Triggers Infiltration of M2 Polarized Macrophages via the Circhipk3/PTK2 Immunosuppressive Circuit. *Sci Rep* (2021) 11:15455. doi: 10.1038/s41598-021-94671-x
135. Ma X, Xu J, Lu Q, Feng X, Liu J, Cui C, et al. Hsa_circ_0087352 Promotes the Inflammatory Response of Macrophages in Abdominal Aortic Aneurysm by Adsorbing hsa-miR-149-5p. *Int Immunopharmacol* (2022) 107:108691. doi: 10.1016/j.intimp.2022.108691
136. Lu X, Liu Y, Xuan W, Ye J, Yao H, Huang C, et al. Circ_1639 Induces Cells Inflammation Responses by Sponging miR-122 and Regulating TNFRSF13C Expression in Alcoholic Liver Disease. *Toxicol Lett* (2019) 314:89–97. doi: 10.1016/j.toxlet.2019.07.021
137. Deng Q, Huang J, Yan J, Mao E, Chen H, Wang CJT. Circ_0001490/miR-579-3p/FSTL1 Axis Modulates the Survival of Mycobacteria and the Viability, Apoptosis and Inflammatory Response in Mycobacterium Tuberculosis-Infected Macrophages. *Tuberculosis (Edinb)* (2021) 131:102123. doi: 10.1016/j.tube.2021.102123
138. Luo H, Pi J, Zhang J, Yang E, Xu H, Luo H, et al. Mycobacterium Tuberculosiscircular RNA TRAPPC6B Inhibits Intracellular Growth While Inducing Autophagy in Macrophages by Targeting microRNA-874-3p. *Clin Transl Immunol* (2021) 10:. doi: 10.1002/cti2.1254
139. Wu M, Liu Z, Zhang S. Down-Regulation of Hsa_Circ_0045474 Induces Macrophage Autophagy in Tuberculosis *via* miR-582-5p/TNKS2 Axis. *Innate Immun* (2022) 28:11–8. doi: 10.1177/17534259211064285
140. Deng T, Yang L, Zheng Z, Li Y, Ren W, Wu C, et al. Calcitonin Gene–Related Peptide Induces IL–6 Expression in RAW264.7 Macrophages Mediated by Mmu_circRNA_007893. *Mol Med Rep* (2017) 16:9367–74. doi: 10.3892/mmr.2017.7779
141. Li S, Chen Z, Zhou R, Wang S, Wang W, Liu D, et al. Hsa_circ_0048674 Facilitates Hepatocellular Carcinoma Progression and Natural Killer Cell Exhaustion Depending on the Regulation of miR-223-3p/PDL1. *Histol Hisphatol* (2022) 18440. doi: 10.14670/HH-18-440
142. Ma Y, Zhang C, Zhang B, Yu H, Yu Q. circRNA of AR-Suppressed PABPC1 91 Bp Enhances the Cytotoxicity of Natural Killer Cells Against Hepatocellular Carcinoma *via* Upregulating UL16 Binding Protein 1. *Oncol Lett* (2019) 17:388–97. doi: 10.3892/ol.2018.9606
143. Ou Z, Luo Z, Wei W, Liang S, Gao T, Lu Y. Hypoxia-Induced Shedding of MICA and HIF1A-Mediated Immune Escape of Pancreatic Cancer Cells From NK Cells: Role of Circ_0000977/miR-153 Axis. *RNA Biol* (2019) 16:1592–603. doi: 10.1080/15476286.2019.1649585
144. Ke H, Zhang J, Wang F, Xiong Y. ZNF652-Induced Circrhot1 Promotes SMAD5 Expression to Modulate Tumorigenic Properties and Nature Killer Cell-Mediated Toxicity in Bladder Cancer *via* Targeting miR-3666. *J Immunol Res* (2021) 2021:7608178. doi: 10.1155/2021/7608178
145. Luan J, Jiao C, Kong W, Fu J, Qu W, Chen Y, et al. circHLA-C Plays an Important Role in Lupus Nephritis by Sponging miR-150. *Mol Ther Nucleic Acids* (2018) 10:245–53. doi: 10.1016/j.omtn.2017.12.006
146. Wang B, Zhou Q, Li A, Li S, Greasley A, Skaro A, et al. Preventing Alloimmune Rejection Using Circular RNA FSCN1-Silenced Dendritic Cells in Heart Transplantation. *J Heart Lung Transpl* (2021) 40:584–94. doi: 10.1016/j.healun.2021.03.025
147. Zhang Y, Zhang G, Liu Y, Chen R, Zhao D, McAlister V, et al. GDF15 Regulates Malat-1 Circular RNA and Inactivates Nfkb Signaling Leading to Immune Tolerogenic DCs for Preventing Alloimmune Rejection in Heart Transplantation. *Front Immunol* (2018) 9:2407. doi: 10.3389/fimmu.2018.02407
148. Zhang C, Wang X, Chen Y, Wu Z, Zhang C, Shi W. The Down-Regulation of hsa_circ_0012919, the Sponge for miR-125a-3p, Contributes to DNA Methylation of CD11a and CD70 in CD4 + T Cells of Systemic Lupus Erythematous. *Clin Sci (Lond)* (2018) 132:2285–98. doi: 10.1042/CS20180403
149. Zhu X, Wang X, Wang Y, Zhao Y. The Regulatory Network Among CircHIPK3, LncGAS5, and miR-495 Promotes Th2 Differentiation in Allergic Rhinitis. *Cell Death Dis* (2020) 11:216. doi: 10.1038/s41419-020-2394-3
150. Huang Z, Fu B, Qi X, Xu Y, Mou Y, Zhou M, et al. Diagnostic and Therapeutic Value of Hsa_circ_0002594 for T Helper 2-Mediated Allergic Asthma. *Int Arch Allergy Immunol* (2021) 182:388–98. doi: 10.1159/000511612
151. Liu Z, Wang T, She Y, Wu K, Gu S, Li L, et al. N-Methyladenosine-Modified Circigf2bp3 Inhibits CD8 T-Cell Responses to Facilitate Tumor Immune Evasion by Promoting the Deubiquitination of PD-L1 in Non-Small Cell Lung Cancer. *Mol Cancer* (2021) 20:105. doi: 10.1186/s12943-021-01398-4
152. Yang C, Wu S, Mou Z, Zhou Q, Dai X, Ou Y, et al. Exosome-Derived Circtrps1 Promotes Malignant Phenotype and CD8+ T Cell Exhaustion in Bladder Cancer Microenvironments. *Mol Ther* (2022) 30:1054–70. doi: 10.1016/j.ymthe.2022.01.022
153. Wang Y, Yu X, Luo S, Han H. Comprehensive Circular RNA Profiling Reveals That Circular RNA100783 is Involved in Chronic CD28-Associated CD8(+)T Cell Ageing. *Immun Ageing* (2015) 12:17. doi: 10.1186/s12979-015-0042-z
154. Chen S, Zhu S, Pei X, Qiu B, Xiong D, Long X, et al. Cancer Cell-Derived Exosomal Circusp7 Induces CD8 T Cell Dysfunction and Anti-PD1 Resistance by Regulating the miR-934/SHP2 Axis in NSCLC. *Mol Cancer* (2021) 20:144. doi: 10.1186/s12943-021-01448-x
155. Li M, Chi C, Zhou L, Chen Y, Tang X. Circular PVT1 Regulates Cell Proliferation and Invasion *via* miR-149-5p/FOXM1 Axis in Ovarian Cancer. *J Cancer* (2021) 12:611–21. doi: 10.7150/jca.52234
156. Sekar S, Cuyugan L, Adkins J, Geiger P, Liang W. Circular RNA Expression and Regulatory Network Prediction in Posterior Cingulate Astrocytes in Elderly Subjects. *BMC Genomics* (2018) 19:340. doi: 10.1186/s12864-018-4670-5
157. Xia P, Wang S, Ye B, Du Y, Li C, Xiong Z, et al. A Circular RNA Protects Dormant Hematopoietic Stem Cells From DNA Sensor cGAS-Mediated Exhaustion. *Immunity* (2018) 48:688–701.e7. doi: 10.1016/j.immuni.2018.03.016
158. Wesselhoeft R, Kowalski P, Anderson D. Engineering Circular RNA for Potent and Stable Translation in Eukaryotic Cells. *Nat Commun* (2018) 9:2629. doi: 10.1038/s41467-018-05096-6
159. De-lai K, Yi-fan Z, Wen-jun Z, Ai-zhen G, Ying-yu C. Research Progress on Circular RNA. *Chin Vet Sci* (2021) 51(03):1–7. doi: 10.16656/j.issn.1673-4696.2021.0027
160. Morad G, Helmink B, Sharma P, Wargo J. Hallmarks of Response, Resistance, and Toxicity to Immune Checkpoint Blockade. *Cell* (2021) 184 (21):5309–37. doi: 10.1016/j.cell.2021.09.020
161. Song H, Liu Q, Liao Q. Circular RNA and Tumor Microenvironment. *Cancer Cell Int* (2020) 20:211. doi: 10.1186/s12935-020-01301-z
162. Li W, Liu J, Chen M, Xu J, Zhu D. Circular RNA in Cancer Development and Immune Regulation. *J Cell Mol Med* (2020) 26(6):1785–98. doi: 10.1111/jcmm.16102
163. Shang Q, Yang Z, Jia R, Ge S. The Novel Roles of circRNAs in Human Cancer. *Mol Cancer* (2019) 18:6. doi: 10.1186/s12943-018-0934-6
164. Xu Z, Li P, Fan L, Wu M. The Potential Role of circRNA in Tumor Immunity Regulation and Immunotherapy. *Front Immunol* (2018) 9:9. doi: 10.3389/fimmu.2018.00009
165. Hegde P, Chen D. Top 10 Challenges in Cancer Immunotherapy. *Immunity* (2020) 52:17–35. doi: 10.1016/j.immuni.2019.12.011
166. Billan S, Kaidar-Person O, Gil Z. Treatment After Progression in the Era of Immunotherapy. *Lancet Oncol* (2020) 21:e463–e76. doi: 10.1016/S1470-2045(20)30328-4
167. Wang R, Wang H. Immune Targets and Neoantigens for Cancer Immunotherapy and Precision Medicine. *Cell Res* (2017) 27:11–37. doi: 10.1038/cr.2016.155
168. Lu J, Zhang P, Huang X, Guo X, Gao C, Zeng H, et al. Amplification of Spatially Isolated Adenosine Pathway by Tumor-Macrophage Interaction Induces Anti-PD1 Resistance in Hepatocellular Carcinoma. *J Hematol Oncol* (2021) 14:200. doi: 10.1186/s13045-021-01207-x
169. Qu L, Yi Z, Shen Y, Lin L, Chen F, Xu Y, et al. Circular RNA Vaccines Against SARS-CoV-2 and Emerging Variants. *Cell* (2022) 185(10):1728–44.e16. doi: 10.1016/j.cell.2022.03.044

Conflict of Interest: The authors declare that the research was conducted in the absence of any commercial or financial relationships that could be construed as a potential conflict of interest.

this article, or claim that may be made by its manufacturer, is not guaranteed or endorsed by the publisher.

frontiers | Frontiers in Immunology

ORIGINAL RESEARCH
published: 15 July 2022
doi: 10.3389/fimmu.2022.910136

Heterologous saRNA Prime, DNA Dual-Antigen Boost SARS-CoV-2 Vaccination Elicits Robust Cellular Immunogenicity and Cross-Variant Neutralizing Antibodies

Adrian Rice[1†], Mohit Verma[1†], Emily Voigt[2†], Peter Battisti[2], Sam Beaver[2], Sierra Reed[2], Kyle Dinkins[1], Shivani Mody[1], Lise Zakin[1], Shiho Tanaka[1], Brett Morimoto[1], C. Anders Olson[1], Elizabeth Gabitzsch[1], Jeffrey T. Safrit[1], Patricia Spilman[1], Corey Casper[2,3] and Patrick Soon-Shiong[1]*

[1] ImmunityBio, Inc., Culver City, CA, United States, [2] Access to Advanced Health Institute (AAHI), Seattle, WA, United States, [3] Departments of Medicine and Global Health, University of Washington, Seattle, WA, United States

OPEN ACCESS

Edited by:
Ingo Drexler, Heinrich Heine University, Germany

Reviewed by:
Juan Pablo Jaworski, Consejo Nacional de Investigaciones Científicas y Técnicas (CONICET), Argentina
Srinivasa Reddy Bonam, University of Texas Medical Branch at Galveston, United States

***Correspondence:**
Patrick Soon-Shiong
Patrick@Nantworks.com

[†]These authors have contributed equally to this work

Specialty section:
This article was submitted to Vaccines and Molecular Therapeutics, a section of the journal Frontiers in Immunology

Received: *31 March 2022*
Accepted: *22 June 2022*
Published: *15 July 2022*

Citation:
Rice A, Verma M, Voigt E, Battisti P, Beaver S, Reed S, Dinkins K, Mody S, Zakin L, Tanaka S, Morimoto B, Olson CA, Gabitzsch E, Safrit JT, Spilman P, Casper C and Soon-Shiong P (2022) Heterologous saRNA Prime, DNA Dual-Antigen Boost SARS-CoV-2 Vaccination Elicits Robust Cellular Immunogenicity and Cross-Variant Neutralizing Antibodies. Front. Immunol. 13:910136. doi: 10.3389/fimmu.2022.910136

We assessed if immune responses are enhanced in CD-1 mice by heterologous vaccination with two different nucleic acid-based COVID-19 vaccines: a next-generation human adenovirus serotype 5 (hAd5)-vectored dual-antigen spike (S) and nucleocapsid (N) vaccine (AdS+N) and a self-amplifying and -adjuvanted S RNA vaccine (AAHI-SC2) delivered by a nanostructured lipid carrier. The AdS+N vaccine encodes S modified with a fusion motif to increase cell-surface expression and an N antigen modified with an Enhanced T-cell Stimulation Domain (N-ETSD) to direct N to the endosomal/lysosomal compartment and increase MHC class I and II stimulation potential. The S sequence in the AAHI-SC2 vaccine comprises the D614G mutation, two prolines to stabilize S in the prefusion conformation, and 3 glutamines in the furin cleavage region to confer protease resistance. CD-1 mice received vaccination by homologous and heterologous prime > boost combinations. Humoral responses to S were the highest with any regimen that included the AAHI-SC2 vaccine, and IgG bound to wild type and Delta (B.1.617.2) variant S1 at similar levels. An AAHI-SC2 prime followed by an AdS+N boost particularly enhanced CD4+ and CD8+ T-cell responses to both wild type and Delta S peptides relative to all other vaccine regimens. Sera from mice receiving AAHI-SC2 homologous or heterologous vaccination were found to be highly neutralizing for all pseudovirus strains tested: Wuhan, Beta, Delta, and Omicron strains. The findings here, taken in consideration with the availability of both vaccines in thermostable formulations, support the testing of heterologous vaccination by an AAHI-SC2 > AdS+N regimen in animal models of SARS-CoV-2 infection to assess its potential to provide increased protection against emerging SARS-CoV-2 variants particularly in regions of the world where the need for cold-chain storage has limited the distribution of other vaccines.

Keywords: self-amplifying RNA, DNA, vaccine, dual antigen, heterologous, spike, nucleocapsid

INTRODUCTION

Impressive efforts of the scientific and pharmaceutical community have resulted in the design, testing and successful deployment of several COVID-19 vaccines that have shown high levels of efficacy (1–5). Nonetheless, SARS-CoV-2 viral variants have continued to emerge and spread throughout the globe – most recently the highly transmissible Omicron variant (6) – pointing to the need for delivery of vaccines to populations that are currently underserved.

To address the need for a vaccine regimen that would be highly efficacious against predominating and emerging variants as well as distributable in currently underserved areas, we previously developed a next-generation human adenovirus serotype 5 (hAd5)-vectored dual-antigen spike (S) plus nucleocapsid (N) vaccine (AdS+N) (7, 8) to leverage the resilience of cell-mediated immunity against variants. This vaccine, encoding Wuhan strain or 'wild type' (wt) SARS-CoV-2 S and modified with a fusion sequence (S-Fusion) to enhance cell-surface expression (7, 8), as well as N modified with an Enhanced T-cell Stimulation Domain (N-ETSD) (9) for increased MHC class I and II stimulation (10–12), has been shown to elicit humoral and T-cell responses in mice (8), non-human primates (NHP) (7), and participants in Phase 1b trials (9). The AdS+N vaccine given as a subcutaneous (SC) prime with two oral boosts protected NHP from SARS-CoV-2 infection (7), and a single prime vaccination of clinical trial participants generated T-cell responses that were sustained against a series of variant S peptide sequences, including those for the B.1.351, B.1.1.7, P.1, and B.1.426 variants (9).

Despite the promising findings with the AdS+N vaccine candidate, we wish to continue to investigate vaccine regimens with the potential to maximize immune responses – both humoral and cellular. One such approach is by heterologous vaccination utilizing multiple nucleic acid-based vaccine platforms, such as ImmunityBio's hAd5-vectored DNA vaccine and the Access to Advanced Health Institute's (AAHI) RNA-based vaccine (13). Heterologous vaccination using vaccine constructs expressing the same or different antigens vectored by different platforms has previously been reported to significantly increase immune responses (14–16), and specifically for COVID-19 vaccines, heterologous prime-boost regimens including the available mRNA and adenovirus-based vaccines elicit humoral and cellular responses in human subjects that are at least as good as or better than homologous vaccination (17–20).

To assess the potential for enhanced immune responses by heterologous vaccination, we tested prime > boost combinations of the AdS+N vaccine with a self-amplifying and self-adjuvanted S(wt) RNA-based vaccine (AAHI-SC2) delivered in a nanostructured lipid carrier (NLC) (21, 22) that has recently been reported to elicit robust, virus-neutralizing humoral responses, establishment of long-lived antibody-secreting plasma cell populations, and polyfunctional CD4+ and CD8+ T-cell responses after both prime and prime-boost regimens in C57BL/6 mice (13). The NLC stabilizes the self-amplifying RNA (23–25) and delivers it to cells, where the vaccine RNA is then amplified and S protein is expressed. The S sequence in the AAHI-SC2 vaccine comprises a codon-optimized sequence with the D614G mutation (26) that increases SARS-CoV-2 susceptibility to neutralization (27), a diproline modification to stabilize S in the pre-fusion conformation that increases antigenicity (28), and a tri-glutamine (3Q) repeat in the furin cleavage region to render it protease resistant (29).

In this work, the two aforementioned vaccines were tested by homologous and heterologous AdS+N > AAHI-SC2 and AAHI-SC2 > AdS+N prime > boost regimens. The findings reported here support our hypothesis that heterologous vaccination with the AAHI-SC2 and AdS+N vaccines enhances immune responses, particularly T-cell responses.

METHODS

The AdS+N and AAHI-SC2 Vaccines

For studies here, the next generation hAd5 [E1-, E2b-, E3-] vector was used to create the viral vaccine candidate construct (7). This hAd5 [E1-, E2b-, E3-] vector is primarily distinguished from other first-generation [E1-, E3-] recombinant Ad5 platforms (30, 31) by having additional deletions in the early gene 2b (E2b) region that remove the expression of the viral DNA polymerase (pol) and in preterminal protein (pTP) genes, and by its propagation in the E.C7 human cell line (32–35).

The AdS+N vaccine expresses a wild type spike (S) sequence [accession number YP009724390] modified with a proprietary 'fusion' linker peptide sequence as well as a wild type nucleocapsid (N) sequence [accession number YP009724397] with an Enhanced T-cell Stimulation Domain (ETSD) signal sequence that directs translated N to the endosomal/lysosomal pathway (9) as described in Gabitzsch *et al.*, 2021 (7).

The AAHI-SC2 vaccine comprises an saRNA replicon composed of an 11.7 kb construct expressing the SARS-CoV-2 S protein, along with the non-structural proteins 1-4 derived from the Venezuelan equine encephalitis virus (VEEV) vaccine strain TC-83 (**Figure 1**). The S RNA sequence is codon-optimized and expresses a protein with the native sequence of the original Wuhan strain plus the dominant D614G mutation, with the prefusion conformation-stabilizing diproline (pp) mutation (consistent with other vaccine antigens) and replacement of the furin cleavage site RRAR sequence with a QQAQ sequence.

The RNA is generated by T7 promoter-mediated *in vitro* transcription using a linearized DNA template. *In vitro* transcription is performed using an in house-optimized protocol (13, 36, 37) using T7 polymerase, RNase inhibitor, and pyrophosphatase enzymes. The DNA plasmid is digested with DNase I, and the RNA is capped by vaccinia capping enzyme, guanosine triphosphate, and S-adenosyl-methionine. RNA is then purified from the transcription and capping reaction components by chromatography using a CaptoCore 700 resin (GE Healthcare) followed by diafiltration and concentration using tangential flow filtration into 10 mM Tris buffer. The RNA material is terminally filtered with a 0.22 μm polyethersulfone filter and stored at -80°C until use.

The RNA-delivering NLC is comprised of particles with a hybrid liquid and solid oil core, providing colloidal stability (21),

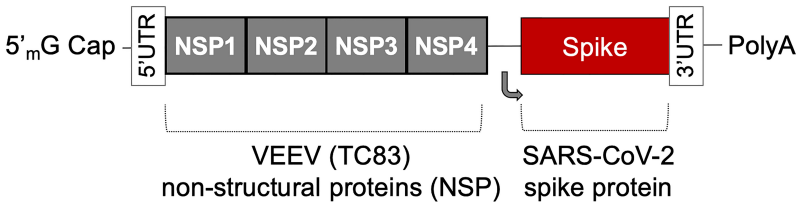

FIGURE 1 | *The saRNA(D614G)-2P-3Q-NLC (AAHI-SC2) vaccine*. The AAHI-SC2 vaccine comprises an saRNA replicon backbone consisting of the non-structural proteins (NSPs) 1-4 derived from the Venezuelan equine encephalitis virus (VEEV) vaccine strain TC-83 and an independent open reading frame under the control of a subgenomic promoter sequence that contains Wuhan sequence S with a diproline (pp) mutation and a QQAQ furin cleavage site sequence.

surrounded by non-ionic hydrophobic and hydrophilic surfactants to help maintain a stable nanoparticle droplet and the cationic lipid DOTAP to provide positive charge for electrostatic binding with RNA. This RNA binding on the surface of the nanoparticles protects the RNA from RNase degradation and allows effective delivery to cells.

NLC is manufactured by mixing the lipids in an oil phase, dissolving the Tween 80 in citrate buffer aqueous phase, and homogenizing the two phases by micro-fluidization. The resulting emulsion is sterile-filtered and vialed until dilution in a sucrose-citrate solution and complexing with vaccine saRNA.

Murine Immunization and Blood/ Tissue Collection

The design of vaccination study performed using CD-1 mice is shown in **Figure 2**.

All *in vivo* experiments described were carried out at the Omeros Inc. vivarium (Seattle, WA) in strict accordance with good animal practice according to NIH recommendations. All procedures for animal use were done under an animal use protocol (#19-08) approved by the IACUC at Omeros, Inc. (Seattle, WA, USA).

CD-1 female mice (Charles River Laboratories) 6-8 weeks of age were used for immunological studies. The adenovirus-vectored vaccines were administered by subcutaneous (SC) injections at 1x10e^{10} viral particles (VP) in 50 µL ARM buffer (20 mM Tris pH 8.0, 25 mM NaCl, with 2.5% glycerol). The AAHI-SC2 vaccine was administered intramuscularly (IM) in 10% sucrose, 5 mM sodium citrate solution at a dose of 10 µg.

On the final day of each study, blood was collected submandibularly from isoflurane-anesthetized mice, and sera were isolated using a microtainer tube. Mice were then euthanized for collection of spleens. Spleens were placed in 5 mL of sterile media (RPMI/HEPES/Pen/Strep/10% FBS). Splenocytes were isolated (38) within 2 hours of collection and used fresh or cryopreserved for later analysis.

Intracellular Cytokine Stimulation

ICS assays were performed using 10^6 live splenocytes per well in 96-well U-bottom plates. Splenocytes in RPMI media supplemented with 10% FBS were stimulated by the addition of pools of overlapping peptides spanning the SARS-CoV-2 S protein (both wild type Wuhan strain, wt, or Delta sequence) or N antigens at 1-2 µg/mL/peptide for 6 h at 37°C in 5% CO_2, with protein transport inhibitor, GolgiStop (BD) added two hours after initiation of incubation. The S peptide pool (wild type, JPT Cat #PM-WCPV-S-1; Delta, JPT cat# PM-SARS2-SMUT06-1) is a total of 315 spike peptides split into two pools, S1 and S2, comprised of 158 and 157 peptides each. The N peptide pool

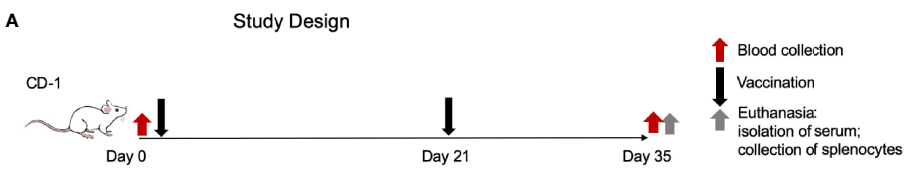

B

N #	Prime	Dose (Route)	Boost	Dose (Route)	Code
4	Untreated		untreated		UnTx
7	hAd5 S-Fusion+N-ETSD	1x10^{10} VP (SC)	hAd5 S-Fusion+N-ETSD	1x10^{10} VP (SC)	AdS+N > AdS+N
6	saRNA(D614G-2P-3Q)-NLC	10 µg (IM)	saRNA(D614G-2P-3Q)-NLC	10 µg (IM)	AAHI-SC2 > AAHI-SC2
7	hAd5 S-Fusion+N-ETSD	1x10^{10} VP (SC)	saRNA(D614G-2P-3Q)-NLC	10 µg (IM)	AdS+N > AAHI-SC2
7	saRNA(D614G-2P-3Q)-NLC	10 µg (IM)	hAd5 S-Fusion+N-ETSD	1x10^{10} VP (SC)	AAHI-SC2 > AdS+N

FIGURE 2 | *Study design and vaccine description*. **(A)** CD-1 mice received prime vaccination on Day 0 after blood collection and boost vaccination on Day 21; mice were euthanized and tissues/blood collected on Day 35. **(B)** The various combinations of prime > boost are shown, including: AdS+N homologous; saRNA(D614G-2P-3Q)-NLC (AAHI-SC2) homologous; AdS+N prime, AAHI-SC2 boost; and AAHI-SC2 prime, AdS+N boost. Untreated mice were used as controls. All groups were n = 7 with the exception of untreated n = 4 and AAHI-SC2 homologous n = 6. The color code for each group is shown.

(JPT; Cat # PM-WCPV-NCAP-1) was also used to stimulate cells. A SIV-Nef peptide pool (BEI Resources) was used as an off-target negative control. Stimulated splenocytes were then stained with a fixable cell viability stain (eBioscience™ Fixable Viability Dye eFluor™ 506 Cat# 65-0866-14) followed by the lymphocyte surface markers CD8β and CD4, fixed with CytoFix (BD), permeabilized, and stained for intracellular accumulation of interferon-gamma (IFN-γ), tumor necrosis factor-alpha (TNF-α), and interleukin-2 (IL-2). Fluorescent-conjugated anti-mouse antibodies used for labeling included CD8β antibody (clone H35-17.2, ThermoFisher), CD4 (clone RM4-5, BD), IFN-γ (clone XMG1.2, BD), TNF-α (clone MP6-XT22, BD) and IL-2 (clone JES6-5H4; BD), and staining was performed in the presence of unlabeled anti-CD16/CD32 antibody (clone 2.4G2; BD). Flow cytometry was performed using a Beckman-Coulter Cytoflex S flow cytometer and analyzed using Flowjo software.

ELISpot Assay

ELISpot assays were used to detect cytokines secreted by splenocytes from inoculated mice. Fresh splenocytes were used on the same day as harvest, and cryopreserved splenocytes containing lymphocytes were used on the day of thawing. The cells (2-4 x 10^5 cells per well of a 96-well plate) were added to the ELISpot plate containing an immobilized primary antibody to either IFN-γ or IL-4 (BD Cat# 551881 and BD Cat# 551878, respectively), and were exposed to various stimuli (e.g. control peptides SIV and ConA, S-WT and N peptides pools – see catalog numbers above) at a concentration of 1-2 μg/mL peptide pools for 36-40 hours. After aspiration and washing to remove cells and media, extracellular cytokines were detected by a biotin-conjugated secondary antibody to either IFN-γ or IL-4 (BD Cat# 551881 and BD Cat# 551878, respectively), followed by a streptavidin/horseradish peroxidase conjugate (BD Cat# 557630) to detect the biotin-conjugated secondary antibody. The number of spots per well, or per 2-4 x 10^5 cells, was counted using an ELISpot plate reader. Quantification of Th1/Th2 bias was calculated by dividing the IFN-γ spot forming cells (SFC) per million splenocytes with the IL-4 SFC per million splenocytes for each animal.

ELISA for Detection of Antibodies

For IgG antibody detection in inoculated mouse sera and lung homogenates, ELISAs for spike-binding (including S1 Delta) and nucleocapsid-binding IgG and IgG subclass (IgG1, IgG2a, IgG2b, and IgG3 antibodies were used. A microtiter plate was coated overnight with 100 ng of either purified recombinant SARS-CoV-2 S-FTD (FL S with fibritin trimerization domain, constructed and purified in-house by ImmunityBio), purified recombinant Spike S1 domain (S1(wt)) (Sino; Cat # 40591-V08B1), purified recombinant Delta variant Spike S1 domain (S1(Delta)) (Sino; Cat # 40591-V08H23), or purified recombinant SARS-CoV-2 nucleocapsid (N) protein (Sino; Cat # 40588-V08B) in 100 μL of coating buffer (0.05 M Carbonate Buffer, pH 9.6). The wells were washed three times with 250 μL PBS containing 1% Tween 20 (PBST) to remove unbound protein, and the plate was blocked for 60 minutes at room temperature with 250 μL PBST. After blocking, the wells were washed with PBST, 100 μL of either diluted serum or diluted lung homogenate samples was added to each well, and samples were incubated for 60 minutes at room temperature. After incubation, the wells were washed with PBST and 100 μL of a 1/5000 dilution of anti-mouse IgG2a HRP (GE Health Care; Cat # NA9310V), anti-mouse IgG2b HRP (Sigma; Cat # SAB3701171), anti-mouse IgG_{2a} HRP (Sigma; Cat # SAB3701178), anti-mouse IgG_{2b} HRP (Sigma; catalog# SAB3701185), or anti-mouse IgG3 HRP conjugated antibody (Sigma; Cat # SAB3701192), (Sigma: Cat #SAB3701192) was added to wells. For positive controls, 100 μL of a 1/5000 dilution of rabbit anti-N IgG Ab or 100 μL of a 1/25 dilution of mouse anti-S serum (from mice immunized with purified S antigen in adjuvant) were added to appropriate wells. After incubation at room temperature for 1 hour, the wells were washed with PBST and incubated with 200 μL o-phenylenediamine-dihydrochloride (OPD substrate, Thermo Scientific Cat # A34006) until appropriate color development. The color reaction was stopped with addition of 50 μL 10% phosphoric acid solution (Fisher Cat # A260-500) in water, and the absorbance at 490 nm was determined using a microplate reader (SoftMax Pro, Molecular Devices).

Calculation of Relative ng Amounts of Antibodies and the Th1/Th2 IgG Subclass Bias

A standard curve of IgG for OD vs. ng mouse IgG was generated using purified mouse IgG (Sigma Cat #15381); absorbance values from this standard curve were used to convert sample absorbance signals into mass equivalents for both anti-S and anti-N antibodies. Using these values, we calculated the geometric mean value for S- and N-specific IgG per milliliter of serum induced by vaccination. These values were also used to quantify the Th1/Th2 bias for the humoral responses by dividing the sum total of Th1 biased antigen-specific IgG subclasses (IgG2a, IgG2b and IgG3) with the total Th2 indicative IgG1, for each mouse. For mice that lacked anti-S and/or anti-N specific IgG responses, Th1/Th2 ratio was not calculated. Some responses, particularly for anti-N responses in IgG2a and IgG2b (both Th1 biased subclasses), were above the limit of quantification with OD values higher than those observed in the standard curve. These data points were therefore reduced to values within the standard curve, and thus the reported Th1/Th2 bias is lower than would otherwise be reported.

Endpoint titers

Serial dilutions were prepared from each serum sample, with dilution factors ranging from 400 to 6,553,600 in 4-fold steps. These dilution series were characterized by whole IgG ELISA assays against both recombinant S1(wt) and recombinant S1 (Delta), as described above. Half maximal response values (Ab_{50}) were calculated by non-linear least squares fit analysis on the values for each dilution series against each recombinant S1 in GraphPad Prism. Serum samples from mice without anti-S responses were removed from Ab_{50}, μg IgG/mL sera, and endpoint titer analyses and reported as N/D on the graphs. Endpoint titers were defined as the last dilution with an absorbance value at least 3 standard deviations higher than the standard deviation of all readings from serum of untreated animals (n = 32 total negative samples). Quantitative titration

values (μg IgG/mL sera) were calculated against a standard curve as described above.

Pseudovirus Neutralization Assay

SARS-CoV-2 pseudovirus neutralization assays were conducted on immunized mouse serum samples using procedures adapted from Crawford *et al.*, 2020 (39). In brief, lentiviral pseudoviruses expressing SARS-CoV-2 spike protein variants were prepared by co-transfecting HEK293 cells (ATCC CRL-3216) seeded at $4x10^{e5}$ cells/mL with a plasmid containing a lentiviral backbone expressing luciferase and ZsGreen (BEI Resources NR-52516), plasmids containing lentiviral helper genes (BEI Resources NR-52517, NR-52518, NR-52519), a delta19 cytoplasmic tail-truncated SARS-CoV-2 spike protein expression plasmid (Wuhan strain, B.1.1.7, and B.1.351 spike variant plasmids were a gift from Jesse Bloom of Fred Hutchinson Cancer Research Center; B.1.617.2 Delta and Omicron variant plasmids were a gift from Thomas Peacock of Imperial College London) and Bio-T transfection reagent (Bioland Scientific B0101). The transfection was incubated for 72 hours at 37°C, 5% CO_2. Pseudovirus stocks were harvested from the cell culture media, (Gibco DMEM + GlutaMAX + 10% FBS) filtered through a 0.2 μm filter, and frozen at -80°C until titering and use.

Mouse serum samples were diluted 1:10 in media (Gibco DMEM + GlutaMAX + 10% FBS) and then serially diluted 1:2 for 11 total dilutions, and incubated for 1 hour at 37°C, 5% CO_2.with a mixture of 5 μg/mL polybrene (Sigma TR-1003-G) and pseudovirus diluted to a titer that produces 1×10^{e8} total integrated intensity units/mL. The serum-virus mix was then added in duplicate to human Angiotensin-Converting Enzyme 2 expressing HEK293 cells (BEI Resources NR-52511, NIAID, NIH) seeded at 4 x 10^{e5} cells/mL on a 96 well plate.

The plates were incubated at 37°C, 5% CO_2 for 72 hours. Plates were imaged on a high content fluorescent imager (Molecular Devices ImageXpress Pico) for ZsGreen expression. Total integrated intensity units per well quantified using ImageXpress software (Molecular Devices) was used to calculate % pseudovirus inhibition in each well. Neutralization curves were fit with a four-parameter sigmoidal curve which was used to calculate 50% inhibitory concentration dilution (IC50) values.

Statistical Analyses and Graph Generation

All statistical analyses were performed and figures and graphs generated using GraphPad Prism software. Data that did not have a normal distribution as determined by a Shapiro-Wilks test were analyzed using a non-parametric Kruskal-Wallis test with Dunn's *post-hoc* comparison of groups and were graphed as the mean and standard deviation (SD). Data graphed on a log scale were log-normalized, analyzed using one-way ANOVA and Tukey's comparison of groups, and were graphed as the geometric mean and the geometric SD. Statistical analyses of Endpoint Titers for anti-S1 IgG were performed by assigning a value of 200 – one half the Level of Detection (LOD) of 400 – to the 4 animals with serum values below the LOD. P values for each comparison are listed in **Supplementary Table S1**.

RESULTS

The AAHI-SC2 Vaccine Enhances Generation of Anti-S(wt) IgG

Mice that received either AAHI-SC2 homologous or AAHI-SC2 > AdS+N heterologous vaccination had the higher levels of anti-full length S(wt) (FL S) IgG2a and 2b when compared to untreated or AdS+N homologous vaccinated mice, as determined by ELISA OD readouts OD at 490 nm (**Figure 3A**). Only mice receiving the N antigen generated anti-N IgG (also determined by ELISA 490 nm OD readouts at 490 nm); there were no significant differences between the groups that received AdS+N homologous, prime, or boost vaccination (**Figure 3B**). Determination of the IgG2a + IgG2b + IgG3/IgG1 ratio using ng amounts calculated from the OD reading (see *Methods*) revealed responses were highly T helper cell 1 (Th1)-biased, with calculated values being one or greater (**Figure 3C**).

Humoral Responses Against Wildtype and Delta S1 Were Similar in all AAHI-SC2 Groups

To assess serum antibody production specific for Delta B.1.617.2 variant as compared to wild type (wt) S, ELISAs were performed using either the wt or B.1.617.2 sequence S1 domain of S, which contains the RBD.

There were no statistical differences among groups that received the AAHI-SC2 vaccine in any regimen for anti-S1(wt) or -S1(Delta) Ab_{50} or μg IgG/mL (**Figures 4A, B**, respectively); statistical comparison of the AdS+N homologous group to other groups was not performed in **Figure 4A** or **B** because 4 of 7 values were below the LOD. For the endpoint titer reciprocal dilution (**Figure 4C**), AdS+N sera below the LOD were assigned the value of 200 (half the LOD of 400) to allow statistical analysis. Anti-S1(wt) IgG responses were higher for AAHI-SC2 homologous and AAHI-SC2 > AdS+N group mice compared with AdS+N homologous vaccination. Anti-S1(Delta) IgG responses were significantly higher in animals in the AAHI-SC2 homologous group versus the AdS+N homologous group. Other comparisons were not significant due to variation among individual mice.

An AdS+N Boost After AAHI-SC2 Prime Vaccination Enhances CD4+ and CD8+ T-Cell Responses to S Peptides

Significantly higher percentages of CD4+ T-cells secreting IFN-γ alone, IFN-γ and tumor necrosis factor-α (TNF-α), or IFN-γ, TNF-α, and interleukin-2 (IL-2) as detected by intracellular cytokine staining (ICS) in response to S(wt) peptides were detected in the AAHI-SC2 > AdS+N - but not AdS+N > AAHI-SC2 - group mice as compared to the untreated and AdS+N homologous group (**Figures 5A, C, E**). Although mean values for the AdS+N > AAHI-SC2 group were lower than those for the AAHI-SC2 > AdS+N group, the differences were not statistical significant due to individual variation among mice.

Only cytokine production by CD8+T cells from AAHI-SC2 > AdS+N group mice was significantly greater than the untreated

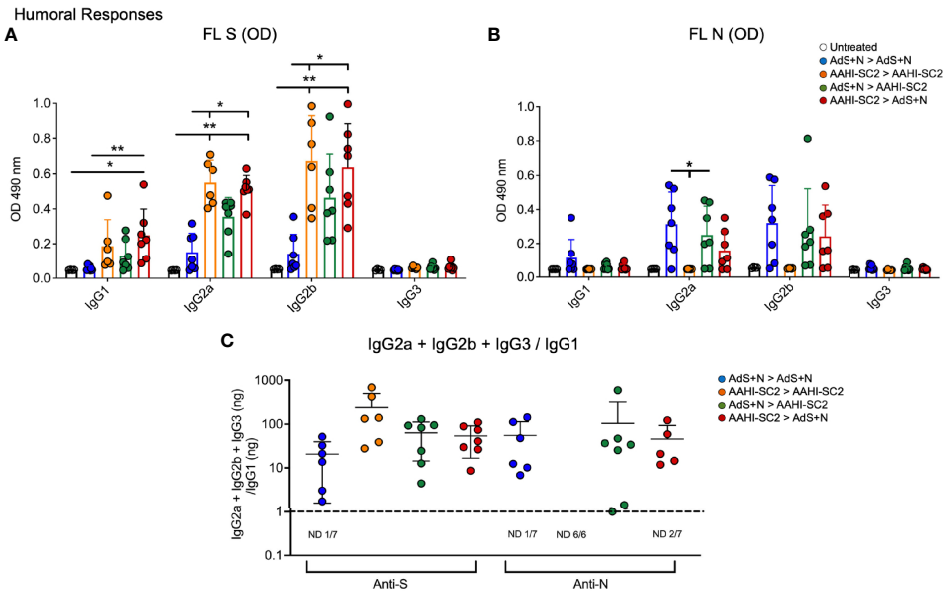

FIGURE 3 | *Anti-full length (FL) spike wild type (Swt) and -nucleocapsid (N) IgG antibody levels in sera show T helper cell 1 (Th1) bias*. **(A)** Levels of anti-FL Swt and **(B)** anti-N IgG1, IgG2a, IgG2b and IgG3 subtypes represented by OD at 490 nm from ELISA of sera are shown. Statistical analyses were performed using a non-parametric Kruskal-Wallis test and Dunn's *post-hoc* comparison of all groups where *p ≤.05 and **p <.01. In instances of similar significance, the tick marks indicate groups compared to the group without a tick mark; for example in panel A, both the AAHI-SC2 homozygous (orange) and AAHI-SC2 > AdS+N (red) groups showed **p <.01 signifcant increases as compared to the untreated group (clear) for IgG2a. P values are listed in Table 1. The legend in B applies to panels **(A, B)**. All dilutions were 1:400. **(C)** The IgG2a+IgG2b+IgG3/IgG1 ratio calculated using the ng equivalents for each is shown with a dashed line at 1. Values > 1 reflect Th1 bias. The number (n) of animals in which the ratio was not determined due to very low antibody levels is shown below the x-axis for each group. The homologous AAHI-SC2 group did not receive an N antigen. Data graphed as the mean and SD.

group (**Figures 5B, D, F**), and the level of significance was greater than that observed for CD4+ T cells (**Figures 5A, C, E**).

Only T cells from mice receiving vaccination regimens that included delivery of the N antigen by the AdS+N vaccine produced cytokines in response to N peptide stimulation. For CD4+ T cells, IFN-γ (IFN-γ) production was significantly greater for AdS+N homologous and AAHI-SC2 > AdS+N groups (but not the AdS+N > AAHI-SC2 group) compared to the AAHI-SC2 homologous group (**Figure 5A**), and IFN-γ, tumor necrosis factor-α (TNF-α) as well as IFN-γ, TNF-α, and interleukin-1 (IL-2) production were greater for the same two groups as compared to either the untreated or AAHI-SC2 homologous groups (**Figures 5C, E**, respectively). For CD8+ T cells, only the AdS+N homologous group had significantly greater cytokine production than the groups that did not receive N (**Figures 5B, D, F**).

CD4+ and CD8+ T-Cell Production of IFN-γ Was Similar in Response to Either S(wt) or S(Delta) Peptides

CD4+ and CD8+ T cells show similar levels of IFN-γ production by ICS in response to either S(wt) or S(Delta) sequence peptides (**Figures 6A, B**, respectively). Patterns of CD4+ and CD8+ T-cell stimulation by S protein peptides between the vaccination regimens were also similar between the S(wt) and S(Delta) peptides. Compared to the untreated control, the increase in IFN-γ production was again the highest for the AAHI-SC2 > AdS+N group for both CD4+ and CD8+ T cells, in response to either S(wt) or S(Delta) peptides.

Numbers of IFN-γ-Secreting Splenocytes in Response to S Peptides Were the Highest From Mice Receiving AAHI-SC2 > AdS+N Heterologous Vaccination

As shown in **Figure 7A**, ELISpot detection of cytokine secreting cells in response to S peptide stimulation revealed that animals receiving either homologous AAHI-SC2 or heterologous AAHI-SC2 > AdS+N vaccination developed significantly higher levels of S peptide-reactive IFN-γ-secreting T cells than untreated group animals; the level of significance was greater with heterologous vaccination. Numbers of IFN-γ-secreting T cells in response to the N peptide pool were similar for AdS+N homologous and AAHI-SC2 > AdS+N groups. T cells from AAHI-SC2 > AAHI-SC2 group animals did not secrete IFN-γ in response to the N peptide pool, as expected, because the AAHI-SC2 vaccine does not deliver the N antigen. There was some skew seen for data in **Figure 7A**, with values for S WT/N of untreated = 2.0/0.0, AdS+N > AdS+N = 1.27/0.27, AAHI-SC2 > AAHI-SC2 = -0.53/2.45, AdS+N > AAHI-SC2 = 1.89/1.4, and AAHI-SC2 > AdS+N = 0.35/-0118. We note these are outbred mice with variance in MHC haplotype and variable T-cell data not unexpected.

Reflecting the Th1 bias of T-cell responses, induction of interleukin-4 (IL-4) secreting T cells was low for all animals in

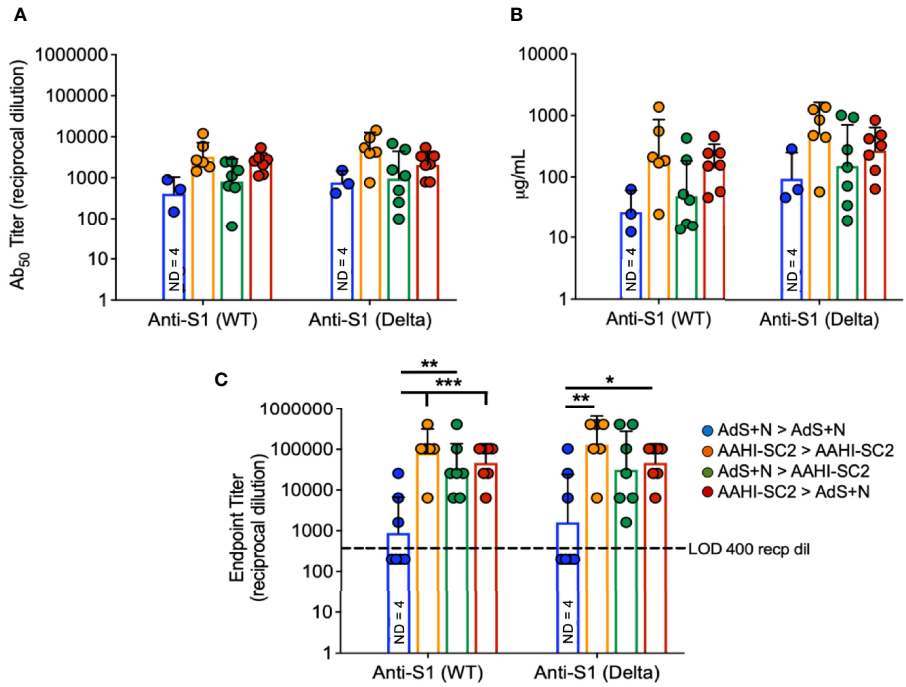

FIGURE 4 | *Wildtype and B.1.617.2 'Delta' S1-specific IgG endpoint titers*. Levels of anti-S1(wt) and -Delta S1 IgG are shown by **(A)** Ab_{50} reciprocal dilution, **(B)** µg/mL sera, and **(C)** endpoint titer reciprocal dilution. Values were below the level of detection in 4 of 7 AdS+N homologous group mice. Statistical analyses were performed on log-normalized data using one-way ANOVA and Tukey's *post-hoc* comparison of all groups for anti-S1 (WT) or -S1 (Delta) where *p ≤.05, **p <.01 and ***p <.001; in **(C)**, sera without detectable levels of anti-S1 IgG were assigned a value of 200, one-half the Limit of Detection (LOD) of 400. In instances of similar significance, the tick marks indicate groups compared to the group without a tick mark; p values are listed in Table 1. Data graphed as the geometric mean and geometric SD. The legend in C applies to all figure panels.

all groups (**Figure 7B**); therefore the IFN-γ/IL-4 ratio was above 1 for all animals for which the ratio could be calculated, with the exception of 1 animal in the AdS+N > AAHI-SC2 group in response to N (**Figure 7C**).

Sera From Mice Receiving the AAHI-SC2 Vaccine Neutralize SARS-CoV-2 Wuhan, Delta, Beta and Omicron Pseudoviruses

As represented in **Figure 8A**, sera from AAHI-SC2 homologous and AAHI-SC2 > AdS+N heterologous group mice showed the highest neutralization capability against the four SARS-CoV-2 lentiviral pseudoviruses: Wuhan (D614G), Beta (B.1.351), Delta (B.1.617.2), and Omicron (B.1.1.529) variants. Neutralizing antibody titers were significantly higher than for sera from untreated and AdS+N > AdS+N group mice.

Comparison of SARS-CoV-2 variant neutralizing antibody titers between groups (**Figure 8B**) demonstrate that sera from AAHI-SC2 homologous, AdS+N > AAHI-SC2 and AAHI-SC2 > AdS+N heterologous vaccinated mice all have high Wuhan-strain neutralization capacity. There were no significant differences in the capability of sera from AAHI-SC2 homologous vaccinated mice to neutralize the 4 strains tested, but sera from both heterologously vaccinated groups showed a greater capability to neutralize the Wuhan strain than the Omicron strain.

DISCUSSION

The immune responses observed in the present study support our hypothesis, and that of others, that heterologous vaccination provides an opportunity for increased humoral and cell-mediated responses to vaccination. These results are consistent with recently-published data reporting enhanced antibody and T-cell responses in patients who received heterologous vaccination with the currently available COVID-19 vaccines (17–20).

Perhaps the most intriguing finding in the present study was that the increases in S-specific CD4+ and CD8+ T-cell responses from heterologous AAHI-SC2 > AdS+N group mice as compared to untreated mice had the highest level of significance, with greater than 5% of CD8+ T cells accumulating both IFN-γ and TNF-α in response to S peptides, on average. Enhancement of T-cell responses when an adenovirus vaccine is used as a boost for an RNA vaccine prime is consistent with both Liu *et al.* (18), who assessed humoral and cellular responses in participants who received ChAdOx or BNT162b2 in various heterologous and homologous prime-boost combinations and concluded the BNT prime > ChAdOx boost regimen resulted in the greatest expansion of vaccine-antigen responsive T cells; and with Atmar *et al.* (20), who found that with various prime > boost regimens with the Ad26.COV2.S and mRNA1273 or BNT162b2 vaccines, heterologous boosting with the Ad26.COV2.S vaccine

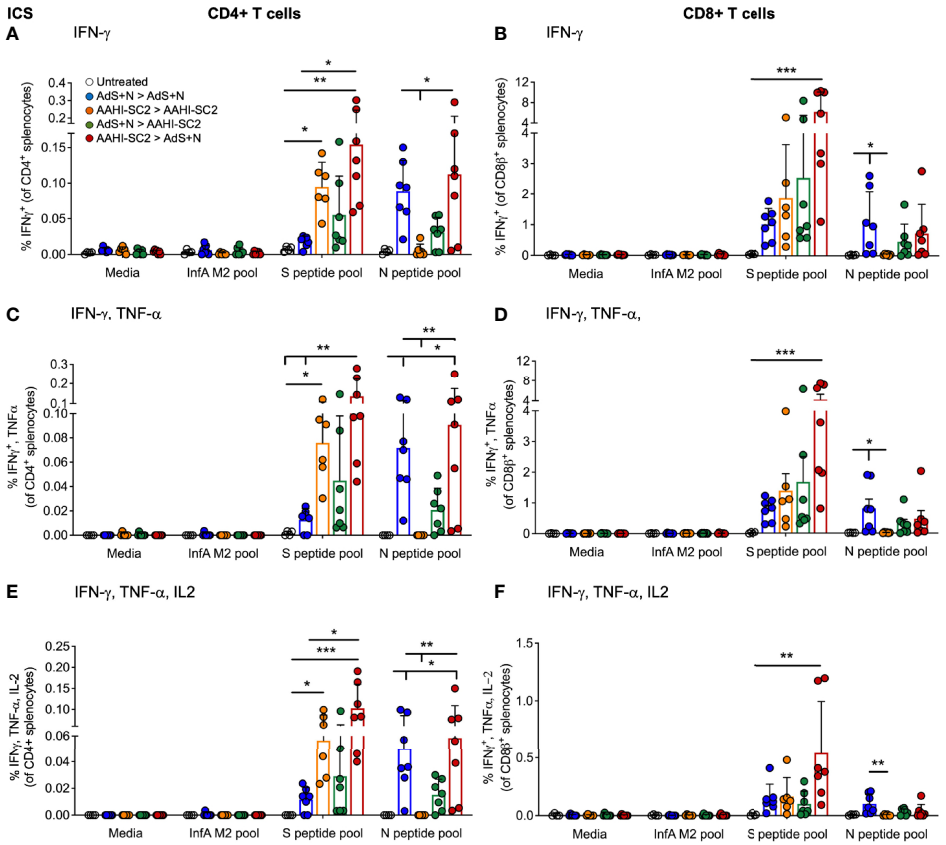

FIGURE 5 | *CD4+ and CD8+ T cell intracellular cytokine staining (ICS) in response to S(wt) and N peptides*. **(A, B)** ICS for interferon-γ (IFN-γ), **(C, D)** IFN-γ and tumor necrosis factor-α (TNF-α), and **(E, F)** IFN-γ, TNF-α and interleukin-2 (IL-2) are shown for CD4+ and CD8+ T cells, respectively. Statistical analyses performed using a non-parametric Kruskal-Wallis test and Dunn's *post-hoc* comparison of all groups to all other groups where *p ≤.05, **p <.01, and ***p <.001. In instances of similar significance, the tick marks indicate groups compared to the group without a tick mark; p values are listed in Table 1. Data graphed as the mean and SD. The legend in A applies to all figure panels.

substantially increased spike-specific CD8+ T cells in the mRNA vaccine-primed recipients.

The enhanced T-cell activity in the AAHI-SC2 > AdS+N group mice was observed in both ICS and ELISpot and for CD8+ T-cells, was seen in response to both wild type and Delta S peptides. Responses of CD4+ T cells to S(wt) and S(Delta) were similar for AAHI-SC2 homologous and AAHI-SC2 > AdS+N heterologous group mice. We hypothesize that because the AAHI-SC2 vaccine elicits the greatest humoral response to S when given in any order – possibly reaching the upper detection limit for our ELISA - it enhances CD4+ T-cell activation as such activation is closely related to humoral/B cell responses. Therefore, CD4+ T-cell activation might be expected to be higher after a boost if there are stronger pre-existing, prime-induced B cell responses, that is, when AAHI-SC2 is the prime. Adenovirus vectors such as that used for the AdS+N vaccine are good at eliciting CD8+ T-cell responses (40), an effect that likely also benefits from more robust pre-existing CD4+ T-cell and B cell responses, a condition that exists most prominently when the AAHI-SC2 vaccine is given as the prime.

Effectively, enhanced CD4+-specific T-helper responses seen with AAHI-SC2 prime dosing might have provided conditions for the enhanced CD8+ specific response upon AdS+N boost. Confirmation of this hypothesis awaits further investigation.

Importantly, all of the vaccination regimens that included the AAHI-SC2 vaccine neutralized SARS-CoV-2 variant pseudoviruses – Wuhan, Beta, Delta, and – for AAHI-SC2 homologous vaccination - the highly transmissible Omicron (BA.1) variant. The heterologous vaccine regimens resulted in lower capability of neutralizing Omicron BA.1 variant, reported to be more resistant to neutralization than the BA.2 variant (41) now displacing BA.1. This neutralization capability reflects the strength of humoral responses to the AAHI-SC2 vaccine and is consistent with reported findings for this vaccine (13). The validity of such pseudovirus-based assay results and their correlation to live virus assays has been reported elsewhere (42, 43). We observed that the geometric mean IC50s for reciprocal dilutions of sera from mice receiving the heterologous AAHI-SC2 > AdS+N regimen were consistently higher than those for AdS+N > AAHI-SC2, and speculate that the AAHI-SC2 as a

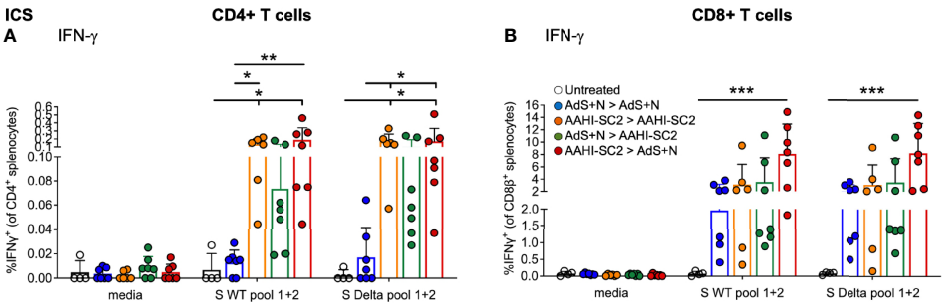

FIGURE 6 | *CD4+ and CD8+ T-cell responses to S(wt) and S(Delta) peptides are similar*. Both CD4+ **(A)** and CD8+ **(B)** T cells show similar levels of interferon-γ (IFN-γ) production in ICS in response to either S(wt) or S(Delta) sequence peptides. For both T-cell types, the greatest responses were seen with AAHI-SC2 > AdS+N vaccination. Statistical analyses performed using a non-parametric Kruskal-Wallis test with Dunn's comparison of groups where *p ≤.05, **p <.01, and ***p <.001. In instances of similar significance, the tick marks indicate groups compared to the group without a tick mark; p values are listed in Table 1. Data graphed as the mean and SD. The legend in B applies to both figure panels.

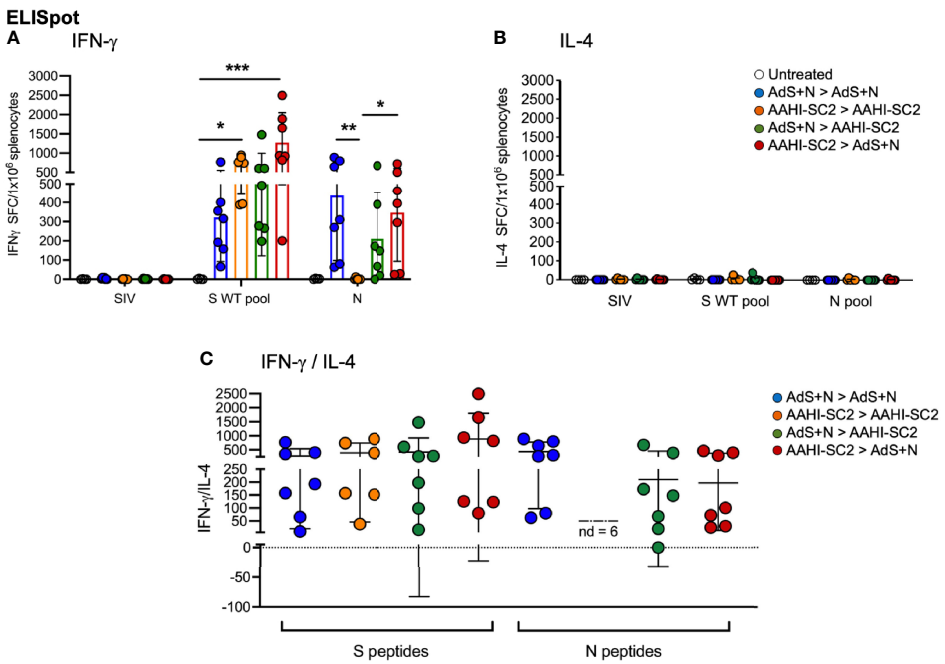

FIGURE 7 | *Heterologous vaccination increases T-cell cytokine secretion in ELISpot*. **(A)** Numbers of interferon-γ (IFN-γ) and **(B)** interleukin-4 (IL-4) secreting T cells in response to S WT and N peptides pools. The legend in B applies to panels A and B. **(C)** The IFN-γ/IL-4 ratio; value of 1 indicated by dashed line. The ratio was not determined (ND) for animals with very low IL-4 secretion. Statistical analyses performed using a non-parametric Kruskal Wallis test and Dunn's *post-hoc* comparison of all groups to all other groups where *p ≤.05, **p <.01 and ***p<.001. Data graphed as the mean and SD.

prime triggers greater B cell priming and development (as compared to AdS+N as the prime) which then results in enhanced recall when the AdS+N boost is delivered.

The lower capability of sera from AdS+N homologously vaccinated mice to neutralize the S-expressing pseudovirus does not necessarily indicate that the predominantly T-cell inducing AdS+N vaccine would not be effective in protecting against SARS-CoV-2 challenge. The pseudovirus assay does not reveal the protection conferred by T-cells and non-neutralizing antibodies against natural infection, which may be enhanced by addition of the N antigen. In fact, we have previously reported that homologous AdS+N prime-boost vaccination of non-human primates confers protection against viral challenge (7). In the *in vivo* viral challenge testing paradigm, cell-mediated immunity - not accessed in the pseudovirus assay that tests sera - conferred by AdS+N vaccination likely plays a key role in

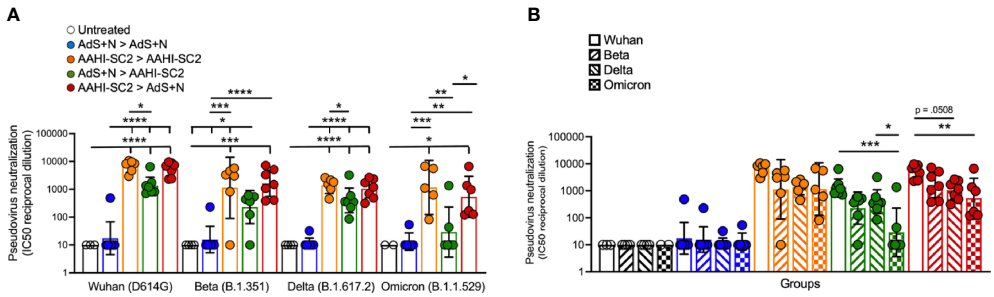

FIGURE 8 | *Sera from AAHI-SC2 > AdS+N heterologously vaccinated mice neutralize Wuhan, Delta, Beta, and Omicron SARS-CoV-2 pseudoviruses*. **(A)** IC50 reciprocal dilution for pseudovirus neutralization grouped by pseudovirus variant assay is shown. Statistical differences are shown for comparison of each vaccinated group for a specific variant (not between variants). **(B)** IC50 reciprocal dilution for neutralization of all strains/variants tested compared for each group is shown. The color code legend in **(A)** applies also to **(B)**. Statistical comparison of IC50 values for untreated and AdS+N homologous group mice with values < the LOD was not performed. Statistical analyses were performed on log-normalized data using one-way ANOVA and Tukey's *post-hoc* comparison where *p ≤.05, **p <.01, ***p <.001, and ****p <.0001. In instances of similar significance, the tick marks indicate groups compared to the group without a tick mark; p values are listed in Table 1. Data graphed as the geometric mean and the geometric SD.

protection, as has been reported for natural infection of patients (44–47). Others have reported that combination of S and N increased provided enhanced protection against infection by variants with highly mutated spike in a hamster model (48), and thus, in future studies, we plan to assess protection against infection by SARS-CoV-2 variants *in vivo* by the dual-antigen vaccine as compared to S or N alone.

There were limitations to the study performed, including there being a single time interval between prime and boost tested (21 days) and a single time point for sample collection (35 days). Our goal was to elicit vigorous T-cell responses while also detecting humoral responses, but the relatively short prime-boost interval as well as time to tissue collection may have favored saRNA-induced over adenovirus (AdS+N) generated humoral responses. In addition, a limitation may be that the S antigen in both vaccines is not the Omicron sequence, given that Omicron is currently the predominant variant in many regions. But recent reports suggest Omicron infection does not produce sera that is highly cross-reactive for other Variants of Concern (VOCs) and that a vaccine delivering an Omicron-based spike immunogen is unlikely to be superior to existing vaccines for prime vaccination (49).

The findings here support ongoing study of heterologous vaccination with the AAHI-SC2 and AdS+N vaccines. In our continued efforts, we are designing vaccines with Omicron S sequences and an saRNA vaccine that delivers both an S and N antigen. Further testing in pre-clinical models of SARS-CoV-2 challenge and clinical trials should be conducted to assess the capability of this vaccine regimen to provide increased protection against COVID-19 and SARS-CoV-2 variants by combining the ability of AAHI-SC2 to elicit vigorous humoral responses with AdS+N's second, highly antigenic N antigen and T-cell response enhancement. In addition to the opportunity for a high level of efficacy, the availability of both the AAHI-SC2 and AdS+N vaccines in thermostable formulations addresses a critical issue in vaccine technology - freedom from cold-chain limitations on distribution - and provides further justification for their continued development.

DATA AVAILABILITY STATEMENT

The datasets presented in this study are within the manuscript, online at doi: 10.1101/2021.11.29.470440, and available by request.

ETHICS STATEMENT

The animal study was reviewed and approved by the Institutional Animal Care and Use Committee (IACUC) at Omeros, Inc. (Seattle, WA, USA).

AUTHOR CONTRIBUTIONS

AR and MV contributed to the study design, co-wrote the manuscript and, with KD and SM, performed the *in vivo* studies and co-analyzed data. EV is co-inventor of the RNA technology used for the AAHI-SC2 saRNA vaccine, contributed to design of the study, co-analyzed data and data interpretation, and edited the manuscript. SB performed the pseudovirus neutralization assay, with the assistance of PB and SR, and edited the manuscript. LZ, CO, ST, and BM contributed to the design, production, and testing of the AdS+N vaccine. EG co-designed the AdS+N vaccine vector. JS contributed to the study design and provided expert immunological/biological insight for interpretation of data. PS analyzed data, generated figures and tables, and wrote the manuscript. CC contributed to the study design and data analysis, and edited the manuscript. PS-S co-designed and developed the AdS+N vaccine, co-conceptualized the study, reviewed all data, and edited the manuscript. All authors contributed to the article and approved the submitted version.

FUNDING

The original development of the AAHI-SC2 vaccine was funded by the Infectious Disease Research Institute (IDRI).

ACKNOWLEDGMENTS

We would like to thank Jesse Bloom (Fred Hutchinson Cancer Research Center) and Thomas Peacock (Imperial College London) for sharing the SARS-CoV-2 spike protein plasmids used for pseudovirus production.

SUPPLEMENTARY MATERIAL

The Supplementary Material for this article can be found online at: https://www.frontiersin.org/articles/10.3389/fimmu.2022.910136/full#supplementary-material

REFERENCES

1. Polack FP, Thomas SJ, Kitchin N, Absalon J, Gurtman A, Lockhart S, et al. Safety and Efficacy of the BNT162b2 mRNA Covid-19 Vaccine. *N Engl J Med* (2020) 383(27):2603–15. doi: 10.1056/NEJMoa2034577
2. Ewer KJ, Barrett JR, Belij-Rammerstorfer S, Sharpe H, Makinson R, Morter R, et al. T Cell and Antibody Responses Induced by a Single Dose of ChAdOx1 Ncov-19 (AZD1222) Vaccine in a Phase 1/2 Clinical Trial. *Nat Med* (2021) 27 (2):270–8. doi: 10.1038/s41591-020-01194-5
3. Shinde V, Bhikha S, Hoosain Z, Archary M, Bhorat Q, Fairlie L, et al. Efficacy of NVX-CoV2373 Covid-19 Vaccine Against the B.1.351 Variant. *N Engl J Med* (2021) 384(20):1899–909. doi: 10.1056/NEJMoa2103055
4. Sadoff J, Gray G, Vandebosch A, Cárdenas V, Shukarev G, Grinsztejn B, et al. Safety and Efficacy of Single-Dose Ad26.Cov2.S Vaccine Against Covid-19. *N Engl J Med* (2021) 384:2187–201. doi: 10.1056/NEJMoa2101544
5. Voysey M, Clemens SAC, Madhi SA, Weckx LY, Folegatti PM, Aley PK, et al. Safety and Efficacy of the ChAdOx1 Ncov-19 Vaccine (AZD1222) Against SARS-CoV-2: An Interim Analysis of Four Randomised Controlled Trials in Brazil, South Africa, and the UK. *Lancet* (2021) 397(10269):99–111. doi: 10.1016/S0140-6736(20)32661-1
6. Araf Y, Akter F, Tang YD, Fatemi R, Parvez MSA, Zheng C, et al. Omicron Variant of SARS-CoV-2: Genomics, Transmissibility, and Responses to Current COVID-19 Vaccines. *J Med Virol* (2022) 94:1825–32. doi: 10.1002/jmv.27588
7. Gabitzsch E, Safrit JT, Verma M, Rice A, Sieling P, Zakin L, et al. Dual-Antigen COVID-19 Vaccine Subcutaneous Prime Delivery With Oral Boosts Protects NHP Against SARS-CoV-2 Challenge. *Front Immunol* (2021) 12:729837. doi: 10.3389/fimmu.2021.729837
8. Rice A, Verma M, Shin A, Zakin L, Sieling P, Tanaka S, et al. Intranasal Plus Subcutaneous Prime Vaccination With a Dual Antigen COVID-19 Vaccine Elicits T-Cell and Antibody Responses in Mice. *Sci Rep* (2021) 11(1):14917. doi: 10.1038/s41598-021-94364-5
9. Sieling P, King T, Wong R, Nguyen A, Wnuk K, Gabitzsch ER, et al. Prime Had5 Spike Plus Nucleocapsid Vaccination Induces Ten-Fold Increases in Mean T-Cell Responses in Phase 1 Subjects That are Sustained Against Spike Variants. *medRxiv* (2021). doi: 10.1101/2021.04.05.21254940
10. Niazi KR, Ochoa M-T, Sieling PA, Rooke NE, Peter AK, Mollahan P, et al. Activation of Human CD4+ T Cells by Targeting MHC Class II Epitopes to Endosomal Compartments Using Human CD1 Tail Sequences. *Immunology* (2007) 122(4):522–31. doi: 10.1111/j.1365-2567.2007.02666.x
11. Lin KY, Guarnieri FG, Staveley-O'Carroll KF, Levitsky HI, August JT, Pardoll DM, et al. Treatment of Established Tumors With a Novel Vaccine That Enhances Major Histocompatibility Class II Presentation of Tumor Antigen. *Cancer Res* (1996) 56(1):21–6. Available at: https://aacrjournals.org/cancerres/article/56/1/21/502219/Treatment-of-Established-Tumors-with-a-Novel
12. Wu TC, Guarnieri FG, Staveley-O'Carroll KF, Viscidi RP, Levitsky HI, Hedrick L, et al. Engineering an Intracellular Pathway for Major Histocompatibility Complex Class II Presentation of Antigens. *Proc Natl Acad Sci USA* (1995) 92(25):11671–5. doi: 10.1073/pnas.92.25.11671
13. Voigt EA, Gerhardt A, Hanson D, Battisti P, Reed S, Singh J, et al. A Self-Amplifying RNA Vaccine Against COVID-19 With Long-Term Room-Temperature Stability. *bioRxiv* (2022). doi: 10.1101/2022.03.22.485230
14. Spencer AJ, McKay PF, Belij-Rammerstorfer S, Ulaszewska M, Bissett CD, Hu K, et al. Heterologous Vaccination Regimens With Self-Amplifying RNA and Adenoviral COVID Vaccines Induce Robust Immune Responses in Mice. *Nat Commun* (2021) 12(1):2893. doi: 10.1038/s41467-021-23173-1
15. Wu L, Kong WP, Nabel GJ. Enhanced Breadth of CD4 T-Cell Immunity by DNA Prime and Adenovirus Boost Immunization to Human Immunodeficiency Virus Env and Gag Immunogens. *J Virol* (2005) 79 (13):8024–31. doi: 10.1128/JVI.79.13.8024-8031.2005
16. Kardani K, Bolhassani A, Shahbazi S. Prime-Boost Vaccine Strategy Against Viral Infections: Mechanisms and Benefits. *Vaccine* (2016) 34(4):413–23. doi: 10.1016/j.vaccine.2015.11.062
17. Nordström P, Ballin M, Nordström A. Effectiveness of Heterologous ChAdOx1 Ncov-19 and mRNA Prime-Boost Vaccination Against Symptomatic Covid-19 Infection in Sweden: A Nationwide Cohort Study. *Lancet Reg Health Eur* (2021) 11:100249. doi: 10.1016/j.lanepe.2021.100249
18. Liu X, Shaw RH, Stuart ASV, Greenland M, Aley PK, Andrews NJ, et al. Safety and Immunogenicity of Heterologous Versus Homologous Prime-Boost Schedules With an Adenoviral Vectored and mRNA COVID-19 Vaccine (Com-COV): A Single-Blind, Randomised, non-Inferiority Trial. *Lancet* (2021) 398(10303):856–69. doi: 10.1016/S0140-6736(21)01694-9
19. Chiu NC, Chi H, Tu YK, Huang YN, Tai YL, Weng SL, et al. To Mix or Not to Mix? A Rapid Systematic Review of Heterologous Prime-Boost Covid-19 Vaccination. *Expert Rev Vaccines* (2021) 20(10):1211–20. doi: 10.1080/14760584.2021.1971522
20. Atmar RL, Lyke KE, Deming ME, Jackson LA, Branche AR, El Sahly HM, et al. Homologous and Heterologous Covid-19 Booster Vaccinations. *N Engl J Med* (2022) 386(11):1046–57. doi: 10.1056/NEJMoa2116414
21. Gerhardt A, Voigt E, Archer M, Reed S, Larson E, Van Hoeven N, et al. A Flexible, Thermostable Nanostructured Lipid Carrier Platform for RNA Vaccine Delivery. *Mol Ther Methods Clin Dev* (2022) 25:205–14. doi: 10.1016/j.omtm.2022.03.009
22. Erasmus JH, Khandhar AP, Guderian J, Granger B, Archer J, Archer M, et al. A Nanostructured Lipid Carrier for Delivery of a Replicating Viral RNA Provides Single, Low-Dose Protection Against Zika. *Mol Ther* (2018) 26 (10):2507–22. doi: 10.1016/j.ymthe.2018.07.010
23. Bloom K, van den Berg F, Arbuthnot P. Self-Amplifying RNA Vaccines for Infectious Diseases. *Gene Ther* (2021) 28(3-4):117–29. doi: 10.1038/s41434-020-00204-y
24. Sandbrink JB, Shattock RJ. RNA Vaccines: A Suitable Platform for Tackling Emerging Pandemics? *Front Immunol* (2020) 11:608460. doi: 10.3389/fimmu.2020.608460
25. Zhang C, Maruggi G, Shan H, Li J. Advances in mRNA Vaccines for Infectious Diseases. *Front Immunol* (2019) 10:594. doi: 10.3389/fimmu.2019.00594
26. Zhang L, Jackson CB, Mou H, Ojha A, Peng H, Quinlan BD, et al. SARS-CoV-2 Spike-Protein D614G Mutation Increases Virion Spike Density and Infectivity. *Nat Commun* (2020) 11(1):6013. doi: 10.1038/s41467-020-19808-4
27. Weissman D, Alameh M-G, de Silva T, Collini P, Hornsby H, Brown R, et al. D614G Spike Mutation Increases SARS CoV-2 Susceptibility to Neutralization. *Cell Host Microbe* (2021) 29(1):23–31.e24. doi: 10.1016/j.chom.2020.11.012
28. Kirchdoerfer RN, Wang N, Pallesen J, Wrapp D, Turner HL, Cottrell CA, et al. Stabilized Coronavirus Spikes are Resistant to Conformational Changes Induced by Receptor Recognition or Proteolysis. *Sci Rep* (2018) 8:15701–1. doi: 10.1038/s41598-018-34171-7
29. Bangaru S, Ozorowski G, Turner HL, Antanasijevic A, Huang D, Wang X, et al. Structural Analysis of Full-Length SARS-CoV-2 Spike Protein From an Advanced Vaccine Candidate. *Science* (2020) 370(6520):1089–94. doi: 10.1126/science.abe1502

30. van Doremalen N, Lambe T, Spencer A, Belij-Rammerstorfer S, Purushotham JN, Port JR, et al. ChAdOx1 Ncov-19 Vaccine Prevents SARS-CoV-2 Pneumonia in Rhesus Macaques. *Nature* (2020) 586(7830):578–82. doi: 10.1038/s41586-020-2608-y
31. Zhu F-C, Li Y-H, Guan X-H, Hou L-H, Wang W-J, Li J-X, et al. Safety, Tolerability, and Immunogenicity of a Recombinant Adenovirus Type-5 Vectored COVID-19 Vaccine: A Dose-Escalation, Open-Label, non-Randomised, First-in-Human Trial. (2020) *Lancet* (2020) 395(10240):1845–54. doi: 10.1016/S0140-6736(20)31208-3
32. Amalfitano A, Begy CR, Chamberlain JS. Improved Adenovirus Packaging Cell Lines to Support the Growth of Replication-Defective Gene-Delivery Vectors. *Proc Natl Acad Sci USA* (1996) 93(8):3352–6. doi: 10.1073/pnas.93.8.3352
33. Amalfitano A, Chamberlain JS. Isolation and Characterization of Packaging Cell Lines That Coexpress the Adenovirus E1, DNA Polymerase, and Preterminal Proteins: Implications for Gene Therapy. *Gene Ther* (1997) 4 (3):258–63. doi: 10.1038/sj.gt.3300378
34. Amalfitano A, Hauser MA, Hu H, Serra D, Begy CR, Chamberlain JS. Production and Characterization of Improved Adenovirus Vectors With the E1, E2b, and E3 Genes Deleted. *J Virol* (1998) 72(2):926. doi: 10.1128/JVI.72.2.926-933.1998
35. Seregin SS, Amalfitano A. Overcoming Pre-Existing Adenovirus Immunity by Genetic Engineering of Adenovirus-Based Vectors. *Expert Opin Biol Ther* (2009) 9(12):1521–31. doi: 10.1517/14712590903307388
36. Erasmus JH, Archer J, Fuerte-Stone J, Khandhar AP, Voigt E, Granger B, et al. Intramuscular Delivery of Replicon RNA Encoding ZIKV-117 Human Monoclonal Antibody Protects Against Zika Virus Infection. *Mol Ther Methods Clin Dev* (2020) 18:402–14. doi: 10.1016/j.omtm.2020.06.011
37. Voigt EA, Fuerte-Stone J, Granger B, Archer J, Van Hoeven N. Live-Attenuated RNA Hybrid Vaccine Technology Provides Single-Dose Protection Against Chikungunya Virus. *Mol Ther* (2021) 29(9):2782–93. doi: 10.1016/j.ymthe.2021.05.018
38. Skordos I, Demeyer A, Beyaert R. Analysis of T Cells in Mouse Lymphoid Tissue and Blood With Flow Cytometry. *STAR Protoc* (2021) 2(1):100351–1. doi: 10.1016/j.xpro.2021.100351
39. Crawford KHD, Eguia R, Dingens AS, Loes AN, Malone KD, Wolf CR, et al. Protocol and Reagents for Pseudotyping Lentiviral Particles With SARS-CoV-2 Spike Protein for Neutralization Assays. *Viruses* (2020) 12:513. doi: 10.3390/v12050513
40. Cupovic J, Ring SS, Onder L, Colston JM, Lütge M, Cheng HW, et al. Adenovirus Vector Vaccination Reprograms Pulmonary Fibroblastic Niches to Support Protective Inflating Memory CD8(+) T Cells. *Nat Immunol* (2021) 22(8):1042–51. doi: 10.1038/s41590-021-00969-3
41. Bruel T, Hadjadj J, Maes P, Planas D, Seve A, Staropoli I, et al. Serum Neutralization of SARS-CoV-2 Omicron Sublineages BA.1 and BA.2 in Patients Receiving Monoclonal Antibodies. *Nat Med* (2022) 28(6):1297–302. doi: 10.1038/s41591-022-01792-5
42. Hyseni I, Molesti E, Benincasa L, Piu P, Casa E, Temperton NJ, et al. Characterisation of SARS-CoV-2 Lentiviral Pseudotypes and Correlation Between Pseudotype-Based Neutralisation Assays and Live Virus-Based Micro Neutralisation Assays. *Viruses* (2020) 12(9):1011–29. doi: 10.3390/v12091011
43. Tolah AMK, Sohrab SS, Tolah KMK, Hassan AM, El-Kafrawy SA, Azhar EI. Evaluation of a Pseudovirus Neutralization Assay for SARS-CoV-2 and Correlation With Live Virus-Based Micro Neutralization Assay. *Diagn (Basel)* (2021) 11(6):994–1003. doi: 10.3390/diagnostics11060994
44. Grifoni A, Sidney J, Vita R, Peters B, Crotty S, Weiskopf D, et al. SARS-CoV-2 Human T Cell Epitopes: Adaptive Immune Response Against COVID-19. *Cell Host Microbe* (2021) 29(7):1076–92. doi: 10.1016/j.chom.2021.05.010
45. Tarke A, Sidney J, Kidd CK, Dan JM, Ramirez SI, Yu ED, et al. Comprehensive Analysis of T Cell Immunodominance and Immunoprevalence of SARS-CoV-2 Epitopes in COVID-19 Cases. *Cell Rep Med* (2021) 2(2):100204. doi: 10.1016/j.xcrm.2021.100204
46. Sekine T, Perez-Potti A, Rivera-Ballesteros O, Strålin K, Gorin J-B, Olsson A, et al. Robust T Cell Immunity in Convalescent Individuals With Asymptomatic or Mild COVID-19. *Cell* (2020) 183(1):158–68. doi: 10.1016/j.cell.2020.08.017
47. Tan AT, Linster M, Tan CW, Le Bert N, Chia WN, Kunasegaran K, et al. Early Induction of Functional SARS-CoV-2-Specific T Cells Associates With Rapid Viral Clearance and Mild Disease in COVID-19 Patients. *Cell Rep* (2021) 34 (6):108728. doi: 10.1016/j.celrep.2021.108728
48. McCafferty S, Haque A, Vandierendonck A, Weidensee B, Plovyt M, Stuchlíková M, et al. A Dual-Antigen Self-Amplifying RNA SARS-CoV-2 Vaccine Induces Potent Humoral and Cellular Immune Responses and Protects Against SARS-CoV-2 Variants Through T Cell-Mediated Immunity. *Mol Ther* (2022) S1525-0016(22):00243–X. doi: 10.1016/j.ymthe.2022.1004.1014
49. Richardson SI, Madzorera VS, Spencer H, Manamela NP, van der Mescht MA, Lambson BE, et al. SARS-CoV-2 Omicron Triggers Cross-Reactive Neutralization and Fc Effector Functions in Previously Vaccinated, But Not Unvaccinated, Individuals. *Cell Host Microbe* (2022) S1931-3128(22):00159–7. doi: 10.1016/j.chom.2022.1003.1029

Author Disclaimer: All authors with an ImmunityBio, Inc., affiliation contribution to the design, production or testing of the AdS+N vaccine that may become a commercial product. Emily Voigt is an inventor on a patent related to the RNA vaccine technology.

Conflict of Interest: Author EV is one of the inventors of the AAHI-SC2 vaccine and all authors with an ImmunityBio, Inc. affiliation are employees of and/or hold shares of ImmunityBio, Inc. stock, which is developing the AdS+N vaccine as a potential product.

The remaining authors declare that the research was conducted in the absence of any commercial or financial relationships that could be constructed as a potential conflict of interest.

This study received funding from ImmunityBio, Inc. The funder had the following involvement with the study: design and manufacturing of the AdS+N vaccine, design and performance of the in vivo study, including tissue collection and analysis; and the writing of the manuscript and decision to publish.

Publisher's Note: All claims expressed in this article are solely those of the authors and do not necessarily represent those of their affiliated organizations, or those of the publisher, the editors and the reviewers. Any product that may be evaluated in this article, or claim that may be made by its manufacturer, is not guaranteed or endorsed by the publisher.

frontiers | Frontiers in Immunology

TYPE Review
PUBLISHED 23 September 2022
DOI 10.3389/fimmu.2022.1002742

OPEN ACCESS

EDITED BY
Hamid Reza Mirzaei,
Tehran University of Medical Sciences, Iran

REVIEWED BY
Maryam Azimi,
Iran University of Medical Sciences, Iran
Annalisa Santucci,
University of Siena, Italy

*CORRESPONDENCE
Shenglong Li,
lishenglong@cancerhosp-ln-cmu.com;
slli@cmu.edu.cn

†These authors have contributed equally to this work

SPECIALTY SECTION
This article was submitted to Cancer Immunity and Immunotherapy, a section of the journal Frontiers in Immunology

RECEIVED 25 July 2022
ACCEPTED 12 September 2022
PUBLISHED 23 September 2022

CITATION
Gao X, Gao B and Li S (2022) Extracellular vesicles: A new diagnostic biomarker and targeted drug in osteosarcoma.
Front. Immunol. 13:1002742.
doi: 10.3389/fimmu.2022.1002742

Extracellular vesicles: A new diagnostic biomarker and targeted drug in osteosarcoma

Xiaozhuo Gao[1†], Bo Gao[1†] and Shenglong Li[2*]

[1]Department of Pathology, Liaoning Cancer Hospital & Institute, Cancer Hospital of Dalian University of Technology, Cancer Hospital of China Medical University, Shenyang, China, [2]Department of Bone and Soft Tissue Tumor Surgery, Liaoning Cancer Hospital & Institute, Cancer Hospital of Dalian University of Technology, Cancer Hospital of China Medical University, Shenyang, China

Osteosarcoma (OS) is a primary bone cancer that is highly prevalent among adolescents and adults below the age of 20 years. The prognostic outcome of metastatic OS or relapse is extremely poor; thus, developing new diagnostic and therapeutic strategies for treating OS is necessary. Extracellular vesicles (EVs) ranging from 30–150 nm in diameter are commonly produced in different cells and are found in various types of body fluids. EVs are rich in biologically active components like proteins, lipids, and nucleic acids. They also strongly affect pathophysiological processes by modulating the intercellular signaling pathways and the exchange of biomolecules. Many studies have found that EVs influence the occurrence, development, and metastasis of osteosarcoma. The regulation of inflammatory communication pathways by EVs affects OS and other bone-related pathological conditions, such as osteoarthritis and rheumatoid arthritis. In this study, we reviewed the latest findings related to diagnosis, prognosis prediction, and the development of treatment strategies for OS from the perspective of EVs.

KEYWORDS

EVs, osteosarcoma, biomarkers, treatment, diagnosis

Abbreviations: OS, Osteosarcoma; ALP, alkaline phosphatase; LDH, lactate dehydrogenase; lncRNAs, long non-coding RNAs; miRNAs, microRNAs; mRNAs, messenger RNAs; circRNAs, circular RNAs; ASMCs, airway smooth muscle cells; NSCLC, non-small-cell lung cancer; LUAD lung adenocarcinoma; EVs, extracellular vesicles, ILVs, luminal vesicles; MVBs, multivesicular bodies; Aiix, ALG-2 interacting protein X; ESCRT, endosomal sorting complex required for transport; HGG, high-grade gliomas; PSA, prostate-specific antigen; EMT, epithelial-mesenchymal transition; MSCs, mesenchymal stem cell; CAFs, cancer-associated fibroblasts; BMSCs, bone marrow-derived mesenchymal stem cells; OS, overall survival; DFS, disease-free survival; NGS, next-generation sequencing; CDDP, cisplatin-resistant.

Introduction

Osteosarcoma (OS) predominantly occurs among individuals below 20 years and is a form of aggressive primary bone cancer (1, 2). The etiology of OS is mainly characterized by epidemiological, genetic, and environmental factors (3). Several risk factors are associated with tumorigenesis of OS, such as alkylating agents, hereditary retinoblastoma, Paget's disease, ionizing radiation, and chromosomal abnormalities (4, 5). The diagnosis of OS relies mainly on clinical manifestations, medical imaging, tissue biopsy, and laboratory tests. The standard treatment regimens for OS include neoadjuvant chemotherapy, surgical resection, chemotherapy, and interventional therapy (6, 7). Recent developments related to the treatment of OS include extensive research on stem cell therapy, immunotherapy, and gene therapy (8–10). However, due to the complexity of therapeutic interventions and the genetic differences between laboratory animals and humans, these strategies are limited to preclinical studies. Additionally, patients with OS have a high incidence of early lung metastasis, except for other bone tissue metastasis. About 18% of OS patients show signs of micrometastasis at the time of diagnosis, and the five-year survival rate of patients with stage III OS or higher stages of OS is very low (11–13). Moreover, the treatment outcomes are suboptimal because of the difficulty in early diagnosis, the early onset of metastasis, and high malignancy (14, 15). The five-year survival of OS patients who do not receive chemotherapy is below 30%. Pulmonary metastasis is the main cause of OS-related mortality. Moreover, the chemotherapeutic intervention can partially control pulmonary metastasis of OS and increase the five-year survival to 50%. For OS cases with pulmonary metastasis, the two-year survival is less than 25%. Additionally, although there are several alternatives, the survival period during treatment might stabilize without any improvement. Therefore, implementing traditional treatment strategies might not yield the best results (16, 17). Hence, determining the mechanism of the occurrence and metastasis of OS might help to find new clinical diagnostic markers and efficient therapeutic targets.

Extracellular vesicles (EVs) are specialized membranous vesicles originating from endonuclear bodies with particles ranging from 30 to 100 nm in diameter (18, 19). EVs were first identified as a component of blood erythrocytes. They appeared as a lipid bilayer structure surrounded by cytoplasm and devoid of any organelles (20). These EVs were discovered approximately 40 years ago (20). The understanding of the role of EVs in human pathophysiological processes has improved significantly.

Several studies have shown that EVs are produced by various cancer and healthy cells (21–23). When EVs were discovered, their primary function was thought to be the excretion of metabolic wastes from cells (24). However, various studies highlighted the ability of EVs to perform cellular communication, which is essential during various biological processes and disease progression. This communication is possible due to the presence of various nucleic acids and proteins that are responsible for distinguishing the transmission of important biological information between cells (25–28). Thus, EVs can be used as nano-cargos for delivering nucleic acids (such as messenger RNA) (29) and therapeutic agents (such as paclitaxel) (30). Cells within the tumor microenvironment (TME) of OS can secrete EVs, which can deliver non-coding RNAs (ncRNAs) and proteins within the tumor matrix essential for cellular communication. Thus, EVs can effectively regulate the TME within OS and accelerate cell proliferation and metastasis. Additionally, EVs show high systemic stability and are not susceptible to cellular enzymes. They also have good therapeutic and diagnostic potential. In this article, we reviewed the different types of EVs and their biological properties, along with their potential in the diagnosis and treatment of OS.

The sources of EVs involved in osteosarcoma

Extracellular vesicles secreted by drug-resistant cells facilitate and transfer drug resistance to different types of tumors, including breast, prostate, colon, lung, and gastric cancer, as well as, osteosarcoma (31). Doxorubicin and cisplatin resistance are transferred from OS resistant cells to sensitive cells through EVs that carry P-glycoprotein, MDR-1 mRNA, or the circular RNA hsa_circ_103801 [178.179]. Bone marrow-derived mesenchymal stem cell-derived extracellular vesicles (BMSC-EVs) can promote the proliferation, invasion, and migration of osteosarcoma cells *via* the MALAT1/miR-143/NRSN2/Wnt/β-catenin axis (32). Additionally, EVs secreted by the osteosarcoma 143B cell line contain a pro-osteoclastogenic cargo, which includes MMPs (MMP-1 and MMP-13), RANK-L (Receptor Activator of Nuclear Factor κ B Ligand), CD-9, and TGF-β. These findings highlighted that EVs from different sources exhibit different biological activities.

The characteristics of EVs

Extracellular vesicles released from most cells contain various proteins, RNA, genomic DNA (gDNA), non-coding RNAs (ncRNAs), lipids, and metabolites (33, 34). EVs can be categorized into three types based on their size and release mechanisms and include EVs, microvesicles, and apoptotic vesicles, with vesicle sizes ranging from 30 to 150 nm, 100 to 1,000 nm, and 50 to 1,500 nm, respectively (35, 36). EVs are cultured from OS cells obtained *in vivo* and purified by differential centrifugation. The separated and purified EVs are assessed according to their purity and morphology, followed by protein profiling and sequencing of the components. The assessment of the morphology of EVs by electron microscopy remains a gold

standard. Additionally, flow cytometry (FCM) might also be performed for assessing EVs. For particle size analysis of EVs, Nanoparticle Tracking Analysis Technology (NTA) is frequently used. The production of EVs involves the initiation of endocytosis, the formation of multivesicular bodies (MVBs), and the production of exosomes (37, 38). EVs start to develop with the initial formation of plasma membrane invaginations into a cup-like structure containing cell surface proteins, soluble proteins, and endoplasmic reticulum (ER). This cup-shaped structure, together with trans Golgi, promotes the formation of early endonucleosomes (39). Early intranucleosomes mature into late intranucleosomes, resulting in the formation of MVBs. These MVBs may fuse with the plasma membrane to release the intraluminal vesicles (ILVs) associated with EVs or may fuse with autophagosomes or lysosomes for degradation (40, 41). EVs are found in different types of body fluids, such as urine, plasma, breast milk, and ascites (42, 43), which makes EVs a significant tool with great diagnostic potential.

The process of the formation of EVs

Extracellular vesicles are usually formed by endosomal endocytosis, in contrast to other conventional membrane outgrowth processes, which deform membranes from organelles into the cytoplasm. The endosomal limiting membrane undergoes multiple depressions with inward growth resulting in the formation ILVs. These ILVs are then converted into MVBs, which have a dynamic subcellular architecture. Interestingly, MVB formation can occur at the endosomal limiting membrane by the endosomal sorting complex required for the transport (ESCRT) mechanism (44, 45). The ESCRT machinery functions through a set of cytoplasmic protein complexes by recognizing the ubiquitinylated modified membrane proteins. The first ESCRT complex (ESCRT-0) can recognize ubiquitin markers, showing high levels of enrichment in the endosomal membrane during the transport of ubiquitinated complex into ESCRT I/II. Within ESCRT I, tumor susceptibility gene 101 protein (TSG101) can detect disulfide bonds and induce depression of the endosomal membrane. They function as shears in the bud neck under the influence of ESCRT III and lead to the formation of MVBs (46, 47). However, MVBs can still be formed in the absence of ESCRT. The process is initiated by an accessory protein ALG-2 interacting protein X (AIix). AIix directly binds to the intracellular bridging protein syntenin, which is further involved in EV formation (48, 49). Such ESCRT-independent MVBs are produced under the action of the abundant tetra-transmembrane protein CD63-α on MVBs and by ceramide-mediated cell membrane outgrowth (50, 51). These MVBs can fuse with lysosomes, degrade their contents, and recirculate them. The sorting of MVBs is significantly regulated by their cholesterol levels. For example, MVBs rich in cholesterol are targeted to cell membranes to be released as EVs, whereas, MVBs with low cholesterol levels are targeted for transport toward lysosomes (52).

Mechanism of action of EVs

Extracellular vesicles are generally responsible for inducing functional responses in receptor cells by delivering their contents, promoting phenotypic changes in receptor cells, and affecting their physiological state (25, 53). EV-mediated intercellular communication within plasma membrane relies on the activation of surface receptors on recipient cells and initiates cell signaling. The uptake of EVs by recipient cells is facilitated by cytokinesis (54, 55). The mechanisms of exosome cell membrane interaction and the transport of exosomes and endosomes are not fully understood. However, some studies have shown that these mechanisms are associated with the origin of EVs, receptor cells, and downstream processes involved in the same. Some studies have shown the activity of EVs derived from certain cells along with their application in the treatment of diseases (56, 57). The interaction between proteins significantly expressed on EVs and surface receptors of the recipient cell membrane can be used to assess the target cell specificity (58, 59). The known mediators of cell communication also include transmembrane tetraspanins, integrins, lipids, and extracellular matrix components (60, 61).

Extracellular vesicles in tumor diagnosis and treatment

Extracellular vesicles influence the exclusion of redundant and nonfunctional cellular components (62, 63). They can also act as intercellular linkers for protein, nucleic acid, and lipid transport between host and recipient cells. They strongly affect different biological processes, such as antigen presentation, angiogenesis, inflammation, and apoptosis (64–67). These processes might be related to the metastasis of biomolecules and cell crosstalk that leads to cancer-related events (47, 68, 69). The constituent nucleic acids, proteins, and lipids captured by EVs during production might reflect their cellular origin and physiological state.

These biomolecules have high disease specificity and might act as potential biomarkers. Additionally, EVs function as carriers for these biomolecules and prevent their enzymatic degradation. Various tumor-associated events involve EVs for cell proliferation, apoptosis, metastasis, and angiogenesis, and thus, may be used as a noninvasive diagnostic biomarker in various types of cancer (70–72). For example, miR-21, miR-124–3p, and miR-222 in serum EVs might be used as molecular biomarkers for assessing early cancer development during postsurgical management of high-grade gliomas (HGG) (73). Shin et al. reported the expression of miR-

21, miR-451, and miR-636 in urinary EVs in prostate cancer patients, which indicated a close resemblance with preoperative prostate-specific antigen (PSA) levels. Thus, urinary exosome-derived miRNAs might be used as noninvasive markers for predicting prostate cancer prognostic outcomes and metastasis (74). Wang et al. showed that plasma exosome-derived miR-363–5p was necessary for differentiating LN-positive breast cancer (BC) patients from LN-negative patients. Additionally, upregulation of miR-363–5p was strongly associated with overall survival (75). Exosome therapeutic research is focused on three main areas, which include biomedicine, drug delivery, and regenerative medicine. EVs are promising for treating disorders due to their nontumorigenic risk and bactericidal infiltration. Due to their small size, EVs can reach the site of injury through internal circulation and lower immunogenicity, which makes them an ideal candidate for developing treatment against various disorders (76, 77). EVs also facilitate gene delivery to recipient cells, thus alteringtheir biological activity. They are also capable of carrying therapeutic payloads such as proteins, RNAs, and chemotherapeutic agents and delivering them to the target site across different biological barriers (47, 78, 79). EVs can be engineered to target cell signaling pathways or specific recipient cells using a ligand-targeted approach (27, 80). Chemotherapeutic loaded EVs can target tumors with a significant reduction in dose-dependent side effects of chemotherapeutic agents and an increase in their efficacy in cancer treatment (55, 68, 81). Mesenchymal stem cell (MSC)-derived EVs can be used in the field of regeneration and repair. Additionally, some *in vitro* and *in vivo* studies have investigated its regenerative potential and therapeutic applications. In some studies, EVs were found to outperform MSCs in the treatment of various diseases (19, 82, 83).

Role of EVs in tumor growth and metastasis of osteosarcoma (OS)

Extracellular vesicles affect cellular communication between cells within the TME, thus influencing cell proliferation and metastasis in cancer. Bone marrow-derived mesenchymal stem cell-derived extracellular vesicles (BMSC-EVs) can promote proliferation, invasion, and migration of osteosarcoma cells *via* the MALAT1/miR-143/NRSN2/Wnt/β-catenin axis (32). This enhancement in cell proliferation and metastasis is facilitated by the epithelial-mesenchymal transition (EMT) in related cell types. Moreover, the TME significantly accelerates tumor neovascularization, immunosuppression through stromal cells, and the transformation of cancer-associated fibroblasts (84–87). In conclusion, EVs have a strong effect on OS cell proliferation, migration, invasion, and angiogenesis by participating in intercellular communication and controlling cellular signaling (Figure 1).

Extracellular vesicles are involved in osteosarcoma proliferation

Cancer cells undergo indefinite proliferation (88). In contrast, normal tissues have precise and controlled release of pro-growth signals, which cyclically initiate cell proliferation and differentiation up to a finite number of cell divisions. However, tumor cells can inherently produce growth factor receptors, thus escaping negative feedback regulation against proliferation (89, 90). EVs also have an important effect on proliferation in OS (Table 1). Zhang et al. reported the effect of exosomal miR-208a obtained from bone marrow-derived mesenchymal stem cells (BMSCs) on OS cell proliferation and apoptosis. They found that OS cell growth was enhanced and apoptosis was inhibited when PDCD4 expression was suppressed. This, in turn, activated the Hippo and ERK1/2 pathways. In contrast, the exosomal miR-206 obtained from BMSCs suppressed cell growth, invasion, and migration. It also promoted apoptosis by targeting TRA2B in OS cells (102). Additionally, BMSC-derived EVs could encapsulate and translocate PVT1 in OS cells, and PVT1 promoted cancer development and migration by binding to miR-183–5p and facilitating the expression of ERG (94). BMSC-EVs could enhance OS cell growth, migration, and invasion through MALAT1/miR-143/NRSN2/Wnt/β-catenin signaling (93). Huang et al. showed the effect of EVs obtained from hBMSCs on tumorigenesis and migration. The EVs showed enhanced tumorigenesis and migration by promoting oncogenic autophagy in OS (95). EVs derived from ADSC could enhance OS cell growth, invasion, and migration by delivering COLGALT2 to OS cells, leading to the malignant progression of OS (96). Li et al. found that OS cells that showed AXL upregulation promoted the secretion of EVs into cells with downregulated AXL, and this promoted cell growth, invasion, and migration *via* the linc00852/miR-7–5p/AXL regulatory axis (103). Ge et al. found that BMSC-derived EVs translocate into OS cells and promote OS growth and migration by LCP1/JAK2/STAT3 signaling and inhibit OS progression *via* miR-135a-5p/LCP1 signaling (98). The MG-63 cell-derived EVs, which were co-cultured using HOS and MG-63 cell lines, significantly enhanced OS cell growth and inhibited apoptosis. This effect might be related to the interaction of Hic-5 with smad4 and a decrease in the expression of TCF/LEF that regulates Wnt/β-catenin signaling (99). Han et al. found that exosomal miR-1307 obtained from OS cells can promote OS cell growth, invasion, and migration by inhibiting AGAP1 expression. This finding indicated that the miR-1307-AGAP1 axis might act as an anti-OS therapeutic target (100). Wu et al. found that exosomal miR-15a expression decreased in plasma EVs, and exosomal miR-15a was absorbed by OS cells, which suppressed GATA2/MDM2 signaling *via* the p53 pathway. This inhibited OS cell growth and migration *in vitro* (104).

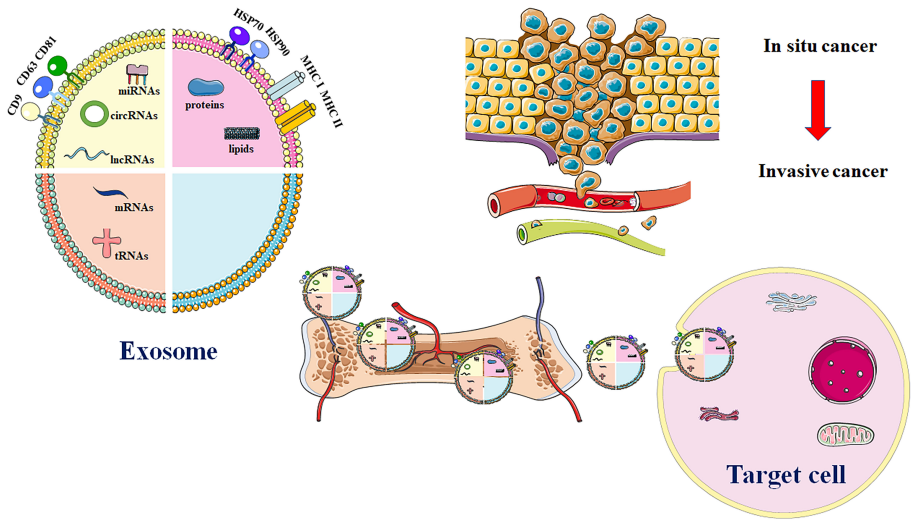

FIGURE 1
Major exosome release process in OS. EVs are comprised of various proteins and nucleic acids. These evolutionarily conserved proteins that can be used as biomarkers, like HSP70, CD9, CD63, and CD81. Additionally, exosomal cargos are also involved in transport of multiple biomolecules such as DNA or RNA. EVs that carry genetic materials are utilized in development of treatment for OS through enhancing drug resistance, immune evasion, migration, invasion, and angiogenesis. Source cell-derived exosomal cargos are also carried into recipient cells *via* blood circulation. Highly invasive OS cells enhance cell migration and invasion through production of exosomes.

TABLE 1 Biological activity of exosomes in OS proliferation.

EV content	Parent cells	Target cells	Mechanism	Biological activity	Ref.
miR-208	BMSCs	OS cells	PDCD4/ERK1/2	Enhance OS cell invasion, viability as well as clone formation ability	(91)
miR-206	BMSCs	OS cells	TRA2B	Suppress OS cell growth, invasion, and migration, while inducing their apoptosis	(92)
MALAT1	BMSCs	OS cells	MALAT1/miR-143/NRSN2/Wnt/β-catenin	Promote OS cell proliferation, metastasis, and invasion	(93)
PVT1	BMSCs	OS cells	PVT1/miR-183–5p/ERG	Promote OS proliferation and invasion	(94)
ATG5	BMSCs	OS cells	/	Enhance OS cell growth, invasion, and migration,	(95)
COLGALT2	ADSCs	OS cells	/	Enhance OS cell growth, invasion, and migration	(96)
Linc00852	high AXL expression in OS cells	low AXL expression in OS cells	Linc00852/miR-7–5p/AXL	Promote cell proliferation, migration and invasion	(97)
LCP1	BMSCs	OS cells	miR-135a-5p/LCP1/JAK2/STAT3	Enhance OS cell growth, and migration	(98)
Hic-5	MG-63	MG-63 and HOS cells	Hic-5/smad4-TCF/LEF-Wnt/β-catenin	Promote cell proliferation and inhibit cell apoptosis	(99)
miR-1307	OS cells	OS cells	AGAP1	Enhance OS cell growth, invasion, and migration	(100)
miR-15a	Serum-derived exosome	OS cells	miR-15a/p5/GATA2/MDM2	Inhibit OS cell growth, invasion, and migration	(101)

EVs have an important effect on OS metastasis

In epithelial-mesenchymal transition (EMT), the epithelial properties of epithelial cells are lost, while the mesenchymal phenotype is acquired. This phenomenon is widely involved in physiological regulation and pathological changes and is closely related to embryogenesis, tissue regeneration, invasion, and metastasis of cancer tissue (105–107). When EMT occurs, the main features of epithelial cells are lost, resulting in a change from polygonal to spindle-shaped fibroblast-like morphology. Additionally, the cells also lose their polarity, show reduced adhesion, and gain the ability to invade and metastasize (108, 109). EVs have a strong effect on OS invasive metastasis (Table 2). When *in-vitro* synthesized miR-143 was transported into OS cells *via* EVs, they significantly inhibited the invasive ability of the cells (110). Gong et al. found that highly invasive OS cells secreted exosomal miR-675 into recipient cells and further suppressed CALN1 expression to enhance migration and invasion of OS cells. Additionally, serum exosomal miR-675 levels among OS cases are strongly associated with the prognosis of OS (111). Mazumdar et al. found that EVs derived from 143-B cells with high metastasis capacity and SAOS-2 cells with low metastasis capacity could induce the recruitment of BMCs into the lungs. The components of EVs might inhibit distant metastasis of OS (113). Zhong et al. showed that the Rab22a-NeoF1 fusion protein with PYK2 could be sorted into EVs in OS. The exosomal Rab22a-NeoF1 fusion protein promotes premetastatic lung niche generation by recruiting bone marrow-derived macrophages (BMDMs) (112). Han et al. showed that exosomal miR-1307 obtained from OS cells enhanced OS cell growth, invasion, and migration by inhibiting AGAP1 expression; thus, targeting miR-1307 might inhibit the malignant progression of OS (100).

EVs are essential for angiogenesis in osteosarcoma

Angiogenesis is the formation of new blood vessels in capillaries or venules behind capillaries (114, 115). This process is regulated by the interaction between proangiogenic and antiangiogenic factors. Although these factors are stable under normal physiological conditions, they can be activated or inactivated by external stimuli (12, 116). Different types of cells (cancer and healthy cells) require nutrients, which are supplied through blood capillaries. These capillaries can also excrete metabolic waste generated within cells (117, 118). Tumor-derived EVs are associated with an important mechanism that promotes angiogenesis. Moreover, EVs have a critical effect on angiogenesis in OS (Table 3). Yoshida et al. found that the expression of miR-25–3p increased in OS tissues, which promoted cancer development, drug resistance, and invasion by inhibiting the expression of DKK3. Embedding synthetic miR-25–3p into tumor-derived EVs significantly promoted the capillary formation and vascular endothelial cell (EC) invasion (119). Tao et al. showed that angiogenesis in OS could be promoted by EWSAT1. Therefore, including exosomes increases the sensitivity of vascular endothelial cells, which directly induces an increase in the secretion of angiogenic factors (120). Li et al. showed that osteosarcoma cells with high exosome abundance could modulate autophagy and angiogenesis in OS *via* ATG and miR-153 by secreting exosomal lnc-OIP5-AS1 into other OS cells (121).

TABLE 2 Biological functions of exosomes during the metastasis of OS.

EV content	Parent cells	Target cell	Mechanism	Biological activity	Ref.
synthetic miR-143	/	OS cells	/	Inhibit cell invasion	(110)
miR-675	OS cells	hFOB1.19	CALN1	Enhance OS cell invasion, and migration	(111)
Rab22a-NeoF1/PYK2	PYK2-positive osteosarcoma cells	macrophages	RhoA	Facilitate the pre-metastatic niche formation	(112)
miR-1307	OS cells	OS cells	AGAP1	Enhance OS cell growth, invasion, and migration	(100)

TABLE 3 The biological function of exosome in the angiogenesis of OS.

EV content	Parent cells	Target cells	Mechanism	Biological activity	Ref.
synthetic miR-25–3p	/	OS cells	DKK3	Enhance angiogenesis and vascular endothelial cell migration	(119)
EWSAT1	/	OS cells	/	Increase in sensitivity/reactivity of vascular endothelial cells	(120)
OIP5-AS1	OS cells	OS cells	miR-153/ATG5	Increase in the angiogenesis level	(121)

Extracellular vesicles are essential for the immune activity of osteosarcoma

The natural response of the body to any foreign material is expressed by immune system activation and production of EVs (22, 83, 122). EVs can also regulate and modulate immune cells and participate in the immune response (21, 123, 124). EVs obtained from cancer cells can deliver tumor-associated antigens (TAAs) to stimulate immune cells and generate antitumor immune responses. However, they can also interfere with immune recognition and inhibit tissue-associated cells, T cells, immune-related cells, and natural killer (NK) cells, thus accelerating tumor cell escape and metastasis (25, 125). Moreover, EVs are responsible for regulating cancer cell development *via* TME-derived immune cells (126, 127). Additionally, the immune microenvironment within OS cells is strongly affected by EVs (Table 4). Cancer-associated fibroblast (CAFs)-secreted exosomal miR-1228 can enhance OS migration and invasion *via* SCAI. This can be further used in the development of miR-1228-based anti-OS therapy (119). Raimondi et al. found that EVs can promote osteoclast bone resorption and differentiation. EVs can also enhance tube formation in ECs while increasing the expression of angiogenic markers. Specific miRNAs, including miR-21–5p and miR-148a, have important effects on the tumor microenvironment, as determined by second-generation sequencing (128). The EVs of metastatic OS cells secrete exosomal TGFβ2 into tumor-associated macrophages, which in turn promote the M2 phenotype and contribute to immunosuppression and tumorigenesis (129). Mazumdar et al. showed that EVs obtained from OS cells can promote the differentiation of myofibroblasts/CAF, the generation of fibronectin, and the expression of smooth muscle actin. They can also significantly promote the invasive ability of human lung fibroblasts (130). Cheng et al. showed that OS-obtained EVs can promote the polarization of M2 macrophages *via* Tim-3, which in turn can promote the invasion of OS cells and metastasis (135). Zhang et al. showed that OS cell-derived exosomal COL6A1 can convert normal fibroblasts into CAFs by secreting proinflammatory cytokines. After activation, CAFs can mediate the TGF-β/COL6A1 pathway to enhance the migration and invasion of OS cells (132). Zhang et al. showed that exosomal LIFR-AS1 obtained from macrophages could promote the OS malignancy grade by combining with miR-29a, which promoted the NFIA level (133).

Potential clinical application of EVs in osteosarcoma

Extracellular vesicles consist of various biomolecules, which are biologically active. They circulate through systemic circulation and are also found in various body fluids capable of mediating long-distance intercellular communication (40, 136). Tumor-derived EVs are rich in biomolecules, such as proteins, nucleotides, and lipids, which indicate the origin of the pathophysiological status of the cells (137, 138). EVs can provide a specialized lipid bilayer covering, thus preventing the degradation of RNA molecules (137, 139). Hence, the detection of tumor EVs in patients provides significant advantages to liquid biopsy, and EVs might also be used for early diagnosis. EVs might also be used to develop efficacious treatment strategies and monitor the prognosis of different diseases [181.182]. A specific collection of RNAs in the EV cargo might also serve as new or supplementary biomarkers in the diagnosis

TABLE 4 The biological functions of exosome in the immuno-modulation of OS.

EV content	Parent cell	Target cell	Mechanism	Biological function	Ref.
miR-1228	cancer-associated fibroblasts	OS cells	SCAI	Promote OS cell migration and invasion	(119)
miR-148a-3p and miR-21–5p	OS cells	Raw264.7 and Huvec cells	/	Influence osteoclast formation, tumor angiogenesis, and bone resorption	(128)
TGFβ2	Metastatic OS cells	Tumor-associated macrophages	/	Enhance M2 phenotype while creating the tumor-promoting, Immunosuppressive TME	(129)
TGFβ1	OS cells	Resident lung cells	/	Drive myofibroblast/cancer-associated fibroblast differentiation	(130)
Tim-3	MG63	Macrophages	/	Induce M2 type differentiation of macrophages	(131)
COL6A1	OS cells	cancer-associated fibroblasts	IL-6, IL-8 and STAT1	Convert normal fibroblasts to cancer-associated fibroblasts	(132)
LIFR-AS1	Macrophages	OS cells	miR-29a/NFIA	Enhance OS cell growth, invasion, and migration While promoting their apoptosis	(133)
miR-221–3p	M2-polarized tumor-associated macrophages	OS cells	SOCS3/JAK2/STAT3	Promote growth of OS cells	(134)

and progression of OS (31). Another study showed dysregulated levels of several miRNAs and mRNAs in EVs isolated from the serum of OS patients with a poor chemotherapeutic response compared to that of patients who responded positively to chemotherapy (140). A pilot study showed a higher tumor mutation burden in the RNA isolated from the plasma samples with metastatic EVs compared to that isolated from the plasma samples with non-metastatic ones (141). These findings highlighted the clinical application of EVs in OS.

Extracellular vesicles are promising tools for developing osteosarcoma biomarkers

The diagnostic and prognostic assessment of OS improved considerably with the application of EVs as a biomarker for the disease. Next-generation sequencing was conducted, and eight novel miRNAs were identified from OS cells, out of which five miRNAs were present in circulating EVs among OS patients. However, the biological activity in the pathogenesis of OS and the diagnostic and therapeutic potential of these miRNAs need to be further investigated (142). The expression levels of plasma EV-miR-101 in OS patients and normal participants were determined by performing qRT–PCR. The results indicated a significant decrease in EV-miR-101 levels in OS patients relative to that in normal participants. Moreover, the EV-miR-101 plasma levels in OS patients with metastases were lower than those in patients without metastases. Hence, EV-miR-101 might be a diagnostic marker for OS (143). Ye et al. identified 57 differentially expressed miRNAs in plasma samples obtained from OS patients and normal participants *via* high-throughput sequencing. Among these miRNAs, 20 were upregulated, and 37 were downregulated. The expression of miR-92a-3p, miR-130a-3p, miR-195–3p, let-7i-3p, and miR-335–5p increased significantly within EVs from OS patients relative to their expression in controls. The findings suggested that these miRNAs might be used as potential diagnostic markers for OS (144). Zhang et al. reported high levels of CASC15 in OS cells and tissues along with a significant increase in the levels of CASC15 in the OS plasma EVs compared to their levels in controls (145). Cambier et al. described the significant diagnostic potential of overexpressed biomarkers such as HSATII, HSATI, Charlie 3, and LINE1-P1 at the DNA level rather than the RNA level in serum EVs from OS patients compared to their levels in serum EVs of the control (146). Huo et al. described significant upregulation of hsa_circ_0056285 in serum EVs in OS patients. They also showed the great diagnostic ability of hsa_circ_0056285 based on the ROC curve analysis (147). The expression of SENP1 obtained from plasma exosomes of OS patients was closely related to the tumor size, tumor location, necrosis rate, lung metastasis, and surgical staging. Moreover, patients with higher SENP1 expression had poorer overall survival, and disease-free survival (DFS) compared to OS patients with downregulated SENP1 (148). Han et al. analyzed EVs from plasma samples of OS patients with and without metastases and compared the results to those of normal controls using MALDI-TOF MS. They identified seven exosomal protein markers that were associated with OS lung metastasis (11). Also, noninvasive liquid biopsy using MALDI-TOF MS fingerprinting and SERS for the identification of EVs can be applied for the rapid diagnosis of OS (149).

Potentials of EVs in the treatment of osteosarcoma

Treatment options for OS were either surgery or radiotherapy until the 1970s. Patients with OS also showed high resistance to radiotherapy (150, 151). Clinical results showed that surgical intervention, including tumor resection and/or amputation, cannot improve the survival rate (the operative mortality was about 80%) (152). The five-year survival rate of tumor resection cases is only 20% (153). Additionally, chemotherapeutic interventions can improve the survival rate of OS and reduce the amputation rate, thus improving the limb rescue score. The long-term survival rate of OS patients without metastasis is as high as 75%, compared to 20% before the 1970s (154, 155). However, the long-term survival rate of patients with recurrence or metastasis is still low (Figure 2).

Kyung et al. showed that EVs have antitumor effects on osteosarcoma cells. EVs from canine macrophages can activate the apoptosis pathway of canine OS cells, which is an effective anti-cancer treatment (156). Additionally, MSC-derived EVs carrying miR-150 can reduce the proliferation and migration of osteosarcoma cells by targeting IGF2BP1 (insulin-like growth factor-2 mRNA binding protein 1) (157) Exosomes might also be used as a carrier to deliver chemotherapeutic drugs to osteosarcoma cells [188.189]. Exosomes can be directly charged with drugs [190.191].

Conclusion

The advanced metastasized tumors, in contrast to primary tumors, often pose a major hindrance to the success of treatment outcomes in OS and increase patient mortality. Therefore, early diagnosis is the key to improving the prognosis and survival of OS patients (123, 158). EVs are stable, diverse, nano-sized vesicles that are found in most tissues, organs, and body fluids (124, 159). Moreover, EVs containing transmembrane proteins and some intracellular proteins, such as integrins or genetic material from the cells of origin, display a high level of identity within cells. This identity is associated with the identification of the tissue of origin, suggesting the importance of EVs and their potential as biomarkers in the early diagnosis and prognosis of OS (22, 160, 161). The

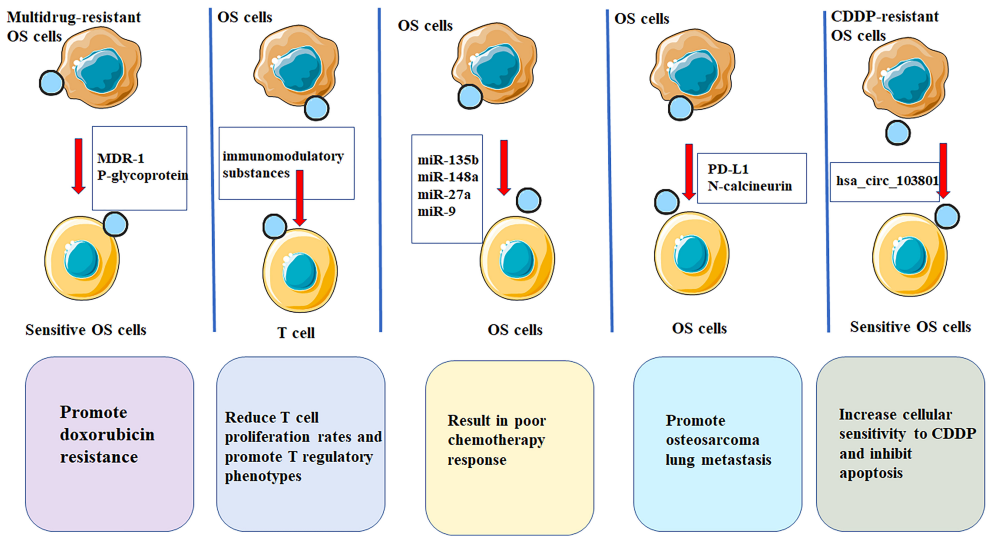

FIGURE 2
EVs have potential applications in treatment of OS. EVs are multifunctional nanostructured carriers which can be used as drug delivery systems with low immunogenicity as well as high biocompatibility and efficacy. OS-derived EVs contain immunomodulation properties that significantly reduces T cell proliferation rates and promote T regulatory phenotypes, thereby promoting OS progression. OS cases showing low chemosensitivity in patients showing favorable chemosensitivity. miR-9, miR-27a, miR-135b and miR-148a show marked up-regulation within serum EVs of OS patients. OS cells could promote osteosarcoma lung metastasis by releasing EVs that contained PD-L1 and N-calcineurin. EVs from cisplatin-resistant (CDDP)-resistant OS cells decreased P-glycoprotein and MDR-associated protein 1 levels in MG63 and U2OS cells, increases cellular sensitivity to CDDP and inhibits apoptosis through exosomal-hsa_circ_103801.

surface proteins of EVs can be targeted and captured by recipient cells, and the contents of EVs can alter the physiological state of recipient cells (162, 163). Tumor EVs can also modulate cancer progression, immune evasion, metastasis, and angiogenesis by interacting with other cells within the TME (125, 164, 165). Additionally, the exosome-mediated pathological processes also highlight the great potential of EVs as biomarkers. Also, a better understanding of the mechanisms of exosome action is necessary to screen, diagnose, and assess patient prognosis.

There are still many problems in the development of EVs. For example, a standardized approach is needed for the quick, easy, and specific isolation of EVs in liquid biopsy. Moreover, EVs can serve as potential biomarkers for the diagnosis of OS, predict its prognosis, and monitor real-time treatment response. Clinical studies with a small sample size have shown reproducibility of EVs (166–168). However, more multicenter trials with large sample sizes are required for developing more accurate liquid biopsies. For evaluating the biological functions of EVs, determining whether they have similar regulatory functions *in vivo* and *in vitro* is challenging. The reason for this heterogeneity is that numerous assays have been performed *in vitro*, however, similar culture conditions cannot be replicated *in vivo*. Additionally, for therapeutic purposes, exosome-derived cells need to be selected carefully to ensure safe treatment. Due to their availability and non-nucleated and non-genetic nature, erythrocytes are the most promising cells for producing exosomes.

Besides their potential as good biomarkers, EVs are promising for precise and targeted cancer therapy (169–171). The development of a novel drug-loading system is a barrier to enhancing the effectiveness of antitumor drug therapy. Therefore, as a natural therapeutic carrier, EVs might be used for their low immunogenicity and various therapeutic bioactive molecules contained within (21, 161). Moreover, exogenous drugs carried by EVs can maintain drug stability *in vivo*. These advantages make EVs a better drug loading system than traditional drug delivery models. Hence, EVs are important for developing precision medicine for OS and other cancers. Han et al. constructed the iRGD-Lamp2b-modified MSC fusion gene for isolating and purifying EVs, as well as, loading the anti-miRNA-221 oligonucleotides into EVs. AMO-loaded EVs are effective in inhibiting *in-vitro* colon cancer (CC) cell growth and clone-forming ability (172). Exosomal ANXA6 levels in the sera of TNBC patients can predict the efficacy of gemcitabine chemotherapy (173). CC cells can produce exosomal miR-208b to receptor T-cells and promote the expansion of Treg cells *via* programmed cell death factor 4 (PDCD4), leading to malignant tumor growth and oxaliplatin resistance (174).

In this study, we highlighted and reviewed the advancements in the research on the biological functions of EVs during the occurrence and development of OS, along with its clinical applications. Moreover, EVs from OS can promote the progression of OS by regulating cancer drug resistance,

immunity, angiogenesis, and metastasis. These findings highlight the role of EVs as anti-OS targets. Additionally, due to their abnormal expression in tumor-derived exosomal inclusions and their ability to reflect the tumor status, EVs might be used as markers for the diagnosis and prognosis of OS. Exosomal drug carriers and immunomodulatory therapy are promising therapeutic strategies in the treatment of OS.

Author contributions

SL, XG, and BG were responsible for original drafting, supplementation, allocation as well as editing. The authors have carefully read and approved the final version for submission.

Funding

The present study was funded by Fundamental Research Funds for the Central Universities (LD202110) and Natural Science Foundation of Liaoning Province (2020-MS-058) and Shenyang Young and Middle-age Scientific and Technological Innovation Talent Support Plan (RC190456).

Acknowledgments

The present study was funded by Liaoning Cancer Hospital & Institute (Shenyang) and China Medical University (Shenyang).

Conflict of interest

The authors declare that the research was conducted in the absence of any commercial or financial relationships that could be construed as a potential conflict of interest.

Publisher's note

References

1. Chen Y, Cao J, Zhang N, Yang B, He Q, Shao X, et al. Advances in differentiation therapy for osteosarcoma. *Drug Discovery Today* (2020) 25 (3):497–504. doi: 10.1016/j.drudis.2019.08.010

2. Dean DC, Shen S, Hornicek FJ, Duan Z. From genomics to metabolomics: emerging metastatic biomarkers in osteosarcoma. *Cancer Metastasis Rev* (2018) 37 (4):719–31. doi: 10.1007/s10555-018-9763-8

3. Zheng C, Tang F, Min L, Hornicek F, Duan Z, Tu C. PTEN in osteosarcoma: Recent advances and the therapeutic potential. *Biochim Biophys Acta Rev Cancer* (2020) 1874(2):188405. doi: 10.1016/j.bbcan.2020.188405

4. Hattinger CM, Patrizio MP, Fantoni L, Casotti C, Riganti C, Serra M. Drug resistance in osteosarcoma: Emerging biomarkers, therapeutic targets and treatment strategies. *Cancers (Basel)* (2021) 13(12):2878. doi: 10.3390/cancers13122878

5. Czarnecka AM, Synoradzki K, Firlej W, Bartnik E, Sobczuk P, Fiedorowicz M, et al. Molecular biology of osteosarcoma. *Cancers (Basel)* (2020) 12(8):2130. doi: 10.3390/cancers12082130

6. Lin Z, Wu Z, Luo W. Chimeric antigen receptor T-cell therapy: The light of day for osteosarcoma. *Cancers (Basel)* (2021) 13(17):4469. doi: 10.3390/cancers13174469

7. Brookes MJ, Chan CD, Baljer B, Wimalagunaratna S, Crowley TP, Ragbir M, et al. Surgical advances in osteosarcoma. *Cancers (Basel)* (2021) 13(3):388. doi: 10.3390/cancers13030388

8. Gill J, Gorlick R. Advancing therapy for osteosarcoma. *Nat Rev Clin Oncol* (2021) 18(10):609–24. doi: 10.1038/s41571-021-00519-8

9. Huang Q, Liang X, Ren T, Huang Y, Zhang H, Yu Y, et al. The role of tumor-associated macrophages in osteosarcoma progression-therapeutic implications. *Cell Oncol (Dordr)* (2021) 44(3):525–39. doi: 10.1007/s13402-021-00598-w

10. Marchandet L, Lallier M, Charrier C, Baud'huin M, Ory B, Lamoureux F. Mechanisms of resistance to conventional therapies for osteosarcoma. *Cancers (Basel)* (2021) 13(4):683. doi: 10.3390/cancers13040683

11. Cui J, Dean D, Hornicek FJ, Chen Z, Duan Z. The role of extracelluar matrix in osteosarcoma progression and metastasis. *J Exp Clin Cancer Res* (2020) 39 (1):178. doi: 10.1186/s13046-020-01685-w

12. Liu Y, Huang N, Liao S, Rothzerg E, Yao F, Li Y, et al. Current research progress in targeted anti-angiogenesis therapy for osteosarcoma. *Cell Prolif* (2021) 54(9):e13102. doi: 10.1111/cpr.13102

13. Prudowsky ZD, Yustein JT. Recent insights into therapy resistance in osteosarcoma. *Cancers (Basel)* (2020) 13(1):83. doi: 10.3390/cancers13010083

14. Laskar S, Kakoti S, Khanna N, Manjali JJ, Mangaj A, Puri A, et al. Outcomes of osteosarcoma, chondrosarcoma and chordoma treated with image guided-intensity modulated radiation therapy. *Radiother Oncol* (2021) 164:216–22. doi: 10.1016/j.radonc.2021.09.018

15. Christie JD, Appel N, Canter H, Achi JG, Elliott NM, de Matos AL, et al. Systemic delivery of TNF-armed myxoma virus plus immune checkpoint inhibitor eliminates lung metastatic mouse osteosarcoma. *Mol Ther Oncolytics* (2021) 22:539–54. doi: 10.1016/j.omto.2021.07.014

16. Synoradzki KJ, Bartnik E, Czarnecka AM, Fiedorowicz M, Firlej W, Brodziak A, et al. TP53 in biology and treatment of osteosarcoma. *Cancers (Basel)* (2021) 13(17):4284. doi: 10.3390/cancers13174284

17. Chen C, Xie L, Ren T, Huang Y, Xu J, Guo W. Immunotherapy for osteosarcoma: Fundamental mechanism, rationale, and recent breakthroughs. *Cancer Lett* (2021) 500:1–10. doi: 10.1016/j.canlet.2020.12.024

18. Pathania AS, Prathipati P, Challagundla KB. New insights into exosome mediated tumor-immune escape: Clinical perspectives and therapeutic strategies. *Biochim Biophys Acta Rev Cancer* (2021) 1876(2):188624. doi: 10.1016/j.bbcan.2021.188624

19. Psaraki A, Ntari L, Karakostas C, Korrou-Karava D, Roubelakis MG. Extracellular vesicles derived from mesenchymal Stem/Stromal cells: The regenerative impact in liver diseases. *Hepatology* (2021) 75(6):1590–1603. doi: 10.1002/hep.32129

20. Trams EG, Lauter CJ, Salem NJr., Heine U. Exfoliation of membrane ecto-enzymes in the form of micro-vesicles. *Biochim Biophys Acta* (1981) 645(1):63–70. doi: 10.1016/0005-2736(81)90512-5

21. Bondhopadhyay B, Sisodiya S, Alzahrani FA, Bakhrebah MA, Chikara A, Kasherwal V, et al. EVs: A forthcoming era of breast cancer therapeutics. *Cancers (Basel)* (2021) 13(18):4672. doi: 10.3390/cancers13184672

22. Vautrot V, Bentayeb H, Causse S, Garrido C, Gobbo J. Tumor-derived EVs: Hidden players in PD-1/PD-L1 resistance. *Cancers (Basel)* (2021) 13(18):4537. doi: 10.3390/cancers13184537

23. Thakur A, Ke X, Chen YW, Motallebnejad P, Zhang K, Lian Q, et al. The mini player with diverse functions: Extracellular vesicles in cell biology, disease, and therapeutics. *Protein Cell* (2021) 13(9):631–54. doi: 10.1007/s13238-021-00863-6

24. Johnstone RM, Ahn J. A common mechanism may be involved in the selective loss of plasma membrane functions during reticulocyte maturation. *BioMed Biochim Acta* (1990) 49:S70–5. doi: 10.1007/BF02789143

25. Jiang C, Zhang N, Hu X, Wang H. Tumor-associated EVs promote lung cancer metastasis through multiple mechanisms. *Mol Cancer* (2021) 20(1):117. doi: 10.1186/s12943-021-01411-w

26. Piffoux M, Volatron J, Cherukula K, Aubertin K, Wilhelm C, Silva AKA, et al. Engineering and loading therapeutic extracellular vesicles for clinical translation: A data reporting frame for comparability. *Adv Drug Delivery Rev* (2021) 178:113972. doi: 10.1016/j.addr.2021.113972

27. Kim H, Jang H, Cho H, Choi J, Hwang KY, Choi Y, et al. Recent advances in exosome-based drug delivery for cancer therapy. *Cancers (Basel)* (2021) 13 (17):4435. doi: 10.3390/cancers13174435

28. Isaac R, Reis FCG, Ying W, Olefsky JM. EVs as mediators of intercellular crosstalk in metabolism. *Cell Metab* (2021) 33(9):1744–62. doi: 10.1016/j.cmet.2021.08.006

29. Ding Y, Cao F, Sun H, Wang Y, Liu S, Wu Y, et al. EVs derived from human umbilical cord mesenchymal stromal cells deliver exogenous miR-145–5p to inhibit pancreatic ductal adenocarcinoma progression. *Cancer Lett* (2019) 442:351–61. doi: 10.1016/j.canlet.2018.10.039

30. Kim MS, Haney MJ, Zhao Y, Yuan D, Elena V. Engineering macrophage-derived EVs for targeted paclitaxel delivery to pulmonary metastases: *In vitro* and *in vivo* evaluations. *Nanomedicine.* (2018) 14:195–204. doi: 10.1016/j.nano.2017.09.011

31. Perut F, Roncuzzi L, Baldini N. The emerging roles of extracellular vesicles in osteosarcoma. *Front Oncol* (2019) 9:1342. doi: 10.3389/fonc.2019.01342

32. Li F, Chen X, Shang C, Ying Q, Zhou X, Zhu R, et al. Bone marrow mesenchymal stem cells-derived extracellular vesicles promote proliferation, invasion and migration of osteosarcoma cells *via* the lncRNA MALAT1/miR-143/NRSN2/Wnt/β-Catenin axis. *Onco Targets Ther* (2021) 14:737–49. doi: 10.2147/OTT.S283459

33. Hur JY, Lee KY. Characteristics and clinical application of extracellular vesicle-derived DNA. *Cancers (Basel)* (2021) 13(15):3827. doi: 10.3390/cancers13153827

34. Jiang X, You L, Zhang Z, Cui X, Zhong H, Sun X, et al. Biological properties of milk-derived extracellular vesicles and their physiological functions in infant. *Front Cell Dev Biol* (2021) 9:693534. doi: 10.3389/fcell.2021.693534

35. Poupardin R, Wolf M, Strunk D. Adherence to minimal experimental requirements for defining extracellular vesicles and their functions. *Adv Drug Delivery Rev* (2021) 176:113872. doi: 10.1016/j.addr.2021.113872

36. Burgos-Ravanal R, Campos A, Diaz-Vesga MC, Gonzalez MF, Leon D, Lobos-Gonzalez L, et al. Extracellular vesicles as mediators of cancer disease and as nanosystems in theranostic applications. *Cancers (Basel)* (2021) 13(13):3324. doi: 10.3390/cancers13133324

37. Mittal R, Bencie N, Langlie J, Mittal J, Eshraghi AA. EVs as drug delivery vehicles and biomarkers for neurological and auditory systems. *J Cell Physiol* (2021) 236(12):8035–49. doi: 10.1002/jcp.30484

38. Chen J, Zhang Q, Liu D, Liu Z. EVs: Advances, development and potential therapeutic strategies in diabetic nephropathy. *Metabolism* (2021) 122:154834. doi: 10.1016/j.metabol.2021.154834

39. Ruan S, Greenberg Z, Pan X, Zhuang P, Erwin N, He M. Extracellular vesicles as an advanced delivery biomaterial for precision cancer immunotherapy. *Adv Healthc Mater* (2021) 11(5):e2100650. doi: 10.1002/adhm.202100650

40. Sun SJ, Wei R, Li F, Liao SY, Tse HF. Mesenchymal stromal cell-derived EVs in cardiac regeneration and repair. *Stem Cell Rep* (2021) 16(7):1662–73. doi: 10.1016/j.stemcr.2021.05.003

41. Kostallari E, Valainathan S, Biquard L, Shah VH, Rautou PE. Role of extracellular vesicles in liver diseases and their therapeutic potential. *Adv Drug Delivery Rev* (2021) 175:113816. doi: 10.1016/j.addr.2021.05.026

42. Fu P, Zhang J, Li H, Mak M, Xu W, Tao Z. Extracellular vesicles as delivery systems at nano-/micro-scale. *Adv Drug Delivery Rev* (2021) 179:113910. doi: 10.1016/j.addr.2021.113910

43. Tang XH, Guo T, Gao XY, Wu XL, Xing XF, Ji JF, et al. Exosome-derived non-coding RNAs in gastric cancer: Functions and clinical applications. *Mol Cancer* (2021) 20(1):99. doi: 10.1186/S12943-021-01396-6

44. Gurunathan S, Kang MH, Qasim M, Khan K, Kim JH. Biogenesis, membrane trafficking, functions, and next generation nanotherapeutics medicine of extracellular vesicles. *Int J Nanomed* (2021) 16:3357–83. doi: 10.2147/IJN.S310357

45. Chivero ET, Dagur RS, Peeples ES, Sil S, Liao K, Ma R, et al. Biogenesis, physiological functions and potential applications of extracellular vesicles in substance use disorders. *Cell Mol Life Sci* (2021) 78(11):4849–65. doi: 10.1007/s00018-021-03824-8

46. Zhang Z, Xu R, Yang Y, Liang C, Yu X, Liu Y, et al. Micro/nano-textured hierarchical titanium topography promotes exosome biogenesis and secretion to improve osseointegration. *J Nanobiotech* (2021) 19(1):78. doi: 10.1186/s12951-021-00826-3

47. Song H, Liu B, Dong B, Xu J, Zhou H, Na S, et al. Exosome-based delivery of natural products in cancer therapy. *Front Cell Dev Biol* (2021) 9:650426. doi: 10.3389/fcell.2021.650426

48. Gurunathan S, Kang MH, Kim JH. A comprehensive review on factors influences biogenesis, functions, therapeutic and clinical implications of EVs. *Int J Nanomed* (2021) 16:1281–312. doi: 10.2147/IJN.S291956

49. Chen P, Wang L, Fan X, Ning X, Yu B, Ou C, et al. Targeted delivery of extracellular vesicles in heart injury. *Theranostics* (2021) 11(5):2263–77. doi: 10.7150/thno.51571

50. Shehzad A, Islam SU, Shahzad R, Khan S, Lee YS. Extracellular vesicles in cancer diagnostics and therapeutics. *Pharmacol Ther* (2021) 223:107806. doi: 10.1016/j.pharmthera.2021.107806

51. Tosar JP, Witwer K, Cayota A. Revisiting extracellular RNA release, processing, and function. *Trends Biochem Sci* (2021) 46(6):438–45. doi: 10.1016/j.tibs.2020.12.008

52. Schubert A, Boutros M. Extracellular vesicles and oncogenic signaling. *Mol Oncol* (2021) 15(1):3–26. doi: 10.1002/1878-0261.12855

53. Morrissey SM, Zhang F, Ding C, Montoya-Durango DE, Hu X, Yang C, et al. Tumor-derived EVs drive immunosuppressive macrophages in a pre-metastatic niche through glycolytic dominant metabolic reprogramming. *Cell Metab* (2021) 33(10):2040–58.e10. doi: 10.1016/j.cmet.2021.09.002

54. Sun Z, Yang J, Li H, Wang C, Fletcher C, Li J, et al. Progress in the research of nanomaterial-based exosome bioanalysis and exosome-based nanomaterials tumor therapy. *Biomaterials* (2021) 274:120873. doi: 10.1016/j.biomaterials.2021.120873

55. Mohammadi M, Zargartalebi H, Salahandish R, Aburashed R, Wey Yong K, Sanati-Nezhad A. Emerging technologies and commercial products in exosome-based cancer diagnosis and prognosis. *Biosens Bioelectron* (2021) 183:113176. doi: 10.1016/j.bios.2021.113176

56. Fraga de Andrade I, Mehta C, Bresnick EH. Post-transcriptional control of cellular differentiation by the RNA exosome complex. *Nucleic Acids Res* (2020) 48 (21):11913–28. doi: 10.1093/nar/gkaa883

57. Kumar A, Deep G. Hypoxia in tumor microenvironment regulates exosome biogenesis: Molecular mechanisms and translational opportunities. *Cancer Lett* (2020) 479:23–30. doi: 10.1016/j.canlet.2020.03.017

58. Jafari D, Malih S, Eini M, Jafari R, Gholipourmalekabadi M, Sadeghizadeh M, et al. Improvement, scaling-up, and downstream analysis of exosome production. *Crit Rev Biotechnol* (2020) 40(8):1098–112. doi: 10.1080/07388551.2020.1805406

59. Nakamura K, Sawada K, Kobayashi M, Miyamoto M, Shimizu A, Yamamoto M, et al. Role of the exosome in ovarian cancer progression and its potential as a therapeutic target. *Cancers (Basel)* (2019) 11(8):1147. doi: 10.3390/cancers11081147

60. Zhao X, Wu D, Ma X, Wang J, Hou W, Zhang W. EVs as drug carriers for cancer therapy and challenges regarding exosome uptake. *BioMed Pharmacother* (2020) 128:110237. doi: 10.1016/j.biopha.2020.110237

61. Li C, Hou X, Zhang P, Li J, Liu X, Wang Y, et al. Exosome-based tumor therapy: Opportunities and challenges. *Curr Drug Metab* (2020) 21(5):339–51. doi: 10.2174/1389200221666200515103354

62. Han C, Zhang C, Wang H, Zhao L. Exosome-mediated communication between tumor cells and tumor-associated macrophages: Implications for tumor microenvironment. *Oncoimmunology* (2021) 10(1):1887552. doi: 10.1080/2162402X.2021.1887552

63. Shao J, Zaro J, Shen Y. Advances in exosome-based drug delivery and tumor targeting: From tissue distribution to intracellular fate. *Int J Nanomed* (2020) 15:9355–71. doi: 10.2147/IJN.S281890

64. He C, Li L, Wang L, Meng W, Hao Y, Zhu G. Exosome-mediated cellular crosstalk within the tumor microenvironment upon irradiation. *Cancer Biol Med* (2021) 18(1):21–33. doi: 10.20892/j.issn.2095-3941.2020.0150

65. Yu W, Hurley J, Roberts D, Chakrabortty SK, Enderle D, Noerholm M, et al. Exosome-based liquid biopsies in cancer: Opportunities and challenges. *Ann Oncol* (2021) 32(4):466–77. doi: 10.1016/j.annonc.2021.01.074

66. Xu Z, Zeng S, Gong Z, Yan Y. Exosome-based immunotherapy: A promising approach for cancer treatment. *Mol Cancer* (2020) 19(1):160. doi: 10.1186/s12943-020-01278-3

67. Mughees M, Kumar K, Wajid S. Exosome vesicle as a nano-therapeutic carrier for breast cancer. *J Drug Target* (2021) 29(2):121–30. doi: 10.1080/1061186X.2020.1808001

68. Gonzalez MJ, Kweh MF, Biava PM, Olalde J, Toro AP, Goldschmidt-Clermont PJ, et al. Evaluation of exosome derivatives as bio-informational reprogramming therapy for cancer. *J Transl Med* (2021) 19(1):103. doi: 10.1186/s12967-021-02768-8

69. Kim YK, Choi Y, Nam GH, Kim IS. Functionalized exosome harboring bioactive molecules for cancer therapy. *Cancer Lett* (2020) 489:155–62. doi: 10.1016/j.canlet.2020.05.036

70. Wu Q, Zhou L, Lv D, Zhu X, Tang H. Exosome-mediated communication in the tumor microenvironment contributes to hepatocellular carcinoma development and progression. *J Hematol Oncol* (2019) 12(1):53. doi: 10.1186/s13045-019-0739-0

71. Wortzel I, Dror S, Kenific CM, Lyden D. Exosome-mediated metastasis: Communication from a distance. *Dev Cell* (2019) 49(3):347–60. doi: 10.1016/j.devcel.2019.04.011

72. Meng W, Hao Y, He C, Li L, Zhu G. Exosome-orchestrated hypoxic tumor microenvironment. *Mol Cancer* (2019) 18(1):57. doi: 10.1186/s12943-019-0982-6

73. Olioso D, Caccese M, Santangelo A, Lippi G, Zagonel V, Cabrini G, et al. Serum exosomal microRNA-21, 222 and 124–3p as noninvasive predictive biomarkers in newly diagnosed high-grade gliomas: A prospective study. *Cancers (Basel)* (2021) 13(12):3006. doi: 10.3390/cancers13123006

74. Shin S, Park YH, Jung SH, Jang SH, Kim MY, Lee JY, et al. Urinary exosome microRNA signatures as a noninvasive prognostic biomarker for prostate cancer. *NPJ Genom Med* (2021) 6(1):45. doi: 10.1038/s41525-021-00212-w

75. Wang X, Qian T, Bao S, Zhao H, Chen H, Xing Z, et al. Circulating exosomal miR-363–5p inhibits lymph node metastasis by downregulating PDGFB and serves as a potential noninvasive biomarker for breast cancer. *Mol Oncol* (2021) 15 (9):2466–79. doi: 10.1002/1878-0261.13029

76. Yang E, Wang X, Gong Z, Yu M, Wu H, Zhang D. Exosome-mediated metabolic reprogramming: the emerging role in tumor microenvironment remodeling and its influence on cancer progression. *Signal Transduct Target Ther* (2020) 5(1):242. doi: 10.1038/s41392-020-00359-5

77. Gholipour E, Sarvarian P, Samadi P, Talebi M, Movassaghpour A, Motavalli R, et al. Exosome: From leukemia progression to a novel therapeutic approach in leukemia treatment. *Biofactors* (2020) 46(5):698–715. doi: 10.1002/biof.1669

78. Peswani Sajnani SL, Zhang Y, Vllasaliu D. Exosome-based therapies for mucosal delivery. *Int J Pharm* (2021) 608:121087. doi: 10.1016/j.ijpharm.2021.121087

79. Li B, Cao Y, Sun M, Feng H. Expression, regulation, and function of exosome-derived miRNAs in cancer progression and therapy. *FASEB J* (2021) 35 (10):e21916. doi: 10.1096/fj.202100294RR

80. Santos P, Almeida F. Exosome-based vaccines: History, current state, and clinical trials. *Front Immunol* (2021) 12:711565. doi: 10.3389/fimmu.2021.711565

81. Jan AT, Rahman S, Badierah R, Lee EJ, Mattar EH, Redwan EM, et al. Expedition into exosome biology: A perspective of progress from discovery to therapeutic development. *Cancers (Basel)* (2021) 13(5):1157. doi: 10.3390/cancers13051157

82. Shen M, Chen T. Mesenchymal stem cell-derived EVs and their potential agents in hematological diseases. *Oxid Med Cell Longev* (2021) 2021:4539453. doi: 10.1155/2021/4539453

83. Yang C, Sun J, Tian Y, Li H, Zhang L, Yang J, et al. Immunomodulatory effect of MSCs and MSCs-derived extracellular vesicles in systemic lupus erythematosus. *Front Immunol* (2021) 12:714832. doi: 10.3389/fimmu.2021.714832

84. Tang LB, Ma SX, Chen ZH, Huang QY, Wu LY, Wang Y, et al. Exosomal microRNAs: Pleiotropic impacts on breast cancer metastasis and their clinical perspectives. *Biol (Basel)* (2021) 10(4):307. doi: 10.3390/biology10040307

85. Giordano C, La Camera G, Gelsomino L, Barone I, Bonofiglio D, Ando S, et al. The biology of EVs in breast cancer progression: Dissemination, immune evasion and metastatic colonization. *Cancers (Basel)* (2020) 12(8):2179. doi: 10.3390/cancers12082179

86. Kim H, Lee S, Shin E, Seong KM, Jin YW, Youn H, et al. The emerging roles of EVs as EMT regulators in cancer. *Cells* (2020) 9(4):861. doi: 10.3390/cells9040861

87. Mashouri L, Yousefi H, Aref AR, Ahadi AM, Molaei F, Alahari SK. EVs: Composition, biogenesis, and mechanisms in cancer metastasis and drug resistance. *Mol Cancer* (2019) 18(1):75. doi: 10.1186/s12943-019-0991-5

88. Hanahan D, Weinberg RA. Hallmarks of cancer: The next generation. *Cell* (2011) 144(5):646–74. doi: 10.1016/j.cell.2011.02.013

89. Huang T, Song X, Yang Y, Wan X, Alvarez AA, Sastry N, et al. Autophagy and hallmarks of cancer. *Crit Rev Oncog* (2018) 23(5–6):247–67. doi: 10.1615/CritRevOncog.2018027913

90. Sasahira T, Kirita T. Hallmarks of cancer-related newly prognostic factors of oral squamous cell carcinoma. *Int J Mol Sci* (2018) 19(8):2413. doi: 10.3390/ijms19082413

91. Qin F, Tang H, Zhang Y, Zhang Z, Huang P, Zhu J. Bone marrow-derived mesenchymal stem cell-derived exosomal microRNA-208a promotes osteosarcoma cell proliferation, migration, and invasion. *J Cell Physiol* (2020) 235(5):4734–45. doi: 10.1002/jcp.29351

92. Zhang H, Wang J, Ren T, Huang Y, Liang X, Yu Y, et al. Bone marrow mesenchymal stem cell-derived exosomal miR-206 inhibits osteosarcoma progression by targeting TRA2B. *Cancer Lett* (2020) 490:54–65. doi: 10.1016/j.canlet.2020.07.008

93. Li F, Chen X, Shang C, Ying Q, Zhou X, Zhu R, et al. Bone marrow mesenchymal stem cells-derived extracellular vesicles promote proliferation, invasion and migration of osteosarcoma cells *via* the lncRNA MALAT1/miR-143/NRSN2/Wnt/beta-Catenin axis. *Onco Targets Ther* (2021) 14:737–49. doi: 10.2147/OTT.S283459

94. Zhao W, Qin P, Zhang D, Cui X, Gao J, Yu Z, et al. Long non-coding RNA PVT1 encapsulated in bone marrow mesenchymal stem cell-derived EVs promotes osteosarcoma growth and metastasis by stabilizing ERG and sponging miR-183–5p. *Aging (Albany NY)* (2019) 11(21):9581–96. doi:10.18632/aging.102406

95. Huang Y, Liu W, He B, Wang L, Zhang F, Shu H, et al. EVs derived from bone marrow mesenchymal stem cells promote osteosarcoma development by activating oncogenic autophagy. *J Bone Oncol* (2020) 21:100280. doi: 10.1016/j.jbo.2020.100280

96. Wang Y, Chu Y, Li K, Zhang G, Guo Z, Wu X, et al. EVs secreted by adipose-derived mesenchymal stem cells foster metastasis and osteosarcoma proliferation by increasing COLGALT2 expression. *Front Cell Dev Biol* (2020) 8:353. doi: 10.3389/fcell.2020.00353

97. Li Q, Wang X, Jiang N, Xie X, Liu N, Liu J, et al. Exosome-transmitted linc00852 associated with receptor tyrosine kinase AXL dysregulates the proliferation and invasion of osteosarcoma. *Cancer Med* (2020) 9(17):6354–66. doi: 10.1002/cam4.3303

98. Ge X, Liu W, Zhao W, Feng S, Duan A, Ji C, et al. Exosomal transfer of LCP1 promotes osteosarcoma cell tumorigenesis and metastasis by activating the JAK2/STAT3 signaling pathway. *Mol Ther Nucleic Acids* (2020) 21:900–15. doi: 10.1016/j.omtn.2020.07.025

99. Sha L, Ma D, Chen C. Exosome-mediated hic-5 regulates proliferation and apoptosis of osteosarcoma *via* wnt/beta-catenin signal pathway. *Aging (Albany NY)* (2020) 12(23):23598–608. doi: 10.18632/aging.103546

100. Han F, Pu P, Wang C, Ding X, Zhu Z, Xiang W, et al. Osteosarcoma cell-derived exosomal miR-1307 promotes tumorgenesis *via* targeting AGAP1. *BioMed Res Int* (2021) 2021:7358153. doi: 10.1155/2021/7358153

101. Wu C, Li Z, Feng G, Wang L, Xie J, Jin Y, et al. Tumor suppressing role of serum-derived exosomal microRNA-15a in osteosarcoma cells through the GATA binding protein 2/murine double minute 2 axis and the p53 signaling pathway. *Bioengineered* (2021) 12(1):8378–95. doi: 10.1080/21655979.2021.1987092

102. Zhang H, Wang J, Ren T, Huang Y, Liang X, Yu Y, et al. Bone marrow mesenchymal stem cell-derived exosomal miR-206 inhibits osteosarcoma progression by targeting TRA2B. *Cancer Lett* (2020) 490:54–65. doi: 10.1016/j.canlet.2020.07.008

103. Li Q, Wang X, Jiang N, Xie X, Liu N, Liu J, et al. Exosome-transmitted linc00852 associated with receptor tyrosine kinase AXL dysregulates the proliferation and invasion of osteosarcoma. *Cancer Med* (2020) 9(17):6354–66. doi: 10.1002/cam4.3303

104. Wu C, Li Z, Feng G, Wang L, Xie J, Jin Y, et al. Tumor suppressing role of serum-derived exosomal microRNA-15a in osteosarcoma cells through the GATA binding protein 2/murine double minute 2 axis and the p53 signaling pathway. *Bioengineered* (2021) 12(1):8378–95. doi: 10.1080/21655979.2021.1987092

105. Chong ZX, Yeap SK, Ho WY. Unraveling the roles of miRNAs in regulating epithelial-to-mesenchymal transition (EMT) in osteosarcoma. *Pharmacol Res* (2021) 172:105818. doi: 10.1016/j.phrs.2021.105818

106. Zhang N, Ng AS, Cai S, Li Q, Yang L, Kerr D. Novel therapeutic strategies: Targeting epithelial-mesenchymal transition in colorectal cancer. *Lancet Oncol* (2021) 22(8):e358–e68. doi: 10.1016/S1470-2045(21)00343-0

107. Gonzalez-Martinez S, Perez-Mies B, Pizarro D, Caniego-Casas T, Cortes J, Palacios J. Epithelial mesenchymal transition and immune response in metaplastic breast carcinoma. *Int J Mol Sci* (2021) 22(14):7398. doi: 10.3390/ijms22147398

108. Pal A, Barrett TF, Paolini R, Parikh A. Puram SV. partial EMT in head and neck cancer biology: A spectrum instead of a switch. *Oncogene* (2021) 40(32):5049–65. doi: 10.1038/s41388-021-01868-5

109. Chattopadhyay I, Ambati R, Gundamaraju R. Exploring the crosstalk between inflammation and epithelial-mesenchymal transition in cancer. *Mediators Inflammation* (2021) 2021:9918379. doi: 10.1155/2021/9918379

110. Shimbo K, Miyaki S, Ishitobi H, Kato Y, Kubo T, Shimose S, et al. Exosome-formed synthetic microRNA-143 is transferred to osteosarcoma cells and inhibits their migration. *Biochem Biophys Res Commun* (2014) 445(2):381–7. doi: 10.1016/j.bbrc.2014.02.007

111. Gong L, Bao Q, Hu C, Wang J, Zhou Q, Wei L, et al. Exosomal miR-675 from metastatic osteosarcoma promotes cell migration and invasion by targeting

CALN1. *Biochem Biophys Res Commun* (2018) 500(2):170–76. doi: 10.1016/j.bbrc.2018.04.016

112. Zhong L, Liao D, Li J, Liu W, Wang J, Zeng C, et al. Rab22a-NeoF1 fusion protein promotes osteosarcoma lung metastasis through its secretion into EVs. *Signal Transduct Target Ther* (2021) 6(1):59. doi: 10.1038/s41392-020-00414-1

113. Mazumdar A, Urdinez J, Boro A, Arlt MJE, Egli FE, Niederost B, et al. Exploring the role of osteosarcoma-derived extracellular vesicles in pre-metastatic niche formation and metastasis in the 143-b xenograft mouse osteosarcoma model. *Cancers (Basel)* (2020) 12(11):3457. doi: 10.3390/cancers12113457

114. Liu CG, Li J, Xu Y, Li W, Fang SX, Zhang Q, et al. Long non-coding RNAs and circular RNAs in tumor angiogenesis: From mechanisms to clinical significance. *Mol Ther Oncolytics* (2021) 22:336–54. doi: 10.1016/j.omto.2021.07.001

115. Aspritoiu VM, Stoica I, Bleotu C, Diaconu CC. Epigenetic regulation of angiogenesis in development and tumors progression: Potential implications for cancer treatment. *Front Cell Dev Biol* (2021) 9:689962. doi: 10.3389/fcell.2021.689962

116. Martin P, Gurevich DB. Macrophage regulation of angiogenesis in health and disease. *Semin Cell Dev Biol* (2021) 119:101–10. doi: 10.1016/j.semcdb.2021.06.010

117. Zhu L, Yu X, Wang L, Liu J, Qu Z, Zhang H, et al. Angiogenesis and immune checkpoint dual blockade in combination with radiotherapy for treatment of solid cancers: Opportunities and challenges. *Oncogenesis* (2021) 10(7):47. doi: 10.1038/s41389-021-00335-w

118. Montanino A, Manzo A, Carillio G, Palumbo G, Esposito G, Sforza V, et al. Angiogenesis inhibitors in small cell lung cancer. *Front Oncol* (2021) 11:655316. doi: 10.3389/fonc.2021.655316

119. Yoshida A, Fujiwara T, Uotani K, Morita T, Kiyono M, Yokoo S, et al. Clinical and functional significance of intracellular and extracellular microRNA-25–3p in osteosarcoma. *Acta Med Okayama* (2018) 72(2):165–74. doi: 10.18926/AMO/55857

120. Tao SC, Huang JY, Wei ZY, Li ZX, Guo SC. EWSAT1 acts in concert with EVs in osteosarcoma progression and tumor-induced angiogenesis: The "Double stacking effect". *Adv Biosyst* (2020) 4(9):e2000152. doi: 10.1002/adbi.202000152

121. Li Y, Lin S, Xie X, Zhu H, Fan T, Wang S. Highly enriched exosomal lncRNA OIP5-AS1 regulates osteosarcoma tumor angiogenesis and autophagy through miR-153 and ATG5. *Am J Transl Res* (2021) 13(5):4211–23.

122. Mao W, Wang K, Wu Z, Xu B, Chen M. Current status of research on EVs in general, and for the diagnosis and treatment of kidney cancer in particular. *J Exp Clin Cancer Res* (2021) 40(1):305. doi: 10.1186/s13046-021-02114-2

123. Wang M, Zhang B. The immunomodulation potential of EVs in tumor microenvironment. *J Immunol Res* (2021) 2021:3710372. doi: 10.1155/2021/3710372

124. Liu J, Ren L, Li S, Li W, Zheng X, Yang Y, et al. The biology, function, and applications of EVs in cancer. *Acta Pharm Sin B* (2021) 11(9):2783–97. doi: 10.1016/j.apsb.2021.01.001

125. Chen H, Chengalvala V, Hu H, Sun D. Tumor-derived EVs: Nanovesicles made by cancer cells to promote cancer metastasis. *Acta Pharm Sin B* (2021) 11(8):2136–49. doi: 10.1016/j.apsb.2021.04.012

126. Zheng H, Siddharth S, Parida S, Wu X, Sharma D. Tumor microenvironment: Key players in triple negative breast cancer immunomodulation. *Cancers (Basel)* (2021) 13(13):3357. doi: 10.3390/cancers13133357

127. Whiteside TL, Diergaarde B, Hong CS. Tumor-derived EVs (TEX) and their role in immuno-oncology. *Int J Mol Sci* (2021) 22(12):6234. doi: 10.3390/ijms22126234

128. Raimondi L, De Luca A, Gallo A, Costa V, Russelli G, Cuscino N, et al. Osteosarcoma cell-derived EVs affect tumor microenvironment by specific packaging of microRNAs. *Carcinogenesis* (2020) 41(5):666–77. doi: 10.1093/carcin/bgz130

129. Wolf-Dennen K, Gordon N, Kleinerman ES. Exosomal communication by metastatic osteosarcoma cells modulates alveolar macrophages to an M2 tumor-promoting phenotype and inhibits tumoricidal functions. *Oncoimmunology* (2020) 9(1):1747677. doi: 10.1080/2162402X.2020.1747677

130. Mazumdar A, Urdinez J, Boro A, Migliavacca J, Arlt MJE, Muff R, et al. Osteosarcoma-derived extracellular vesicles induce lung fibroblast reprogramming. *Int J Mol Sci* (2020) 21(15):5451. doi: 10.3390/ijms21155451

131. Cheng Z, Wang L, Wu C, Huang L, Ruan Y, Xue W. Tumor-derived EVs induced M2 macrophage polarization and promoted the metastasis of osteosarcoma cells through Tim-3. *Arch Med Res* (2021) 52(2):200–10. doi: 10.1016/j.arcmed.2020.10.018

132. Zhang Y, Liu Z, Yang X, Lu W, Chen Y, Lin Y, et al. H3K27 acetylation activated-COL6A1 promotes osteosarcoma lung metastasis by repressing STAT1 and activating pulmonary cancer-associated fibroblasts. *Theranostics* (2021) 11(3):1473–92. doi: 10.7150/thno.51245

133. Zhang H, Yu Y, Wang J, Han Y, Ren T, Huang Y, et al. Macrophages-derived exosomal lncRNA LIFR-AS1 promotes osteosarcoma cell progression *via* miR-29a/NFIA axis. *Cancer Cell Int* (2021) 21(1):192. doi: 10.1186/s12935-021-01893-0

134. Liu W, Long Q, Zhang W, Zeng D, Hu B, Liu S, et al. miRNA-221–3p derived from M2-polarized tumor-associated macrophage EVs aggravates the growth and metastasis of osteosarcoma through SOCS3/JAK2/STAT3 axis. *Aging (Albany NY)* (2021) 13(15):19760–75. doi: 10.18632/aging.203388

135. Cheng Z, Wang L, Wu C, Huang L, Ruan Y, Xue W. Tumor-derived EVs induced M2 macrophage polarization and promoted the metastasis of osteosarcoma cells through Tim-3. *Arch Med Res* (2020) 52(2):200–10. doi: 10.21203/rs.2.23484/v1

136. Hwang S, Yang YM. Exosomal microRNAs as diagnostic and therapeutic biomarkers in non-malignant liver diseases. *Arch Pharm Res* (2021) 44(6):574–87. doi: 10.1007/s12272-021-01338-2

137. Wen H, Peng L, Chen Y. The effect of immune cell-derived EVs in the cardiac tissue repair after myocardial infarction: Molecular mechanisms and preclinical evidence. *J Cell Mol Med* (2021) 25(14):6500–10. doi: 10.1111/jcmm.16686

138. Hosseini R, Asef-Kabiri L, Yousefi H, Sarvnaz H, Salehi M, Akbari ME, et al. The roles of tumor-derived EVs in altered differentiation, maturation and function of dendritic cells. *Mol Cancer* (2021) 20(1):83. doi: 10.1186/s12943-021-01376-w

139. Huda MN, Nafiujjaman M, Deaguero IG, Okonkwo J, Hill ML, Kim T, et al. Potential use of EVs as diagnostic biomarkers and in targeted drug delivery: Progress in clinical and preclinical applications. *ACS Biomater Sci Eng* (2021) 7(6):2106–49. doi: 10.1021/acsbiomaterials.1c00217

140. Xu JF, Wang YP, Zhang SJ, Chen Y, Gu HF, Dou XF, et al. Exosomes containing the differential expression of microRNA and mRNA in osteosarcoma that can predict response to chemotherapy. *Oncotarget.* (2017) 8(44):75968–78. doi: 10.18632/oncotarget.18373

141. Ayers L, Pink R, Carter DRF, Nieuwland R. Clinical requirements for extracellular vesicle assays. *J Extracell Vesicles.* (2019) 8(1):1593755. doi: 10.1080/20013078.2019.1593755

142. Cuscino N, Raimondi L, De Luca A, Carcione C, Russelli G, Conti L, et al. Gathering novel circulating exosomal microRNA in osteosarcoma cell lines and possible implications for the disease. *Cancers (Basel)* (2019) 11(12):1924. doi: 10.3390/cancers11121924

143. Zhang K, Dong C, Chen M, Yang T, Wang X, Gao Y, et al. Extracellular vesicle-mediated delivery of miR-101 inhibits lung metastasis in osteosarcoma. *Theranostics* (2020) 10(1):411–25. doi: 10.7150/thno.33482

144. Ye Z, Zheng Z, Peng L. MicroRNA profiling of serum EVs in patients with osteosarcoma by high-throughput sequencing. *J Investig Med* (2020) 68(4):893–901. doi: 10.1136/jim-2019-001196

145. Zhang H, Wang J, Ren T, Huang Y, Yu Y, Chen C, et al. LncRNA CASC15 is upregulated in osteosarcoma plasma EVs and CASC15 knockdown inhibits osteosarcoma progression by regulating miR-338–3p/RAB14 axis. *Onco Targets Ther* (2020) 13:12055–66. doi: 10.2147/OTT.S282053

146. Cambier L, Stachelek K, Triska M, Jubran R, Huang M, Li W, et al. Extracellular vesicle-associated repetitive element DNAs as candidate osteosarcoma biomarkers. *Sci Rep* (2021) 11(1):94. doi: 10.1038/s41598-020-77398-z

147. Huo S, Dou D. Circ_0056285 regulates proliferation, apoptosis and glycolysis of osteosarcoma cells *via* miR-1244/TRIM44 axis. *Cancer Manag Res* (2021) 13:1257–70. doi: 10.2147/CMAR.S290645

148. Wang L, Wu J, Song S, Chen H, Hu Y, Xu B, et al. Plasma exosome-derived sentrin SUMO-specific protease 1: A prognostic biomarker in patients with osteosarcoma. *Front Oncol* (2021) 11:625109. doi: 10.3389/fonc.2021.625109

149. Han Z, Yi J, Yang Y, Li D, Peng C, Long S, et al. SERS and MALDI-TOF MS based plasma exosome profiling for rapid detection of osteosarcoma. *Analyst* (2021) 146(21):6496–505. doi: 10.1039/d1an01163d.

150. Anderson PM. Effectiveness of radiotherapy for osteosarcoma that responds to chemotherapy. *Mayo Clin Proc* (2003) 78:145–6. doi: 10.4065/78.2.145

151. Schwarz R, Bruland Øyvind S, Cassoni A, Schomberg P, Bielack S. The role of radiotherapy in oseosarcoma. *Cancer Treat Res* (2009) 152:147–64. doi: 10.1007/978-1-4419-0284-9_7

152. Majó J, Cubedo R, Pardo N. Treatment of osteosarcoma. a review. *Rev Esp. Cir. Ortop. Traumatol.* (2010) 54:329–36. doi: 10.1016/S1988-8856(10)70255-8

153. Saraf AJ, Fenger JM, Roberts RD. Osteosarcoma: Accelerating progress makes for a hopeful future. *Front Oncol* (2018) 8:4. doi: 10.3389/fonc.2018.00004

154. Ferrari S, Palmerini E. Adjuvant and neoadjuvant combination chemotherapy for osteogenic sarcoma. *Curr Opin Oncol* (2007) 19:341–6. doi: 10.1097/CCO.0b013e328122d73f

155. Mialou V, Philip T, Kalifa C, Perol D, Gentet J-C, Marec-Berard P, et al. Metastatic osteosarcoma at diagnosis: Prognostic factors and long-term outcom–the French pediatric experience. *Cancer* (2005) 104:1100–9. doi: 10.1002/cncr.21263

156. Lee KM, An JH, Yang SJ, Park SM, Lee JH, Chae HK, et al. Influence of canine macrophage-derived extracellular vesicles on apoptosis in canine melanoma and osteosarcoma cell lines. *Anticancer. Res* (2021) 41:719–30. doi: 10.21873/anticanres.14823

157. Xu Z, Zhou X, Wu J, Cui X, Wang M, Wang X, et al. Mesenchymal stem cell-derived exosomes carrying microRNA-150 suppresses the proliferation and migration of osteosarcoma cells *via* targeting IGF2BP1. *Transl Cancer Res* (2020) 9:5323–35. doi: 10.21037/tcr-20-83

158. Killingsworth B, Welsh JA, Jones JC. EV translational horizons as viewed across the complex landscape of liquid biopsies. *Front Cell Dev Biol* (2021) 9:556837. doi: 10.3389/fcell.2021.556837

159. Clark RA, Garman ZG, Price RJ, Sheybani ND. Functional intersections between extracellular vesicles and oncolytic therapies. *Trends Pharmacol Sci* (2021) 42(11):883–96. doi: 10.1016/j.tips.2021.09.001

160. Gaglani S, Gonzalez-Kozlova E, Lundon DJ, Tewari AK, Dogra N, Kyprianou N. EVs as a next-generation diagnostic and therapeutic tool in prostate cancer. *Int J Mol Sci* (2021) 22(18):131. doi: 10.3390/ijms221810131

161. Mkhobongo B, Chandran R, Abrahamse H. The role of melanoma cell-derived EVs (MTEX) and photodynamic therapy (PDT) within a tumor microenvironment. *Int J Mol Sci* (2021) 22(18):131. doi: 10.3390/ijms221810131

162. Prieto-Vila M, Yoshioka Y, Ochiya T. Biological functions driven by mRNAs carried by extracellular vesicles in cancer. *Front Cell Dev Biol* (2021) 9:620498. doi: 10.3389/fcell.2021.620498

163. Deng Y, Sun Z, Wang L, Wang M, Yang J, Li G. Biosensor-based assay of exosome biomarker for early diagnosis of cancer. *Front Med* (2021) 16(2):157–75. doi: 10.1007/s11684-021-0884-z

164. Nie H, Liao Z, Wang Y, Zhou J, He X, Ou C. Exosomal long non-coding RNAs: Emerging players in cancer metastasis and potential diagnostic biomarkers for personalized oncology. *Genes Dis* (2021) 8(6):769–80. doi: 10.1016/j.gendis.2020.12.004

165. Jing Z, Chen K, Gong L. The significance of EVs in pathogenesis, diagnosis, and treatment of esophageal cancer. *Int J Nanomed* (2021) 16:6115–27. doi: 10.2147/IJN.S321555

166. Torreggiani E, Roncuzzi L, Perut F, Zini N, Baldini N. Multimodal transfer of MDR by exosomes in human osteosarcoma. *Int J Oncol* (2016) 49(1):189–96. doi: 10.3892/ijo.2016.3509

167. Nawaz M, Fatima F, Nazarenko I, Ekström K, Murtaza I, Anees M, et al. Extracellular vesicles in ovarian cancer: Applications to tumor biology, immunotherapy and biomarker discovery. *Expert Rev Proteomics.* (2016) 13:395–409. doi: 10.1586/14789450.2016.1165613

168. Mc Namee N, O'Driscoll L. Extracellular vesicles and anti-cancer drug resistance. *Biochim Biophys Acta* (2018) 1870:123–36. doi: 10.1016/j.bbcan.2018.07.003

169. Ng CY, Chai JY, Foo JB, Mohamad Yahaya NH, Yang Y, Ng MH, et al. Potential of EVs as cell-free therapy in articular cartilage regeneration: A review. *Int J Nanomed* (2021) 16:6749–81. doi: 10.2147/IJN.S327059

170. Claridge B, Lozano J, Poh QH, Greening DW. Development of extracellular vesicle therapeutics: Challenges, considerations, and opportunities. *Front Cell Dev Biol* (2021) 9:734720. doi: 10.3389/fcell.2021.734720

171. Matheakakis A, Batsali A, Papadaki HA, Pontikoglou CG. Therapeutic implications of mesenchymal stromal cells and their extracellular vesicles in autoimmune diseases: From biology to clinical applications. *Int J Mol Sci* (2021) 22(18):132. doi: 10.3390/ijms221810132

172. Han S, Li G, Jia M, Zhao Y, He C, Huang M, et al. Delivery of anti-miRNA-221 for colorectal carcinoma therapy using modified cord blood mesenchymal stem cells-derived EVs. *Front Mol Biosci* (2021) 8:743013. doi: 10.3389/fmolb.2021.743013

173. Li T, Tao Z, Zhu Y, Liu X, Wang L, Du Y, et al. Exosomal annexin A6 induces gemcitabine resistance by inhibiting ubiquitination and degradation of EGFR in triple-negative breast cancer. *Cell Death Dis* (2021) 12(7):684. doi: 10.1038/s41419-021-03963-7

174. Ning T, Li J, He Y, Zhang H, Wang X, Deng T, et al. Exosomal miR-208b related with oxaliplatin resistance promotes treg expansion in colorectal cancer. *Mol Ther* (2021) 29(9):2723–36. doi: 10.1016/j.ymthe.2021.04.028

frontiers | Frontiers in Immunology

TYPE Original Research
PUBLISHED 06 October 2022
DOI 10.3389/fimmu.2022.942192

OPEN ACCESS

EDITED BY
Nimesh Gupta,
National Institute of Immunology (NII), India

REVIEWED BY
Yongjun Sui,
National Cancer Institute (NIH), United States
Maryna Skok,
Palladin Institute of Biochemistry (NAS Ukraine), Ukraine

*CORRESPONDENCE
Beatriz Suarez-Alvarez
beatriz.suarez@ispasturias.es;
bsuarez@hca.es

†These authors have contributed equally to this work

SPECIALTY SECTION
This article was submitted to Viral Immunology, a section of the journal Frontiers in Immunology

RECEIVED 12 May 2022
ACCEPTED 16 September 2022
PUBLISHED 06 October 2022

CITATION
Salgado Del Riego E, Saiz ML, Corte-Iglesias V, Leoz Gordillo B, Martin-Martin C, Rodríguez-Pérez M, Escudero D, Lopez-Larrea C and Suarez-Alvarez B (2022) Divergent SARS-CoV-2-specific T cell responses in intensive care unit workers following mRNA COVID-19 vaccination. *Front. Immunol.* 13:942192. doi: 10.3389/fimmu.2022.942192

Divergent SARS-CoV-2-specific T cell responses in intensive care unit workers following mRNA COVID-19 vaccination

Estefanía Salgado Del Riego[1,2†], María Laura Saiz[3†], Viviana Corte-Iglesias[3], Blanca Leoz Gordillo[1], Cristina Martin-Martin[3], Mercedes Rodríguez-Pérez[4,5], Dolores Escudero[1,5], Carlos Lopez-Larrea[3,6] and Beatriz Suarez-Alvarez[3*]

[1]Servicio de Medicina Intensiva, Hospital Universitario Central de Asturias, Oviedo, Spain, [2]Instituto de Investigación Sanitaria del Principado de Asturias (ISPA), Oviedo, Spain, [3]Translational Immunology, Instituto de Investigación Sanitaria del Principado de Asturias (ISPA), Hospital Universitario Central de Asturias, Oviedo, Spain, [4]Servicio de Microbiología, Hospital Universitario Central de Asturias, Oviedo, Spain, [5]Translational Microbiology, Instituto de Investigación Sanitaria del Principado de Asturias (ISPA), Hospital Universitario Central de Asturias, Oviedo, Spain, [6]Servicio de Inmunología, Hospital Universitario Central De Asturias, Oviedo, Spain

The cellular immune response to severe acute respiratory syndrome coronavirus 2 (SARS-CoV-2) in response to full mRNA COVID-19 vaccination could be variable among healthy individuals. Studies based only in specific antibody levels could show an erroneous immune protection at long times. For that, we analyze the antibody levels specific to the S protein and the presence of SARS-CoV-2-specific T cells by ELISpot and AIM assays in intensive care unit (ICU) workers with no antecedents of COVID-19 and vaccinated with two doses of mRNA COVID-19 vaccines. All individuals were seronegative for the SARS-CoV-2 protein S before vaccination (Pre-v), but 34.1% (14/41) of them showed pre-existing T lymphocytes specific for some viral proteins (S, M and N). One month after receiving two doses of COVID-19 mRNA vaccine (Post-v1), all cases showed seroconversion with high levels of total and neutralizing antibodies to the spike protein, but six of them (14.6%) had no T cells reactive to the S protein. Specifically, they lack of specific $CD8^+$ T cells, but maintain the contribution of $CD4^+$ T cells. Analysis of the immune response against SARS-CoV-2 at 10 months after full vaccination (Post-v10), exhibited a significant reduction in the antibody levels ($p<0.0001$) and protein S-reactive T cells ($p=0.0073$) in all analyzed individuals, although none of the individuals become seronegative and 77% of them maintained a competent immune response. Thus, we can suggest that the immune response to SARS-CoV-2 elicited by the mRNA vaccines was highly variable among ICU workers. A non-negligible proportion of individuals did not develop a specific T cell response mediated by $CD8^+$ T cells after vaccination, that may condition the susceptibility to further viral infections with SARS-CoV-2. By contrast, around 77% of individuals developed strong humoral and cellular immune responses to SARS-CoV-2 that persisted even after 10 months. Analysis of the cellular

10.3389/fimmu.2022.942192

immune response is highly recommended for providing exact information about immune protection against SARS-CoV-2.

KEYWORDS

SARS-CoV-2, specific T-cell response, intensive care unit workers, vaccination, ELISpot, $CD4^+$ T cells, $CD8^+$ T cells

Introduction

Since the first vaccine against SARS-CoV-2 was approved by the regulatory agencies and millions of people around the world were vaccinated, the pandemic has been analyzed from a different perspective. New questions arising about such matters as the long-term effectiveness of the vaccines, the number of doses or boosters needed, and how interindividual variability is affected, have only been partially answered. We know that mRNA vaccines, in particular Pfizer-BioNTech (BNT162b2, Comirnaty) and Moderna (mRNA-1273, Spikevax), provide up to 95% protection against COVID-19 (1, 2), but the level of specific neutralizing antibodies against the S protein diminish over time. Consequently, a third booster dose, even fourth, is being administered to the most vulnerable population, including aged people and health care workers, as well as to the general population (3, 4).

Most of the relevant studies done so far have been based on antibody levels but it remains partially unclear whether the individuals who have received two doses of vaccine have developed a long-term protective cellular response against SARS-CoV-2 and, more important still, whether all healthy people are adequately immunized after these two doses. To investigate this, we focus on a cohort of COVID-19 intensive care unit (ICU) workers, who are one of the groups who have been at high risk of infection from the start of the pandemic until the present time. The seroprevalence of SARS-CoV-2 antibodies among these workers has been extensively analyzed, not only to measure the effectiveness of vaccines since they were one of the earliest groups to be vaccinated, but also to ensure their safety and the success of the measures adopted to contain the infection against new variants (5).

Studies in healthcare workers, who are comparable to other healthy individuals, showed that vaccination induces higher antibodies levels in people previously exposed to SARS-CoV-2, and that one dose is enough to produce the maximum antibodies levels and to maintain them for up to 1 year (6). However, in unexposed healthy workers, two doses are required to obtain robust humoral immunity, and this declines over time, leading to the advocation of the administration of a booster vaccine shot (7). In relation to the cellular immune response, numerous studies have evaluated its strength and durability after mRNA vaccination in healthy people (8–13), but also in older people (14, 15), or in patients with some immunodeficiencies (16–19). Studies in unexposed healthy people showed that a robust humoral and cellular response is triggered in response to second vaccination, although first-dose mRNA vaccination is enough to trigger the immunological memory in COVID-19-recovered subjects (20, 21). Combined analysis of SARS-CoV-2 mRNA vaccines revealed a coordinated immune response mediated by a rapid antigen-specific $CD4^+$ T cell response followed by a gradual development of $CD8^+$ T cells more variable in magnitude (22). Specifically, circulating T follicular helper (Tfh) cells represent a key fraction of specific $CD4^+$ T cells being crucial for the development of memory B cells, plasma cells and support antibody response following vaccination (23). First studies with BNT162b1 showed that two doses are required to elicit a robust $CD4^+$ (100% responders) and $CD8^+$ T (85% responders) cell response, with a favorable Th1 profile that enhances the quality of cytotoxic cells (12). Spike-specific $CD4^+$ (100% responders) and $CD8^+$ T (87% responders) cells responses peaked after the second dose of the mRNA-1273 vaccine and were largely maintained up to 6 months after vaccination, with a decline mainly in $CD8^+$ T cells (9). Memory spike-specific $CD8^+$ T cells produce mainly IFN-γ and co-express granzyme B exhibiting an effector memory surface phenotype. Oberhardt V et al. (24) showed that these vaccine-elicited $CD8^+$ T cells are early mobilized, one week after the first dose, when $CD4^+$ T cells and antibodies are undetectable and undergo a robust expansion after the second dose generating a pool of highly differentiated $CD8^+$ T cells with a relevant effector function. Recently, it has also been reported that the frequency of stem cell-like memory (T_{SCM}) cells one-two weeks post-second vaccination determinates the longevity of memory $CD8^+$ T cells induced by SARS-CoV-2 mRNA vaccines (25). SARS-CoV-2-reactive T and B cells persist over time even as the levels of antibodies decline, suggesting that the vaccines do provide durable protection against severe disease (26) and against new variants (27). However, we cannot discount the possibility that interindividual variability might lead to heterogeneous immune responses that will condition the durability of the protection from SARS-CoV-2 infection and COVID-19 disease, even in individuals who are not of older ages or immunocompromised (28).

The aim of this study was to establish the genuine degree of protection against SARS-CoV-2 in ICU workers who have been highly exposed to the virus, and to determine how long the protection lasts after vaccination. Using the T ELISpot and flow cytometry activation induced marker (AIM) assays, we analyzed the SARS-CoV-2- T cells that are reactive against the main structural viral proteins —spike (S), membrane (M) and nucleocapsid (N) — before vaccination, to establish the influence of a pre-existing response, and 1 and 10 months after full vaccination with mRNA vaccines, to analyze the durability of the anti-viral immune response and the requirement for additional boosters.

Results

Pre-existing T cells against SARS-CoV-2 proteins in highly exposed ICU workers

The primary aim of this study was to analyze the presence of SARS-CoV-2-specific T cells in COVID-19 ICU workers who had been highly exposed to the virus during the first (March 2020) and second (November 2020) pandemic waves in Spain and who remained unvaccinated (Figure 1A). None of the participants (n=41) had a history of SARS-CoV-2, COVID-19 disease, or household contact with SARS-CoV-2-positive people (Table 1). Initially, we determined the number of SARS-CoV-2-specific memory T cells by using the ELISpot assay to determine the IFN-γ-producing cells. For that, PBMCs were stimulated with overlapping peptides pools spanning the three main structural proteins of SARS-CoV-2, the spike (S), membrane (M) and nucleocapsid (N) proteins. We found 14 of the 41 individuals (34.1%) to have pre-existing T lymphocytes specific for at least one of the three analyzed SARS-CoV-2 structural proteins (Figure 1B). The dominant target of the pre-existing SARS-CoV-2-specific T cells was the M protein (detected in 9/41 of the samples; 22.0%), followed by the S protein (7/41; 17.1%) and the N protein (5/41; 12.2%) (Figure 1B). The distribution of these specific T cells varied considerably between individuals: some showed reactivity against one or two proteins, and two individuals reacted against all three SARS-CoV-2 proteins (Supplementary Figure 1A). Moreover, we determined the presence of antibodies specific to the S and N proteins (Figure 2A), showing absence of both antibodies in all individuals and corroborating the lack of asymptomatic COVID-19.

To elucidate whether the presence of pre-existing T cells against SARS-CoV-2 proteins are due to the continuous exposition to the virus in COVID-19 ICUs, we assayed a cohort of 20 healthy donors obtained in pre-pandemic time, between 2007 and 2013 years (Table 1). A total of 7 out of 20 (35%) pre-pandemic donors showed reactivity and respond to the viral proteins with a similar frequency to the one detected in ICU workers (Figure 1C). Again, the specific T cell response against the M protein was the majority (25% of samples) followed by the one against the N (15%) and S proteins (10%), suggesting a major role of the M protein in the development of cross-reactivity against other coronaviruses. To further understand the magnitude of the cellular immune response developed after exposition to the SARS-CoV-2 virus, we compared the levels of these pre-existing T cells with the observed in COVID-19 convalescent patients with mild or severe infection (Table 1). All patients were diagnosed by PCR and have S- and N-reactive IgG antibodies. The development of specific T lymphocytes against the three structural proteins of the virus was detected in all COVID-19 patients at high levels, indicating that the cellular response triggered under virus exposition was clearly higher than the one observed in unexposed individuals, ICU workers and pre-pandemic donors (Figure 1D).

In order to corroborate the results obtained by ELISpot assay and discriminate the contribution of SARS-CoV-2-specific $CD4^+$ and $CD8^+$ T cell responses, we performed AIM assay in samples obtained from ICU workers. The gating strategy used and representative flow cytometry plots of one ICU worker and one COVID-19 patient is showed in Supplementary Figure 2 and Figure 1E. We detect the presence of antigen-specific T cells in all analyzed samples, being in some individuals mediated by $CD4^+$ T (Figure 1F) cells and by $CD8^+$ T (Figure 1G) lymphocytes in others, but no correlation between them was observed for any protein (Supplementary Figure 1B). However, when the contribution of $CD4^+$ and $CD8^+$ T cells for each individual was added, all individuals showed a positive response (Figure 1H), and the distribution of positive specific T cells was identical between ELISpot and AIM assays (Supplementary Figure 1C), showing the utility of both methods to detect pre-existing T cells against SARS-CoV-2 and their effector ability secreting IFN-γ. As we have previously reported by ELISpot assay, the magnitude of cellular response determined by AIM assay was slightly higher against M protein, and mainly mediated by $CD4^+$ T cells.

Altogether, some ICU workers showed a specific cellular response against SARS-CoV-2 proteins, at similar levels to pre-pandemic donors, probably because of the cross-reactivity between SARS-CoV-2 and other coronaviruses or viruses, and not by the continuous exposition to the virus in the COVID-19 units. That pre-existing immunity is associated with the contribution of both $CD4^+$ and $CD8^+$ T cells, but variable among individuals.

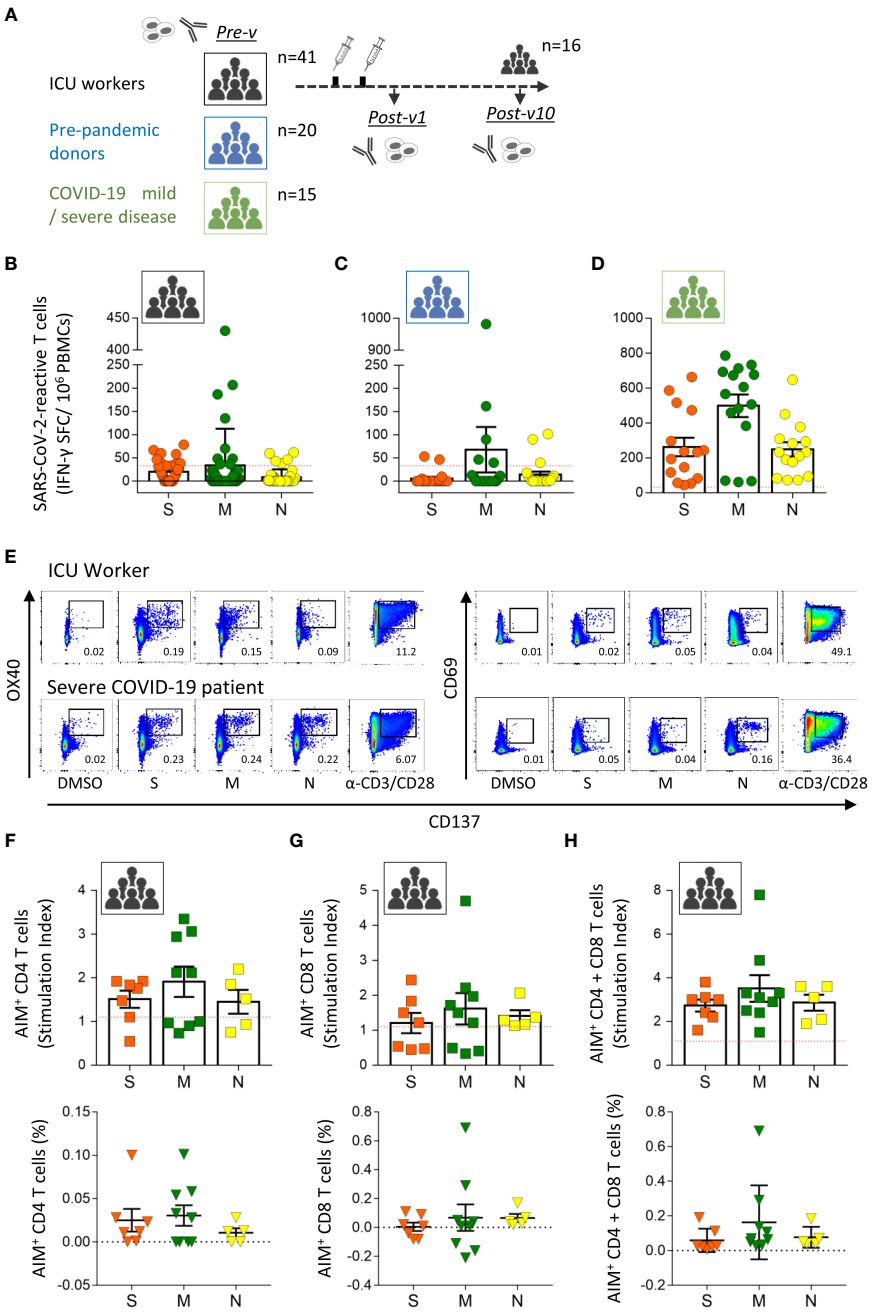

FIGURE 1
Pre-existing SARS-CoV-2-specific T cells in healthy ICU workers. **(A)** Study design. Blood samples were taken from intensive care unit workers with no known antecedents of COVID-19 before vaccination (n=41, Pre-v), and 1 month (n=41, Post-v1) and 10 months (n=16, Post-v10) after receiving two doses of the mRNA vaccine. Pre-pandemic healthy donors (n=20) and COVID-19 convalescent patients (n=15) with mild and severe disease were used as control groups. Antibody levels and SARS-CoV-2-reactive T cells were assayed at the indicated times. Frequencies of IFN-γ-producing T cells assayed by ELISpot assay against spike (S, orange circles), membrane (M, green circles) and nucleocapsid (N, yellow circles) proteins in samples from ICU workers **(B)** taken before vaccination, pre-pandemic healthy donors **(C)** and convalescent patients recovered from COVID-19 **(D)**. Data from ELISpot assays are depicted as the number of spot-forming cells (SFCs) per 1 x 10^6 PBMCs. The red dashed line shows the established cut-off (≥33.3 SFCs/10^6 cells) after subtraction of negative control values. **(E)** Flow cytometry dot plots from one ICU workers showing the representative gating strategy to identify antigen specific $CD4^+$ ($CD3^-$ $CD4^+$ $OX40^+$ $CD137^+$) and $CD8^+$ ($CD3^-$ $CD8^+$ $CD69^+$ $CD137^+$) T cells by AIM assay. A patient with severe COVID-19 was reference as positive control. DMSO and polyclonal induction with anti-CD3/CD28 antibodies were used as negative and positive controls of stimulation for each sample. Numbers in dot plots represent the percentage of AIM^+ cells in each indicated square. Number of CD4+ **(F)**, $CD8^+$ **(G)** T cells or both **(H)** detected by AIM assay against spike (S, orange squares, n=7), membrane (M, green squares, n=9) and nucleocapsid (N, yellow squares, n=5) proteins in samples from ICU workers that were positive by ELISpot assay. Data from AIM assay are represented as stimulation index (SI, squares) and frequency (triangles). Red dashed line represents the limit of positivity for SI > 1.1. All data are represented as mean ± SEM.

10.3389/fimmu.2022.942192

TABLE 1 Characteristics of individuals groups under study.

	ICU workers	Pre-pandemic	Mild/Severe COVID-19
N° of participants; n	41	20	15
Male/Female; n	9/32	12/8	12/3
Age; median ± SD	39 ± 12.31	40 ± 12.09	62 ± 9.08
SARS-CoV-2 infection by RT-PCR, n (%)	0	0	15 (100%)
Comorbidities, n (%)			
Heart disease	0	0	2 (13.3)
Diabetes Mellitus	1 (2.4)	0	4 (26.6)
Hypertension	0	0	10 (66.6)
Cancer	0	0	0
Pulmonary disease	0	0	5 (33.3)
Medications, n (%)			
Statins	3 (7.3)	–	4 (26.6)
Levothyroxine	6 (14.6)	–	0
ARA II	0	–	9 (60)
Immunosuppressant	0	–	0

(-) not determined.

Divergent cell-mediated immune response induced by SARS-CoV-2 mRNA vaccination

Following these results, the humoral and cellular immune responses were analyzed in the same individuals 1 month (Post-v1) after receiving two doses of COVID-19 vaccine, with the aim of determining whether the pre-existing immunity might condition the immune response to the vaccines. Only the reactivity against the S protein could be analyzed since all the approved mRNA COVID19 vaccines have been designed to act on the S protein. To corroborate the effectiveness of vaccination, we measured seroconversion, and found that all individuals developed high levels of anti-S protein antibodies, with titers >200 AU/ml in all cases, although the levels varied among samples (Figure 2A). Moreover, SARS-CoV-2 nucleocapsid-reactive IgG was not detected in any sample showing that no asymptomatic COVID19 infection was experimented by these ICU workers during the time of the study (Figure 2B). As positive control group, we determine the presence of anti-S and anti-N immunoglobulins in five COVID19 patients, being all the detected values upper than the superior limit of the assays (Figures 2A, B). Besides, we analyzed the presence of neutralizing antibodies using a surrogate virus neutralization assay based on the ability of the antibodies to neutralize the RBD (receptor binding domain of the spike protein)-ACE2 interaction. Results are shown as the percentage of neutralization potential (Figure 2C) and the antibodies titers (Figure 2D). In both cases, we observed the induction of high levels of neutralizing antibodies in all ICU workers after one moth having received the full vaccination. Moreover, a significant correlation between the titers of neutralizing and anti-S IgG antibodies (Figure 2E) suggest that most of the antibodies induced after vaccination are able to block the virus entry.

Next, we analyzed the presence of S-protein-specific T cells by ELISpot assay and most of the individuals developed a strong cellular response; IFN-γ-Spot Forming Cells (SFC), Pre-v: 19.8 ± 20.64; Post-v1: 108 ± 97.86; $p<0.0001$ (Figure 3A). Surprisingly, we observed that six individuals (6/41; 14.6%) did not develop any SARS-CoV-2-reactive T cells showing a number of S-protein-reactive T cells below of the established detection limit (SFC ≤ $33.3/10^6$ of PBMCs) (Figure 3B). These individuals were named "Null responders". Moreover, to analyze the cellular immune response specific against SARS-CoV-2 only as consequence of vaccination, we compared the number of pre-existing specific-T cells against the S protein (Pre-v) from the number of S protein-reactive T cells obtained 1 month after vaccination (Post-v1). We observed that of the seven individuals with pre-existing T cells against S protein, five showed similar levels of SARS-CoV-2-specific T cells to those they had before vaccination (Figure 3B), suggesting there was no increased response to vaccination ("Equal to Pre-v" group), and only two developed a stronger cellular immune response after vaccination, despite the presence of pre-existing T cells. Together, these results indicated that whereas 30 individuals (73.2%, named "Responders") developed a moderate or elevated number of S-specific T cells, 11 (26.8%), showed a number of specific-T cells below the established cut-off or at equal levels before vaccination (named "Non-responders") (Figures 3B, C). Thus, nearly one out of four healthy individuals do not reach a strong and effective cellular immunity against SARS-CoV-2 after receiving two doses of the vaccine, despite the high titer of specific antibodies developed.

According to this, no significant correlation was found between the humoral and cellular immune responses assayed by ELISpot assay one month after full vaccination (Supplemental Figure 3A). Moreover, the absence of SARS-CoV-2-specific T cells was not associated with any clinical parameter, treatment or diagnosed immune condition in these ICU workers (data not shown). However, patient chronological age was significantly correlated with the antibody titer, although not with the cellular immune response (Supplemental Figures 3B, C). Younger ICU workers showed a higher titer of S protein-specific antibodies. These correlations were similar when neutralizing antibodies were taken into account, showing a significant correlation with age but not with the cellular response (Supplemental Figures 3D, E).

To corroborate the results found in the cellular response by a different method, we performed AIM assay in seven samples from "Responders" and six samples from "Null responders" groups.

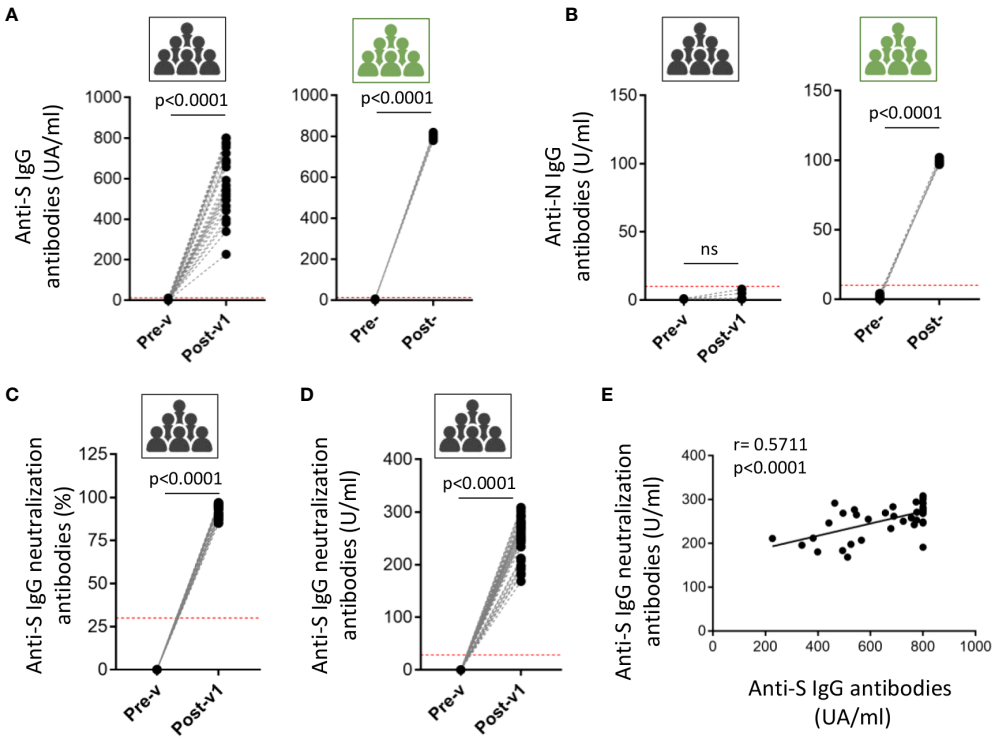

FIGURE 2
Induced humoral response in ICU workers after COVID-19 mRNA vaccination. The antibodies titer against full-length spike (S) protein **(A)** and nucleocapsid (N) protein **(B)** was quantified in serum samples from ICU workers (black icons) at times previous to vaccination (Pre-v) and one month after full vaccination (Post-v1), and from five COVID-19 convalescent patients with severe disease (green icons) determined before (Pre-) and after (Post-) infection. Neutralizing antibodies were measured in serum samples from ICU workers (black icons) at times previous to vaccination (Pre-v) and one month after full vaccination (Post-v1) and data are represented as the inhibition percentage **(C)** and quantified by units per ml (U/ml) **(D)**. Red dotted-lines in panels **(A-D)** mark the limit of positivity. Statistical comparisons were performed by Wilcoxon test. **(E)** Correlation between frequencies of the titers of neutralizing and total anti-S IgG antibodies in ICU workers one month after full vaccination. Statistical by Spearman correlation coefficient. ns, not significant.

Unexpectedly, we detect that both ICU workers groups developed AIM$^+$ CD4$^+$ T cells ("Responders": 0.1629 ± 0.0241; "Null-responders": 0.1317 ± 0.0322; p=0.4679) (Figure 3D), whereas only "Responders" individuals showed a strong AIM$^+$ CD8$^+$ T cell-mediated response cells ("Responders": 0.2271 ± 0.0249; "Null-responders": 0.03167 ± 0.0047; p=0.0012) (Figure 3E). That is supported by the significant correlation observed between S-protein reactive T cells assayed by ELISpot and spike AIM$^+$ CD8$^+$ T cells (p=0.011), and not with spike AIM$^+$ CD4$^+$ T cells (p=0.9291) (Figures 3F, G). Moreover, in these analyzed individuals, no significant correlation between AIM$^+$ CD4+ T cells and total IgG and neutralizing antibodies titers was observed (data not shown). Thus, these results suggest that the absence of cellular response detected in the "Null responders" group by ELISpot assay could be consequence of the lack of a specific immune response against the S protein mediated by CD8$^+$ T cells, the main effector cells producing IFN-γ.

An early immune response might condition the durability of the immunological memory to SARS-CoV-2

Subsequently, the persistence of the long-term immune response to SARS-CoV-2 was assayed in a small number of individuals (n=16), from the collection of samples 10 months after full vaccination (Post-v10). Overall significant decreases in anti-spike immunoglobulins (p<0.0001), percentage (p<0.0001) and titer of neutralizing antibodies (p<0.0001) in plasma samples were observed in all individuals (Figures 4A–C). As expected, no anti-nucleocapsid antibodies were observed in ICU workers (data not shown), because of mRNA vaccines are aimed against spike protein and no one was infected with SARS-CoV-2 during this time after vaccination. The specific antibody levels declined in the long term, but any samples became seronegative during this time.

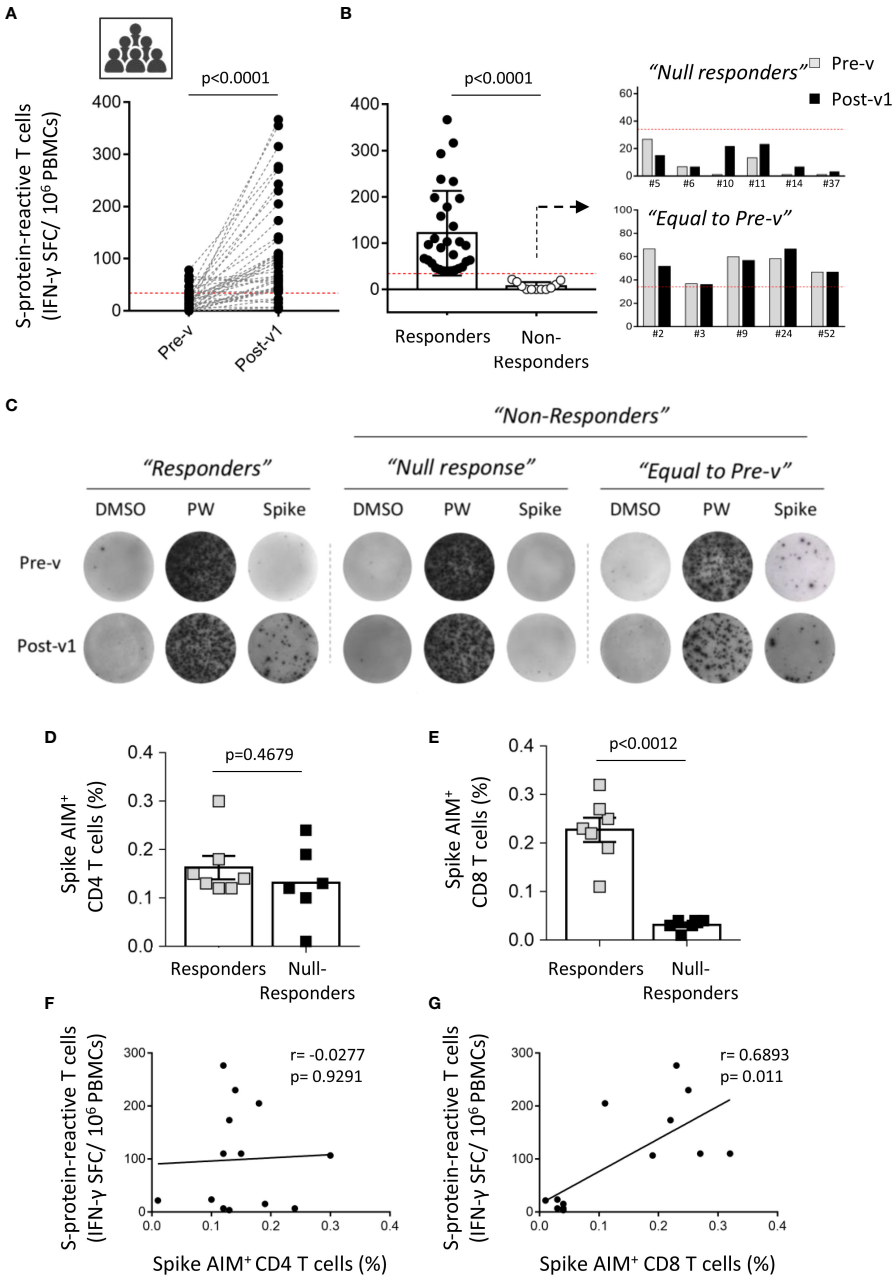

FIGURE 3
Interindividual variation of the cellular immune response to SARS-CoV-2 after COVID-19 mRNA vaccination. **(A)** Paired graph showing the number of specific T cells reactive against the S protein was evaluated by ELISpot assay in PBMCs from ICU workers (n=41) obtained before vaccination (Pre-v) and 1 month (Post-v1) after full vaccination. Statistical comparisons were performed by Wilcoxon test. **(B)** Frequency of spike-specific T cells detected by ELISpot assay in samples with a positive response ("Responders") o those with a null response ("Non-responders"). The latter were divided in "Null responders" when the number of specific T cells was below the cut-off (<33.3 SFCs/10^6 PBMCs) and "Equal to Pre-v" when the number of specific T cells is not enhanced after vaccination. **(C)** Representative images of IFN-γ-inducing spots in "Responders" and "Non-responders" groups. **(D, E)** Percentage of spike AIM$^+$ CD4$^+$ and CD8$^+$ T cells in seven individuals from "Responders" group and six samples that lack of cellular response to SARS-CoV-2 ("Null responders" group). Statistical comparisons were performed by two tail Mann Whitney test. **(F, G)** Correlation between frequencies of spike AIM$^+$ CD4$^+$ and CD8$^+$ T cells and the number of spike-reactive T cells evaluated by ELISpot assay in the individuals corresponding to "Responders" (n=7) and "Null responders" (n=6) groups. Statistical was performed by Spearman correlation coefficient.

10.3389/fimmu.2022.942192

Again, the correlation between total anti-spike IgG and neutralizing antibodies was highly significant (p=0.0003; Figure 4D), suggesting that the decrease in the number of specific antibodies goes in hand with the reduction in their neutralizing ability. When the cellular response was analyzed, we also observed a significant contraction or reduction of the specific T cell number over time (p=0.0073) (Figure 4E). The comparison of the humoral and cellular immune responses detected at ten months after vaccination (Post-v10), revealed that all individuals showed a reduction in the antibody and specific T cells levels, but maintain neutralizing antibodies levels upper than the detection limit. Moreover, only three individuals showed a decline in the specific-T cell count to levels below the cut-off compared with the number of specific T cells elicited at one month after vaccination (Figure 4F). On the other hand, 76.9% (10/13) of individuals with a positive cellular response after 1 month still had a competent immune response 10 months after receiving their second dose. As expected, individuals (n=3) who lacked positive T cells against the S protein one month after vaccination (Post-v1) remained

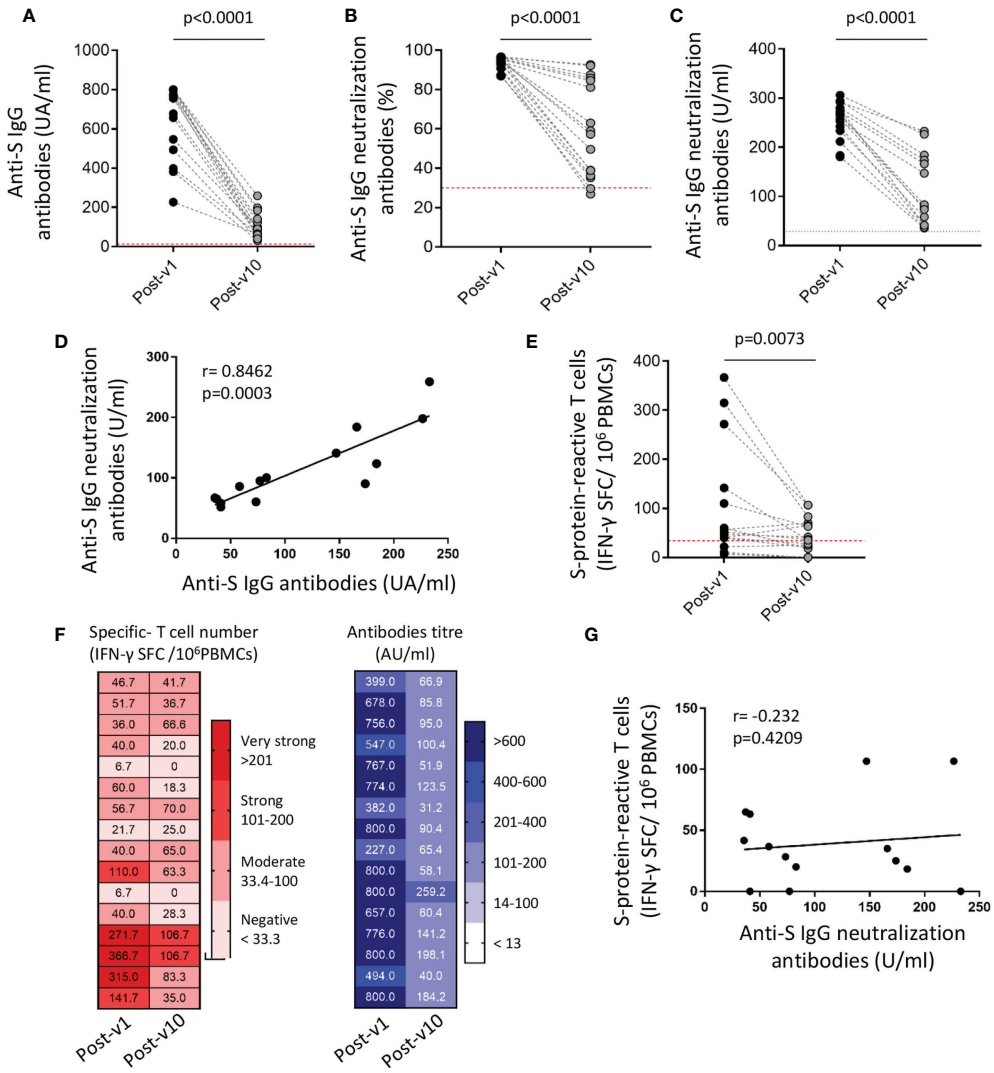

FIGURE 4
SARS-COV-2-specific humoral and cellular immune responses decline over time but persist 10 months after vaccination. The titer of anti-S IgG and neutralizing antibodies **(A–C)**, the correlation between them **(D)** and the frequency of S protein-specific T cells **(E)** were assayed in blood samples (n=16) obtained 1 month (Post-v1) and 10 months (Post-v10) after full vaccination. **(F)** Global distribution of the number of specific T cells (left) and total S IgG titers (right) in samples (n=16) obtained at 10 months (Post-v10) after receiving the second dose of the vaccine, and comparison with the values obtained at 1 month (Post-v1) after vaccination. Numbers indicate the S-specific T cells number and antibodies titers and each line represents one ICU worker. **(G)** Correlation between neutralizing antibodies and the number of spike-reactive T cells in ICU workers at 10 months after full vaccination. Statistical comparisons were performed by Wilcoxon test and correlation with Spearman correlation coefficient.

negative. Despite that both humoral and cellular immune responses are decreased, again no correlation between them was observed (Figure 4G).

In conclusion, most of the individuals maintain a stable repertoire of T cells and antibodies specific to SARS-CoV-2 ten months after having received full vaccination, and those with the highest levels of specific antibodies and cells one month after vaccination are the ones who experienced the least reduction over time. Although more studies are required to ensure strong conclusions, our results provide insights that the immune response reached initially after vaccination could condition the durability of an effective immune response.

Discussion

Although progress continues to be made to understand the humoral and immune responses arising from the administration of COVID-19 mRNA vaccines, many questions remain unanswered and may only be resolved with time and as the pandemic naturally evolves. In the meantime, a range of scenarios need to be analyzed, taking into account the diversity among individuals and the immune history of each. Here, we analyzed the immune response against SARS-CoV-2 over time in healthy individuals, COVID-19 intensive care unit workers who were not infected during the first or second waves of the pandemic in Spain and who received two doses of vaccine by February/March 2021.

The main findings of our study were that: (i) before vaccination, and in the absence of specific antibodies, 34.1% of individuals had T cells that reacted against some of the main structural proteins of SARS-CoV-2, mainly the M protein, and remarkably, this percentage resembles to that one detected in pre-pandemic healthy donors; (ii) all individuals showed high neutralizing antibody titers 1 month after full vaccination, although 14.6% of them had not developed any S-specific T cells by ELISpot assay; (iii) when the contribution of $CD4^+$ and $CD8^+$ T cells was independently analyzed, we observe a lack of cellular response mediated by $CD8^+$ T cells in these "Null responders" individuals; (iv) there were clear long-term declines in the humoral and cellular immune responses, although negative seroconversion was not detected in any individual 10 months after full vaccination, and of greater relevance, still 76.9% of the individuals with a positive cellular response at 1 month after vaccination showed values of specific T cells above the limit of positivity at long-term; and (v) no correlation between humoral and cellular immune responses was observed at any time after full vaccination. Thus, our findings indicate that in healthy individuals whose immune system responded properly to the vaccination against the SARS-CoV-2 S protein, the humoral and cellular immunity that developed early on are specific and durable; however, a small but far from negligible proportion of people, around 15%, did not develop a T cell response, regardless of their age or known history of immunodeficiency.

Several studies have reported the existence of SARS-CoV-2-reactive T cells in SARS-CoV-2-unexposed healthy people (29–34). Braun and colleagues (35) reported that around 35% of seronegative SARS-CoV-2-unexposed healthy donors had $CD4^+$ T cells that were reactive mainly against the C-terminal portion of the SARS-CoV-2-S protein, although this was a lower proportion than in COVID-19 patients. Similarly, in our cohort of ICU healthy workers, around 34% of the samples showed T cells reactive against SARS-CoV-2 proteins, and the number of specific T cells was considerably reduced compared to the observed in COVID-19 convalescent patients. Additional studies of geographically diverse cohorts reported that 20-50% of healthy donors unexposed to SARS-CoV-2 had detectable levels of specific T cells against structural (S, M, N) and non-structural (ORF1a and ORF1b) proteins of SARS-CoV-2 (32). In our study, and according to these previous results, SARS-CoV-2-specific T cells mainly directed against the M protein were detected in SARS-CoV-2-seronegative ICU workers.

Initially, we postulated that the continuous exposition of ICU workers to patients with severe COVID-19 could trigger a slight but efficient cellular immune response specific to SARS-CoV-2 that might influence the response against further SARS-CoV-2 infections. However, the presence of pre-existing T cells in ICU workers was similar to the one detected in samples obtained from healthy donors before the pandemic, who were not exposed to the SARS-CoV-2. Thus, we guess that the origin of these cross-reactive T cells against SARS-CoV-2 proteins is not generated by the virus itself, but the possible recognition of SARS-CoV-2 epitopes shared with other seasonal viruses as it has been shown in previous studies (36, 37). One of the hypotheses suggested is that these unexposed individuals could have developed a variable, short-lived antibody response to another coronavirus but supplemented by a more sustained cellular immune response. Whereas the humoral cross-immunity is weak and decay rapidly (38), the cross-reactivity cellular immunity persists and contributes to SARS-CoV-2 immune responses upon infection or vaccination. Accordingly, SARS-CoV-2-reactive T cells respond to the restimulation with peptide pools obtained from other common coronaviruses (229E and OC43), which is evidence of their origin as an earlier immune response to an endemic human coronavirus (39). However, additional studies using different MHC-II epitopes reported that the high frequency of these cells in unexposed individuals cannot be completely explained by the homology among seasonal coronaviruses, and even that some might be naive and respond to unrelated pathogens (32). In our study, both crossreactive CD4+ and CD8+ T cells subsets were detected. Moreover, there are some discordances between the diverse reported studies. For instance, we and others observed a higher prevalence of pre-existing T cells with cross-reactive against membrane protein, whilst other studies showed the cellular response to the nucleoprotein as the most prevalent. These differences could be due to the varied geographical

origin of the studied cohorts and the differential exposition to diverse human coronavirus.

The presence of pre-existing cross-reactive T cells has been suggested to contribute to the variation in COVID-19 disease outcome (40, 41), increase the strength of the immune response in SARS-CoV-2 infection and vaccination (42), or even give rise to new therapeutic options that could be built upon and used as passive cell immunotherapy (43). But until now, few studies have evaluated whether these pre-existing T cells contribute to the host defense against SARS-CoV-2 or conversely, impair the development of an effective immune response. Only studies evaluating the severity of SARS-CoV-2 infection in individuals with pre-existing SARS-CoV-2-specific T cells will allow assessing the truly biological relevance of these cells. Meanwhile, Loyal et al. (18) identified a peptide (S816-830) located within the fusion peptide domain of spike protein that is recognized by CD4+ T cells in 20% of the unexposed individuals. Most of the individuals, but not all, increased the frequency of cross-reactive T cells after infection or vaccination, suggesting their reactivation and role to mediate the secondary response. By contrast, we showed that only two of the seven ICU workers enhanced the frequency of pre-existing T cells after vaccination, while five maintained similar levels to the ones detected before vaccination though always above the limit of positivity stablished. Therefore, we postulated that cross-reactive T cells can be generated by the previous exposure to diverse human coronaviruses but only some generated against specific peptides might be boosted upon SARS-CoV-2 infection or vaccination. However, a better phenotypical and functional characterization of pre-existing cross-reactive T cells versus a newly induced SARS-CoV-2-specific T cell response is required to further comprehend their differences and in consequence, whether they could modulate the severity and outcome of the disease.

Following the immune response upon SARS-CoV-2 vaccination, we observed high S protein and neutralizing IgG titers in all individuals only 1 month after complete administration as a consequence of the high efficacy of SARS-CoV-2 mRNA vaccines (1, 2). Antibody levels decline was slightly associated with age, although we should point out that there were no elderly people in our cohort. However, we detected strong variability in the cellular immune response triggered after full vaccination. It is quite remarkable that six (14.6%) individuals, all under 40 years of age, had not developed a cellular response against the S protein. COVID-19 disease is characterized by the great variability of its severity, from asymptomatic to severe, or in the worst cases, with a fatal outcome. In addition, however, the magnitude of the innate and adaptive immune responses to SARS-CoV-2 among people could condition the immune response to further infections, variants or to the vaccination (44). Thus, it is worth considering immunological heterogeneity in all situations, rather than just in the transplant, autoimmunity, and oncological contexts in which immune dysregulation is clearly established by the received therapy. One of the first studies reported by Sahin U et al. (12) showed that most of the vaccinated individuals, but not all, developed Th1-skewed immune responses and IFN-γ-producing $CD4^+$ and $CD8^+$ T cells. However, not all individuals responded to the vaccination, remaining the interindividual variability in response to vaccination poorly understood, whereas most studies have tried to understand the durability of the immunological memory. Multiple factors could condition the T cell response to vaccination or to any new viral infection, such as the repertory of naive T cells, which declines substantially with age but also with the persistent activation of T cells by other chronic viruses, such as cytomegalovirus; deficient ability of cytotoxic T cells to induce an effector response mediated by IFN-γ and cytolytic granules production or the induction of antigen-specific regulatory T cells under subimmunogenic conditions (45), among others.

Our study was designed to analyze for differences in the overall cellular immune response to vaccines, but the specific contribution mediated by $CD4^+$ or $CD8^+$ T cells was also determined. Cassaniti I et al. (46) showed that the overall SARS-CoV-2 specific T-cell response in convalescent patients was reduced to about 95% and 80% after CD4 or CD8 T-cell depletion, respectively. By using activation assays and cytokine production determinations, other studies showed that upon SARS-CoV-2 exposition the immune responses mediated by $CD4^+$ cells are predominant, but SARS-CoV-2-specific $CD8^+$ T cells were also reported (47). Most of the studies are commonly carried out upon infection and not after vaccination, and some differences could be observed compared to natural infection although are not fully understood. Goel RR et al. (8) described that after the second dose of SARS-CoV-2 mRNA vaccine, all individuals generated high levels of $CD4^+$ T cells, regardless of any prior SARS-CoV-2 infection, and most of them produced a $CD8^+$ T cell response. After an initial contraction, these specific memory T cells stabilized and began to decline but remain at least 6 months after vaccination. In addition, the early $CD4^+$ T cells response detected in those individuals correlated with the intensity of humoral immunity at long-term. Likewise, in our study, the humoral and cellular responses to SARS-CoV-2 weakened by 10 months after administration of the complete vaccine regime. Nonetheless, we do not detect such correlation neither at 1 month or 10 months after vaccination. On the other hand, we observed that those patients with the highest responses after 1 month of vaccination, undergo a lessened reduction in the antibody titer and specific T cells number, suggesting that the intensity of the early immune response after vaccination may condition their durability and that a third, booster dose is not required so early for all people. Initially, there was a little controversy about whether mRNA vaccines generated CD8+ T cell responses and at what time were produced. Oberhardt et al. (24) reported that $CD8^+$ T cells are early generated after vaccination, even when

antibodies and $CD4^+$ T cells are scarcely detectable and there are highly differentiated effector $CD8^+$ T cells. These cells remain stable and fully functional at long-term and together with antibodies and $CD4^+$ T cells act in coordination to maintain a full protection. Thus, a combined response mediated by both, $CD4^+$ and $CD8^+$ T cells, is triggered after vaccination and required to confer protection at different times. In this respect, we observed that the six ICU workers who does not developed IFN-γ-producing specific T cells 1 month after vaccination, are the same that lacked AIM^+ $CD8^+$ T cells. However, they do maintain a modest cellular response mediated by $CD4^+$ T cells, like the one detected in the "Responders" ICU workers group with a positive determination by ELISpot assay. Thus, our results suggest that early after vaccination, $CD8^+$ T cells are mostly contributing to the IFN-γ production. In this sense, it has been previously reported that the time of antigen exposure required to trigger effector cells is different between $CD4^+$ and $CD8^+$ T cells, showing these latter a faster rate of cell division and a lower threshold of activation (48). Moreover, we cannot rule out that the length of peptides used for the technical approaches could be also conditioning the MHC-I or MHC-II presentation, although this needs further confirmation.

We recognize that our study is limited by the relatively small number of individuals considered. It would be desirable to have more subjects to enable firm conclusions to be drawn, but to our knowledge, that is one of the scary studies evaluating the complete immune protection (humoral and cellular immunity) against SARS-CoV-2 in highly exposed COVID-19 ICU workers. Although our results demonstrated no correlation between the humoral and cellular responses after vaccination, it should be required to analyze the frequency of Tfh cells to understand the direct association between these cells and the neutralizing antibodies, such as it has been reported by Vikkurthi R et al. (49) with BBV152 vaccine in an Indian cohort. Unfortunately, this kind of studies require a greater number of PBMCs that were not available in our samples. Our results nevertheless suggest that the pattern of the cellular immune response to SARS-CoV-2 after vaccination is highly variable among healthy individuals. Some individuals lack an effective cellular response after receiving two doses of vaccine, but others may be sufficiently protected 10 months after vaccination and so might not require a booster dose. Although we demonstrated that the absence of IFN-γ-producing T cells is mainly mediated by $CD8^+$ T cells, an exhaustive functional characterization of these cytotoxic T cells could help to understand the lack of specific cellular response in these individuals.

In summary, after receiving two-doses of COVID-19 vaccine, a strong humoral immune response is produced in all individuals, but the cellular immune response, mainly mediated by $CD8^+$ T cells, is more variable. This supports the notion that it exists an interindividual variability to SARS-CoV-2 vaccination among healthy people that could condition their protection at long-term and thus, determining the SARS-CoV-2-specific T cell response might be of great value not only for establishing real immune competence after vaccination, but also for scheduling subsequent booster doses in highly exposed healthy workers, given that the cellular immune response can be detected in most individuals even 10 months after full vaccination.

Materials and methods

Population, samples and data collection

The observational and prospective study includes COVID-19 ICU workers (n=41, 26 nurses and 15 doctors) at the Central University Hospital of Asturias (Oviedo, Spain), with no antecedents of COVID-19 according to previous COVID-19 symptoms and household contacts. Moreover, we analyzed the humoral and cellular immune response against SARS-CoV-2 proteins in 20 healthy blood donors collected before pandemic (pre-pandemic group) and 15 convalescent patients with mild or severe COVID-19 disease diagnosed by viral RT-PCR test on respiratory samples. The demographic and clinical characteristics of the three groups are provided in Table 1.

Whole blood was collected from all individuals in appropriate collection tubes, serum samples were stored at -80°C until analysis, and peripheral blood mononuclear cells (PBMCs) were isolated by Ficoll (Lymphoprep) density-gradient centrifugation using standard protocols and frozen, maintaining their viability, until use. Samples from ICU workers group were collected between December 2020 and November 2021, specifically, one-week before SARS-CoV-2 vaccination (Pre-v) and then about 1 month (4-5 weeks) after their second dose (Post-v1) (Figure 1A). In 16 patients, an additional sample was taken 10 months after full vaccination (Post-v10). All participants received vaccination with Comirnaty (BNT162b2) except one, who received Spikevax (mRNA1273). Pre-pandemic samples were collected in two times, during 2007 and between December 2012 and January 2013. Another groups of COVID-19 convalesvent individuals was diagnosed by viral RT-PCR test and all required hospitalization.

All participants gave their written informed consent for inclusion. The study was approved by the ethic committee of research of Principality of Asturias (CEImPA, n° 2020.521 "*Study of the cellular immunity against SARS-CoV-2 in high-risk healthy workers*") and informed consent was obtained from all participants in compliance with the Helsinki Declaration of 1975

SARS-CoV-2-specific antibodies

Serum samples were tested for SARS-CoV-2 antibodies against the S protein using an automated commercial

chemiluminescent system on the LIAISONXL® platform. The LIAISON® SARS-CoV-2 TrimericS IgG assay (DiaSorin, VC, Italy) was used to quantify IgG antibodies to the anti-trimeric spike glycoprotein of SARS-CoV-2. This test has a clinical sensitivity of 98.7% and specificity of 99.5%, and a good correlation with microneutralization test results (PPA: 100% and NPS: 96.9%). Results are presented in arbitrary units per ml (AU/ml), with a cutoff of 13 AU/ml, and a maximum response of 800 AU/ml. Antibodies against nucleocapsid protein were determined using the BioPlex2200 SARS-CoV-2 IgG panel (Biorad) following the manufacturer´s instructions. This test has a clinical sensitivity of 96.3% and specificity of 99.8% and results are shown in units per ml (U/ml), being values ≤ 9 U/ml considered negative and positive for ≥10 U/ml.

For detection of neutralizing antibodies, we used the cPass SARS-CoV-2 Neutralization Antibody Detection Kit (Genscript) following the manufacturer´s instructions. This test allows to determinate the ability of antibodies to block the interaction of the SARS-CoV-2 receptor-binding domain (RBD) and the human ACE2 receptor. Samples were diluted 1:10 and the percentage of inhibition was determined using the formula: (1-OD value of sample/OD value of negative control) x 100%. Samples were run by duplicate and percentage of inhibition below 30% were considered as no detectable neutralizing antibodies. Additionally, we used the SARS-CoV-2 neutralizing antibody calibrator (Genscript) to generate a calibration curve and show the semi-quantitative results as units per ml (U/ml). Values ≥ 28.6 U/ml were considered positive.

SARS-CoV-2-reactive T cells detection by ELISpot

The cellular immune response against SARS-CoV-2 was evaluated by the ELISpot assay using the anti-IFN-γ ELISpot kit (AID® GmbH, Strasberg, Germany) to measure counts of IFN-γ- producing T cells that had previously been stimulated with SARS-CoV-2 peptide pools. To achieve this, PBMCs (3 x 10^5/well) in AIM-V medium (Gibco, MA, USA) were cultured for 16-18 h with the specific antigens of interest on plates precoated with an anti-IFN-γ antibody. Overlapping peptide pools (15-mers with an 11-amino acid overlap) against the SARS-CoV-2 S (ref 130-126-700), M (ref 130-126-702) and N (ref 130-126-698) proteins (all from Miltenyi Biotec, Bergisch Gladbach, Germany) were used as a stimulus at a concentration of 0.5μg/ml. Pokeweed mitogen (AID GmbH), with high mitogenic activity on T and B lymphocytes, and AIM-V medium were used as positive and negative controls, respectively. Plates were developed according to the manufacturer's protocol and spot-forming cells (SFCs) were read with an AID iSpot reader system using AIS ELISpot version 7.0 software (AID GmbH, Germany). Samples were assayed in duplicate, and results were obtained as the mean count of spots after subtracting the frequency with medium alone, and expressed as the number of SFCs per million PBMCs. T cell response was considered positive when mean spot counts were >10 SFCs per well or ≥33.3 spots/10^6 cells after subtracting the negative control frequency.

SARS-CoV-2-reactive T cells determination by activation-induced markers

The activation-induced markers (AIM) assay was performed as previously described (50, 51) to determine the antigen-specific $CD4^+$ and $CD8^+$ T cells. For that, PBMCs were thawed in AIM-V medium (Gibco, MA, USA) and stimulated for 24 hours in the presence of SARS-CoV-2 specific megapools (1μg/ml). The megapools consist of peptide pools of 15-mers overlapping by 11-amino acid and aimed against the SARS-CoV-2 S (ref 130-126-700), M (ref 130-126-702) and N (ref 130-126-698) proteins (Miltenyi Biotec). An equimolar concentration of DMSO and a mix of anti-CD3 (3μg/ml) and anti-CD28 (1μg/ml) antibodies were used as negative and positive controls, respectively. After stimulation, cells were washed with PBS containing 2% FBS and 0.05 mM EDTA and further surface stained with a cocktail of antibodies for 1 hour at 4°C in the dark. The following antibodies were used for multiparametric flow cytometry: CD3 APC-Cy7 (SK7), CD8 BV605 (HIT8a), CD137 APC (4B4-1), CD69 PE-Cy7 (FN50), OX40 PE (ACT35) and CD4 PerCP (SK3). All antibodies were purchased from Biolegend, CA, USA. The DNA-binding dye, DAPI (0.1 μg/ml, Santa Cruz Biotechnologies, TX, USA) was used for live/dead discrimination. After staining, cells were washed and resuspended in FACS buffer for further acquisition using Cytek® Aurora 3L Spectral Analyzer (Cytek Biosciences). Data were analyzed using FlowJo version 10.8.1. The percentage of antigen-specific $CD4^+$ and $CD8^+$ T cells was calculated by subtracting the DMSO percentages, set as background. Stimulation Index (SI) was calculated as the ratio between the percentage of AIM^+ cells after stimulation with peptide pools and the percentage of AIM^+ cells after DMSO stimulation, and SI > 1.1 was considered positive.

Statistical analysis

Data are expressed as the mean ± standard error of mean (SEM). Associations between variables were assessed by Spearman correlation and comparisons between samples using Fisher´s exact test, Wilcoxon paired-samples test, or Mann-Whitney test for comparison of unpaired samples. Statistical analyses were carried out with IBM SPSS Statistics v20.0

(Armonk, NY, USA) and GraphPad-Prism v7 (San Diego, CA, USA). Statistical significance was concluded for values of $p<0.05$. Statistical details of the experiments and significance are noted in the respective figures and figure legends.

Data availability statement

The original contributions presented in the study are included in the article/Supplementary Material. Further inquiries can be directed to the corresponding author.

Ethics statement

The studies involving human participants were reviewed and approved by CEImPA, 2020.521 "Study of the cellular immunity against SARS-CoV-2 in high-risk healthy workers". The patients/participants provided their written informed consent to participate in this study.

Author contributions

Conceptualization, BS-A and CL-L; design of the work, BS-A; ESdR; MLS; acquisition of samples, ESdR; CM-M; DE; and BLG; methodology, BS-A; MLS; VC-I; MR-P; interpretation of data and analysis BS-A; MLS and DE; writing the manuscript BS-A; ESdR and VC-I; revision and agree of the manuscript, all authors; funding acquisition BS-A and CL-L. All authors contributed to the article and approved the submitted version.

Funding

This study was supported by the Plan Nacional de I+D+I 2013-2016 ISCIII (Spanish Institute of Health Carlos III; grant numbers PI19/00184 and PI20/00639) and Gobierno del Principado de Asturias, PCTI-Plan de Ciencia, Tecnología e Innovación 2021-2023 (Grant number IDI/2021/000032).

Conflict of interest

The authors declare that the research was conducted in the absence of any commercial or financial relationships that could be construed as a potential conflict of interest.

Publisher's note

All claims expressed in this article are solely those of the authors and do not necessarily represent those of their affiliated organizations, or those of the publisher, the editors and the reviewers. Any product that may be evaluated in this article, or claim that may be made by its manufacturer, is not guaranteed or endorsed by the publisher.

Supplementary material

The Supplementary Material for this article can be found online at: https://www.frontiersin.org/articles/10.3389/fimmu.2022.942192/full#supplementary-material

References

1. Polack FP, Thomas SJ, Kitchin N, Absalon J, Gurtman A, Lockhart S, et al. Safety and efficacy of the BNT162b2 mRNA covid-19 vaccine. *New Engl J Med* (2020) 383(27):2603–15. doi: 10.1056/NEJMoa2034577

2. Baden LR, El Sahly HM, Essink B, Kotloff K, Frey S, Novak R, et al. Efficacy and safety of the mRNA-1273 SARS-CoV-2 vaccine. *New Engl J Med* (2021) 384 (5):403–16. doi: 10.1056/NEJMoa2035389

3. Wolz OO, Kays SK, Junker H, Koch SD, Mann P, Quintini G, et al. A third dose of the COVID-19 vaccine, CVnCoV, increased the neutralizing activity against the SARS-CoV-2 wild-type and delta variant. *Vaccines* (2022) 10(4):508. doi: 10.3390/vaccines10040508

4. Magen O, Waxman JG, Makov-Assif M, Vered R, Dicker D, Hernan MA, et al. Fourth dose of BNT162b2 mRNA covid-19 vaccine in a nationwide setting. *New Engl J Med* (2022) 386(17):1603–14. doi: 10.1056/NEJMoa2201688

5. Evans JP, Zeng C, Carlin C, Lozanski G, Saif LJ, Oltz EM, et al. Neutralizing antibody responses elicited by SARS-CoV-2 mRNA vaccination wane over time and are boosted by breakthrough infection. *Sci Transl Med* (2022) 14(637): eabn8057. doi: 10.1126/scitranslmed.abn8057

6. Moncunill G, Aguilar R, Ribes M, Ortega N, Rubio R, Salmeron G, et al. Determinants of early antibody responses to COVID-19 mRNA vaccines in a cohort of exposed and naive healthcare workers. *EBioMedicine* (2022) 75:103805. doi: 10.1016/j.ebiom.2021.103805

7. Terpos E, Trougakos IP, Karalis V, Ntanasis-Stathopoulos I, Gumeni S, Apostolakou F, et al. Kinetics of anti-SARS-CoV-2 antibody responses 3 months post complete vaccination with BNT162b2; a prospective study in 283 health workers. *Cells* (2021) 10(8):1942. doi: 10.3390/cells10081942

8. Sette A, Crotty S. Immunological memory to SARS-CoV-2 infection and COVID-19 vaccines. *Immunol Rev* (2022). 310(1):27–46. doi: 10.1111/imr.13089

9. Zhang Z, Mateus J, Coelho CH, Dan JM, Moderbacher CR, Galvez RI, et al. Humoral and cellular immune memory to four COVID-19 vaccines. *Cell* (2022) 185(14):2434–51.e17. doi: 10.1016/j.cell.2022.05.022

10. Widge AT, Rouphael NG, Jackson LA, Anderson EJ, Roberts PC, Makhene M, et al. Durability of responses after SARS-CoV-2 mRNA-1273 vaccination. *New Engl J Med* (2021) 384(1):80–2. doi: 10.1056/NEJMc2032195

11. Lozano-Ojalvo D, Camara C, Lopez-Granados E, Nozal P, Del Pino-Molina L, Bravo-Gallego LY, et al. Differential effects of the second SARS-CoV-2 mRNA vaccine dose on T cell immunity in naive and COVID-19 recovered individuals. *Cell Rep* (2021) 36(8):109570. doi: 10.1016/j.celrep.2021.109570

12. Sahin U, Muik A, Derhovanessian E, Vogler I, Kranz LM, Vormehr M, et al. COVID-19 vaccine BNT162b1 elicits human antibody and TH1 T cell responses. *Nature* (2020) 586(7830):594–9. doi: 10.1038/s41586-020-2814-7

13. Tarke A, Sidney J, Methot N, Zhang Y, Dan JM, Goodwin B, et al. Negligible impact of SARS-CoV-2 variants on CD4 (+) and CD8 (+) T cell reactivity in COVID-19 exposed donors and vaccinees. *bioRxiv preprint server Biol* (2021). doi: 10.1101/2021.02.27.433180

14. Jergovic M, Uhrlaub JL, Watanabe M, Bradshaw CM, White LM, LaFleur BJ, et al. Competent immune responses to SARS-CoV-2 variants in older adults

following two doses of mRNA vaccination. *Nat Commun* (2022) 13(1):2891. doi: 10.1038/s41467-022-30617-9

15. Anderson EJ, Rouphael NG, Widge AT, Jackson LA, Roberts PC, Makhene M, et al. Safety and immunogenicity of SARS-CoV-2 mRNA-1273 vaccine in older adults. *New Engl J Med* (2020) 383(25):2427–38. doi: 10.1056/NEJMoa2028436

16. Apostolidis SA, Kakara M, Painter MM, Goel RR, Mathew D, Lenzi K, et al. Cellular and humoral immune responses following SARS-CoV-2 mRNA vaccination in patients with multiple sclerosis on anti-CD20 therapy. *Nat Med* (2021) 27(11):1990–2001. doi: 10.1038/s41591-021-01507-2

17. Tobudic S, Benazzo A, Koblischke M, Schneider L, Bluml S, Winkler F, et al. Immune response after mRNA COVID-19 vaccination in lung transplant recipients: A 6-month follow-up. *Vaccines* (2022) 10(7):1130. doi: 10.3390/vaccines10071130

18. Cuffel A, Maylin S, Le Buanec H, Delaugerre C, Minier M, Bergerat D, et al. Humoral and cellular responses to SARS-CoV-2 BNT162b2 vaccination in allogeneic hematopoietic stem cell transplantation recipients. *Vaccine* (2022) 40 (33):4682–5. doi: 10.1016/j.vaccine.2022.07.006

19. Zaleska J, Kwasnik P, Paziewska M, Purkot J, Szabelak A, Jurek M, et al. Response to anti-SARS-CoV-2 mRNA vaccines in multiple myeloma and chronic lymphocytic leukemia patients. *Int J Cancer* (2022). doi: 10.1002/ijc.34209

20. Mazzoni A, Di Lauria N, Maggi L, Salvati L, Vanni A, Capone M, et al. First-dose mRNA vaccination is sufficient to reactivate immunological memory to SARS-CoV-2 in subjects who have recovered from COVID-19. *J Clin Invest* (2021) 131(12):e149150. doi: 10.1172/JCI149150

21. Laranjeira P, Rodrigues T, Silva A, Barbosa P, Reis T, Lopes C, et al. A single dose of COVID-19 vaccine induces a strong T cell and b cell response in healthcare professionals recovered from SARS-CoV-2 infection. *Clin Exp Med* (2022). doi: 10.1007/s10238-022-00801-8

22. Painter MM, Mathew D, Goel RR, Apostolidis SA, Pattekar A, Kuthuru O, et al. Rapid induction of antigen-specific CD4(+) T cells is associated with coordinated humoral and cellular immunity to SARS-CoV-2 mRNA vaccination. *Immunity* (2021) 54(9):2133–42.e3. doi: 10.1016/j.immuni.2021.08.001

23. Mudd PA, Minervina AA, Pogorelyy MV, Turner JS, Kim W, Kalaidina E, et al. SARS-CoV-2 mRNA vaccination elicits a robust and persistent T follicular helper cell response in humans. *Cell* (2022) 185(4):603–13.e15. doi: 10.1016/j.cell.2021.12.026

24. Oberhardt V, Luxenburger H, Kemming J, Schulien I, Ciminski K, Giese S, et al. Rapid and stable mobilization of CD8(+) T cells by SARS-CoV-2 mRNA vaccine. *Nature* (2021) 597(7875):268–73. doi: 10.1038/s41586-021-03841-4

25. Jung S, Jung JH, Noh JY, Kim WJ, Yoon SY, Jung J, et al. The generation of stem cell-like memory cells early after BNT162b2 vaccination is associated with durability of memory CD8(+) T cell responses. *Cell Rep* (2022) 40(4):111138. doi: 10.1016/j.celrep.2022.111138

26. Goel RR, Painter MM, Apostolidis SA, Mathew D, Meng W, Rosenfeld AM, et al. mRNA vaccines induce durable immune memory to SARS-CoV-2 and variants of concern. *Science* (2021) 374(6572):abm0829. doi: 10.1126/science.abm0829

27. Tarke A, Coelho CH, Zhang Z, Dan JM, Yu ED, Methot N, et al. SARS-CoV-2 vaccination induces immunological T cell memory able to cross-recognize variants from alpha to omicron. *Cell* (2022) 185(5):847–59.e11. doi: 10.1016/j.cell.2022.01.015

28. Chakraborty C, Sharma AR, Bhattacharya M, Zayed H, Lee SS. Understanding gene expression and transcriptome profiling of COVID-19: An initiative towards the mapping of protective immunity genes against SARS-CoV-2 infection. *Front Immunol* (2021) 12:724936. doi: 10.3389/fimmu.2021.724936

29. Mateus J, Grifoni A, Tarke A, Sidney J, Ramirez SI, Dan JM, et al. Selective and cross-reactive SARS-CoV-2 T cell epitopes in unexposed humans. *Science* (2020) 370(6512):89–94. doi: 10.1126/science.abd3871

30. da Silva Antunes R, Pallikkuth S, Williams E, Dawen Yu E, Mateus J, Quiambao L, et al. Differential T-cell reactivity to endemic coronaviruses and SARS-CoV-2 in community and health care workers. *J Infect Dis* (2021) 224(1):70–80. doi: 10.1093/infdis/jiab176

31. Swadling L, Diniz MO, Schmidt NM, Amin OE, Chandran A, Shaw E, et al. Pre-existing polymerase-specific T cells expand in abortive seronegative SARS-CoV-2. *Nature* (2022) 601(7891):110–7. doi: 10.1038/s41586-021-04186-8

32. Le Bert N, Tan AT, Kunasegaran K, Tham CYL, Hafezi M, Chia A, et al. SARS-CoV-2-specific T cell immunity in cases of COVID-19 and SARS, and uninfected controls. *Nature* (2020) 584(7821):457–62. doi: 10.1038/s41586-020-2550-z

33. Grifoni A, Weiskopf D, Ramirez SI, Mateus J, Dan JM, Moderbacher CR, et al. Targets of T cell responses to SARS-CoV-2 coronavirus in humans with COVID-19 disease and unexposed individuals. *Cell* (2020) 181(7):1489–501.e15. doi: 10.1016/j.cell.2020.05.015

34. Ansari A, Arya R, Sachan S, Jha SN, Kalia A, Lall A, et al. Immune memory in mild COVID-19 patients and unexposed donors reveals persistent T cell responses after SARS-CoV-2 infection. *Front Immunol* (2021) 12:636768. doi: 10.3389/fimmu.2021.636768

35. Braun J, Loyal L, Frentsch M, Wendisch D, Georg P, Kurth F, et al. SARS-CoV-2-reactive T cells in healthy donors and patients with COVID-19. *Nature* (2020) 587(7833):270–4. doi: 10.1038/s41586-020-2598-9

36. Grifoni A, Sidney J, Vita R, Peters B, Crotty S, Weiskopf D, et al. SARS-CoV-2 human T cell epitopes: Adaptive immune response against COVID-19. *Cell Host Microbe* (2021) 29(7):1076–92. doi: 10.1016/j.chom.2021.05.010

37. Sette A, Crotty S. Pre-existing immunity to SARS-CoV-2: the knowns and unknowns. *Nat Rev Immunol* (2020) 20(8):457–8. doi: 10.1038/s41577-020-0389-z

38. Ng KW, Faulkner N, Cornish GH, Rosa A, Harvey R, Hussain S, et al. Preexisting and *de novo* humoral immunity to SARS-CoV-2 in humans. *Science* (2020) 370(6522):1339–43. doi: 10.1126/science.abe1107

39. Bonifacius A, Tischer-Zimmermann S, Dragon AC, Gussarow D, Vogel A, Krettek U, et al. COVID-19 immune signatures reveal stable antiviral T cell function despite declining humoral responses. *Immunity* (2021) 54(2):340–54.e6. doi: 10.1016/j.immuni.2021.01.008

40. Sagar M, Reifler K, Rossi M, Miller NS, Sinha P, White LF, et al. Recent endemic coronavirus infection is associated with less-severe COVID-19. *J Clin Invest* (2021) 131(1):e143380. doi: 10.1172/JCI143380

41. Gombar S, Bergquist T, Pejaver V, Hammarlund NE, Murugesan K, Mooney S, et al. SARS-CoV-2 infection and COVID-19 severity in individuals with prior seasonal coronavirus infection. *Diagn Microbiol Infect disease.* (2021) 100(2):115338. doi: 10.1016/j.diagmicrobio.2021.115338

42. Loyal L, Braun J, Henze L, Kruse B, Dingeldey M, Reimer U, et al. Cross-reactive CD4(+) T cells enhance SARS-CoV-2 immune responses upon infection and vaccination. *Science* (2021) 374(6564):eabh1823. doi: 10.1126/science.abh1823

43. Panikkar A, Lineburg KE, Raju J, Chew KY, Ambalathingal GR, Rehan S, et al. SARS-CoV-2-specific T cells generated for adoptive immunotherapy are capable of recognizing multiple SARS-CoV-2 variants. *PloS Pathog* (2022) 18(2): e1010339. doi: 10.1371/journal.ppat.1010339

44. Mathew D, Giles JR, Baxter AE, Oldridge DA, Greenplate AR, Wu JE, et al. Deep immune profiling of COVID-19 patients reveals distinct immunotypes with therapeutic implications. *Science* (2020) 369(6508):eabc8511. doi: 10.1126/science.abc8511

45. Lin PH, Wong WI, Wang YL, Hsieh MP, Lu CW, Liang CY, et al. Vaccine-induced antigen-specific regulatory T cells attenuate the antiviral immunity against acute influenza virus infection. *Mucosal Immunol* (2018) 11(4):1239–53. doi: 10.1038/s41385-018-0004-9

46. Cassaniti I, Percivalle E, Bergami F, Piralla A, Comolli G, Bruno R, et al. SARS-CoV-2 specific T-cell immunity in COVID-19 convalescent patients and unexposed controls measured by ex vivo ELISpot assay. *Clin Microbiol infection Off Publ Eur Soc Clin Microbiol Infect Diseases.* (2021) 27(7):1029–34. doi: 10.1016/j.cmi.2021.03.010

47. Schulien I, Kemming J, Oberhardt V, Wild K, Seidel LM, Killmer S, et al. Characterization of pre-existing and induced SARS-CoV-2-specific CD8(+) T cells. *Nat Med* (2021) 27(1):78–85. doi: 10.1038/s41591-020-01143-2

48. Seder RA, Ahmed R. Similarities and differences in CD4+ and CD8+ effector and memory T cell generation. *Nat Immunol* (2003) 4(9):835–42. doi: 10.1038/ni969

49. Vikkurthi R, Ansari A, Pai AR, Jha SN, Sachan S, Pandit S, et al. Inactivated whole-virion vaccine BBV152/Covaxin elicits robust cellular immune memory to SARS-CoV-2 and variants of concern. *Nat Microbiol* (2022) 7(7):974–85. doi: 10.1038/s41564-022-01161-5

50. Boppana S, Qin K, Files JK, Russell RM, Stoltz R, Bibollet-Ruche F, et al. SARS-CoV-2-specific peripheral T follicular helper cells correlate with neutralizing antibodies and increase during convalescence. *medRxiv preprint server Health Sci* (2020). doi: 10.1101/2020.10.07.20208488

51. Kalimuddin S, Tham CYL, Qui M, de Alwis R, Sim JXY, Lim JME, et al. Early T cell and binding antibody responses are associated with COVID-19 RNA vaccine efficacy onset. *Med* (2021) 2(6):682–8.e4. doi: 10.1016/j.medj.2021.04.003

frontiers | Frontiers in Immunology

TYPE Original Research
PUBLISHED 06 October 2022
DOI 10.3389/fimmu.2022.1004045

OPEN ACCESS

EDITED BY
Elke Bergmann-Leitner,
Walter Reed Army Institute of Research, United States

REVIEWED BY
Tim Luetkens,
University of Maryland, Baltimore, United States
Yanmin Wan,
Fudan University, China

*CORRESPONDENCE
Monika Strengert
monika.strengert@helmholtz-hzi.de
Alex Dulovic
alex.dulovic@nmi.de
Georg M. N. Behrens
behrens.georg@mh-hannover.de

†These authors have contributed equally to this work

‡These authors have contributed equally to this work and share first authorship

SPECIALTY SECTION
This article was submitted to Vaccines and Molecular Therapeutics, a section of the journal Frontiers in Immunology

RECEIVED 26 July 2022
ACCEPTED 12 September 2022
PUBLISHED 06 October 2022

CITATION
Becker M, Cossmann A, Lürken K, Junker D, Gruber J, Juengling J, Ramos GM, Beigel A, Wrenger E, Lonnemann G, Stankov MV, Dopfer-Jablonka A, Kaiser PD, Traenkle B, Rothbauer U, Krause G, Schneiderhan-Marra N, Strengert M, Dulovic A and Behrens GMN (2022) Longitudinal cellular and humoral immune responses after triple BNT162b2 and fourth full-dose mRNA-1273 vaccination in haemodialysis patients. *Front. Immunol.* 13:1004045. doi: 10.3389/fimmu.2022.1004045

Longitudinal cellular and humoral immune responses after triple BNT162b2 and fourth full-dose mRNA-1273 vaccination in haemodialysis patients

Matthias Becker[1‡], Anne Cossmann[2‡], Karsten Lürken[3], Daniel Junker[1], Jens Gruber[1], Jennifer Juengling[1], Gema Morillas Ramos[2], Andrea Beigel[3], Eike Wrenger[3], Gerhard Lonnemann[3], Metodi V. Stankov[2], Alexandra Dopfer-Jablonka[2,4], Philipp D. Kaiser[1], Bjoern Traenkle[1], Ulrich Rothbauer[1,5], Gérard Krause[4,6,7], Nicole Schneiderhan-Marra[1], Monika Strengert[6,7*†], Alex Dulovic[1*†] and Georg M. N. Behrens[2,4,8*†]

[1]NMI Natural and Medical Sciences Institute at the University of Tübingen, Reutlingen, Germany, [2]Department for Rheumatology and Immunology, Hannover Medical School, Hannover, Germany, [3]Department of Internal Medicine and Nephrology, Dialysis Centre Eickenhof, Langenhagen, Germany, [4]German Centre for Infection Research (DZIF), partner site Hannover-Braunschweig, Hannover, Germany, [5]Pharmaceutical Biotechnology, University of Tübingen, Tübingen, Germany, [6]Department Epidemiology, Helmholtz Centre for Infection Research, Braunschweig, Germany, [7]TWINCORE GmbH, Centre for Experimental and Clinical Infection Research, a joint venture of the Hannover Medical School and the Helmholtz Centre for Infection Research, Hannover, Germany, [8]CiiM - Centre for Individualized Infection Medicine, Hannover, Germany

Haemodialysis patients respond poorly to vaccination and continue to be at-risk for severe COVID-19. Therefore, dialysis patients were among the first for which a fourth COVID-19 vaccination was recommended. However, targeted information on how to best maintain immune protection after SARS-CoV-2 vaccinations in at-risk groups for severe COVID-19 remains limited. We provide, to the best of our knowledge, for the first time longitudinal vaccination response data in dialysis patients and controls after a triple BNT162b2 vaccination and in the latter after a subsequent fourth full-dose of mRNA-1273. We analysed systemic and mucosal humoral IgG responses against the receptor-binding domain (RBD) and ACE2-binding inhibition towards variants of concern including Omicron and Delta with multiplex-based immunoassays. In addition, we assessed Spike S1-specific T-cell responses by interferon γ release assay. After triple BNT162b2 vaccination, anti-RBD B.1 IgG and ACE2 binding inhibition reached peak levels in dialysis patients, but remained inferior compared to controls. Whilst we detected B.1-specific ACE2 binding inhibition in 84% of dialysis patients after three BNT162b2 doses, binding inhibition towards the Omicron variant was only detectable in 38% of samples and

declining to 16% before the fourth vaccination. By using mRNA-1273 as fourth dose, humoral immunity against all SARS-CoV-2 variants tested was strongly augmented with 80% of dialysis patients having Omicron-specific ACE2 binding inhibition. Modest declines in T-cell responses in dialysis patients and controls after the second vaccination were restored by the third BNT162b2 dose and significantly increased by the fourth vaccination. Our data support current advice for a four-dose COVID-19 immunisation scheme for at-risk individuals such as haemodialysis patients. We conclude that administration of a fourth full-dose of mRNA-1273 as part of a mixed mRNA vaccination scheme to boost immunity and to prevent severe COVID-19 could also be beneficial in other immune impaired individuals. Additionally, strategic application of such mixed vaccine regimens may be an immediate response against SARS-CoV-2 variants with increased immune evasion potential.

KEYWORDS

dialysis, mRNA vaccination, Omicron variant of concern, protective immunity, immunocompromised, longitudinal response, mixed mRNA vaccination, COVID-19

Introduction

To date, SARS-CoV-2 vaccinations reassuringly provide some degree of protection from severe COVID-19 independent of the currently circulating variants of concern (VoC) for the majority of healthy individuals (1). However, weaker immunogenicity and a faster decline in protection levels to standard two-dose or three-dose booster SARS-CoV-2 immunisation schemes have been widely demonstrated in immunocompromised individuals such as solid organ transplant recipients (2), dialysis patients (3) or patients suffering from other severe chronic conditions such as cancer (4). Starting in mid-2021 and more widely since the beginning of 2022, several countries recommended a fourth dose of SARS-CoV-2 mRNA vaccines for immunosuppressed populations at-risk for severe COVID-19 disease and older individuals to maintain levels of immune protection (5–8). This was driven by weaker peak vaccine responses and waning immunity in those individuals as well as continued evolution of SARS-CoV-2 variants with increasing levels of immune evasion potential as demonstrated for Omicron VoC subspecies BA.1, BA.4, BA.5, and BA.2.12.1 (9–12).

Recent studies reported improved SARS-CoV-2 humoral and cellular responses not only towards the original SARS-CoV-2 B.1 isolate but also Delta and Omicron VoC after a fourth vaccination in haemodialysis patients receiving either mRNA vaccines or vector-based formulations in combination with mRNA vaccines (13–15). However, targeted data on the most efficient dosing and vaccination scheme or even predictors of vaccination success in haemodialysis patients at-risk of severe COVID-19 and its associated mortality is limited. We aimed to comprehensively examine the magnitude and kinetics of both cellular and humoral immunity towards the most recently dominating Delta and Omicron variant's in a well-controlled longitudinal cohort of haemodialysis patients. These patients received a triple dose of BNT162b2 followed by a full-dose of mRNA-1273. Healthcare workers vaccinated three times with BNT162b2 served as controls. Our data provide preliminary evidence that in addition to heterologous vector- and mRNA-based vaccination schemes also heterologous mRNA vaccine regimens may become strategically beneficial for achieving efficient immunity against SARS-CoV-2 in immunosuppressed patients.

Methods

Study design and sample collection

This is a follow-up study in haemodialysis patients and control individuals, for which the results for haemodialysis patients after a complete two-dose BNT162b2 vaccination (16) and subsequent decline (17) have been previously reported. Blood samples were taken before start of dialysis treatment (n=50) or from healthcare workers (n=33), who participated in the COVID-19 contact (CoCo) study served (18) as non-dialysed control population. To be included in the study, participants had to be over the age of 18 and able to give

written informed consent. For the current analysis, we only considered dialysis patients for which results from all time points after either three or four vaccine doses were available. All participants received the standard two-dose regimen of BNT162b2 three weeks apart, followed by a third BNT162b2 vaccination about six (dialysis) or 8.5 months (controls) after the second vaccination. Only dialysis patients were vaccinated a fourth time with 100 µg mRNA-1273 four months after the last BNT162b2 vaccination. The vaccination schedule and blood collection time points are depicted in Figure 1 and Figure S1. Participants with SARS-CoV-2 infection diagnosed by either PCR or anti-nucleocapsid IgG determined by MULTICOV-AB multiplex measurement (19) were excluded from the analysis. Demographic characteristics and medical information are listed in Tables 1, S1, S2. Plasma was obtained from lithium heparin blood (S-Monovette Plasma, Sarstedt, Germany). Whole blood samples were used immediately for interferon γ release assay (IGRA). For saliva collection, all individuals spat directly into a collection tube. To inactivate replication-competent SARS-CoV-2 virus particles potentially present in saliva samples, Tri(n-butyl) phosphate (TnBP) and Triton X-100 were added to final concentrations of 0.3% and 1%, respectively (20). Both plasma and saliva samples were frozen and stored at −80°C until further use.

MULTICOV-AB

IgG binding and levels were analysed using MULTICOV-AB, a multiplex coronavirus immunoassay which contains the trimeric Spike B.1, its subdomains (S1, S2, RBD), nucleocapsid B.1 and RBDs of Delta and Omicron BA.1 antigens as previously described (9, 19). Briefly, antigens were immobilised on spectrally distinct populations of MagPlex beads (Cat #MC10XXX-01, Luminex Corporation) either by EDC/s-NHS coupling (21) or by Anteo coupling (Cat #A-LMPAKMM-10, Anteo Tech Reagents) following the manufacturer's instruction (19). The combined MagPlex beads were then incubated with samples at an effective dilution of 1:3200 for plasma and of 1:12 for saliva. After a wash step to remove unbound antibodies, IgG was detected with R-phycoerythrin labelled goat-anti-human IgG (Jackson ImmunoResearch Labs, Cat #109-116-098, Lot #148837, RRID: AB_2337678) as secondary antibody. After another wash step and bead resuspension, samples were measured once on a FLEXMAP 3D instrument (Luminex Corporation) using the following settings: Timeout 80 sec, Gate: 7500-15000, Reporter Gain: Standard PMT, 50 events. Raw median fluorescence intensity (MFI) values or normalised values (MFI/MFI of quality control (QC) samples (19, 22) are reported. Three QC samples were measured per individual plate to monitor MULTICOV-AB performance.

RBDCoV-ACE2

RBDCoV-ACE2, a multiplex competitive inhibition assay, was performed as previously described (23) as surrogate assay to determine immunoglobulin neutralisation capacity against SARS-CoV-2 B.1 isolate and variants of concern. For this, biotinylated ACE2 was combined with individual samples (and as a control, ACE2 alone) and incubated with the above mentioned MULTICOV-AB bead mix. Before and after ACE2 detection with Strep-PE (Cat #SAPE-001, Moss), washes were carried out. Samples were measured once on a FLEXMAP 3D instrument with the same settings as MULTICOV-AB and analysed by normalisation of MFI values against the control. 100% ACE2 binding inhibition indicates maximum binding inhibition. Responders for ACE2 binding inhibition are classified as above a 20% ACE2 binding threshold as described in Junker et al. (23).

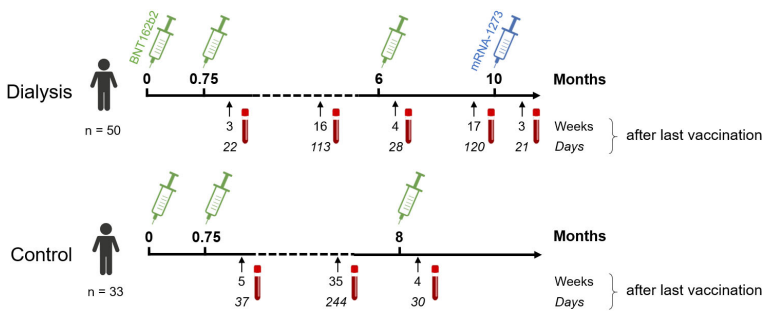

FIGURE 1
Participant recruitment scheme for longitudinal vaccination response analysis in haemodialysis patients after triple BNT162b2 and fourth full-dose mRNA-1273. Patients on haemodialysis (n = 50) and healthcare workers as controls (n = 33) were triple-vaccinated with BNT162b2 (green syringe) followed by a 100 µg (full) dose of mRNA-1273 (blue syringe) for dialysed individuals only. Sampling and vaccination schedule is given in days and weeks as indicated.

10.3389/fimmu.2022.1004045

TABLE 1 Characteristics of study population.

Characteristics	Haemodialysis group (n = 50)	Non-dialysis control group (n =33)	p-value for difference between groups
Age (years), median (IQR)	69.5 (60–79)	42 (32–55)	$1.08*10^{-11}$
Sex (female: n, %)	19 (38.0)	23 (69.7)	$9.26*10^{-3}$
Days since start of haemodialysis (median, IQR)	1263 (753-2314)	n. a.	n. a.
Immunosuppressive medication (n, %)			
2021 (Vaccine dose 1-3)*	7 (14.0)	0 (0.0)	n. a.
2022 (Vaccine dose 4)*	6 (12.0)	n. a.	n. a.
Co-morbidities			
Obesity (BMI, >30)	12 (24.0)	NA	n. a.
Diabetes mellitus (n, %)	14 (28.0)	1 (3.0)	$9.27*10^{-3}$
Cardiovascular disease (n, %)	21 (42.0)	2 (6.1)	$8.69*10^{-4}$
Cancer (n, %)	1 (2.0)	0 (0.0)	n. a.
Chronic conditions (n, %)			
Ulcerative colitis (n, %)	0 (0.0)	1 (3.0)	n. a.
Goiter (n, %)	0 (0.0)	1 (3.0)	n. a.
Hashimoto's thyroiditis (n, %)	0 (0.0)	1 (3.0)	n. a.
Hypothyroidism (n, %)	0 (0.0)	1 (3.0)	n. a.
Other	0 (0.0)	1 (3.0)	n. a.

*Participants on medication when vaccinated and sampled.
IQR, Inter Quartile Range; BMI, Body Mass Index; n, absolute numbers per group; NA, Information not available; n. a., not applicable.

Anti-SARS-CoV-2 QuantiVac ELISA

Plasma samples were additionally analysed using the Anti-SARS-CoV-2-QuantiVac-ELISA IgG (Cat #EI 2606-9601-10G, Euroimmun) as previously described (16).

Interferon γ release assay

SARS-CoV-2-specific T-cell responses from whole blood were analysed by measuring IFNγ production after stimulation with a peptide pool from the SARS-CoV-2 Spike S1 with the SARS-CoV-2 Interferon Gamma Release Assay (Cat #ET-2606-3003, Euroimmun) and the IFNγ ELISA (Cat #EQ-6841-9601, Euroimmun) according to the manufacturer's description and as previously evaluated against alternative assays for antigen-specific T-cell reactivity using intracellular cytokine staining or enzyme linked immuno spot assay (24, 25). Background signals from negative controls were subtracted and final results calculated in mIU/mL using standard curves. IFNγ concentrations >200 mIU/mL were considered as reactive. We defined this arbitrary cut-off by using average background IFNγ activity without antigen-stimulation in all samples multiplied with 10 for the threshold for IGRA-positive. Using this cut-off, we found in all of the 15 controls taken from independent individuals before the COVID-19 pandemic negative IGRA results (26). The upper limit of reactivity was 16,000 mIU/mL.

Data analysis and statistics

RStudio (Version 1.2.5001), with R (version 3.6.1) was used for data analysis and figure generation. Additionally, the R add-on package "beeswarm" was utilised to visualise data as stripcharts with overlaying boxplots and to create non-overlaying data points. A second R add-on package "gplots" was used to generate specific colours for plots. Figures were exported from RStudio and then edited using Inkscape (Inkscape 1.2). Spearman's rho coefficient was calculated to determine correlation between IGRA results and ACE2 binding inhibition using the "cor" function from R's "stats" library. Mann-Whitney-U test and Wilcoxon test were used to determine difference of signal distributions between dialysed and control groups for unpaired and paired samples, respectively using the "wilcox.test" function from R's "stats" library. To assess differences in the study population, Pearson's Chi-squared test with Yates' continuity correction was used for categorical characteristics using the "chisq.test" function from R's "stats" library and Mann-Whitney-U test as above was used for difference in age. The type of statistical analysis performed

(when appropriate) is listed in the figure legends. Pre-processing of data such as matching sample metadata and collecting results from multiple assay platforms was performed in Excel 2016.

Results

Inferior humoral responses in haemodialysis patients after triple BNT162b2 vaccination

To characterise the vaccination response after the third BN162b2 vaccination in 50 patients on maintenance haemodialysis, we had followed immunoglobulin levels longitudinally after the second dose of BNT162b2 using MULTICOV-AB, a multiplex immunoassay containing antigens from the Spike protein of SARS-CoV-2 and selected variants of concern (9). As a novel control group, 33 samples from healthcare workers with triple BNT162b2 vaccination were used for comparison. Detailed information on the study populations can be found in Tables 1, S1, S2. Consistent with our previous reports (16, 17), IgG responses towards the original B.1 isolate in vaccinated dialysis patients were significantly reduced ($p=4.68*10^{-5}$, Mann-Whitney-U test) when compared to the control group and declined after the second vaccination to comparable levels in both groups ($p=7.33*10^{-2}$, Mann-Whitney-U test, Figure 2A). A third BNT162b2 vaccination about six to eight months after the second increased the peak IgG RBD B.1 response in both groups but with higher variability in dialysis patients ($p=4.02*10^{-2}$, Mann-Whitney-U test, Figure 2A). As an additional control, quantitative S1 IgG titres were measured using a commercial assay (Figure S2), which led to a very similar pattern of significantly diminished antibody responses in dialysis patients compared to non-dialysed individuals after the second BNT162b2 dose, declining titres and a robust peak response increase after the third vaccination. There was no significant difference in male or female individuals and we did not find any association to age. Regarding the decline in anti-S IgG after the third dose, we were able to measure this in only n=10 of the control group at a comparable time point after vaccination to the haemodialysis group (Figure S3). Dialysis patients showed a mean 3-fold reduction in anti-S IgG levels 121 days (range 119-129 days) after the third vaccination (from mean 2,314 BAU/mL to mean 771 BAU/mL). This was almost identical to the 3.2-fold decline in healthy controls (from mean 5,430 BAU/mL to mean 1, 662 BAU/mL), although the time point for the follow up was somewhat later.

For a functional characterisation of vaccine-induced antibodies towards the original B.1 RBD isolate, we used RBDCoV ACE2 - a multiplex competitive inhibition assay (23). ACE2 binding inhibition was significantly reduced in dialysed compared to non-dialysed individuals ($p=2.42*10^{-6}$, Mann-Whitney-U test) after the second vaccination (Figure 2B). Responses were comparably diminished in both groups four to eight months after the second vaccination, with only 12% and 6% of samples being above the 20% responder threshold in patients on haemodialysis and controls, respectively. However, comparable to IgG binding levels, the

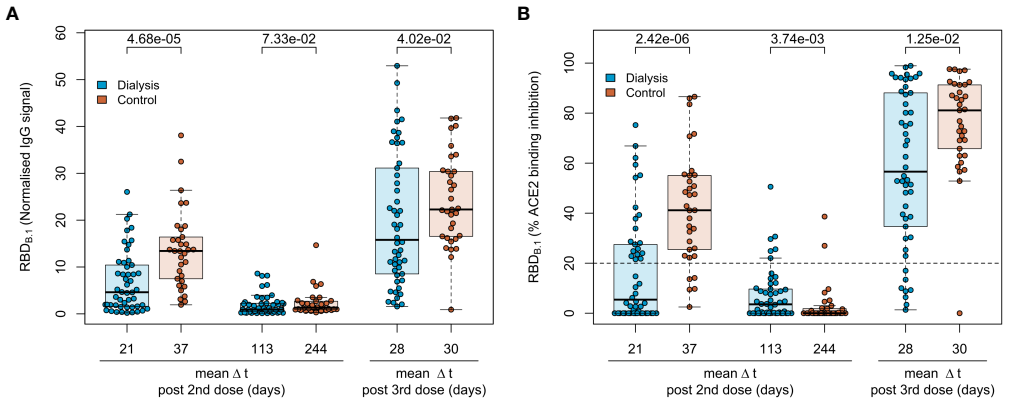

FIGURE 2
Humoral immune response in haemodialysis patients after a triple vaccination with BNT162b2. IgG response **(A)** and ACE2 binding inhibition **(B)** towards the SARS-CoV-2 B.1 RBD isolate were measured in plasma from haemodialysis patients (blue circles, n = 50) and controls (orange circles, n=33) using MULTICOV-AB **(A)** or an ACE2-RBD competition assay **(B)** after double or triple vaccination with BNT162b2 at the indicated time points. Data is displayed as normalised median fluorescence intensity (MFI) signal **(A)** for IgG binding or as % ACE2 binding inhibition where 100% indicates maximum inhibition and 0% no inhibition **(B)**. Samples with an ACE2 binding inhibition of less than 20% (dashed line) are classified as non-responders. Boxes represent the median, 25th and 75th percentiles, whiskers show the largest and smallest non-outlier values. Outliers were determined by 1.5 times IQR. Mean sampling time in days after two-dose BNT162b2 vaccination as Δt is displayed on the x-axis. Statistical significance was calculated by two-sided Mann-Whitney-U test. P-values for relevant comparisons are given above the sample groups. Significance was defined as $p < 0.05$. Response data from dialysed individuals from day 21 and day 113 after the second BNT162b2 dose were already published before as part of Strengert et al. (16) and Dulovic et al. (17).

10.3389/fimmu.2022.1004045

third BNT162b2 vaccination restored and even augmented ACE2 binding inhibition against the B.1 variant in both populations.

Strong immune responses after a fourth mRNA-1273 vaccination in haemodialysis patients

Next, we followed the anti-Spike RBD IgG levels in haemodialysis patients after the third vaccination over time and after a fourth vaccination with a full 100 µg dose of mRNA-1273, which was considered by German guidelines for immunocompromised individuals. As expected, IgG responses against the original B.1 isolate had again declined within approximately 4 months after the third vaccination (Figure 3A; Figure S2) as did the ACE2 binding inhibition activity as a surrogate for virus neutralisation (Figure 3B). Whilst the decline was not as severe as after the second BNT162b2 dose with now 64% of samples remaining above the 20% ACE2 binding inhibition threshold, only the fourth vaccination with mRNA-1273 markedly raised both anti-Spike RBD IgG levels (Figures 3A, S2; Table S3 for a complete statistical evaluation) and ACE2 binding inhibition (Figure 3B) towards the B.1 isolate above levels seen at peak response after the second and third dose of BNT162b2. 96% of samples from individuals on haemodialysis were now classified as above the 20% ACE2 responder threshold. Further, we also analysed the longitudinal development of ACE2 binding inhibition towards the dominantly circulating SARS-CoV-2 of 2021 (Delta) and 2022 (Omicron) (Figures 3C, D). ACE2 binding inhibition towards the Delta variant was slightly reduced over time compared to levels observed with the B.1 isolate. Overall, the third dose resulted in a clear increase in Delta ACE2 responder rates from 24% after two-dose BNT162b2 scheme to 64%, which was further increased to 94% after the subsequent dose of mRNA-1273 (Figure 3C). Importantly, neutralisation against the Omicron BA.1 variant, which was largely absent after the second vaccination and only transiently above threshold in 38% of dialysis patients after the third vaccination, reached high levels of ACE2 binding inhibition with an 80% responder rate at peak response after the fourth vaccination with mRNA-1273. This coincided with Omicron being the dominant SARS-CoV-2 variant circulating in Germany (Figure 3D).

We also analysed IgG binding longitudinally after a triple dose of BNT162b2 towards the RBD of B.1, Delta and Omicron

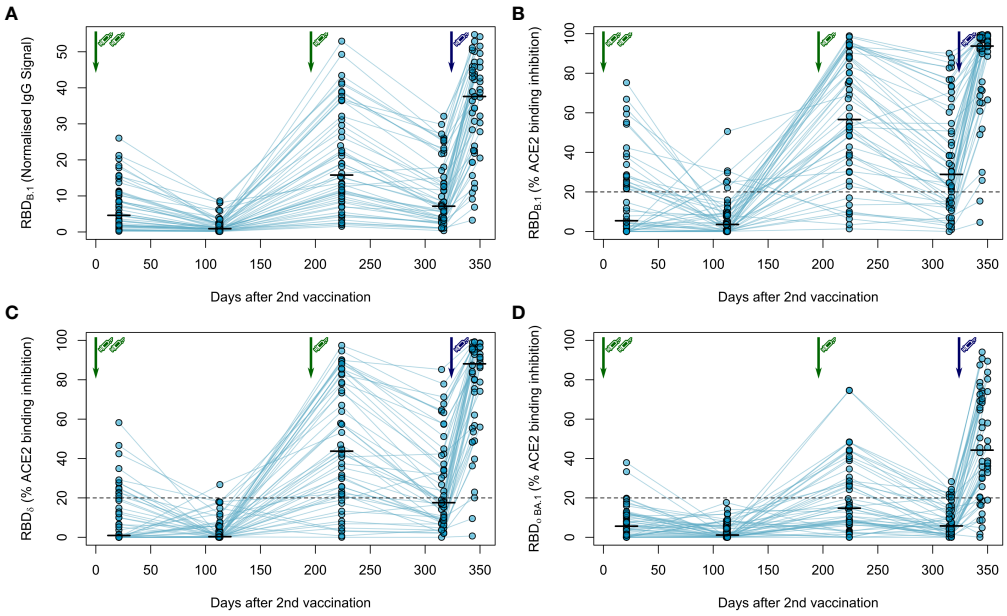

FIGURE 3
Longitudinal humoral immune response in haemodialysis patients after a triple vaccination with BNT162b2 and a fourth full-dose of mRNA-1273. IgG response **(A)** and ACE2 binding inhibition **(B–D)** towards the SARS-CoV-2 RBD of B.1 **(A, B)**, δ **(C)** and O BA.1 **(D)** isolates were measured in plasma from haemodialysis patients (n = 50) using MULTICOV-AB **(A)** or an ACE2-RBD competition assay **(B–D)** after immunisation with a triple dose of BNT162b2 (green syringe) and a fourth full-dose of mRNA-1273 (blue syringe). Data is displayed as normalised median fluorescence intensity (MFI) signal for IgG binding **(A)** or as % ACE2 binding inhibition where 100% indicates maximum inhibition and 0% no inhibition **(B–D)**. Samples with an ACE2 binding inhibition of less than 20% (dashed line) are classified as non-responders **(B–D)**. Interconnecting lines represent samples from the same individual. Sampling time points in days after the standard complete two-dose BNT162b2 vaccination is stated below the graph. Statistical significance was calculated by two-sided paired Wilcoxon rank test. Significance was defined as $p < 0.05$. All p-values for relevant comparisons are listed in Table S3.

BA.1 VoC in saliva of haemodialysis patients to determine protection levels at the primary side of SARS-CoV-2 replication. Although anti-RBD specific IgG was readily detectable both in the peak and plateau response phase following the complete two-dose and the third booster dose of BNT162b2, IgG binding towards the Delta and Omicron BA.1 RBD was significantly reduced compared to the B.1 RBD across all time points (Figure S4). Interestingly, saliva responses across vaccinated individuals were much more widespread in saliva than in plasma.

As clinical studies suggested that both cellular and humoral response can confer protection from COVID-19 (27), we also assessed vaccination-induced T-cell responses by IFNγ release assay longitudinally. Overall, these responses were more stable over time (Figure 4A). After two BNT162b2 vaccinations, IFNγ release after *in vitro* re-stimulation was readily detectable in haemodialysis patients, but declined slightly thereafter. The third BNT162b2 vaccination increased cellular responses to levels comparable to after the second vaccination. Similar to the humoral responses, the fourth vaccination with mRNA-1273 further increased IFNγ release after Spike S1 peptide restimulation of T-cells (Figure 4A; Table S3 for a complete statistical evaluation).

Finally, we correlated B- and T-cell responses after each vaccination within our longitudinal cohort of haemodialysis patients. We overall observed moderate correlation between peak T-cell responses (measured by IGRA) and B-cell responses [determined by % ACE2 binding inhibition of the B.1 variant (Spearman's rho=0.561, Figure 4B, upper panel)], which did not increase after the third (Spearman's rho=0.405) and fourth (Spearman's rho=0.371) vaccination. We further described responder rates for T- and B-cell response by a combined cut-off as displayed in Figure 4B. Notably, responder rates among haemodialysis patients strongly increased to 72% after the triple BNT162b2 dose and further to 86% after the fourth full-dose mRNA-1273. Importantly, whilst we observed a similar trend for the correlation coefficient between Delta and Omicron BA.1 % ACE2 binding inhibition and T-cell responses (Figure 4B; middle and lower panel, Table S3 for a complete statistical evaluation), dual cellular (>200mIU/mL) and humoral (>20% ACE inhibition) responders levels equally strongly increased for both VoC after the third and fourth vaccination to a final 84% and 74%, respectively.

Discussion

Although overall case mortality rates for SARS-CoV-2 have significantly decreased since the initial wave of the pandemic, maintaining high levels of vaccine-induced protection is of paramount importance for at-risk individuals for severe COVID-19 such as haemodialysis patients. Ensuring that these and other similarly vulnerable individuals are sufficiently protected remains challenging, with high case numbers throughout 2022 as a result of successive occurrence of Omicron subvariants. Despite clear recommendations on the need for a fourth dose, worryingly this fourth dose uptake among haemodialysis patients has decreased compared to the first three doses, with disparities among demographic groups remaining in place (28). At present, recommendations by the German Standing Committee on Vaccination (STIKO) clearly endorse a fourth SARS-CoV-2 vaccine dose including a full dose of mRNA-1273 for immunocompromised individuals (5), which contrasts WHO guidelines recommending 50 µg mRNA-1273 for fourth vaccinations (29).

Several studies report of superior immunity after initial mRNA-1273 prime/boost vaccination when compared to BNT162b2 in haemodialyis patients (30, 31) or in the general population (32–34) and further improved humoral responses after triple vaccination in dialysis patients (35–39). Third dose vaccination with mRNA-1273 or BNT162b2 provided comparable protection against symptomatic SARS-CoV-2 infection in the general population, although differences between both vaccines were observed after the second dose (40). Finally, Caillard et al. found that a four-dose mRNA-1273 compared to a four-dose BNT162b2 results in increased levels of binding antibodies in kidney transplant recipients (41). In general, COVID-19 vaccine-induced humoral immune responses tend to be higher in females and lower in elderly people. Differences in anti-S IgG were prominent after the second but not after the third vaccination, whilst males remained to have inferior neutralisation activity even after the third vaccination (42). We did not find such association most likely due to the smaller samples size of our cohort.

Two studies found more durable neutralising antibody titers four or six months after a third dose of mRNA vaccine compared to two doses (43, 44). For the BNT162b2 vaccine the decline was 1.6-fold at four months. These findings indicate robust long-lived antibody production after three doses, but the durability of neutralising activity against different SARS-CoV-2 variants could be variable (43). In a third study in an Israeli population receiving the BNT162b2 vaccine, the decline over approximately four months after the third dose was much higher (5.5-fold). We observed an about 3-fold decline in both groups, which is in line with the current literature and indicates that the peak anti-S IgG responses are the main drivers for the differences between groups over time and that the anti-S IgG kinetics are likely similar in dialysis patients and controls. However, conclusions about durability of antibody responses after 3-doses mRNA vaccination remain uncertain, particularly after combination of different vaccines (45). With regard to the T-cell responses, we (24, 25, 46, 47) and others (48, 49) have described that Spike-specific T-cell responses (CD4+ or CD8+ T-lymphocytes) after infection or prime/boost vaccination are more stable as compared to the respective humoral responses in healthy

10.3389/fimmu.2022.1004045

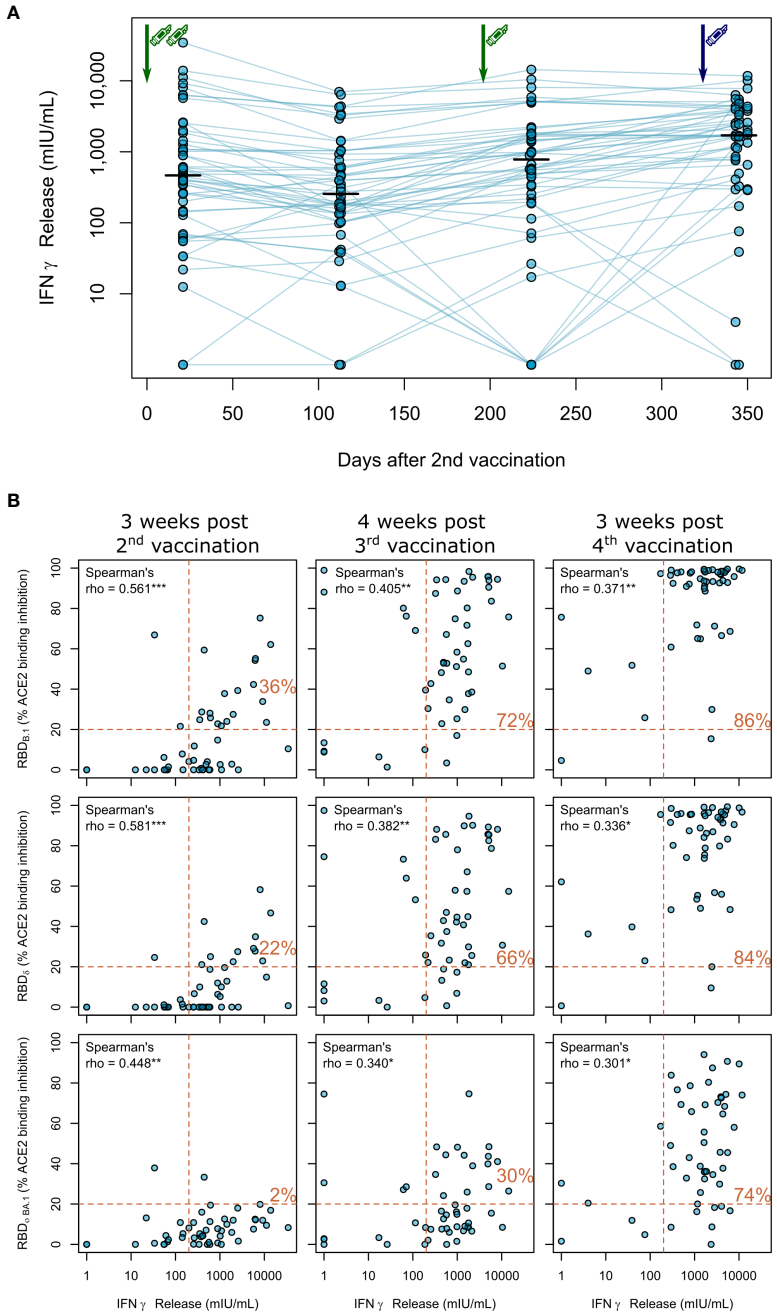

FIGURE 4
Impact of triple vaccination with BNT162b2 and a fourth full-dose of mRNA-1273 on cellular immune response in haemodialysis patients. **(A)** Whole blood from longitudinally-sampled vaccinated haemodialysis patients (n = 50) was *ex vivo* stimulated using a SARS-CoV-2 Spike S1-specific peptide pool. Supernatant fractions were then analysed by interferon γ release assay (IGRA). Interconnecting lines represent samples from the same individual. Sampling time points in days after two-dose BNT162b2 vaccination is displayed on the x-axis. Statistical significance was calculated by two-sided paired Wilcoxon rank test. Significance was defined as $p<0.05$. All p-values for relevant comparisons are listed in Table S3. Response data from dialysed individuals from day 21 after the second BNT162b2 dose were already published before as part of Strengert et al. (16) and Dulovic et al. (17). **(B)** T-cell responses assessed by IGRA and B-cell responses assessed by ACE2-RBD competition assay towards the RBD of B.1, Delta, Omicron BA.1 isolates were plotted for correlation analysis **(B)**. Correlation was calculated using Spearman's coefficient rho. P values are marked as * <0.05, ** <0.01, *** <0.001. Dashed lines indicated the respective responder thresholds for IGRA (IFNγ release >200 mIU/mL) and RBD-ACE2 binding assay (20%). Responder rates (%) for both cellular and humoral response are shown in the upper right quadrant.

individuals. Thus, vaccine-induced long-lasting T-cell memory after two or three COVID-19 vaccination are most likely not a specific response in dialysis patients COVID-19 (45). The IGRA employed in this study reliably detects vaccine-induced Spike-specific T-cell responses and showed good correlation to other techniques for studying post-vaccination T-cell immunity including ELISpot and intracellular cytokine staining (24, 26).

Potential causes for our observations may include the higher dose of mRNA-1273. Similar doses of mRNA-1273 (25 µg) to the BNT162b2 dose (30 µg) generated comparable Spike-specific memory CD4 T-cell frequencies to natural infection and about half as strong as those seen with high-dose vaccination (100 µg) indicating that differences between cellular and humoral immunity after two mRNA vaccines most likely result from the different doses of the vaccine (48). In addition, Spike and RBD IgG+ memory B-cell frequencies increase between 3 and 6 months after immunisation with mRNA vaccine (50) and germinal centers appear to be central to the immune responses to COVID-19 vaccines (45). Kidney transplant recipients, unlike healthy subjects, presented deeply blunted SARS-CoV-2-specific germinal center B-cell responses coupled with severely hindered neutralising antibody responses. These data indicate impaired germinal center-derived immunity in immunocompromised individuals (51). Germinal centers can persist and be productive for more than six months after two doses of COVID-19 mRNA vaccines and that the quality of neutralising antibodies can improve over three to six months (52). We speculate that diminished B-cell memory generation and germinal center formation is one feature of the immune dysfunction in dialysis patients and that repetitive vaccination, mix of mRNA vaccines or increase in vaccine dose may help to overcome these limitations. Finally, we specifically looked at dialysis patients with IGRA results below threshold after the third vaccination (n=12), of which almost all were among individuals with lowest IGRA results also after the second and fourth vaccination. We classified these as “low responders”, since also their anti-S IgG responses were persistently very low. These low responders comprised all patients with organ-transplantation (n=4) and 7 out of 8 individuals with immunosuppressive therapy at the time of the third vaccination. We found no other association to co-morbidities or clinical conditions in the low responder subgroup. Thus, immunosuppression as listed in Table S2 is a further explanation for the inferior humoral and cellular vaccine response in many of the low responders.

We can only speculate about the effects of mixing mRNA-based vaccines. Janssen et al. compared heterologous and homologous mRNA-1273 and BNT162b2 vaccination after the respective first vaccination in a randomised trial (53). They found the geometric mean titers of anti-Spike IgG antibodies for each heterologous regimen to be higher relative to the corresponding homologous regimen. This is consistent with data from Israel (54) and the COV-BOOST study (55), in which even half-dose mRNA-1273 as fourth dose after triple BNT162b2 vaccination appeared to have higher immunogenicity than full-dose BNT162b2. The authors suggested that this result might be due to a heterologous schedule effect or the vaccine dose. Interestingly, differences between both mRNA vaccines could be more complex, since mRNA-1273 is reported to induce higher concentrations of RBD- and N-terminal domain-specific IgA and more antibodies eliciting neutrophil phagocytosis and natural killer cell activation as compared to BNT162b2 (56).

Our study is, to our knowledge, the only study examining the longitudinal humoral and cellular immune response towards the most recent SARS-CoV-2 isolates in haemodiaylsis patients after administration of consistent vaccination regimens starting with a triple dose of BNT162b2 followed by a fourth full-dose of mRNA-1273. Whilst other studies principally support the beneficial impact of a fourth vaccination dose on both antibody titers and neutralising potency towards SARS-CoV-2 B.1 and VoC isolates, often various vaccination regimens including heterologous vector-based/mRNA regimens were pooled in cohorts (14) or vaccine dosages not provided (13).

Our data provide solid evidence that the triple vaccination resulted in mean antibody concentration and neutralising activity above levels to after the second vaccination. Interestingly, we identified significant further increases in both humoral and cellular response rates following the fourth dose, compared to the second and third. The increase in response rate from 30% to 74% from third to fourth dose for Omicron is particularly important considering it comprises almost all currently circulating variants of SARS-CoV-2. We consider this as a valid argument for a fourth vaccination in at-risk patients, especially, since T-cell immunity elicited by current vaccines is also effective against VoC including Omicron (57–59). The large range in both humoral and cellular responses illustrates however the variable nature of SARS-CoV-2 vaccination responses in dialysis patients and may be of relevance for identifying individuals with inferior responses in need for further doses.

Our study has several limitations. The number of participants within our cohort was limited, with only 50 patients on haemodialysis and a further 33 control participants, although our sample size is larger than similar studies examining the effect of the fourth dose within haemodialysis patients (15). The use of longitudinal cohort also allows us to directly identify the responses and their decline following each individual dose. Unfortunately, we were unable to obtain samples post-fourth dose for our control population, since many individuals were meanwhile infected with Omicron, additional booster vaccinations are not generally recommended and a full dose mRNA-1273 vaccination would be the unlikely regimen for the healthy controls. Although our control group was well-matched for sample collection at peak antibody levels after the second and third vaccination, they were not optimally matched for age and gender. A potential limitation of our study is that we used only peptides from a single SARS-

CoV-2 S1 protein for T-cell analysis, not taking into account reactivity against other variants including Omicron. To investigate the extent to which substitutions in spike and non-spike proteins affect T-cell recognition, several studies examined T-cells in vaccinated and convalescent individuals (49, 60–62). Overall, these studies show a high degree of preservation of T-cell epitopes between the ancestral strain, Omicron and other variants of concern. However, the degree of cross-reactivity varied among individuals, possibly as a consequence of genetic aspects of antigen presentation. Finally, it would have been interesting to directly compare homologous fourth BNT162b2 dose to mRNA-1273 in haemodialysis patients and to assess the reactogenicity, but this would have required a prospective study design for an interventional study.

Overall, a fourth full-dose of the mRNA-1273 vaccine elicits improved cellular and humoral responses compared to the triple BNT162b2 vaccination and appears to be an advisable strategy for immunocompromised patients, such as haemodialysis patients. Nevertheless, the decline after fourth vaccination and the effectivity against emerging SARS-CoV-2 variants will have to be monitored to assess the immune response duration and requirement for further booster vaccinations.

Data availability statement

The raw data supporting the conclusions of this article will be made available by the authors, without undue reservation.

Ethics statement

The studies involving human participants were reviewed and approved by the Internal Review Board of Hannover Medical School (MHH, approval number 8973_BO-K_2020, amendment Dec. 2020). The patients/participants provided their written informed consent to participate in this study.

Author contributions

GMNB, NS-M, AD, and MS conceived the study. MB, AD, MS, AD-J, GMNB, AC, NS-M, DJ, and MVS designed the experiments. NS-M, MS, GMNB, AD-J, and GK procured funding. GR, JG, JJ, DJ, and MVS performed experiments. KL, AB, EW, GL, AC, and GMNB collected samples or organised their collection. PK, BT, and UR produced and designed recombinant assay proteins. MB, KL, AD, MS, GR, MVS, and AC performed data collection and analysis. MB generated the figures. MB, MS, AD, and GMNB verified the underlying data. GMNB and MS wrote the first draft of the manuscript with input from MB, AC, KL, and AD. All authors critically reviewed and approved the final manuscript.

Funding

This work was financially supported by the Initiative and Networking Fund of the Helmholtz Association of German Research Centres (grant number SO-96), the EU Horizon 2020 research and innovation program (grant agreement number 101003480 - CORESMA), the State Ministry of Baden-Württemberg for Economic Affairs, Labour and Tourism (grant numbers FKZ 3-4332.62-NMI-67 and FKZ 3-4332.62-NMI-68) and the European Regional Development Fund (ZW7-8515131 and ZW7-85151373). The funders had no role in study design, data collection, data analysis, interpretation, writing or submission of the manuscript. All authors had complete access to the data and hold responsibility for the decision to submit for publication.

Acknowledgments

We sincerely thank all patients for their continued contribution and willingness to participate in this study. We also thank all clinical staff at the Eickenhof Dialysis Centre for their efforts to make this study possible.

Conflict of interest

NS-M was a speaker at Luminex user meetings in the past. The Natural and Medical Sciences Institute at the University of Tübingen is involved in applied research projects as a fee for services with the Luminex Corporation. GMNB was a speaker on a symposium sponsored by Moderna.

The remaining authors declare that the research was conducted in the absence of any commercial or financial relationships that could be construed as a potential conflict of interest.

Publisher's note

Supplementary material

The Supplementary Material for this article can be found online at: https://www.frontiersin.org/articles/10.3389/fimmu.2022.1004045/full#supplementary-material

References

1. Zeng B, Gao L, Zhou Q, Yu K, Sun F. Effectiveness of COVID-19 vaccines against SARS-CoV-2 variants of concern: A systematic review and meta-analysis. *BMC Med* (2022) 20(1):200. doi: 10.1186/s12916-022-02397-y

2. Manothummetha K, Chuleerarux N, Sanguankeo A, Kates OS, Hirankarn N, Thongkam A, et al. Immunogenicity and risk factors associated with poor humoral immune response of SARS-CoV-2 vaccines in recipients of solid organ transplant: A systematic review and meta-analysis. *JAMA Netw Open* (2022) 5(4):e226822. doi: 10.1001/jamanetworkopen.2022.6822

3. Galmiche S, Luong Nguyen LB, Tartour E, de Lamballerie X, Wittkop L, Loubet P, et al. Immunological and clinical efficacy of COVID-19 vaccines in immunocompromised populations: A systematic review. *Clin Microbiol Infect* (2022) 28(2):163–77. doi: 10.1016/j.cmi.2021.09.036

4. Kuderer NM, Lyman GH. COVID-19 vaccine effectiveness in patients with cancer: remaining vulnerabilities and uncertainties. *Lancet Oncol* (2022) 23(6):693–5. doi: 10.1016/S1470-2045(22)00252-2

5. Epidemiologisches Bulletin.Ständige Impfkommission: Beschluss der STIKO zur 20. Aktualisierung der COVID-19-Impfempfehlung. *Epid Bull* (2022) 21:3–19. doi: 10.25646/10076.2

6. *Update: FDA authorizes additional vaccine dose for certain immunocompromised individuals* (2021). Available at: https://www.fda.gov/news-events/press-announcements/coronavirus-covid-19-update-fda-authorizes-additional-vaccine-dose-certain-immunocompromised.

7. *Direction générale de la santé DGS precisions sur la vaccination IMD*. Available at: https://solidarites-sante.gouv.fr/IMG/pdf/dgs_urgent_52_precisions_sur_la_vaccination_imd.pdf.

8. Burki TK. Fourth dose of COVID-19 vaccines in Israel. *Lancet Respir Med* (2022) 10(2):e19. doi: 10.1016/S2213-2600(22)00010-8

9. Junker D, Becker M, Wagner TR, Kaiser PD, Maier S, Grimm TM, et al. Antibody binding and ACE2 binding inhibition is significantly reduced for both the BA1 and BA2 omicron variants. *Clin Infect Dis* (2022), ciac498. doi: 10.1093/cid/ciac498

10. van Gils MJ, Lavell A, van der Straten K, Appelman B, Bontjer I, Poniman M, et al. Antibody responses against SARS-CoV-2 variants induced by four different SARS-CoV-2 vaccines in health care workers in the Netherlands: A prospective cohort study. *PloS Med* (2022) 19(5):e1003991. doi: 10.1371/journal.pmed.1003991

11. Gruell H, Vanshylla K, Korenkov M, Tober-Lau P, Zehner M, Münn F, et al. SARS-CoV-2 Omicron sublineages exhibit distinct antibody escape patterns. *Cell Host Microbe* (2022) 30(9):1231–1241.e6. doi: 10.1101/2022.04.06.487257

12. van der Straten K, Guerra D, van Gils MJ, Bontjer I, Caniels TG, van Willigen HDG, et al. Antigenic cartography using sera from sequence-confirmed SARS-CoV-2 variants of concern infections reveals antigenic divergence of Omicron. *Immunity*. (2022) 55(9):1725–1731.e4. doi: 10.1016/j.immuni.2022.07.018

13. Anft M, Blazquez-Navarro A, Frahnert M, Fricke L, Meister TL, Roch T, et al. Inferior cellular and humoral immunity against omicron and delta variants of concern compared with SARS-CoV-2 wild type in hemodialysis patients immunized with 4 SARS-CoV-2 vaccine doses. *Kidney Int* (2022) 102(1):207–8. doi: 10.1016/j.kint.2022.05.004

14. Cheng CC, Platen L, Christa C, Tellenbach M, Kappler V, Bester R, et al. Improved SARS-CoV-2 neutralization of Delta and Omicron BA.1 variants of concern after fourth vaccination in hemodialysis patients. *Vaccines (Basel)* (2022) 10(8):1328. doi: 10.3390/vaccines10081328

15. Housset P, Kubab S, Hanafi L, Pardon A, Vittoz N, Bozman D-F, et al. Humoral response after a fourth "booster" dose of a coronavirus disease 2019 vaccine following a 3-dose regimen of mRNA-based vaccination in dialysis patients. *Kidney Int* (2022) 101(6):1289–90. doi: 10.1016/j.kint.2022.04.006

16. Strengert M, Becker M, Ramos GM, Dulovic A, Gruber J, Juengling J, et al. Cellular and humoral immunogenicity of a SARS-CoV-2 mRNA vaccine in patients on haemodialysis. *EBioMedicine*. (2021) 70:103524. doi: 10.1016/j.ebiom.2021.103524

17. Dulovic A, Strengert M, Ramos GM, Becker M, Griesbaum J, Junker D, et al. Diminishing immune responses against variants of concern in dialysis patients 4 months after SARS-CoV-2 mRNA vaccination. *Emerg Infect Dis* (2022) 28(4):743–50. doi: 10.3201/eid2804.211907

18. Behrens GMN, Cossmann A, Stankov MV, Schulte B, Streeck H, Förster R, et al. Strategic anti-SARS-CoV-2 serology testing in a low prevalence setting: The COVID-19 contact (CoCo) study in healthcare professionals. *Infect Dis Ther* (2020) 9(4):837–49. doi: 10.1007/s40121-020-00334-1

19. Becker M, Dulovic A, Junker D, Ruetalo N, Kaiser PD, Pinilla YT, et al. Immune response to SARS-CoV-2 variants of concern in vaccinated individuals. *Nat Commun* (2021) 12(1):3109. doi: 10.1038/s41467-021-23473-6

20. Rabenau HF, Biesert L, Schmidt T, Bauer G, Cinatl J, Doerr HW. SARS-coronavirus (SARS-CoV) and the safety of a solvent/detergent (S/D) treated immunoglobulin preparation. *Biologicals*. (2005) 33(2):95–9. doi: 10.1016/j.biologicals.2005.01.003

21. Becker M, Strengert M, Junker D, Kaiser PD, Kerrinnes T, Traenkle B, et al. Exploring beyond clinical routine SARS-CoV-2 serology using MultiCoV-ab to evaluate endemic coronavirus cross-reactivity. *Nat Commun* (2021) 12(1):1152. doi: 10.1038/s41467-021-20973-3

22. Planatscher H, Rimmele S, Michel G, Potz O, Joos T, Schneiderhan-Marra N. Systematic reference sample generation for multiplexed serological assays. *Sci Rep* (2013) 3:3259–64. doi: 10.1038/srep03259

23. Junker D, Dulovic A, Becker M, Wagner TR, Kaiser PD, Traenkle B, et al. COVID-19 patient serum less potently inhibits ACE2-RBD binding for various SARS-CoV-2 RBD mutants. *Sci Rep* (2022) 12(1):7168. doi: 10.1038/s41598-022-10987-2

24. Barros-Martins J, Hammerschmidt SI, Cossmann A, Odak I, Stankov MV, Morillas Ramos G, et al. Immune responses against SARS-CoV-2 variants after heterologous and homologous ChAdOx1 nCoV-19/BNT162b2 vaccination. *Nat Med* (2021) 27(9):1525–9. doi: 10.1038/s41591-021-01449-9

25. Behrens GMN, Barros-Martins J, Cossmann A, Ramos GM, Stankov MV, Odak I, et al. BNT162b2-boosted immune responses six months after heterologous or homologous ChAdOx1nCoV-19/BNT162b2 vaccination against COVID-19. *Nat Commun* (2022) 13(1):4872. doi: 10.1038/s41467-022-32527-2

26. Stankov MV, Cossmann A, Bonifacius A, Dopfer-Jablonka A, Ramos GM, Godecke N, et al. Humoral and cellular immune responses against severe acute respiratory syndrome coronavirus 2 variants and human coronaviruses after single BNT162b2 vaccination. *Clin Infect Dis* (2021) 73(11):2000–8. doi: 10.1093/cid/ciab555

27. Forni G, Mantovani A, Forni G, Mantovani A, Moretta L, Rappuoli R, et al. COVID-19 vaccines: where we stand and challenges ahead. *Cell Death Differentiation*. (2021) 28(2):626–39. doi: 10.1038/s41418-020-00720-9

28. Parker EPK, Tazare J, Hulme WJ, Bates C, Beale R, Carr EJ, et al. Factors associated with COVID-19 vaccine uptake in people with kidney disease: An OpenSAFELY cohort study. *medRxiv*. (2022), 2022.06.14.22276391. doi: 10.1101/2022.06.14.22276391

29. WHO. *The moderna COVID-19 (mRNA-1273) vaccine: what you need to know* (2022). Available at: https://www.who.int/news-room/feature-stories/detail/the-moderna-covid-19-mrna-1273-vaccine-what-you-need-to-know.

30. Van Praet J, Reynders M, De Bacquer D, Viaene L, Schoutteten MK, Caluwé R, et al. Predictors and dynamics of the humoral and cellular immune response to SARS-CoV-2 mRNA vaccines in hemodialysis patients: A multicenter observational study. *J Am Soc Nephrol* (2021) 32(12):3208. doi: 10.1681/ASN.2021070908

31. Yau K, Chan CT, Abe KT, Jiang Y, Atiquzzaman M, Mullin SI, et al. Differences in mRNA-1273 (Moderna) and BNT162b2 (Pfizer-BioNTech) SARS-CoV-2 vaccine immunogenicity among patients undergoing dialysis. *Can Med Assoc J* (2022) 194(8):E297. doi: 10.1503/cmaj.211881

32. Dulovic A, Kessel B, Harries M, Becker M, Ortmann J, Griesbaum J, et al. Comparative magnitude and persistence of humoral SARS-CoV-2 vaccination responses in the adult population in Germany. *Front Immunol* (2022) 13. doi: 10.3389/fimmu.2022.828053

33. Montoya JG, Adams AE, Bonetti V, Deng S, Link NA, Pertsch S, et al. Differences in IgG antibody responses following BNT162b2 and mRNA-1273 SARS-CoV-2 vaccines. *Microbiol spectrum*. (2021) 9(3):e0116221. doi: 10.1128/Spectrum.01162-21

34. Steensels D, Pierlet N, Penders J, Mesotten D, Heylen L. Comparison of SARS-CoV-2 antibody response following vaccination with BNT162b2 and mRNA-1273. *Jama*. (2021) 326(15):1533–5. doi: 10.1001/jama.2021.15125

35. Benning L, Klein K, Morath C, Bartenschlager M, Kim H, Buylaert M, et al. Neutralizing antibody activity against the B.1.617.2 (delta) variant before and after a third BNT162b2 vaccine dose in hemodialysis patients. *Front Immunol* (2022) 13. doi: 10.3389/fimmu.2022.840136

36. Espi M, Charmetant X, Barba T, Mathieu C, Pelletier C, Koppe L, et al. A prospective observational study for justification, safety, and efficacy of a third dose of mRNA vaccine in patients receiving maintenance hemodialysis. *Kidney Int* (2022) 101(2):390–402. doi: 10.1016/j.kint.2021.10.040

37. Tillmann F-P, Figiel L, Ricken J, Still H, Korte C, Plaßmann G, et al. Effect of third and fourth mRNA-based booster vaccinations on SARS-CoV-2 neutralizing antibody titer formation, risk factors for non-response, and outcome after SARS-CoV-2 omicron breakthrough infections in patients on chronic hemodialysis: A

prospective multicenter cohort study. *J Clin Med* (2022) 11(11):3187–201. doi: 10.3390/jcm11113187

38. Patyna S, Eckes T, Koch BF, Sudowe S, Oftring A, Kohmer N, et al. Impact of moderna mRNA-1273 booster vaccine on fully vaccinated high-risk chronic dialysis patients after loss of humoral response. *Vaccines* (2022) 10(4):585–94. doi: 10.3390/vaccines10040585

39. Bensouna I, Caudwell V, Kubab S, Acquaviva S, Pardon A, Vittoz N, et al. SARS-CoV-2 antibody response after a third dose of the BNT162b2 vaccine in patients receiving maintenance hemodialysis or peritoneal dialysis. *Am J Kidney Diseases.* (2022) 79(2):185–92.e1. doi: 10.1053/j.ajkd.2021.08.005

40. Niesen Michiel JM, Matson R, Puranik A, O'Horo John C, Pawlowski C, Vachon C, et al. Third dose vaccination with mRNA-1273 or BNT162b2 vaccines improves protection against SARS-CoV-2 infection. *PNAS Nexus* (2022) 1(2): pgac042. doi: 10.1093/pnasnexus/pgac042

41. Benotmane I, Gautier G, Perrin P, Olagne J, Cognard N, Fafi-Kremer S, et al. Antibody response after a third dose of the mRNA-1273 SARS-CoV-2 vaccine in kidney transplant recipients with minimal serologic response to 2 doses. *JAMA.* (2021) 326(11):1063–5. doi: 10.1001/jama.2021.12339

42. Lustig Y, Gonen T, Meltzer L, Gilboa M, Indenbaum V, Cohen C, et al. Superior immunogenicity and effectiveness of the third compared to the second BNT162b2 vaccine dose. *Nat Immunol* (2022) 23(6):940–6. doi: 10.1038/s41590-022-01212-3

43. Pajon R, Doria-Rose NA, Shen X, Schmidt SD, O'Dell S, McDanal C, et al. SARS-CoV-2 omicron variant neutralization after mRNA-1273 booster vaccination. *N Engl J Med* (2022) 386(11):1088–91. doi: 10.1056/NEJMc2119912

44. Xia H, Zou J, Kurhade C, Cai H, Yang Q, Cutler M, et al. Neutralization and durability of 2 or 3 doses of the BNT162b2 vaccine against omicron SARS-CoV-2. *Cell Host Microbe* (2022) 30(4):485–8.e3. doi: 10.1016/j.chom.2022.02.015

45. Sette A, Crotty S. Immunological memory to SARS-CoV-2 infection and COVID-19 vaccines. *Immunol Rev* (2022) 310(1):27–46. doi: 10.1111/imr.13089

46. Bonifacius A, Tischer-Zimmermann S, Dragon AC, Gussarow D, Vogel A, Krettek U, et al. COVID-19 immune signatures reveal stable antiviral T cell function despite declining humoral responses. *Immunity.* (2021) 54(2):340–54.e6. doi: 10.1016/j.immuni.2021.01.008

47. Guerrera G, Picozza M, D'Orso S, Placido R, Pirronello M, Verdiani A, et al. BNT162b2 vaccination induces durable SARS-CoV-2-specific T cells with a stem cell memory phenotype. *Sci Immunol* (2021) 6(66):eabl5344. doi: 10.1126/sciimmunol.abl5344

48. Mateus J, Dan JM, Zhang Z, Rydyznski Moderbacher C, Lammers M, Goodwin B, et al. Low-dose mRNA-1273 COVID-19 vaccine generates durable memory enhanced by cross-reactive T cells. *Science* (2021) 374(6566):eabj9853. doi: 10.1126/science.abj9853

49. Tarke A, Coelho CH, Zhang Z, Dan JM, Yu ED, Methot N, et al. SARS-CoV-2 vaccination induces immunological T cell memory able to cross-recognize variants from alpha to omicron. *Cell.* (2022) 185(5):847–59.e11. doi: 10.1016/j.cell.2022.01.015

50. Zhang Z, Mateus J, Coelho CH, Dan JM, Moderbacher CR, Galvez RI, et al. Humoral and cellular immune memory to four COVID-19 vaccines. *Cell.* (2022) 185(14):2434–51.e17. doi: 10.1016/j.cell.2022.05.022

51. Lederer K, Bettini E, Parvathaneni K, Painter MM, Agarwal D, Lundgreen KA, et al. Germinal center responses to SARS-CoV-2 mRNA vaccines in healthy and immunocompromised individuals. *Cell.* (2022) 185(6):1008–24.e15. doi: 10.1016/j.cell.2022.01.027

52. Turner JS, O'Halloran JA, Kalaidina E, Kim W, Schmitz AJ, Zhou JQ, et al. SARS-CoV-2 mRNA vaccines induce persistent human germinal centre responses. *Nature.* (2021) 596(7870):109–13. doi: 10.1038/s41586-021-03738-2

53. Janssen C, Cachanado M, Ninove L, Lachatre M, Michon J, Epaulard O, et al. Immunogenicity and reactogenicity of heterologous and homologous mRNA-1273 and BNT162b2 vaccination: A multicenter non-inferiority randomized trial. *eClinicalMedicine.* (2022) 48:101444. doi: 10.1016/j.eclinm.2022.101444

54. Regev-Yochay G, Gonen T, Gilboa M, Mandelboim M, Indenbaum V, Amit S, et al. Efficacy of a fourth dose of covid-19 mRNA vaccine against omicron. *New Engl J Med* (2022) 386(14):1377–80. doi: 10.1056/NEJMc2202542

55. Munro APS, Janani L, Cornelius V, Aley PK, Babbage G, Baxter D, et al. Safety and immunogenicity of seven COVID-19 vaccines as a third dose (booster) following two doses of ChAdOx1 nCov-19 or BNT162b2 in the UK (COV-BOOST): a blinded, multicentre, randomised, controlled, phase 2 trial. *Lancet* (2021) 398(10318):2258–76. doi: 10.1016/S0140-6736(21)02717-3

56. Kaplonek P, Cizmeci D, Fischinger S, A-r C, Suscovich T, Linde C, et al. mRNA-1273 and BNT162b2 COVID-19 vaccines elicit antibodies with differences in fc-mediated effector functions. *Sci Trans Med* (2022) 14(645):eabm2311. doi: 10.1126/scitranslmed.abm2311

57. De Marco L, D'Orso S, Pirronello M, Verdiani A, Termine A, Fabrizio C, et al. Assessment of T-cell reactivity to the SARS-CoV-2 omicron variant by immunized individuals. *JAMA Network Open* (2022) 5(4):e2210871–e. doi: 10.1001/jamanetworkopen.2022.10871

58. Jung MK, Jeong SD, Noh JY, Kim D-U, Jung S, Song JY, et al. BNT162b2-induced memory T cells respond to the omicron variant with preserved polyfunctionality. *Nat Microbiol* (2022) 7(6):909–17. doi: 10.1038/s41564-022-01123-x

59. Jergović M, Coplen CP, Uhrlaub JL, Beitel SC, Burgess JL, Lutrick K, et al. Cutting edge: T cell responses to B.1.1.529 (Omicron) SARS-CoV-2 variant induced by COVID-19 infection and/or mRNA vaccination are largely preserved. *J Immunol* (2022) 208(11):2461–5. doi: 10.4049/jimmunol.2200175

60. Naranbhai V, Nathan A, Kaseke C, Berrios C, Khatri A, Choi S, et al. T Cell reactivity to the SARS-CoV-2 omicron variant is preserved in most but not all individuals. *Cell.* (2022) 185(6):1041–51.e6. doi: 10.1016/j.cell.2022.01.029

61. Keeton R, Tincho MB, Ngomti A, Baguma R, Benede N, Suzuki A, et al. T Cell responses to SARS-CoV-2 spike cross-recognize omicron. *Nature.* (2022) 603 (7901):488–92. doi: 10.1038/s41586-022-04460-3

62. GeurtsvanKessel CH, Geers D, Schmitz KS, Mykytyn AZ, Lamers MM, Bogers S, et al. Divergent SARS-CoV-2 omicron-reactive T and b cell responses in COVID-19 vaccine recipients. *Sci Immunol* (2022) 7(69):eabo2202. doi: 10.1126/sciimmunol.abo2202

frontiers | Frontiers in Immunology

TYPE Review
PUBLISHED 10 October 2022
DOI 10.3389/fimmu.2022.984252

OPEN ACCESS

EDITED BY
Francesca Re,
University of Milano Bicocca, Italy

REVIEWED BY
Morgan Brittany Johnson,
University of North Carolina at Charlotte, United States
Shengshuang Zhu,
Eli Lilly, United States

*CORRESPONDENCE
Marina A. Dobrovolskaia
marina@mail.nih.gov

SPECIALTY SECTION
This article was submitted to Molecular Innate Immunity, a section of the journal Frontiers in Immunology

RECEIVED 01 July 2022
ACCEPTED 23 August 2022
PUBLISHED 10 October 2022

CITATION
Dobrovolskaia MA (2022) Lessons learned from immunological characterization of nanomaterials at the Nanotechnology Characterization Laboratory. *Front. Immunol.* 13:984252. doi: 10.3389/fimmu.2022.984252

Lessons learned from immunological characterization of nanomaterials at the Nanotechnology Characterization Laboratory

Marina A. Dobrovolskaia*

Nanotechnology Characterization Laboratory, Cancer Research Technology Program, Frederick National Laboratory for Cancer Research, Sponsored by the National Cancer Institute, Frederick, MD, United States

Nanotechnology carriers have become common in pharmaceutical products because of their benefits to drug delivery, including reduced toxicities and improved efficacy of active pharmaceutical ingredients due to targeted delivery, prolonged circulation time, and controlled payload release. While available examples of reduced drug toxicity through formulation using a nanocarrier are encouraging, current data also demonstrate that nanoparticles may change a drug's biodistribution and alter its toxicity profile. Moreover, individual components of nanoparticles and excipients commonly used in formulations are often not immunologically inert and contribute to the overall immune responses to nanotechnology-formulated products. Said immune responses may be beneficial or adverse depending on the indication, dose, dose regimen, and route of administration. Therefore, comprehensive toxicology studies are of paramount importance even when previously known drugs, components, and excipients are used in nanoformulations. Recent data also suggest that, despite decades of research directed at hiding nanocarriers from the immune recognition, the immune system's inherent property of clearing particulate materials can be leveraged to improve the therapeutic efficacy of drugs formulated using nanoparticles. Herein, I review current knowledge about nanoparticles' interaction with the immune system and how these interactions contribute to nanotechnology-formulated drug products' safety and efficacy through the lens of over a decade of nanoparticle characterization at the Nanotechnology Characterization Laboratory.

KEYWORDS

nanoparticles, nucleic acids, immunotoxicity, characterization, trends, methods

Introduction

Nanotechnology is often used to formulate various drugs to improve their solubility, prolong circulation time, achieve delivery to the target organs and tissues, direct the route of particle uptake into and intracellular distribution within a target cell, and benefit from multifunctional capabilities (1–6). Many nanotechnology-based concepts are already used in the clinic and include, among others, anticancer formulations (e.g., Onivyde, Doxil, Abraxane, Daunoxome), anti-microbial agents (e.g., Ambisome), therapeutic nucleic acids (e.g., Onpattro), and vaccines (e.g., Comirnaty). Some industry reports suggest that the global nanomedicine market is rapidly increasing at a compound annual growth rate of 12.6% and will reach $258.11 billion in 2025 (7). Indeed, many nanotechnology-based concepts are in various stages of drug development, including clinical trials. As a recent example, in August 2020, ClinicalTrials.gov reported 1,200 various nanoparticle-based treatments for over 200 indications (8); these numbers continue to grow every year. Most of these concepts (~72%) in 2020 were intended to treat different cancer types, while a small percentage covered indications for body weight, non-cancerous diseases affecting various systems, and infectious diseases (Figure 1). The dominance of anti-cancer nanomedicines is not surprising due to the extensive research in the past three decades demonstrating the role of the enhanced permeability and retention (EPR) phenomenon in nanoparticle trafficking to and accumulation in solid tumors. The initial EPR concept implied that due to their size, nanoparticles readily pass the leaky vasculature of tumors and stay in the tumor milieu, unable to exit quickly due to altered lymphatic drainage; as such, they accumulate and release drugs in tumors, reducing the exposure of healthy tissues to cytotoxic drugs. However, more recently, the complexity of EPR became evident in that this phenomenon was more pronounced in some but not all solid tumors and varied considerably between patients. This recent notion stimulated cancer nanomedicine researchers to develop strategies, such as quantifying the degree of EPR in individual patients by non-invasive imaging techniques prior to administering the treatment, with the overall goal of improving the delivery of nanomedicines to tumors. The controversy surrounding EPR and various strategies for improving cancer nanomedicine targeting and efficacy have been recently discussed by Lammers and the team (9). Verifying the clinical utility of these strategies is expected to result in more cancer nanomedicine concepts going into clinical trials.

Given the current global emergency use of lipid-nanoparticle (LNP)-based COVID-19 vaccines to combat the COVID-19 pandemic, some experts expect more nanotechnology applications in infectious diseases (10).

Many studies have demonstrated that the reformulation of a drug using a nanocarrier helps to reduce the drug's toxicity. For example, the anticancer drug doxorubicin (DXR) is known for its accumulation in cardiomyocytes and in relation to its cardiotoxicity; this toxicity is overcome when DXR is delivered using a polyethylene glycol (PEG)-modified liposome (Doxil) (11). The removal of toxic excipient Cremophor and reformulation of another anticancer drug, paclitaxel, using nanoalbumin particles, resulted in an improved safety profile. As a result, the original, Cremophor-EL-based formulation of paclitaxel (Taxol) requires slow infusion and premedication to avoid anaphylactoid reactions, whereas nanoalbumin-formulated paclitaxel (Abraxane) is injected without premedication and does

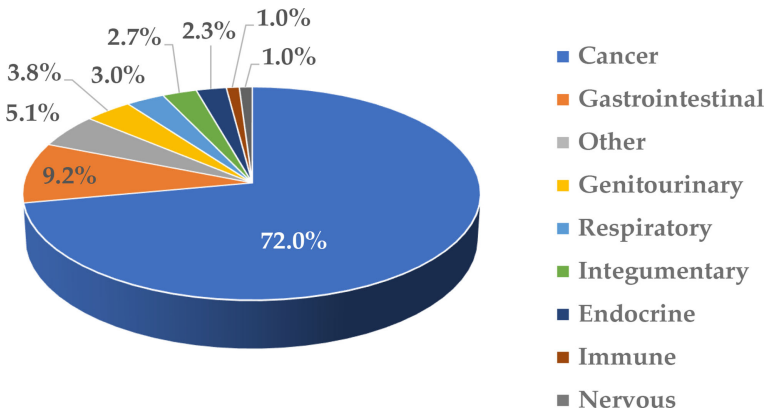

FIGURE 1
Clinical trials involving nanotechnology-based formulations. This figure was prepared based on data downloaded from ClinicalTrials.gov (8) on August 5, 2020; the accessibility of the site was verified on March 2, 2022. The data were grouped based on disease type and the percentage of total (1,200) was calculated. The cancer category included malignancies affecting various organs and systems. Non-cancerous diseases were grouped based on the type of affected system. "Other" includes communicable diseases, congenital abnormalities, body weight, musculoskeletal, death, fibrosis, infectious and stomatognathic diseases, tissue adhesion, blister, and breast and otorhinolaryngologic diseases.

not induce anaphylaxis (12, 13). The formulation of therapeutic proteins TNFα and coagulation factor VIII (FVIII) using colloidal gold and liposome, respectively, helped to overcome systemic inflammatory response to TNFα and generation of neutralizing antibodies to FVIII (14–16).

While reduced drug toxicity through formulation with a nanocarrier is encouraging, available data also suggest that a change in the drug's biodistribution due to the carrier may also occur and lead to the "relocation" of toxicity from one target organ to another. For example, the liposomal formulation of DXR helped to overcome DXR's cardiotoxicity (11); however, due to the liposomal drug's accumulation in the skin's dendritic cells, it created new toxicity, palmar-plantar erythrodysesthesia (PPE, also known as Hand-and-Foot Syndrome) (17). Reformulation of the same active pharmaceutical ingredient (API) DXR using cyanoacrylate nanoparticles eliminated cardiotoxicity and PPE but resulted in nephrotoxicity due to the drug's accumulation in the kidneys (18). These studies emphasize the importance of performing comprehensive toxicology studies even when a previously known drug is used in formulations using nanoparticles because nanocarriers may change the distribution of the drug and, hence, alter its toxicity profile.

For decades, the efforts of the nanotechnology drug delivery community were focused on masking nanoparticles from immune recognition (19–21). However, recent evidence shows that this intrinsic ability of the immune system to clear particulate materials —one that researchers have tried to work around for years—is one that can be modulated to synergize with the primary mechanism of action of drugs delivered by nanocarriers. This creates limitless opportunities to harness this property and direct it against disease-causing mechanisms (22). For example, PEGylated liposomal DXR (Doxil), initially approved for cancer therapy due to its ability to decrease DXR-mediated cardiotoxicity, is now known to stimulate the anticancer immune response, through a mechanism that is not completely understood, that allows for improved anticancer efficacy when Doxil is combined with immune-checkpoint inhibitors (23). A study in a colorectal cancer model in immunocompetent but not immunocompromised mice demonstrated that a combination of Doxil and anti-PD1 resulted in a complete response in 11 out of 12 animals (23). In another study, the same API DXR, formulated using polymeric-LNPs, was effective against breast cancer in treated animals by reducing immunosuppression in the tumor microenvironment (24). RGD-targeted LNPs co-delivering API (a-GalCer) and an immunomodulatory agent (PI3K inhibitor) improved therapeutic outcomes against breast tumors (25). Nanoalbumin-formulated paclitaxel (Abraxane) that has already been approved for clinical use as monotherapy is also undergoing clinical testing in combination with immune-checkpoint inhibitors to improve the outcome of anti-tumor therapy (26, 27).

The mechanisms through which nanocarriers contribute to immunomodulation are incompletely understood. One mechanism commonly discussed in cancer therapy literature includes the induction of so-called immunogenic cell death (ICD) by APIs, which are more precisely delivered to tumors by nanocarriers (28). The studies that favor this mechanism include those demonstrating that APIs, such as paclitaxel, oxaliplatin, gemcitabine, DXR, 5-fluorouracil, and gemcitabine, to name a few, activate apoptotic pathways that lead to the release of so-called danger signals or danger-associated molecular patterns [DAMPs (e.g., ATP, calreticulin and high-mobility group-B1 protein)] that activate tumor-infiltrating antigen-presenting cells, thereby contributing to immunogenicity of tumor-specific antigens released by dying cancer cells; these studies have been discussed in detail elsewhere (29–31). In contrast, some studies clearly demonstrate that cytotoxic APIs do not have the same efficacy as their nanoparticle-formulated counterparts when used in immunocompetent animals and combined with immune-checkpoint inhibitors (23). Therefore, ICD induction by cytotoxic APIs alone does not entirely explain the observed improvement in anti-tumor efficacy.

The existing data suggest that nanocarriers may contribute to this phenomenon through other mechanisms than delivering an ICD-inducing drug to tumors. Some of such mechanisms may include nanocarriers inducing chemokines. For example, I reported earlier that liposomes and lipid nanocarriers commonly induce chemokine IL-8 (32), which is responsible for the recruitment of leukocytes (33). Other mechanisms may be linked to intracellular complement activation. For example, our team found that dendrimers and other cationic polymeric molecules activate an intracellular complement (34) that plays a critical role in regulating T-cell activation (35–37).

Moreover, nanocarriers can be loaded with immunomodulatory agents that improve the therapeutic outcome of cytotoxic agents. For example, liposomes formulated to co-deliver a PI3K inhibitor with an API (a-GalCer) activated anti-tumor T-cell responses (25). In another recent study, nanoscale coordination polymer core-shell nanoparticles were designed to co-deliver oxaliplatin and dihydroartemesinin; these particles induced reactive oxygen species (ROS), which activated the immune cells and improved the anti-tumor response to anti-PD-1 immunotherapy (38). Interestingly, chemokine induction by lipid-based nanocarriers has also been attributed to their ability to induce ROS (39). Besides activating the chemokine responses, oxidative stress also negatively regulates the complement factor H (a complement system inhibitor), thereby further contributing to inflammatory responses (40). Therefore, oxidative stress induced by a nanocarrier may be an important mechanism contributing to the observed efficacy of nanoformulated drugs in immunotherapy applications.

It is well established now that nanoparticle physicochemical properties such as size, aspect ratio, zeta potential, hydrophobicity, surface area, and functionalization determine interactions between nanoparticles and immune cells. By optimizing these properties, researchers could control undesirable immunotoxicity and achieve desirable immunomodulatory effects. More studies are needed to fully understand the mechanisms by which nanocarriers contribute

to API therapeutic efficacy (besides their primary role as drug-delivery vehicles).

Regardless of the indication, all new formulations must undergo rigorous safety testing prior to their approval for clinical use. Even after receiving initial approval, drugs undergo post-marketing surveillance and can be removed from the market due to toxicity (41). One reason for drug discontinuation in clinical practice is immunotoxicity, with hypersensitivity reactions (HSRs) being named frequently (42, 43). Herein, I will focus on available information relevant to HSRs and immunosuppression and review the current literature about nanoparticle-mediated immunotoxicity and available methodologies to study it.

Infusion reactions

Infusion reactions (IRs) are HSRs that occur within minutes to hours of nanoparticle administration (44). The mechanisms underlying IRs to nanomedicines are complex and often involve overlapping pathways and systems (Figure 2). Some of the currently known mechanisms include activation of the complement system and so-called complement activation related pseudoallergy (CARPA), activation of platelets that release secondary mediators contributing to the overall response, and production of cytokines by immune cells, including but not limited to macrophages (44–48). Interestingly, IR symptoms in patients receiving intravenous (i.v.) injection or infusion of nanomedicines overlap with that of HSR in individuals immunized with LNP-based mRNA vaccines (49). It is generally agreed that the same pro-inflammatory properties of LNPs required for vaccine efficacy also contribute to the HSR. More detailed mechanisms and safety roadmaps for IRs to nanomedicine and HSRs to LNP-based mRNA vaccines have been discussed elsewhere (44, 49). Below I will focus on the complement system, the coagulation system, and cytokines that are recognized among leading contributors to nanoparticle-mediated IRs and HSRs.

Complement system

The complement system plays an essential role in both innate and adaptive immunity (50). It is complex and includes a large group of proteins that are produced by different cells in the body, act in different compartments, get activated by different mechanisms, and contribute to different types of immune responses (Figure 3). The discussion below focuses on current knowledge about plasma and intracellular complement systems.

Plasma complement

The plasma complement is a group of more than 30 proteins produced by the liver and secreted into the blood, where they "complement" cellular immune defense mechanisms. Activation

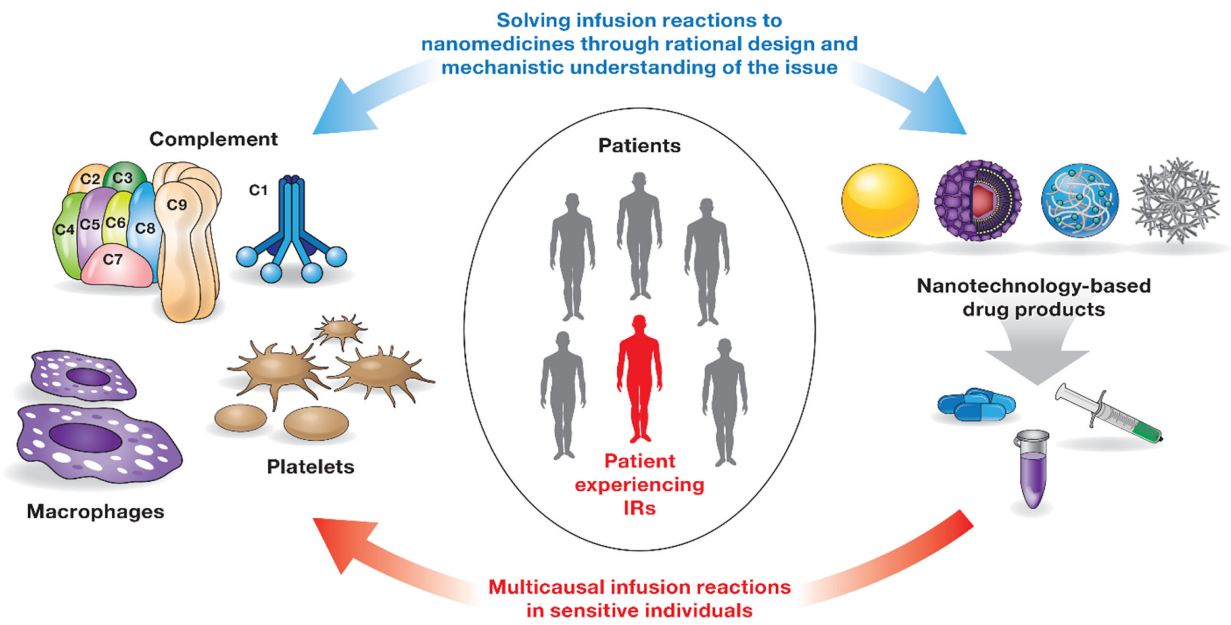

FIGURE 2
Infusion reactions to nanomedicines. IRs to nanomedicines involve multiple players (immune cells, coagulation, and complement systems) and complex, often overlapping mechanisms. Not all patients are sensitive to these responses. Interaction between one or several components of the immune system and the nanocarrier triggers these responses in sensitive individuals. Timely detection and appropriate management of IRs are critical to avoid severe health consequences for patients undergoing therapy with nanomedicines. IRs are not unique to nanomedicines and have been documented for other types of drug products (44). Rational design of nanocarriers and understanding of mechanisms underlying nanoparticle-mediated immunotoxicity are currently considered a solution to overcome the issue of IRs to nanomedicines.

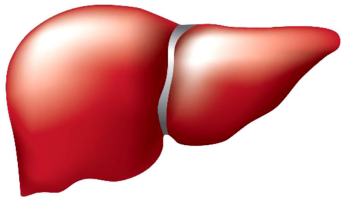

Plasma Complement

1. Produced by the liver
2. Required for the detection and removal of pathogens
3. Activation occurs in plasma
4. Activated via formation of convertase
5. Essential component of innate immunity
6. Undesirable activation leads to acute toxicity, which can be resolved by removing exposure to activating agent
7. Undesirable activation leads to anaphylactoid reactions and CARPA

Intracellular Complement

1. Resides inside of T cells
2. Required for sustaining T-cell function
3. Activation occurs inside the cell
4. Activated by cathepsin L
5. Essential component of adaptive immunity
6. Undesirable activation may lead to chronic toxicity, which cannot be resolved by removing exposure to activating agent*
7. Undesirable activation may lead to autoimmunity*

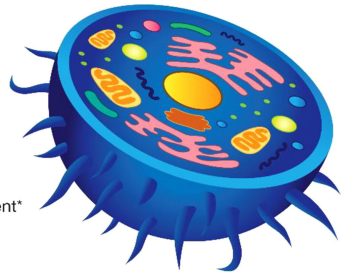

FIGURE 3
The main characteristics of the complement system. The main characteristics of plasma and intracellular complement are summarized. The intracellular complement system is discussed in the figure in the context of T lymphocytes due to a better understanding of its function in the currently available literature. The intracellular complement system has also been detected in other cell types; its role in other cells is less understood and, therefore, not mentioned in the figure. Statements highlighted with an asterisk (*) were hypothesized based on the role of lymphocytes in which the intracellular complement system was described; experimental verification is still required for these statements and represents one of the future directions of research in this field.

of the plasma complement system occurs *via* three main mechanisms—the lectin pathway, initiated by mannose-binding lectin; the classical pathway, initiated by the antibody; and the alternative pathway initiated by C3b binding. Additionally, autoactivation can occur *via* the so-called C3-tickover mechanism (51). Once triggered, these pathways result in sequential proteolytic cleavage of complement proteins organized in a cascade that converges on the C3 component of the complement. The activation culminates with the formation of terminal, or so-called membrane-attack complex, sC5b-9, which is perforin disrupting a microbe membrane and "killing" the microbe. Activation of the plasma complement results in production of anaphylatoxins—C3a, C4a, and C5a—that act like cytokines and activate immune cells, thereby promoting the immune response (51). The action of the plasma complement system is tightly connected to that of the blood coagulation and kinin/kallikrein systems, collectively acting to stop the infection and restore homeostasis. The same components of the complement system intended for the elimination of the pathogen—anaphylatoxins and terminal complex—are also responsible for adverse effects: tissue swelling, redness, pain, and cardiopulmonary changes. When complement activation is triggered by drug products (e.g., PEGylated liposomal DXR or Cremophor-EL formulated drugs), it leads to CARPA. CARPA symptoms overlap with that of immediate type I HSRs triggered by antigen-specific IgE. When left uncontrolled, CARPA may be fatal. Janos Szebeni of the Semmelweis University in Hungary pioneered the research on CARPA; he coined the term, described the mechanism, and developed *in vitro* and *in vivo* models used by other researchers worldwide to understand this phenomenon further and find the means for controlling it to prevent adverse health effects. Plasma complement activation and CARPA in response to pharmaceuticals, including those formulated using nanotechnology, have been extensively discussed in the literature (most recent references: (44, 46, 48, 52–54); Dr. Szebeni published more than 100 papers on this subject). Understanding the immunogenicity of drug products and their components, as detailed in the immunogenicity section of this review, provides mechanistic insights in understanding the CARPA phenomenon due to the known role of certain types of antibodies in activating the classical complement pathway.

Herein, I want to briefly summarize key structure-activity relationships and current approaches for minimizing the ill effects of CARPA on patients receiving nanomedicines to lay the foundation for the next section pertaining to the lesser-known intracellular complement system. Factors influencing complement activation by PEGylated liposomes include lipid composition and structure, zeta potential, surface and PEG phospholipid anchor charge, density, and the molecular weight of PEG (55). Similar findings were described in another study demonstrating that conformation and density of glycopolymer

coating on polystyrene nanoparticles can serve as "molecular switches" of complement activation (56). An increase in the surface load of cationic moieties on perfluorocarbon nanoparticles was associated with an increase in complement activation, whereas the addition of PEG-3000, but not PEG-350, decreased the reactogenicity (57). Moreover, drug release and crystal formation at the particle surface and contamination with endotoxin may further contribute to the reactogenicity of nanoparticles with the complement system, as was discussed in a liposome study (55). Decreasing nanomedicine infusion rate *in vivo*, applying complement inhibitors, and injecting empty nanocarriers (e.g., Doxebo) before administering drug-loaded nanoparticles (e.g., Doxil) were proposed as effective means of inhibiting complement activation by nanoparticles *in vitro* and *in vivo* (58–60).

Among nanoparticles that passed characterization in the Nanotechnology Characterization Laboratory (NCL; https://ncl.cancer.gov/) assay cascade, PEGylated liposomes, especially those with elongated shapes, had more significant complement activation responses than spherical PEGylated liposomes and other PEGylated nanomaterials, which is consistent with the literature (55). The significant factors determining the nanoparticles' complement activating ability in the NCL assay cascade include composition, shape, and dose. While we found that anti-PEG antibodies contribute to complement activation by PEGylated liposomal DXR, we observed no correlation between the anti-PEG antibody titer in the normal donors' blood and the magnitude of the complement activation (61). We concluded that the presence of antibodies might be monitored for mechanistic purposes when the reaction occurs, but it should not be used to predict the reaction; instead, functional assays such as an *in vitro* complement activation assay are a more accurate tool to identify nanoparticles that trigger complement activation *in vitro*, and, as such, have a greater risk of causing CARPA *in vivo*.

Intracellular complement

Unlike the plasma complement proteins produced in the liver and secreted into the blood, the intracellular complement system is expressed by and remains inside the cells (Figure 3). The expression is either constitutive or induced by stimuli that activate the cells (35–37, 62). Once activated, intracellular complement split products are transported outside the cell and are exposed on the cellular membrane (34–37). Both C3 and C5 components of the complement system were described in cells. Even though the intracellular complement system is more extensively studied in T cells, it is not specific to T-lymphocytes and is found in other cell types including immune cells (monocytes, neutrophils, and B cells), non-immune cells (epithelial cells, endothelial cells, fibroblasts, and adipocytes), and cells that have undergone malignant transformation (62–64). The intracellular C3 component of the complement system produced by dendritic cells contributes to T-cell activation (65); when expressed by cancer cells, it promotes tumor growth *via* a mechanism involving the PI3K/Akt pathway (64). The autocrine activation of CD46 and C3aR by intracellular complement directs the metabolic reprogramming of T-cells and determines the Th1 polarization phenotype of activated T-lymphocytes (63, 66).

The study by Liszewski et al. identified the protease cathepsin L as the enzyme responsible for cleaving the C3 protein and generating the C3a split product to be exposed on the cellular membrane (63). Another study was unable to reproduce this mechanism despite analyzing the same activating stimulus (a-CD3 antibody) (34), suggesting that multiple mechanisms of intracellular complement activation likely exist.

Nanoparticles activate intracellular complement based on their surface charge. A recent study investigated a large group of nanomaterials for their ability to trigger intracellular complement activation in human cells (34). The study organized test nanomaterials into several groups based on current knowledge of their involvement in different types of immunotoxicity. One group included materials known for their ability to activate the plasma complement system and cause CARPA in sensitive individuals (e.g., PEGylated liposome, amphotericin-loaded liposome Ambisome, and iron oxide nanoparticles (IONPs) Feraheme, polyethoxylated castor oil Cremaphor-EL, and Propofol). Another group included nanomaterials with an established record of delayed-type HSR and contribution to protein immunogenicity (e.g., nickel, zinc oxide, gold, and silver nanoparticles). The third group was based on materials with a known record of perturbation or disruption of cellular organelles (silica, silicon, nano-silica particles, and dendrimers). Among these materials, only amine- and guanidine-terminated polyamidoamine (PAMAM) and amine-terminated triazine dendrimers activated the intracellular complement system in manner dependent on size and density of surface groups (34). In all cases, complement split products C3c and C3d were detected on the surface of activated T-lymphocytes (34).

Interestingly, unlike the original study describing intracellular complement activation in T cells (63), this study with dendrimers demonstrated that the mechanism underlying nanoparticle-mediated intracellular complement activation involves membrane damage and does not induce substantial changes in cell functionality as was assessed by cytokine production in and proliferative responses of leukocytes (34). Functional consequences of dendrimer-mediated intracellular complement activation remain largely unknown. However, complement split product deposition on lymphocyte surfaces may represent a process of so-called self-opsonization, which nanoparticle-damaged cells use to alarm other cells about the presence of danger. Further investigation is required to

determine whether the cell surface-exposed intracellular complement system represents another DAMP contributing to immunity. It also remains unknown whether intracellular complement system activation by dendrimers observed *in vitro* in healthy human donor lymphocytes (34) is also responsible for the delayed-type HSRs observed in a human subject after occupational exposure to cationic PAMAM dendrimers (67). To my knowledge, our team's study (34) represents the only currently available structure-activity relationship and mechanistic investigation of nanoparticle-mediated activation of the intracellular complement system. Therefore, more studies are needed to improve current knowledge about nanoparticle effects on intracellular complement activation and its functional consequences.

Cytokines

The communication between various immune cells and between the immune cells and other cells in the body can be direct *via* cell-to-cell contact and indirect *via* messenger molecules. Cytokines are a large group of such messenger molecules with diverse structures and functions produced and released by cells in response to inflammatory stimuli or damage. The earliest phase of the innate immune response operates with cytokines produced by macrophages and plasmacytoid dendritic cells (DCs). Other cell types, including platelets, some T cells (mainly regulatory T cells), fibroblasts, endothelial cells, and epithelial cells, can also contribute to the cytokine response during the early phase of inflammation. During this early phase, cytokines act on the nearest cells *via* the paracrine mechanism and, upon entry into systemic circulation, send the message to cells at other locations *via* the endocrine mechanism. Cytokines can have similar, overlapping, and unique functions and stimulate the production of other cytokines and secondary messengers, which amplify the response and initiate new responses. Examples of cytokines produced in the early phase of innate immune responses include tumor necrosis factor-alpha (TNFα), interleukins (IL-1, IL-12, IL-10, IL-6, IL-15, IL-18, IL-23, and IL-27), type I interferons (IFNα and IFNβ), and chemokines (IL-8, MIP-1a, MCP-1). Cytokines coordinate innate and adaptive immune responses; some of them (e.g., IFNγ, TNF, IL-5, and IL-17) are also produced by activated T lymphocytes during the adaptive immune response. Understanding cytokine responses helps interpret the results of both safety and efficacy studies. Other aspects of nanoparticle immunocompatibility, such as the immunogenicity topic described later in this review, may provide mechanistic insight into the cytokine responses to nanomaterials due to the known role of antibodies in activating the immune cells and biochemical immune pathways such as the complement pathway.

Beneficial cytokine responses

Activation of specific cytokines by nanotechnology carriers to direct desirable immune responses is determined by the nanoparticle composition and physicochemical properties (e.g., size, charge, shape and hydrophobicity) (68) and has been extensively studied in the field of vaccines and immunotherapies (69). For example, fibrous TiO_2 particles with a large aspect ratio were more potent at activating NLRP3 inflammasome and promoting LPS-induced IL-1β induction than their spherical and fibrous low aspect ratio counterparts (70). In another study, smaller carbon black and TiO2 nanoparticles were more potent inducing cytokines than larger particles of the same composition and surface functionality (71). An interesting example demonstrating the importance of the cell type is the study of sheet-like zinc oxide particles that induced higher levels of TNF than their spherical counterparts in murine dendritic cells but not in macrophages (72). More examples of structure-activity relationships in nanoparticle-mediated cytokine responses are reviewed elsewhere (68).

Iron, silica, chitosan, poly(lactic,glycolic) acid (PLGA), liposomes, emulsions, virus-like particles, peptide- and poly (amino acids)-based carriers, synthetic polymers (e.g., polyethyleneimine, PEI), and DNA origami have been shown in various models to improve the antigen uptake, processing, and presentation, and result in overall better vaccine and immunotherapy performance (73–86). For example, Veneziano et al., designed virus-like particles using DNA-origami technology for presenting antigens to B-cells; in this concept, the antigens were spaced out on the origami surface at a controlled distance (25-30 nm) that allowed for the most optimal activation of the B-cell receptor (85).

Using nanoparticles, researchers were able to direct specific Th1 versus Th2 polarization and major histocompatibility complex (MHC)-restricted cytotoxic T-cell responses that traditional vaccines and therapies could not achieve (73, 86–88). Through nanoparticle-mediated regulation of inflammatory pathways and cytokine production by the cells residing in the tumor microenvironment, researchers have also been able to direct the activation status of macrophages from immunosuppressive M2 to inflammatory M1 phenotypes and thereby contribute to a better outcome of cancer therapy (89–91). Likewise, nanoparticles have been used to achieve repolarization of macrophages from M1 to M2 phenotype to benefit therapy of autoinflammatory and inflammation-mediated neurodegenerative conditions (92–95). Besides inducing desirable host cytokine response supportive of either M2/M1 or M1/M2 repolarization, nanoparticles have been successfully used to deliver cytokines (such as IL-4 and TNFα) that, upon release from a nanocarrier, triggered desirable responses without toxicity to the host (16, 93, 96, 97). Nanoparticle-mediated delivery of TNFα tested in phase I clinical trials demonstrated that, unlike free cytokine, nanoparticle-bound

TNFα does not induce a systemic inflammatory response and is also not immunogenic (16).

Other examples of beneficial cytokine response to nanoparticles and nanoparticle-formulated drugs include a recent study of CpG oligonucleotides delivered using particle replication in non-wetting templates (PRINT) nanoparticles. This concept resulted in particle accumulation in the lungs, where local cytokine response to delivered CpG oligonucleotides resulted in a reduction in the tumor size (98). Unlike free oligonucleotides, the PRINT nanoparticle-formulated CpG oligos did not elicit a systemic cytokine response (98). In another study, local application of doxycycline-loaded PLGA nanoparticles in the oral cavity resulted in an induction of anti-inflammatory (IL-10) and reduction in pro-inflammatory (IL-8, IL-6, IL-17, and IFNγ) cytokines, which contributed to resolving inflammation in patients with type 2 diabetes-associated periodontitis (99). Chitosan/polyglutamic-acid-formulated interferon-gamma induced the secretion of IL-12, IL-6, and TNFα, which modified the tumor microenvironment such that the invasion of colorectal cancer cells was hampered (100).

Overt cytokine responses

In contrast to studies discussed above, an overt production of inflammatory cytokines in response to systemically administered nanoparticles has also been described for certain nanoformulations. For example, adverse immune-mediated reactions to liposomal microRNA formulation MRX34 were so severe that they led to four patient deaths and subsequent discontinuation of the clinical trial (101). The same study reported that the toxicity could be managed using immunosuppressive therapy with dexamethasone (101). Another lipid-based nanoparticle formulation of siRNA, ONPATTRO, resulted in IRs in more than 20% of patients. This response was not attributed to cytokines and, in one case, was due to the complement activation (102). The mechanism underlying these reactions in other patients remains unknown. These studies emphasize the importance of considering each nanoformulation in the context of the intended route of administration and indication and conducting extensive physicochemical characterization along with immunotoxicity assessment for the nanocarrier, API, and a final formulation containing both components.

Cytokine responses to nucleic acid nanoparticles

Unlike traditional therapeutic nucleic acids (TNA) such as siRNA, anti-sense DNA oligonucleotides, and CpG oligonucleotides, nucleic acid nanoparticles (NANPs) are immunoquiescent in that adding these particles to immune cells does not result in a cytokine response (103). However, cytokine response to NANPs can be observed after they are delivered to immune cells using a lipid carrier (e.g., lipofectamine 2000). Earlier studies demonstrated that NANPs, after complexation with a lipid-based carrier, are internalized *via* Scavenger Receptor A-mediated phagocytosis, and this uptake culminates with the production of type I and type III interferons (103). Another remarkable difference between NANPs and TNA is that endosomal TLR7, but not TLR3 or TLR9, triggers the interferon response to RNA and DNA NANPs (104).

The expression of TLR7 is abundant in airways, and the activation of this innate immune receptor has a bronchodilating effect, decreases allergy-mediating Th2 responses, eosinophilic inflammation, and goblet-cell hyperplasia that make it a therapeutic target in asthma (105). Since the activation of TLR7 pathway inhibits viral replication in lungs and reduces airway hyperreactivity triggered by viral infections, synthetic TLR7 agonists [e.g., imiquimod (R837), resiquimod (R848), and 8-hydroxyadenine derivatives] have also been investigated as antiviral drugs (105). Collectively, the existing knowledge of targeting TLR7 for therapeutic indications opens the opportunity for NANPs to be used as antiviral and anti-asthmatic drugs.

While the initial studies are encouraging, more research is needed to fully evaluate the safety of NANP-mediated TLR7 activation because a recent study provided the first causation link between TLR7 activation and systemic lupus erythematosus (SLE), an autoimmune disorder (106), which is in line with the earlier clinical observation of TLR7-agonist association with psoriasis, an autoinflammatory skin disorder (107).

Structure-activity relationship studies revealed that the magnitude of the interferon response to NANPs could be controlled by the type of nucleic acids used to create these particles, with RNA-based NANPs being more potent interferon inducers; three-dimensional shape, with the globular NANPs being more potent than planar and fibrous NANPs; and size, but not sequence complementarity (103). More interestingly, the spectrum of cytokine response to NANPs could be controlled by the type of delivery carrier. Particularly, when amine-terminated dendrimers were used instead of lipofectamine, pro-inflammatory cytokines IL-1, TNF, and IL-6 were observed, whereas type I and type III interferons were not (108). Therefore, both the quantity (e.g., cytokine levels) and the quality (e.g., cytokine spectrum) of the innate immune responses to NANPs can be controlled by using different carriers to deliver these materials.

An extensive discussion regarding the immunotoxicity of traditional TNAs and NANPs; the role of nanocarriers in mitigating this toxicity; and translational challenges, opportunities, and barriers due to the immunological properties of NANPs are available elsewhere (109–115).

Trends in cytokine responses to nanomaterials

Cytokines are commonly used in preclinical studies as biomarkers of inflammation. Previously, NCL reported an interesting trend showing that lipid-based nanomaterials analyzed in the NCL standardized assay cascade between 2005 and 2015 induced chemokine IL-8 without inducing other pro-inflammatory cytokines such as TNF, IL-1, and IL-6 (32). The data were acquired using in-house developed single-plex ELISAs and several commercial multiplex platforms, including Meso Scale Discovery, BD Biosciences Cytometric Bead Array, Rules-Based Medicine MAP, and Bender MedSystems Flocytomix Multiplex Kit, and showed comparable results. In 2016, NCL switched to using chemiluminescent multiplex cytokine panels by Quansys Biosciences; these new custom multiplex assays cover 29 cytokines, including several chemokines (IL-6, MCP-1, MCP-2, MIP-1α, MIP-1β, and RANTES). During the past five years, the NCL assay cascade detected nanoformulations that induced a broad spectrum of cytokines and continued observing a trend in nanoformulations that exclusively induce chemokines, i.e., without other pro-inflammatory cytokines (Figure 4A). Nanoparticle composition analysis reveals that most concepts inducing chemokines are made of polymers, lipids, or containing both polymers and lipids, either as core nanoparticle carriers or excipients in the formulation (Figure 4B). Formulations inducing a broad spectrum of cytokines are often those that contain another cytokine as either API or targeting moiety, a TLR agonist as an adjuvant, or CpG oligonucleotide(s) as either an API or structural component of the nanoparticle.

Coagulation system

The coagulation system's two main components are platelets and the plasma coagulation system.

Platelets, also known as thrombocytes, are the smallest among peripheral blood cells (116). The main role of these cells is to maintain hemostasis. Physical damage to blood vessels and inflammation are among the factors that activate platelets and promote their aggregation (116). The contribution of activated platelets to IRs was described in patients undergoing therapy with a perioperative neuromuscular blocking agent and in a humanized mouse model of IgG-dependent anaphylaxis (117). Earlier studies demonstrated that nanoparticle size, charge, and density of surface functional groups determine nanoparticle interaction with platelets (118–121). For example, PAMAM and triazine dendrimers with cationic surface moieties (amine or guanidine) activated platelets and resulted in platelet aggregation; this activity was size-dependent in that larger particles were more potent than smaller particles with the same surface functionality (119). In contrast to amine-terminated PAMAM dendrimers, particles with hydroxy- or carboxy-functionalized surfaces did not activate platelets regardless of the particle size (119). PAMAM dendrimers were more potent at activating platelets than triazine dendrimers of equivalent size and surface charge (121).

It has also been demonstrated that traditional sterilization methods such as gamma irradiation and autoclaving may change nanoparticle surfaces so that the particles become pro-thrombogenic and activate platelets (122). However, the contribution of platelets to IRs in response to nanoparticles has not yet been fully investigated.

The coagulation factor family is a group of thirteen proteins that, like the complement system, are organized in a proteolytic cascade. When analyzed under *in vitro* conditions, this cascade can be divided into three pathways: an extrinsic (prothrombin time [PT]) pathway, an intrinsic (activated partial thromboplastin time [aPTT]) pathway, and a common (thrombin time) pathway. Nanoparticle interaction with plasma coagulation depends on particle composition, surface functionalization, and size. For example, amine-terminated polystyrene nanoparticles inhibited plasma coagulation by depleting plasma coagulation factors VII and IX (123). This property was size-dependent in that smaller nanoparticles were more effective than their larger counterparts (123). Surface functional groups significantly contributed to the nanoparticle interaction with the coagulation pathway in that polystyrene nanoparticles with a negatively-charged surface coating activated the intrinsic pathway; this property was also size-dependent, with large particles being more effective than their smaller counterparts (123). In contrast, anionic liposomes inhibited plasma coagulation *via* interaction with coagulation factors XII and XI (124).

The number of concepts characterized in the NCL assay cascade and affecting coagulation is growing with the increasing general trend of using polymer-based drug delivery systems and prodrugs (Figure 5A). Most of the particles affecting coagulation pathways contain polymers as a part of the carrier or as an excipient (Figure 5B). Common features these polymers share with traditional anti-coagulant heparin are that these polymers are polar, long, charged, and hydrophilic. This observation deserves attention for several reasons. First, because many tumors have prothrombogenic properties (125), delivering cancer therapeutics using nanotechnology platforms with anti-coagulant properties may have a collateral benefit for cancer therapy. Second, it has been demonstrated that due to its polyanionic nature, heparin binds to various proteins (126). This property contributes to heparin's biological effects beyond blood coagulation. Particularly, heparin inhibits viral infection by competing with the virus for binding sites on target cells (127). The S1 subunit of the SARS-CoV-2 spike protein containing a receptor-binding domain was shown to bind to heparin (128). Moreover, heparin antagonizes histones released from damaged cells, thereby reducing endothelial injury during viral infection (129, 130).

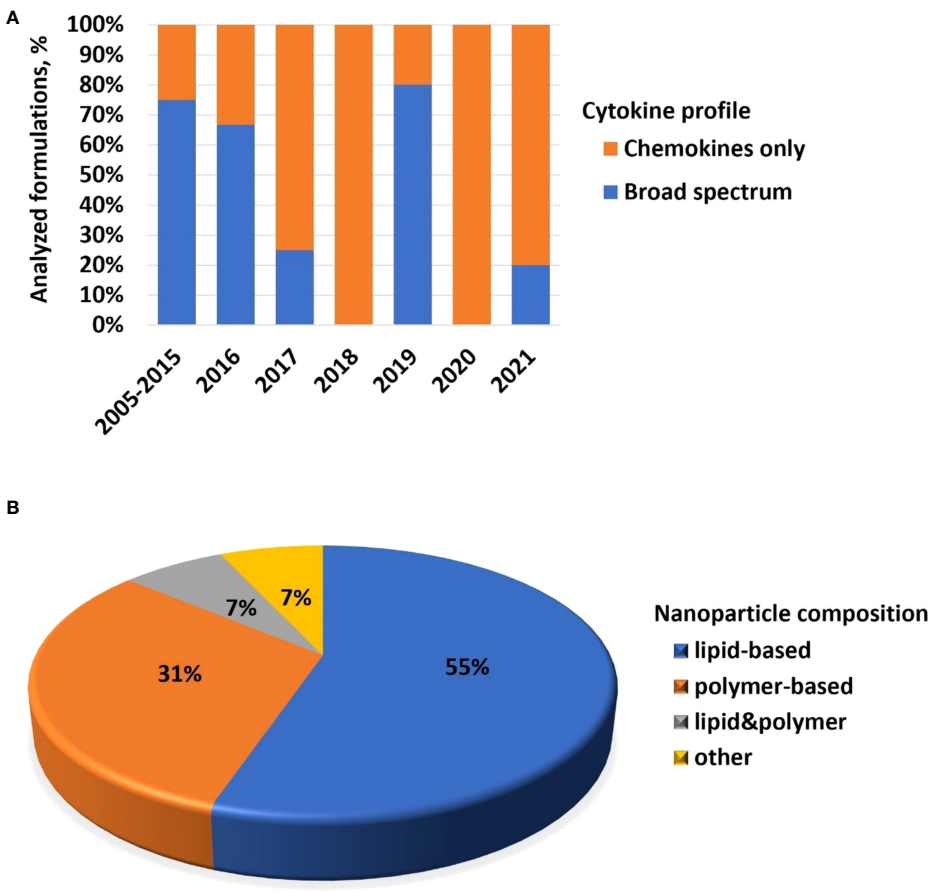

FIGURE 4
NCL assay cascade experience with cytokine analysis. Between 2005 and 2021, NCL has characterized over 450 nanotechnology formulations using assay cascade protocols (https://ncl.cancer.gov/resources/assay-cascade-protocols) that include six assays for the assessment of cytokines (ITA-10, ITA-22, ITA-23, ITA-24, ITA-25, and ITA-27). **(A)** Breakdown of formulations by cytokine profile (i.e., formulations that induced broad-spectrum cytokines versus those that exclusively induced chemokines). Percentage reflects the total number of formulations subjected to cytokine analysis. The data for 2005–2015 are pooled; during this time, IL-8 was the only chemokine on the NCL cytokine panel; other cytokines in the NCL 2005–2015 panel include TNF, IL-1β, IL-6, and IFNλ. The panel was expanded and, since 2016, includes chemokines MIP-1α, MIP-1β, MCP-1, MCP-2, and RANTES, in addition to the IL-8. Other cytokines in the extended panel are TNF, IL-1α, IL-1β, IL-2, IL-4, IL-5, IL-6, IL-7, IL-10, IL-12, IL-13, IL-15, IL-17, IL-22, IL-23, IL-27, IFNγ, IFNα, IFNβ, and IFNλ. "Broad-spectrum" refers to all or any combination of these cytokines where the combination includes cytokines of different functional types (e.g., pro-inflammatory and chemokines; pro-inflammatory and interferons; interferons and chemokines, or all of the above). Chemokines only refer to formulations that induce all or any chemokines in the absence of other functional cytokine types. **(B)** Breakdown of formulations that exclusively induce chemokines by nanoparticle composition. Most of the chemokine-inducing formulations are lipid-based, polymer-based, or contain both lipids and polymers either in the nanoparticle core or as the excipient or both. NCL, Nanotechnology Characterization Laboratory; ITA, immunotoxicity assay.

Therefore, I hypothesize that nanotechnology platforms with heparin-like behavior, when used for the delivery of SARS-CoV-2 therapeutics, may have collateral benefits (like that of heparin) by inhibiting viral interaction with cellular receptors and antagonizing histone-release-mediated endothelial injury.

Immunogenicity

One of the consequences of immunogenicity significant for therapeutic products is the formation of anti-drug antibodies (ADA). The ADA can increase or decrease the product's efficacy, cause alterations in the drug's pharmacokinetics (PK), accelerate the drug clearance, and mediate systemic and local antibody-mediated toxicities such as anaphylaxis, HSR, kidney toxicity, and neutralization of non-redundant endogenous proteins with overlapping epitopes (131). The frequency of ADA occurrence and their clinical impact anti-correlate in that binding antibodies are the most frequent but have the least clinical impact, whereas neutralizing cross-reacting antibodies are the least frequent but have the most clinical impact. Therefore, detection of ADA and understanding their functional type

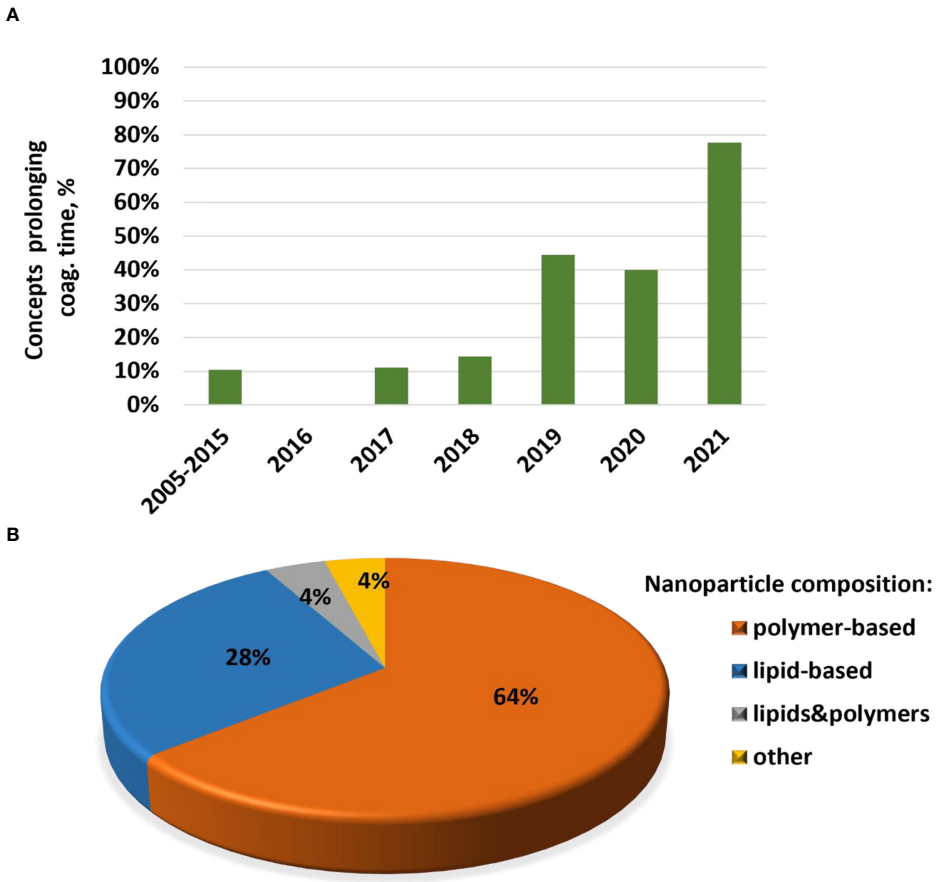

FIGURE 5
NCL assay cascade experiences with nanoparticle effects on blood coagulation. NCL has characterized more than 450 nanotechnology formulations using assay cascade protocols (https://ncl.cancer.gov/resources/assay-cascade-protocols) that include two assays for the assessment of the coagulation system (ITA-2 and ITA-12). Shown on the graph is a proportion of formulations that induced prolongation of plasma coagulation time in the NCL assay ITA-12 **(A)** and breakdown by nanoparticle composition of formulations resulting in APTT prolongation, a feature shared with traditional blood-thinning agent heparin **(B)**. Most of these concepts are polymer-based, contain lipids, or both lipids and polymers either as the core nanoparticle or excipient or both. NCL, Nanotechnology Characterization Laboratory; ITA, immunotoxicity assay.

(e.g., binding, PK-altering, neutralizing, HSR-causing, cross-reacting neutralizing) and isotype (e.g., IgM, IgG, IgE) are recommended by the US Food and Drug Administration for certain drug products (e.g., protein, antibody, and peptide-containing products including nanotechnology concepts) (132). Understanding the functional type of the ADA helps to estimate the risk of adverse events and their severity in the context of PK, safety, and efficacy studies. Knowing the ADA isotype provides a mechanistic insight; for example, IgE is associated with true allergy, whereas IgM and IgG are known for their ability to mediate complement activation and CARPA, as detailed in the complement section above.

Nanoparticle immunogenicity has been extensively studied using fullerenes, dendrimers, and liposomes. These studies demonstrated that nanoparticles are poor antigens and do not induce antibody responses even in the presence of potent adjuvants. For example, C60 fullerene derivatives in the presence of Freund adjuvant did not induce generation-fullerene-specific antibodies (133). However, conjugation of nanoparticles to proteins and/or administration in the presence of microbial ligands that activate toll-like receptors (TLRs) resulted in the formation of particle-specific antibodies. For example, C60 fullerenes derivatives conjugated to thyroglobulin administered in the presence of an adjuvant resulted in generation-fullerene-specific antibodies (134–136). Interestingly, C60 fullerene-specific antibodies reacted to the core and not to the terminal groups (136) and cross-reacted with C70 fullerenes and single-wall carbon nanotubes (134, 137).

Most importantly, unconjugated fullerenes, even in the presence of Freud adjuvants, were not immunogenic (133). Similar results were obtained with PAMAM dendrimers (138, 139). Dendrimer conjugation to a protein (hIL-3 or BSA) resulted in the formation of a dendrimer-specific antibody response (139). The induced antibodies reacted with

dendrimer surface groups (139). Collectively these studies indicated that nanoparticles behave as haptens and that both T and B lymphocytes are involved in the immunogenicity of protein-conjugated nanomaterials.

Like fullerenes and dendrimers, liposomes alone were not immunogenic (140); however, in contrast to fullerenes and dendrimers, liposomes induced antibodies in the presence of TLR4 agonist, lipid A, which was used as an adjuvant (140–142). Pre-existing (naturally occurring) antibodies to liposome components such as phosphatidylcholine (PC), cholesterol (Chol), and dicetyl phosphate (DCP) were found in human blood (143). The mechanism underlying the formation of these antibodies is not well understood but potentially involves a prior exposure to these lipids coinciding with or related to infectious agents supplying TLR ligands as adjuvants. For example, in an experimental rabbit model, Trypanosoma rhodesiense infection led to the formation of antibodies specific to several lipids, including PC, PI, PIP, and Chol; these lipids were also detected in the pathogen used in this animal model (144). Immunization of immunologically competent but not athymic mice with liposomes and an adjuvant resulted in a liposome-specific IgM response; this finding pointed to the thymus-independent mechanism (145). Interestingly, liposome-specific antibodies also recognized phospholipids, DNA, and lipoteichoic acids (141).

Recently, the immunogenicity of hydrophilic polymer coating, particularly that of PEG, on nanoparticle surfaces became a hot topic due to the contribution of these antibodies to infusion reactions and HSRs to nanoformulations, as was discussed above in the complement section. The original intention of including PEG and other hydrophilic polymers on the particle surface was to improve nanoparticle solubility and shield them from clearance by the mononuclear phagocytic system. It was expected that extended circulation time and decreased clearance would also prevent the immunogenicity of both the particles and their therapeutic payload. Surprisingly to many researchers, PEG itself was found to be immunogenic, and various antibodies, including IgM, IgG, and IgE, specific to this polymer, were described in the blood of healthy individuals and patients treated with PEGylated or PEG-containing products (146–148). Anti-PEG IgG and IgM were primarily reviewed in the literature in the context of CARPA because antibody-antigen complexes trigger activation of the classical pathway of complement (47); these antibodies were also shown to induce premature drug release from and reduce the therapeutic efficacy of PEGylated liposomes, underline accelerated blood clearance of PEGylated products, and alter biodistribution and mobility in the mucus of PEGylated nanoparticles (149–151). Anti-PEG IgEs correlated with immediate-type HSRs (true allergy) to PEGylated products (147, 148). Importantly, anti-PEG antibodies cross-reacted with polysorbate and were found to be responsible for allergic reactions to polysorbate-containing products (147). Likewise, in another study, anti-PEG antibodies cross-reacted with other C-C-O-containing polymers, including polypropylene glycol, polyethyleneimine, and polytetramethylene ether glycol (152). The mechanism underlying PEG immunogenicity is not completely understood, but two recent reviews have discussed the application of general knowledge regarding T-independent antigens to PEG immunogenicity through the passive immunization resulting from environmental exposure and food (153, 154). Interestingly, two recent reports demonstrated anti-PEG IgG and IgM induction *via* active immunization with mRNA-PEG-LNPs in a pig model (155) and humans (156).

For many years, the hydrophilic nature of PEG made some scientists doubt the existence of anti-PEG antibodies and suggested that the unspecific antibodies are cross-reacting with ELISA components. However, structural investigation of the antibody-PEG interaction (157), along with studies linking the presence of these antibodies to HSR (47, 147, 148, 155) and premature drug release (60, 158), softened these doubts. Additional studies investigating the crystal structure of PEG-anti-PEG antibody complexes will further improve the understanding of antibody interactions with hydrophilic polymers and are urgently needed.

These unexpected but quickly expanding findings prompted many researchers to reconsider PEG use in nanomedicine and promoted the investigation of other polymers as PEG alternatives with the hope of overcoming the problem of PEG immunogenicity. Despite initially exciting findings of many such alternatives to improve solubility and increase circulation time of modified nanoparticles, they also discovered immunogenicity of these polymers, very much like earlier studies of PEG. More details about the immunogenicity of PEG alternatives (e.g., polyvinyl pyrrolidone and polyglutamic acid) and other immunological responses to polymers (e.g., heparin, polyoxazoline, and polycarboxybetaine, to name a few) used in pharmaceutical products and nanomedicines have been reviewed in detail elsewhere (154). Overall, it was concluded that no ideal PEG alternative exists; immunogenicity, allergy, and HSRs to various PEG alternatives are common. Moreover, thorough studies of immunological properties of PEG alternatives both alone and in the context of the whole product, which may contain nanoparticle carriers, APIs (e.g., protein, antibody, therapeutic nucleic acid, and small molecule), and excipients appear to be key to understanding immune-mediated reactions to this product and designing safe and effective formulations.

Immunosuppression

Immunosuppression is a condition in which an individual's immune response is lowered. It can result from genetic mutations affecting receptors, adaptor proteins, or transcription factors involved in the normal innate and adaptive immunity (159, 160). For example, the mutation in IRAK4 increases

susceptibility to infections (161, 162). Immunosuppression may also be due to environmental factors (e.g., xenobiotics) and certain types of drug products (163–165). Drug-mediated immunosuppression can be desirable [i.e., used to suppress a known overt activation of the immune system to prevent host damage (e.g., dexamethasone helps to prevent damaging effects of cytokine storm during bacterial or viral sepsis, rejection of organ transplant, or for suppressing an autoimmune response)] (164, 166) or adverse(i.e., when it is not intended but weakens the host's response to microbes and cancer [e.g., chemo and radiation therapy target cancer cells but also damage nontarget immune cells]) (163, 165, 167). Drugs intended to modulate the function of immune cells may also cause adverse immunosuppression. For example, cyclosporin, intended to prevent transplant rejection, when taken for a long time, may also increase the risk of bacterial and viral infections (168). To reduce the negative consequences of immunosuppressive therapies, vaccination and prophylactic anti-microbial therapies are often considered for patients receiving such drugs (167, 169).

Cytotoxic oncology drugs intend to stop cancer cell proliferation but also affect lymphocytes, thereby decreasing lymphocyte-mediated immune responses (170). When such APIs are delivered using nanotechnology platforms, final formulations may inherit the immunosuppressive properties of APIs. For example, among nanotechnology-formulated drugs that were characterized by NCL between 2005 and 2020, the majority (92%) were immunosuppressive due to the APIs, while only a small proportion (8%) was due to the nanocarrier (Figure 6).

Below, I review some examples of drug-mediated immunosuppression due to bone marrow (BM) and blood lymphocyte inhibition and discuss whether and how nanotechnology platforms influence this toxicity. Whenever available, I will also discuss the immunosuppressive properties of nanocarriers themselves.

Bone marrow

Nanocarriers may influence drug distribution to BM, thereby diminishing or enhancing the drug-mediated toxicity. For example, in one early study, DXR, formulated on polyisobutyl (PIBCA)- and polyisohexyl (PIHCA)- cyanoacrylate nanoparticles, demonstrated differential distribution and toxicity (171). DXR-PIBCA suppressed the formation of granulocyte–macrophage progenitor (CFU-GM) after i.v. injection in mice, and this toxicity was comparable to the effect of free DXR; however, at an equivalent drug dose, DXR-PIHCA were more immunosuppressive. Similar effects were observed on spleen cells with a decrease in granulocytes and lymphocytes being more pronounced with DXR-PICHA formulation. Both PIBCA and PICHA carriers alone were not toxic. The authors linked greater toxicity of PICHA- versus PIBCA-formulated DXR to the more significant accumulation of PICHA-formulated drug in BM and spleen; however, the mechanisms underlying such differential biodistribution were not identified but were hypothesized to relate to different rates of opsonization that determined the greater uptake of nanoparticle-formulated drug by phagocytic cells in target organs (171). Another study found that the uptake of unfunctionalized- and citrate-stabilized IONPs by BM cells *in vitro* exceeded the uptake of iron citrate used as a control. Greater uptake, however, did not influence cell viability and expression of surface markers (172). Unlike PICHA and PIBCA nanoparticles in the study by Gibaud et al. (171), IONPs were not loaded with an oncology drug; therefore, the lack of difference in toxicity may be

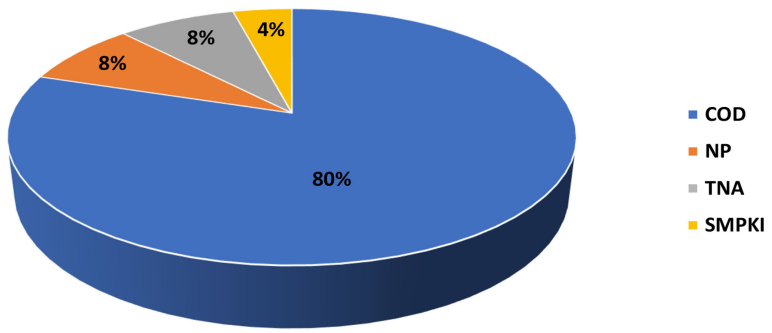

FIGURE 6
Immunosuppressive properties of nanotechnology formulations characterized at NCL. NCL has characterized more than 450 nanotechnology formulations using assay cascade protocols (https://ncl.cancer.gov/resources/assay-cascade-protocols) that include two assays for the assessment of immunosuppression (ITA-6 and ITA-18). Shown on the graph is a proportion of formulations that were immunosuppressive in these *in vitro* assays due to either API or carrier. The immunosuppressive properties attributed to APIs included those due to small molecules: cytotoxic oncology drugs (COD), therapeutic nucleic acids (TNA), small-molecule protein kinase inhibitor (SMPKI), or nanoparticle platform (NP). API, active pharmaceutical ingredient; NCL, Nanotechnology Characterization Laboratory; ITA, immunotoxicity assay.

explained by the generally biocompatible nature of the iron oxide platform (172). Provided the greater accumulation of IONPs in BM remains after the drug conjugation, I expect a similar increase in the BM cytotoxicity of the drug-formulated IONPs. Apart from biodistribution, drug-mediated myelosuppression may be influenced by the rates of drug release from nanocarriers. For example, docetaxel conjugated to solid LNPs was less myelosuppressive than docetaxel at equivalent concentrations *in vitro* in a colony-forming unit assay (173).

Accumulation of some nanoparticles in BM resulted in myelosuppressive effects due to particle-mediated apoptosis and hypoplasia. For example, intraperitoneal administration of aluminum oxide nanoparticles to mice decreased total and differential BM counts and altered erythropoiesis (174). The same study also reported myeloid hyperplasia due to the inflammation-associated increase in neutrophil precursors. The damaging effects of aluminum oxide nanoparticles on BM were neutralized by co-treatment with curcumin nanoparticles; the protective effects of nanocurcumin were attributed to its anti-inflammatory properties (174).

Blood lymphocytes

Suppression of lymphocyte function may occur due to either immunosuppressive drug payload or nanocarrier per se. Examples of drug-mediated immunosuppression include PLGA-betamethasone and nanoalbumin-paclitaxel (Abraxane), among others (175–177). Drug-mediated immunosuppression is common for nanotechnology concepts delivering cytotoxic oncology drugs.

Inhalation of carbon nanotubes suppressed B-lymphocytes' function *via* TGFβ produced by alveolar macrophages (178). An interesting example is the iron-oxide formulation Feraheme (ferumoxytol) used for iron deficiency in chronic kidney disease patients. While adverse effects of this formulation commonly discussed in the literature include HSRs and CARPA, both attributed to the dextran coating on the surface of IONPs (179–181), this formulation was also found to be immunosuppressive and inhibited human T-cell function *in vitro* (182) and *in vivo* (183). Feraheme inhibited cytokine secretion and antigen-induced proliferation of T cells by inducing mitochondrial oxidative stress (182). Interestingly, Th17 function inhibition and IL-17 secretion by these cells in response to Feraheme *in vitro* (182) was suggested for potential use in relieving inflammation leading to psoriatic skin lesions *in vivo*. In a subsequent study, using a mouse model of chemically induced psoriasis, topical application of Feraheme was almost as effective as hydrocortisone in reducing skin inflammation (183). Another study demonstrated that Feraheme's ability to suppress myeloid-derived suppressor cells has beneficial effects on recovery from endotoxin tolerance following sepsis (184).

Available methods and models to study immunotoxicity

This section will discuss assays for assessing nanoparticle effects on the integrity and function of immune cells commonly used in preclinical research. Nanoparticles must undergo analysis for sterility and contamination with innate immunity-modulating impurities prior to *in vitro* and *in vivo* immunotoxicity studies since microbes and their components (e.g., endotoxin, beta-glucans, and CpG DNA) may confound the results of such studies (185). Challenges with endotoxin and beta-glucans detection in nanomaterials from NCL's experience have been described earlier (19, 32, 186–190). Reports on methodologies for endotoxin detection in nanomaterials from other laboratories are also available (191–196).

In vitro methods

Hemolysis

An *in vitro* hemolysis test is conducted to assess nanoparticles' effects on the integrity of red blood cells. Various experimental protocols for hemolysis studies using human and animal blood are available and have been discussed in more detail elsewhere (197). The *in vitro* method that incubates human whole blood with test nanomaterials and then detects plasma-free hemoglobin (198) shows a good *in vitro-in vivo* correlation. As reported earlier, as low as 5% of hemolysis detected by this method *in vitro* correlates with hemoglobin and hematocrit alterations *in vivo* (199). Nanoparticles that are found hemolytic in the NCL assay cascade possess common structural properties, including cationic surface moieties and the presence of detergents and detergent-like molecules as APIs or excipients.

Complement activation

This assay is used to assess nanoparticles' propensity of causing CARPA. Several formats of this method exist. One of the commonly used methods employs plasma or serum from human donors or animals, which, after exposure to test nanomaterials or controls, are analyzed by western blot or ELISA for the presence of the complement split products (C3a, iC3b, C4a, C5a, Bb, and/or sC5b-9) (200, 201). Szebeni's laboratory established good *in vitro-in vivo* correlation for this method both in the human and animal (pig, rats) matrix (202–205).

When the *in vitro* complement activation assay is used for nanoparticle characterization, it is essential to consider both inter- and intra-species variability in complement activation, which may influence the assay sensitivity and overall conclusions. For example, when mouse plasma from several strains (Balb/c, CD-1, C3H/HeN, C57BL/6, and DBA1) was used as a matrix to study complement activation by liposomal amphotericin (Ambisome), the highest complement activation

was observed in the plasma of Balb/c and CD-1 mice, whereas the lowest activation was seen in plasma of C57BL/6 mice; the activation in plasma of other strains was moderate (206). Interestingly, Balb/c and CD-1 mice are known for their Th-2 bias and preferred for sensitization studies, whereas C57BL/6 mice are Th-1-biased animals and are preferred in vaccine and autoimmunity studies (207). Another interesting observation is the difference in magnitude of complement activation by various agents. For example, human, but not mouse, plasma is susceptible to the complement activation by cobra venom factor (CVF) that is commonly used as a positive control for *in vitro* studies; however, the magnitude of the complement activation by Ambisome is comparable between human and mouse plasma (206). Another topic commonly discussed in the context of *in vitro* complement activation assay is the anticoagulant used to generate blood plasma. Hirudin is generally agreed as the best anticoagulant (208–210); however, this anticoagulant is not widely available. In the absence of hirudin, sodium citrate or EDTA-anticoagulated plasma can be used as long as veronal buffer is also used to supply divalent cations required for the complement activation.

Coagulation system

When analyzing the coagulation system in preclinical studies, it is essential to recognize that all components of this system are closely connected *via* positive and negative regulation loops. Plasma coagulation controls the activity of the zymogen prothrombin and a serine protease thrombin; Factor IIa (α-thrombin) is a final product of prothrombin activation that results in platelet activation and fibrinogen-to-fibrin conversion. Thrombin activates transamidase Factor XIIIa, which stabilizes the fibrin network with activated platelets, thereby forming a blood clot. Positive feedback of thrombin activation includes the activation of coagulation factors XI, IX, V, and VIII. The negative feedback controls the thrombin activity: thrombin binding to thrombomodulin expressed on the surface of endothelial cells activates protein C and stops further procoagulant activity. Activated protein C and its cofactor protein S activate proteolytic degradation of activated coagulation factors Va and VIIIa, which function to accelerate the thrombin-generation pathway. Thrombin also activates complement, leukocytes, and other cell types. Activated by thrombin and complement cells contribute to the plasma coagulation by producing cytokines and expressing the phospholipid-protein procoagulant activity complex. This complex initiates plasma coagulation by activating coagulation factor VII.

Nanoparticle effects on the coagulation system are commonly assessed *in vitro* using platelet aggregation, plasma coagulation, and leukocyte procoagulant activity assays (211). Platelet aggregation can be accessed using light transmission aggregometry and direct counting of single (unaggregated) platelets. Common plasma coagulation assays include APTT, prothrombin time (PT), thrombin time (TT), and reptilase time (RT) assays. The APTT assay assesses functionality of factors XII, XI, IX, VIII, X, V, II; the PT assay does so for factors VII, X, V and II; TT and RT assess the role of fibrinogen. Alteration in the fibrinogen conversion to fibrin can also be detected in all of these assays. The PT assay is also used to access the procoagulant activity of leukocytes and endothelia cells; in this case, the cells are used instead of the Neoplastin-TM reagent to activate the plasma coagulation.

Despite their common use in nanoparticle hemocompatibility studies, abnormal results of these *in vitro* assays are often challenging to interpret due to the complex effects of nanoparticles on individual components of plasma coagulation, often synergistic and antagonistic effects, and generally low specificity or sensitivity for discrimination between individual pathways of nanoparticle interactions with the coagulation system. Other methodological aspects of thromboelastography, synthetic substrate-based assays, ELISA, fibrinolytic, thrombolytic activity, and other assays for coagulation assessment have been discussed elsewhere (212).

Cytokines

Two types of primary cell-based systems are available to cytokine researchers. They include whole blood cultures and peripheral blood mononuclear cells (PBMCs). If the cytokine of interest is expressed by cells of low abundance in the whole blood and even in PBMCs (e.g., plasmacytoid dendritic cells or γδT-cells), researchers could isolate these cells from the blood and concentrate them prior to analysis *in vitro*. Both negative and positive selection reagents are available when enrichment of a particular cell population is of interest. When such enrichment is not needed, the decision between whole blood and PBMCs could be made based on the type of cytokines one wants to detect (Figure 7). Table 1 summarizes human cytokines that are commonly analyzed in preclinical and clinical studies and included in the NCL multiplex panel. The information in this table could be used to guide both study design and data interpretation.

Leukocyte proliferation

Leukocytes can be activated by mitogens such as plant lectin phytohemagglutinin (PHA) for T cells and lipopolysaccharide for B cells. Antigen-specific lymphocytes can also proliferate in response to their cognate antigens (e.g., flu antigens). Proliferating cell expansion can be detected by several commercially available kits and reagents with (3-(4,5-dimethylthiazol-2-yl)-2,5-diphenyltetrazolium bromide (MTT), bromodeoxyuridine, (BrdU) and carboxyfluorescein diacetate succinimidyl ester (CFSC), being broadly used (215, 216). BrdU is preferable as it detects proliferating cells that incorporate this molecule into their DNA. While increased cell viability detected by the MTT assay generally reflects

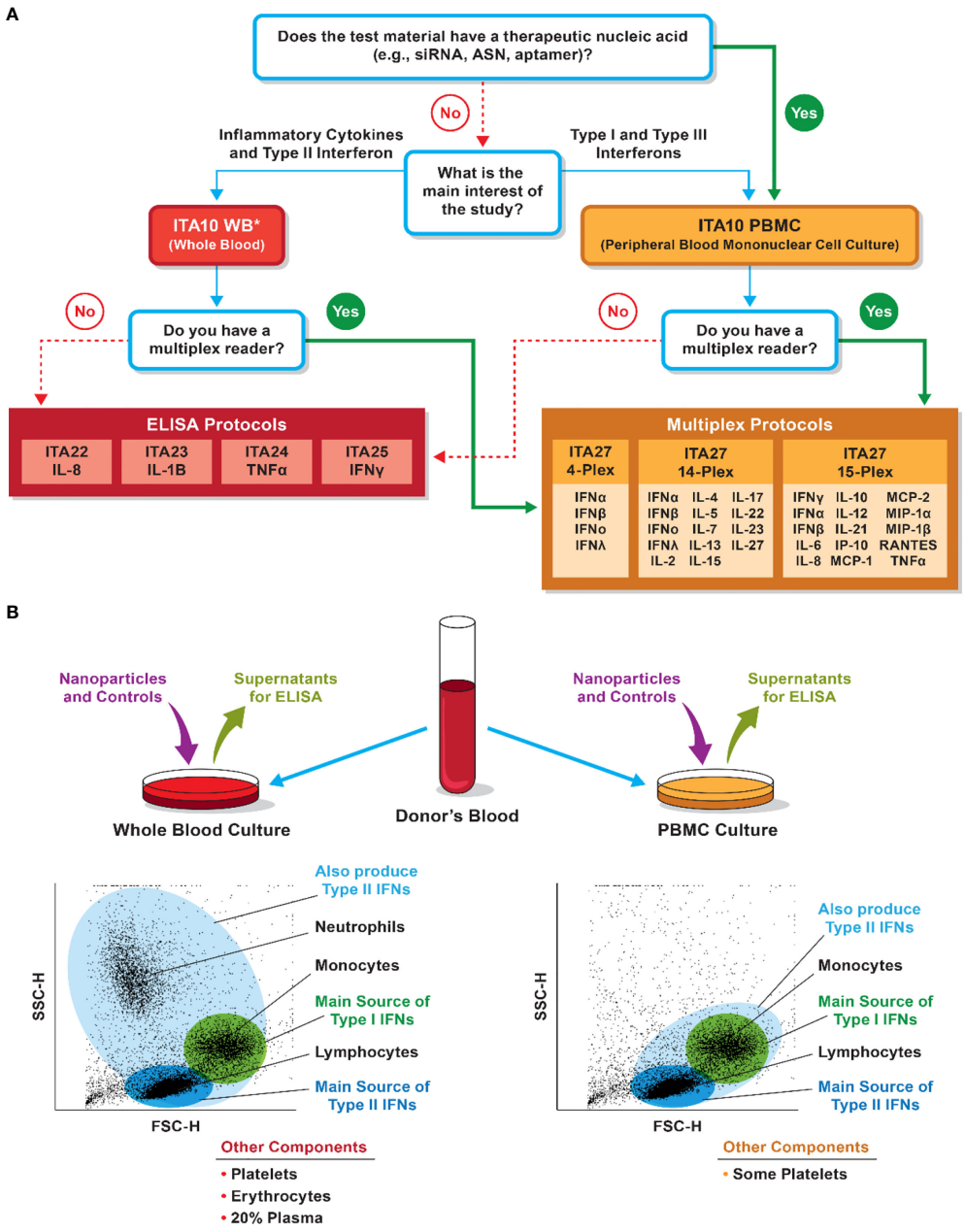

FIGURE 7
Considerations for selection of whole blood versus PBMC cultures for cytokine analysis. **(A)** NCL decision tree for model selection. The decision is influenced by the nanoparticle composition, study questions, and instrument availability. *PBMC could be used to assess pro-inflammatory cytokines and answer questions related to the risk of the cytokine storm. Whole blood, however, is a better system if type II interferon induction is of interest. **(B)** Differences in immune-cell populations between the whole-blood and PBMC cultures may influence the detection of various cytokines. Bullet points at the bottom list other cells or matrices present in the culture but not shown in the forward and side-scatter cytometry plots.

on the number of viable and expanded cells, the MTT signal may also go up when nanoparticles do not induce proliferation but rather improve cell viability by supplying nutrients into the culture medium; for example, nanoformulations containing sucrose are often seen as those increasing the MTT signal. However, such an increase in the cell viability is usually minor and can be easily distinguished from a true mitogenic effect. Nanoparticles may activate the cells and promote proliferation induced by traditional stimuli, and this property is used to estimate their mitogenic activity. Some nanoparticles,

TABLE 1 Human cytokine panel used at NCL.

Cytokine	Primary cell source	Effector target and function
IL-1α	Monocytes, DCs, macrophages, endothelial cells, hepatocytes	Endothelial cells (activation, inflammation, coagulation) Hypothalamus (fever)
IL-1β	DC, macrophages	Endothelial cells, hypothalamus (fever); liver (synthesis of acute-phase protein); Th17 (differentiation)
IL-2	T cells	T cells (activation, proliferation, and differentiation) NK cells (proliferation and activation) B cells: proliferation, antibody synthesis (*in vitro*)
IL-4	CD4+ T cells, mast cells	B cell (activation, proliferation, and differentiation)
IL-5	T cells, mast cells	B cell (isotype switching to IgE) T cells (Th2 differentiation, proliferation) Macrophages (alternative activation and inhibition of IFNγ-mediated classical activation)
IL-6	T cells, macrophages	Liver (synthesis of acute-phase protein); B cells (proliferation of antibody-producing cells); Th17 (differentiation)
IL-8	Monocytes	Neutrophil recruitment
IL-10	T cells, primarily T regs	Macrophages, DCs (inhibition of IL-12 expression, co-stimulators, and class II MHC)
IL-12	DCs, macrophages	Th1 differentiation; NK and T cells (IFNg synthesis, increased cytotoxicity)
IL-13	Th2, NKT, ILC2, mast cells	B cells (isotype switching to IgE); Epithelial cells (increased mucus production); Macrophages (alternative activation)
IL-15	Monocytes	CD8+ memory T cells (survival and proliferation) NK cells (proliferation)
IL-21	Th2, Th17	B cells (activation, proliferation, and differentiation); Tfh-cells (development); Th17 (increased generation)
IL-22	γ/δ T cells, ILC3	Epithelial cells (production of defensins, increased barrier function); hepatocytes (survival)
IL-23	Monocytes, DCs	Th17 (differentiation and expansion)
IL-27	DCs, macrophages	T cells (enhancement of Th1 and inhibition of Th17 differentiation) NK cells (IFNγ synthesis)
MIP-1α	Monocytes, macrophages	Mixed leukocyte recruitment
MIP-1β	Monocytes, macrophages	T cells, monocytes, NK recruitment
MCP-1	Monocytes, macrophages	Mixed leukocyte recruitment except for eosinophils (monocytes, T lymphocytes, NK cells, basophils, mast cells)
MCP-2	Monocytes, macrophages	Mixed leukocyte recruitment, including eosinophils (monocytes, T lymphocytes, NK cells, basophils, mast cells, and eosinophils)
RANTES	T cells	Mixed leukocytes recruitment
TNFα	NK cells, T cells, monocytes, macrophages	Endothelial cells, neutrophils (activation); hypothalamus (fever); muscle, fat (catabolism, cachexia)
IP-10	Monocytes, macrophages	Effector T-cell recruitment
IFNα (Type I)	Plasmacytoid dendritic cells (pDCs)	All cells (antiviral state, increased class I MHC); NK cells (activation)
IFNβ (Type I)	pDCs	All cells (antiviral state), increased class I MHC; NK cells (activation)
IFNω (Type I)	pDCs	All cells (antiviral state, increased class I MHC); NK cells (activation)
IFNγ (Type II)	T cells (Th1, CD8+), NK cells	Macrophages (classical activation); B cells (isotype switch to opsonizing and complement-fixing IgG subclasses); Th1 differentiation; various cells (increase in class II MHC expression, Ag processing, and presentation to T cells)
IFNλ (Type III)	pDC	DCs, neutrophils, CD4+ T cells, and B cells

This table summarizes cytokines, their origin, and their effector function. The information about these cytokines is based on references (213, 214). Knowing the primary cell source and effector/target function of the cytokines induced by nanoparticles helps to identify cell types affected by the analyzed formulations and to predict the biological effect(s) of such induction. This information aids both safety and efficacy studies.

especially those formulated to deliver cytotoxic drugs, inhibit or suppress the proliferation induced by mitogens (e.g., PHA-M) or antigens (e.g., flu antigen). Identification of nanomaterials' ability to suppress mitogen- or antigen-induced proliferation is commonly used to identify immunosuppression (216). A popular *in vitro* assay that is a surrogate of the *in vivo* T-cell-dependent antibody response (TDAR) for immunosuppression screening is the human lymphocyte activation (HuLa) test that employs PBMCs of healthy donors immunized with the current-year flu vaccine. The HuLa assay

was initially developed and validated across immunosuppressive drugs with various mechanisms of action and showed consistent performance (217, 218). This method is also instrumental in identifying nanoparticles with immunosuppressive properties (216).

CFU-GM

Hematopoietic stem cells present in the BM proliferate and differentiate to form so-called colony-forming units (CFU). Depending on the growth factors present in the culture medium, these CFU can be of different cell linage. CFU-GM, for example, assesses the formation of granulocytes and macrophages; CFU-E, erythrocytes; and CFU-GEMM, erythroid and mixed myeloid cells. This method is commonly used to assess the functionality of BM stem cells and the potential effects of test substances on these cells. The method can be conducted *in vitro* and ex vivo. In the *in vitro* protocol, the BM stem cells are isolated from untreated animals or human-donor volunteers, followed by the *in vitro* treatment with nanoparticles. In the ex vivo format, the BM cells are obtained from animals exposed to nanoparticles. Although the *in vitro* method does not account for nanoparticle biodistribution, it allows for rapid identification of potentially toxic formulations and is helpful in cases when amounts of nanoparticles are limited, and the dose information is unavailable, i.e., early in preclinical development. When BM cells are cultured in a methylcellulose-based medium in the presence of SCF, IL-3, and IL-6, it results in the formation of the CFU-GM that can be enumerated. Therefore, the *in vitro* CFU-GM protocol is used to assess the myelosuppressive properties of cytotoxic oncology drugs or nanoformulations delivering these compounds. The comparison between CFU-GM in the untreated sample (the baseline) and nanoparticle-treated sample (test) allows for the identification of nanomaterials with myelosuppressive properties (219). When conducted *in vitro* using murine or human BM cells, the CFU-GM assay was also found to accurately predict a drug's clinical maximum tolerated dose (MTD) in human patients (220, 221).

Phagocytic function

Phagocytes' primary function is to engulf and eliminate foreign particles, microbes, and abnormal host cells. Drug- or xenobiotic-mediated alterations in phagocytosis may lower the host's response to pathogens and transformed cells. Therefore, investigation of nanoparticle effects on phagocytosis is commonly included in experimental frameworks used to assess the safety of nanotechnology-based drug products. Tracking the uptake of model foreign bodies (e.g., yeast zymosan or heat-killed *E. coli*) could be done by flow cytometry or confocal microscopy; in this case, the model particulates are conjugated to a fluorescent label. When unconjugated particulates are used as model foreign bodies for monitoring phagocytic function, a luminescence-producing reagent, luminol, is used to detect their uptake by a plate-reader-based assay (222, 223).

NK cytotoxicity

Natural killer (NK) cells are staffed with cytoplasmic granules containing cytotoxic proteins, such as perforin and granzymes. These proteins form pores in tumor and virus-infected cells when released, thereby contributing to the innate immune response against abnormal and infected cells. Alterations in the NK cytotoxicity may impair immunity; therefore, NK cell function analysis is an integral part of immunotoxicity studies. Both model cell lines and primary NK cells are used for such studies. For example, NK92 and HepG2 cell lines are frequently used as effector and target cells, respectively; the viability of HepG2 cells in the presence of untreated or nanoparticle-treated NK92 cells can be monitored in real-time using label-free technology (224). Other experimental approaches include whole-blood and PBMC cytotoxicity assays in which CFSE-labeled K562 target cells are monitored by flow cytometry to assess the cytotoxicity of primary effector NK cells. Another flow-cytometry-based approach includes the CD107a degranulation assay, in which whole blood or PBMCs serve as the source of primary NK cells (225, 226).

In vivo models

After the initial immunotoxicity assessment using general toxicity studies, specialized immune function tests can be employed to further interrogate adverse effects on the immune system. Some of these specialized immune function tests are described below. In these methods, test nanomaterials are administered as the dose level, using the dosing regimen and *via* the route of administration relevant to the intended clinical use of these materials.

Rabbit pyrogen test

Systemic exposure to pyrogens (i.e., fever-causing substances) results in an elevation in body temperature. As such, the rabbit pyrogen test (RPT) was established to detect fever-causing drugs and other medical products to prevent overt responses in patients. The experimental procedure involves the injection of a test material into the ear vein of a rabbit; the animal's body temperature is monitored before the injection and three hours after the injection with 30-minute intervals. The RPT is standardized for worldwide use in the field of drug development and pharmaceutical analysis for pyrogenicity and

is documented in pharmacopoeias of various countries. However, some discrepancies exist between protocols used in various countries with regards of the required number of rabbits, the acceptable initial body temperature, the determination of baseline temperature, and the decision algorithm (227–229). Historically, the RPT was used to detect endotoxin, a pyrogenic component of the cell wall of gram-negative bacteria that is a common contaminant in pharmaceutical products. However, after the discovery of the *in vitro* limulus amoebocyte lysate (LAL) assay (230, 231), the pharmaceutical community largely switched to this *in vitro* method to detect endotoxin. Later, the *in vitro* PBMC and whole-blood cytokine test, also known as monocyte activation test (MAT), has been validated as a reliable surrogate for LAL and RPT to test not only for endotoxin but for non-endotoxin pyrogens (228, 232–238). Moreover, the experience with some biotechnology-derived therapeutics demonstrated that product processing such as lyophilization may affect the ability of LAL and RPT to accurately detect endotoxin resulting in a product that passes these traditional tests but results in a fever in human patients; in contrast, incubation of the product with PBMC reliably detected "leukocytic pyrogen" produced in response to the endotoxin that was present in the product but remained undetectable by LAL and RPT (239). Currently, all methods—*in vivo* RPT and *in vitro* LAL and MAT—are used for pyrogenicity screening, though LAL remains the most popular.

Murine local lymph node proliferation

Guinea Pig Maximization Test, Buehler's test, and local lymph node assay (LLNA) have been developed to test for delayed-type hypersensitivity (DTH) reactions. More recently, the local lymph node proliferation assay (LLNP) was proposed for the prediction of DTH; this method accurately predicted DTH reactions to systemically administered pharmaceuticals (240). In LLNP protocol, test materials and controls are subcutaneously injected to mice once a day for three consecutive days; next, the animals are allowed to rest for two days before intravenous administration of ^{3}H-thymidine; five hours after the thymidine injection, the animals are sacrificed, and their draining lymph nodes are analysed by scintillation counting to detect thymidine incorporation into the DNA of proliferating leukocytes. An increase in the thymidine incorporation points to T-cell activation that occurs during allergic sensitization. The LLNA protocol is identical to that of LLNP except for the route of test-material administration. In the LLNA assay, the test material is topically applied to the animal's skin; this test is applicable to nanomaterials formulated as creams or lotions. *In vitro* assays myeloid U937 skin sensitization test (U-SENS also known as MUSST) and human cell line activation test (h-CLAT) were developed as surrogates for LLNA/LLNP and showed consistent performance in interlaboratory studies (241–243). However, when applied to nanomaterials testing, the results of these *in vitro* assays do not always correlate with that of the *in vivo* LLNP studies. For example, greater rate of positive response was observed using *in vitro* methods than using *in vivo* tests with MUSST/U-SENS being more sensitive in identifying positive responses than h-CLAT (244). Therefore, the *in vitro* assays are recommended when rapid screening of multiple nanoformulations is needed, but once positive responders are identified, they need to be re-tested using an *in vivo* method.

T-Cell-dependent antibody response

This method is used to assess the immunosuppressive properties of a test material. The assay is conducted in mice. First, the animals are exposed to the test nanomaterials. Next, they are injected with a substance known to produce a TDAR (e.g., keyhole limpet hemocyanin). Finally, the levels of the antigen-specific IgM and IgG are assessed one and three weeks from the antigen administration (216). A decrease in the antibody titer indicates immunosuppressive properties of the test material. The results of this *in vivo* test for iron oxide formulation Feraheme correlated with the *in vitro* HuLa assay discussed above; of note, a sex-dependent difference was detected by the TDAR method (216). Inhibition of the T-cell function by Feraheme has also been confirmed both *in vitro* and *in vivo* in other models (182, 183). However, as with any study, differences may be observed between *in vitro* and *in vivo* tests for various nanomaterials. Therefore, like the strategy mentioned above for the DTH studies, every nanoformulation should be considered on a case-by-case basis; the *in vitro* method is suitable for quick screening, whereas the *in vivo* study should be considered to verify the *in vitro* findings.

Porcine model for CARPA

Pigs are infused or injected with nanomedicines, and hemodynamic changes are monitored in real-time, followed by ex vivo blood sample analysis for the presence of complement split products and other inflammatory mediators such as thromboxane; the model reproduces symptoms and molecular markers induced in response to various nanomedicines known to cause IRs in human patients (48, 245, 246). Clinical relevance of this animal model has been extensively discussed elsewhere (52).

Genetically engineered, humanized, and naturalized models

Genetically engineered and humanized models have been developed to assess human-like immune responses in

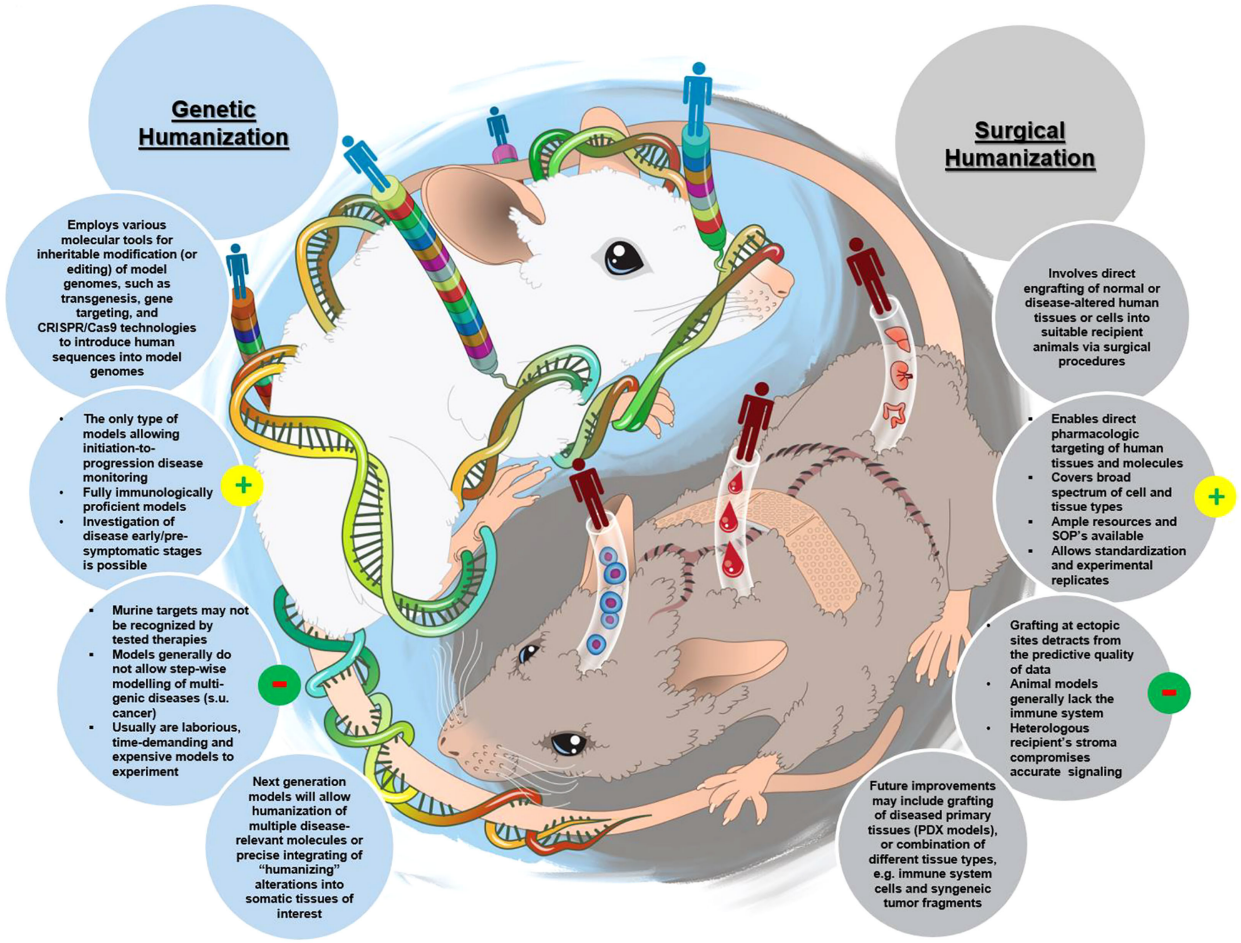

FIGURE 8
Complementary approaches in establishing humanized animal models for basic and translational research purposes. Key benefits (highlighted as yellow circle with a plus sign inside) versus shortcomings (highlighted as a green circle with a minus sign inside) of both strategies are listed, as well as anticipated future directions toward improved utility of these models for preclinical drug-assessment studies. This figure is reproduced with permission from (254).

TABLE 2 Differences between standard husbandry conditions and the natural environment.

Condition	Standard Husbandry	Natural Environment
Optimal temperature	21°C	29–31°C
Light/Dark Cycle	12h/12h	Varies with season
Food	Less diverse	More diverse
Physical activity	Low	High
Likelihood of exposure to microbes, parasites, and allergens	Low	High
Behavioral complexity (ability to navigate or maintain vigilance for predators)	Low	High
Leukocytes	Less mature	More mature
Immune repertoire	Less diverse	More diverse

The table summarizes various conditions for C57BL/6 mice based on reviewed literature (258). Naturalizing or rewilding the animals by exposing them to the natural environment increased the maturity and diversity of lymphocytes and diversified the gut microflora (259).

animals (247–251). Such assessment in preclinical studies is often needed when animals do not express the target for nanoparticle-formulated drugs or when drug efficacy requires immunocompetent animals. Genetically engineered mouse models (GEMMs) are ideal for studies of cancer and other diseases due to unique mechanistic insights that traditional models cannot provide; these models were reviewed in detail elsewhere (252). An example demonstrating the utility of these models in preclinical studies of nanomaterials is the Taxane-resistant GEMM strain FVB/NJ containing C3(1)SV40 T-antigen (C3Tag) transgene used to demonstrate the efficacy of PRINT nanoparticles against taxane-resistant triple-negative breast cancer (253). However, their high costs and complex logistics limit their use in research and development to specialized facilities equipped to support such models. Humanized animal models were developed by surgical transplantation of human cells or tissues, or by genetic engineering to express desired human proteins, and are more widely used in preclinical research due to their wider accessibility (Figure 8) (254). In one such study, PRINT nanoparticles were tested in NOD.Rag1−/−Il2rg−/− (NRG) mice, which, after irradiation, received an intrahepatic injection of CD34+ cells from human fetal liver tissues to produce human blood cells. This study found PRINT

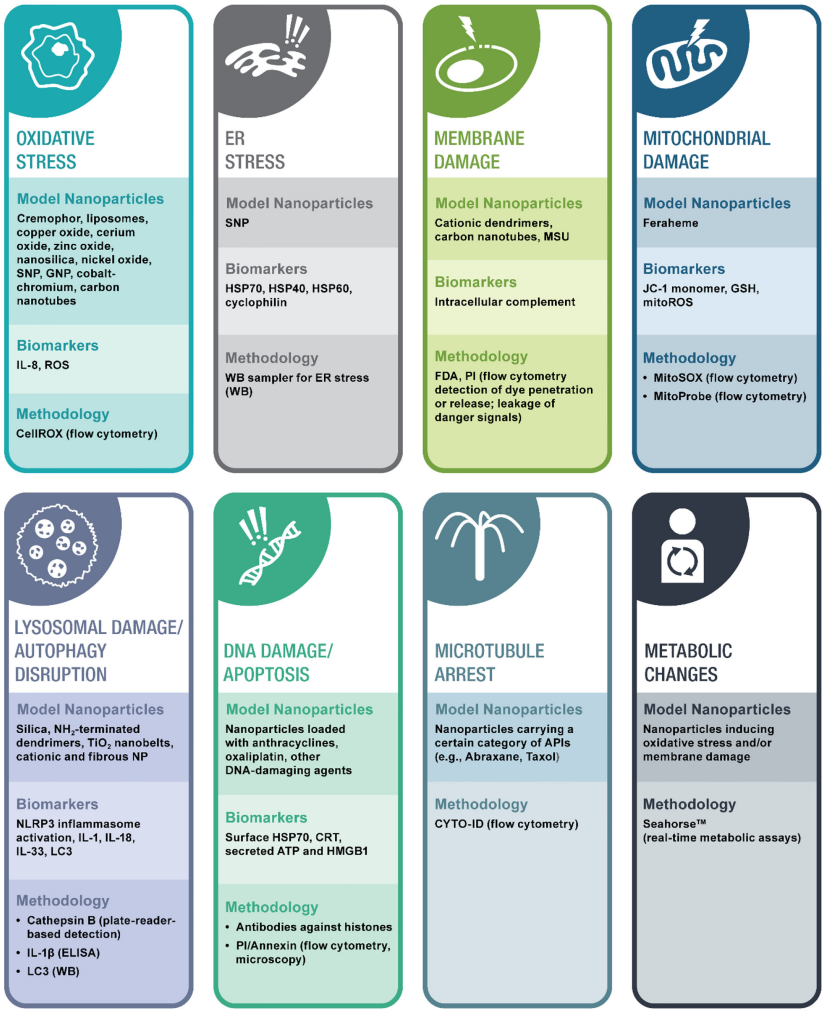

FIGURE 9
A framework of mechanistic studies. Types of mechanistic studies, model nanoparticles that could be used as controls, methodologies, and intrumentation, and, whenever available, relevant biomarkers are summarized. API, active pharmaceutical ingredient; ATP, adenosine triphosphate; CRT, calreticulin; ER, endoplasmic reticulum; ELISA, enzyme-linked immunosirbent assay; FDA, fluorescein diacetate; GNP, gold nanoparticles; GSH, glutathion; Histones, Phospho-Histone H2AX (Ser139); HSP, heat shock protein; HMG, high mobility group; ID, identifier; LC, light chain; MSU, monosodium urate; NP, nanoparticles; PI, propidium iodine; ROS, reactive oxygen species; SNP, silver nanoparticles; TM, trade mark; WB, western blot.

nanoparticles' preferential uptake by human CD14+ monocytes without induction of systemic inflammation; these data in the humanized animals correlated with the *in vitro* uptake studies performed using human PBMCs (255). Another study utilized NOD/*scid*/*IL2r* common γ chain null (NSG) mice following the transfer of human PBMCs to analyze the functionality of the antigen-specific human regulatory T cells induced by PLGA nanoparticles co-delivering IL-2 and TGF-β to produce the tolerogenic response for lupus therapy (256). Similarly, NSG mice engrafted after the irradiation with human CD34+ peripheral blood stem cells derived from granulocyte colony-stimulating-factor-mobilized healthy donors were found instrumental for the *in vivo* efficacy analysis of protein subunit vaccines delivered by self-assembling protein-based nanoparticles to prevent Epstein-Barr virus infection (257).

Another interesting and thought-provoking idea for improving animal model relevance to humans is so-called "rewilding" or naturalizing the animals (258). One study demonstrated that naturalizing or rewilding animals by exposing them to the natural environment increased the maturity and diversity of lymphocytes and diversified the gut microflora (259). Graham reviewed multiple studies across several animal species, demonstrating that transitioning animals from standard husbandry conditions to a natural environment diversified the immune repertoire of the naturalized animals and suggested considering these animals for preclinical studies (258). A comparison between standard husbandry and the natural environment for C57BL/6 mice, as an example, is provided in Table 2. Moving preclinical studies in this direction would increase data variability, logistical challenges, and costs of such studies; however, such costs may be warranted, especially if this approach helps improve the predictability of preclinical animal studies and their relevance to humans. It would be interesting to compare biodistribution, safety, and efficacy of the same nanoformulation in the same laboratory animal strain when it is kept under standard husbandry conditions versus when it is naturalized.

Conclusion and future directions

After almost two decades of researching immunological properties of nanomaterials, common trends have been identified for certain nanoparticles based on their composition (e.g., polymer- and lipid-based nanomaterials induce chemokine response and prolong plasma coagulation time), surface moieties (e.g., the presence of PEG increases the risk of anti-PEG antibody-mediated responses), zeta potential (e.g., cationic materials are pro-thrombogenic and cytotoxic), shape (e.g., fibrous nanomaterials cause lysosomal rupture with subsequent activation of inflammasome), and size (e.g., large [< 300 nm] materials regardless of their surface coating are quickly eliminated by the phagocytic cells) as reviewed in this manuscript and earlier reports from NCL (32, 199, 260, 261) and other groups (22, 262–271). Knowing these trends helps prioritize safety studies and select nanoparticle platforms for formulating non-immunologically inert APIs. However, each component of nanoformulation has a role and unique properties; therefore, each nanoparticle must be considered on a case-by-case basis and in the context of APIs, excipients, route of administration, and indication.

The investigation of nanoparticle immunological properties progresses toward mechanistic studies involving new technological modalities, such as real-time imaging, advanced immunophenotyping, and immunometabolomics. Some examples of mechanistic studies and relevant methods are summarized in Figure 9. The increased use of nucleic acid therapeutics (e.g., mRNA), especially when delivered using nanocarriers with intrinsic pro-inflammatory properties (e.g., LNPs) *via* local routes traditionally used for immunization (e.g., i.m.), in the presence of adjuvants (e.g., TLR agonists, CpG oligos, saponins and other natural products) and intended for use in healthy individuals (e.g., to prevent infections) warrants studies investigating the risk of autoimmunity. Improving *in vitro* and *in vivo* models for assessing nanoparticle immunotoxicity along with harmonization of testing approaches is another important direction in this field. Sharing high quality data generated by "wet" laboratories with bioinformatics researchers is also expected to improve quality of nanotherapeutics, streamline the selection of nanocarriers and aid in developing safer nanomedicines by generating supporting computer-based algorithms and analysis tools.

Author contributions

The author confirms being the sole contributor of this work and has approved it for publication.

Funding

This study was funded in whole by federal funds from the National Cancer Institute, National Institutes of Health, under contract 75N91019D00024.

Acknowledgments

I am grateful to Allen Kane and Karolina Wilk for the help with manuscript preparation.

Conflict of interest

The author declares that the research was conducted in the absence of any commercial or financial relationships that could be construed as a potential conflict of interest.

Publisher's note

All claims expressed in this article are solely those of the authors and do not necessarily represent those of their affiliated organizations, or those of the publisher, the editors and the reviewers. Any product that may be evaluated in this article, or claim that may be made by its manufacturer, is not guaranteed or endorsed by the publisher.

Author disclaimer

The content of this publication does not necessarily reflect the views or policies of the Department of Health and Human Services, nor does mention of trade names, commercial products, or organizations imply endorsement by the U.S. Government.

References

1. Akhter MH, Ahmad I, Alshahrani MY, Al-Harbi AI, Khalilullah H, Afzal O, et al. Drug delivery challenges and current progress in nanocarrier-based ocular therapeutic system. *Gels* (2022) 8:1–50. doi: 10.3390/gels8020082

2. Ayub A, Wettig S. An overview of nanotechnologies for drug delivery to the brain. *Pharmaceutics* (2022) 14:1–30. doi: 10.3390/pharmaceutics14020224

3. Jiang Y, Lin W, Zhu L. Targeted drug delivery for the treatment of blood cancers. *Molecules* (2022) 27:1–16. doi: 10.3390/molecules27041310

4. Khan MI, Hossain MI, Hossain MK, Rubel MHK, Hossain KM, Mahfuz A, et al. Recent progress in nanostructured smart drug delivery systems for cancer therapy: A review. *ACS Appl Bio Mater* (2022) 5:971–1012. doi: 10.1021/acsabm.2c00002

5. Nazir F, Tabish TA, Tariq F, Iftikhar S, Wasim R, Shahnaz G. Stimuli-sensitive drug delivery systems for site-specific antibiotic release. *Drug Discovery Today* (2022) 6:1698–705. doi: 10.1016/j.drudis.2022.02.014

6. Song H, Jiang C. Recent advances in targeted drug delivery for the treatment of pancreatic ductal adenocarcinoma. *Expert Opin Drug Delivery* (2022) 19:281–301. doi: 10.1080/17425247.2022.2045943

7. Research AM. *Nanomedicine market overview* (2017). Available at: https://www.thepharmaletter.com/article/global-nanomedicine-market-to-be-worth-258-billion-by-2025-says-report (Accessed March 2 2022).

8. Medicine NLO. *Clinical trials* (2020). Available at: https://clinicaltrials.gov/ct2/results/browse?term=nanoparticle&recrs=abcd&cond=Cancer&brwse=cond_alpha_all.

9. Shi Y, van der Meel R, Chen X, Lammers T. The EPR effect and beyond: Strategies to improve tumor targeting and cancer nanomedicine treatment efficacy. *Theranostics* (2020) 10:7921–4. doi: 10.7150/thno.49577

10. Kirtane AR, Verma M, Karandikar P, Furin J, Langer R, Traverso G. Nanotechnology approaches for global infectious diseases. *Nat Nanotechnol* (2021) 16:369–84. doi: 10.1038/s41565-021-00866-8

11. O'brien ME, Wigler N, Inbar M, Rosso R, Grischke E, Santoro A, et al. Reduced cardiotoxicity and comparable efficacy in a phase III trial of pegylated liposomal doxorubicin HCl (CAELYX/Doxil) versus conventional doxorubicin for first-line treatment of metastatic breast cancer. *Ann Oncol* (2004) 15(3):440–9. doi: 10.1093/annonc/mdh097

12. Sparreboom A, Baker SD, Verweij J. Paclitaxel repackaged in an albumin-stabilized nanoparticle: handy or just a dandy? *J Clin Oncol* (2005) 23:7765–7. doi: 10.1200/JCO.2005.03.7135

13. De Leon MC, Bolla S, Greene B, Hutchinson L, Del Priore G. Successful treatment with nab-paclitaxel after hypersensitivity reaction to paclitaxel and docetaxel. *Gynecol Oncol Case Rep* (2013) 5:70–1. doi: 10.1016/j.gynor.2013.05.003

14. Paciotti GF, Myer L, Weinreich D, Goia D, Pavel N, Mclaughlin RE, et al. Colloidal gold: a novel nanoparticle vector for tumor directed drug delivery. *Drug Delivery* (2004) 11:169–83. doi: 10.1080/10717540490433895

15. Ramani K, Miclea RD, Purohit VS, Mager DE, Straubinger RM, Balu-Iyer SV. Phosphatidylserine containing liposomes reduce immunogenicity of recombinant human factor VIII (rFVIII) in a murine model of hemophilia a. *J Pharm Sci* (2008) 97:1386–98. doi: 10.1002/jps.21102

16. Libutti SK, Paciotti GF, Byrnes AA, Alexander HRJr., Gannon WE, Walker M, et al. Phase I and pharmacokinetic studies of CYT-6091, a novel PEGylated colloidal gold-rhTNF nanomedicine. *Clin Cancer Res* (2010) 16:6139–49. doi: 10.1158/1078-0432.CCR-10-0978

17. Lorusso D, Di Stefano A, Carone V, Fagotti A, Pisconti S, Scambia G. Pegylated liposomal doxorubicin-related palmar-plantar erythrodysesthesia ('hand-foot' syndrome). *Ann Oncol* (2007) 18:1159–64. doi: 10.1093/annonc/mdl477

18. Manil L, Couvreur P, Mahieu P. Acute renal toxicity of doxorubicin (adriamycin)-loaded cyanoacrylate nanoparticles. *Pharm Res* (1995) 12:85–7. doi: 10.1023/A:1016290704772

19. Dobrovolskaia MA, Aggarwal P, Hall JB, Mcneil SE. Preclinical studies to understand nanoparticle interaction with the immune system and its potential effects on nanoparticle biodistribution. *Mol Pharm* (2008) 5:487–95. doi: 10.1021/mp800032f

20. Aggarwal P, Hall JB, Mcleland CB, Dobrovolskaia MA, Mcneil SE. Nanoparticle interaction with plasma proteins as it relates to particle biodistribution, biocompatibility and therapeutic efficacy. *Adv Drug Delivery Rev* (2009) 61:428–37. doi: 10.1016/j.addr.2009.03.009

21. Bao J, Zhang Q, Duan T, Hu R, Tang J. The fate of nanoparticles *In vivo* and the strategy of designing stealth nanoparticle for drug delivery. *Curr Drug Targets* (2021) 22:922–46. doi: 10.2174/1389450122666210118105122

22. Magadán S, Mikelez-Alonso I, Borrego F, González-Fernández Á. Nanoparticles and trained immunity: Glimpse into the future. *Adv Drug Delivery Rev* (2021) 175:113821. doi: 10.1016/j.addr.2021.05.031

23. Rios-Doria J, Durham N, Wetzel L, Rothstein R, Chesebrough J, Holoweckyj N, et al. Doxil synergizes with cancer immunotherapies to enhance antitumor responses in syngeneic mouse models. *Neoplasia* (2015) 17:661–70. doi: 10.1016/j.neo.2015.08.004

24. Amini MA, Abbasi AZ, Cai P, Lip H, Gordijo CR, Li J, et al. Combining tumor microenvironment modulating nanoparticles with doxorubicin to enhance chemotherapeutic efficacy and boost antitumor immunity. *J Natl Cancer Inst* (2019) 111:399–408. doi: 10.1093/jnci/djy131

25. Zhang F, Stephan SB, Ene CI, Smith TT, Holland EC, Stephan MT. Nanoparticles that reshape the tumor milieu create a therapeutic window for effective T-cell therapy in solid malignancies. *Cancer Res* (2018) 78:3718–30. doi: 10.1158/0008-5472.CAN-18-0306

26. Cyprian FS, Akhtar S, Gatalica Z, Vranic S. Targeted immunotherapy with a checkpoint inhibitor in combination with chemotherapy: A new clinical paradigm in the treatment of triple-negative breast cancer. *Bosn J Basic Med Sci* (2019) 19:227–33. doi: 10.17305/bjbms.2019.4204

27. Medicine NLO. *Abraxane with anti-PD1/PDL1 in patients with advanced urothelial cancer (ABLE)* (2022). Available at: https://clinicaltrials.gov/ct2/show/NCT03240016 (Accessed March 2 2022).

28. Lim S, Park J, Shim MK, Um W, Yoon HY, Ryu JH, et al. Recent advances and challenges of repurposing nanoparticle-based drug delivery systems to enhance cancer immunotherapy. *Theranostics* (2019) 9:7906–23. doi: 10.7150/thno.38425

29. Galluzzi L, Buqué A, Kepp O, Zitvogel L, Kroemer G. Immunological effects of conventional chemotherapy and targeted anticancer agents. *Cancer Cell* (2015) 28:690–714. doi: 10.1016/j.ccell.2015.10.012

30. Zhao X, Yang K, Zhao R, Ji T, Wang X, Yang X, et al. Inducing enhanced immunogenic cell death with nanocarrier-based drug delivery systems for pancreatic cancer therapy. *Biomaterials* (2016) 102:187–97. doi: 10.1016/j.biomaterials.2016.06.032

31. Gondhowiardjo SA, Handoko, Jayalie VF, Apriantoni R, Barata AR, Senoaji F, et al. Tackling resistance to cancer immunotherapy: What do we know? *Molecules* (2020) 25:1–20. doi: 10.3390/molecules25184096

32. Dobrovolskaia MA. Pre-clinical immunotoxicity studies of nanotechnology-formulated drugs: Challenges, considerations and strategy. *J Control Release* (2015) 220:571–83. doi: 10.1016/j.jconrel.2015.08.056

33. Taub DD, Anver M, Oppenheim JJ, Longo DL, Murphy WJ. T Lymphocyte recruitment by interleukin-8 (IL-8). IL-8-induced degranulation of neutrophils releases potent chemoattractants for human T lymphocytes both *in vitro* and *in vivo*. *J Clin Invest* (1996) 97:1931–41. doi: 10.1172/JCI118625

34. Ilinskaya AN, Shah A, Enciso AE, Chan KC, Kaczmarczyk JA, Blonder J, et al. Nanoparticle physicochemical properties determine the activation of intracellular complement. *Nanomedicine* (2019) 17:266–75. doi: 10.1016/j.nano.2019.02.002

35. West EE, Afzali B, Kemper C. Unexpected roles for intracellular complement in the regulation of Th1 responses. *Adv Immunol* (2018) 138:35–70. doi: 10.1016/bs.ai.2018.02.001

36. West EE, Kolev M, Kemper C. Complement and the regulation of T cell responses. *Annu Rev Immunol* (2018) 36:309–38. doi: 10.1146/annurev-immunol-042617-053245

37. Hansen CB, Willer A, Bayarri-Olmos R, Kemper C, Garred P. Expression of complement C3, C5, C3aR and C5aR1 genes in resting and activated CD4(+) T cells. *Immunobiology* (2019) 224:307–15. doi: 10.1016/j.imbio.2018.12.004

38. Duan X, Chan C, Han W, Guo N, Weichselbaum RR, Lin W. Immunostimulatory nanomedicines synergize with checkpoint blockade immunotherapy to eradicate colorectal tumors. *Nat Commun* (2019) 10:1899. doi: 10.1038/s41467-019-09221-x

39. Ilinskaya AN, Clogston JD, Mcneil SE, Dobrovolskaia MA. Induction of oxidative stress by taxol® vehicle cremophor-EL triggers production of interleukin-8 by peripheral blood mononuclear cells through the mechanism not requiring *de novo* synthesis of mRNA. *Nanomedicine* (2015) 11:1925–38. doi: 10.1016/j.nano.2015.07.012

40. Tezel G, Yang X, Luo C, Kain AD, Powell DW, Kuehn MH, et al. Oxidative stress and the regulation of complement activation in human glaucoma. *Invest Ophthalmol Vis Sci* (2010) 51:5071–82. doi: 10.1167/iovs.10-5289

41. Smith DA, Schmid EF. Drug withdrawals and the lessons within. *Curr Opin Drug Discovery Devel* (2006) 9(1):38–46.

42. Wysowski DK, Swartz L. Adverse drug event surveillance and drug withdrawals in the united states 1969-2002: the importance of reporting suspected reactions. *Arch Intern Med* (2005) 165:1363–9. doi: 10.1001/archinte.165.12.1363

43. Craveiro NS, Lopes BS, Tomás L, Almeida SF. Drug withdrawal due to safety: A review of the data supporting withdrawal decision. *Curr Drug Saf* (2020) 15:4–12. doi: 10.2174/1574886314666191004092520

44. Szebeni J, Simberg D, González-Fernández Á., Barenholz Y, Dobrovolskaia MA. Roadmap and strategy for overcoming infusion reactions to nanomedicines. *Nat Nanotechnol* (2018) 13:1100–8. doi: 10.1038/s41565-018-0273-1

45. Fülöp T, Kozma GT, Vashegyi I, Mészáros T, Rosivall L, Urbanics R, et al. Liposome-induced hypersensitivity reactions: Risk reduction by design of safe infusion protocols in pigs. *J Control Release* (2019) 309:333–8. doi: 10.1016/j.jconrel.2019.07.005

46. Mohamed M, Abu Lila AS, Shimizu T, Alaaeldin E, Hussein A, Sarhan HA, et al. PEGylated liposomes: immunological responses. *Sci Technol Adv Mater* (2019) 20:710–24. doi: 10.1080/14686996.2019.1627174

47. Kozma GT, Shimizu T, Ishida T, Szebeni J. Anti-PEG antibodies: Properties, formation, testing and role in adverse immune reactions to PEGylated nano-biopharmaceuticals. *Adv Drug Delivery Rev* (2020) 154-155:163–75. doi: 10.1016/j.addr.2020.07.024

48. Milosevits G, Mészáros T, Őrfi E, Bakos T, Garami M, Kovács G, et al. Complement-mediated hypersensitivity reactions to an amphotericin b-containing lipid complex (Abelcet) in pediatric patients and anesthetized rats: Benefits of slow infusion. *Nanomedicine* (2021) 34:102366. doi: 10.1016/j.nano.2021.102366

49. Szebeni J, Storm G, Ljubimova JY, Castells M, Phillips EJ, Turjeman K, et al. Applying lessons learned from nanomedicines to understand rare hypersensitivity reactions to mRNA-based SARS-CoV-2 vaccines. *Nat Nanotechnol* (2022) 17:337–46. doi: 10.1038/s41565-022-01071-x

50. Sunyer JO, Boshra H, Lorenzo G, Parra D, Freedman B, Bosch N. Evolution of complement as an effector system in innate and adaptive immunity. *Immunol Res* (2003) 27:549–64. doi: 10.1385/IR:27:2-3:549

51. Szebeni J. Complement activation-related pseudoallergy: a stress reaction in blood triggered by nanomedicines and biologicals. *Mol Immunol* (2014) 61:163–73. doi: 10.1016/j.molimm.2014.06.038

52. Szebeni J, Bawa R. Human clinical relevance of the porcine model of pseudoallergic infusion reactions. *Biomedicines* (2020) 8:1–24. doi: 10.3390/biomedicines8040082

53. Vigne J, Cabella C, Dézsi L, Rustique E, Couffin AC, Aid R, et al. Nanostructured lipid carriers accumulate in atherosclerotic plaques of ApoE(-/-) mice. *Nanomedicine* (2020) 25:102157. doi: 10.1016/j.nano.2020.102157

54. Pethő Á., Piecha D, Mészáros T, Urbanics R, Moore C, Canaud B, et al. A porcine model of hemodialyzer reactions: roles of complement activation and rinsing back of extracorporeal blood. *Ren Fail* (2021) 43:1609–20. doi: 10.1080/0886022X.2021.2007127

55. Szebeni J, Bedocs P, Rozsnyay Z, Weiszhár Z, Urbanics R, Rosivall L, et al. Liposome-induced complement activation and related cardiopulmonary distress in pigs: factors promoting reactogenicity of doxil and AmBisome. *Nanomedicine* (2012) 8:176–84. doi: 10.1016/j.nano.2011.06.003

56. Yu K, Lai BF, Foley JH, Krisinger MJ, Conway EM, Kizhakkedathu JN. Modulation of complement activation and amplification on nanoparticle surfaces by glycopolymer conformation and chemistry. *ACS Nano* (2014) 8:7687–703. doi: 10.1021/nn504186b

57. Pham CT, Thomas DG, Beiser J, Mitchell LM, Huang JL, Senpan A, et al. Application of a hemolysis assay for analysis of complement activation by perfluorocarbon nanoparticles. *Nanomedicine* (2014) 10:651–60. doi: 10.1016/j.nano.2013.10.012

58. Szebeni J, Muggia F, Gabizon A, Barenholz Y. Activation of complement by therapeutic liposomes and other lipid excipient-based therapeutic products: prediction and prevention. *Adv Drug Delivery Rev* (2011) 63:1020–30. doi: 10.1016/j.addr.2011.06.017

59. Szebeni J, Bedőcs P, Urbanics R, Bünger R, Rosivall L, Tóth M, et al. Prevention of infusion reactions to PEGylated liposomal doxorubicin *via* tachyphylaxis induction by placebo vesicles: a porcine model. *J Control Release* (2012) 160:382–7. doi: 10.1016/j.jconrel.2012.02.029

60. Bavli Y, Winkler I, Chen BM, Roffler S, Cohen R, Szebeni J, et al. Doxebo (doxorubicin-free doxil-like liposomes) is safe to use as a pre-treatment to prevent infusion reactions to PEGylated nanodrugs. *J Control Release* (2019) 306:138–48. doi: 10.1016/j.jconrel.2019.06.007

61. Neun BW, Barenholz Y, Szebeni J, Dobrovolskaia MA. Understanding the role of anti-PEG antibodies in the complement activation by doxil *in vitro*. *Molecules* (2018) 23:1–19. doi: 10.3390/molecules23071700

62. Morgan BP, Gasque P. Extrahepatic complement biosynthesis: where, when and why? *Clin Exp Immunol* (1997) 107:1–7. doi: 10.1046/j.1365-2249.1997.d01-890.x

63. Liszewski MK, Kolev M, Le Friec G, Leung M, Bertram PG, Fara AF, et al. Intracellular complement activation sustains T cell homeostasis and mediates effector differentiation. *Immunity* (2013) 39:1143–57. doi: 10.1016/j.immuni.2013.10.018

64. Cho MS, Vasquez HG, Rupaimoole R, Pradeep S, Wu S, Zand B, et al. Autocrine effects of tumor-derived complement. *Cell Rep* (2014) 6:1085–95. doi: 10.1016/j.celrep.2014.02.014

65. Peng Q, Li K, Patel H, Sacks SH, Zhou W. Dendritic cell synthesis of C3 is required for full T cell activation and development of a Th1 phenotype. *J Immunol* (2006) 176:3330–41. doi: 10.4049/jimmunol.176.6.3330

66. Kolev M, Dimeloe S, Le Friec G, Navarini A, Arbore G, Povoleri GA, et al. Complement regulates nutrient influx and metabolic reprogramming during Th1 cell responses. *Immunity* (2015) 42:1033–47. doi: 10.1016/j.immuni.2015.05.024

67. Toyama T, Matsuda H, Ishida I, Tani M, Kitaba S, Sano S, et al. A case of toxic epidermal necrolysis-like dermatitis evolving from contact dermatitis of the hands associated with exposure to dendrimers. *Contact Dermatitis* (2008) 59:122–3. doi: 10.1111/j.1600-0536.2008.01340.x

68. Elsabahy M, Wooley KL. Cytokines as biomarkers of nanoparticle immunotoxicity. *Chem Soc Rev* (2013) 42:5552–76. doi: 10.1039/c3cs60064e

69. Pati R, Shevtsov M, Sonawane A. Nanoparticle vaccines against infectious diseases. *Front Immunol* (2018) 9:2224. doi: 10.3389/fimmu.2018.02224

70. Hamilton RF, Wu N, Porter D, Buford M, Wolfarth M, Holian A. Particle length-dependent titanium dioxide nanomaterials toxicity and bioactivity. *Part Fibre Toxicol* (2009) 6:35. doi: 10.1186/1743-8977-6-35

71. Hussain S, Boland S, Baeza-Squiban A, Hamel R, Thomassen LC, Martens JA, et al. Oxidative stress and proinflammatory effects of carbon black and titanium dioxide nanoparticles: role of particle surface area and internalized amount. *Toxicology* (2009) 260:142–9. doi: 10.1016/j.tox.2009.04.001

72. Heng BC, Zhao X, Tan EC, Khamis N, Assodani A, Xiong S, et al. Evaluation of the cytotoxic and inflammatory potential of differentially shaped zinc oxide nanoparticles. *Arch Toxicol* (2011) 85:1517–28. doi: 10.1007/s00204-011-0722-1

73. Xiang SD, Wilson KL, Goubier A, Heyerick A, Plebanski M. Design of peptide-based nanovaccines targeting leading antigens from gynecological cancers to induce HLA-A2.1 restricted CD8(+) T cell responses. *Front Immunol* (2018) 9:2968. doi: 10.3389/fimmu.2018.02968

74. Grippin AJ, Wummer B, Wildes T, Dyson K, Trivedi V, Yang C, et al. Dendritic cell-activating magnetic nanoparticles enable early prediction of antitumor response with magnetic resonance imaging. *ACS Nano* (2019) 13:13884–98. doi: 10.1021/acsnano.9b05037

75. Wilson KL, Pouniotis D, Hanley J, Xiang SD, Ma C, Coppel RL, et al. A synthetic nanoparticle based vaccine approach targeting MSP4/5 is immunogenic and induces moderate protection against murine blood-stage malaria. *Front Immunol* (2019) 10:331. doi: 10.3389/fimmu.2019.00331

76. Dai CC, Yang J, Hussein WM, Zhao L, Wang X, Khalil ZG, et al. Polyethylenimine: An intranasal adjuvant for liposomal peptide-based subunit vaccine against group a streptococcus. *ACS Infect Dis* (2020) 6:2502–12. doi: 10.1021/acsinfecdis.0c00452

77. Fotoran WL, Kleiber N, Müntefering T, Liebau E, Wunderlich G. Production of glycosylphosphatidylinositol-anchored proteins for vaccines and directed binding of immunoliposomes to specific cell types. *J Venom Anim Toxins Incl Trop Dis* (2020) 26:e20200032. doi: 10.1590/1678-9199-jvatitd-2020-0032

78. Hong X, Zhong X, Du G, Hou Y, Zhang Y, Zhang Z, et al. The pore size of mesoporous silica nanoparticles regulates their antigen delivery efficiency. *Sci Adv* (2020) 6:eaaz4462. doi: 10.1126/sciadv.aaz4462

79. Lee JY, Kim MK, Nguyen TL, Kim J. Hollow mesoporous silica nanoparticles with extra-Large mesopores for enhanced cancer vaccine. *ACS Appl Mater Interfaces* (2020) 12:34658–66. doi: 10.1021/acsami.0c09484

80. Li X, Wang X, Ito A, Tsuji NM. A nanoscale metal organic frameworks-based vaccine synergises with PD-1 blockade to potentiate anti-tumour immunity. *Nat Commun* (2020) 11:3858. doi: 10.1038/s41467-020-17637-z

81. Ringe RP, Cruz Portillo VM, Dosenovic P, Ketas TJ, Ozorowski G, Nogal B, et al. Neutralizing antibody induction by HIV-1 envelope glycoprotein SOSIP trimers on iron oxide nanoparticles may be impaired by mannose binding lectin. *J Virol* (2020) 94:1–32. doi: 10.1128/JVI.01883-19

82. Skwarczynski M, Zhao G, Boer JC, Ozberk V, Azuar A, Cruz JG, et al. Poly (amino acids) as a potent self-adjuvanting delivery system for peptide-based nanovaccines. *Sci Adv* (2020) 6:eaax2285. doi: 10.1126/sciadv.aax2285

83. Sosa-Acosta JR, Iriarte-Mesa C, Ortega GA, Díaz-García AM. DNA-Iron oxide nanoparticles conjugates: Functional magnetic nanoplatforms in biomedical applications. *Top Curr Chem (Cham)* (2020) 378:13. doi: 10.1007/s41061-019-0277-9

84. Theobald N. Emerging vaccine delivery systems for COVID-19: Functionalised silica nanoparticles offer a potentially safe and effective alternative delivery system for DNA/RNA vaccines and may be useful in the hunt for a COVID-19 vaccine. *Drug Discovery Today* (2020) 25:1556–8. doi: 10.1016/j.drudis.2020.06.020

85. Veneziano R, Moyer TJ, Stone MB, Wamhoff EC, Read BJ, Mukherjee S, et al. Role of nanoscale antigen organization on b-cell activation probed using DNA origami. *Nat Nanotechnol* (2020) 15:716–23. doi: 10.1038/s41565-020-0719-0

86. Wilson KL, Howard GP, Coatsworth H, Dinglasan RR, Mao HQ, Plebanski M. Biodegradable PLGA-b-PEG nanoparticles induce T helper 2 (Th2) immune responses and sustained antibody titers *via* TLR9 stimulation. *Vaccines (Basel)* (2020) 8:1–14. doi: 10.3390/vaccines8020261

87. Wusiman A, Xu S, Ni H, Gu P, Liu Z, Zhang Y, et al. Immunomodulatory effects of alhagi honey polysaccharides encapsulated into PLGA nanoparticles. *Carbohydr Polym* (2019) 211:217–26. doi: 10.1016/j.carbpol.2019.01.102

88. Shim S, Soh SH, Im YB, Park HE, Cho CS, Kim S, et al. Elicitation of Th1/Th2 related responses in mice by chitosan nanoparticles loaded with brucella abortus malate dehydrogenase, outer membrane proteins 10 and 19. *Int J Med Microbiol* (2020) 310:151362. doi: 10.1016/j.ijmm.2019.151362

89. Zhang X, Tian W, Cai X, Wang X, Dang W, Tang H, et al. Hydrazinocurcumin encapsuled nanoparticles "re-educate" tumor-associated macrophages and exhibit anti-tumor effects on breast cancer following STAT3 suppression. *PloS One* (2013) 8:e65896. doi: 10.1371/journal.pone.0065896

90. Perisé-Barrios AJ, Gómez R, Corbí AL, de la Mata J, Domínguez-Soto A, Muñoz-Fernandez MA. Use of carbosilane dendrimer to switch macrophage polarization for the acquisition of antitumor functions. *Nanoscale* (2015) 7:3857–66. doi: 10.1039/C4NR04038D

91. Kumari M, Purohit MP, Pahuja R, Patnaik S, Shukla Y, Kumar P, et al. Pro-inflammatory macrophage polarization enhances the anti-cancer efficacy of self-assembled galactomannan nanoparticles entrapped with hydrazinocurcumin. *Drug Delivery Transl Res* (2019) 9:1159–88. doi: 10.1007/s13346-019-00661-y

92. Gan J, Dou Y, Li Y, Wang Z, Wang L, Liu S, et al. Producing anti-inflammatory macrophages by nanoparticle-triggered clustering of mannose receptors. *Biomaterials* (2018) 178:95–108. doi: 10.1016/j.biomaterials.2018.06.015

93. Li M, Gao L, Chen J, Zhang Y, Wang J, Lu X, et al. Controllable release of interleukin-4 in double-layer sol-gel coatings on TiO(2) nanotubes for modulating macrophage polarization. *BioMed Mater* (2018) 13:045008. doi: 10.1088/1748-605X/aa9526

94. Ren C, Li D, Zhou Q, Hu X. Mitochondria-targeted TPP-MoS(2) with dual enzyme activity provides efficient neuroprotection through M1/M2 microglial polarization in an alzheimer's disease model. *Biomaterials* (2020) 232:119752. doi: 10.1016/j.biomaterials.2019.119752

95. Yang Y, Guo L, Wang Z, Liu P, Liu X, Ding J, et al. Targeted silver nanoparticles for rheumatoid arthritis therapy *via* macrophage apoptosis and re-polarization. *Biomaterials* (2020) 264:120390. doi: 10.1016/j.biomaterials.2020.120390

96. Pedro RN, Thekke-Adiyat T, Goel R, Shenoi M, Slaton J, Schmechel S, et al. Use of tumor necrosis factor-alpha-coated gold nanoparticles to enhance radiofrequency ablation in a translational model of renal tumors. *Urology* (2010) 76:494–8. doi: 10.1016/j.urology.2010.01.085

97. Powell AC, Paciotti GF, Libutti SK. Colloidal gold: a novel nanoparticle for targeted cancer therapeutics. *Methods Mol Biol* (2010) 624:375–84. doi: 10.1007/978-1-60761-609-2_25

98. Perry JL, Tian S, Sengottuvel N, Harrison EB, Gorentla BK, Kapadia CH, et al. Pulmonary delivery of nanoparticle-bound toll-like receptor 9 agonist for the treatment of metastatic lung cancer. *ACS Nano* (2020) 14:7200–15. doi: 10.1021/acsnano.0c02207

99. Lecio G, Ribeiro FV, Pimentel SP, Reis AA, Da Silva RVC, Nociti-Jr F, et al. Novel 20% doxycycline-loaded PLGA nanospheres as adjunctive therapy in chronic periodontitis in type-2 diabetics: randomized clinical, immune and microbiological trial. *Clin Oral Investig* (2020) 24:1269–79. doi: 10.1007/s00784-019-03005-9

100. Castro F, Pinto ML, Almeida R, Pereira F, Silva AM, Pereira CL, et al. Chitosan/poly(γ-glutamic acid) nanoparticles incorporating IFN-γ for immune response modulation in the context of colorectal cancer. *Biomater Sci* (2019) 7:3386–403. doi: 10.1039/c9bm00393b

101. Hong DS, Kang YK, Borad M, Sachdev J, Ejadi S, Lim HY, et al. Phase 1 study of MRX34, a liposomal miR-34a mimic, in patients with advanced solid tumours. *Br J Cancer* (2020) 122:1630–7. doi: 10.1038/s41416-020-0802-1

102. Urits I, Swanson D, Swett MC, Patel A, Berardino K, Amgalan A, et al. A review of patisiran (ONPATTRO®) for the treatment of polyneuropathy in people with hereditary transthyretin amyloidosis. *Neurol Ther* (2020) 9:301–15. doi: 10.1007/s40120-020-00208-1

103. Hong E, Halman JR, Shah AB, Khisamutdinov EF, Dobrovolskaia MA, Afonin KA. Structure and composition define immunorecognition of nucleic acid nanoparticles. *Nano Lett* (2018) 18:4309–21. doi: 10.1021/acs.nanolett.8b01283

104. Hong E, Halman JR, Shah A, Cedrone E, Truong N, Afonin KA, et al. Toll-like receptor-mediated recognition of nucleic acid nanoparticles (NANPs) in human primary blood cells. *Molecules* (2019) 24:1–13. doi: 10.3390/molecules24061094

105. Drake MG, Kaufman EH, Fryer AD, Jacoby DB. The therapeutic potential of toll-like receptor 7 stimulation in asthma. *Inflammation Allergy Drug Targets* (2012) 11:484–91. doi: 10.2174/187152812803589967

106. Bernard NJ. TLR7 drives human lupus. *Nat Immunol* (2022) 23:817–7. doi: 10.1038/s41590-022-01235-w

107. Gilliet M, Conrad C, Geiges M, Cozzio A, Thürlimann W, Burg G, et al. Psoriasis triggered by toll-like receptor 7 agonist imiquimod in the presence of dermal plasmacytoid dendritic cell precursors. *Arch Dermatol* (2004) 140:1490–5. doi: 10.1001/archderm.140.12.1490

108. Avila YI, Chandler M, Cedrone E, Newton HS, Richardson M, Xu J, et al. Induction of cytokines by nucleic acid nanoparticles (NANPs) depends on the type of delivery carrier. *Molecules* (2021) 26:1–18. doi: 10.3390/molecules26030652

109. Dobrovolskaia MA, Mcneil SE. Immunological and hematological toxicities challenging clinical translation of nucleic acid-based therapeutics. *Expert Opin Biol Ther* (2015) 15:1023–48. doi: 10.1517/14712598.2015.1014794

110. Dobrovolskaia MA, Mcneil SE. Strategy for selecting nanotechnology carriers to overcome immunological and hematological toxicities challenging clinical translation of nucleic acid-based therapeutics. *Expert Opin Drug Delivery* (2015) 12:1163–75. doi: 10.1517/17425247.2015.1042857

111. Dobrovolskaia MA. Nucleic acid nanoparticles at a crossroads of vaccines and immunotherapies. *Molecules* (2019) 24:1–20. doi: 10.3390/molecules24244620

112. Afonin KA, Dobrovolskaia MA, Church G, Bathe M. Opportunities, barriers, and a strategy for overcoming translational challenges to therapeutic nucleic acid nanotechnology. *ACS Nano* (2020) 14:9221–7. doi: 10.1021/acsnano.0c04753

113. Weng Y, Huang Q, Li C, Yang Y, Wang X, Yu J, et al. Improved nucleic acid therapy with advanced nanoscale biotechnology. *Mol Ther Nucleic Acids* (2020) 19:581–601. doi: 10.1016/j.omtn.2019.12.004

114. Bila D, Radwan Y, Dobrovolskaia MA, Panigaj M, Afonin KA. The recognition of and reactions to nucleic acid nanoparticles by human immune cells. *Molecules* (2021) 26. doi: 10.3390/molecules26144231

115. Afonin KA, Dobrovolskaia MA, Ke W, Grodzinski P, Bathe M. Critical review of nucleic acid nanotechnology to identify gaps and inform a strategy for accelerated clinical translation. *Adv Drug Delivery Rev* (2022) 181:114081. doi: 10.1016/j.addr.2021.114081

116. Fountain JH, Lappin SL. Physiology, platelet. In: *StatPearls*. Treasure Island (FL: StatPearls Publishing Copyright © 2020, StatPearls Publishing LLC (2020).

117. Beutier H, Hechler B, Godon O, Wang Y, Gillis CM, De Chaisemartin L, et al. Platelets expressing IgG receptor FcγRIIA/CD32A determine the severity of experimental anaphylaxis. *Sci Immunol* (2018) 3:1–11. doi: 10.1126/sciimmunol.aan5997

118. Lo ST, Stern S, Clogston JD, Zheng J, Adiseshaiah PP, Dobrovolskaia M, et al. Biological assessment of triazine dendrimer: toxicological profiles, solution behavior, biodistribution, drug release and efficacy in a PEGylated, paclitaxel construct. *Mol Pharm* (2010) 7:993–1006. doi: 10.1021/mp100104x

119. Dobrovolskaia MA, Patri AK, Simak J, Hall JB, Semberova J, De Paoli Lacerda SH, et al. Nanoparticle size and surface charge determine effects of PAMAM dendrimers on human platelets *in vitro*. *Mol Pharm* (2012) 9:382–93. doi: 10.1021/mp200463e

120. Adiseshaiah P, Dellinger A, Macfarland D, Stern S, Dobrovolskaia M, Ileva L, et al. A novel gadolinium-based trimetasphere metallofullerene for application as a magnetic resonance imaging contrast agent. *Invest Radiol* (2013) 48:745–54. doi: 10.1097/RLI.0b013e318294de5d

121. Enciso AE, Neun B, Rodriguez J, Ranjan AP, Dobrovolskaia MA, Simanek EE. Nanoparticle effects on human platelets *in vitro*: A comparison between PAMAM and triazine dendrimers. *Molecules* (2016) 21:428. doi: 10.3390/molecules21040428

122. Zheng J, Clogston JD, Patri AK, Dobrovolskaia MA, Mcneil SE. Sterilization of silver nanoparticles using standard gamma irradiation procedure affects particle integrity and biocompatibility. *J Nanomed Nanotechnol* (2011) 2011:001. doi: 10.4172/2157-7439.S5-001

123. Oslakovic C, Cedervall T, Linse S, Dahlbäck B. Polystyrene nanoparticles affecting blood coagulation. *Nanomedicine* (2012) 8:981–6. doi: 10.1016/j.nano.2011.12.001

124. Zbinden G, Wunderli-Allenspach H, Grimm L. Assessment of thrombogenic potential of liposomes. *Toxicology* (1989) 54:273–80. doi: 10.1016/0300-483X(89)90063-2

125. Dipasco PJ, Misra S, Koniaris LG. Thrombophilic state in cancer, part I: biology, incidence, and risk factors. *J Surg Oncol* (2011) 104:316–22. doi: 10.1002/jso.21925

126. Mulloy B, Hogwood J, Gray E, Lever R, Page CP. Pharmacology of heparin and related drugs. *Pharmacol Rev* (2016) 68:76–141. doi: 10.1124/pr.115.011247

127. Shukla D, Spear PG. Herpesviruses and heparan sulfate: an intimate relationship in aid of viral entry. *J Clin Invest* (2001) 108:503–10. doi: 10.1172/JCI200113799

128. Mycroft-West CJ, Su D, Pagani I, Rudd TR, Elli S, Gandhi NS, et al. Heparin inhibits cellular invasion by SARS-CoV-2: Structural dependence of the interaction of the spike S1 receptor-binding domain with heparin. *Thromb Haemost* (2020) 120:1700–15. doi: 10.1055/s-0040-1721319

129. Iba T, Hashiguchi N, Nagaoka I, Tabe Y, Kadota K, Sato K. Heparins attenuated histone-mediated cytotoxicity *in vitro* and improved the survival in a rat model of histone-induced organ dysfunction. *Intensive Care Med Exp* (2015) 3:36. doi: 10.1186/s40635-015-0072-z

130. Zhu C, Liang Y, Li X, Chen N, Ma X. Unfractionated heparin attenuates histone-mediated cytotoxicity *in vitro* and prevents intestinal microcirculatory dysfunction in histone-infused rats. *J Trauma Acute Care Surg* (2019) 87:614–22. doi: 10.1097/TA.0000000000002387

131. Sauna ZE, Lagassé D, Pedras-Vasconcelos J, Golding B, Rosenberg AS. Evaluating and mitigating the immunogenicity of therapeutic proteins. *Trends Biotechnol* (2018) 36:1068–84. doi: 10.1016/j.tibtech.2018.05.008

132. US Food and Drug Administration. *"Guidance for industry immunogenicity assessment for therapeutic protein products"*. Silver Spring, Maryland, USA: US FDA (2014).

133. Andreev SM, Babakhin AA, Petrukhina AO, Romanova VS, Parnes ZN, Petrov RV. Immunogenic and allergenic properties of fulleren conjugates with aminoacids and proteins. *Doklady Biochem* (2000) 370(1–6):4–7.

134. Chen BX, Wilson SR, Das M, Coughlin DJ, Erlanger BF. Antigenicity of fullerenes: antibodies specific for fullerenes and their characteristics. *Proc Natl Acad Sci U.S.A.* (1998) 95:10809–13. doi: 10.1073/pnas.95.18.10809

135. Braden BC, Goldbaum FA, Chen BX, Kirschner AN, Wilson SR, Erlanger BF. X-Ray crystal structure of an anti-buckminsterfullerene antibody fab fragment: biomolecular recognition of C(60). *Proc Natl Acad Sci U.S.A.* (2000) 97:12193–7. doi: 10.1073/pnas.210396197

136. Hendrickson O, Fedyunina N, Zherdev A, Solopova O, Sveshnikov P, Dzantiev B. Production of monoclonal antibodies against fullerene C60 and development of a fullerene enzyme immunoassay. *Analyst* (2012) 137:98–105. doi: 10.1039/C1AN15745K

137. Erlanger BF, Chen BX, Zhu M, Brus L. Binding of an anti-fullerene IgG monoclonal antibody to single wall carbon nanotubes. *Nano Lett* (2001) 1:465–7. doi: 10.1021/nl015570r

138. Roberts JC, Bhalgat MK, Zera RT. Preliminary biological evaluation of polyamidoamine (PAMAM) starburst dendrimers. *J BioMed Mater Res* (1996) 30:53–65. doi: 10.1002/(SICI)1097-4636(199601)30:1<53::AID-JBM8>3.0.CO;2-Q

139. Lee SC, Parthasarathy R, Duffin TD, Botwin K, Zobel J, Beck T, et al. Recognition properties of antibodies to PAMAM dendrimers and their use in immune detection of dendrimers. *Biomed Microdevices* (2001) 3:53–9. doi: 10.1023/A:1011429404950

140. Schuster BG, Neidig M, Alving BM, Alving CR. Production of antibodies against phosphocholine, phosphatidylcholine, sphingomyelin, and lipid a by injection of liposomes containing lipid A. *J Immunol* (1979) 122(3):900–5.

141. Alving CR. Antibodies to liposomes, phospholipids and phosphate esters. *Chem Phys Lipids* (1986) 40:303–14. doi: 10.1016/0009-3084(86)90075-7

142. Alving CR, Swartz GMJr., Wassef NM, Ribas JL, Herderick EE, Virmani R, et al. Immunization with cholesterol-rich liposomes induces anti-cholesterol antibodies and reduces diet-induced hypercholesterolemia and plaque formation. *J Lab Clin Med* (1996) 127:40–9. doi: 10.1016/S0022-2143(96)90164-X

143. Alving CR. Natural antibodies against phospholipids and liposomes in humans. *Biochem Soc Trans* (1984) 12:342–4. doi: 10.1042/bst0120342

144. Richards RL, Aronson J, Schoenbechler M, Diggs CL, Alving CR. Antibodies reactive with liposomal phospholipids are produced during experimental trypanosoma rhodesiense infections in rabbits. *J Immunol* (1983) 130(3):1390–4.

145. Banerji B, Kenny JJ, Scher I, Alving CR. Antibodies against liposomes in normal and immune-defective mice. *J Immunol* (1982) 128(4):1603–7.

146. Chen BM, Su YC, Chang CJ, Burnouf PA, Chuang KH, Chen CH, et al. Measurement of pre-existing IgG and IgM antibodies against polyethylene glycol in healthy individuals. *Anal Chem* (2016) 88:10661–6. doi: 10.1021/acs.analchem.6b03109

147. Stone CAJr., Liu Y, Relling MV, Krantz MS, Pratt AL, Abreo A, et al. Immediate hypersensitivity to polyethylene glycols and polysorbates: More common than we have recognized. *J Allergy Clin Immunol Pract* (2019) 7:1533–1540.e1538. doi: 10.1016/j.jaip.2018.12.003

148. Zhou ZH, Stone CAJr., Jakubovic B, Phillips EJ, Sussman G, Park J, et al. Anti-PEG IgE in anaphylaxis associated with polyethylene glycol. *J Allergy Clin Immunol Pract* (2021) 9:1731–1733.e1733. doi: 10.1016/j.jaip.2020.11.011

149. Henry CE, Wang YY, Yang Q, Hoang T, Chattopadhyay S, Hoen T, et al. Anti-PEG antibodies alter the mobility and biodistribution of densely PEGylated nanoparticles in mucus. *Acta Biomater* (2016) 43:61–70. doi: 10.1016/j.actbio.2016.07.019

150. Hsieh YC, Wang HE, Lin WW, Roffler SR, Cheng TC, Su YC, et al. Pre-existing anti-polyethylene glycol antibody reduces the therapeutic efficacy and pharmacokinetics of PEGylated liposomes. *Theranostics* (2018) 8:3164–75. doi: 10.7150/thno.22164

151. Chang TC, Chen BM, Wu JY, Cheng TL, Roffler S. Impact of anti-PEG antibody affinity on accelerated blood clearance of pegylated epoetin beta in mice. *BioMed Pharmacother* (2022) 146:112502. doi: 10.1016/j.biopha.2021.112502

152. Mccallen J, Prybylski J, Yang Q, Lai SK. Cross-reactivity of select PEG-binding antibodies to other polymers containing a c-C-O backbone. *ACS Biomater Sci Eng* (2017) 3:1605–15. doi: 10.1021/acsbiomaterials.7b00147

153. Chen BM, Cheng TL, Roffler SR. Polyethylene glycol immunogenicity: Theoretical, clinical, and practical aspects of anti-polyethylene glycol antibodies. *ACS Nano* (2021) 15:14022–48. doi: 10.1021/acsnano.1c05922

154. Shi D, Beasock D, Fessler A, Szebeni J, Ljubimova JY, Afonin KA, et al. To PEGylate or not to PEGylate: Immunological properties of nanomedicine's most popular component, polyethylene glycol and its alternatives. *Adv Drug Delivery Rev* (2022) 180:114079. doi: 10.1016/j.addr.2021.114079

155. Dézsi L, Mészáros T, Kozma G, M HV, Oláh CZ, Szabó M, et al. A naturally hypersensitive porcine model may help understand the mechanism of COVID-19 mRNA vaccine-induced rare (pseudo) allergic reactions: complement activation as a possible contributing factor. *Geroscience* (2022) 44:597–618. doi: 10.1007/s11357-021-00495-y

156. Ju Y, Lee WS, Kelly HG, Pilkington EH, Wragg KM, Subbarao K, et al. Anti-PEG antibodies boosted in humans by SARS-CoV-2 lipid nanoparticle mRNA vaccine. *MedRxiv* (2021) 27:acsnano.2c04543. doi: 10.1021/acsnano.2c04543

157. Lee CC, Su YC, Ko TP, Lin LL, Yang CY, Chang SS, et al. Structural basis of polyethylene glycol recognition by antibody. *J BioMed Sci* (2020) 27:12. doi: 10.1186/s12929-019-0589-7

158. Chang TC, Chen BM, Lin WW, Yu PH, Chiu YW, Chen YT, et al. Both IgM and IgG antibodies against polyethylene glycol can alter the biological activity of methoxy polyethylene glycol-epoetin beta in mice. *Pharmaceutics* (2019) 12:1–16. doi: 10.3390/pharmaceutics12010015

159. Murphy M, Pattabiraman G, Manavalan TT, Medvedev AE. Deficiency in IRAK4 activity attenuates manifestations of murine lupus. *Eur J Immunol* (2017) 47:880–91. doi: 10.1002/eji.201646641

160. Pattabiraman G, Murphy M, Agliano F, Karlinsey K, Medvedev AE. IRAK4 activity controls immune responses to intracellular bacteria listeria monocytogenes and mycobacterium smegmatis. *J Leukoc Biol* (2018) 104:811–20. doi: 10.1002/JLB.2A1117-449R

161. Medvedev AE, Thomas K, Awomoyi A, Kuhns DB, Gallin JI, Li X, et al. Cutting edge: expression of IL-1 receptor-associated kinase-4 (IRAK-4) proteins with mutations identified in a patient with recurrent bacterial infections alters normal IRAK-4 interaction with components of the IL-1 receptor complex. *J Immunol* (2005) 174:6587–91. doi: 10.4049/jimmunol.174.11.6587

162. Vogel SN, Awomoyi AA, Rallabhandi P, Medvedev AE. Mutations in TLR4 signaling that lead to increased susceptibility to infection in humans: an overview. *J Endotoxin Res* (2005) 11:333–9. doi: 10.1177/09680519050110060801

163. Descotes J. Importance of immunotoxicity in safety assessment: a medical toxicologist's perspective. *Toxicol Lett* (2004) 149:103–8. doi: 10.1016/j.toxlet.2003.12.024

164. Wiseman AC. Immunosuppressive medications. *Clin J Am Soc Nephrol* (2016) 11:332–43. doi: 10.2215/CJN.08570814

165. Anderson SE, Shane HL. Investigative immunotoxicology. *Methods Mol Biol* (2018) 1803:27–46. doi: 10.1007/978-1-4939-8549-4_3

166. Brogan PA, Dillon MJ. The use of immunosuppressive and cytotoxic drugs in non-malignant disease. *Arch Dis Child* (2000) 83:259–64. doi: 10.1136/adc.83.3.259

167. Kubeček O, Paterová P, Novosadová M. Risk factors for infections, antibiotic therapy, and its impact on cancer therapy outcomes for patients with solid tumors. *Life (Basel)* (2021) 11:1–25. doi: 10.3390/life11121387

168. Kim JH, Perfect JR. Infection and cyclosporine. *Rev Infect Dis* (1989) 11:677–90. doi: 10.1093/clinids/11.5.677

169. Taplitz RA, Kennedy EB, Bow EJ, Crews J, Gleason C, Hawley DK, et al. Antimicrobial prophylaxis for adult patients with cancer-related immunosuppression: ASCO and IDSA clinical practice guideline update. *J Clin Oncol* (2018) 36:3043–54. doi: 10.1200/JCO.18.00374

170. Mackall CL, Fleisher TA, Brown MR, Magrath IT, Shad AT, Horowitz ME, et al. Lymphocyte depletion during treatment with intensive chemotherapy for cancer. *Blood* (1994) 84:2221–8. doi: 10.1182/blood.V84.7.2221.2221

171. Gibaud S, Andreux JP, Weingarten C, Renard M, Couvreur P. Increased bone marrow toxicity of doxorubicin bound to nanoparticles. *Eur J Cancer* (1994) 30a:820–6. doi: 10.1016/0959-8049(94)90299-2

172. Paik SY, Kim JS, Shin SJ, Ko S. Characterization, quantification, and determination of the toxicity of iron oxide nanoparticles to the bone marrow cells. *Int J Mol Sci* (2015) 16:22243–57. doi: 10.3390/ijms160922243

173. Yuan Q, Han J, Cong W, Ge Y, Ma D, Dai Z, et al. Docetaxel-loaded solid lipid nanoparticles suppress breast cancer cells growth with reduced myelosuppression toxicity. *Int J Nanomed* (2014) 9:4829–46. doi: 10.2147/IJN.S70919

174. Alghriany A, Omar H.E.L.D.M., Mahmoud AM, Atia MM. Assessment of the toxicity of aluminum oxide and its nanoparticles in the bone marrow and liver of Male mice: Ameliorative efficacy of curcumin nanoparticles. *ACS Omega* (2022) 7:13841–52. doi: 10.1021/acsomega.2c00195

175. Blum JL, Savin MA, Edelman G, Pippen JE, Robert NJ, Geister BV, et al. Phase II study of weekly albumin-bound paclitaxel for patients with metastatic breast cancer heavily pretreated with taxanes. *Clin Breast Cancer* (2007) 7:850–6. doi: 10.3816/CBC.2007.n.049

176. Stinchcombe TE, Socinski MA, Walko CM, O'neil BH, Collichio FA, Ivanova A, et al. Phase I and pharmacokinetic trial of carboplatin and albumin-bound paclitaxel, ABI-007 (Abraxane) on three treatment schedules in patients with solid tumors. *Cancer Chemother Pharmacol* (2007) 60:759–66. doi: 10.1007/s00280-007-0423-x

177. Ishihara T, Kubota T, Choi T, Higaki M. Treatment of experimental arthritis with stealth-type polymeric nanoparticles encapsulating betamethasone phosphate. *J Pharmacol Exp Ther* (2009) 329:412–7. doi: 10.1124/jpet.108.150276

178. Mitchell LA, Lauer FT, Burchiel SW, Mcdonald JD. Mechanisms for how inhaled multiwalled carbon nanotubes suppress systemic immune function in mice. *Nat Nanotechnol* (2009) 4:451–6. doi: 10.1038/nnano.2009.151

179. Achebe M, Deloughery TG. Clinical data for intravenous iron - debunking the hype around hypersensitivity. *Transfusion* (2020) 60:1154–9. doi: 10.1111/trf.15837

180. Blumenstein I, Shanbhag S, Langguth P, Kalra PA, Zoller H, Lim W. Newer formulations of intravenous iron: a review of their chemistry and key safety aspects - hypersensitivity, hypophosphatemia, and cardiovascular safety. *Expert Opin Drug Saf* (2021) 20:757–69. doi: 10.1080/14740338.2021.1912010

181. Trumbo H, Kaluza K, Numan S, Goodnough LT. Frequency and associated costs of anaphylaxis- and hypersensitivity-related adverse events for intravenous iron products in the USA: An analysis using the US food and drug administration adverse event reporting system. *Drug Saf* (2021) 44:107–19. doi: 10.1007/s40264-020-01022-2

182. Shah A, Mankus CI, Vermilya AM, Soheilian F, Clogston JD, Dobrovolskaia MA. Feraheme® suppresses immune function of human T lymphocytes through mitochondrial damage and mitoROS production. *Toxicol Appl Pharmacol* (2018) 350:52–63. doi: 10.1016/j.taap.2018.04.028

183. Shah A, Cedrone E, Sanders C, Butcher D, Defrancesco A, Degrange C, et al. The potential utility of iron oxide nanoparticles for the treatment of skin inflammation in a mouse model of psoriasis. *Precis Nanomed* (2019) 2:249–52. doi: 10.33218/prnano2(1).181218.1

184. Xue Y, Xu Y, Liu X, Sun Z, Pan Y, Lu X, et al. Ferumoxytol attenuates the function of MDSCs to ameliorate LPS-induced immunosuppression in sepsis. *Nanoscale Res Lett* (2019) 14:379. doi: 10.1186/s11671-019-3209-2

185. Holley CK, Dobrovolskaia MA. Innate immunity modulating impurities and the immunotoxicity of nanobiotechnology-based drug products. *Molecules* (2021) 26:1–23. doi: 10.3390/molecules26237308

186. Dobrovolskaia MA, Neun BW, Clogston JD, Ding H, Ljubimova J, Mcneil SE. Ambiguities in applying traditional limulus amebocyte lysate tests to quantify endotoxin in nanoparticle formulations. *Nanomed (Lond)* (2010) 5:555–62. doi: 10.2217/nnm.10.29

187. Neun BW, Dobrovolskaia MA. Detection and quantitative evaluation of endotoxin contamination in nanoparticle formulations by LAL-based assays. *Methods Mol Biol* (2011) 697:121–30. doi: 10.1007/978-1-60327-198-1_12

188. Dobrovolskaia MA, Neun BW, Clogston JD, Grossman JH, Mcneil SE. Choice of method for endotoxin detection depends on nanoformulation. *Nanomed (Lond)* (2014) 9:1847–56. doi: 10.2217/nnm.13.157

189. Neun BW, Dobrovolskaia MA. Detection of endotoxin in nanoformulations using limulus amoebocyte lysate (LAL) assays. *J Vis Exp* (2019) (143). doi: 10.3791/58830

190. Neun BW, Cedrone E, Potter TM, Crist RM, Dobrovolskaia MA. Detection of beta-glucan contamination in nanotechnology-based formulations. *Molecules* (2020) 25:1–16. doi: 10.3390/molecules25153367

191. Smulders S, Kaiser JP, Zuin S, Van Landuyt KL, Golanski L, Vanoirbeek J, et al. Contamination of nanoparticles by endotoxin: evaluation of different test methods. *Part Fibre Toxicol* (2012) 9:41. doi: 10.1186/1743-8977-9-41

192. Unger RE, Peters K, Sartoris A, Freese C, Kirkpatrick CJ. Human endothelial cell-based assay for endotoxin as sensitive as the conventional limulus amebocyte lysate assay. *Biomaterials* (2014) 35:3180–7. doi: 10.1016/j.biomaterials.2013.12.059

193. Li Y, Italiani P, Casals E, Tran N, Puntes VF, Boraschi D. Optimising the use of commercial LAL assays for the analysis of endotoxin contamination in metal colloids and metal oxide nanoparticles. *Nanotoxicology* (2015) 9:462–73. doi: 10.3109/17435390.2014.948090

194. Li Y, Boraschi D. Endotoxin contamination: a key element in the interpretation of nanosafety studies. *Nanomed (Lond)* (2016) 11:269–87. doi: 10.2217/nnm.15.196

195. Giannakou C, Aimonen K, Bloois LV, Catalán J, Geertsma RE, Gremmer ER, et al. Sensitive method for endotoxin determination in nanomedicinal product samples. *Nanomed (Lond)* (2019) 14:1231–46. doi: 10.2217/nnm-2018-0339

196. Pang G, Liu Y, Wang Y, Wang Y, Wang F, Zhao J, et al. Endotoxin contamination in ovalbumin as viewed from a nano-immunotherapy perspective. *Wiley Interdiscip Rev Nanomed Nanobiotechnol* (2022) 14:e1747. doi: 10.1002/wnan.1747

197. Wildt B, Malinauskas RA, Brown RP. "The effects of engineered nanomaterials on erythrocytes,". In: MA Dobrovolskaia and SE Mcneil, editors. *Immunological properties of engineered nanomaterials*. Singapore: World Scientific Publishing (2013). p. 173–206.

198. Neun BW, Ilinskaya AN, Dobrovolskaia MA. Updated method for *In vitro* analysis of nanoparticle hemolytic properties. *Methods Mol Biol* (2018) 1682:91–102. doi: 10.1007/978-1-4939-7352-1_9

199. Dobrovolskaia MA, Mcneil SE. Understanding the correlation between *in vitro* and *in vivo* immunotoxicity tests for nanomedicines. *J Control Release* (2013) 172:456–66. doi: 10.1016/j.jconrel.2013.05.025

200. Mészáros T, Kozma GT, Shimizu T, Miyahara K, Turjeman K, Ishida T, et al. Involvement of complement activation in the pulmonary vasoactivity of polystyrene nanoparticles in pigs: unique surface properties underlying alternative pathway activation and instant opsonization. *Int J Nanomed* (2018) 13:6345–57. doi: 10.2147/IJN.S161369

201. Neun BW, Ilinskaya AN, Dobrovolskaia MA. Analysis of complement activation by nanoparticles. *Methods Mol Biol* (2018) 1682:149–60. doi: 10.1007/978-1-4939-7352-1_13

202. Szebeni J, Muggia FM, Alving CR. Complement activation by cremophor EL as a possible contributor to hypersensitivity to paclitaxel: an *in vitro* study. *J Natl Cancer Inst* (1998) 90:300–6. doi: 10.1093/jnci/90.4.300

203. Chanan-Khan A, Szebeni J, Savay S, Liebes L, Rafique NM, Alving CR, et al. Complement activation following first exposure to pegylated liposomal doxorubicin (Doxil): possible role in hypersensitivity reactions. *Ann Oncol* (2003) 14:1430–7. doi: 10.1093/annonc/mdg374

204. Merkel OM, Urbanics R, Bedocs P, Rozsnyay Z, Rosivall L, Toth M, et al. *In vitro* and *in vivo* complement activation and related anaphylactic effects associated with polyethylenimine and polyethylenimine-graft-poly(ethylene glycol) block copolymers. *Biomaterials* (2011) 32:4936–42. doi: 10.1016/j.biomaterials.2011.03.035

205. Fülöp T, Nemes R, Mészáros T, Urbanics R, Kok RJ, Jackman JA, et al. Complement activation *in vitro* and reactogenicity of low-molecular weight dextran-coated SPIONs in the pig CARPA model: Correlation with physicochemical features and clinical information. *J Control Release* (2018) 270:268–74. doi: 10.1016/j.jconrel.2017.11.043

206. Neun BW, Szenasi G, Szebeni J, Dobrovolskaia MA. Plasma samples from mouse strains and humans demonstrate different *in vitro* susceptibilities to complement activation. *Precis Nanomed* (2018) 1:208–17. doi: 10.33218/prnano1(3).181029.2

207. Watanabe H, Numata K, Ito T, Takagi K, Matsukawa A. Innate immune response in Th1- and Th2-dominant mouse strains. *Shock* (2004) 22:460–6. doi: 10.1097/01.shk.0000142249.08135.e9

208. Kopp R, Bernsberg R, Kashefi A, Mottaghy K, Rossaint R, Kuhlen R. Effect of hirudin versus heparin on hemocompatibility of blood contacting biomaterials: an *in vitro* study. *Int J Artif Organs* (2005) 28:1272–7. doi: 10.1177/039139880502801211

209. Bexborn F, Engberg AE, Sandholm K, Mollnes TE, Hong J, Nilsson Ekdahl K. Hirudin versus heparin for use in whole blood *in vitro* biocompatibility models. *J BioMed Mater Res A* (2009) 89:951–9. doi: 10.1002/jbm.a.32034

210. Cedrone E, Neun BW, Rodriguez J, Vermilya A, Clogston JD, Mcneil SE, et al. Anticoagulants influence the performance of *In vitro* assays intended for characterization of nanotechnology-based formulations. *Molecules* (2017) 23:1–17. doi: 10.3390/molecules23010012

211. Potter TM, Rodriguez JC, Neun BW, Ilinskaya AN, Cedrone E, Dobrovolskaia MA. *In vitro* assessment of nanoparticle effects on blood coagulation. *Methods Mol Biol* (2018) 1682:103–24. doi: 10.1007/978-1-4939-7352-1_10

212. Simak J, De Paoli S. The effects of nanomaterials on blood coagulation in hemostasis and thrombosis. *Wiley Interdiscip Rev Nanomed Nanobiotechnol* (2017) 9:1–16. doi: 10.1002/wnan.1448

213. Abbas A, Lichtman A, Pillai S. *Cellular and molecular immunology. 9th Edition*. (Philadelphia, Pennsylvania, USA: Elsevier) (2017).

214. Opdal SH. Cytokines, infection, and immunity. In: JR Duncan and RW Byard, editors. *SIDS Sudden infant and early childhood death: The past, the present and the future*. Adelaide (AU: University of Adelaide Press (2018).

215. Quah BJ, Parish CR. The use of carboxyfluorescein diacetate succinimidyl ester (CFSE) to monitor lymphocyte proliferation. *J Vis Exp* (2010) (44):2259. doi: 10.3791/2259

216. Potter TM, Neun BW, Dobrovolskaia MA. Methods for analysis of nanoparticle immunosuppressive properties *In vitro* and *In vivo*. *Methods Mol Biol* (2018) 1682:161–72. doi: 10.1007/978-1-4939-7352-1_14

217. Collinge M, Cole SH, Schneider PA, Donovan CB, Kamperschroer C, Kawabata TT. Human lymphocyte activation assay: an *in vitro* method for predictive immunotoxicity testing. *J Immunotoxicol* (2010) 7:357–66. doi: 10.3109/1547691X.2010.523881

218. Collinge M, Schneider P, Li D, Parish S, Dumont C, Freebern W, et al. Cross-company evaluation of the human lymphocyte activation assay. *J Immunotoxicol* (2020) 17:51–8. doi: 10.1080/1547691X.2020.1725694

219. Neun BW, Cedrone E, Dobrovolskaia MA. *NCL method ITA-3: Mouse granulocyte-macrophage colony-forming unit assay* (2020) (Accessed June 2022).

220. Pessina A, Albella B, Bayo M, Bueren J, Brantom P, Casati S, et al. *In vitro* tests for haematotoxicity: prediction of drug-induced myelosuppression by the CFU-GM assay. *Altern Lab Anim* (2002) 30 Suppl 2:75–9. doi: 10.1177/026119290203002S11

221. Pessina A, Albella B, Bayo M, Bueren J, Brantom P, Casati S, et al. Application of the CFU-GM assay to predict acute drug-induced neutropenia: an international blind trial to validate a prediction model for the maximum tolerated dose (MTD) of myelosuppressive xenobiotics. *Toxicol Sci* (2003) 75:355–67. doi: 10.1093/toxsci/kfg188

222. Skoczen SL, Potter TM, Dobrovolskaia MA. *In vitro* analysis of nanoparticle uptake by macrophages using chemiluminescence. *Methods Mol Biol* (2011) 697:255–61. doi: 10.1007/978-1-60327-198-1_27

223. Potter TM, Skoczen SL, Rodriguez JC, Neun BW, Ilinskaya AN, Cedrone E, et al. *In vitro* analysis of nanoparticle effects on the zymosan uptake by phagocytic cells. *Methods Mol Biol* (2018) 1682:125–33. doi: 10.1007/978-1-4939-7352-1_11

224. Potter TM, Cedrone E, Neun BW, Dobrovolskaia MA. NCL method ITA-11. In: *Measurement of nanoparticle effects on cytotoxic activity of NK cells by label-free RT-CES system*. (Frederick, Maryland, USA: Nanotechnology Characterization Lab., National Cancer Institute) (2020). Available at: https://www.cancer.gov/nano/research/ncl/protocols-capabilities/ncl-method-ita-11.pdf.

225. Shabrish S, Gupta M, Madkaikar M. A modified NK cell degranulation assay applicable for routine evaluation of NK cell function. *J Immunol Res* (2016) 2016:3769590. doi: 10.1155/2016/3769590

226. Kim J, Phan MT, Kweon S, Yu H, Park J, Kim KH, et al. A flow cytometry-based whole blood natural killer cell cytotoxicity assay using overnight cytokine activation. *Front Immunol* (2020) 11:1851. doi: 10.3389/fimmu.2020.01851

227. Hoffmann S, Luderitz-Puchel U, Montag T, Hartung T. Optimisation of pyrogen testing in parenterals according to different pharmacopoeias by probabilistic modelling. *J Endotoxin Res* (2005) 11:25–31. doi: 10.1177/09680519050110010701

228. Hoffmann S, Peterbauer A, Schindler S, Fennrich S, Poole S, Mistry Y, et al. International validation of novel pyrogen tests based on human monocytoid cells. *J Immunol Methods* (2005) 298:161–73. doi: 10.1016/j.jim.2005.01.010

229. Du Y, Li XJ, Tan DJ. Comparison of temperature rise interpretations in the rabbit pyrogen test among Chinese, Japanese, European, and united states pharmacopeias and 2-2-2 theoretical models proposed by s. hoffmann. *Innate Immun* (2011) 17:486–95. doi: 10.1177/1753425910384754

230. Cooper JF, Pearson SM. Detection of endotoxin in biological products by the limulus test. *Dev Biol Stand* (1977) 34:7–13.

231. Ronneberger HJ. Comparison of the pyrogen tests in rabbits and with limulus lysate. *Dev Biol Stand* (1977) 34:27–36.

232. Schindler S, Asmus S, Von Aulock S, Wendel A, Hartung T, Fennrich S. Cryopreservation of human whole blood for pyrogenicity testing. *J Immunol Methods* (2004) 294:89–100. doi: 10.1016/j.jim.2004.08.019

233. Schindler S, Von Aulock S, Daneshian M, Hartung T. Development, validation and applications of the monocyte activation test for pyrogens based on human whole blood. *Altex* (2009) 26:265–77. doi: 10.14573/altex.2009.4.265

234. Hasiwa N, Daneshian M, Bruegger P, Fennrich S, Hochadel A, Hoffmann S, et al. Evidence for the detection of non-endotoxin pyrogens by the whole blood monocyte activation test. *Altex* (2013) 30:169–208. doi: 10.14573/altex.2013.2.169

235. Hartung T. The human whole blood pyrogen test - lessons learned in twenty years. *Altex* (2015) 32:79–100. doi: 10.14573/altex.1503241

236. Da Silva CC, Presgrave OA, Hartung T, De Moraes AM, Delgado IF. Applicability of the monocyte activation test (MAT) for hyperimmune sera in the routine of the quality control laboratory: Comparison with the rabbit pyrogen test (RPT). *Toxicol In Vitro* (2016) 32:70–5. doi: 10.1016/j.tiv.2015.12.004

237. Brown J, Clippinger AJ, Fritz Briglia C, Casey W, Coleman K, Fritsch A, et al. Using the monocyte activation test as a stand-alone release test for medical devices. *Altex* (2021) 38:151–6. doi: 10.14573/altex.2012021

238. Hartung T. Pyrogen testing revisited on occasion of the 25th anniversary of the whole blood monocyte activation test. *Altex* (2021) 38:3–19. doi: 10.14573/altex.2101051

239. Dinarello CA, O'connor JV, Lopreste G, Swift RL. Human leukocytic pyrogen test for detection of pyrogenic material in growth hormone produced by recombinant escherichia coli. *J Clin Microbiol* (1984) 20:323–9. doi: 10.1128/jcm.20.3.323-329.1984

240. Weaver JL, Chapdelaine JM, Descotes J, Germolec D, Holsapple M, House R, et al. Evaluation of a lymph node proliferation assay for its ability to detect pharmaceuticals with potential to cause immune-mediated drug reactions. *J Immunotoxicol* (2005) 2:11–20. doi: 10.1080/15476910590930100

241. Nukada Y, Ashikaga T, Sakaguchi H, Sono S, Mugita N, Hirota M, et al. Predictive performance for human skin sensitizing potential of the human cell line activation test (h-CLAT). *Contact Dermatitis* (2011) 65:343–53. doi: 10.1111/j.1600-0536.2011.01952.x

242. Piroird C, Ovigne JM, Rousset F, Martinozzi-Teissier S, Gomes C, Cotovio J, et al. The myeloid U937 skin sensitization test (U-SENS) addresses the activation of dendritic cell event in the adverse outcome pathway for skin sensitization. *Toxicol In Vitro* (2015) 29:901–16. doi: 10.1016/j.tiv.2015.03.009

243. Gilmour N, Reynolds J, Przybylak K, Aleksic M, Aptula N, Baltazar MT, et al. Next generation risk assessment for skin allergy: Decision making using new approach methodologies. *Regul Toxicol Pharmacol* (2022) 131:105159. doi: 10.1016/j.yrtph.2022.105159

244. Potter TM, Neun BW, Dobrovolskaia MA. *In vitro* and *In vivo* methods for analysis of nanoparticle potential to induce delayed-type hypersensitivity reactions. *Methods Mol Biol* (2018) 1682:197–210. doi: 10.1007/978-1-4939-7352-1_17

245. Dézsi L, Mészáros T, Őrfi E, Fülöp TG, Hennies M, Rosivall L, et al. Complement activation-related pathophysiological changes in anesthetized rats: Activator-dependent variations of symptoms and mediators of pseudoallergy. *Molecules* (2019) 24:1–12. doi: 10.3390/molecules24183283

246. Dézsi L, Mészáros T, Kozma G, M HV, Oláh CZ, Szabó M, et al. A naturally hypersensitive porcine model may help understand the mechanism of COVID-19 mRNA vaccine-induced rare (pseudo) allergic reactions: complement activation as a possible contributing factor. *Geroscience* (2022) 44:597–618. doi: 10.1007/s11357-021-00495-y

247. Day CP, Merlino G, Van Dyke T. Preclinical mouse cancer models: a maze of opportunities and challenges. *Cell* (2015) 163:39–53. doi: 10.1016/j.cell.2015.08.068

248. Dobrolecki LE, Airhart SD, Alferez DG, Aparicio S, Behbod F, Bentires-Alj M, et al. Patient-derived xenograft (PDX) models in basic and translational breast cancer research. *Cancer Metastasis Rev* (2016) 35:547–73. doi: 10.1007/s10555-016-9653-x

249. Gengenbacher N, Singhal M, Augustin HG. Preclinical mouse solid tumour models: status quo, challenges and perspectives. *Nat Rev Cancer* (2017) 17:751–65. doi: 10.1038/nrc.2017.92

250. Kersten K, De Visser KE, Van Miltenburg MH, Jonkers J. Genetically engineered mouse models in oncology research and cancer medicine. *EMBO Mol Med* (2017) 9:137–53. doi: 10.15252/emmm.201606857

251. Walsh NC, Kenney LL, Jangalwe S, Aryee KE, Greiner DL, Brehm MA, et al. Humanized mouse models of clinical disease. *Annu Rev Pathol* (2017) 12:187–215. doi: 10.1146/annurev-pathol-052016-100332

252. Gopinathan A, Morton JP, Jodrell DI, Sansom OJ. GEMMs as preclinical models for testing pancreatic cancer therapies. *Dis Model Mech* (2015) 8:1185–200. doi: 10.1242/dmm.021055

253. Bowerman CJ, Byrne JD, Chu KS, Schorzman AN, Keeler AW, Sherwood CA, et al. Docetaxel-loaded PLGA nanoparticles improve efficacy in taxane-resistant triple-negative breast cancer. *Nano Lett* (2017) 17:242–8. doi: 10.1021/acs.nanolett.6b03971

254. Zamboni WC, Szebeni J, Kozlov SV, Lucas AT, Piscitelli JA, Dobrovolskaia MA. Animal models for analysis of immunological responses to nanomaterials: Challenges and considerations. *Adv Drug Delivery Rev* (2018) 136-137:82–96. doi: 10.1016/j.addr.2018.09.012

255. Robbins GR, Roberts RA, Guo H, Reuter K, Shen T, Sempowski GD, et al. Analysis of human innate immune responses to PRINT fabricated nanoparticles with cross validation using a humanized mouse model. *Nanomedicine* (2015) 11:589–99. doi: 10.1016/j.nano.2014.11.010

256. Giang S, Horwitz DA, Bickerton S, La Cava A. Nanoparticles engineered as artificial antigen-presenting cells induce human CD4(+) and CD8(+) tregs that are functional in humanized mice. *Front Immunol* (2021) 12:628059. doi: 10.3389/fimmu.2021.628059

257. Malhi H, Homad LJ, Wan Y-H, Poudel B, Fiala B, Borst AJ, et al. Immunization with a self-assembling nanoparticle vaccine displaying EBV gH/gL protects humanized mice against lethal viral challenge. *bioRxiv* (2022) 2017:480914. doi: 10.1016/j.xcrm.2022.100658

258. Graham AL. Naturalizing mouse models for immunology. *Nat Immunol* (2021) 22:111–7. doi: 10.1038/s41590-020-00857-2

259. Yeung F, Chen YH, Lin JD, Leung JM, Mccauley C, Devlin JC, et al. Altered immunity of laboratory mice in the natural environment is associated with fungal colonization. *Cell Host Microbe* (2020) 27:809–22.e806. doi: 10.1016/j.chom.2020.02.015

260. Zolnik BS, González-Fernández A, Sadrieh N, Dobrovolskaia MA. Nanoparticles and the immune system. *Endocrinology* (2010) 151:458–65. doi: 10.1210/en.2009-1082

261. Dobrovolskaia MA, Shurin M, Shvedova AA. Current understanding of interactions between nanoparticles and the immune system. *Toxicol Appl Pharmacol* (2016) 299:78–89. doi: 10.1016/j.taap.2015.12.022

262. Moghimi SM, Hunter AC. Capture of stealth nanoparticles by the body's defences. *Crit Rev Ther Drug Carrier Syst* (2001) 18:527–50. doi: 10.1615/CritRevTherDrugCarrierSyst.v18.i6.30

263. Xiang SD, Scalzo-Inguanti K, Minigo G, Park A, Hardy CL, Plebanski M. Promising particle-based vaccines in cancer therapy. *Expert Rev Vaccines* (2008) 7:1103–19. doi: 10.1586/14760584.7.7.1103

264. Cavadas M, González-Fernández A, Franco R. Pathogen-mimetic stealth nanocarriers for drug delivery: a future possibility. *Nanomedicine* (2011) 7:730–43. doi: 10.1016/j.nano.2011.04.006

265. Boraschi D, Costantino L, Italiani P. Interaction of nanoparticles with immunocompetent cells: nanosafety considerations. *Nanomed (Lond)* (2012) 7:121–31. doi: 10.2217/nnm.11.169

266. Mohamud R, Xiang SD, Selomulya C, Rolland JM, O'hehir RE, Hardy CL, et al. The effects of engineered nanoparticles on pulmonary immune homeostasis. *Drug Metab Rev* (2014) 46:176–90. doi: 10.3109/03602532.2013.859688

267. David CA, Owen A, Liptrott NJ. Determining the relationship between nanoparticle characteristics and immunotoxicity: key challenges and approaches. *Nanomed (Lond)* (2016) 11:1447–64. doi: 10.2217/nnm-2016-0017

268. Őrfi E, Szebeni J. The immune system of the gut and potential adverse effects of oral nanocarriers on its function. *Adv Drug Delivery Rev* (2016) 106:402–9. doi: 10.1016/j.addr.2016.09.009

269. Boraschi D, Italiani P, Palomba R, Decuzzi P, Duschl A, Fadeel B, et al. Nanoparticles and innate immunity: new perspectives on host defence. *Semin Immunol* (2017) 34:33–51. doi: 10.1016/j.smim.2017.08.013

270. Ernst LM, Casals E, Italiani P, Boraschi D, Puntes V. The interactions between nanoparticles and the innate immune system from a nanotechnologist perspective. *Nanomaterials (Basel)* (2021) 11:1–20. doi: 10.3390/nano11112991

271. Mikelez-Alonso I, Magadán S, González-Fernández Á., Borrego F. Natural killer (NK) cell-based immunotherapies and the many faces of NK cell memory: A look into how nanoparticles enhance NK cell activity. *Adv Drug Delivery Rev* (2021) 176:113860. doi: 10.1016/j.addr.2021.113860

frontiers | Frontiers in Immunology

TYPE Brief Research Report
PUBLISHED 13 October 2022
DOI 10.3389/fimmu.2022.1016927

OPEN ACCESS

EDITED BY
Mrinmoy Sanyal,
Stanford University, United States

REVIEWED BY
Maria Alice Freitas Queiroz,
Federal University of Pará, Brazil
Khalid Muhammad,
United Arab Emirates University,
United Arab Emirates
Pasquale Stefanizzi,
University of Bari Aldo Moro, Italy

*CORRESPONDENCE
Andrea Rubbert-Roth
Andrea.Rubbert-Roth@kssg.ch

SPECIALTY SECTION
This article was submitted to Vaccines and Molecular Therapeutics, a section of the journal Frontiers in Immunology

RECEIVED 11 August 2022
ACCEPTED 20 September 2022
PUBLISHED 13 October 2022

CITATION
Raptis CE, Berger CT, Ciurea A, Andrey DO, Polysopoulos C, Lescuyer P, Maletic T, Riek M, Scherer A, von Loga I, Safford J, Lauper K, Möller B, Vuilleumier N, Finckh A and Rubbert-Roth A (2022) Type of mRNA COVID-19 vaccine and immunomodulatory treatment influence humoral immunogenicity in patients with inflammatory rheumatic diseases. *Front. Immunol.* 13:1016927. doi: 10.3389/fimmu.2022.1016927

Type of mRNA COVID-19 vaccine and immunomodulatory treatment influence humoral immunogenicity in patients with inflammatory rheumatic diseases

Catherine E. Raptis[1], Christoph T. Berger[2,3], Adrian Ciurea[4], Diego O. Andrey[5,6], Christos Polysopoulos[1], Pierre Lescuyer[5], Tanja Maletic[1], Myriam Riek[1], Almut Scherer[1], Isabell von Loga[1], Judith Safford[7], Kim Lauper[6,8], Burkhard Möller[9], Nicolas Vuilleumier[5,6], Axel Finckh[6,8] and Andrea Rubbert-Roth[10]*

[1]SCQM Foundation (Swiss Clinical Quality Management in Rheumatic Diseases), Zurich, Switzerland, [2]University Center for Immunology and Immunization Clinic, University Hospital Basel, Basel, Switzerland, [3]Translational Immunology, Department of Biomedicine, University of Basel, Basel, Switzerland, [4]Department of Rheumatology, Zurich University Hospital, University of Zurich, Zurich, Switzerland, [5]Laboratory Medicine Division, Geneva University Hospitals, Geneva, Switzerland, [6]Faculty of Medicine, University of Geneva, Geneva, Switzerland, [7]RheumaCura Foundation, Bern, Switzerland, [8]Division of Rheumatology, Geneva University Hospitals, Geneva, Switzerland, [9]Division of Rheumatology and Immunology, Inselspital, Bern University Hospital, Bern, Switzerland, [10]Division of Rheumatology and Immunology, St. Gallen Cantonal Hospital, St. Gallen, Switzerland

Patients with inflammatory rheumatic diseases (IRD) are at increased risk for worse COVID-19 outcomes. Identifying whether mRNA vaccines differ in immunogenicity and examining the effects of immunomodulatory treatments may support COVID-19 vaccination strategies. We aimed to conduct a long-term, model-based comparison of the humoral immunogenicity following BNT162b2 and mRNA-1273 vaccination in a cohort of IRD patients. Patients from the Swiss IRD cohort (SCQM), who assented to mRNA COVID-19 vaccination were recruited between 3/2021-9/2021. Blood samples at baseline, 4, 12, and 24 weeks post second vaccine dose were tested for anti-SARS-CoV-2 spike IgG (anti-S1). We examined differences in antibody levels depending on the vaccine and treatment at baseline while adjusting for age, disease, and past SARS-CoV-2 infection. 565 IRD patients provided eligible samples. Among monotherapies, rituximab, abatacept, JAKi, and TNFi had the highest odds of reduced anti-S1 responses compared to no medication. Patients on specific combination therapies showed significantly lower antibody responses than those on monotherapy. Irrespective of the disease, treatment, and past SARS-CoV-2 infection, the odds of higher antibody levels at 4, 12, and 24 weeks post second vaccine dose were, respectively, 3.4, 3.8, and 3.8 times higher with mRNA-1273 versus BNT162b2 ($p < 0.0001$). With

10.3389/fimmu.2022.1016927

every year of age, the odds ratio of higher peak humoral immunogenicity following mRNA-1273 versus BNT162b2 increased by 5% ($p < 0.001$), indicating a particular benefit for elderly patients. Our results suggest that in IRD patients, two-dose vaccination with mRNA-1273 versus BNT162b2 results in higher anti-S1 levels, even more so in elderly patients.

KEYWORDS

SARS-CoV-2, vaccination, mRNA-1273, BNT162b2, anti-spike-IgG, waning immunity, rheumatic disease, immunosuppression

Introduction

Patients with inflammatory rheumatic diseases (IRD) requiring immunomodulatory therapies represent a vulnerable population during the COVID-19 pandemic and may have an increased risk of poor COVID-19 outcomes (1, 2). Two mRNA COVID-19 vaccines, BNT162b2 (Comirnaty, Pfizer-BioNTech) and mRNA-1273 (Spikevax, Moderna), are currently available and have proven to be highly effective in preventing severe COVID-19 disease, including hospitalizations and deaths (3). However, patients on specific immunomodulatory treatments mount an attenuated antibody response following mRNA COVID-19 vaccination compared to healthy individuals and may be less protected (4–9). Data on whether the risk of breakthrough infections is increased as the immune response wanes over time and the impact of certain immunomodulatory medication on the level of antibodies in patients with different diseases are still under discussion (10–12).

The efficacy of therapeutic and prophylactic antibodies against the spike protein further supports the importance of a robust humoral immune response (13, 14). Vaccine-induced immune responses in immunocompromized individuals may, among other factors, depend on the type of vaccine received. The available mRNA vaccines both encode for the SARS-CoV2 spike protein but contain different amounts of mRNA. Moreover, the mRNA incorporates distinct proprietary nucleotide and sequence modifications to stabilise the mRNA and modulate its immune activation profile (15). There is evidence that these differences may be clinically relevant, as, compared to BNT162b2, vaccination with mRNA-1273 resulted in significantly lower infection and hospitalization rates in non-immunocompromized adults and US veterans and higher antibody levels in healthcare workers (16–18). To our knowledge, relevant studies comparing the vaccine-induced immune responses following a two-dose regimen of the mRNA COVID-19 vaccines in patients with rheumatic diseases mostly involved a single sampling timepoint, or have reported results in terms of the proportion of patients achieving seroconversion or passing a predefined threshold (5, 19, 20). However, since they used relatively low antibody thresholds, it is difficult to explore differences between BNT162b2 and mRNA-1273 induced immunity. As strong, antibody-mediated neutralizing activity increases with higher vaccine-induced anti-S1-antibody levels, comprehensively and longitudinally quantifying a potential difference in the humoral immunogenicity resulting from the approved mRNA vaccines in IRD patients and examining the effects of immunomodulatory treatments thereon may help to optimize COVID-19 vaccination strategies for this vulnerable patient population. Our aim was, therefore, to carry out a long-term, model-based comparative analysis of the magnitude and kinetics of the humoral immune response following two-dose vaccination with BNT162b2 and mRNA-1273 in patients with IRD on different immunomodulatory treatments.

Methods

Study set-up and participants

Between 1 March and 30 September 2021, adult patients from the Swiss cohort for patients with IRD (SCQM, Swiss Clinical Quality Management) who planned to receive an mRNA COVID-19 vaccine and were active users of the mySCQM patient application (21) were recruited into the study. The Geneva Ethics Committee approved the study protocol (BASEC-ID: 2020-01708), and all participants provided written informed consent. Participants' demographics and clinical characteristics were extracted from physician- and patient-reported data from the SCQM cohort database. In addition, at predefined intervals, patients were asked to answer study-specific questionnaires *via* the patient app. These included questions regarding testing for active SARS-CoV-2 infections (if any), COVID-19 vaccination details, changes in medication intake, pausing of immunomodulatory therapies around the vaccination dates, and serious vaccine-related adverse events. The detailed study schedule and questionnaire are available in Supplementary Figure S1 and

Table S1, respectively. Participants received blood collection kits for the self-collection of capillary blood samples (Labonovum, NL), along with instructions for use. Participants were required to collect samples at baseline (i.e., before the first vaccine dose) and 4, 12, and 24 weeks post the second vaccine dose. Some patients with a past SARS-CoV-2 infection, were only given a single dose of an mRNA vaccine according to the Swiss immunization recommendations; others received two doses despite their previous infection. Samples were sent to the centralized laboratory in Geneva with a maximum allowed storage of 2 days at 2-8 °C before shipping and a postal time of ≤ 24 hours to ensure that anti-SARS-CoV-2 spike IgG antibodies were stable in the samples upon reception by the laboratory (22). Samples were tested for IgG antibodies against the S1 domain of the spike protein of SARS-CoV-2 using the EUROIMMUN ELISA. The assay read-out is a unitless index, calculated as the ratio of the optical density of the sample over that of the calibrator. We applied previously validated cut-offs: indices < 0.8 were considered negative, those ≥ 0.8 < 2.5 indeterminate and subsequently confirmed positive/negative with recombinant immunofluorescence (those ≥2.5 considered positive) (23). Prior SARS-CoV-2 infection was defined by records of a past positive anti-SARS-CoV-2 IgG or PCR test in the SCQM cohort database or a positive baseline anti-SARS-CoV2 IgG result.

Final dataset for analysis

Only patients who received an mRNA COVID-19 vaccine, who provided an eligible baseline sample plus at least one subsequent sample, who fully answered the study questionnaires, and for whom the data regarding demographics and clinical characteristics extracted from the SCQM registry database were complete, were included in the analysis. Samples were considered eligible if enough serum for the assay could be extracted and if they were collected within the window of predefined collection timepoints (Figure S2). Samples taken after breakthrough infections or after receiving additional vaccine doses were excluded from the analysis. Samples not yet collected/tested at the time of writing were also not included in the analysis.

Outcomes and objectives

The anti-SARS-CoV-2 spike IgG levels (anti-S1; expressed as a unitless optical density ratio) at 4, 12, and 24 weeks post second vaccine dose were our outcomes of interest. The primary and secondary study objectives were to compare these outcomes depending on the vaccine received (BNT162b2 vs mRNA-1273) and the immunomodulatory treatment at baseline while adjusting for age, disease, and past SARS-CoV-2 infection.

Statistical methods

Models: We applied mixed-effects continuous outcome logistic regression models to the anti-S1 levels obtained at 4, 12, and 24 weeks post second vaccine dose to analyze differences depending on the vaccine and immunomodulatory treatment while accounting for inter-lot and inter-batch variability. These models are appropriate for the ELISA output, which is bounded (by a lower bound > 0 and an upper saturation limit), and, with the assumption of proportional odds, permit the comparison of the immunogenicity, following different vaccines and treatments, in relation to a given antibody cut-off, without the need to predefine it (24). Specifically, at each timepoint considered and for the covariates included, these models return the odds ratios of the vaccine-induced antibody levels being higher than a given cut-off without needing to pre-specify it. This is important since, to date, no absolute correlate of protection against severe COVID-19 has been established, and cut-offs may shift with the emergence of new variants (25). Since the true optical density ratios at the assay upper saturation limit are higher than this limit by an unknown amount, which we did not quantify through sample dilution, we treated the few observations at the saturation limit as right-censored.

Covariates: The following covariates assessed at baseline were included in the models applied at each timepoint: age, disease, past-SARS-CoV-2 infection, vaccine, immunomodulatory treatment as mono/combination therapy, as well as the interaction of vaccine with age (the odds ratios reported are therefore adjusted). Multiple other interactions were investigated prior to the final modelling, including those between vaccine and treatment, but only significant ones were retained in the final model. The majority (89%) of the study population indicated no reduction or pause in their immunomodulatory therapy during vaccination. Therefore, we decided not to include treatment changes in the analysis.

Confounding: In Switzerland, the BNT162b2 vaccine rollout began before that of mRNA-1273, at a time when the vaccination of the elderly and immunocompromized was prioritized. By including age and treatment as covariates in the model, we adjusted for this potential confounding of the vaccine effect by the timing of the vaccination.

Contextualization of absolute antibody levels: In addition to the relative comparisons emerging from the application of the models mentioned above, we sought to contextualize our results as it has been demonstrated that anti-S1 levels expressed as optical density ratios ≥ 5 (using the same EUROIMMUN assay) allowed to identify sera from SARS-CoV-2 convalescent plasma donors with strong neutralizing capacity (90% inhibition plaque reduction neutralization test (PRNT90) titers ≥ 1:20) with high specificity (26). Accordingly, at the different timepoints considered, we compared the proportion of SARS-CoV-2

naïve BNT162b2 and mRNA-1273 recipients with optical density ratios equal to or greater than this cut-off.

Results

Between 4 March and 16 September 2021, 917 patients consented to participate in the study (Table S2). Five hundred and sixty-five patients received an mRNA COVID-19 vaccine, provided eligible samples and had complete data (Figure S3 and Table 1). The total number of eligible samples that were tested were 565, 552, 542, and 513 at baseline, 4, 12, and 24 weeks post second vaccine dose, respectively (Figure S3). At the 4-, 12-, and 24-week post-second vaccine dose timepoints, only 3.6%, 1.5%, and 1.2% of the optical density ratios, respectively, were at the upper saturation limit and were treated as right-censored.

TABLE 1 Demographics and clinical characteristics of the study population.

	Total (n = 565)	BNT162b2 (n = 305)	mRNA-1273 (n = 260)
Age at baseline, years [median (IQR)]	53 (44 – 62)	54 (43 – 62)	52 (45 – 61)
Sex, n (%)			
Female	374 (66)	204 (67)	170 (65)
Male	191 (34)	101 (33)	90 (35)
Disease duration at baseline, years [median (IQR)]	15 (8 – 22)	14 (8 – 22)	15 (8 – 21)
Evidence of SARS-CoV-2 infection, n (%)			
Past infection	58 (10)	30 (10)	28 (11)
No past infection	507 (90)	275 (90)	232 (89)
Vaccine, n (%)			
BNT162b2; mRNA-1273	305 (54); 260 (46)	305 (100)	260 (100)
of which one dose*	*4; 7*	*4*	*7*
interval between doses [median (IQR)]	28 (28 – 29)	28 (28 – 29)	28 (28 – 29)
Diagnosis, n (%)			
Rheumatoid arthritis	204 (36.1)	112 (36.7)	92 (35.4)
Axial spondyloarthritis	207 (36.6)	107 (35.1)	100 (38.5)
Psoriatic arthritis	120 (21.2)	62 (20.3)	58 (22.3)
Undifferentiated arthritis	34 (6.0)	24 (7.9)	10 (3.8)
Treatment at baseline, n (%)			
no medication	84 (14.9)	42 (13.8)	42 (16.2)
csDMARD	52 (9.2)	23 (7.5)	29 (11.2)
of which combination therapy with GC	*4*	*1*	*3*
GC monotherapy	5 (0.9)	4 (1.3)	1 (0.4)
TNFi	273 (48.3)	152 (49.8)	121 (46.5)
of which combination therapy$^{\pm}$, n	*76*	*47*	*29*
JAKi	36 (6.4)	21 (6.9)	15 (5.8)
of which combination therapy$^{\perp}$, n	*12*	*7*	*5*
IL-6/17/23i	77 (13.6)	45 (14.8)	32 (12.3)
of which combination therapy$^{\perp}$, n	*20*	*11*	*9*
Rituximab	20 (3.5)	9 (3.0)	11 (4.2)
of which combination therapy$^{\perp}$, n	*10*	*5*	*5*
time since last infusion, days [median (IQR)]	267 (179 – 568)	262 (215 – 372)	286 (142 – 706)
Abatacept	14 (2.5)	8 (2.6)	6 (2.3)
of which combination therapy$^{\perp}$, n	*6*	*5*	*1*
PDE4i	4 (0.7)	1 (0.3)	3 (1.2)
of which combination therapy$^{\times}$, n	*1*	-	*1*
Total GC use over all patients			
in mono- and combination therapy, n (%)	32 (5.7)	20 (6.6)	12 (4.2)
Dose, mg [median (IQR)]	5 (2.5 - 7.5)	5 (2.5 - 6)	7.5 (5 – 10)

*Due to past SARS-CoV-2 infection. No medication, currently on no immunomodulatory medication; csDMARD, conventional synthetic disease-modifying antirheumatic drug; GC, glucocorticoids; TNFi, tumor necrosis factor inhibitor; JAKi, Janus kinase inhibitor; IL-6/17/23i, interleukin 6/17/23 inhibitors; PDE4i, phosphodiesterase-4 inhibitor. $^{\pm}$with csDMARD/GC/csDMARD & GC; $^{\perp}$with csDMARD/csDMARD & GC; $^{\times}$with csDMARD. The 32 patients receiving GCs are double counted, i.e. included in individual treatment groups and the entire GC group, to show the extent of GC use over the entire study population.

10.3389/fimmu.2022.1016927

BNT162b2 and mRNA-1273 recipients had comparable demographics and clinical characteristics (Table 1).

We analyzed how participants' treatments affected humoral immunogenicity in SARS-CoV-2 naïve IRD patients (Figure 1A; Table 2). As monotherapy, the use of abatacept, JAKi, rituximab, and TNFi resulted in significantly lower antibody levels compared to those observed in the group of patients who were not on immunomodulatory medication at baseline (Table 2), with the latter group of patients currently not on medication presenting anti-S1 levels comparable to those previously

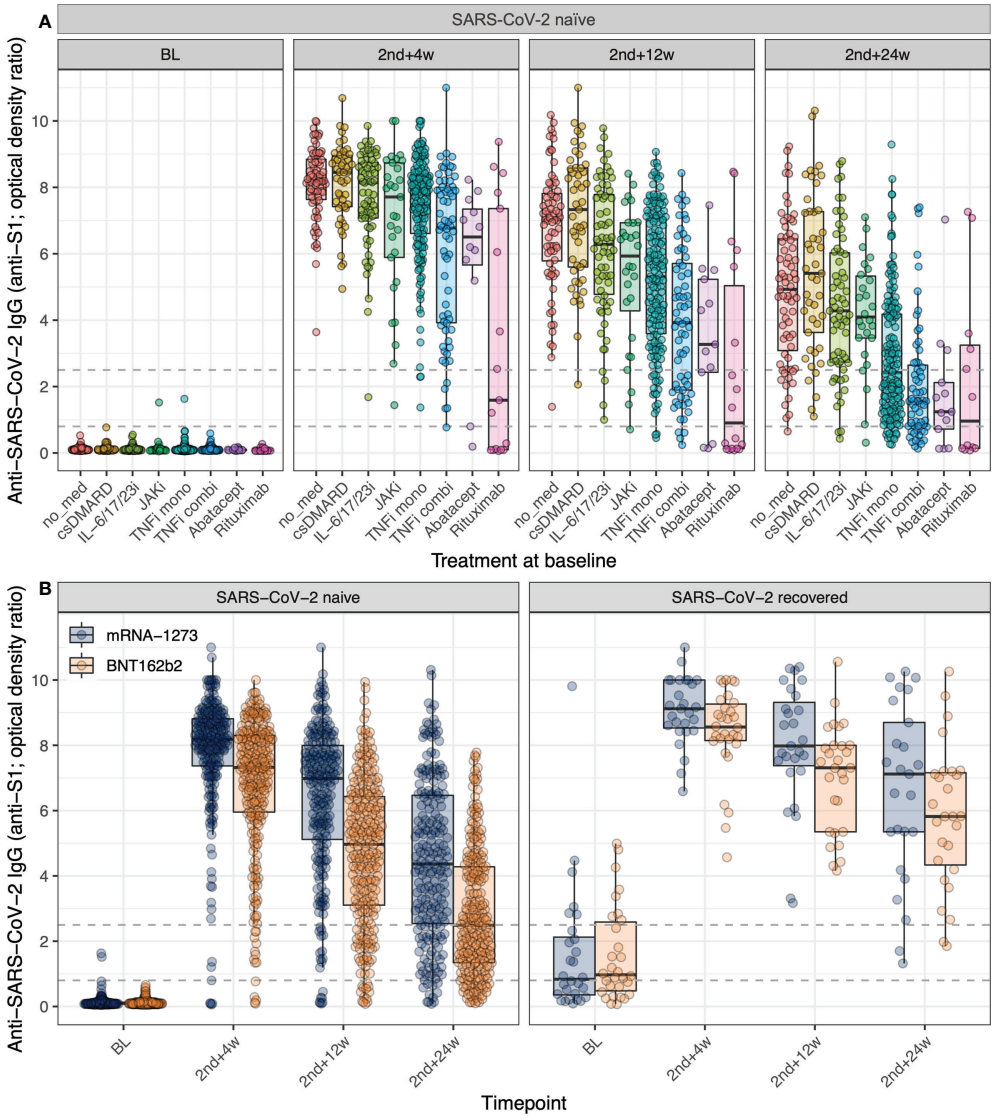

FIGURE 1
Impact of treatment for IRD and mRNA COVID-19 vaccine on anti-S1 antibody levels. **(A)** The variation over time of anti-S1 antibodies post mRNA COVID-19 vaccination in adult SARS-CoV-2 naïve IRD patients disaggregated by treatment group at baseline. No med = currently on no medication; csDMARD = conventional synthetic disease-modifying antirheumatic drugs in mono or combination therapy with GC (glucocorticoids); IL-6/17/23i = interleukin 6/17/23 inhibitors in mono or combination therapy with csDMARD/csDMARD & GC; JAKi = janus kinase inhibitors in mono or combination therapy with csDMARD/csDMARD & GC; TNFi mono = tumor necrosis factor inhibitor as monotherapy, TNFi combi = TNFi in combination therapy with csDMARD/GC/csDMARD & GC; Abatacept in mono or combination therapy with csDMARD/csDMARD & GC; Rituximab in mono or combination therapy with csDMARD/csDMARD & GC. The following treatment groups with five or fewer participants are not shown here: GC monotherapy and PDE4i (phosphodiesterase-4 inhibitor) in mono or combination therapy with csDMARD. **(B)** The variation over time of anti-S1 antibodies post mRNA COVID-19 vaccination in adult IRD patients disaggregated by vaccine and evidence of SARS-CoV-2 infection. For both panels: The dashed lines indicate the assay thresholds (see Methods). Individual points are overlaid on boxplots, with whiskers extending to 1.5*IQR. BL = baseline (day of 1st vaccine dose, before vaccination), 2nd+4w/12w/24w = 4/12/24 weeks post 2nd vaccine dose. For the full, adjusted model outcomes, see Table 2.

10.3389/fimmu.2022.1016927

TABLE 2 The (adjusted) odds ratios of higher antibody levels (regardless of the threshold) up to 24 weeks post 2nd vaccine dose for IRD patients.

Weeks post 2nd vacc. dose: (Total number of samples available for analysis)	4 (552)		12 (542)		24 (513)	
	OR (95% CI)	p-value	OR (95% CI)	p-value	OR (95% CI)	p-value
Age[×]	**0.96** (0.94 - 0.97)	< 0.0001	**0.98** (0.96 - 0.99)	0.0045	0.99 (0.97 -1.0)	0.074
mRNA-1273 vs BNT162b2	**3.3** (2.4 - 4.6)	< 0.0001	**3.8** (2.7 - 5.4)	< 0.0001	**3.8** (2.7 - 5.2)	< 0.0001
Past SARS-CoV-2 infection vs none	**8.2** (4.8 - 14)	< 0.0001	**8.6** (5.1 - 15)	< 0.0001	**13** (7.2 - 22)	< 0.0001
Abatacept monotherapy*	**0.13** (0.035 - 0.45)	0.0013	**0.081** (0.020 - 0.32)	0.00036	**0.082** (0.021 - 0.32)	0.00034
cDMARD monotherapy*	1.3 (0.66 - 2.4)	0.49	1.8 (0.93 - 3.4)	0.083	**2.2** (1.1 - 4.4)	0.022
IL-6/17/23i monotherapy*	0.97 (0.54 - 1.7)	0.92	1.0 (0.55 - 1.9)	0.97	1.0 (0.56 - 1.9)	0.95
JAKi monotherapy*	**0.37** (0.16 - 0.84)	0.018	**0.36** (0.15 - 0.85)	0.020	0.64 (0.27 - 1.5)	0.29
Rituximab monotherapy*	**0.12** (0.022 - 0.62)	0.012	**0.074** (0.014 - 0.40)	0.0025	**0.11** (0.025 - 0.51)	0.0046
TNFi monotherapy*	**0.41** (0.26 - 0.65)	0.00014	**0.28** (0.18 - 0.45)	< 0.0001	**0.16** (0.098 - 0.26)	< 0.0001
RA vs axSpA	1.0 (0.65 - 1.5)	0.98	1.1 (0.72 - 1.7)	0.68	0.89 (0.58 - 1.5)	0.59
PsA vs axSpA	0.98 (0.64 - 1.5)	0.93	0.94 (0.61 - 1.4)	0.78	0.95 (0.61 - 1.5)	0.82
UA vs axSpA	0.90 (0.48 - 1.7)	0.75	1.3 (0.65 - 2.4)	0.50	1.0 (0.53 – 1.9)	0.98
Abatacept combi[#]	0.97 (0.14 - 6.8)	0.98	0.49 (0.070 - 3.5)	0.48	0.36 (0.055 - 2.4)	0.29
IL-6/17/23i combi[#]	**0.34** (0.12 - 0.95)	0.039	**0.26** (0.094 - 0.73)	0.011	**0.24** (0.086 - 0.68)	0.0070
JAKi combi[#]	1.2 (0.31 - 4.9)	0.77	1.2 (0.37 - 4.0)	0.75	1.1 (0.35 - 3.6)	0.85
Rituximab combi[#]	**0.044** (0.0051 - 0.37)	0.0040	**0.091** (0.012 - 0.71)	0.022	0.14[$] (0.015- 1.3)	0.087[$]
TNFi combi[±#]	**0.39** (0.23 - 0.65)	0.00039	**0.36** (0.22 - 0.60)	< 0.0001	**0.38** (0.22 - 0.64)	0.00029
Interaction of age with vaccine[+]	**1.05** (1.02 - 1.07)	0.00078	1.02 (0.995 - 1.05)	0.11	**1.03** (1.01 - 1.06)	0.018

[×]For 1 y increase with BNT162b2. The following treatments are considered at baseline: *vs no medication (= currently on no medication). csDMARD, conventional synthetic disease-modifying antirheumatic drugs; IL-6/17/23i, interleukin 6/17/23 inhibitors; JAKi, janus kinase inhibitors; TNFi, tumor necrosis factor inhibitors. RA, rheumatoid arthritis; axSpA, axial spondyloarthritis; PsA, psoriatic arthritis; UA, undifferentiated arthritis. Combi, combination therapy with csDMARD/csDMARD & GC; ±combination therapy with csDMARD/GC/csDMARD & GC; #vs respective monotherapy [+]Interaction term showing how the OR of mRNA-1273 vs BNT162b2 increased with increasing age (indicatively, at 4 and 24 weeks post 2nd vaccine dose, for every increase in age of 1 year, the odds ratio of higher antibody levels with mRNA-1273 vs BNT162b2 increased by 5% and 3%, respectively). The following treatment groups with five or fewer participants were included in the model but are not shown here: GC (glucocorticoid) monotherapy, PDE4i (phosphodiesterase-4 inhibitor) monotherapy and combination therapy, and csDMARD combination therapy. [$]At the time of analysis, only five samples from participants in this group were available from this timepoint.
Bold values indicate odds ratio estimates that were statistically significant.

reported for healthy individuals (Figure S4). Of note, compared to the untreated IRD group, monotherapy with biologics targeting other cytokines than TNF (i.e. IL-6/17/23i) did not negatively affect the humoral immune response (Table 2). In combination therapy, interleukin inhibitors and TNFi led to significantly lower antibody levels than respective monotherapy over all timepoints. Table S3 provides the summary statistics (median, range and IQR) of the absolute antibody levels expressed as optical density ratios for each medication group and timepoint.

Comparing the humoral immunogenicity of the two administered mRNA vaccines (Figure 1B; Table 2), we observed that the odds of having higher antibody levels than any given threshold at 4, 12, and 24 weeks post second vaccine dose were, respectively, 3.4, 3.8, and 3.8 times higher following vaccination with mRNA-1273 compared to BNT162b2 for the average-aged

patient (53 y) in this study ($p < 0.0001$, Table 2). This was irrespective of the disease, immunomodulatory treatment, and past SARS-CoV-2 infection. Moreover, for every one-year increase in age, the odds ratio of higher peak antibody levels following mRNA-1273 versus BNT162b2 vaccination increased by 5% (age – vaccine interaction at 4 weeks post second vaccine dose, $p < 0.001$, Table 2). This effect was cumulative (Figure 2, panel '4 weeks post 2nd vaccine dose') ratio of higher peak antibody levels with mRNA-1273 versus BNT162b2 were over two times greater for patients ≥ 62 y (the eldest 25% of the population) versus patients ≤ 44 y (the youngest 25% of the population; Figure 2, panel '4 weeks post 2nd vaccine dose'). Vaccination of patients with a past SARS-CoV-2 infection led to strikingly higher peak antibody levels than in SARS-CoV-2 naïve IRD patients (odd ratios 8.2, 8.6, and 13 at 4, 12, and 24 weeks post second vaccine dose, respectively; $p < 0.0001$, Table 2). Table S4 provides the summary statistics (median, range and IQR) of the absolute antibody levels in optical density ratios for each vaccine, SARS-CoV-2 infection status, and timepoint.

In spite of the independence of the model-based results from any priorly defined cut-off, the absolute antibody levels (Figure 1; Tables S3, S4) can also be contextualized in terms of the optical density ratio cut-off of 5, which has previously been described to identify sera from SARS-CoV-2 convalescent plasma donors with strong neutralizing capacity against the original Wuhan strain of SARS-CoV2 (26). We observed differences in the proportion of SARS-CoV-2 naïve patients with sera reaching an optical density ratio of ≥ 5 in recipients of mRNA-1273 compared to BNT162b2. Specifically, the proportion of samples with an optical density ratio ≥ 5 from mRNA-1273 recipients was 93%, 75%, and 40% at 4, 12, and 24 weeks post second vaccine dose, whereas, during the same respective period, this was only the case in 84%, 50%, and 15% of samples from BNT162b2 recipients (Figure 1B, SARS-CoV-2 naïve patients). While potentially not applicable to the neutralization of more recent variants of concern, this finding suggests that it can be assumed that the higher absolute antibody levels were associated with more robust virus neutralization.

Discussion

Longitudinal data on anti-SARS-CoV-2 vaccine-induced immune responses beyond three months for patients on

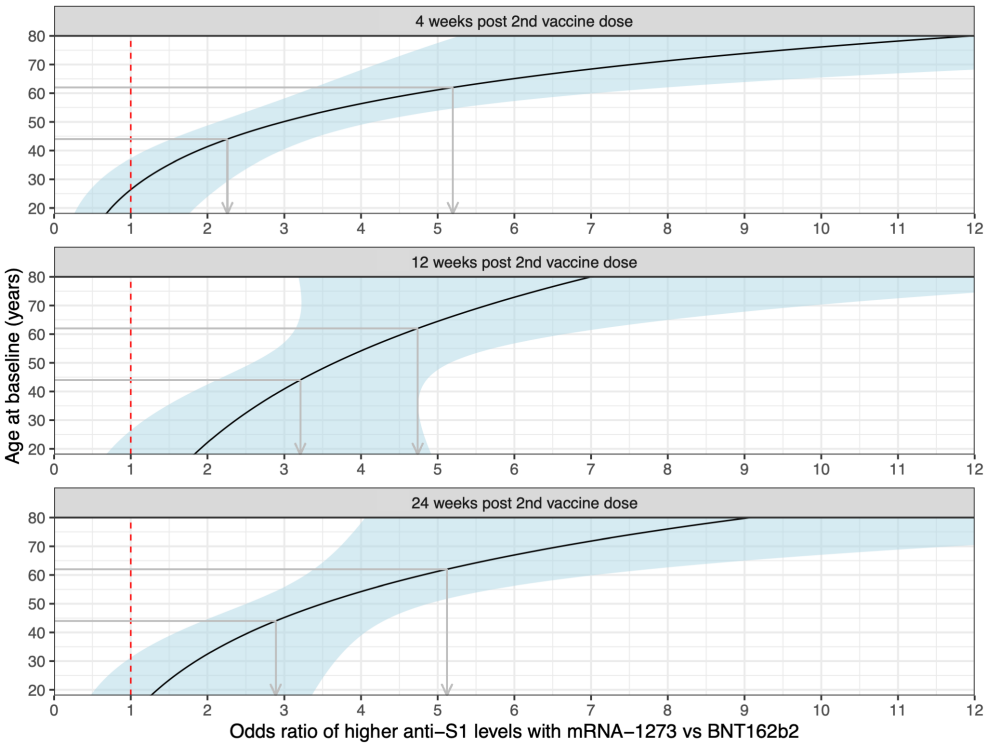

FIGURE 2
Age-dependent odds of higher antibody levels following mRNA-1273 vs BNT162b2 vaccination at the different timepoints. The dashed red line indicates the location of odds ratio = 1, and the light blue-shaded areas the pointwise 95% confidence intervals. The grey arrows demonstrate, at the different timepoints, the increased benefit (in terms of higher odds of higher antibody levels) from vaccination with mRNA-1273 vs BNT162b2 for an IRD patient of 62 y vs 44 y (an interval coinciding with the study population age IQR).

immunomodulatory therapies are still limited but of high clinical relevance given the widespread use of the latter in a variety of immune-mediated diseases. Our results confirmed differences in vaccine-induced antibody responses driven by distinct treatment modalities as others have reported (4, 5, 7, 27, 28). Impaired antibody responses were observed in patients on rituximab, abatacept, TNFi and JAKi supporting the view that the formation of a robust vaccine-induced immune response depends on complex interactions between distinct components of the immune system that may be differentially affected depending on the mode of action of the treatment used. Of note, irrespective of the underlying diagnosis and of the treatment modality, we observed higher odds of increased anti-S1 antibody levels at all timepoints following vaccination with mRNA-1273 versus BNT162b2 in the patients of our cohort. Moreover, our results suggest that in IRD patients the benefit – in terms of humoral immune response – of vaccination with mRNA-1273 versus BNT162b2 increases with age. The higher humoral immunogenicity could be due to the higher dose of mRNA in the mRNA-1273 vaccine, differences in the immune activation by the proprietary mRNA modifications introduced by each manufacturer, or a combination thereof (29). In Switzerland, both vaccines were given at a four weeks interval, excluding a difference introduced by dosing schedules.

The observation that the effect of higher antibodies in mRNA-1273- vs BNT162b2-vaccinated patients increased with age is of special interest. Age is an important factor for reduced immunogenicity and vaccine-induced protection due to immunosenescence (30). Higher antigen doses of influenza or hepatitis B vaccines enable to increase vaccine responses in older adults or patients at risk for vaccine non response (31, 32). Therefore, it can be speculated that the higher dose of the mRNA-1273 may overcome an age-related decrease in immunogenicity. Indeed, for an increase in age of 10 years, the odds of higher antibody levels following BNT162b2 vaccination at peak immunogenicity decreased by a factor of 0.65 (95% CI 0.54, 0.77), while following mRNA-1273 vaccination the change in the odds with 10 more years was estimated as 1.02 (95% CI: 0.83, 1.25). With BNT162b2 therefore, we have evidence that the odds decrease with age (confidence interval entirely below 1), whereas with mRNA-1273 the odds decrease at a lower rate with age compared to BNT162b2, or might even increase (confidence interval includes 1 and does not overlap with the confidence interval for BNT162b2). Consequently, we observe an increasing benefit of mRNA-1273 over BNT162b2 with age.

Strong vaccine-induced anti-S1 antibody responses have been shown to correspond to neutralization of viral variants and correlated with a better clinical outcome (33–35). Yet, to date, no anti-S1 cut-off has been established that correlates with protection from severe COVID-19. Moreover, higher antibody levels are deemed necessary to protect against different variants of concern compared to the wild-type virus (36). With the assumption of proportional odds, the statistical models applied in this study permit the effective comparison of the impact of different mRNA vaccines and treatments on the antibody levels within a bounded range, without the need to predefine a formal cut-off (24). Furthermore, the applied models also enable adjusting for confounding, allowing for an informative comparison. To our knowledge, a longitudinal comparison of the humoral immunogenicity following two-dose mRNA COVID-19 vaccination in patients with rheumatic diseases has not been performed in this level of detail to date, with relevant studies reporting results in terms of the proportion of individuals achieving seroconversion or passing a relatively low antibody threshold, making it difficult to investigate differences between the BNT162b2 and mRNA-1273 vaccines (5, 19, 20).

Despite the independence of the model-based results from any priorly defined cut-off, the absolute optical density ratios were also contextualized in terms of the cut-off of 5, that has been demonstrated to correspond to strong neutralization capacity against the original Wuhan strain of SARS-CoV2 in plasma derived from convalescent patients (26). While this cut-off is potentially not applicable to the neutralization of more recent variants of concern, the comparison of the proportion of samples per vaccine passing this threshold suggests a higher neutralization capacity of mRNA-1273 compared to BNT162b2. Specifically, while the proportion of SARS-CoV-2 naïve mRNA-1273 and BNT162b2 recipients with antibody levels equal to or above this cut-off is comparable at the timepoint of peak immunogenicity (93% versus 84%, respectively), by 12 and 24 weeks post second vaccine dose 25% more mRNA-1273 recipients achieve this antibody cut-off compared to BNT162b2 recipients. Unlike the adjusted statistical models that form the principal analysis in this study, the comparison in terms of proportions of patients achieving this cut-off is unadjusted. Nevertheless, it is worth noting that the demographic and clinical characteristics of both vaccine recipients were comparable (Table 1).

The limitations of this study include the sampling by capillary blood self-collection, which, while maximizing participation due to its convenience, provided limited serum volumes and restricted the assay choice to the semi-quantitative EUROIMMUN ELISA that requires a small amount of serum. Nevertheless, in terms of accuracy of results for a series of biomarkers, capillary blood self-sampling did not suffer compared to venous blood draws, as demonstrated by a recent randomized controlled trial (37). Another limitation of this study was the inability to perform neutralization or cellular assays or measure antibody responses to other SARS-CoV-2 antigens. Consequently, we have no data on how the vaccination-induced T cell responses compare between the two mRNA vaccines in patients with IRD. Interestingly, in a recent study on RA patients vaccinated with BNT162b2, significant impairment of the humoral immune response but less so of the T cell response was found at six months post vaccination (38).

Moreover, we did not include a matched healthy control group, although we were able to establish that the group of IRD patients on no immunomodulatory medication at baseline had vaccine-induced antibody responses comparable to those reported for healthy individuals (Figure S4). Finally, the study results warrant a comparison of potential vaccine-associated side effects, which were not systematically captured in this study (the questionnaire involved questions on severe vaccine-related adverse events only; Table S1). We were also unable to systematically assess disease activity, however recent studies support the safety of mRNA anti-SARS-CoV2 vaccines in patients and report on infrequent flares of the underlying rheumatic disease (39, 40).

In conclusion, our results suggest that in patients with IRD, who are at risk of a poor vaccine response, two-dose vaccination with mRNA-1273 versus BNT162b2 results in higher peak anti-S1 levels, even more so in elderly patients, and longer antibody persistence. Immunogenicity is only a potential surrogate for vaccine effectiveness and future studies will show whether the observed difference in immunogenicity has an impact on breakthrough infections and whether it persists or levels out after further mRNA COVID-19 vaccine doses.

Data availability statement

Study-related data can be made available from the SCQM Foundation according to the SCQM Rules of Research after the publication of all study-related research objectives. Researchers interested in further analyzing the data resulting from this study can contact the SCQM Foundation (scqm@hin.ch). Data can only be used for scientific research. SCQM is an ongoing, long-term registry with no end date for data collection and data provision.

Ethics statement

This study involving human participants was reviewed and approved by the Geneva Ethics Committee. Patients provided their written informed consent to participate in this study.

Author contributions

CR was involved in project administration, funding acquisition, supervision, conceptualization, investigation, methodology, formal analysis, visualization, and writing the original manuscript draft. CB was involved in the study conceptualization, formal analysis, and writing of the original manuscript draft. AC was involved in funding acquisition, conceptualization, and reviewing & editing of the manuscript. CP was involved in data curation, software, methodology, formal analysis, visualization, and reviewing & editing of the manuscript. DA, PL, and NV contributed to resources, investigation, validation, and reviewing & editing of the manuscript. TM contributed to project administration, supervision, funding acquisition, resources, investigation, data curation, and reviewing & editing of the manuscript. MR was involved in conceptualization, formal analysis, methodology, and reviewing & editing of the manuscript. AS contributed to the conceptualization, and reviewing & editing of the manuscript. IvL and JS were patient representatives involved in conceptualization and reviewing & editing of the manuscript. KL, BM, and AF contributed to conceptualization, and reviewing & editing of the manuscript. AR-R was the principal investigator involved in funding acquisition, study conceptualization, formal analysis, and writing the original manuscript draft. All authors contributed to the article and approved the submitted version.

Funding

This study was investigator-initiated and received independent financial support from an anonymous donation from a research foundation and Moderna Switzerland GmbH. The study sponsors had no role in the study design or in the collection, analysis and interpretation of the data, the writing of the manuscript or the decision to submit the manuscript for publication. The following pharmaceutical industries financially support the SCQM: Abbvie, iQone Healthcare, Janssen, Eli Lilly, MSD Merck Sharp & Dohme, Novartis, Pfizer, Samsung Bioepis, Sandoz, and Biogen.

Acknowledgments

A list of rheumatology offices and hospitals contributing to the SCQM registries can be found on www.scqm.ch/institutions. The SCQM thanks the patients for their participation in this study.

Conflict of interest

KL reports personal fees from Gilead-Galapagos, Pfizer, Viatris, Celltrion, outside of the submitted work. AF has received research support from Abbvie, Eli-Lilly, Galapagos, and Pfizer outside of the submitted work, and consultancies or speaker honoraria for Abbvie, BMS, Eli-Lilly, Gilead, Pfizer, Sanofi, and UCB outside of the submitted work. AR-R reports honoraria for consultation and lectures from Abbvie, Amgen, Pfizer, Gilead, Novartis, Janssen, Eli-Lilly, Sanofi, Roche, UCB, BMS outside of the submitted work.

The remaining authors declare that the research was conducted in the absence of any commercial or financial

relationships that could be construed as a potential conflict of interest.

Publisher's note

All claims expressed in this article are solely those of the authors and do not necessarily represent those of their affiliated organizations, or those of the publisher, the editors and the reviewers. Any product that may be evaluated in this article, or claim that may be made by its manufacturer, is not guaranteed or endorsed by the publisher.

Supplementary material

The Supplementary Material for this article can be found online at: https://www.frontiersin.org/articles/10.3389/fimmu.2022.1016927/full#supplementary-material

References

1. Grainger R, Kim AHJ, Conway R, Yazdany J, Robinson PC. COVID-19 in people with rheumatic diseases: risks, outcomes, treatment considerations. *Nat Rev Rheumatol* (2022) 18:191–204. doi: 10.1038/S41584-022-00755-X

2. Conway R, Grimshaw AA, Konig MF, Putman M, Duarte-García A, Tseng LY, et al. SARS-CoV-2 infection and COVID-19 outcomes in rheumatic diseases: a systematic literature review and meta-analysis. *Arthritis Rheumatol (Hoboken NJ)* (2022) 74:766–75. doi: 10.1002/ART.42030

3. Embi PJ, Levy ME, Naleway AL, Patel P, Gaglani M, Natarajan K, et al. Effectiveness of 2-dose vaccination with mRNA COVID-19 vaccines against COVID-19–associated hospitalizations among immunocompromised adults — nine states, January–September 2021. *MMWR Morb Mortal Wkly Rep* (2021) 70:1553–9. doi: 10.15585/MMWR.MM7044E3

4. Deepak P, Kim W, Paley MA, Yang M, Carvidi AB, Demissie EG, et al. Effect of immunosuppression on the immunogenicity of mRNA vaccines to SARS-CoV-2. *A prospective cohort study. Ann Intern Med* (2021) 174:1572–85. doi: 10.7326/M21-1757

5. Wieske L, van Dam KPJ, Steenhuis M, Stalman EW, Kummer LYL, van Kempen ZLE, et al. Humoral responses after second and third SARS-CoV-2 vaccination in patients with immune-mediated inflammatory disorders on immunosuppressants: a cohort study. *Lancet Rheumatol* (2022) 4:e338–e350. doi: 10.1016/s2665-9913(22)00034-0

6. Lee ARYB, Wong SY, Chai LYA, Lee SC, Lee MX, Muthiah MD, et al. Efficacy of COVID-19 vaccines in immunocompromised patients: Systematic review and meta-analysis. *BMJ* (2022) 376:e068632. doi: 10.1136/BMJ-2021-068632

7. Furer V, Eviatar T, Zisman D, Peleg H, Paran D, Levartovsky D, et al. Immunogenicity and safety of the BNT162b2 mRNA COVID-19 vaccine in adult patients with autoimmune inflammatory rheumatic diseases and in the general population : A multicentre study. *Ann Rheum Dis* (2021) 80:1330–8. doi: 10.1136/annrheumdis-2021-220647

8. Ahmed S, Mehta P, Paul A, Anu S, Cherian S, Shenoy V, et al. Postvaccination antibody titres predict protection against COVID-19 in patients with autoimmune diseases: Survival analysis in a prospective cohort. *Ann Rheum Dis* (2022) 0:1–7. doi: 10.1136/annrheumdis-2021-221922

9. Boekel L, Stalman EW, Wieske L, Hooijberg F, van Dam KPJ, Besten YR, et al. Breakthrough SARS-CoV-2 infections with the delta (B.1.617.2) variant in vaccinated patients with immune-mediated inflammatory diseases using immunosuppressants: A substudy of two prospective cohort studies. *Lancet Rheumatol* (2022) 4:e417–29. doi: 10.1016/S2665-9913(22)00102-3

10. Furer V, Eviatar T, Freund T, Peleg H, Paran D, Levartovsky D, et al. Immunogenicity induced by two and three doses of the BNT162b2 mRNA vaccine in patients with autoimmune inflammatory rheumatic diseases and immunocompetent controls: A longitudinal multicentre study. *Ann Rheum Dis* (2022), annrheumdis–2022-222550. doi: 10.1136/ARD-2022-222550

11. Venerito V, Stefanizzi P, Fornaro M, Cacciapaglia F, Tafuri S, Perniola S, et al. Immunogenicity of BNT162b2 mRNA SARS-CoV-2 vaccine in patients with psoriatic arthritis on TNF inhibitors. *RMD Open* (2022) 8:e001847. doi: 10.1136/RMDOPEN-2021-001847

12. Rabinowitz KM, Navon M, Edelman-Klapper H, Zittan E, Bar-Gil Shitrit A, Goren I, et al. Anti-TNFα treatment impairs long-term immune responses to COVID-19 mRNA vaccine in patients with inflammatory bowel diseases. *Vaccines* (2022) 10:1186. doi: 10.3390/VACCINES10081186

13. Abani O, Abbas A, Abbas F, Abbas M, Abbasi S, Abbass H, et al. Casirivimab and imdevimab in patients admitted to hospital with COVID-19 (RECOVERY): a randomised, controlled, open-label, platform trial. *Lancet* (2022) 399:665–76. doi: 10.1016/S0140-6736(22)00163-5

14. Goulenok T, Delaval L, Delory N, François C, Papo T, Descamps D, et al. Pre-exposure anti-SARS-CoV-2 monoclonal antibodies in severely immunocompromised patients with immune-mediated inflammatory diseases. *Lancet Rheumatol* (2022) 4:e458–e461. doi: 10.1016/S2665-9913(22)00099-6

15. Pardi N, Hogan MJ, Porter FW, Weissman D. mRNA vaccines — a new era in vaccinology. *Nat Rev Drug Discovery* (2018) 17:261–79. doi: 10.1038/nrd.2017.243

16. Self WH, Tenforde MW, Rhoads JP, Gaglani M, Ginde AA, Douin DJ, et al. Comparative effectiveness of moderna, pfizer-BioNTech, and janssen (Johnson & Johnson) vaccines in preventing COVID-19 hospitalizations among adults without immunocompromising conditions - united states, march-august 2021. *MMWR Morb Mortal Wkly Rep* (2021) 70:1337–43. doi: 10.15585/MMWR.MM7038E1

17. Dickerman BA, Gerlovin H, Madenci AL, Kurgansky KE, Ferolito BR, Figueroa Muñiz MJ, et al. Comparative effectiveness of BNT162b2 and mRNA-1273 vaccines in U.S. veterans. *N Engl J Med* (2022) 386:105–15. doi: 10.1056/NEJMOA2115463

18. Steensels D, Pierlet N, Penders J, Mesotten D, Heylen L. Comparison of SARS-CoV-2 antibody response following vaccination with BNT162b2 and mRNA-1273. *JAMA* (2021) 326:1533–5. doi: 10.1001/JAMA.2021.15125

19. Frey S, Connolly CM, Chiang TPY, Teles M, Alejo JL, Boyarsky BJ, et al. Antibody kinetics in patients with rheumatic diseases after SARS-CoV-2 mRNA vaccination. *Lancet Rheumatol* (2021) 3:e753–4. doi: 10.1016/S2665-9913(21)00282-4

20. Mitchell J, Connolly CM, Chiang TPY, Alejo JL, Werbel WA, Segev DL, et al. Comparison of SARS-CoV-2 antibody response after 2-dose mRNA-1273 vs BNT162b2 vaccines in incrementally immunosuppressed patients. *JAMA Netw Open* (2022) 5:e2211897–e2211897. doi: 10.1001/JAMANETWORKOPEN.2022.11897

21. SCQM Foundation. *The "mySCQM" patient app* . Available at: https://www.scqm.ch/patienten/patienten-apps/ (Accessed June 14, 2022).

22. Kanji JN, Bailey A, Fenton J, Robbin Lindsay L, Dibernardo A, Toledo NP, et al. Stability of SARS-CoV-2 IgG in multiple laboratory conditions and blood sample types. *J Clin Virol* (2021) 142:104933. doi: 10.1016/J.JCV.2021.104933

23. Meyer B, Torriani G, Yerly S, Mazza L, Calame A, Arm-Vernez I, et al. Validation of a commercially available SARS-CoV-2 serological immunoassay. *Clin Microbiol Infect* (2020) 26:1386. doi: 10.1016/J.CMI.2020.06.024

24. Hothorn T, Lohse T, Rohrmann S, Faeh D. Continuous outcome logistic regression for analyzing body mass index distributions. *F1000Research* (2017) 6:1933. doi: 10.12688/F1000RESEARCH.12934.1

25. Edara V-V, Pinsky BA, Suthar MS, Lai L, Davis-Gardner ME, Floyd K, et al. Infection and vaccine-induced neutralizing-antibody responses to the SARS-CoV-2 B.1.617 variants. *N Engl J Med* (2021) 385:664–6. doi: 10.1056/NEJMC2107799

26. Jahrsdörfer B, Groß R, Seidel A, Wettstein L, Ludwig C, Schwarz T, et al. Characterization of the SARS-CoV-2 neutralization potential of COVID-19-convalescent donors. *J Immunol* (2021) 206:2614–22. doi: 10.4049/JIMMUNOL.2100036

27. Moor MB, Suter-Riniker F, Horn MP, Aeberli D, Amsler J, Möller B, et al. Humoral and cellular responses to mRNA vaccines against SARS-CoV-2 in patients with a history of CD20 b-cell-depleting therapy (RituxiVac): An investigator-initiated, single-centre, open-label study. *Lancet Rheumatol* (2021) 3:e789–97. doi: 10.1016/S2665-9913(21)00251-4

28. Haberman RH, Herati R, Simon D, Samanovic M, Blank RB, Tuen M, et al. Methotrexate hampers immunogenicity to BNT162b2 mRNA COVID-19 vaccine in immune-mediated inflammatory disease. *Ann Rheum Dis* (2021) 80:1339–44. doi: 10.1136/annrheumdis-2021-220597

29. Fang E, Liu X, Li M, Zhang Z, Song L, Zhu B, et al. Advances in COVID-19 mRNA vaccine development. *Signal Transduct Target Ther* (2022) 7:1–31. doi: 10.1038/s41392-022-00950-y

30. Crooke SN, Ovsyannikova IG, Poland GA, Kennedy RB. Immunosenescence and human vaccine immune responses. *Immun Ageing* (2019) 16:25. doi: 10.1186/S12979-019-0164-9

31. DiazGranados CA, Dunning AJ, Kimmel M, Kirby D, Treanor J, Collins A, et al. Efficacy of high-dose versus standard-dose influenza vaccine in older adults. *N Engl J Med* (2014) 371:635–45. doi: 10.1056/NEJMOA1315727

32. Vargas JI, Jensen D, Martínez F, Sarmiento V, Peirano F, Acuña P, et al. Comparative efficacy of a high-dose vs standard-dose hepatitis b revaccination schedule among patients with HIV: A randomized clinical trial. *JAMA Netw Open* (2021) 4:e2120929. doi: 10.1001/JAMANETWORKOPEN.2021.20929

33. Cromer D, Steain M, Reynaldi A, Schlub TE, Wheatley AK, Juno JA, et al. Neutralising antibody titres as predictors of protection against SARS-CoV-2 variants and the impact of boosting: A meta-analysis. *Lancet Microbe* (2022) 3: e52–61. doi: 10.1016/S2666-5247(21)00267-6

34. Khoury DS, Cromer D, Reynaldi A, Schlub TE, Wheatley AK, Juno JA, et al. Neutralizing antibody levels are highly predictive of immune protection from symptomatic SARS-CoV-2 infection. *Nat Med* (2021) 27:1205–11. doi: 10.1038/s41591-021-01377-8

35. Feng S, Phillips DJ, White T, Sayal H, Aley PK, Bibi S, et al. Correlates of protection against symptomatic and asymptomatic SARS-CoV-2 infection. *Nat Med* (2021) 27:2032–40. doi: 10.1038/s41591-021-01540-1

36. Schmidt F, Muecksch F, Weisblum Y, Da Silva J, Bednarski E, Cho A, et al. Plasma neutralization of the SARS-CoV-2 omicron variant. *N Engl J Med* (2022) 386:599–601. doi: 10.1056/NEJMC2119641

37. Knitza J, Tascilar K, Vuillerme N, Eimer E, Matusewicz P, Corte G, et al. Accuracy and tolerability of self-sampling of capillary blood for analysis of inflammation and autoantibodies in rheumatoid arthritis patients-results from a randomized controlled trial. *Arthritis Res Ther* (2022) 24:125. doi: 10.1186/S13075-022-02809-7

38. Farroni C, Picchianti-Diamanti A, Aiello A, Nicastri E, Laganà B, Agrati C, et al. Kinetics of the b- and T-cell immune responses after 6 months from SARS-CoV-2 mRNA vaccination in patients with rheumatoid arthritis. *Front Immunol* (2022) 13:846753/BIBTEX. doi: 10.3389/FIMMU.2022.846753/BIBTEX

39. Machado PM, Lawson-Tovey S, Strangfeld A, Mateus EF, Hyrich KL, Gossec L, et al. Safety of vaccination against SARS-CoV-2 in people with rheumatic and musculoskeletal diseases: Results from the EULAR coronavirus vaccine (COVAX) physician-reported registry. *Ann Rheum Dis* (2022) 81:695–709. doi: 10.1136/ANNRHEUMDIS-2021-221490

40. Fornaro M, Venerito V, Iannone F, Cacciapaglia F. Safety profile and low risk of disease relapse after BNT162b2 mRNA SARS-COV-2 vaccination in patients with rare rheumatic diseases. *J Rheumatol* (2022) 49:334–5. doi: 10.3899/JRHEUM.210863

frontiers | Frontiers in Immunology

TYPE Original Research
PUBLISHED 08 November 2022
DOI 10.3389/fimmu.2022.948335

OPEN ACCESS

EDITED BY
Jennifer Dan,
University of California, San Diego,
United States

REVIEWED BY
Matthew Siggins,
Imperial College London,
United Kingdom
Wayne Robert Thomas,
University of Western Australia,
Australia
Shyh Poh Teo,
Raja Isteri Pengiran Anak Saleha
Hospital, Brunei

*CORRESPONDENCE
Kapil Bahl
Kapil.bahl@modernatx.com

†These authors have contributed
equally to this work

SPECIALTY SECTION
This article was submitted to
Vaccines and Molecular Therapeutics,
a section of the journal
Frontiers in Immunology

RECEIVED 19 May 2022
ACCEPTED 13 October 2022
PUBLISHED 08 November 2022

CITATION
Garcia-Dominguez D, Henry C, Ma L,
Jani H, Amato NJ, Manning T, Freyn A,
Davis H, Hsiao CJ, Li M, Koch H,
Elbashir S, DiPiazza A, Carfi A,
Edwards D and Bahl K (2022)
Altering the mRNA-1273 dosing
interval impacts the kinetics,
quality, and magnitude of immune
responses in mice.
Front. Immunol. 13:948335.
doi: 10.3389/fimmu.2022.948335

Altering the mRNA-1273 dosing interval impacts the kinetics, quality, and magnitude of immune responses in mice

Dario Garcia-Dominguez†, Carole Henry†, LingZhi Ma, Hardik Jani, Nicholas J. Amato, Taylor Manning, Alec Freyn, Heather Davis, Chiaowen Joyce Hsiao, Mengying Li, Hillary Koch, Sayda Elbashir, Anthony DiPiazza, Andrea Carfi, Darin Edwards and Kapil Bahl*

Moderna, Inc., Cambridge, MA, United States

For a vaccine to achieve durable immunity and optimal efficacy, many require a multi-dose primary vaccination schedule that acts to first "prime" naive immune systems and then "boost" initial immune responses by repeated immunizations (ie, prime-boost regimens). In the context of the global coronavirus disease 2019 (COVID-19) pandemic caused by severe acute respiratory syndrome coronavirus 2 (SARS-CoV-2), 2-dose primary vaccination regimens were often selected with short intervals between doses to provide rapid protection while still inducing robust immunity. However, emerging post-authorization evidence has suggested that longer intervals between doses 1 and 2 for SARS-CoV-2 vaccines may positively impact robustness and durability of immune responses. Here, the dosing interval for mRNA-1273, a messenger RNA based SARS-CoV-2 vaccine administered on a 2-dose primary schedule with 4 weeks between doses, was evaluated in mice by varying the dose interval between 1 and 8 weeks and examining immune responses through 24 weeks after dose 2. A dosing interval of 6 to 8 weeks generated the highest level of antigen-specific serum immunoglobulin G binding antibody titers. Differences in binding antibody titers between mRNA-1273 1 μg and 10 μg decreased over time for dosing intervals of ≥4 weeks, suggesting a potential dose-sparing effect. Longer intervals (≥4 weeks) also increased antibody-dependent cellular cytotoxicity activity and numbers of antibody-secreting cells (including long-lived plasma cells) after the second dose. An interval of 6 to 8 weeks elicited the strongest CD8+ T-cell responses, while an interval of 3 weeks elicited the strongest CD4+ T-cell response. Overall, these results suggest that in a non-pandemic setting, a longer interval (≥6 weeks) between the doses of the primary series for mRNA-1273 may induce more durable immune responses.

KEYWORDS

SARS-CoV-2, mRNA-1273, COVID-19, dosing interval, dosing regimen

Introduction

Vaccination aims to provide protection against infection and/or disease when an individual is subsequently exposed to the causative pathogen (1). Achievement of vaccine-mediated protection relies on the ability of a vaccine to elicit potent and durable immune responses to a specific pathogen (1); this can be affected by a multitude of vaccine-specific variables, including the immunizing antigen, antigen-delivery system (ie, nucleic acid, viral vector, recombinant protein, or inactivated pathogen), immunization route, adjuvant, dosing level, and regimen, as well as characteristics of the vaccine recipient, including prior infection, race/ethnicity, age, and gender (2, 3).

Vaccine-mediated protection often correlates with the magnitude of antibody responses (1, 4, 5), with T cells playing a potentially equally important role, particularly in the context of waning antibody responses (6). Upon pathogen exposure after vaccination, antigen-specific B and T cells increase in frequency and differentiate into antigen-specific memory cells (ie, immunological memory), enabling the immune system to respond quickly and robustly to a re-encountered antigen (1, 7–9).

To establish immunity, vaccines are typically administered on a multi-dose primary vaccination schedule, first to "prime" a naive immune system and subsequently to "boost" immune responses through repeated administrations (ie, prime-boost regimens) (10, 11). However, defining the ideal interval between the doses of the primary vaccination series remains difficult and is not well understood. Current recommendations from the World Health Organization indicate that routine immunizations among children worldwide typically have a minimum 4-week interval between doses 1 and 2 (12); however, the exact interval can vary by vaccine type, antigen, regional location, and population age, among other factors. Understanding how the dosing interval impacts vaccine-elicited immune responses is thus of significant importance for ensuring robust and durable vaccine-mediated protection.

Since the emergence of severe acute respiratory syndrome coronavirus 2 (SARS-CoV-2) and the ensuing coronavirus disease 2019 (COVID-19) pandemic, several SARS-CoV-2 vaccines have been developed, including mRNA-1273 (SPIKEVAX; Moderna, Inc., Cambridge, MA, USA), an mRNA-based COVID-19 vaccine encoding for the SARS-CoV-2 spike protein (13). In the pivotal phase 3 clinical trial (NCT04470427), mRNA-1273 100 µg administered intramuscularly with a 4-week interval between dose 1 and 2 resulted in 93.2% efficacy against disease (14). However, emerging studies on other 2-dose SARS-CoV-2 vaccines have indicated that extending the dose interval beyond the standard 4-week schedule improved antibody and B-cell responses as well as vaccine efficacy and effectiveness, but reduced interferon γ (IFNγ)-producing T-cell responses (15–19).

We therefore evaluated how the interval between dose 1 and dose 2 of mRNA-1273 affects vaccine-elicited immunogenicity in mice, assessing multiple aspects of the kinetics, magnitude, and durability of mRNA-1273–induced immune responses across dosing intervals (from 1-8 weeks), including characterizing antigen-specific antibody and T-cell responses as well as long-term memory cell maintenance.

Abbreviations: ADCC, antibody-dependent cellular toxicity; ASC, antibody secreting cell; COVID-19, coronavirus disease 2019; ELISA, enzyme-linked immunosorbent assay; FBS, fetal bovine serum; GAM, generalized additive model; IFN, interferon; Ig, immunoglobulin; IL, interleukin; LLPC, long lived plasma cell; LNP, lipid nanoparticle; PBS, phosphate-buffered saline; PEG, polyethylene glycol; PerCP, peridinin-chlorophyll-protein; RBD, receptor binding domain; S-2P, SARS-CoV-2 spike protein with 2 proline mutations; SARS-CoV-2, severe acute respiratory syndrome coronavirus 2; Th1, T helper type 1; TMB, 3,3',5,5'-tetramethylbenzidine; TNF, tumor necrosis factor.

Materials and methods

Mice

Specific pathogen-free, 6- to 8-week-old BALB/c mice were purchased from Charles River Laboratories and housed in microisolator cages in a BSL-2 facility with sterile water and food provided ad libitum. Animal experiments were carried out in compliance with approval from the Institutional Animal Care and Use Committee of Moderna, Inc. Mice were immunized with mRNA-1273 1 µg or 10 µg (preclinical batch [non-GMP]) diluted in phosphate-buffered saline (PBS) 50 µL *via* intramuscular injection into the same hind leg for both dose 1 and dose 2. Mice (n=8-10 mice per group) were immunized with 2 doses of mRNA-1273 (1 µg or 10 µg) at varying dosing intervals (1-, 2-, 3-, 4-, 6-, or 8-week intervals between doses; Figure 1); for the purposes of comparing to a single dose regimen, an additional group of mice received only a single mRNA-1273 immunization at the time of dose 2 (prime-only group). For immunogenicity assessments, samples were collected as detailed in Figure 1.

Preclinical mRNA and lipid nanoparticle production

A sequence-optimized mRNA encoding the prefusion-stabilized SARS-CoV-2 spike protein with 2 proline mutations (S-2P) was synthesized *in vitro* as previously described (20). The mRNA then underwent oligo-dT affinity purification, buffer exchange by tangential flow filtration into sodium acetate (pH 5.0), sterile filtration, and stored at −20°C until use. As described previously (21), mRNA was lipid nanoparticle (LNP) encapsulated through a modified ethanol-drop nanoprecipitation process.

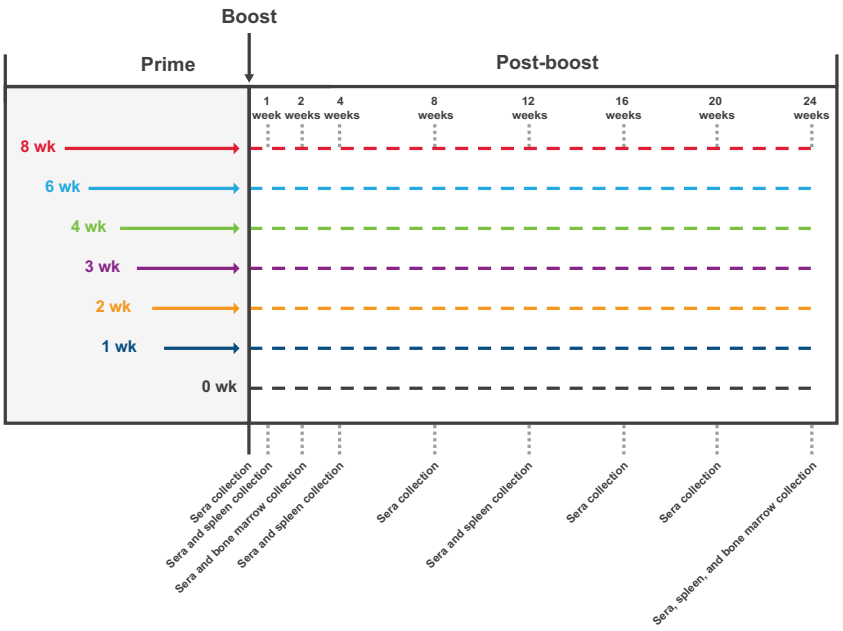

FIGURE 1
Study Design. The impact of the dosing interval on mRNA-1273 vaccine immunogenicity was evaluated by administering 2 doses of mRNA-1273 (1 µg or 10 µg) to mice on a schedule of 1-, 2-, 3-, 4-, 6-, or 8-week intervals between doses; a prime-only group (only administered first dose of mRNA-1273 at time of dose 2) was also evaluated for comparison purposes. Sera were collected from mice (n=8-10 per group) before dose 2 and 1, 2, 4, 8, 12, 16, 20, and 24 weeks following dose 2. Spleens were collected 1, 4, 12, and 24 weeks after dose 2 from a subgroup of mice (n=8-10 per group) administered mRNA-1273 10 µg; bone marrow samples were collected 2 and 24 weeks after dose 2 from the same subgroup of mice. mRNA, messenger RNA.

Ionizable, structural, helper, and polyethylene glycol (PEG) lipids were mixed at a 2.5:1 ratio with mRNA (lipids:mRNA) in acetate buffer (pH 5.0). The drug product was not intended for clinical use; the product underwent analytical characterization (ie, mRNA purity, double-stranded RNA content, particle size and polydispersity determination, encapsulation, osmolality, pH, endotoxin, and bioburden) and was deemed acceptable for *in vivo* study.

S-2P–specific enzyme-linked immunosorbent assay

Microtiter plates were coated with S-2P protein 1 µg/mL (GenScript), corresponding to the spike protein of the Wuhan-Hu-1 virus stabilized with 2 proline mutations, and incubated overnight at 4°C. Plates were then washed 4 times with PBS/0.05% Tween-20 and blocked for 1.5 hours at 37°C using SuperBlock (Thermo). After washing, 5-fold serial dilutions of mouse serum were added (assay diluent: TBS + 5% BSA + 0.05% Tween-20 [Boston Bioproducts]) and incubated for 2 hours at 37°C. Plates were washed and then horseradish peroxidase-conjugated goat anti-mouse immunoglobulin G (IgG) (Southern Biotech) was added at a 1:30,000 dilution in assay diluent. After incubation for 1 hour at 37°C, plates were washed and bound antibody was detected with a 3,3',5,5'-tetramethylbenzidine (TMB) substrate (Thermo). After a 10-minute incubation at room temperature, TMB stop solution (Invitrogen) was added to stop the reaction and absorbance at 450 nm was measured. Titers were determined using a 4-parameter logistic curve fit in Prism v.8 (GraphPad 112 Software, Inc.), defined as the reciprocal dilution at approximately optical density 450 = 1 (normalized to a mouse standard on each plate).

Anti-polyethylene glycol enzyme-linked immunosorbent assay

Carboxy-modified latex beads (Molecular Probes, Life Technologies) were aliquoted to 100 µL per tube and washed 3 times with 50 mM MES 1 mM EDTA (pH 6.0). Beads were coupled with 1-ethyl-3-(3-dimethylaminopropyl) carbodiimide HCl 5 mg (Thermo Fisher Scientific) on a plate shaker at maximum rpm for 15 minutes at room temperature. Coupled beads were incubated with PEG2K-DMG 400 µg in PBS for 2 hours (at room temperature shaking at 800 rpm), washed 2 times with PBS, and resuspended in PBS + 2% BSA for either direct usage or storage at 4°C. PEG-coupled beads were

incubated with serum samples diluted 1:100 at room temperature for 45 minutes. Beads were then washed and incubated with either anti-mouse IgM APC (1:1000; clone Il-41; BD Pharmingen) or anti-mouse IgG Alexa Fluor 488 (1:1000; polyclonal; Abcam) for 30 minutes in the dark. After washing, beads were resuspended in PBS 100 µL + 2% BSA for analysis on a ThermoFisher Scientific Attune NXT. Forward scatter and side scatter gatings were adjusted so that the field captured the 10-µm PEG-coupled carboxy-modified latex beads; 60 µL of the sample was collected at a speed of 200 µL/s. Bead population was gated around in FlowJo 10.8, eliminating debris, and median fluorescence intensity for either APC or FITC was applied to appropriate serum samples or controls. Antibody levels for respective IgM and IgG samples were quantified using a standard curve obtained with a monoclonal mouse anti-PEG IgM (AGP4-PABM-A; Academia Sinica, Taipei, Taiwan) or a monoclonal mouse anti-PEG IgG (3.3-PABG-A; Academia Sinica, Taipei, Taiwan).

B-cell ELISpot

Ninety-six well plates were incubated overnight at 4°C with SARS-CoV-2 S-2P protein 2 µg/mL (GenScript). On the next day, plates were washed 3 times with PBS and blocked for 2 hours at 37°C with RPMI complete medium (RPMI + 10% fetal calf serum + 1% penicillin/streptomycin + 1% HEPES + 1% L-Glutamine). Freshly isolated splenocytes or bone marrow cells were washed 3 times then resuspended in RPMI complete medium, added to each plate, and serially diluted 2-fold down the plate. After overnight incubation at 37°C, plates were washed extensively with PBS + 0.05% Tween-20 and antibody-secreting cells (ASCs) were detected with biotinylated anti-mouse IgG (1:10,000, Southern Biotech; 1030-08), followed by streptavidin-alkaline phosphatase (1:500, Southern Biotech; 7105-04), and developed with nitroblue tetrazolium–5-bromo-4-chloro-3-indolylphosphate (Thermo Scientific). Plates were imaged (Cellular Technologies) and spots were manually counted to determine the number of ASCs.

T-cell assessments by intracellular cytokine staining

A gentleMACS tissue dissociator (Miltenyi Biotec) was used to generate mononuclear single-cell suspensions from BALB/c mouse whole spleens. Following tissue dissociation, cells were sieved through a 70-µm filter. Cells from each mouse were resuspended in R10 media (RPMI 1640 medium supplemented with L-glutamine, penicillin/streptomycin, and 10% HI–fetal bovine serum [FBS]) and incubated at 37°C for 6 hours with protein transport inhibitors GolgiStop and GolgiPlug (BD Biosciences) and 1 µg/mL spike glycoprotein peptide pools (JPT; PM–WCPV-S-1; divided into peptide pools, S1 and S2), 1 µg/mL spike RBD peptide pool (JPT; PM-WCPV-S-RBD), or 1 µg/mL spike NTD peptide pool (JPT; custom order). All pools were derived from the Wuhan-Hu-1 strain and contained peptides of 15 amino acids in length overlapped by 11 amino acids (70% purity). Control cells were incubated with an equivalent concentration of DMSO as contained in the peptide pools. Cells were washed with PBS then stained with LIVE/DEAD Fixable Aqua Dead Cell Stain (Invitrogen) for 20 minutes at room temperature. Cells were subsequently washed with FC stain buffer (PBS supplemented with 3% HI-FBS and 0.05% sodium azide) and resuspended in Becton, Dickinson and Company (BD) Fc Block (clone 2.4G2) for 5 minutes at room temperature. Staining was performed at 4°C for 30 minutes with a surface stain cocktail of the following antibodies: CD4 APC (Biolegend; 100412, clone GK1.5), CD8 Alexa Fluor 700 (Biolegend; 126618, clone YTS156.7.7), and CD44 BV421 (BD; 563970, clone IM7). After this step, cells were washed with FC buffer and then fixed and permeabilized using the BD Cytofix/Cytoperm kit according to the manufacturer's instructions. Cells were washed with permeabilized and wash solution and then intracellular staining was performed at 4°C for 30 minutes using the following cocktail of antibodies in 1X permeabilized and wash solution: IFNγ APC-Cy7 (Biolegend; 505850, clone XMG1.2), tumor necrosis factor α (TNFα) PE-Dazzle594 (Biolegend; 506345, clone MP6-XT22), interleukin-2 (IL-2) BV711 (Biolegend; 503837, clone JES6-5H4), IL-4 PE-Cy7 (Biolegend; 504117, clone 11B11), IL-5 PE (Biolegend; 504303, clone TRFK5), IL-9 PerCP-Cy5.5 (Biolegend; 514112, clone RM9A4), IL-10 BV605 (Biolegend; 505031, clone JES5-16E3), and IL-13 Alexa Fluor 488 (ThermoFisher; 53-7133-82, clone eBio13A). Cells were then washed with permeabilized and wash solution, filtered through a 96-well plate 30-µm filter (Pall), and resuspended in FC stain buffer prior to running on a LSR Fortessa flow cytometer (BD). Analysis was done using FlowJo software (version 10.7.1). Background cytokine expression in the control cells was subtracted from that measured in the peptide pools for each individual mouse.

ADCC reporter assay

CHO-K1 cells constitutively expressing SARS-CoV-2 S protein (GenScript) were cultured in Ham's F-12K media containing 10% FBS and puromycin 8 µg/mL (Gibco). Cells were seeded at 1.5E4 cells/well in white-walled 96-well dishes (Corning) and incubated overnight at 37°C and 5% CO_2. Serum was serially diluted in assay medium (RPMI 16-40 containing 4% Ultra-low IgG FBS [Gibco]), including a high-positive control and wells lacking serum as a negative control. Media was aspirated from the wells and 25 µL of assay medium was added to each well; 25 µL of diluted serum was then added to corresponding wells. Jurkat cells expressing murine FcγRIV with

an NFAT-driven firefly luciferase reporter gene (Promega) were diluted in warm assay medium and 25 µL of the cell solution was added to each well. Plates were incubated for 6 hours at 37°C and 5% CO_2 and then removed from the incubator to rest at room temperature for 10 to 15 minutes. Room temperature BioGlo luciferase substrate (Promega) was added at 75 µL per well and plates were read immediately on a Pherastar FS plate reader (BMG Labtech). Data were analyzed using Prism 9 (GraphPad) and were processed by subtracting the average plus 3 times the standard deviation of negative wells and normalizing to the average of positive control wells. Curves were fit to the data using the [Inhibitor] versus response – Variable slope (4 parameters) function, and area under the curve was determined and reported for each group.

Statistical modeling and hypothesis testing

A generalized additive model (GAM) (22) was applied to enzyme-linked immunosorbent assay (ELISA) S-specific IgG antibody titers, with a dose- and dosing interval group-specific smooth nonlinear trend in days, and 9-dimensional thin plate spline basis. Animal-specific random effects were included to estimate group-specific time curves after dose 2. Two-way and 3-way interactions of dose, days after dose 2, and dosing interval were included to allow for interval-varying effects of dose levels between days following dose 2. For hypothesis testing of ELISA titers, we opted for a linear mixed effect model and included days following dose 2 as a categorical variable. The linear mixed effect model and the GAM model of ELISA included similar covariates. mgcv R package (23) was used for GAM and lme4 (24) was used for linear mixed model (described in Supplementary Methods).

ADCC activity was modeled using a Bayesian GAM using brms R package (25, 26) with the default weakly informative priors. A Bayesian model was selected over a frequentist model as a better test for group-specific differences while accounting for heterogeneous variances due to days after dose 2 and simultaneous accounting for data points falling below limit of detection. Dose- and dosing interval-specific non-linear terms, as well as day, dose, and interval interactions, were used to predict ADCC activity. To capture the heterogeneous variance observed across days following dose 2, residual variance was estimated to change linearly in days after dose 2. See Supplementary Methods for details.

To compare anti-PEG IgM and IgG levels between dosing interval groups, a linear mixed model (lme4) was used separately for IgM or IgG levels, modeling the effect of dosing interval groups and dose levels on titers. For comparisons of spike-specific ASCs and LLPCs, we transformed ASC and LLPC counts/million cells using a Box-Cox transformation (27). Generalized linear regression was used to model the transformed count by $g(counts) = \beta_0 + \beta_1\ interval$ for both spleen and bone marrow data, where g(.) denotes the Box-Cox transformation.

For comparisons of cytokine polyfunctionality and spike-specific CD4+ and CD8+ T-cell IFNγ responses, we used zero-inflated beta regression models (28). Cytokine polyfunctionality thresholded composition data were analyzed (see Supplementary Methods for thresholding details). A separate model was fit for each cell type, peptide, and each type of polyfunctionality (ie, a separate model was fit to predict the proportion of single expressors, dual expressors, and triple expressors). The model was constructed using default link functions for all 3 components of the zero-inflated beta distribution in the gamlss (22, 28) R package. The dosing interval, days following dose 2, and their interactions were used as linear predictors for the mean component; the dosing interval was used as the linear predictor for the scale parameter σ. Zero-inflated beta regression was similarly used to model spike-specific CD4+ and CD8+ T-cell IFNγ responses (see Supplementary Methods for details).

Statistical analyses were conducted with R version 4.1.2 (29). Statistical comparisons were conducted using the emmeans package in R (30), with multivariate t adjustment at alpha level of 0.05, except when noted otherwise. Residual diagnostics and goodness-of-fit criteria were examined for all models to affirm satisfactory model fit.

Results

S2-P–specific serum binding antibody titers

To evaluate the impact of the dosing intervals on mRNA-1273 elicited immunogenicity, mice were immunized with 2 doses of mRNA-1273 (1 µg or 10 µg) on varying dosing schedules of 1-, 2-, 3-, 4-, 6-, or 8-week intervals between doses 1 and 2; a single dose group (administered dose 1 only at time of dose 2) was also evaluated for comparison purposes (Figure 1). S2-P–specific serum binding IgG antibody titers were evaluated through 24 weeks after dose 2. Because mRNA vaccines induce robust and long-lasting germinal center (GC) responses (31, 32), and the formation of memory B cells and LLPCs has been associated with durable humoral immune responses (33), we assessed the persistence of serum antibodies through 24 weeks after dose 2.

At 2 weeks following dose 2, all assessed dosing intervals of mRNA-1273 (1 µg or 10 µg dose levels) showed increased S2-P–specific antibody titers relative to titers before the second dose (Figure 2A; Figure S1), with largest fold changes observed for the 6- and 8-week intervals (Figure S2; Table S1; Figure S3). Increased antibody titers were also observed at 24 weeks following dose 2 for all dosing intervals except for the 2-week interval; for the 8-week

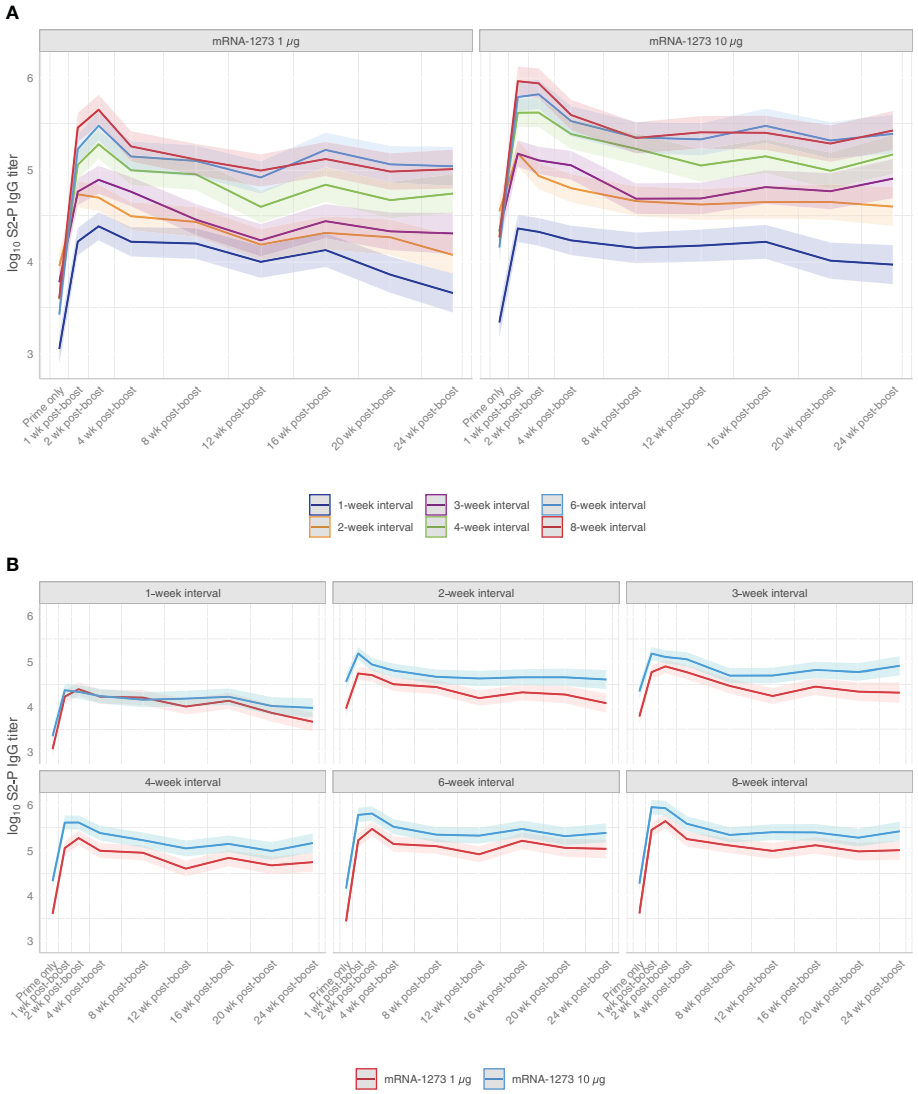

FIGURE 2
S2-P–specific Serum Binding IgG Antibody Titers. Predicted S2-P serum binding IgG antibody titers (with corresponding 95% CIs [shaded region]; based on GAM with days after dose 2 as a continuous variable [see Methods for details]) from before dose 2 through 24 weeks following dose 2 are presented according to **(A)** mRNA-1273 dosing level (1 μg or 10 μg) or by **(B)** dosing intervals (1-, 2-, 3-, 4-, 6-, or 8-week intervals between doses) with n=8-10 mice per group. Results of statistical comparisons between groups based on GAM are presented in Table S1 and Figure S3. Observed data at individual animal level are shown in Figure S1. CI, confidence interval; GAM, generalized additive model; IgG, immunoglobulin G; mRNA, messenger RNA.

interval, S2-P–specific serum-binding antibody titers at 24 weeks were approximately 30-fold and 10-fold higher relative to before dose 2 for mRNA-1273 1-μg and 10-μg dose levels, respectively (Figure S2). Throughout the 24-week period after dose 2, the 6- and 8-week intervals elicited the highest antibody titers, particularly in comparison to the shorter 1-, 2-, and 3-week intervals. Overall, S2-P–specific serum binding antibody titers after dose 2 were generally comparable between the 6- and 8-week intervals at all evaluated time points.

Across mRNA-1273 dose levels, S2-P–specific serum-binding antibody titers were higher at the 10-μg dose than 1-μg dose level at all time points following dose 2 for dosing intervals of ≥2 weeks (Figure 2B; Figure S1). However, differences in antibody titers between mRNA-1273 dose levels with ≥4-week intervals became progressively less observable over the 24-week study duration.

Antibody Fc-effector responses

Fc-functional antibody responses through 24 weeks after dose 2 of mRNA-1273 (1 μg or 10 μg dose levels) were evaluated using

a reporter assay for ADCC activity, a regulated antibody-centric immune response that is Fc-mediated (Figure S4). Antibody Fc-effector responses improved with longer dosing intervals (ie, 4-, 6-, and 8-week intervals), showing significantly higher activity than ≤3-week intervals at both the 1-µg and 10-µg dose levels (adjusted *P*-value <0.001; Figure 3; Table S2; Figure S5). In mice immunized with mRNA-1273 10 µg, antibody responses peaked 1 week after dose 2, with longer dosing intervals showing steadily waning responses through 24 weeks after dose 2.

Induction of S2-P–specific ASCs and LLPCs

To evaluate the impact of the mRNA-1273 dosing interval on S2-P–specific ASC and LLPC induction, mice were immunized with mRNA-1273 10 µg at varying times between dose 1 and 2 and spleens and bone marrow were collected after dose 2 (Figure 1). Based on ELISpot assay, 2 doses of mRNA-1273 10 µg administered on 6- and 8-week intervals induced the highest number of S2-P–specific ASCs in spleen 1 week following dose 2 (Figure 4; Table S3; Figure S6). At this time point, the number of S2-P–specific ASCs induced by the 6- and 8-week dosing intervals were generally similar and higher than shorter dosing intervals (≤4 weeks).

At 4 weeks and 24 weeks following dose 2, the 4-, 6-, and 8-week dosing intervals of mRNA-1273 10 µg induced the greatest number of S2-P–specific IgG ASCs (including LLPCs) in the bone marrow (Figure 4; Table S4; Figure S6), although notably, the number of ASCs induced by the 4-week interval declined from 4 weeks to 24 weeks following dose 2, which was not observed with the 6- and 8-week intervals.

Spike-specific CD4+ and CD8+ T-cell responses

Mice were immunized with 2 doses of mRNA-1273 10 µg at varying dosing intervals and spike-specific CD4+ and CD8+ T-cell responses were evaluated after dose 2. At 24 weeks after dose 2, the 3-week interval elicited the strongest CD4+ IFNγ response to the S2 peptide pool (Figure 5; Table S5; Figure S7), with a similar trend observed for IL-2 (Table S5; Figure S7), although responses overall were low. A 3-week interval between first and second doses elicited the highest percentage of polyfunctional CD4+ T helper type 1 (Th1) cells (adjusted *P*-value <0.05; Figure 5, Table S6; Figures S8, S9). Both the 6- and 8-week intervals produced the strongest CD8+ IFNγ response to the S1 peptide pool 24 weeks post-dose 2, which were significantly higher than those elicited by a 4-week interval (adjusted *P*-value <0.01; Figure 5; Table S7; Figure S10). A similar trend was also observed for IL-2 and TNF (Table S7; Figure S10). In CD8+ Th1 cells, the greatest percentage of polyfunctional cells was induced by a 6-week dosing interval of mRNA-1273 (Figure 5; Table S6; Figure S11).

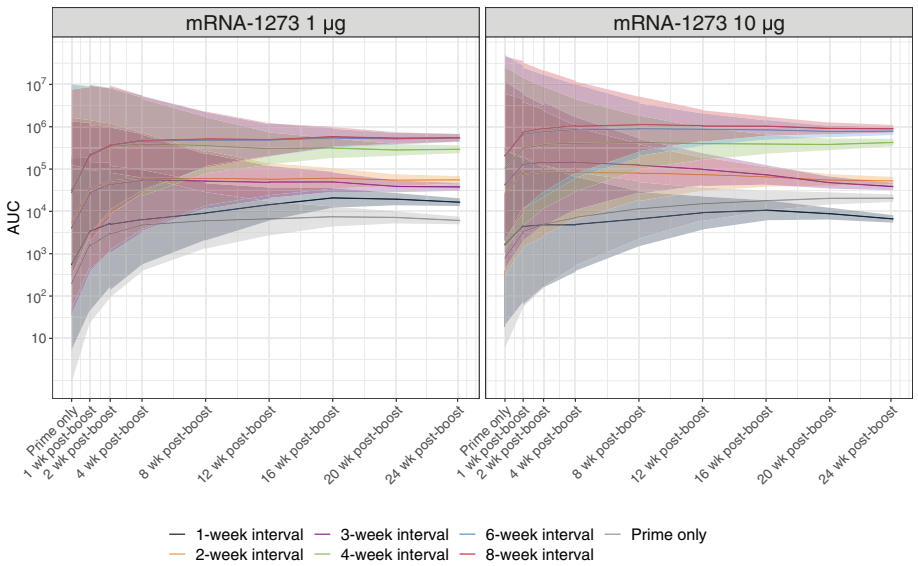

FIGURE 3
Antibody Fc-effector Function Responses. Antibody Fc-effector function was assessed using reporter cells expressing the murine FcγRIV. Predicted serum Fc-effector responses from before dose 2 through 24 weeks after dose 2 (with corresponding 95% CIs [shaded region]; based on a Bayesian GAM with days after dose 2 as a continuous variable [see Methods for details]) are presented by dosing interval (prime only, 1-, 2-, 3-, 4-, 6-, or 8-week intervals between doses) for 1-µg or 10-µg dosing levels (n=8-10 mice per group). Results of statistical comparisons between groups based on the Bayesian GAM are presented in Table S2 and Figure S5. Observed data at individual animal level are shown in Figure S4. AUC, area under the curve; CI, confidence interval; GAM, generalized additive model; mRNA, messenger RNA.

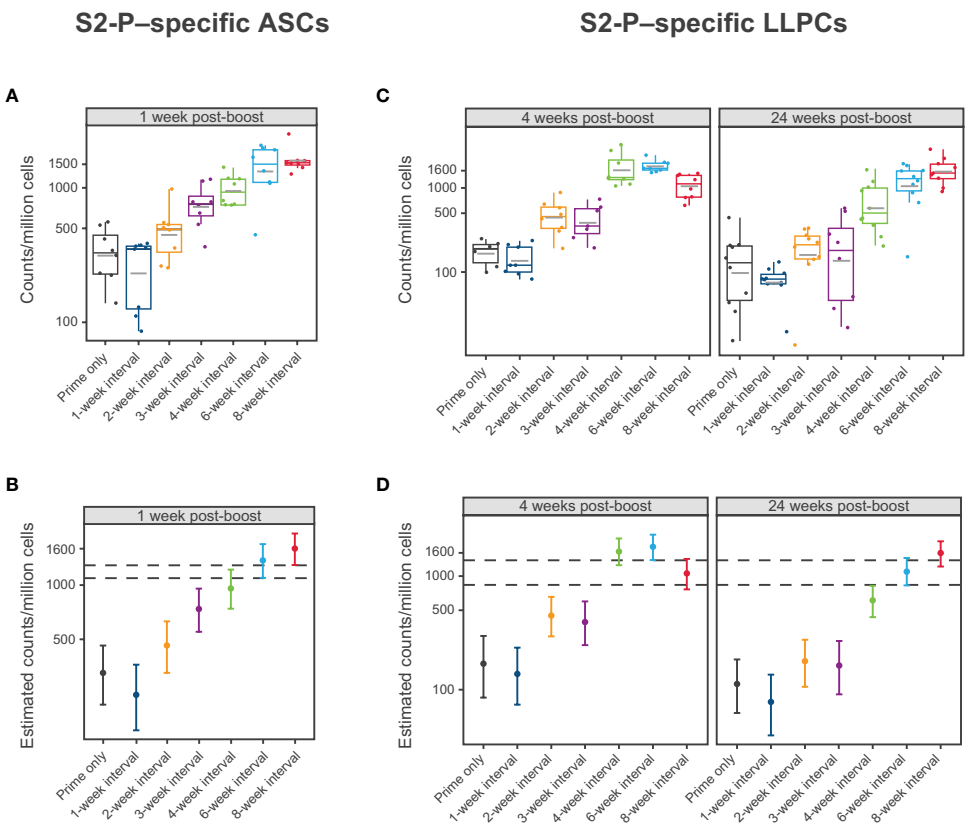

FIGURE 4
S2-P–specific Antibody Secreting Cells and Long-Lived Plasma Cells. **(A, B)** Levels of S2-P–specific ASCs 1 week following dose 2 of mRNA-1273 10 μg are presented by dosing intervals (prime only or 1-, 2-, 3-, 4-, 6-, or 8-week intervals between doses). Panel **(A)** presents individual animal-level data with dots corresponding to individual animals and grey horizontal lines denoting the average within each group. Panel **(B)** presents the estimated mean and associated 95% CIs based on a statistical model (see Methods), with error bars representing the 95% CI of the estimated mean. **(C, D)** Levels of S2-P–specific LLPCs 4 weeks and 24 weeks after dose 2 of mRNA-1273 10 μg are presented by dosing intervals (prime only or 1-, 2-, 3-, 4-, 6-, or 8-week intervals between doses). Individual animal-level data (dots corresponding to individual animals and grey horizontal line denoting the average within each group) are shown in panel **(C)**. Panel **(D)** presents the corresponding estimated means and associated 95% CIs based on a statistical model (see Methods), with error bars representing the 95% CI of the estimated mean (n=8-10 mice per group). Results of statistical comparisons between groups based on the statistical models are presented in Table S3, Table S4, and Figure S6. ASC, antibody-secreting cell; CI, confidence interval; LLPC, long-lived plasma cell; mRNA, messenger RNA.

Anti-PEG antibody levels

Polyethylene glycol is a hydrophilic, biocompatible polymer that is acknowledged to significantly reduce recognition and clearance of nanoparticles (34, 35). Nevertheless, the generation of anti-PEG antibodies has been associated with considerably faster clearance of PEG-containing drugs and nanocarrier systems upon repeated administration, potentially hindering drug product efficacy (36). Therefore, to evaluate whether elevated levels of anti-PEG antibodies were detected at shorter intervals, mice were immunized with dose 1 of mRNA-1273 (1-μg and 10-μg dose levels) at varying dosing intervals and antibodies to PEG (IgG and IgM) were evaluated before dose 2. Control mice were instead administered PBS. At both the 1-μg and 10-μg dose levels, anti-PEG antibodies (IgG and IgM) were significantly elevated relative to controls after dose 1 and prior to administering dose 2; the greatest anti-PEG antibody titers were observed in mice administered mRNA-1273 1 and 2 weeks (IgG and IgM) and 3 weeks (IgM only) prior to dose 2 (adjusted P-value < 0.05; Figure 6; Table S8; Figure S12), which is consistent with the lower levels of immunogenicity observed previously. No significant differences in anti-PEG (IgG and IgM) relative to control were observed for dosing intervals of ≥4 weeks regardless of mRNA-1273 dose level.

Discussion

This study assessed how the interval between dose 1 and dose 2 of mRNA-1273, an mRNA-based SARS-CoV-2 vaccine, impacted the robustness and durability of immune responses in mice. Overall, longer dosing intervals of mRNA-1273 (ie, 6 to

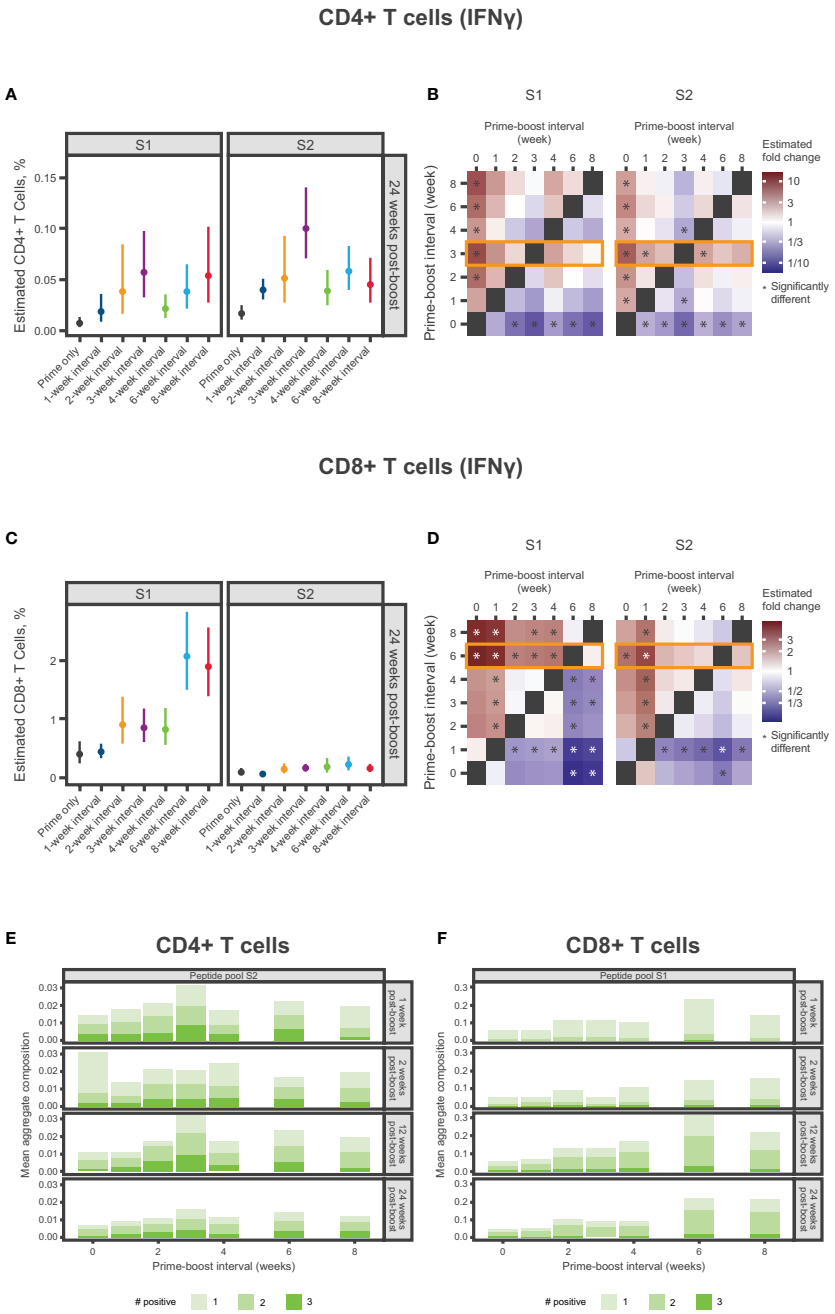

FIGURE 5
Spike-specific CD4+ and CD8+ T-Cell Responses. **(A-D)** Percentage of SARS-CoV-2 spike-specific IFNγ-producing **(A)** CD4+ T cells or **(C)** CD8 + T cells at 24 weeks after dose 2 according to antigen (S1 and S2) and mRNA-1273 dosing interval (prime only or 1-, 2-, 3-, 4-, 6-, or 8-week intervals). Panels **(A, C)** present the estimated mean and associated 95% CIs based on a statistical model (see Methods), with error bars representing the 95% CIs of estimated means. Panels **(B, C)** present the same results in heatmaps showing fold change between percentages of spike-specific IFNγ-producing **(B)** CD4+ T cells or **(D)** CD8+ T cells at 24 weeks after dose 2. Significant differences denoted by an asterisk if the *P*-value was less than 0.05. Results of statistical comparisons between groups are presented in Table S5, Table S7, Figure S7, and Figure S10. **(E, F)** Mean aggregate composition of CD4+ T-cell IFNγ response to the S2 peptide pool or CD8+ T-cell IFNγ response to the S1 peptide pool are presented by mRNA-1273 dosing interval at 1, 2, 12, and 24 weeks following dose 2. Data are presented as averages of individual mice (n=8-10) within each dosing interval group and time point. These compositions were obtained from a thresholding modeling that accounted for day- and cell type–specific differences (see Methods and Supplementary Methods). Results of statistical comparisons between groups based on a zero-inflated beta regression model (see Methods) and shown in Table S6, Figure S9, and Figure S11. Individual animal-level data are presented in Figure S8. CI, confidence interval; IFNγ, interferon γ; mRNA, messenger RNA; S1, subunit 1; S2, subunit 2; SARS-CoV-2, severe acute respiratory syndrome coronavirus 2.

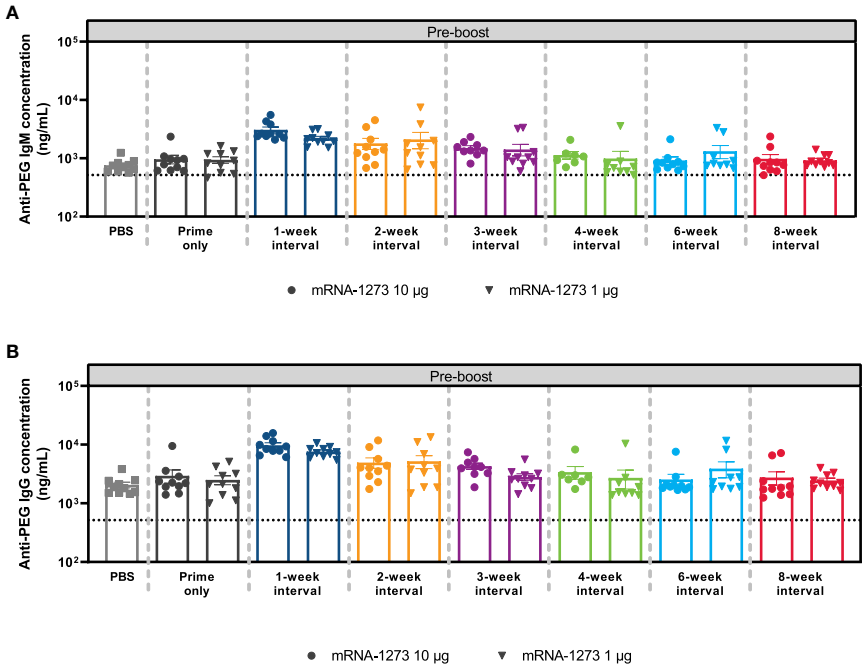

FIGURE 6
Anti-PEG Antibody Responses. The mean ± SEM concentrations of **(A)** anti-PEG IgM and **(B)** anti-PEG IgG antibodies at Day 56 (before dose 2) are presented by mRNA-1273 dosing interval schedule (prime only or 1-, 2-, 3-, 4-, 6-, and 8-week intervals) with n=8-10 mice per group. Results of corresponding statistical comparisons between groups are shown in Table S8 and Figure S12. IgG, immunoglobulin G; IgM, immunoglobulin M; mRNA, messenger RNA; PEG, polyethylene glycol; PBS, phosphate-buffered saline; SEM, standard error of the mean.

8 weeks between doses 1 and 2 of the primary vaccination series) generated higher levels of S2-P–specific binding antibodies, higher numbers of S2-P–specific ASCs in the spleen and LLPCs in the bone marrow, as well as increased effector function and polyfunctional CD8+ T cells through 24 weeks following dose 2. Our findings are in agreement with prior studies of mRNA-vaccines as well as other vaccine platforms (15–18, 37, 38), further highlighting that the length of the interval between vaccine prime and boost doses can directly impact multiple aspects of elicited immune responses.

To understand the impact of the dosing interval on immunogenicity elicited by mRNA-1273, we first examined levels of antigen-specific serum binding antibodies through 24 weeks after the second dose. Notably, binding antibody titers elicited by mRNA-1273 have been previously shown as strongly correlated with neutralizing antibody titers (39), a proposed correlate of protection for SARS-CoV-2 vaccines (4, 40). In our study, longer dosing intervals consistently produced more robust S2-P–specific serum binding IgG titers regardless of the mRNA-1273 dose level tested. Relative to levels before dose 2, both 6- and 8-week intervals increased antibody levels at 24 weeks following the second dose, with 30-fold and 10-fold increases for the 1 µg and 10 µg doses, respectively. Overall, the mRNA-1273 10-µg dose level induced greater antibody responses than the 1-µg dose level regardless of the dosing interval; however, this distinction between the 2 different dose levels was reduced over time for animals dosed on a ≥4-week interval, suggesting potential for a dose-sparing effect (Figure 2B). To extend upon these findings, we also evaluated ADCC activity, which has been suggested as a correlate of the host immune response to SARS-CoV-2 infection or vaccination (41). Similarly, improved antibody Fc-effector responses were observed with longer (≥4 weeks) over shorter intervals.

The generation of antigen-specific antibodies, produced by ASCs and non-proliferating bone marrow resident LLPCs, is required for durable humoral immunity (42). We therefore evaluated production of S2-P–specific ASCs in the spleen and ASCs including LLPCs in the bone marrow following varying mRNA-1273 dosing intervals. Overall, longer dosing intervals up to 8 weeks elicited higher antigen-reactive ASC counts 1 week after dose 2. Longer dosing intervals were also associated with increased numbers of antigen-reactive ASCs in the bone marrow at 4 weeks and 24 weeks following dose 2, indicative of a more durable long-lived response (42). These results are in alignment with those observed by a clinical study on another mRNA-based SARS-CoV-2 vaccine, BNT162b2, which showed a nearly 7-fold increase in B-cell responses after a 10-week versus a 4-week interval between doses 1 and 2 (17), indicating continued B-cell development beyond 4 weeks after dose 1 and a benefit of longer intervals in the primary dosing regimens.

CD4+ and CD8+ T-cell responses have important roles in resolving SARS-CoV-2 infection and reducing disease severity, with memory T-cells associated with persistent protection over time (43). In this analysis, dosing intervals of 6 weeks or longer elicited the strongest antigen-specific IFNγ CD8+ responses to the S1 peptide pool. Further, measurements of T-cell cytokine polyfunctionality, performed to gain insight to the robustness of the response (44), indicated that the 6-week interval elicited the highest percentage of polyfunctional CD8+ Th1 cells. Comparatively, a dosing interval of 3 weeks elicited the strongest antigen-specific IFNγ CD4+ responses to the S2 peptide pool and the highest percentage of polyfunctional CD4+ Th1 cells, which is consistent with a prior study showing CD4+ T-cell responses to the S2 peptide pool were higher than to the S1 peptide pool in mice vaccinated with 2 doses of mRNA-1273 (45). While it remains difficult to draw overall conclusions, as CD4+ T-cell responses were generally low in our study, it is notable that a recent study in participants older than 80 years found that peak cellular responses after vaccination with the mRNA-based BNT162b2 vaccine against SARS-CoV-2 was observed with the standard 3-week interval as opposed to extended (11-12 weeks) prime-dose intervals (19). However, a separate BNT162b2 real-world study indicated that longer (6- to 14-week) dosing intervals increased IL-2 and IFNγ CD4+ T-cell responses and decreased IFNγ CD8+ T-cell responses (17). Our study also evaluated the impact of the mRNA-1273 dosing interval on immune responses to PEG, a common lipid conjugate of mRNA-LNP vaccines. Anti-PEG antibodies were significantly elevated relative to controls with a dosing interval of 1 and 2 weeks for IgG and 1, 2, and 3 weeks for IgM, which parallels the low levels of immunogenicity detected following dose 2 for these dosing regimens. We speculate that these elevated anti-PEG titers might contribute to the reduced anti-spike antibody responses observed for short dosing intervals. Nevertheless, further investigation is required to evaluate this correlation.

Overall, our findings further illustrate that the interval between vaccine doses can impact mRNA-1273-induced immunogenicity and potentially mRNA vaccines in general. It is notable that during the COVID-19 pandemic, wherein the distribution and administration of safe and efficacious vaccines were paramount to combat a pervasive and deadly disease, it was essential to consider the risk-benefit of the shortest dosing interval of SARS-CoV-2 vaccines that induced potent immune responses and conferred efficacy against infection and disease. However, our findings indicate that a longer (6- to 8-week) interval between mRNA-1273 doses 1 and 2 elicits more robust and durable binding antibody responses with increased effector function and CD8+ T cell polyfunctionality, suggesting that a longer dosing interval could be used to optimize the immune responses elicited by mRNA-1273 in an endemic setting.

Our results are supported by multiple studies reporting that longer dosing intervals for SARS-CoV-2 vaccines may improve vaccine-elicited immunogenicity, effectiveness, and tolerability. A recent study among healthcare workers showed mRNA-1273 induced significantly higher humoral immunogenicity than BNT162b2 regardless of SARS-CoV-2 infection status and age, which the authors suggested might result from the higher antigenic content and longer dosing interval of mRNA-1273 compared with BNT162b2 (4 weeks vs 3 weeks, respectively) (16). Notably, a study found that antibody responses among BNT162b2 recipients were 10-fold higher using a 65- to 84-day versus a 19- to 29-day interval between doses 1 and 2, with consistently higher vaccine effectiveness observed with longer dosing intervals (>45 days) (18). A recent pooled analysis of 4 clinical trials of the ChAdOx1 nCoV-19 adenoviral-vectored vaccine also showed that higher vaccine efficacy against symptomatic COVID-19 was observed, with longer dosing intervals (81.3% at ≥12 weeks vs 55.1% at <6 weeks); antibody responses were also >2-fold higher with a ≥12-week versus <6-week dosing interval (15). Notably, extended intervals between doses 1 and 2 may also limit certain rare safety events observed with currently available COVID-19 mRNA vaccines, with the US Centers for Disease Control and Prevention recently recommending extending the interval between doses 1 and 2 for mRNA-1273 and BNT162b2 (from 4- to 8-week intervals and from 3- to 4-week intervals, respectively) for individuals ≥12 years due to reduced risk of myocarditis with longer intervals (46, 47). Of note, myocarditis and pericarditis following mRNA vaccination are rare and most vaccine-associated myocarditis events have been mild and self-limiting (48, 49).

Limitations to this study include that mouse animal models are not optimal for measuring immune response durability; future studies are planned to further assess the impact of dosing intervals on vaccine-elicited immunogenicity in human participants. Notably, while innate immune responses to SARS-CoV-2 mRNA vaccines differ between mouse animal models and humans, these models are potentially predictive of the innate response and immunogenicity profiles of these vaccines in humans (50). Although this study only examined immune responses elicited by mRNA-1273, it might be anticipated that longer dosing intervals for other mRNA vaccines may similarly elicit more robust and durable immune responses, as has been observed for other vaccine modalities (37, 38).

In conclusion, longer intervals (≥6 weeks) between the first and second vaccine dose of mRNA-1273 induced more durable immune responses in mice. Our findings suggest that extending the current dosing interval could improve immune responses for mRNA-1273 and potentially for other mRNA-based vaccines.

Data availability statement

The authors declare that the data supporting the findings of this study are available within this article and its Supplementary

Information. All R code used to produce the results presented in this article are publicly accessible on the Moderna GitHub repository (https://github.com/modernatx/mRNA1273_dosing_Interval_mice_immune_response_kinetics_quality_magnitude.git).

Ethics statement

The animal study was reviewed and approved by Institutional Animal Care and Use Committee of Moderna, Inc.

Author contributions

CH, SE, AC, DE and KB contributed to the study concept and design. Data collection was performed by DG-D, CH, LM, HJ, TM, AF, and HD. All authors besides AC were involved in the analysis and interpretation of the data. All authors were involved in the drafting and critical revision of the manuscript and provided approval for submission. All authors contributed to the article and approved the submitted version.

Acknowledgments

The authors would like to acknowledge the *In Vivo* Pharmacology team at Moderna, Inc. for assisting in tissue and serum collection. Medical writing and editorial assistance were provided by Emily Stackpole, PhD, and Wynand van Losenoord, MSc, of MEDiSTRAVA in accordance with Good Publication Practice (GPP3) guidelines, funded by Moderna, Inc., and under the direction of the authors.

Conflict of interest

All authors are employees of Moderna, Inc., and hold stock/stock options from the company. The authors declare that this study received funding from Moderna, Inc. The funder was involved in the study design, collection, analysis, interpretation of data, and the writing of this article or the decision to submit it for publication.

Publisher's note

Supplementary material

The Supplementary Material for this article can be found online at: https://www.frontiersin.org/articles/10.3389/fimmu.2022.948335/full#supplementary-material

References

1. Pollard AJ, Bijker EM. A guide to vaccinology: from basic principles to new developments. *Nat Rev Immunol* (2021) 21(2):83–100. doi: 10.1038/s41577-020-00479-7

2. Zimmermann P, Curtis N. Factors that influence the immune response to vaccination. *Clin Microbiol Rev* (2019) 32(2):e00084–18. doi: 10.1128/CMR.00084-18

3. Slifka MK, Amanna IJ. Role of multivalency and antigenic threshold in generating protective antibody responses. *Front Immunol* (2019) 10:956. doi: 10.3389/fimmu.2019.00956

4. Earle KA, Ambrosino DM, Fiore-Gartland A, Goldblatt D, Gilbert PB, Siber GR, et al. Evidence for antibody as a protective correlate for COVID-19 vaccines. *Vaccine* (2021) 39(32):4423–8. doi: 10.1016/j.vaccine.2021.05.063

5. Plotkin SA. Updates on immunologic correlates of vaccine-induced protection. *Vaccine* (2020) 38(9):2250–7. doi: 10.1016/j.vaccine.2019.10.046

6. Tarke A, Coelho CH, Zhang Z, Dan JM, Dawen Yu E, Methot N, et al. SARS-CoV-2 vaccination induces immunological memory able to cross-recognize variants from alpha to omicron. *bioRxiv* (2021). doi: 10.1101/2021.12.28.474333

7. McHeyzer-Williams LJ, McHeyzer-Williams MG. Antigen-specific memory b cell development. *Annu Rev Immunol* (2005) 23:487–513. doi: 10.1146/annurev.immunol.23.021704.115732

8. Seder RA, Darrah PA, Roederer M. T-Cell quality in memory and protection: implications for vaccine design. *Nat Rev Immunol* (2008) 8(4):247–58. doi: 10.1038/nri2274

9. Yoshida T, Mei H, Dorner T, Hiepe F, Radbruch A, Fillatreau S, et al. Memory b and memory plasma cells. *Immunol Rev* (2010) 237(1):117–39. doi: 10.1111/j.1600-065X.2010.00938.x

10. Palgen JL, Feraoun Y, Dzangue-Tchoupou G, Joly C, Martinon F, Le Grand R, et al. Optimize Prime/Boost vaccine strategies: Trained immunity as a new player in the game. *Front Immunol* (2021) 12:612747. doi: 10.3389/fimmu.2021.612747

11. Woodland DL. Jump-starting the immune system: prime-boosting comes of age. *Trends Immunol* (2004) 25(2):98–104. doi: 10.1016/j.it.2003.11.009

12. World Health Organization. *Table 2: Summary of WHO position papers - recommended routine immunizations for children* (2021). Available at: https://cdn.who.int/media/docs/default-source/immunization/immunization_schedules/immunization-routine-table2.pdf?sfvrsn=3e27ab48_9&download=true.

13. FDA. *HIGHLIGHTS OF PRESCRIBING INFORMATION* (2022). Available at: https://www.fda.gov/media/155675/download (Accessed 11 March 2022).

14. El Sahly HM, Baden LR, Essink B, Doblecki-Lewis S, Martin JM, Anderson EJ, et al. Efficacy of the mRNA-1273 SARS-CoV-2 vaccine at completion of blinded phase. *N Engl J Med* (2021) 385(19):1774–85. doi: 10.1056/NEJMoa2113017

15. Voysey M, Costa Clemens SA, Madhi SA, Weckx LY, Folegatti PM, Aley PK, et al. Single-dose administration and the influence of the timing of the booster dose on immunogenicity and efficacy of ChAdOx1 nCoV-19 (AZD1222) vaccine: a pooled analysis of four randomised trials. *Lancet* (2021) 397(10277):881–91. doi: 10.1016/S0140-6736(21)00432-3

16. Steensels D, Pierlet N, Penders J, Mesotten D, Heylen L. Comparison of SARS-CoV-2 antibody response following vaccination with BNT162b2 and mRNA-1273. *JAMA* (2021) 326(15):1533–5. doi: 10.1001/jama.2021.15125

17. Payne RP, Longet S, Austin JA, Skelly DT, Dejnirattisai W, Adele S, et al. Immunogenicity of standard and extended dosing intervals of BNT162b2 mRNA vaccine. *Cell* (2021) 184(23):5699–5714 e11. doi: 10.1016/j.cell.2021.10.011

18. Amirthalingam G, Bernal JL, Andrews NJ, Whitaker H, Gower C, Stowe J, et al. Serological responses and vaccine effectiveness for extended COVID-19 vaccine schedules in England. *Nat Commun* (2021) 12(1):7217. doi: 10.1038/s41467-021-27410-5

19. Parry H, Bruton R, Stephens C, Bentley C, Brown K, Amirthalingam G, et al. Extended interval BNT162b2 vaccination enhances peak antibody generation. *NPJ Vaccines* (2022) 7(1):14. doi: 10.1038/s41541-022-00432-w

20. Nelson J, Sorensen EW, Mintri S, Rabideau AE, Zheng W, Besin G, et al. Impact of mRNA chemistry and manufacturing process on innate immune activation. *Sci Adv* (2020) 6(26):eaaz6893. doi: 10.1126/sciadv.aaz6893

21. Hassett KJ, Benenato KE, Jacquinet E, Lee A, Woods A, Yuzhakov O, et al. Optimization of lipid nanoparticles for intramuscular administration of mRNA vaccines. *Mol Ther Nucleic Acids* (2019) 15:1–11. doi: 10.1016/j.omtn.2019.01.013

22. Stasinopoulos DM, Rigby RA. Generalized additive models for location scale and shape (GAMLSS) in r. *J Stat Software* (2007) 23(7):1–46. doi: 10.18637/jss.v023.i07

23. Wood S. Modelling and smoothing parameter estimation with multiple quadratic penalties. *J R Stat Society: Ser B (Statistical Methodol)* (2000) 62(2):413–28. doi: 10.1111/1467-986800240

24. Bates D, Mächler M, Bolker B, Walker S. Fitting linear mixed-effects models using lme4. *J Stat Software* (2015) 67(1):1–48. doi: 10.18637/jss.v067.i01

25. Bürkner P-C. Brms: An r package for Bayesian multilevel models using Stan. *J Stat Software* (2017) 80(1):1–28. doi: 10.18637/jss.v080.i01

26. Stan Development Team. RStan: the r interface to Stan. (2022). Available at: https://mc-stan.org/rstan/articles/rstan.html.

27. Box GEP, Cox DR. An analysis of transformations. *J R Stat Soc Ser B (Methodol)* (1964) 26(2):211–52. doi: 10.1111/j.2517-6161.1964.tb00553.x

28. Rigby R, Stasinopoulos DM. Generalized additive models for location, scale and shape (with discussion). *J R Stat Society: Ser C (Applied Statistics)* (2005) 54 (3):507–54. doi: 10.1111/j1467-9876200500510x

29. Core Team R. *R: A language and environment for statistical computing*. Vienna, Austria: R Foundation for Statistical Computing (2021). Available at: https://www.R-project.org/.

30. Lenth RV. *Emmeans: Estimated marginal means, aka least-squares means. r package version 1.7.2* (2022). Available at: https://CRAN.R-project.org/package=emmeans.

31. Lederer K, Castano D, Gomez Atria D, Oguin TH3rd, Wang S, Manzoni TB, et al. SARS-CoV-2 mRNA vaccines foster potent antigen-specific germinal center responses associated with neutralizing antibody generation. *Immunity* (2020) 53 (6):1281–1295 e5. doi: 10.1016/j.immuni.2020.11.009

32. Turner JS, O'Halloran JA, Kalaidina E, Kim W, Schmitz AJ, Zhou JQ, et al. SARS-CoV-2 mRNA vaccines induce persistent human germinal centre responses. *Nature* (2021) 596(7870):109–13. doi: 10.1038/s41586-021-03738-2

33. Sallusto F, Lanzavecchia A, Araki K, Ahmed R. From vaccines to memory and back. *Immunity* (2010) 33(4):451–63. doi: 10.1016/j.immuni.2010.10.008

34. Hou X, Zaks T, Langer R, Dong Y. Lipid nanoparticles for mRNA delivery. *Nat Rev Mater* (2021) 6(12):1078–94. doi: 10.1038/s41578-021-00358-0

35. Suk JS, Xu Q, Kim N, Hanes J, Ensign LM. PEGylation as a strategy for improving nanoparticle-based drug and gene delivery. *Adv Drug Delivery Rev* (2016) 99(Pt A):28–51. doi: 10.1016/j.addr.2015.09.012

36. Estape Senti M, de Jongh CA, Dijkxhoorn K, Verhoef JJF, Szebeni J, Storm G, et al. Anti-PEG antibodies compromise the integrity of PEGylated lipid-based nanoparticles *via* complement. *J Control Release* (2022) 341:475–86. doi: 10.1016/j.jconrel.2021.11.042

37. Ledgerwood JE, Zephir K, Hu Z, Wei CJ, Chang L, Enama ME, et al. Prime-boost interval matters: a randomized phase 1 study to identify the minimum interval necessary to observe the H5 DNA influenza vaccine priming effect. *J Infect Dis* (2013) 208(3):418–22. doi: 10.1093/infdis/jit180

38. Pitisuttithum P, Nitayaphan S, Chariyalertsak S, Kaewkungwal J, Dawson P, Dhitavat J, et al. Late boosting of the RV144 regimen with AIDSVAX B/E and ALVAC-HIV in HIV-uninfected Thai volunteers: a double-blind, randomised controlled trial. *Lancet HIV* (2020) 7(4):e238–48. doi: 10.1016/S2352-3018(19)30406-0

39. Corbett KS, Nason MC, Flach B, Gagne M, O'Connell S, Johnston TS, et al. Immune correlates of protection by mRNA-1273 vaccine against SARS-CoV-2 in nonhuman primates. *Science* (2021) 373(6561):eabj0299. doi: 10.1126/science.abj0299

40. Khoury D, Cromer D, Reynaldi A, Schlub T, Wheatley A, Juno J, et al. Neutralizing antibody levels are highly predictive of immune protection from symptomatic SARS-CoV-2 infection. *Nat Med* (2021) 27(7):1205–11. doi: 10.1038/s41591-021-01377-8

41. Yu Y, Wang M, Zhang X, Li S, Lu Q, Zeng H, et al. Antibody-dependent cellular cytotoxicity response to SARS-CoV-2 in COVID-19 patients. *Signal Transduct Target Ther* (2021) 6(1):346. doi: 10.1038/s41392-021-00759-1

42. Lightman SM, Utley A, Lee KP. Survival of long-lived plasma cells (LLPC): Piecing together the puzzle. *Front Immunol* (2019) 10:965. doi: 10.3389/fimmu.2019.00965

43. Noh JY, Jeong HW, Kim JH, Shin EC. T Cell-oriented strategies for controlling the COVID-19 pandemic. *Nat Rev Immunol* (2021) 21(11):687–8. doi: 10.1038/s41577-021-00625-9

44. Boyd A, Almeida JR, Darrah PA, Sauce D, Seder RA, Appay V, et al. Pathogen-specific T cell polyfunctionality is a correlate of T cell efficacy and immune protection. *PloS One* (2015) 10(6):e0128714. doi: 10.1371/journal.pone.0128714

45. Corbett KS, Edwards DK, Leist SR, Abiona OM, Boyoglu-Barnum S, Gillespie RA, et al. SARS-CoV-2 mRNA vaccine design enabled by prototype pathogen preparedness. *Nature* (2020) 586(7830):567–71. doi: 10.1038/s41586-020-2622-0

46. CDC. *Interim clinical considerations for use of COVID-19 vaccines currently approved or authorized in the united states* (2022). Available at: https://www.cdc.gov/vaccines/covid-19/clinical-considerations/covid-19-vaccines-us.html (Accessed 08 March 2022).

47. CDC. *Myocarditis and COVID-19 vaccine intervals: International data and policies* (2022). Available at: https://www.cdc.gov/vaccines/acip/meetings/downloads/slides-2022-02-04/11-COVID-Moulia-508.pdf (Accessed 09 March 2022).

48. Witberg G, Barda N, Hoss S, Richter I, Wiessman M, Aviv Y, et al. Myocarditis after covid-19 vaccination in a Large health care organization. *N Engl J Med* (2021) 385(23):2132–9. doi: 10.1056/NEJMoa2110737

49. Patone M, Mei XW, Handunnetthi L, Dixon S, Zaccardi F, Shankar-Hari M, et al. Risks of myocarditis, pericarditis, and cardiac arrhythmias associated with COVID-19 vaccination or SARS-CoV-2 infection. *Nat Med* (2022) 28(2):410–22. doi: 10.1038/s41591-021-01630-0

50. Li C, Lee A, Grigoryan L, Arunachalam PS, Scott MKD, Trisal M, et al. Mechanisms of innate and adaptive immunity to the pfizer-BioNTech BNT162b2 vaccine. *Nat Immunol* (2022) 23(4):543–55. doi: 10.1038/s41590-022-01163-9

frontiers | Frontiers in Immunology

TYPE Clinical Trial
PUBLISHED 13 December 2022
DOI 10.3389/fimmu.2022.1073777

OPEN ACCESS

EDITED BY
Peter Brossart,
University of Bonn, Germany

REVIEWED BY
Jacob Appelbaum,
University of Washington,
United States
Pablo Sarobe,
University of Navarra, Spain

*CORRESPONDENCE
Weston L. Daniel
wes@exicuretx.com

SPECIALTY SECTION
This article was submitted to Cancer Immunity and Immunotherapy, a section of the journal Frontiers in Immunology

RECEIVED 18 October 2022
ACCEPTED 21 November 2022
PUBLISHED 13 December 2022

CITATION
Daniel WL, Lorch U, Mix S and Bexon AS (2022) A first-in-human phase 1 study of cavrotolimod, a TLR9 agonist spherical nucleic acid, in healthy participants: Evidence of immune activation.
Front. Immunol. 13:1073777.
doi: 10.3389/fimmu.2022.1073777

A first-in-human phase 1 study of cavrotolimod, a TLR9 agonist spherical nucleic acid, in healthy participants: Evidence of immune activation

Weston L. Daniel[1]*, Ulrike Lorch[2], Scott Mix[1] and Alice S. Bexon[3]

[1]Research and Development, Exicure, Inc., Chicago, IL, United States, [2]Clinical Research, Richmond Pharmacology, London, United Kingdom, [3]Clinical Research, Bexon Clinical Consulting, Upper Montclair, NJ, United States

Introduction: Tumor immunotherapy is designed to control malignancies through the host immune response but requires circumventing tumor-dysregulated immunomodulation through immunostimulation, relieving immunorepression, or a combination of both approaches. Here we designed and characterized cavrotolimod (formerly AST-008), an immunostimulatory spherical nucleic acid (SNA) compound targeting Toll-like receptor 9 (TLR9). We assessed the safety and pharmacodynamic (PD) properties of cavrotolimod in healthy participants in a first-in-human Phase 1 study under protocol AST-008-101 (NCT03086278; https://clinicaltrials.gov/ct2/show/NCT03086278).

Methods: Healthy participants aged 18 to 40 years were enrolled to evaluate four dose levels of cavrotolimod across four cohorts. Each cohort included four participants, and all received a single subcutaneous dose of cavrotolimod. The dose levels were 5, 10, 12.5 and 18.8 μg/kg.

Results and discussion: Cavrotolimod was well tolerated and elicited no serious adverse events or dose limiting toxicities at the doses tested. The results demonstrated that cavrotolimod is a potent innate immune activator, specifically stimulating Th1-type immune responses, and exhibits PD properties that may result in anti-tumor effects in patients with cancer. This study suggests that cavrotolimod is a promising clinical immunotherapy agent.

KEYWORDS

immunotherapy, cytokines, immunomodulation, Toll-like receptor, clinical trial, cavrotolimod, AST-008, spherical nucleic acid

Introduction

The immune system is the body's defense mechanism against foreign and infectious agents, such as bacteria and viruses. In addition to combating these dangers, the immune system can also fight diseases like cancer. Tumor immunotherapy uses the immune system to recognize and kill cancerous cells. However, tumors can use immune-checkpoint pathways as a major mechanism of immune resistance, particularly against T cells that are specific for tumor antigens. These checkpoint pathways can prevent a latent immune response from acting on the tumor.

Tumor immunotherapy has been revolutionized by checkpoint inhibitors (CPIs) (1) targeting immune checkpoints such as the programmed cell death 1 protein (PD-1)/PD ligand (L)1 axis and cytotoxic T lymphocyte antigen 4 (CTLA-4). Agents targeting both pathways have been approved for use in many cancer types. CPI therapy reduces the inhibition of anti-tumor immunity, allowing the immune system to act more strongly on cancers, resulting in tumor regression and long-term responses in 10–50% of patients (2, 3). Despite these successes, there are two key opportunities for improvement. First, because only a minority of patients treated with CPIs benefit clinically, new approaches including combination therapies increasing the proportion of responders are needed. Second, because there are limited treatment options after disease progression on CPIs, additional therapeutic options are needed in that setting. We hypothesized that combining a potent TLR9 agonist (an immune stimulant) with CPIs (which support immune response expansion) would be a logical approach for capitalizing on the complementary nature of these two therapeutic mechanisms to begin the self-promoting process of immune-mediated tumor cell death, called the cancer-immunity cycle (4), and address the two key therapeutic opportunities outlined above. TLR9 is a pattern recognition receptor (PRR) that recognizes nucleic acids containing unmethylated cytosine-phosphate-guanosine (CpG) dinucleotides present in specific sequence contexts, referred to as CpG motifs (5–9), resulting in T-helper 1 (Th1)-type innate and adaptive immune responses (10, 11). Innate immunity is a rapid response that protects the body during the time required for an adaptive immune response to develop against a given threat, which is usually a few days to weeks. Antigen-presenting cells, including dendritic cells, macrophages, and B cells, play a critical role in the innate immune response by releasing protein signals called cytokines that induce inflammation to fight invading pathogens or foreign bodies. In addition, they direct T cells, which then coordinate the longer-term adaptive immune response, conferring long-term pathogen-specific immunity to the host.

TLR9 agonists have been extensively evaluated preclinically (12–14) and clinically as agents for treating cancers, asthma and allergies, infectious diseases, and as vaccine adjuvants (15, 16). Despite good safety profiles, conventional TLR9 agonists, such as SD-101 and tilsotolimod, have resulted in varied anti-tumor responses as monotherapies or when combined with other anticancer agents following systemic administration (16–18), suggesting a need for more potent TLR9 agonists and better combination approaches. A TLR9 agonist packaged within a virus-like particle called vidutolimod showed substantial clinical activity when administered in combination with pembrolizumab in advanced and metastatic melanoma patients who had previously progressed on anti-PD-1 therapy alone (18), but the complexity of preparing the virus capsid and oligonucleotide components, and assembling the virus-like particle structure, may limit its widespread application.

Spherical nucleic acids (SNAs) are an emerging category of therapeutic agents, showing promise for treating a wide range of diseases and debilitating conditions, spanning glioblastoma multiforme (19, 20), psoriasis (21), diabetic wound healing (22), and nonalcoholic steatohepatitis (23), among others. As illustrated in Figure 1, SNA structures consist of densely packed and radially oriented oligonucleotides around a spherical nanoparticle core (24–27). Since these structures enter cells to a greater extent compared to their conventional oligonucleotide analogues (i.e., unformulated oligonucleotides) and do so *via* endosomal pathways (28), they are ideal for interacting with targets that reside in endosomes, such as TLR9 (28–30). Moreover, since the oligonucleotides on the surface of SNAs are projected in a way that supports facile TLR9 binding (i.e., the oligonucleotides are not sequestered within the nanoparticle), such structures are more potent stimulatory agents compared to unformulated oligonucleotides (23).

We developed cavrotolimod, an SNA modified with type B CpG oligonucleotides designed to agonize TLR9 and elicit

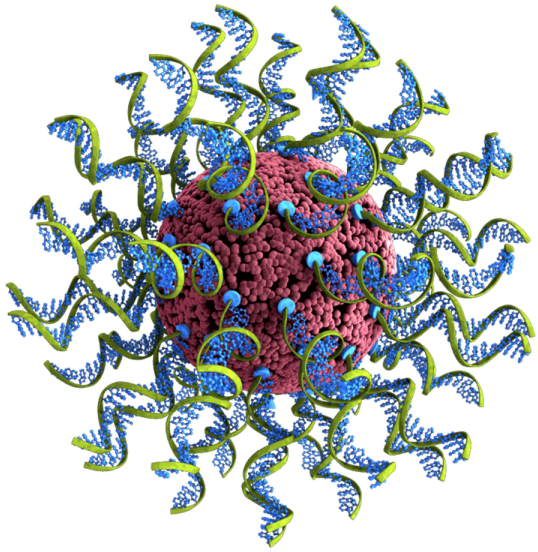

FIGURE 1
Depiction of the cavrotolimod spherical nucleic acid structure.

immune responses useful in oncology applications, and assessed its PD and safety in a Phase 1 study. The results indicated that cavrotolimod produces AEs and a PD response consistent with immune activation, suggesting that cavrotolimod may synergize effectively with anti-PD-1/PD-L1 antibodies. This study, along with data from nonclinical efficacy studies showing tumor regression in mice (31), supported the clinical evaluation of cavrotolimod in combination with CPIs in patients with advanced cancer.

Materials and methods

Study design

This was an open label Phase 1 study which was designed to assess the safety, tolerability, PK and PD of single ascending doses of subcutaneously (SC) administered cavrotolimod in healthy participants. The objectives and endpoints for this study were: (I) to evaluate the safety and tolerability of cavrotolimod; (II) to recommend a dose and regimen for further development; (III) to determine the PK of cavrotolimod in plasma and urine; (IV) to determine the PD of cavrotolimod; and (V) to determine the effect of cavrotolimod on the corrected QT (QTc) interval. The study was conducted at a single clinical study unit in the United Kingdom (UK) and enrolled four cohorts of four participants to receive single ascending doses of cavrotolimod. Participants were assigned into sequential cohorts that received cavrotolimod doses of 5, 10, 12.5 or 18.8 μg/kg. These doses were selected by applying a cautious multiple between these human doses and the no observed adverse event level of cavrotolimod in monkey toxicology studies. In addition, results from a study of TLR9 agonist PF-3512676 in healthy participant were considered (32). No participants received placebo. The study was approved and had oversight by the South Central – Berkshire B Research ethics committee and the Medicines Healthcare Products Regulatory Agency, and was conducted according to the Declaration of Helsinki and Good Clinical Practices.

The main criteria for admission were healthy females or males aged between 18 and 40 years with a body mass index between 18.0 and 25.0 kg/m^2. Participants must have agreed to use effective methods of contraception, if applicable. The main exclusion criteria were any history of cancer and autoimmune or antibody-mediated diseases or any other significant disease or disorder which, in the opinion of the investigator, may have either put the participant at risk because of participation in the study, may have influenced the result of the study or the participant's ability to participate in the study. Participants were screened within 13 days prior to entering the unit on Day -1. Each participant received verbal and written information followed by signing of the Informed Consent Form prior to any screening procedures taking place. Participants were randomized to one dose cohort, admitted to the study unit on Day -1, dosed on Day 1 and discharged on Day 4. All participants attended the unit for outpatient visits on Days 5, 6 and 14 and a follow-up visit on Day 30 (Figure 2).

A mandatory sentinel dosing strategy was used in each cohort, whereby participants were dosed with intervals of 24-96 hours (if safety and tolerability was acceptable) following the prior participant. The Investigator made a judgement whether administration of cavrotolimod to the remaining participants in the cohort could continue based on the clinical safety data available at the time and the protocol toxicity rules. Dose escalation to the subsequent cohort/dose could only occur after satisfactory review of all safety, tolerability, PK and PD data by the Safety Review Committee (SRC) in accordance with the protocol, rules for dose escalation/progression, and toxicity.

Drug supply and administration

A single batch of cavrotolimod was prepared under current Good Manufacturing Practices and released by a Qualified

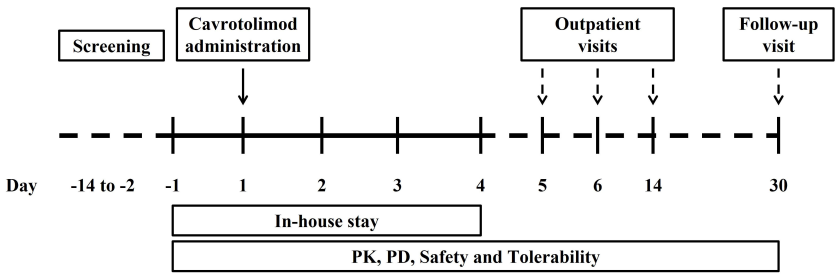

FIGURE 2
Flow chart for the phase 1 study.

Person to support this study. The product was supplied in single use glass vials as a sterile, pH-controlled isotonic solution. To achieve the appropriate doses for each cohort in the study, the pharmacist prepared dilutions of the product in simple saline prior to administration. Cavrotolimod was administered as a SC injection into the abdomen using a 25-gauge, one inch needle.

Safety assessments

Safety and tolerability assessments included AE recording, general health and concomitant medication assessments, and hematology/biochemistry/coagulation parameters during screening, before cavrotolimod dosing, daily during the admission to the study unit, and during the outpatient and follow up visits. At screening and while admitted to the unit, participants were interrogated with continuous 12-lead telemetry starting 1 hour pre-dose through 48 hours post-dose. Further, a Holter electrocardiogram (ECG) was performed during screening to exclude any pre-existing ECG abnormalities. Urinalysis was performed at screening, pre-dose, and Days 3, 14, and 30. Chemokine/cytokine sampling was performed pre- and post-dose during admission, as well as during the outpatient visits and follow up. Lymphocyte sampling was performed pre-dose through Day 3 for the 5 and 10 μg/kg dose groups, and from pre-dose to Day 5 for the 12.5 and 18.8 μg/kg dose groups. PK blood sampling was performed pre- and post-dose through Day 6. PK urine sampling was performed pre-dose and post-dose through Day 2.

Toxicity rules and management algorithm

There were two sets of toxicity rules used in this study. One applied to flu-like symptoms and cytokine release syndrome (CRS), while the second concerned all other adverse events. The rationale for this approach was twofold. First, several constitutional symptoms are present in both flu-like symptoms and CRS, but CRS is a more significant AE, and second, flu-like symptoms were expected after cavrotolimod administration. Therefore, special attention was paid to the toxicity definitions and management of potential CRS reactions.

A CRS management approach based on the literature was used during the first cohort of the study, but for the final three cohorts, a modified algorithm was developed and applied because the approach outlined in the literature was designed for patients who would most likely be in a hospital setting (33). Modifications to the algorithm were therefore made to reflect its application for healthy participants in a non-hospital setting.

The constitutional symptoms and signs of CRS and flu-like symptoms at mild to moderate severity are similar. Table 1 lists the signs and symptoms of CRS and those in bold overlap with the presentation of flu-like symptoms. The management of any AE comprised of the signs or symptoms shown in Table 1 was therefore based on the severity of the overall clinical picture and is illustrated in the algorithm in Figure 3.

The toxicity rules that governed study progression of individual participants, cohorts and the overall study in the event of these AEs were based on the same objective severity scale used in the management algorithm and are shown in Table 2. Based on the desired pharmacology of stimulating a Th1-type immune response, TLR9 agonists are known to cause a range of local and systemic effects that are not necessarily considered adverse. In general, in healthy participant studies of TLR9 agonists administered SC, participants typically experience at least one of the following AEs: injection site induration, erythema, swelling and tenderness, headache, chills, pyrexia/fever, myalgia, arthralgia (constellation of the 5 latter symptoms often described as “flu-like symptoms”).

Pharmacokinetic assessments

Venous blood samples were collected to assess the concentration of cavrotolimod in plasma (K_2EDTA). Blood was collected pre- and post-dose through Day 6. Urine samples for cavrotolimod concentration measurements were taken from the total urine sample provided pre-dose and post-dose through Day 2. Cavrotolimod concentrations were assessed in plasma and urine with validated assays. Non-compartmental analysis was used for calculation of plasma PK parameters. More information about the assays and PK analysis are provided in the Supporting Information.

Pharmacodynamic assessments

Blood samples were taken for the evaluation of the mechanism of action-related cytokines and chemokine markers and immune cell activation. Chemokine and cytokine sampling was performed pre- and post-dose during admission, as well as during the outpatient visits and follow up. Concentrations of cytokines and chemokines were assessed in plasma with a Randox Evidence Investigator or ELISA. The cytokine and chemokines measured were interferon (IFN)α, IFNγ, interleukin (IL)-10, IL-12 p40, IL-1β, IL-1 receptor (R)a, IL-2, IL-6, IL-8, interferon gamma-induced protein (IP)-10, monocyte chemoattractant protein (MCP)-1, and tumor necrosis factor (TNF)α.

Lymphocyte sampling was performed pre-dose through Day 3 for the 5 and 10 μg/kg dose groups, and from pre-dose to Day 5 for the 12.5 and 18.8 μg/kg dose groups. Differential lymphocyte count was performed on a Beckman Coulter Navios flow cytometer to measure abundance of B-cells, T-cells, natural killer (NK) cells, monocytes, macrophages, and plasmacytoid

TABLE 1 Clinical signs and symptoms associated with CRS. Bold indicates signs and symptoms also seen in flu-like symptoms.

Organ system	Symptoms
Constitutional	Fever ± rigors, malaise, fatigue, anorexia, myalgia, arthralgia, nausea, vomiting, and headaches. Additionally, pruritus and dizziness were observed with compounds similar to cavrotolimod and for the purposes of this management algorithm will also be regarded as constitutional, unless another cause for these symptoms is identified.
Skin	Rash.
Gastrointestinal	Nausea, vomiting, diarrhea.
Respiratory	Tachypnoea, hypoxemia.
Cardiovascular	Tachycardia, widened pulse pressure, hypotension, increased cardiac output (early), potentially diminished cardiac output (late).
Coagulation	Elevated D-dimer, hypofibrinogenemia ± bleeding.
Renal	Azotemia.
Hepatic	Transaminitis, hyperbilirubinemia.
Neurologic	Headache, mental status changes, confusion, delirium, word finding difficulty or frank aphasia, hallucinations, tremor, dysmetria, altered gait, seizures.

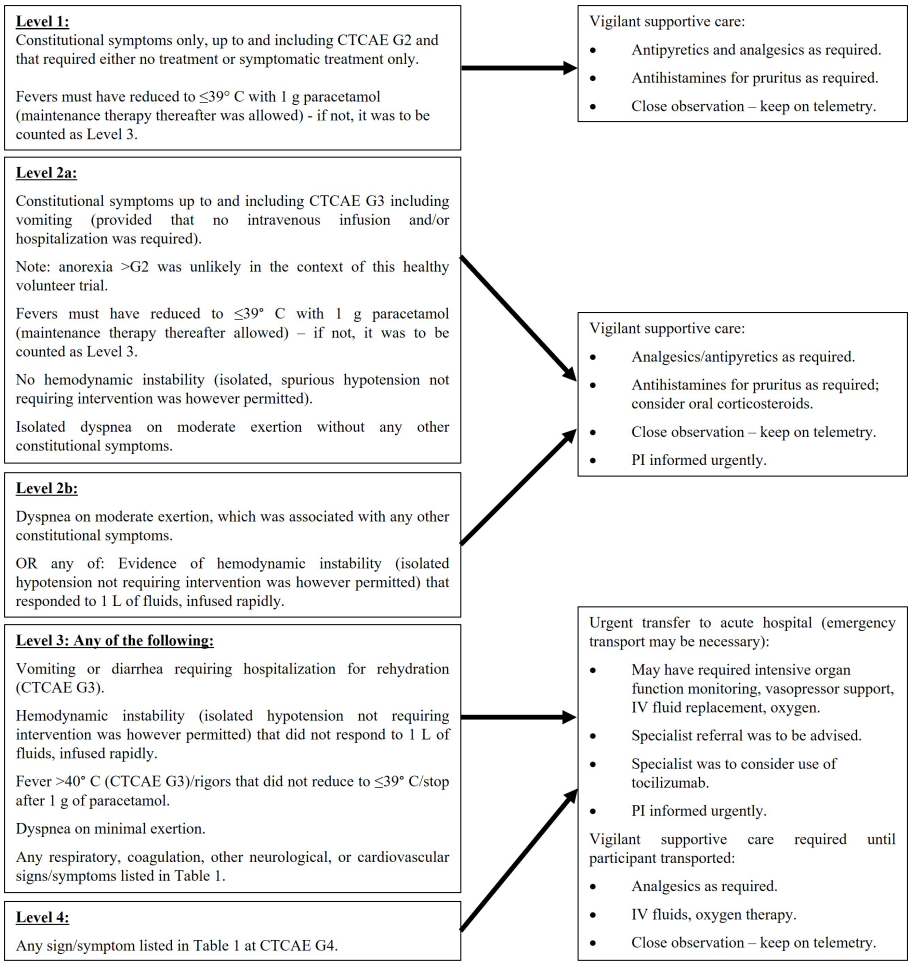

FIGURE 3
Definitions of severity levels and management algorithm for flu-like symptoms/CRS.

10.3389/fimmu.2022.1073777

TABLE 2 Toxicity rules for CRS and Flu-like symptoms.

Level (see Figure 3 for explanation on levels)	DECISION 1 Individuals:	DECISION 2 Continuation within a dosing regimen:	DECISION 3 Study progression:
Level 1 (mild to moderate, not serious)	Continue as per protocol.	Continue as per protocol.	Continue as per protocol.
Level 2a (Severe, not serious)	Cavrotolimod administration was to be discontinued.	1 participant: Continue as per protocol. ≥2 participants: Dosing of the remainder of the dosing regimen suspended. Continuation and extension required substantial amendment.	1 participant: Continue as per protocol. ≥2 participants: Dose escalation and progression to study parts with an equal or higher dose suspended. Dosing regimens on lower dose levels can continue. Progression to successive cohorts or study parts was permitted only with doses below this current level (at which this toxicity was observed). Escalation or progression to study parts with an equal or higher dose requires substantial amendment.
Level 2b (Severe, not serious)	Cavrotolimod administration was to be discontinued.	≥1 participant: Dosing of the remainder of the dosing regimen suspended. Continuation and extension required substantial amendment.	≥1 participant: Dose escalation and progression to study parts with an equal or higher dose suspended. Dosing regimens on lower dose levels can continue. Progression to successive cohorts or study parts was permitted only with doses below this current level (at which this toxicity was observed). Escalation or progression to study parts with an equal or higher dose required substantial amendment.
Level 3 (Severe, serious AE)	Cavrotolimod administration was to be discontinued.		
Level 4 (Life-threatening, serious AE)	Cavrotolimod administration was to be discontinued.	≥1 participants: Dosing of the remainder of the dosing regimen suspended; Continuation and extension requires substantial amendment.	Study suspended (i.e., this dosing regimen AND all ongoing dosing regimens including those at lower doses, and upcoming dosing regimens, were to be immediately suspended). Continuation of the study required a substantial amendment.

dendritic cells. NK and T-cells were identified as CD3-/CD16+/CD19-/CD56+ and CD3+/CD19-/CD45+, respectively. Monocytes were detected as CD14+/CD45+. CD69 was used as the activation marker for these three cell types.

Cytokines, chemokines and flow cytometry analyses were performed by The Doctors' Laboratory (London, UK).

Statistical analysis

A blinded data review meeting was held prior to database lock and completion of the final analyses. AEs, vital signs, ECG parameters and clinical laboratory data were listed and summarized using descriptive statistics. The number and percent of participants who had any AEs were summarized for each dose. All AEs were listed by using system organ class and preferred term assigned to the event using Medical Dictionary for Regulatory Activities (MedDRA). Furthermore, these events were summarized by the maximum intensity and the number of participants who had drug-related AEs. Any serious adverse events (SAEs) and/or AEs that led to withdrawal would have been listed had they occurred.

The statistical analysis of the PD variables consisted of descriptive statistics, listings and graphs of absolute values and fold change from pre- to post-dose time points, and of comparison of pre- to post-dose values by paired t-tests.

Results

Participant characteristics

Cavrotolimod was evaluated in a first-in-human Phase 1 study (34), which was conducted at a single clinical study unit in the UK. The safety, tolerability, PK and PD of single ascending doses of cavrotolimod were studied in healthy participants. Four dose levels of cavrotolimod (5, 10, 12.5, and 18.8 μg/kg) were evaluated in four cohorts. Each cohort included four participants, and all received a single dose of cavrotolimod.

A total of 16 healthy female and male participants were dosed, with the highest single dose of cavrotolimod being 1.4 mg. Among the 16 participants, 13 were male and 3 were female (Table 3). The mean age was 23.9 years (range from 18-37 years), and the mean weight was 69.6 kg (ranging from 54.4 kg to 84.1 kg) at screening. The participants had a mean height of 176.0 cm (ranging from 158 cm to 192 cm). Participants had a mean BMI of 22.4 kg/m^2 (ranging from 19 kg/m^2 to 25 kg/m^2 at screening. A quarter (25%) of the participants who received cavrotolimod were black, while 56.3% were white and 18.8% were of 'other' race. The participants enrolled into the trial were all included in the safety, PK and PD analyses. There were no dropouts.

10.3389/fimmu.2022.1073777

TABLE 3 Demographic data of healthy participants enrolled in AST-008-101.

Demographic Parameter	Statistic	5 µg/kg (N=4)	10 µg/kg (N=4)	12.5 µg/kg (N=4)	18.8 µg/kg (N=4)	Overall (N=16)
Age* [years]	n	4	4	4	4	16
	Mean	21.8	22.5	28.8	22.5	23.9
	SD	2.6	3.7	5.6	1.3	4.4
	Minimum	18	20	25	21	18
	Median	22.5	21.0	26.5	22.5	23.0
	Maximum	24	28	37	24	37
Gender	Female, n (%)	1 (25.0)	0	0	2 (50.0)	3 (18.8)
	Male, n (%)	3 (75.0)	4 (100.0)	4 (100.0)	2 (50.0)	13 (81.3)
Race	Black or African American, n (%)	1 (25.0)	0	1 (25.0)	2 (50.0)	4 (25.0)
	Other, n (%)	0	1 (25.0)	1 (25.0)	1 (25.0)	3 (18.8)
	White, n (%)	3 (75.0)	3 (75.0)	2 (50.0)	1 (25.0)	9 (56.3)
Height [cm]**	n	4	4	4	4	16
	Mean	175.3	185	176.3	167.5	176
	SD	11.6	4.8	5.3	12.3	10.4
	Minimum	158	181	172	158	158
	Median	180.0	183.5	174.5	163.5	180
	Maximum	183	192	184	185	192
Weight [kg]**	n	4	4	4	4	16
	Mean	68.7	77.95	68.58	63.13	69.59
	SD	10.29	7.26	10.60	6.33	9.62
	Minimum	54.4	67.6	55.7	59.6	54.4
	Median	70.75	80.05	69.4	60.15	70.75
	Maximum	78.9	84.1	79.8	72.6	84.1
Body Mass Index [kg/m^2]	n	4	4	4	4	16
	Mean	22.3	22.8	22.0	22.6	22.4
	SD	0.96	1.82	2.57	1.45	1.64
	Minimum	21	20	19	21	19
	Median	22.1	23.4	22.4	22.5	22.6
	Maximum	24	24	25	24	25

N, total number of participants in cohort; n, number of participants for a given statistic; SD, standard deviation. * Age is calculated at the date of informed consent. ** Height, weight, and body mass index are given at screening.

Safety and tolerability assessments

Safety and tolerability assessments included AE recording, general health and concomitant medication assessments, hematology, biochemistry and coagulation parameters measured during screening, before cavrotolimod dosing, daily during the admission to the study unit, and during the outpatient and follow up visits.

All participants at screening, on Day -1, and Day 1 met all inclusion criteria, and none violated any of the exclusion criteria. Two participants reported previous medical history. One participant who received 5 µg/kg of cavrotolimod reported depression and one participant who received 10 µg/kg reported seasonal allergy and depression. Prior and concomitant medication was reported in nine participants. Prior and concomitant medications related to AEs included norfloxacin for urinary tract infections, Strepsils® for sore throat, ibuprofen for toothache and flu-like symptoms, lidocaine for toothache, paracetamol (acetaminophen) for headache, hot flush and pyrexia. Prior and concomitant medication use not related to AEs included loratadine for a runny nose and omega-3 fatty acids for health and well-being.

In the trial, no SAEs or dose limiting toxicities were observed. All 16 participants receiving cavrotolimod experienced at least one drug-related AE, all of which were grade (G) 1 in severity according to the Common Terminology Criteria for Adverse Events (CTCAE) version 4.03 (Table 4). The AEs observed were as expected given the mechanism of action and from other TLR9 agonist clinical trials in healthy participants (32, 35) and in diseased populations (16, 36). The frequency of AEs was similar in the lowest three dose groups but increased in the highest dose group. The most common AEs, in descending order of frequency, were pyrexia, headache, influenza-like illness (i.e., flu-like symptoms), dizziness and myalgia. All 16 participants

TABLE 4 Drug-related adverse events (all Grade 1) observed in AST-008-101.

Preferred Term (MedDRA 21.0)	5 µg/kg (N=4) n (%)	10 µg/kg (N=4) n (%)	12.5 µg/kg (N=4) n (%)	18.8 µg/kg (N=4) n (%)	Overall (N=16) n (%)
Pyrexia	–	–	2 (50.0)	4 (100.0)	6 (37.5)
Influenza like illness	–	3 (75.0)	–	1 (25.0)	4 (25.0)
Headache	1 (25.0)		1 (25.0)	2 (50.0)	4 (25.0)
Myalgia	–	–	–	2 (50.0)	2 (12.5)
Dizziness	–	–	1 (25.0)	1 (25.0)	2 (12.5)
Lymphadenopathy	–	1 (25.0)	–	–	1 (6.3)
Eye pain	1 (25.0)	–	–	–	1 (6.3)
Decreased appetite	–	–	–	1 (25.0)	1 (6.3)
Back pain	–	–	1 (25.0)	–	1 (6.3)
Muscle twitching	1 (25.0)	–	–	–	1 (6.3)
Hyperesthesia	–	–	–	1 (25.0)	1 (6.3)
Cough	–	–	–	1 (25.0)	1 (6.3)
Flushing	–	–	1 (25.0)	–	1 (6.3)

N, total number of participants in cohort; n, number of participants for a given statistic.

experienced mild injection site reactions (i.e., redness, tenderness) that were not considered adverse, and these reactions resolved on their own. Lymphadenopathy was observed in 12 participants but was considered adverse in only one participant. Across all timepoints, the highest grading was 'palpable, normal to mild enlargement'. The inguinal, femoral, and iliac lymph nodes were most often affected, due to the lower right quadrant dosing of cavrotolimod.

Clinical biochemistry and hematology results revealed C-reactive protein increases, neutropenia, and lymphopenia, but these changes were not considered adverse due to their short-lived and asymptomatic nature. Neutropenia and lymphopenia are consistent with the pharmacology of cavrotolimod as they were likely due to the transient margination, or exit, of those cells from the bloodstream.

No clinically significant abnormalities in ECG intervals or morphology were observed. Although minor abnormalities of ECG intervals were reported at all doses, most were either not considered to be changes from the subject's pre-dose baselines or were related to spurious results or anomalies and were not reproducible at subsequent time points. The paired PK/QTc analysis was not conducted because of a lack of change in QTc parameters.

No CRS/flu-like symptoms toxicity rules above Level 1 were met over the course of the study.

Pharmacokinetic assessments

The PK of cavrotolimod was evaluated after single SC administration in healthy adult participants. Eighteen blood samples were collected starting at the pre-dose baseline through 120 hours after the cavrotolimod dose. The samples were used to measure the concentration of the drug in the participant plasma with a plate-based method, utilizing complementary capture and detection probes, and an ECL readout. There were only a few measurable plasma concentrations per participant. Due to this and the small number of participants, these PK results should be interpreted with caution. PK parameters, including $AUC_{0\text{-}24hr}$, $AUC_{0\text{-}tlast}$, C_{max}, the time of maximum plasma concentration (T_{max}) and plasma half-life ($t_{1/2}$) were calculated and are presented by dose in Table 5. The geometric mean $AUC_{0\text{-}24hr}$, $AUC_{0\text{-}tlast}$ and C_{max} values were similar for the 5 and 10 µg/kg dose groups, and increased in a dose proportional manner in the higher dose groups.

The median T_{max} ranged from 2.00 to 2.52 hours over the dose range of 5 µg/kg to 18.8 µg/kg, peaking earlier than the PD effects, which apexed at 24 to 72 hours, depending on the cytokine. Geometric mean $t_{1/2}$ values were 3.881 and 2.370 hours following 12.5 and 18.8 µg/kg administration, while geometric mean apparent clearance (CL) and volume (Vz) were 1.133 L/h/kg and 6.344 L/kg for the 12.5 µg/kg dose level, and 2.266 L/h/kg and 7.748 L/kg for the 18.8 µg/kg dose level, respectively. Inter-participant variability for $AUC_{0\text{-}24h}$, $AUC_{0\text{-}tlast}$, C_{max} were generally low to moderate, except for the 12.5 µg/kg dose level which was generally high.

Cavrotolimod was not detected in any urine samples, so PK parameter analysis was not conducted on those samples.

Pharmacodynamic assessments

The PD effects of cavrotolimod were assessed through the measurement of cytokine and chemokine concentrations and lymphocyte changes. Blood was drawn from the participants before and after dosing with cavrotolimod to measure the

TABLE 5 PK parameters calculated by cavrotolimod dose.

PK Parameter	Cavrotolimod dose			
	5 µg/kg	10 µg/kg	12.5 µg/kg	18.8 µg/kg
$AUC_{0\text{-}24hr}$ (ng × hr/mL)	2.302	2.084	4.762	8.170
$AUC_{0\text{-}tlast}$ (ng × hr/mL)	1.992	1.817	4.241	8.565
C_{max} (ng/mL)	0.74009	0.73726	1.3336	1.8234
T_{max} (hr)	2.52	2.00	2.00	2.04
$T_{1/2}$ (hr)	NC	NC	3.881	2.370
CL (L/h/kg)	NC	NC	1.133	2.266
Vz (L/kg)	NC	NC	6.344	7.748

CL, clearance; hr, hour; kg, kilogram; L, liter; mL, milliliter; NC, not calculated; ng, nanogram; Vz, volume of distribution during the terminal phase.

concentration of a set of cytokines and chemokines in the participant plasma as a function of time. Blood samples were also used for fresh flow cytometry to assess immune cell activation as a percent of the cells detected by flow cytometry.

The cytokine and chemokine markers measured in the study were IL-12 p40, IL-1RA, IP-10, IL-6, MCP-1, TNFα, IFNα, IFNγ, IL-10, IL-1β, IL-2, and IL-8. Approximately 18 blood samples were taken from the participants during a period starting at the pre-dose time point out to 30 days post-dose in each participant. These markers were selected to assess the magnitude and character of the immune response provoked by cavrotolimod. Table 6 shows the peak baseline-subtracted cytokine change with cavrotolimod as a function of dose.

Cavrotolimod elicited a broad Th1-type immune response in an approximately dose-proportional manner. IFNγ, IL-12 p40, IL-1RA, IL-6, IP-10, and MCP-1 were consistently induced across all doses. IFNγ increases were small, but statistically significant, at 20 hours post-dose in all four cohorts. Notably, IP-10 was robustly induced compared to pre-dose levels reaching significance ($p<0.05$) in all four cohorts between 12- and 24-hours post-dose, providing a second indication that IFNγ was elicited, although the latter was not detected at the same magnitude. IFN-γ expression induces PD-L1, a marker positively associated with anti-PD-1 antibody activity (37). TNF-α was also induced, although not consistently or in a dose-proportionate manner. Two participants showed a substantial increase in TNF-α, to 58 and 179 pg/mL above baseline, at the 10 and 18.8 µg/kg dose levels, respectively, while the other participants in the study did not express meaningful levels of the cytokine.

For most of the measured cytokines and chemokines, the peak response was observed about 24 hours after cavrotolimod administration, although IL-12 p40 peaked at 48 to 72 hours after dosing (Figure 4A). Generally, the IL-6 and IFN-γ

TABLE 6 Peak cytokine response by cohort following cavrotolimod administration.

Cytokine	Peak Cytokine Response (expressed in pg/mL)							
	5 µg/kg		10 µg/kg		12.5 µg/kg		18.8 µg/kg	
	mean ± SD	p value	mean ± SD	p value	mean ± SD	p value	mean ± SD	p value
IFNα	11 ± 27	0.4617	7 ± 4	0.0505	4 ± 6	0.2900	1 ± 6	0.8156
IFNγ	2 ± 0	0.0033	12 ± 8	0.0577	3 ± 3	0.1156	5 ± 2	0.0207
IL-1β	1 ± 1	0.3910	0 ± 1	0.3910	0 ± 1	0.3910	2 ± 3	0.2380
IL-1RA	857 ± 288	0.0094	1763 ± 1024	0.0412	1073 ± 576	0.0337	1519 ± 500	0.0089
IL-2	1 ± 2	0.1828	3 ± 4	0.1818	3 ± 2	0.0822	0 ± 3	0.7915
IL-6	20 ± 16	0.0772	123 ± 48	0.0147	64 ± 81	0.2121	66 ± 99	0.2773
IL-8	4 ± 7	0.3557	5 ± 5	0.1512	22 ± 42	0.3634	15 ± 15	0.1457
IL-10	6 ± 9	0.2586	7 ± 9	0.2030	1 ± 1	0.0524	1 ± 1	0.2188
IL-12 p40	99 ± 57	0.0402	192 ± 149	0.0826	266 ± 30	0.0004	263 ± 157	0.0442
IP-10	277 ± 144	0.0309	721 ± 236	0.0088	687 ± 241	0.0107	1007 ± 342	0.0098
MCP-1	276 ± 115	0.0173	753 ± 613	0.0912	303 ± 84	0.0055	420 ± 188	0.0209
TNFα	2 ± 1	0.0180	17 ± 27	0.3037	2 ± 3	0.3233	46 ± 89	0.3788

Peak cytokine response (mean ± standard deviation) and p values (comparison of pre- to post-dose values by paired t-tests) by cohort as a function of dose (baseline subtracted). pg/mL, picogram per milliliter; SD, standard deviation.

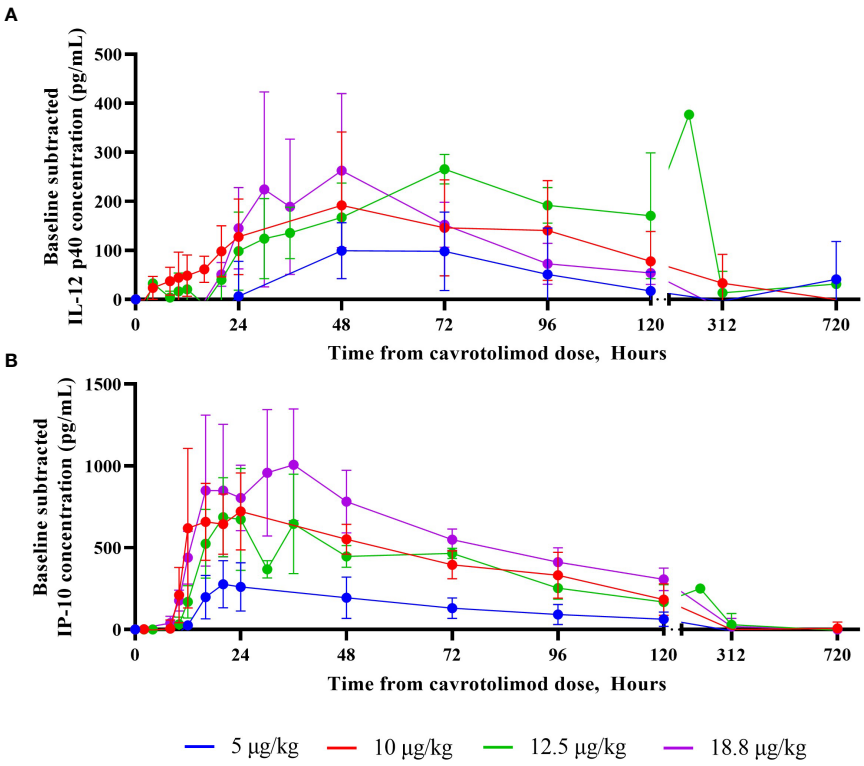

FIGURE 4
IL-12 p40 and IP-10 cytokine responses as a function of time. A Randox Evidence Investigator or ELISA was used to measure concentrations (pg/mL) of IL-12 p40 and IP-10 in peripheral blood following a single SC dose of cavrotolimod. Each point represents averaged, baseline subtracted values from the four participants in each cohort at the sampling time post-dose of cavrotolimod. **(A)** IL-12 p40. **(B)** IP-10.

concentrations returned to baseline approximately 48 hours after cavrotolimod administration, while IL-1RA, IP-10 (Figure 4B), and MCP-1 (at higher doses) required 96 or more hours. Some variability in cytokine response across participants was observed. The non-baseline subtracted peak concentrations of IL-6, IL-12 p40, IL-1RA, IP-10, IFN-γ, and MCP-1 was generally within 2- to 4-fold across participants in one cohort.

Lymphocyte activation was measured using a flow cytometry-based analysis. The results indicate that cavrotolimod activated NK and T cells in participants following administration. NK cell activation, which is indicated by the presence of the CD69 marker in flow cytometry, was observed in all participants (Figure 5A). The NK cell activation peaked at about 48 hours and declined through 96 hours (Figure 5B). Mean NK cell activation for the 12.5 µg/kg dose level was significantly increased at 4-, 12-, 48- and 72-hours post-dose compared to the pre-dose levels ($p<0.05$). T cell activation, which is also measured by the presence of CD69, was also observed in all participants (Figure 5C). It generally peaked between 12 and 24 hours, with the activation tapering off through 96 hours (Figure 5D). T cell activation in each cohort reached significance ($p<0.05$) at least once between 24- and 72-hours post-dose compared to pre-dose levels.

No meaningful changes were observed in activated B cells, macrophages or plasmacytoid dendritic cells. For the 5, 10 and 12.5 µg/kg dose levels, 8, 10 and 3-fold increases in the percent of activated monocytes, respectively, were observed at 48 hours. Although these fold changes were relatively large, they were not dose proportional, did not reach statistical significance, and represented only a small fraction (<2%) of the total number of the total monocytes. Further, similar changes were not observed for the 18.8 µg/kg dose level.

Intraparticipant safety, PK and PD data reveal the kinetics of IP-10 changes, body temperature, cell activation and antipyretic use. Figure 6 contains individual time course participant data through 72 hours post-dose after either a 12.5 µg/kg (Figure 6A) or 18.8 µg/kg (Figure 6B) injection of cavrotolimod. For both participants, cavrotolimod was observed in their plasma before meaningful pharmacodynamic effects, followed later by increased concentrations of IP-10. The chemokine release was followed by increases in body temperature (i.e., fever) and NK and T cell activation. Although the plasma concentrations of cavrotolimod peaked earliest and decayed rapidly, the immune

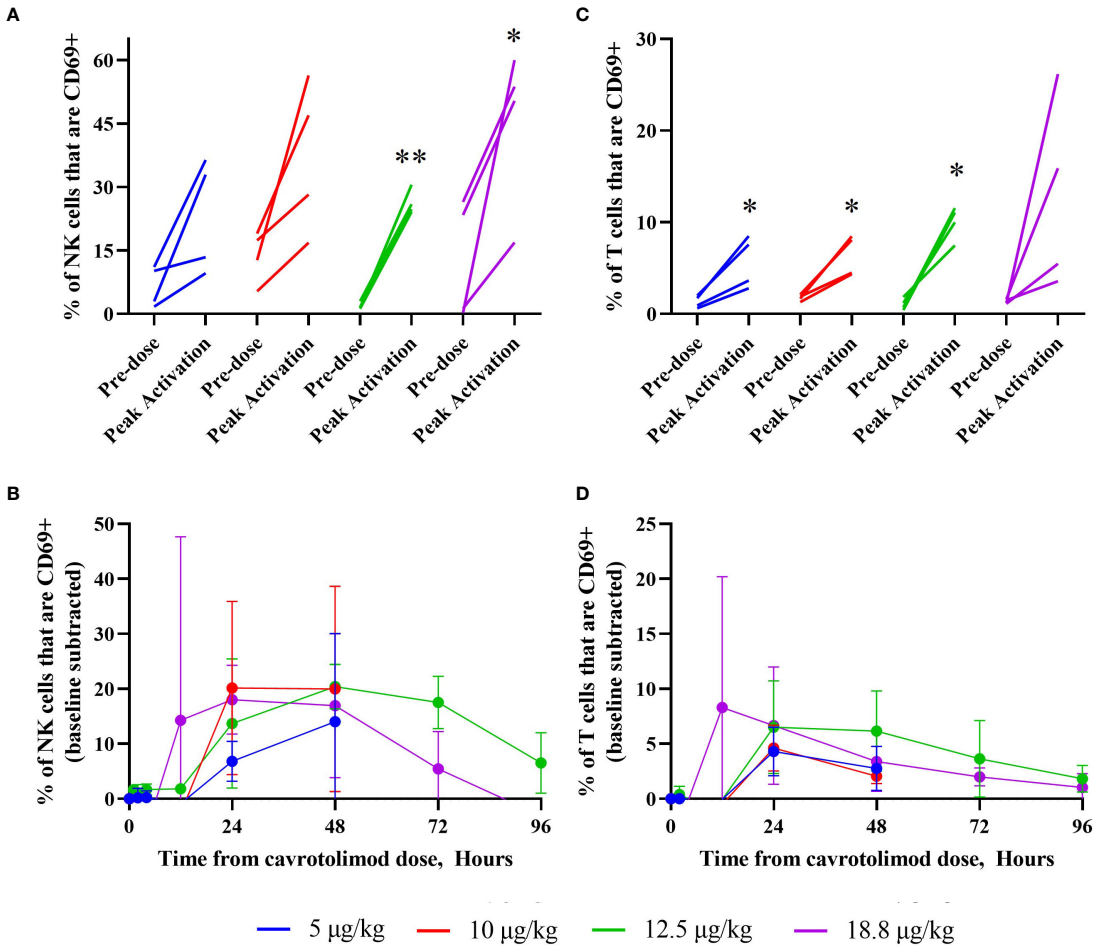

FIGURE 5
NK and T cell activation as a function of cavrotolimod dose and time. Flow cytometry was used to measure NK and T cell activation in peripheral blood following a single SC dose of cavrotolimod. For graphs **(A, C)**, each line represents a single participant. For each participant, the baseline and peak measurements are indicated, independent of time point when the peak cell activation was observed. For graphs **(B, D)**, each line represents averaged, baseline subtracted values from four participants in a cohort at the sampling time points indicated from receiving the dose of cavrotolimod. **(A, B)** Activated NK cells. **(C, D)** Activated T cells. Paired t-test of comparison of pre- to post-dose values; *p < 0.05; **p < 0.01.

cascade elicited by cavrotolimod had a much longer duration, as the activated NK and T cells peaked later with a longer decay to baseline out to 96 hours. When these participants were administered acetaminophen to address fever, in addition to a reduction in body temperature shortly after administration, there were generally corresponding reductions in peripheral chemokine concentrations.

Discussion

To achieve immune-mediated tumor control, cancer cells must be targeted by immune cells, a process which requires a delicate balance of sufficient neoantigen recognition without widespread autoimmunity. CPIs beneficially promote a shift in that balance toward anti-tumor responses, and do so by blocking certain immune-inhibitory proteins, allowing anti-tumor immune responses to develop or expand. In recent years, the United States Food and Drug Administration (FDA) has approved several CPIs targeting CTLA-4, PD-L1, and PD-1 (38), which have become indispensable treatments for many cancers. However, a considerable number of patients do not respond to or relapse on CPI treatments, a process called antigenic escape (2, 3). Tumor escape from CPI treatment is thought to result from exhausted effector T cells, functionally impaired antigen-presenting cells (APCs), and/or infiltration of tumor-supporting regulatory T cells (T_{reg}) and myeloid-derived suppressor cells (MDSCs) (39).

In settings where an anti-tumor response has been initiated but is being repressed, CPI therapies contribute greatly by relieving inhibitory signals. However, CPIs alone cannot promote the

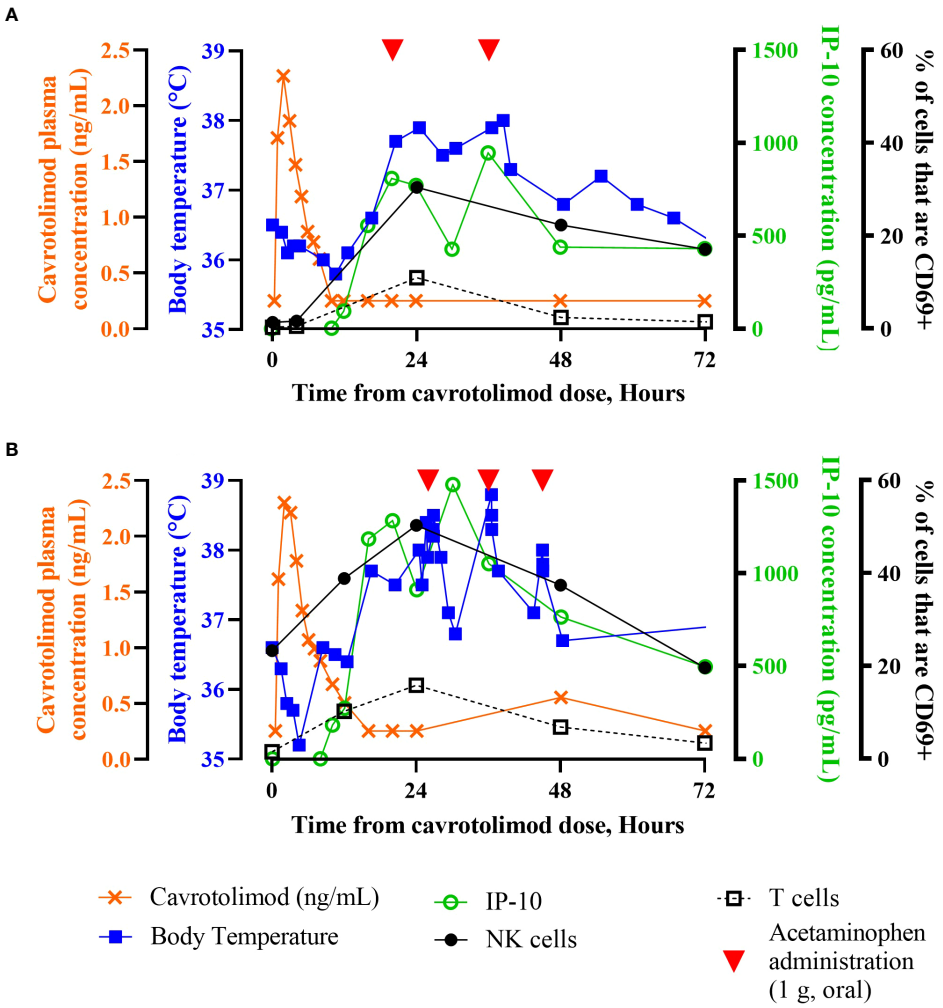

FIGURE 6
Individual participant time course data. Superimposed PK, PD and body temperature data presented as a function of time from receiving the dose of cavrotolimod for group 3 participant 13012 **(A)** and group 4 participant 14013 **(B)**. Participants 13012 and 14013 received 12.5 µg/kg (0.9 mg) and 18.8 µg/kg (1.1 mg) doses of cavrotolimod, respectively. Each line represents a single data set (PK, PD or body temperature) collected while on study for the respective participant. Administration of 1 g acetaminophen to treat related to AEs are indicated (red arrowheads). IP-10 concentrations and % of cells that are CD69+ are baseline subtracted.

initiation of an anti-tumor response, which require immune-stimulating therapies. A rational approach is the use of oligonucleotides containing CpG motifs that can act as activators of TLR9, which is expressed in the endosomes of B and plasmacytoid dendritic cells and induces rapid innate and long-term adaptive immune responses when agonized (5, 8, 11). TLR9 agonists lead to broad activation of immune cells, including APCs and T cells, and suppress T_{reg} and MDSCs in tumor microenvironments (40–42). TLR9-induced immune activation has been extensively characterized in preclinical and clinical studies of cancer (11, 15, 16). TLR9 agonists are often unformulated oligonucleotides. One major challenge associated with use of unformulated oligonucleotides is poor cellular uptake and limited downstream pharmacological activity (43). SNAs are a novel class of therapeutic agents consisting of densely packed and radially oriented oligonucleotides in a 3-dimensional arrangement around a spherical liposomal nanoparticle (23). As a consequence of their 3-D structure (illustrated in Figure 1), SNAs have increased cellular uptake, nuclease stability, and affinity to nucleic acid targets (23), characteristics which address many of the challenges associated with unformulated oligonucleotides. Here we described the activity of cavrotolimod, a novel TLR9-agonist SNA that shows potent TLR9 stimulation in a Phase 1 clinical trial.

The primary objective of this study was to assess the safety and tolerability of cavrotolimod following single ascending doses. To meet this objective and to protect the wellbeing of the participants, a CRS and flu-like symptom management strategy was developed and deployed. There is little guidance

available in literature about managing CRS risk in healthy participant studies, but it is essential to have a process in place before a trial starts to appropriately classify and manage all CRS symptoms without unnecessarily stopping a trial or its progression. This approach may be useful for many clinical trials of advanced therapies or for approaches that use or release cytokines or chemokines, but we note that the algorithm may require tailoring to the environment and resources available to a particular clinical research unit.

Overall, cavrotolimod was considered safe and well tolerated after single SC injections. The AEs observed in the trial were as expected from the TLR9 agonism-based mechanism of action, nonclinical toxicology studies and from other TLR9 agonist clinical trial results. The absence of a placebo arm in the study did not affect this objective because a small number of placebo participants were unlikely to produce statistically meaningful results. Instead, due to the high inter-participant variability of cytokines, chemokines and other immune markers, the use of intra-participant comparisons of PD markers before and after cavrotolimod administration in the statistical analysis of the safety/tolerability (and PD) was expected to yield more robust results than comparing these effects across placebo and cavrotolimod treated participants.

Cavrotolimod's mechanism of action and data from other TLR9 agonists showed that cytokine secretion and lymphocyte activation was an expected and desired PD effect. These PD effects would in turn be expected to produce flu-like symptoms including fevers, injection site reactions and lymphadenopathy, which were observed AEs from this Phase 1 study. Injection site reactions and lymphadenopathy were mild and transitory. The lymphocyte and neutrophil count changes observed reflect a well-documented trafficking phenomenon also associated with the pro-inflammatory TLR9 mechanism of action (44). When looking at the overall clinical picture, taking into account AEs, laboratory abnormalities (CRP, neutrophils and lymphocytes), vital signs and lymphadenopathy, the maximum intensity of the flu-like symptoms was mild. Further, no off-target, systemic effects were observed in this study and no other clinically significant abnormalities on safety assessments were observed and thus there was no evidence of any safety signal.

A secondary objective of this study was to assess the PK of cavrotolimod in plasma and urine. C_{max} values were similar for the 5 and 10 μg/kg dose groups whereas dose-proportionate increases were observed from 10 to 18.8 μg/kg; the highest mean C_{max} was 1.8 ng/mL at the highest dose. T_{max} ranged from 2.00 to 2.52 hours over the dose range tested. The sparse plasma concentration values observed are not unusual for a SC administered TLR9 agonist. Importantly, the PK and PD of cavrotolimod are not expected to be temporally related, as was observed in this Phase 1 study and based on the literature. Therefore, similar cytokine and lymphocyte activation measurements are important markers for inclusion in future studies. In future studies utilizing greater doses of cavrotolimod, the PK data may be more robust and informative.

PD analyses of the cytokine release profile and lymphocyte subset activation confirmed the desired effects of cavrotolimod. Cavrotolimod elicited a broad Th1-type immune response in an approximately dose-proportional manner and activated T cells and NK cells. Regarding the cytokine response, cavrotolimod has robust PD activity but did not trigger CRS. IL-12 p40, IL-1RA, IP-10, and MCP-1 were consistently induced across all doses. IP-10 was robustly induced, while IFN-γ and TNF-α were inconsistently induced. The maximum duration of the cytokine PD effect generally appears to be approximately five days. This duration was an important factor underlying the selection of the weekly dosing interval selected for a follow on clinical trial in patients. NK cells are cytotoxic lymphocytes critical to the innate immune system, while T cells play a central role in cell-mediated immunity, so the activation of these cells bodes well for the hypothesis that cavrotolimod will produce anti-tumor immune responses. The NK cell activation peaked at about 48 hours and declined through to 96 hours. T cell activation, which was measured by the presence of CD69, was observed in all participants and generally peaked between 12 and 24 hours, with the activation tapering off through to 96 hours.

The kinetics of cytokine and chemokine expression, and cell activation observed during this study suggest a weekly dosing interval, thus fulfilling the final secondary objective of this study. Indeed, weekly cavrotolimod dosing was used for the first three cycles in a Phase 1b/2 study of cavrotolimod in advanced cancer patients (45). Similar cytokine and lymphocyte activation measurements were used for the Phase 1b study to help inform the selection of the recommended Phase 2 dose.

Cavrotolimod's PD activity compares favorably to other TLR9 agonists tested in healthy participant studies. PF-03512676, an unformulated TLR9 agonist, did not produce changes in IFNγ or IL-12 cytokine levels after SC administration at a dose of 20 μg/kg (32), while cavrotolimod produced an increase in the plasma concentration of those cytokines at a similar dose of 18.8 μg/kg. IL-12 has been demonstrated to regulate both innate and adaptive immunities in cancer therapy (46), and IFNγ drives PD-L1 expression (47), which correlates to clinical responses to anti-PD-1 and anti-PD-L1 antibody therapy (37). Lefitolimod, another TLR9 agonist previously in a Phase 3 clinical trial, produced a 7-fold increase in cohort mean IP-10 concentrations in participant serum after a 60 mg dose (equivalent to 923 μg/kg for a 65 kg participant) (48). In comparison, cavrotolimod produced a 32-fold increase in IP-10 over baseline at a dose of 18.8 μg/kg. Overall, this Phase 1 study confirmed that cavrotolimod has robust PD activity but did not trigger an immune cascade or CRS.

The PD effects observed in healthy participants in this Phase 1 study suggest that cavrotolimod may synergize effectively with CPI antibodies to initiate and sustain the cancer immunity cycle, which is a seven-step model of how the immune system initiates and propagates anti-tumor immunity (4). Cavrotolimod's activation of NK cells and T cells, along with induction of TNF, IL-12 and IP-10 cytokines, address at least four of the

seven steps in the cycle while CPIs are effective at addressing two other steps. In the context of the cancer immunity cycle and data collected from this Phase 1 study, cavrotolimod has promising PD characteristics for use in combination with CPIs in the first line setting or in patients with disease resistant to PD-1/PD-L1 blockade.

The safety and PD results of this study are compelling support for the use of TLR9-agonist cavrotolimod with CPIs in populations with advanced cancer. On the basis of these results, cavrotolimod was studied in a Phase 1b/2 clinical trial in combination with pembrolizumab or cemiplimab (34, 45) in advanced or metastatic skin cancers.

Data availability statement

The raw data supporting the conclusions of this article will be made available by the authors, without undue reservation.

Ethics statement

The studies involving human participants were reviewed and approved by Health Research Authority - London Bridge Research Ethics Committee Skipton House 80 London Road SE1 6LH. The patients/participants provided their written informed consent to participate in this study.

Author contributions

AB, UL, and WD designed and interpreted the Phase 1 clinical trial study. SM and WD supervised the study as Sponsor, prepared the figures and wrote the manuscript. All authors reviewed the manuscript. All authors contributed to the article and approved the submitted version.

Funding

The study received funding from Exicure, Inc. The funder was involved in the study design, collection, analysis, interpretation of data, the development of the present manuscript and the decision to submit it for publication. The corresponding author had full access to all of the data and the final responsibility to submit for publication.

Acknowledgments

The authors thank Drs. David Giljohann, Matthias Schroff, and Pinal Patel for insightful discussions during the design and execution of the study.

Conflict of interest

Authors SM and WD are employed by Exicure, Inc. and hold company issued stock and stock options. Author AB was employed by Bexon Clinical Consulting. This study received funding from Exicure, Inc. The funder supported the development of this manuscript and paid for medical writing support.

The remaining author declares that the research was conducted in the absence of any commercial or financial relationships that could be construed as a potential conflict of interest.

Publisher's note

Supplementary material

The Supplementary Material for this article can be found online at: https://www.frontiersin.org/articles/10.3389/fimmu.2022.1073777/full#supplementary-material

References

1. Vilgelm AE, Johnson DB, Richmond A. Combinatorial approach to cancer immunotherapy: strength in numbers. *J Leukoc Biol* (2016) 100:275–90. doi: 10.1189/jlb.5RI0116-013RR

2. Topalian SL, Hodi FS, Brahmer JR, Gettinger SN, Smith DC, McDermott DF, et al. Safety, activity, and immune correlates of anti-PD-1 antibody in cancer. *N Engl J Med* (2012) 366:2443–54. doi: 10.1056/NEJMoa1200690

3. Postow MA, Callahan MK, Wolchok JD. Immune checkpoint blockade in cancer therapy. *J Clin Oncol* (2015) 33:1974–82. doi: 10.1200/JCO.2014.59.4358

4. Chen DS, Mellman I. Oncology meets immunology: the cancer-immunity cycle. *Immunity* (2013) 39:1–10. doi: 10.1016/j.immuni.2013.07.012

5. Tokunaga T, Yamamoto H, Shimada S, Abe H, Fukuda T, Fujisawa Y, et al. Antitumor activity of deoxyribonucleic acid fraction from mycobacterium bovis

BCG. i. isolation, physicochemical characterization, and antitumor activity. *J Natl Cancer Inst* (1984) 72:955–62. doi: 10.1093/JNCI/72.4.955

6. Sato Y, Roman M, Tighe H, Lee D, Corr M, Nguyen MD, et al. Immunostimulatory DNA sequences necessary for effective intradermal gene immunization. *Science* (1996) 273:352–4. doi: 10.1126/science.273.5273.352

7. Krieg AM, Yi AK, Matson S, Waldschmidt TJ, Bishop GA, Teasdale R, et al. CpG motifs in bacterial DNA trigger direct b-cell activation. *Nature* (1995) 374:546–9. doi: 10.1038/374546a0

8. Hemmi H, Takeuchi O, Kawai T, Kaisho T, Sato S, Sanjo H, et al. A toll-like receptor recognizes bacterial DNA. *Nature* (2000) 408:740–5. doi: 10.1038/35047123

9. Bauer S, Kirschning CJ, Hacker H, Redecke V, Hausmann S, Akira S, et al. Human TLR9 confers responsiveness to bacterial DNA *via* species-specific CpG motif recognition. *Proc Natl Acad Sci USA* (2001) 98:9237–42. doi: 10.1073/pnas.161293498

10. Klinman DM, Yi AK, Beaucage SL, Conover J, Krieg AM. CpG motifs present in bacteria DNA rapidly induce lymphocytes to secrete interleukin 6, interleukin 12, and interferon gamma. *Proc Natl Acad Sci USA* (1996) 93:2879–83. doi: 10.1073/pnas.93.7.2879

11. Krieg AM. Therapeutic potential of toll-like receptor 9 activation. *Nat Rev Drug Discovery* (2006) 5:471–84. doi: 10.1038/nrd2059

12. Vollmer J, Weeratna R, Payette P, Jurk M, Schetter C, Laucht M, et al. Characterization of three CpG oligodeoxynucleotide classes with distinct immunostimulatory activities. *Eur J Immunol* (2004) 34:251–62. doi: 10.1002/eji.200324032

13. Verthelyi D, Ishii KJ, Gursel M, Takeshita F, Klinman DM. Human peripheral blood cells differentially recognize and respond to two distinct CPG motifs. *J Immunol* (2001) 166:2372–7. doi: 10.4049/jimmunol.166.4.2372

14. Marshall JD, Fearon K, Abbate C, Subramanian S, Yee P, Gregorio J, et al. Identification of a novel CpG DNA class and motif that optimally stimulate b cell and plasmacytoid dendritic cell functions. *J Leukoc Biol* (2003) 73:781–92. doi: 10.1189/jlb.1202630

15. Scheiermann J, Klinman DM. Clinical evaluation of CpG oligonucleotides as adjuvants for vaccines targeting infectious diseases and cancer. *Vaccine* (2014) 32:6377–89. doi: 10.1016/j.vaccine.2014.06.065

16. Krieg AM. CpG still rocks! update on an accidental drug. *Nucleic Acid Ther* (2012) 22:77–89. doi: 10.1089/nat.2012.0340

17. Melisi D, Frizziero M, Tamburrino A, Zanotto M, Carbone C, Piro G, et al. Toll-like receptor 9 agonists for cancer therapy. *Biomedicines* (2014) 2:211–28. doi: 10.3390/biomedicines2030211

18. Dimitriou F, Hauschild A, Mehnert JM, Long GV. Double trouble: Immunotherapy doublets in melanoma–approved and novel combinations to optimize treatment in advanced melanoma. In: *American Society of clinical oncology educational book*, vol. 42 VA: ASCO Publications in Alexandria. (2022). p. 745–66.

19. Jensen SA, Day ES, Ko CH, Hurley LA, Luciano JP, Kouri FM, et al. Spherical nucleic acid nanoparticle conjugates as an RNAi-based therapy for glioblastoma. *Sci Transl Med* (2013) 5:209ra152. doi: 10.1126/scitranslmed.3006839

20. Kouri FM, Hurley LA, Daniel WL, Day ES, Hua Y, Hao L, et al. miR-182 integrates apoptosis, growth, and differentiation programs in glioblastoma. *Genes Dev* (2015) 29:732–45. doi: 10.1101/gad.257394.114

21. Lewandowski KT, Thiede R, Guido N, Daniel WL, Kang R, Guerrero-Zayas MI, et al. Topically delivered tumor necrosis factor-alpha-Targeted gene regulation for psoriasis. *J Invest Dermatol* (2017) 137:2027–30. doi: 10.1016/j.jid.2017.04.027

22. Randeria PS, Seeger MA, Wang XQ, Wilson H, Shipp D, Mirkin CA, et al. siRNA-based spherical nucleic acids reverse impaired wound healing in diabetic mice by ganglioside GM3 synthase knockdown. *Proc Natl Acad Sci USA* (2015) 112:5573–8. doi: 10.1073/pnas.1505951112

23. Radovic-Moreno AF, Chernyak N, Mader CC, Nallagatla S, Kang RS, Hao L, et al. Immunomodulatory spherical nucleic acids. *Proc Natl Acad Sci USA* (2015) 112:3892–7. doi: 10.1073/pnas.1502850112

24. Mirkin CA, Letsinger RL, Mucic RC, Storhoff JJ. A DNA-based method for rationally assembling nanoparticles into macroscopic materials. *Nature* (1996) 382:607–9. doi: 10.1038/382607a0

25. Cutler JI, Auyeung E, Mirkin CA. Spherical nucleic acids. *J Am Chem Soc* (2012) 134:1376–91. doi: 10.1021/ja209351u

26. Banga RJ, Chernyak N, Narayan SP, Nguyen ST, Mirkin CA. Liposomal spherical nucleic acids. *J Am Chem Soc* (2014) 136:9866–9. doi: 10.1021/ja504845f

27. Barnaby SN, Sita TL, Petrosko SH, Stegh AH, Mirkin CA. Therapeutic applications of spherical nucleic acids. *Cancer Treat Res* (2015) 166:23–50. doi: 10.1007/978-3-319-16555-4_2

28. Choi CH, Hao L, Narayan SP, Auyeung E, Mirkin CA. Mechanism for the endocytosis of spherical nucleic acid nanoparticle conjugates. *Proc Natl Acad Sci USA* (2013) 110:7625–30. doi: 10.1073/pnas.1305804110

29. Patel PC, Giljohann DA, Daniel WL, Zheng D, Prigodich AE, Mirkin CA. Scavenger receptors mediate cellular uptake of polyvalent oligonucleotide-functionalized gold nanoparticles. *Bioconjug Chem* (2010) 21:2250–6. doi: 10.1021/bc1002423

30. Wu XA, Choi CH, Zhang C, Hao L, Mirkin CA. Intracellular fate of spherical nucleic acid nanoparticle conjugates. *J Am Chem Soc* (2014) 136:7726–33. doi: 10.1021/ja503010a

31. Nallagatla S, Anderson BR, Anantatmula S, Kandimalla ER. Spherical nucleic acids targeting toll-like receptor 9 enhance antitumor activity in combination with anti-PD-1 antibody in mouse tumor models. *Cancer Res* (2017) 77(13_Supplement):4706. doi: 10.1158/1538-7445.AM2017-4706

32. Krieg AM, Efler SM, Wittpoth M, Al Adhami MJ, Davis HL. Induction of systemic TH1-like innate immunity in normal volunteers following subcutaneous but not intravenous administration of CPG 7909, a synthetic b-class CpG oligodeoxynucleotide TLR9 agonist. *J Immunother* (2004) 27:460–71. doi: 10.1097/00002371-200411000-00006

33. Lee DW, Gardner R, Porter DL, Louis CU, Ahmed N, Jensen M, et al. Current concepts in the diagnosis and management of cytokine release syndrome. *Blood* (2014) 124:188–95. doi: 10.1182/blood-2014-05-552729

34. Exicure. *A phase 1 study of AST 008 in healthy subjects. NCT03086278* (2018). Available at: https://ClinicalTrials.gov/show/NCT03086278.

35. Rynkiewicz D, Rathkopf M, Sim I, Waytes AT, Hopkins RJ, Giri L, et al. Marked enhancement of the immune response to BioThrax(R) (Anthrax vaccine adsorbed) by the TLR9 agonist CPG 7909 in healthy volunteers. *Vaccine* (2011) 29:6313–20. doi: 10.1016/j.vaccine.2011.05.047

36. Aryan Z, Holgate ST, Radzioch D, Rezaei N. A new era of targeting the ancient gatekeepers of the immune system: toll-like agonists in the treatment of allergic rhinitis and asthma. *Int Arch Allergy Immunol* (2014) 164:46–63. doi: 10.1159/000362553

37. Patel SP, Kurzrock R. PD-L1 expression as a predictive biomarker in cancer immunotherapy. *Mol Cancer Ther* (2015) 14:847–56. doi: 10.1158/1535-7163.MCT-14-0983

38. Hargadon KM, Johnson CE, Williams CJ. Immune checkpoint blockade therapy for cancer: An overview of FDA-approved immune checkpoint inhibitors. *Int Immunopharmacol* (2018) 62:29–39. doi: 10.1016/j.intimp.2018.06.001

39. Spranger S. Mechanisms of tumor escape in the context of the T-cell-inflamed and the non-t-cell-inflamed tumor microenvironment. *Int Immunol* (2016) 28:383–91. doi: 10.1093/intimm/dxw014

40. Ashkar AA, Rosenthal KL. Toll-like receptor 9, CpG DNA and innate immunity. *Curr Mol Med* (2002) 2:545–56. doi: 10.2174/1566524023362159

41. Murad YM, Clay TM. CpG oligodeoxynucleotides as TLR9 agonists: therapeutic applications in cancer. *BioDrugs* (2009) 23:361–75. doi: 10.2165/11316930-000000000-00000

42. Zoglmeier C, Bauer H, Norenberg D, Wedekind G, Bittner P, Sandholzer N, et al. CpG blocks immunosuppression by myeloid-derived suppressor cells in tumor-bearing mice. *Clin Cancer Res* (2011) 17:1765–75. doi: 10.1158/1078-0432.CCR-10-2672

43. Juliano RL. The delivery of therapeutic oligonucleotides. *Nucleic Acids Res* (2016) 44:6518–48. doi: 10.1093/nar/gkw236

44. Haining WN, Davies J, Kanzler H, Drury L, Brenn T, Evans J, et al. CpG oligodeoxynucleotides alter lymphocyte and dendritic cell trafficking in humans. *Clin Cancer Res* (2008) 14:5626–34. doi: 10.1158/1078-0432.CCR-08-0526

45. Exicure. *Intratumoral cavrotolimod combined with pembrolizumab in patients with advanced solid tumors. NCT03684785* (2018). Available at: https://clinicaltrials.gov/ct2/show/NCT03684785.

46. Lu X. Impact of IL-12 in cancer. *Curr Cancer Drug Targets* (2017) 17:682–97. doi: 10.2174/1568009617666170427102729

47. Concha-Benavente F, Srivastava RM, Trivedi S, Lei Y, Chandran U, Seethala RR, et al. Identification of the cell-intrinsic and -extrinsic pathways downstream of EGFR and IFNgamma that induce PD-L1 expression in head and neck cancer. *Cancer Res* (2016) 76:1031–43. doi: 10.1158/0008-5472.CAN-15-2001

48. Manuel S, Kerstin K, Detlef O, Matthias S, Burghardt W, Alfredo Z. The immunotherapeutic TLR-9 agonist MGN1703 – pharmacokinetic and pharmacodynamic data from healthy volunteers and cancer patients. *Eur J Cancer* (2015) 51:S12. doi: 10.1016/j.ejca.2015.01.049

frontiers | Frontiers in Immunology

TYPE Mini Review
PUBLISHED 14 December 2022
DOI 10.3389/fimmu.2022.1029069

OPEN ACCESS

EDITED BY
Diana Boraschi,
Shenzhen Institute of Advanced Technology (CAS), China

REVIEWED BY
Yaoying Wu,
Duke University, United States
Wenjie Yang,
Shenzhen Institutes of Advanced Technology (CAS), China

*CORRESPONDENCE
Nikolay V. Dokholyan
dokh@psu.edu

SPECIALTY SECTION
This article was submitted to Molecular Innate Immunity, a section of the journal Frontiers in Immunology

RECEIVED 16 September 2022
ACCEPTED 23 November 2022
PUBLISHED 14 December 2022

CITATION
Vishweshwaraiah YL and Dokholyan NV (2022) mRNA vaccines for cancer immunotherapy. *Front. Immunol.* 13:1029069. doi: 10.3389/fimmu.2022.1029069

mRNA vaccines for cancer immunotherapy

Yashavantha L. Vishweshwaraiah [1]
and Nikolay V. Dokholyan [1,2,3,4]*

[1]Department of Pharmacology, Penn State College of Medicine, Hershey, PA, United States, [2]Department of Biochemistry and Molecular Biology, Penn State College of Medicine, Hershey, PA, United States, [3]Department of Chemistry, Pennsylvania State University, University Park, PA, United States, [4]Department of Biomedical Engineering, Pennsylvania State University, University Park, PA, United States

Immunotherapy has emerged as a breakthrough strategy in cancer treatment. mRNA vaccines are an attractive and powerful immunotherapeutic platform against cancer because of their high potency, specificity, versatility, rapid and large-scale development capability, low-cost manufacturing potential, and safety. Recent technological advances in mRNA vaccine design and delivery have accelerated mRNA cancer vaccines' development and clinical application. In this review, we present various cancer vaccine platforms with a focus on nucleic acid vaccines. We discuss rational design and optimization strategies for mRNA cancer vaccine development. We highlight the platforms available for delivery of the mRNA vaccines with a focus on lipid nanoparticles (LNPs) based delivery systems. Finally, we discuss the limitations of mRNA cancer vaccines and future challenges.

KEYWORDS

mRNA, cancer vaccine, immunotherapy, lipid nanoparticles, nucleic acid, optimization, tumor antigen

1 Introduction

With almost 10 million deaths per year, cancer remains one of the leading causes of death worldwide (1). Finding effective means to fight cancer has been one of the main goals of researchers worldwide for decades and still presents us with enormous challenges. In recent years, immunotherapy has been emerging as a major cancer

Abbreviations: TAs, tumor antigens; MHC, major histocompatibility complex; DCs, dendritic cells; APC, antigen-presenting cell; ROS, reactive oxygen species; LNPs, lipid nanoparticles; UTR, untranslated region; ORF, open reading frame; IVT mRNA, *in vitro* transcribed mRNA; TNFRSF4, tumor necrosis factor receptor superfamily member 4; NGS, next-generation sequencing; PEG, polyethylene glycol; TLR, toll-like receptors; HLA, human leukocyte antigen.

treatment strategy (2–4). Immunotherapy is a therapeutic approach that dynamically modulates the immune system to recognize and destroy cancer cells. Various immunotherapy approaches are being developed to improve clinical outcomes in cancer patients. The development of cancer vaccines is a promising immunotherapy strategy to induce tumor antigens (TAs) specific and long-lasting immune responses. The artificial triggering of an immune response against TAs forms the basis for vaccines against cancers (1, 5).

Cancer vaccines target TAs to elicit both cellular and humoral immune responses which suppress tumor growth and eradicate the tumor (6). TAs can be classified into tumor-associated antigens and tumor-specific antigens. Tumor-associated antigens are nonmutated proteins that are overexpressed or aberrantly expressed in cancer cells (7). Tumor-associated antigens can be differentiation antigens, products of silent genes, universal tumor antigens, and oncoviral antigens. Clinical trials of cancer vaccines targeting tumor-associated antigens have had limited success (8). In some cases, tumor-associated antigens are expressed in normal cells, increasing the risk of vaccine-induced autoimmune toxicity. Tumor-specific antigens are specifically displayed by the tumor cells and are generally not displayed by the normal cells (9). Neoantigens are unique, tumor-specific antigens, resulting from the genetic instability of cancer cells (10). Neoantigens have a higher affinity for major histocompatibility complex (MHC) and potent immunogenicity. They are specifically expressed by tumor cells and elicit a tumor-specific T-cell response with limited "off-target" toxicity. Hence, neoantigens have become the main target for cancer vaccines in recent years (11).

Cancer vaccination strategies are of two types: preventive or prophylactic strategy and therapeutic strategy (12, 13). The preventive strategy aims to induce immune memory by administering vaccines to healthy individuals to prevent morbidity due to virus-associated cancers. There are currently only two prophylactic vaccines that are approved by the FDA to prevent malignancies caused by hepatitis B virus and human papillomavirus (11, 14, 15). However, not all cancers can be avoided by prophylactic vaccinations, as not all cancers are caused by viruses. To date, no preventive vaccine against non-viral cancers has been approved for use in humans. The therapeutic strategy aims to treat the disease by boosting or reactivating the patient's own immune system. Two therapeutic vaccines are currently approved in cancer immunotherapy, namely the Bacillus Calmette-Guérin (BCG) vaccine for bladder cancer and a dendritic cell-based vaccine (Sipuleucel-T) for castration-resistant prostate cancer (11). In addition to the approved cancer vaccines, several other cancer vaccines are either in development or in the preclinical and clinical research phase (16). A complete list of cancer vaccines in clinical trials is available at clinicaltrials.gov.

Despite considerable research into cancer vaccine development, the clinical use of cancer vaccines has been hampered due to the diversity of tumor antigens, systemic toxicity, and low immunogenicity of tumor antigens. In recent years, in-depth studies of immunological mechanisms and the development of various new vaccine platforms have greatly advanced vaccine research. The rapid development and success of RNA-based vaccines against SARS-CoV-2 in response to the COVID-19 pandemic have brought cancer vaccines back into focus.

In this review, we discuss cancer vaccine approaches with a focus on nucleic acid vaccines, compare DNA and mRNA cancer vaccines, and finally discuss on the approaches for designing and optimizing mRNA-based cancer vaccines, delivery formats for mRNA vaccines, and future prospects.

2 Cancer vaccine platform types

In general, cancer vaccine platforms are classified into cell-based vaccines, peptide-based vaccines, viral-based vaccines, and nucleic acid-based vaccines (Figure 1).

2.1 Cell-based cancer vaccines

The tumor cell vaccine approach is a simple and straightforward method in which allogenic or autologous patient-derived tumor cells are used to produce cellular vaccines (17, 18). To enhance the immune response against whole tumor cells, tumor cell lines can be genetically modified by introducing cytokines, chemokines, and co-stimulatory molecule-encoding genes or by silencing immunosuppressive genes. The limitation of this method is that it is sometimes difficult to obtain a sufficient number of cells to induce effective immune response (19).

Dendritic cells (DCs) are highly specialized antigen presenting cells (APCs) that activate naive T cells and are used in the development of cell-based cancer vaccines (20). In DC based vaccine development approach, DCs are loaded with a variety of tumor antigens in the form of DNA, RNA, tumor lysates, tumor-derived proteins, or peptides. Based on the DCs subpopulation, various types of DC vaccines have been developed in recent years. The main types of DCs used in DC vaccines include monocyte-derived DCs (Mo-DCs) and leukemia-derived DCs (DCleu) (20). Since it is possible to culture DCs in adequate numbers, DC cancer vaccines have been tested in phase I, II and III clinical trials (21).

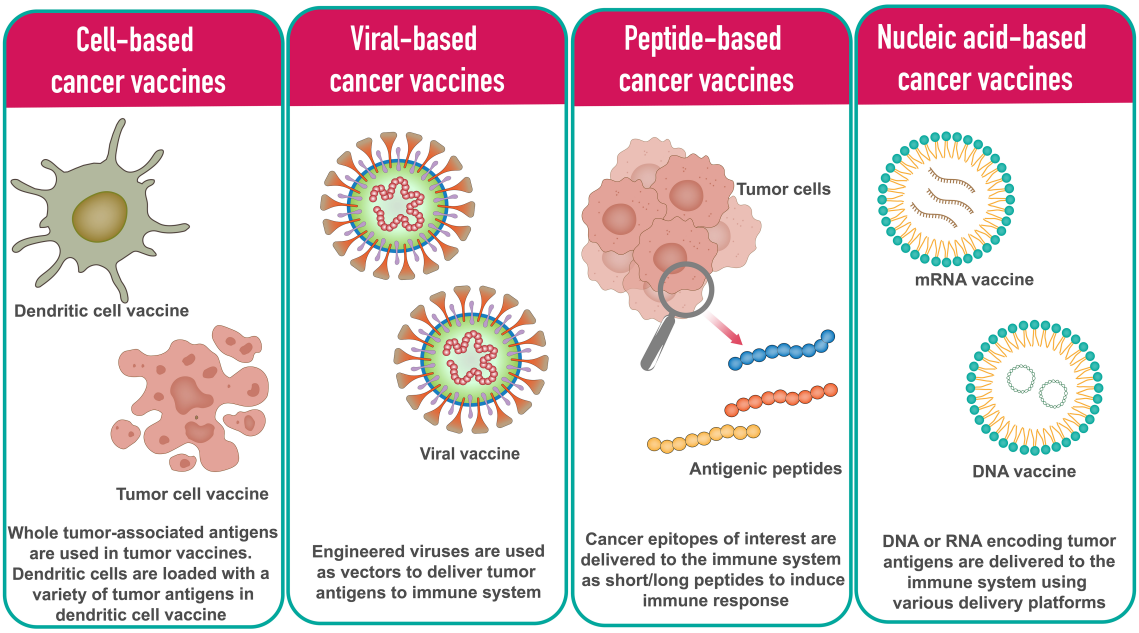

FIGURE 1
Different types of cancer vaccine platforms.

2.2 Peptide-based cancer vaccines

Peptide-based cancer vaccines consist of highly immunogenic tumor-specific peptide antigens to elicit the desired immune response. Using synthetic peptides, peptide vaccination approaches are being used to develop personalized cancer vaccines. Upon administration, peptides antigenic peptides are taken up by APCs and presented in complex with the HLA molecules on the cell surface. T cells recognize the surface antigens, leading to cancer-specific immune responses. The peptide-based vaccine approach has several advantages over other types of vaccines, particularly in terms of safety and ease of manufacturing (22). HBV and HPV vaccines for liver and cervical cancers are two examples of peptide-based vaccines (23).

2.3 Viral-based cancer vaccines

Many viruses are inherently immunogenic, and their genetic content can be manipulated to include sequences encoding TAs. Several viruses have been used as platforms for cancer vaccines. The most common viral vaccine vectors are from adenoviruses, poxviruses, and alphaviruses (24, 25). Most viral vectors are either replication-defective or attenuated versions. A major advantage of virus-based vaccines is that the immune system responds efficiently to viruses, with both innate and adaptive mechanisms working together in the induction of strong and durable immune responses (26). The downside is that the antiviral immune response can neutralize the vector, limiting further repeat immunizations.

Oncolytic virus vaccines represent a novel and exciting approach. Oncolytic viruses identify, infect, and kill tumor cells and promote anti-tumor responses. After infection with the oncolytic virus, tumor cells produce reactive oxygen species (ROS) and cytokines that stimulate immune cells, followed by oncolysis (27–29). T-VEC, a first-generation recombinant herpes simplex virus product, is one such oncolytic virus vaccine (30). Besides herpes simplex virus, adenovirus is another commonly used oncolytic virus due to its ease of handling and a broad spectrum of host cell tropism (11).

2.4 Nucleic acid-based cancer vaccines

Nucleic acid vaccines are vaccines that contain antigens encoded by either DNA or RNA. The nucleic acid vaccine is a promising and attractive vaccine platform because it allows multiple antigens to be easily administered with one immunization and its ability to induce strong MHC I mediated CD8+ T cell responses (31). Compared to traditional vaccines, nucleic acid vaccines have demonstrated advantages such as safety, specificity for inducing the immune response for the antigen of interest, induction of both

humoral and cellular immune responses, relatively low production cost, and ease of manufacturing (32).

DNA cancer vaccines consist of engineered DNAs that code for one or more TAs. DNA vaccines cross the cell membrane of APCs to the cytoplasm and move to the nucleus to start transcription. The resulting mRNAs translocate to the cytoplasm where they are translated into specific TAs by the host machinery. The resulting antigens are then presented to APC to stimulate an immune response (33). Poor immunogenicity of DNA vaccines compared to other vaccine platforms and long-term expression have drawn attention to RNA vaccines (34). Several DNA cancer vaccines have undergone preclinical and clinical trials over the past decade. The DNA vaccine has been extensively studied in cervical cancer. VGX-3100, a DNA vaccine against HPV-16/HPV-18 E6 and E7 oncogenes, has shown promising results in patients with premalignant high-grade cervical intraepithelial neoplasia (35). This vaccine is currently being evaluated in two Phase III clinical trials for safety and efficacy. GX-188E is another cervical cancer DNA vaccine that fuses multiple epitopes (36). GX-188E has the ability to target and activate dendritic cells. Promising results were obtained in a phase II study of GX-188E in cervical cancer (36). Recently, a preclinical study using a synthetic DNA multi-neoantigen vaccine demonstrated a therapeutic antitumor response by inducing a predominant CD8+ T cell response in mouse tumor models (37). In addition, DNA cancer vaccines have demonstrated safety and tolerability in early clinical trials for the treatment of multiple prostate and breast cancers (38, 39).

Like DNA vaccines, mRNA vaccines deliver genetic information encoding TAs in the form of mRNAs. mRNA vaccines do not need to reach the nucleus as they are translated in the cytoplasm (40). The overall immunogenicity of mRNA vaccines is slightly better than that achieved with DNA vaccines. Transient expression of mRNA-encoded antigen allows for more controlled antigen exposure and reduces long-term antigen exposure risk. The disadvantage of the RNA vaccine is that RNA is more easily degraded than DNA (41). However, there are various modifications that can increase stability. Due to challenges related to stability, cost of personalized manufacturing of patient-specific vaccines, and delivery, advances in clinical development of mRNA vaccines have been slow. The COVID-19 pandemic led to the successful development and deployment of multiple mRNA vaccines, confirming the mRNA platform's remarkable versatility, safety, and promising immunogenicity on a global scale (42).

Several mRNA cancer vaccines are in different phases of development. Immunostimulant mRNA vaccine TriMix, encoding CD70, CD40L, and a constitutively active form of TLR4 produced vigorous CD8+ T cell responses in patients with stage III or IV melanoma, showing favorable tumor response rates in phase II clinical trial (43). Another immunostimulant mRNA vaccine, mRNA-252, which encodes human OX40L, IL-23, and IL-36, was developed by Moderna for the treatment of lymphoma and is currently in a clinical trial (NCT03739931). BNT111 mRNA vaccine that encodes four TAAs (NY-ESO-1, MAGE-A3, tyrosinase, and TPTE) has been effective in the treatment of melanoma patients (44). BioNTech and Moderna's personalized mRNA vaccines have shown promising anti-tumor effects in clinical trials. Currently, there are two personalized mRNA cancer vaccines, Moderna vaccine mRNA-4157 (encodes up to 34 neoantigens) and BioNTech vaccine BNT122 (encodes up to 20 neoantigens), in phase II clinical trials (45). A phase II clinical trial with BNT122 for the treatment of colorectal cancer is currently underway (NCT04486378).

For this review, we focus only on mRNA-based vaccines.

3 Rational design and optimization of mRNA cancer vaccines

The typical mRNA consists of a cap flanked by 5′-untranslated regions (UTR), 3′-UTRs, an open reading frame (ORF) encoding cancer antigens in mRNA cancer vaccines, and a poly(A) tail (Figure 2). These components of mRNA can be modified to increase stability, translational efficiency, and immunostimulatory properties. The design and optimization approaches include design and optimization of the coding region, design, and optimization of the noncoding region, and design and optimization of delivery formats.

3.1 Design and optimization of the coding sequence

It is known that codon composition affects translation efficiency. Substituting the rare codons with regular synonymous codons that contain many similar tRNAs in the cytosol accelerates translation and increases yield (46).

However, rare codon optimization for nucleic acid therapies may have potentially serious consequences that should be evaluated (47). Another form of sequence optimization is the enrichment of the GC content. GC enriched sequences are translated at rates 100-fold higher than low GC sequences (48). mRNA can be optimized by incorporating chemically modified nucleosides, which are known to decrease immunogenicity and significantly improve translational efficiency. Nucleotide modifications such as 5-methylcytidine (m5C), 1-methylpseudouridine and pseudouridine (ψ) are generally preferred modifications (49, 50).

3.2 Design and optimization of the noncoding region

The 5′ and 3′ UTR elements adjacent to the coding sequence are critical considerations in optimal vaccine design as they have

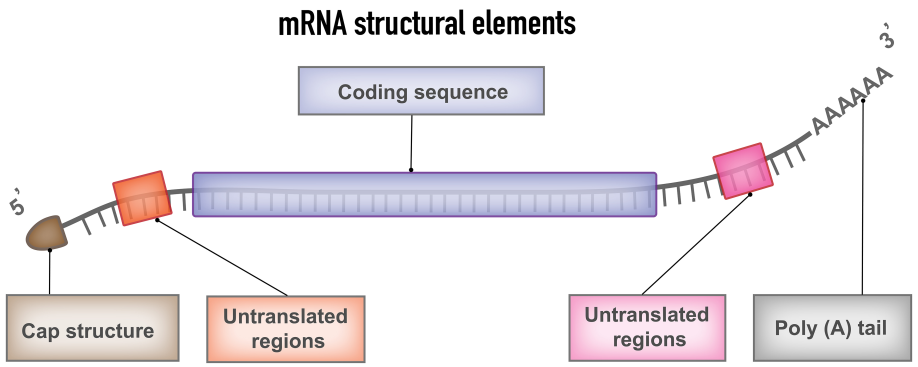

FIGURE 2
mRNA structural elements. Structural elements of mRNA vaccine include coding sequence, flanked by 5′and 3′ untranslated regions (UTRs), 5′ cap structure and 3′poly (A) tail.

a significant impact on mRNA stability, ribosome recognition, and translation (51). Optimizing 5′- and 3′-UTR elements greatly increases the efficiency and half-life of mRNA. The 5′-UTR sequence can be optimized by avoiding the presence of start codons in the 5′-UTR that disrupt ORF translation, by avoiding the presence of highly stable secondary structures that affect ribosome recruitment and codon recognition, by using shorter 5′-UTRs that are ideal for mRNA translation (52, 53). By introducing the 3′-UTRs of α-and β-globin mRNAs, translation and stability of mRNA may be enhanced (54).

The 5′-cap structure is essential for effective mRNA protein synthesis. The 5-cap regulates pre-mRNA splicing and nuclear export acts as a protective structure protecting RNA from exonuclease cleavage and initiates mRNA translation. 5′ capping can be achieved by using a vaccinia virus capping enzyme or by incorporation of synthetic cap or anti-reverse cap analogs during or after the transcription process (52, 55).

The poly(A) tail stabilizes the mRNA and promotes protein translation. The appropriate length of the poly(A) tail is crucial for the regulation of mRNA translation and stability (56). The length of the poly(A) tail is directly proportional to the translational efficacy. The poly(A) tail improves the stability of mRNA by slowing down the degradation of RNA by RNA exonucleases (45). There are two ways to add a poly(A) tail to *in vitro* transcribed (IVT) mRNA *i.e.* (i) extending the IVT mRNA after transcription by using recombinant poly(A) polymerase (ii) including poly(A) tail encoding DNA template from which IVT mRNA is transcribed. mRNA transcribed from a DNA template yields transcripts with a defined poly(A) tail length, whereas the enzymatic polyadenylation process yields mRNA transcripts with variable length poly(A) tails. In addition, deadenylation by poly(A)-specific nucleases can be inhibited by the incorporation of modified nucleotides into the poly(A) tail (52).

3.3 Delivery format optimization

After generating the IVT mRNA transcript, the next step is to administer the RNA vaccine, which should eventually reach the cytoplasm of the target cells. Because of the negatively charged structure of naked RNA and the large molecular size, mRNA is prone to degradation by nucleases and cannot cross the cell membrane. To overcome this obstacle, several mRNA vaccine delivery strategies have been employed, which can be broadly classified into two basic approaches *i.e.* (i) *ex vivo* loading of mRNA into DCs, (ii) direct injection of mRNA with or without a carrier.

3.3.1 *Ex vivo* loading of mRNA into DCs

DCs are the most potent antigen-presenting cells in the immune system. When DCs are used as a vaccination platform, DCs are transfected with mRNA encoding a tumor antigen of interest and then delivered to the host to elicit an immune response against the antigen (57–59). DCs can be transfected with either TAAs mRNA or total tumor RNA (60, 61); both methods have their advantages and disadvantages. DCs can internalize naked mRNA through a variety of endocytic pathways, but *ex vivo* transfection is commonly enhanced by applying electroporation to achieve high transfection efficiency without the need for a carrier molecule (57). Once DCs are loaded with mRNA *ex vivo*, they are reinfused into the recipient of the autologous vaccine to elicit the immune response. Loading of DCs with additional mRNAs, such as mRNAs encoding costimulatory molecules CD83, tumor necrosis factor receptor superfamily member 4 (TNFRSF4), and 4-1BB ligand (4-1BBL), has been shown to result in a substantial increase in the immunostimulatory activities of DCs (59). Most *ex vivo* loaded DC vaccines elicit a predominantly cell-mediated immune response. *Ex vivo* DC loading allows precise control of

transfection efficiency and cellular target. The main disadvantage of this approach is that it is an expensive and labor-intensive vaccination approach (49). An example of this approach is a phase I trial evaluating autologous Langerhans-type dendritic cells with xenogeneic TRP-2 mRNA (62).

3.3.2 Direct injection of mRNA with or without a carrier

Direct injection of mRNA is a comparatively faster and less expensive approach. Recent advances in the direct injection approach have made a lot of progress in precise and efficient cell-type specific delivery of mRNA vaccines.

Naked mRNA has been used successfully for *in vivo* immunizations. Naked mRNA vaccines are formulated in buffer only and without a carrier. In this approach, native mRNA vaccines are injected directly. After administration, naked mRNAs can induce antigen-specific antibodies and T-cell immune responses (61). The limitation of the naked mRNA vaccine platform is the short extracellular half-life of naked mRNA due to rapid degradation caused by ubiquitous RNAases (63). Viral vector-based technologies have been used to deliver nucleic acid vaccines into cells, but their application is limited by pre-existing or vaccine-induced anti-vector immunity, which can reduce vaccine efficacy (64). To overcome some of these limitations, physical methods such as the gene gun method, electroporation, virus-like particles produced in yeast, synthetic delivery vehicles such as liposomes and lipoplexes, and cationic polymers have been developed for IVT mRNA to protect it from RNAase degradation, enhance cellular uptake and improve vaccine delivery (65–69).

Among the various delivery vehicles, LNPs have emerged as one of the advanced and widely used mRNA delivery platforms due to the success of the mRNA-LNP vaccines against SARS-CoV-2 (Figure 3) (70). Lipid nanoparticles are nanosized lipid formulations designed to protect mRNA payloads from degradation and allow for their efficient delivery to target cells.

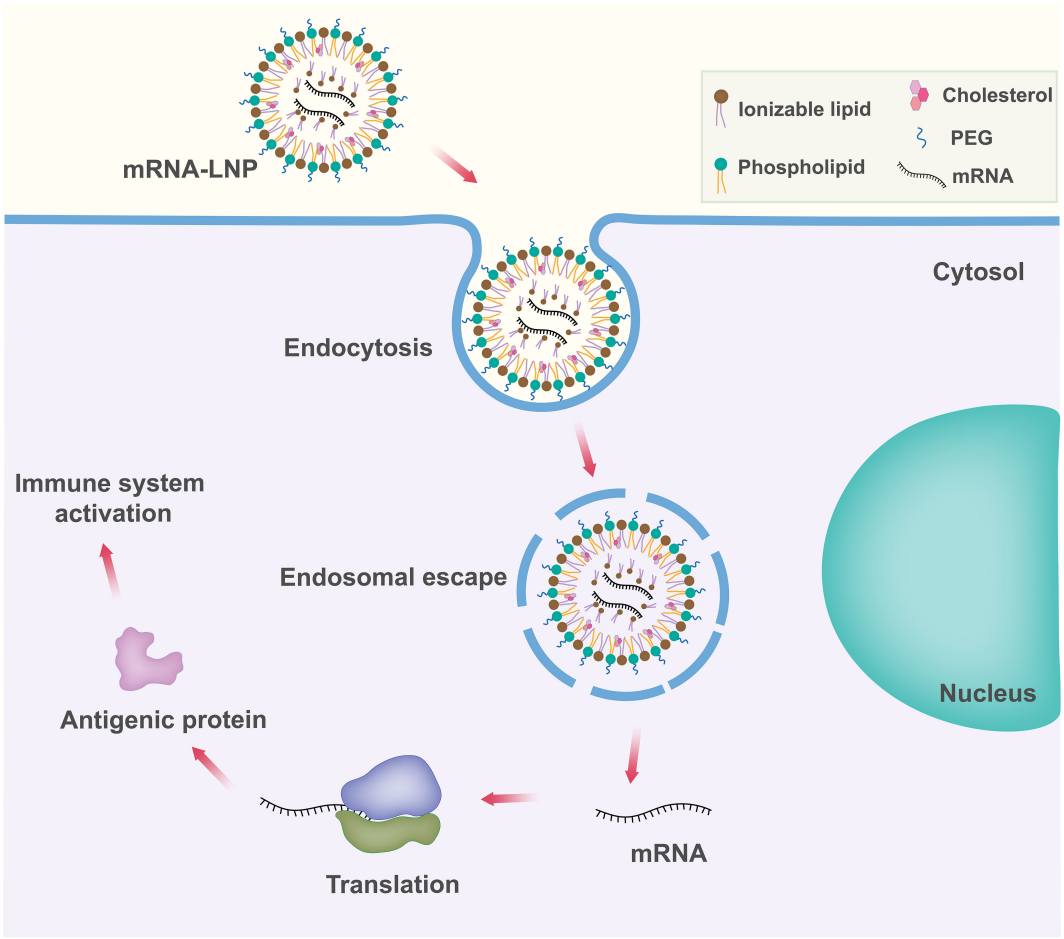

FIGURE 3
Schematic representation of lipid nanoparticle (LNP) based mRNA delivery. Components of the LNP are shown in the upper right box.

These lipid-based nanocarriers can efficiently deliver mRNA intracellularly by fusing with the lipid bilayer of early endosomes, thereby transporting the mRNA into the cytosol. LNPs are typically ~100 nm size carriers and consist of four components: ionizable lipids to form complexation with mRNA and allow the endosomal release of mRNA to the cytoplasm; lipid-linked polyethylene glycol (PEG) to increase the half-life of formulations; cholesterol to stabilize the structure of LNP; and phospholipids to support the lipid bilayer structure (71, 72).

Ionizable lipid. Ionizable lipid is the most important component of LNP as it determines LNP potency. Ionizable lipid generally differentiates different mRNA-LNPs. Ionizable lipids consist of a hydrophilic head group, hydrocarbon chains to enhance self-assembly, and linkers to connect the head groups to the hydrocarbon chains. Ionizable lipids are essential for mRNA complexation. Ionizable lipids are unionized within the LNPs, and they complex with mRNA to form electrostatically stable lipoplex. Ionizable lipids remain neutral in the systemic circulation pH (pH~7.4), but become protonated at early endosomal pH (pH~6.5) and facilitate endosomal membrane fusion followed by cytosolic release (73–75). Ionizable lipids lack a substantial positive charge at physiological pH, resulting in improved pharmacokinetics (76). This property increases the half-life in the bloodstream, allowing for better accumulation in target tissues such as solid tumors. Some ionizable lipids are known to induce inflammation and cell toxicity by activating toll-like receptors (TLR) pathways (77).

Polyethylene glycol (PEG)-lipid. Polyethylene glycol lipids generally comprise <2.5% of the total formulation in LNP. PEG-lipid structure consists of a hydrophilic PEG-polymer, which is conjugated with a hydrophobic lipid anchor. They are found at the surface of LNPs with the lipid domain hidden down in the particle and the PEG domain protruding from the surface. PEG lipids play an important role in balancing circulation time and cellular uptake (71). They are also important for the proper determination of particle size during manufacture (78). PEG-lipid helps to inhibit particle aggregation and in turn improves storage stability (79). Balancing the PEG lipids is important because they are known to prevent the transport of RNA into cells at high concentrations. The development of anti-PEG antibodies has raised concerns about possible allergic reactions to LNPs (80).

Phospholipids and cholesterol. Phospholipids and cholesterol contribute to the structural integrity and phase transition behavior of the LNPs. Cholesterol and phospholipid components of LNPs are unlikely to elicit significant innate immune recognition and inflammatory responses as they are naturally present in mammalian cell membranes (81).

The main advantage of mRNA-LNP vaccines is the modularity and versatility of the platform. LNPs components and their ratios, targeting moieties, and overall lipid-to-mRNA ratios can be tailored and optimized for different targets and applications. LNPs have lower immunogenicity, can deliver larger cargoes, and offer opportunities for rapid and large-scale manufacture. However, more studies should be done on the risks of mRNA-LNP technology. As with most drugs, side effects with mRNA-LNP vaccines often increase with dose. For example, for the mRNA-1273 vaccine, 100 μg of the dose showed good efficacy and minimal side effects, and 250 μg of the vaccine caused severe side effects, while the BNT162b2 vaccine at 30 μg showed better efficacy and minimal side effects (82, 83). Anaphylactic reactions and inflammatory reactions have been observed with some COVID-19 mRNA-LNP vaccines, even at the recommended doses (84–86). In addition, there is a residual risk of toxic side effects associated with the complexing agents and delivery compounds. Long-term immunological changes affecting adaptive immune responses have been reported (87). These data necessitate future studies to optimize the delivery system of mRNA vaccines.

Apart from the platform, the route of administration is also important to the effectiveness of the mRNA vaccines. Intramuscular and intradermal injections are the most commonly used routes of injection because these routes of injection provide the highest level of immunity and the longest duration of effect (71). Intravenous administration involves liver first-pass metabolism and is less convenient, so it is less preferred (71). The systemic route is only preferred in select cases.

4 Concluding remarks

mRNA cancer vaccines are a powerful and versatile form of immunotherapy. mRNA cancer vaccines are able to encode and express TAA, TSA, and their associated cytokines, and these vaccines can induce both humoral and cellular immunity. Appropriate selection of antigens is the basis for the development of mRNA cancer vaccines. mRNA cancer vaccines have several advantages, such as rapid and large-scale production, flexibility, versatility, relatively low production costs, no oncogenic potential, well-tolerated, and the ability to elicit a robust protective immune response. Importantly, mRNA vaccines do not carry the risk of integrating into the host genome, making them a promising therapeutic modality. The viability of mRNA vaccines to fight cancer has been demonstrated by numerous preclinical and clinical studies. Various mRNA cancer vaccines are currently being developed for a variety of cancer treatments. These studies have been extensively reviewed (45, 51, 88, 89).

Personalized mRNA vaccines open a new direction for precision cancer therapy. Personalized mRNA cancer vaccines coding for specific cancer antigens can be produced by utilizing next-generation sequencing (NGS) technology. Various computational approaches can be used to predict neoantigens and their presentation by human leukocyte antigen (HLA). Previously, we demonstrated such an application of computational approaches in epitope prediction and rational vaccine design (42, 90–94). With the increasing number of studies and clinical trials of personalized cancer vaccines, the possibility of developing mRNA vaccines against different types of

cancer is mounting. Despite the promise of mRNA cancer therapy, much more research is needed to develop stable mRNA and safe advanced delivery systems. Further development of personalized vaccines and clinical trials for different tumors are required.

mRNA-based vaccines have gained more and more popularity for the development of novel immunotherapies. However, the instability and *in vivo* delivery of mRNA cancer vaccine have impaired its clinical application. Although progress has been made over the past decades to overcome these limitations, challenges still exist on the development of mRNA cancer vaccines. Another major challenge is the targeted delivery of mRNA to specific tissues and cell types. In addition, future studies could focus on combining mRNA cancer vaccines with other immunotherapies to improve clinical outcomes and cancer treatment.

In summary, given the technological revolution in the field of mRNA vaccines, we can soon expect a leap in cancer immunotherapy and successful clinical translation of mRNA cancer vaccines.

Author contributions

All authors listed have made a substantial, direct, and intellectual contribution to the work and approved it for publication.

Funding

We acknowledge support from the National Institutes of Health (1R35 GM134864 and 1RF1 AG071675) and the Passan Foundation.

Conflict of interest

The authors declare that the research was conducted in the absence of any commercial or financial relationships that could be construed as a potential conflict of interest.

Publisher's note

References

1. Sobhani N, Scaggiante B, Morris R, Chai D, Catalano M, Tardiel-Cyril DR, et al. Therapeutic cancer vaccines: From biological mechanisms and engineering to ongoing clinical trials. *Cancer Treat Rev* (2022) 109:102429. doi: 10.1016/j.ctrv.2022.102429

2. Kruger S, Ilmer M, Kobold S, Cadilha BL, Endres S, Ormanns S, et al. Advances in cancer immunotherapy 2019 – latest trends. *J Exp Clin Cancer Res* (2019) 38:268. doi: 10.1186/s13046-019-1266-0

3. Zhang Y, Zhang Z. The history and advances in cancer immunotherapy: understanding the characteristics of tumor-infiltrating immune cells and their therapeutic implications. *Cell Mol Immunol* (2020) 17:807–21. doi: 10.1038/s41423-020-0488-6

4. Zhao Z, Zheng L, Chen W, Weng W, Song J, Ji J. Delivery strategies of cancer immunotherapy: recent advances and future perspectives. *J Hematol Oncol* (2019) 12:126. doi: 10.1186/s13045-019-0817-3

5. Pandolfi F, Cianci R, Pagliari D, Casciano F, Bagalà C, Astone A, et al. The immune response to tumors as a tool toward immunotherapy. *Clin Dev Immunol* (2011) 2011:894704. doi: 10.1155/2011/894704

6. Finn OJ. Cancer vaccines: between the idea and the reality. *Nat Rev Immunol* (2003) 3:630–41. doi: 10.1038/nri1150

7. Haen SP, Löffler MW, Rammensee H-G, Brossart P. Towards new horizons: characterization, classification and implications of the tumour antigenic repertoire. *Nat Rev Clin Oncol* (2020) 17:595–610. doi: 10.1038/s41571-020-0387-x

8. Buonaguro L, Tagliamonte M. Selecting target antigens for cancer vaccine development. *Vaccines* (2020) 8:615. doi: 10.3390/vaccines8040615

9. Minati R, Perreault C, Thibault P. A roadmap toward the definition of actionable tumor-specific antigens. *Front Immunol* (2020) 11:583287. doi: 10.3389/fimmu.2020.583287

10. Zhang Z, Lu M, Qin Y, Gao W, Tao L, Su W, et al. Neoantigen: A new breakthrough in tumor immunotherapy. *Front Immunol* (2021) 12:672356. doi: 10.3389/fimmu.2021.672356

11. Liu J, Fu M, Wang M, Wan D, Wei Y, Wei X. Cancer vaccines as promising immuno-therapeutics: platforms and current progress. *J Hematol Oncol* (2022) 15:28. doi: 10.1186/s13045-022-01247-x

12. Crews DW, Dombroski JA, King MR. Prophylactic cancer vaccines engineered to elicit specific adaptive immune response. *Front Oncol* (2021) 11:626463. doi: 10.3389/fonc.2021.626463

13. Finn OJ. The dawn of vaccines for cancer prevention. *Nat Rev Immunol* (2018) 18:183–94. doi: 10.1038/nri.2017.140

14. Petrosky E, Bocchini JAJ, Hariri S, Chesson H, Curtis CR, Saraiya M, et al. Use of 9-valent human papillomavirus (HPV) vaccine: updated HPV vaccination recommendations of the advisory committee on immunization practices. *MMWR Morb Mortal Wkly Rep* (2015) 64:300–4.

15. Mast EE, Margolis HS, Fiore AE, Brink EW, Goldstein ST, Wang SA, et al. A comprehensive immunization strategy to eliminate transmission of hepatitis b virus infection in the united states: recommendations of the advisory committee on immunization practices (ACIP) part 1: immunization of infants, children, and adolescents. *MMWR Recomm Rep Morb Mortal Wkly Rep Recomm Rep* (2005) 54:1–31.

16. Saxena M, van der Burg SH, Melief CJM, Bhardwaj N. Therapeutic cancer vaccines. *Nat Rev Cancer* (2021) 21:360–78. doi: 10.1038/s41568-021-00346-0

17. Chiang CL-L, Coukos G, Kandalaft LE. Whole tumor antigen vaccines: Where are we? *Vaccines* (2015) 3:344–72. doi: 10.3390/vaccines3020344

18. de Gruijl TD, van den Eertwegh AJM, Pinedo HM, Scheper RJ. Whole-cell cancer vaccination: from autologous to allogeneic tumor- and dendritic cell-based vaccines. *Cancer Immunol Immunother* (2008) 57:1569–77. doi: 10.1007/s00262-008-0536-z

19. Igarashi Y, Sasada T. Cancer vaccines: Toward the next breakthrough in cancer immunotherapy. *J Immunol Res* (2020) 2020:5825401. doi: 10.1155/2020/5825401

20. Yu J, Sun H, Cao W, Song Y, Jiang Z. Research progress on dendritic cell vaccines in cancer immunotherapy. *Exp Hematol Oncol* (2022) 11:3. doi: 10.1186/s40164-022-00257-2

21. Santos PM, Butterfield LH. Dendritic cell–based cancer vaccines. *J Immunol* (2018) 200:443 LP – 449. doi: 10.4049/jimmunol.1701024

22. Nelde A, Rammensee H-G, Walz JS. The peptide vaccine of the future. *Mol Cell Proteomics* (2021) 20:100022. doi: 10.1074/mcp.R120.002309

23. Slingluff CLJ. The present and future of peptide vaccines for cancer: single or multiple, long or short, alone or in combination? *Cancer J* (2011) 17:343–50. doi: 10.1097/PPO.0b013e318233e5b2

24. Hollingsworth RE, Jansen K. Turning the corner on therapeutic cancer vaccines. *NPJ Vaccines* (2019) 4:7. doi: 10.1038/s41541-019-0103-y

25. Larocca C, Schlom J. Viral vector-based therapeutic cancer vaccines. *Cancer J* (2011) 17:359–71. doi: 10.1097/PPO.0b013e3182325e63

26. Paston SJ, Brentville VA, Symonds P, Durrant LG. Cancer vaccines, adjuvants, and delivery systems. *Front Immunol* (2021) 12:627932. doi: 10.3389/fimmu.2021.627932

27. Santos Apolonio J, Lima de Souza Gonçalves V, Cordeiro Santos ML, Silva Luz M, Silva Souza JV, Rocha Pinheiro SL, et al. Oncolytic virus therapy in cancer: A current review. *World J Virol* (2021) 10:229–55. doi: 10.5501/wjv.v10.i5.229

28. Russell SJ, Peng K-W, Bell JC. Oncolytic virotherapy. *Nat Biotechnol* (2012) 30:658–70. doi: 10.1038/nbt.2287

29. Fu L-Q, Wang S-B, Cai M-H, Wang X-J, Chen J-Y, Tong X-M, et al. Recent advances in oncolytic virus-based cancer therapy. *Virus Res* (2019) 270:197675. doi: 10.1016/j.virusres.2019.197675

30. Russell SJ, Barber GN. Oncolytic viruses as antigen-agnostic cancer vaccines. *Cancer Cell* (2018) 33:599–605. doi: 10.1016/j.ccell.2018.03.011

31. Qin F, Xia F, Chen H, Cui B, Feng Y, Zhang P, et al. A guide to nucleic acid vaccines in the prevention and treatment of infectious diseases and cancers: From basic principles to current applications. *Front Cell Dev Biol* (2021) 9:633776. doi: 10.3389/fcell.2021.633776

32. Vishweshwaraiah YL, Dokholyan NV. Toward rational vaccine engineering. *Adv Drug Delivery Rev* (2022) 183:114142. doi: 10.1016/j.addr.2022.114142

33. Bai H, Lester GMS, Petishnok LC, Dean DA. Cytoplasmic transport and nuclear import of plasmid DNA. *Biosci Rep* (2017) 37. doi: 10.1042/BSR20160616

34. Kutzler MA, Weiner DB. DNA Vaccines: ready for prime time? *Nat Rev Genet* (2008) 9:776–88. doi: 10.1038/nrg2432

35. Trimble CL, Morrow MP, Kraynyak KA, Shen X, Dallas M, Yan J, et al. Safety, efficacy, and immunogenicity of VGX-3100, a therapeutic synthetic DNA vaccine targeting human papillomavirus 16 and 18 E6 and E7 proteins for cervical intraepithelial neoplasia 2/3: a randomised, double-blind, placebo-controlled phase 2b trial. *Lancet (London England)* (2015) 386:2078–88. doi: 10.1016/S0140-6736(15)00239-1

36. Choi YJ, Hur SY, Kim T-J, Hong SR, Lee JK, Cho C-H, et al. Prospective, randomized, multicenter, open-label study of GX-188E, an HPV DNA vaccine, in patients with cervical intraepithelial neoplasia 3. *Clin Cancer Res an Off J Am Assoc Cancer Res* (2020) 26:1616–23. doi: 10.1158/1078-0432.CCR-19-1513

37. Duperret EK, Perales-Puchalt A, Stoltz R, Hiranjith GH, Mandloi N, Barlow J, et al. A synthetic DNA, multi-neoantigen vaccine drives predominately MHC class I CD8(+) T-cell responses, impacting tumor challenge. *Cancer Immunol Res* (2019) 7:174–82. doi: 10.1158/2326-6066.CIR-18-0283

38. Eriksson F, Tötterman T, Maltais A-K, Pisa P, Yachnin J. DNA Vaccine coding for the rhesus prostate specific antigen delivered by intradermal electroporation in patients with relapsed prostate cancer. *Vaccine* (2013) 31:3843–8. doi: 10.1016/j.vaccine.2013.06.063

39. Tiriveedhi V, Tucker N, Herndon J, Li L, Sturmoski M, Ellis M, et al. Safety and preliminary evidence of biologic efficacy of a mammaglobin-a DNA vaccine in patients with stable metastatic breast cancer. *Clin Cancer Res an Off J Am Assoc Cancer Res* (2014) 20:5964–75. doi: 10.1158/1078-0432.CCR-14-0059

40. Ulmer JB, Mason PW, Geall A, Mandl CW. RNA-Based vaccines. *Vaccine* (2012) 30:4414–8. doi: 10.1016/j.vaccine.2012.04.060

41. Miao L, Zhang Y, Huang L. mRNA vaccine for cancer immunotherapy. *Mol Cancer* (2021) 20:41. doi: 10.1186/s12943-021-01335-5

42. Vishweshwaraiah YL, Hnath B, Rackley B, Wang J, Gontu A, Chandler M, et al. Adaptation-proof SARS-CoV-2 vaccine design. *Adv Funct Mater* (2022) 32:2206055. doi: 10.1101/2022.05.17.492310

43. Wilgenhof S, Van Nuffel AMT, Benteyn D, Corthals J, Aerts C, Heirman C, et al. A phase IB study on intravenous synthetic mRNA electroporated dendritic cell immunotherapy in pretreated advanced melanoma patients. *Ann Oncol Off J Eur Soc Med Oncol* (2013) 24:2686–93. doi: 10.1093/annonc/mdt245

44. Sahin U, Oehm P, Derhovanessian E, Jabulowsky RA, Vormehr M, Gold M, et al. An RNA vaccine drives immunity in checkpoint-inhibitor-treated melanoma. *Nature* (2020) 585:107–12. doi: 10.1038/s41586-020-2537-9

45. Deng Z, Tian Y, Song J, An G, Yang P. mRNA vaccines: The dawn of a new era of cancer immunotherapy. *Front Immunol* (2022) 13:887125. doi: 10.3389/fimmu.2022.887125

46. Hanson G, Coller J. Codon optimality, bias and usage in translation and mRNA decay. *Nat Rev Mol Cell Biol* (2018) 19:20–30. doi: 10.1038/nrm.2017.91

47. Mauro VP, Chappell SA. A critical analysis of codon optimization in human therapeutics. *Trends Mol Med* (2014) 20:604–13. doi: 10.1016/j.molmed.2014.09.003

48. Kudla G, Lipinski L, Caffin F, Helwak A, Zylicz M. High guanine and cytosine content increases mRNA levels in mammalian cells. *PloS Biol* (2006) 4:e180. doi: 10.1371/journal.pbio.0040180

49. Pardi N, Hogan MJ, Porter FW, Weissman D. mRNA vaccines — a new era in vaccinology. *Nat Rev Drug Discovery* (2018) 17:261–79. doi: 10.1038/nrd.2017.243

50. Weng Y, Li C, Yang T, Hu B, Zhang M, Guo S, et al. The challenge and prospect of mRNA therapeutics landscape. *Biotechnol Adv* (2020) 40:107534. doi: 10.1016/j.biotechadv.2020.107534

51. Wei J, Hui A-M. The paradigm shift in treatment from covid-19 to oncology with mRNA vaccines. *Cancer Treat Rev* (2022) 107:102405. doi: 10.1016/j.ctrv.2022.102405

52. Kim SC, Sekhon SS, Shin W-R, Ahn G, Cho B-K, Ahn J-Y, et al. Modifications of mRNA vaccine structural elements for improving mRNA stability and translation efficiency. *Mol Cell Toxicol* (2022) 18:1–8. doi: 10.1007/s13273-021-00171-4

53. Leppek K, Das R, Barna M. Functional 5' UTR mRNA structures in eukaryotic translation regulation and how to find them. *Nat Rev Mol Cell Biol* (2018) 19:158–74. doi: 10.1038/nrm.2017.103

54. Sahin U, Karikó K, Türeci Ö. mRNA-based therapeutics — developing a new class of drugs. *Nat Rev Drug Discovery* (2014) 13:759–80. doi: 10.1038/nrd4278

55. Pollard C, De Koker S, Saelens X, Vanham G, Grooten J. Challenges and advances towards the rational design of mRNA vaccines. *Trends Mol Med* (2013) 19:705–13. doi: 10.1016/j.molmed.2013.09.002

56. Jalkanen AL, Coleman SJ, Wilusz J. Determinants and implications of mRNA poly(A) tail size–does this protein make my tail look big? *Semin Cell Dev Biol* (2014) 34:24–32. doi: 10.1016/j.semcdb.2014.05.018

57. Kastenmüller W, Kastenmüller K, Kurts C, Seder RA. Dendritic cell-targeted vaccines — hope or hype? *Nat Rev Immunol* (2014) 14:705–11. doi: 10.1038/nri3727

58. Perez CR, De Palma M. Engineering dendritic cell vaccines to improve cancer immunotherapy. *Nat Commun* (2019) 10:5408. doi: 10.1038/s41467-019-13368-y

59. Gu Y, Zhao X, Song X. Ex vivo pulsed dendritic cell vaccination against cancer. *Acta Pharmacol Sin* (2020) 41:959–69. doi: 10.1038/s41401-020-0415-5

60. Dörrie J, Schaft N, Schuler G, Schuler-Thurner B. Therapeutic cancer vaccination with ex vivo RNA-transfected dendritic cells-an update. *Pharmaceutics* (2020) 12:92. doi: 10.3390/pharmaceutics12020092

61. Beck JD, Reidenbach D, Salomon N, Sahin U, Türeci Ö, Vormehr M, et al. mRNA therapeutics in cancer immunotherapy. *Mol Cancer* (2021) 20:69. doi: 10.1186/s12943-021-01348-0

62. Huff AL, Jaffee EM, Zaidi N. Messenger RNA vaccines for cancer immunotherapy: progress promotes promise. *J Clin Invest* (2022) 132:e156211. doi: 10.1172/JCI156211

63. Houseley J, Tollervey D. The many pathways of RNA degradation. *Cell* (2009) 136:763–76. doi: 10.1016/j.cell.2009.01.019

64. Geall AJ, Mandl CW, Ulmer JB. RNA: the new revolution in nucleic acid vaccines. *Semin Immunol* (2013) 25:152–9. doi: 10.1016/j.smim.2013.05.001

65. Kallen K-J, Heidenreich R, Schnee M, Petsch B, Schlake T, Thess A, et al. A novel, disruptive vaccination technology: self-adjuvanted RNActive(®) vaccines. *Hum Vaccin Immunother* (2013) 9:2263–76. doi: 10.4161/hv.25181

66. Johansson DX, Ljungberg K, Kakoulidou M, Liljeström P. Intradermal electroporation of naked replicon RNA elicits strong immune responses. *PloS One* (2012) 7:e29732. doi: 10.1371/journal.pone.0029732

67. Qiu P, Ziegelhoffer P, Sun J, Yang NS. Gene gun delivery of mRNA *in situ* results in efficient transgene expression and genetic immunization. *Gene Ther* (1996) 3:262–8.

68. Malone RW, Felgner PL, Verma IM. Cationic liposome-mediated RNA transfection. *Proc Natl Acad Sci U.S.A.* (1989) 86:6077–81. doi: 10.1073/pnas.86.16.6077

69. Qin S, Tang X, Chen Y, Chen K, Fan N, Xiao W, et al. mRNA-based therapeutics: powerful and versatile tools to combat diseases. *Signal Transduct Target Ther* (2022) 7:166. doi: 10.1038/s41392-022-01007-w

70. Tenchov R, Bird R, Curtze AE, Zhou Q. Lipid Nanoparticles─From liposomes to mRNA vaccine delivery, a landscape of research diversity and advancement. *ACS Nano* (2021) 15:16982–7015. doi: 10.1021/acsnano.1c04996

71. Hou X, Zaks T, Langer R, Dong Y. Lipid nanoparticles for mRNA delivery. *Nat Rev Mater* (2021) 6:1078–94. doi: 10.1038/s41578-021-00358-0

72. Guevara ML, Persano F, Persano S. Advances in lipid nanoparticles for mRNA-based cancer immunotherapy. *Front Chem* (2020) 8:589959. doi: 10.3389/fchem.2020.589959

73. Hajj KA, Whitehead KA. Tools for translation: non-viral materials for therapeutic mRNA delivery. *Nat Rev Mater* (2017) 2:17056. doi: 10.1038/natrevmats.2017.56

74. Kowalski PS, Rudra A, Miao L, Anderson DG. Delivering the messenger: Advances in technologies for therapeutic mRNA delivery. *Mol Ther* (2019) 27:710–28. doi: 10.1016/j.ymthe.2019.02.012

75. Meng C, Chen Z, Li G, Welte T, Shen H. Nanoplatforms for mRNA therapeutics. *Adv Ther* (2021) 4:2000099. doi: 10.1002/adtp.202000099

76. Kon E, Elia U, Peer D. Principles for designing an optimal mRNA lipid nanoparticle vaccine. *Curr Opin Biotechnol* (2022) 73:329–36. doi: 10.1016/j.copbio.2021.09.016

77. Igyártó BZ, Jacobsen S, Ndeupen S. Future considerations for the mRNA-lipid nanoparticle vaccine platform. *Curr Opin Virol* (2021) 48:65–72. doi: 10.1016/j.coviro.2021.03.008

78. Ryals RC, Patel S, Acosta C, McKinney M, Pennesi ME, Sahay G. The effects of PEGylation on LNP based mRNA delivery to the eye. *PloS One* (2020) 15: e0241006. doi: 10.1371/journal.pone.0241006

79. Thevenot J, Troutier A-L, David L, Delair T, Ladavière C. Steric stabilization of Lipid/Polymer particle assemblies by poly (ethylene glycol)-lipids. *Biomacromolecules* (2007) 8:3651–60. doi: 10.1021/bm700753q

80. Shi D, Beasock D, Fessler A, Szebeni J, Ljubimova JY, Afonin KA, et al. To PEGylate or not to PEGylate: Immunological properties of nanomedicine's most popular component, polyethylene glycol and its alternatives. *Adv Drug Delivery Rev* (2022) 180:114079. doi: 10.1016/j.addr.2021.114079

81. Samaridou E, Heyes J, Lutwyche P. Lipid nanoparticles for nucleic acid delivery: Current perspectives. *Adv Drug Delivery Rev* (2020) 154–155:37–63. doi: 10.1016/j.addr.2020.06.002

82. Rouf NZ, Biswas S, Tarannum N, Oishee LM, Muna MM. Demystifying mRNA vaccines: an emerging platform at the forefront of cryptic diseases. *RNA Biol* (2022) 19:386–410. doi: 10.1080/15476286.2022.2055923

83. Tian Y, Deng Z, Yang P. mRNA vaccines: A novel weapon to control infectious diseases. *Front Microbiol* (2022) 13:1008684. doi: 10.3389/fmicb.2022.1008684

84. Tahtinen S, Tong A-J, Himmels P, Oh J, Paler-Martinez A, Kim L, et al. IL-1 and IL-1ra are key regulators of the inflammatory response to RNA vaccines. *Nat Immunol* (2022) 23:532–42. doi: 10.1038/s41590-022-01160-y

85. Marković I, Božan M, Perković T, Paušek K, Nedeljković V, Perković M, et al. Incidence of immediate allergic reactions to mRNA COVID-19 vaccines in adults with drug allergies and other allergic disorders. *Medicine* (2022) 101:e29571. doi: 10.1097/MD.0000000000029571

86. Bigini P, Gobbi M, Bonati M, Clavenna A, Zucchetti M, Garattini S, et al. The role and impact of polyethylene glycol on anaphylactic reactions to COVID-19 nano-vaccines. *Nat Nanotechnol* (2021) 16:1169–71. doi: 10.1038/s41565-021-01001-3

87. Qin Z, Bouteau A, Herbst C, Igyártó BZ. Pre-exposure to mRNA-LNP inhibits adaptive immune responses and alters innate immune fitness in an inheritable fashion. *PloS Pathog* (2022) 18:e1010830. doi: 10.1371/journal.ppat.1010830

88. He Q, Gao H, Tan D, Zhang H, Wang J. mRNA cancer vaccines: Advances, trends and challenges. *Acta Pharm Sin B* (2022) 12:2969–89. doi: 10.1016/j.apsb.2022.03.011

89. Ladak RJ, He AJ, Huang Y-H, Ding Y. The current landscape of mRNA vaccines against viruses and cancer-a mini review. *Front Immunol* (2022) 13:885371. doi: 10.3389/fimmu.2022.885371

90. Zhu C, Dukhovlinova E, Council O, Ping L, Faison EM, Prabhu SS, et al. Rationally designed carbohydrate-occluded epitopes elicit HIV-1 env-specific antibodies. *Nat Commun* (2019) 10:1–10. doi: 10.1038/s41467-019-08876-w

91. Ding F, Tsao D, Nie H, Dokholyan NV. Ab initio folding of proteins with all-atom discrete molecular dynamics. *Structure* (2008) 16:1010–8. doi: 10.1016/j.str.2008.03.013

92. Shirvanyants D, Alexandrova AN, Dokholyan NV. Rigid substructure search. *Bioinformatics* (2011) 27:1327–9. doi: 10.1093/bioinformatics/btr129

93. Kota P, Ding F, Ramachandran S, Dokholyan NV. Gaia: Automated quality assessment of protein structure models. *Bioinformatics* (2011) 27:2209–15. doi: 10.1093/bioinformatics/btr374

94. Yin S, Ding F, Dokholyan NV. Eris: an automated estimator of protein stability. *Nat Methods* (2007) 4:466–7. doi: 10.1038/nmeth0607-466

TYPE Original Research
PUBLISHED 17 January 2023
DOI 10.3389/fimmu.2022.1099991

OPEN ACCESS

EDITED BY
Bingdong Zhu,
Lanzhou University, China

REVIEWED BY
Leo Visser,
Leiden University Medical Center (LUMC), Netherlands
Jennifer Serwanga,
Uganda Virus Research Institute (UVRI), Uganda

*CORRESPONDENCE
Xiaoyan Zhang
zhangxiaoyan@fudan.edu.cn
Jianqing Xu
xujianqing@fudan.edu.cn
Chen Zhao
chen_zhao72@163.com

†These authors have contributed equally to this work

SPECIALTY SECTION
This article was submitted to Vaccines and Molecular Therapeutics, a section of the journal Frontiers in Immunology

RECEIVED 16 November 2022
ACCEPTED 28 December 2022
PUBLISHED 17 January 2023

CITATION
Bai S, Yang T, Zhu C, Feng M, Zhang L, Zhang Z, Wang X, Yu R, Pan X, Zhao C, Xu J and Zhang X (2023) A single vaccination of nucleoside-modified Rabies mRNA vaccine induces prolonged highly protective immune responses in mice. *Front. Immunol.* 13:1099991. doi: 10.3389/fimmu.2022.1099991

A single vaccination of nucleoside-modified Rabies mRNA vaccine induces prolonged highly protective immune responses in mice

Shimeng Bai[1†], Tianhan Yang[1†], Cuisong Zhu[1], Meiqi Feng[1], Li Zhang[1], Ziling Zhang[1], Xiang Wang[1], Rui Yu[1], Xinghao Pan[1], Chen Zhao[1*], Jianqing Xu[1,2*] and Xiaoyan Zhang[1,2*]

[1]Shanghai Public Health Clinical Center & Institutes of Biomedical Sciences, Fudan University, Shanghai, China, [2]Clinical Center of Biotherapy, Zhongshan Hospital, Fudan University, Shanghai, China

Background: Rabies is a lethal zoonotic disease that kills approximately 60,000 people each year. Although inactivated rabies vaccines are available, multiple-dose regimensare recommended for pre-exposure prophylaxis or post-exposure prophylaxis,which cuts down the cost- and time-effectiveness, especially in low- and middle incomecountries.

Methods: We developed a nucleoside-modified Rabies mRNA-lipid nanoparticle vaccine (RABV-G mRNA-LNP) encoding codon-optimized viral glycoprotein and assessed the immunogenicity and protective efficacy of this vaccine in mice comparing to a commercially available inactivated vaccine.

Results: We first showed that, when evaluated in mice, a single vaccination of RABV-G mRNA with a moderate or high dose induces more potent humoral and T-cell immune responses than that elicited by three inoculations of the inactivated vaccine. Importantly, mice receiving a single immunization of RABV-G mRNA, even at low doses, showed full protection against the lethal rabies challenge. We further demonstrated that the humoral immune response induced by single RABV-G mRNA vaccination in mice could last for at least 25 weeks, while a two-dose strategy could extend the duration of the highly protective response to one year or even longer. In contrast, the three-dose regimen of inactivated vaccine failed to do so.

Conclusion: Our study confirmed that it is worth developing a single-dose nucleoside-modified Rabies mRNA-LNP vaccine, which could confer much prolonged and more effective protection.

KEYWORDS

rabies, mRNA vaccine, rabies virus glycoprotein, virus-neutralizing antibodies, challenge model

Introduction

Rabies is a fatal zoonotic disease that claims about 60,000 lives annually (1). It is a neurological illness caused by the Rabies virus (RABV), a single-stranded non-segmented negative-sense virus belonging to the genus Lyssavirus, in the family Rhabdoviridae (2). The genome of RABV encodes only five proteins, including nucleoprotein (N), phosphoprotein (P), matrix protein (M), glycoprotein (G), and large polymerase protein (L) (2). The glycoprotein, located on the surface of rabies virions, is the major inducer of virus-neutralizing antibodies (VNA) against RABV infection (3, 4). Dog biting accounts for 95% of human infections, with the virus spreading through bites or scratches, usually in the saliva (5). After its replication in the muscle tissue, the virus could infect the peripheral nerves; when the invasion of the brain occurs, the mortality rate is 100% as soon as the clinical symptoms appear (6).

Nowadays, inactivated rabies vaccines are the most widely used. However, they required repeated injections or adjuvants to induce sufficient neutralizing antibody titers against infection. For pre-exposure prophylaxis (PrEP), a 2-dose PrEP schedule on day 0 and day 7 was needed to elicit virus-neutralizing antibody titers greater than 0.5 international units (IU) (7–10); for post-exposure prophylaxis (PEP), 4 to 5 shots are required (11). Given the high financial costs associated with repeated vaccinations and limited access to medical resources in developing countries, particularly in Asia and Africa, developing novel rabies vaccines effective with single-dose would be a desirable step for curing rabies.Recently, messenger RNA (mRNA)-based vaccines have shown great promise as a non-traditional vaccine platform against many infectious diseases. The realization of such a promise depends on the advancement of various methods that enhance the potency of mRNA vaccines, including modified nucleoside incorporation (12, 13)and coding sequence optimization (14). Non-replicating mRNA-based rabies vaccines with exclusively unmodified nucleosides have been developed (15, 16), mainly by CureVac AG (Tübingen, Germany). The mRNA vaccine platform of CureVac AG, the RNActive platform, has been founded onusing a complex sequence optimization algorithm to alter the GC content of the mRNA coding sequence, intending toincrease the protein translation efficacy (14). A major improvement of the mRNA vaccine is the employment of modified nucleosides as blocks for mRNA synthesis, which confer important beneficial effects, particularly the increased antigen expression due to the enhanced mRNA stability and the prevention of unnecessary activation of innate immunity (17, 18). The effectiveness of nucleoside-modified mRNA vaccines against virus-causing diseases has been demonstratedin numerous preclinical investigations (19–24), culminated in its use as a major vaccine typelicensed for human vaccination against SARS-CoV-2 (25, 26). Despite ongoing studies on Rabies mRNA vaccines, like CV7201 or CV7202 from the CureVac AG, which required a single high-dose or two doses to achieve protective virus-neutralizing titers (VNTs) in preclinical studies (16, 27) and phase 1 clinical trial (28), no Rabies mRNA vaccine has been licensed for human use. In addition, there is a lack of investigation of the efficacy in the induction of virus-neutralizing antibodies and antiviral protectivity of nucleoside-modified Rabies mRNA vaccine, and its dose dependency, in animal models.

This study mainly evaluated the immunogenicity of a single vaccination with nucleoside-modified RABV-G mRNA vaccine versus a commercially available inactivated vaccine in BALB/c mice. We demonstrated that the mRNA vaccine could induce higher VNA production in a dose-dependent manner to protect vaccinated mice against lethal rabies challenges and has a better T-cell response in the spleen than the commercially available inactivated vaccine. Moreover, we investigated the duration of the humoral immune response following a single vaccination and two immunization doses in mice.

Methods

Cells, viruses, vaccines, and animals

HEK293 cells (ATCC) were cultured in complete Dulbecco's modified Eagle's medium supplemented with 10% fetal bovine serum (BI, Utah, USA) and 2% penicillin and streptomycin (BI, Utah, USA), and maintained at 37°C in 5% CO_2 incubator. Purified Vero cell culture vaccine (a rabies vaccine made from aGV strain for human use, freeze-dried, labeled potency is 1 dose ≥ 2.5 IU)) was kindly donated by Rongan Biological Co., Ltd (Ningbo, China) and was used as a positive control for the vaccine efficacy comparison. Wuxi Xin Lianxin Biotech co. LTD (Wuxi, China) kindly donated the CVS-11 rabies challenge virus, which was cultivated in BHK-21 cells and titrated in BALB/c mice. The CVS-11 strain has been approved as a challenge virus in RABV-neutralizing antibody tests (29). Female BALB/c mice (6–8 week-old, Specific pathogen-free) purchased from Suzhou Huachang Biological Co., Ltd were housed in the Shanghai Public Health Clinical Center (SPHCC) animal facility.

mRNA and LNP preparation

The mRNA vaccine described here was based on our conventional optimized non-amplifying mRNA platform (CN202211129466.2 and CN 202211129212.0).

T7 RNA polymerase synthesized mRNA using the linearized plasmid (synthesized by GENEWIZ) encoding a codon-optimized Pitman-Moore (PM) strain glycoprotein (accession number AJ871962) as a template. The 3' untranslated region (UTR) of the synthetic plasmid has 250 poly-A inserted at the end of it, eliminating the requirement for poly(A) tailing with poly(A) polymerase during *in vitro* transcription. 1-methylpseudourine-5'-triphosphate (Nanjing Synthgene Medical Technology Co., Ltd.) instead of UTP was used to generate mRNA incorporating a modified nucleoside. Then, the *in vitro* transcribed mRNAs were capped using the Vaccinia Capping System and an mRNA Cap 2'-O-methyltransferase (Novo protein Shanghai, China). The mRNA was precipitated overnight with 2.5 moles or more of LiCl at −20°C for 30 min, and then centrifuged at maximum speed; the mRNA pellets were washed with 70% ethanol and finally suspended with RNase-free water. The nucleoside-modified mRNAs were identified by agarose gel and stored frozen at −20°C until use.

Using the self-assembly method mentioned earlier (24), a mixture of nucleoside-modified RABV-G mRNA and LNP was made. An aqueous solution containing mRNA at acidic pH4.0 was rapidly

mixed with a lipid mixture in ethanol. LNPs contained the ionizable lipid (Dlin-MC3-DMA) AVT (Shanghai) Pharmaceutical Tech Co., Ltd., di-stearoyl phosphatidylcholine (DSPC), cholesterol, and PEG-lipid (PEG2000-DMG) at a ratio of 50:10:38:2 mol/mol. The mRNA and lipid mixture percentage were 3:1. After being dialyzed in PBS, the LNP-encapsulated mRNA was filtered by a 0.22m microfilter, then stored at 4°C. The encapsulation efficiency was analyzed using a Quanti-T RiboGreen RNA Assay Kit (Thermo Fisher Scientific). The particle size was detected by dynamic light scattering (DLS), and the zeta potential of mRNA RABV-G LNPs was measured through a Zetasizer instrument.

mRNA transfection and protein expression

According to the manufacturer's instructions, the RABV-G mRNA was transfected into HEK293T cells with Lipofectamine 3000 Reagent (Life Technologies). Briefly, 1 μg mRNA in 25 μL Opti-MEM (GIBCO, Gaithersburg, MD, USA) was mixed with 2 μL Lipofectamine 3000 in 25 μL Opti-MEM for 5 min, and then the Lipofectamine 3000-mRNA complex mixture was immediately added to the 24-well plates. Cells were harvested after transfection for 24 h and were lysed in RIPA lysis buffer (Life Technologies) for 30 min on ice. The expression of RABV-G protein was detected by Western blot. Samples were mixed with 4×SDS buffer (Takara), and boiled for 5 minutes, then transferred to PVDF membrane following separation on a 10% polyacrylamide gel. The membrane was blocked with 5% non-fat milk dissolved in PBS containing 0.01% Tween at room temperature for two hours. The RABV-G (glycoprotein) protein was detected using primary antibody Rab-50 (Santa Cruz) for 1 h, followed by secondary peroxidase-conjugated goat anti-mouse IgG (H+L) (Yeasen) for 1 h. The protein signals were detected by the SuperSignal West Pico Plus chemiluminescent substrate (Thermo Fisher Scientific).

Mouse immunization experiments

In this study, there were three distinct immunization protocols.

In the first immunization protocol, female BALB/c mice were divided into five groups (n = 5), and vaccinations were performed *via* intramuscular(I.M.) route by injecting into the thigh muscles of the two hind limbs, 0.3 μg, 1 μg, 3 μg, or 10 μg RABV-G mRNA-LNP in 100μl volume, with empty LNP as the negative control. For a prime-boost regimen schedule, the animals were vaccinated twice with the same vaccine at a 3-week interval.

In the second immunization protocol, mice (n = 5) were I.M. immunized with 10 μg of RABV-G mRNA-LNP, and I.M. boosted with 10 μg or 1 μg. Then the antibody titers were monitored until 53 weeks.

In the third immunization protocol, a total of 26 mice were I.M. immunized once with 0.3 μg, 1 μg, or 3 μg of RABV-G mRNA, or the negative control (empty-LNP). Furthermore, a licensed inactivated vaccine (the positive control) (n = 26) was injected intramuscularly three times on days 0, 7, and 21 with 100 μl (0.1 human dose). Then spleens of each group of four mice were collected to detect RABV-G-specific T-cell responses at 10 or 30 days. For the rabies virus challenge, 13 mice of each group were challenged with 20-fold MLD_{50} (50 μl per mouse) of rabies virus CVS-11 (challenge virus standard-11) *via* the I.M. route. Then the body weight was monitored daily to evaluate the survival rate. Mice were euthanized at seven days post-infection (dpi). The brain tissues of infected mice were collected for viral RNA loads, pathological examination, and detection of viral RNA expression in the brain (three mice per group). To assess the endurance of the humoral immune response, the remaining five mice in each vaccinated group were monitored for at least 25 weeks.

ELISA

RABV-G-specific antibodies were detected by ELISA. The specific ELISA plates were coated with 100 ng/well of RABV-G protein (AtaGenix) overnight at 4°C and blocked with 5% skim milk in PBST at room temperature for two hours. After two washes in PBST, coated plates were sequentially incubated with 2-fold serially diluted mouse sera for 3 hours at room temperature, followed by HRP-conjugated anti-mouse IgG (1:5,000) (Yeasen) for 1 hour at room temperature. If analyzing the subclass of antibodies, biotin-conjugated goat anti-mouse IgG1 (1:5,000) or IgG2a (1:5,000) antibodies (Abcam) were added and incubated at room temperature for 1 hour and then incubated with SA-HRP (1:5,000) (Yeasen) for another 1 h at room temperature. Finally, after five PBST washes, the plates were incubated with the substrate OPD (Sigma) and followed by H_2SO_4 (1 M) to stop the reaction. As previously mentioned, we measured the absorbance at 490 nm with a Synergy Microplate Reader (Bio-Tek) (30). The ELISA endpoint titers were considered the highest serum dilution, with an absorbance over two times that of the negative control mice sera.

Enzyme-linked immunospot assay

The manufacturer's protocol (BD Bioscience) assessed T-cell responses with the mouse IFN-γ ELISpot assay set. In short, the spleens were harvested from vaccinated BALB/c mice at 10- or 30-days post-vaccination. The plates of PVDF membrane were pre-coated with anti-mouse IFN-γ antibodies (5 μg/ml) overnight at 4°C and then blocked for 2 hours at room temperature. Next, the 2×10^5 viable isolated splenocytes were added to each well, followed by stimulation with the RABV-G peptide pool (Chinapeptides Co., Ltd) for 18–24 h at 37°C. Then the plate was incubated with biotin-labeled IFN-γ antibodies (2 μg/ml) for 1 h following addition with SA-HRP (1:100 dilution). Finally, the plate was washed in PBS and reacted with an AEC substrate reagent. Reactions were stopped with water until the spots could be clearly observed. The numbers of spots were read and analyzed with a Bio-spot plate reader (ChampSpot 437III, Beijing Sage Creation Science Co., Ltd).

Flow cytometry assay

To assess antigen-specific T-cell immune responses, we isolated the mouse splenocytes and stimulated them with the RABV-G peptide pool (1 μg/ml of individual peptide, 1×10^6 cells/well).

Golgiplug (BD Biosciences) was mixed with the cells after 1 h and incubated for another 5 h. Then cells were harvested, washed in PBS, and stained with Amcyan Live Dead Kit or antibodies to surface markers, including CD3 (Percpcy5.5, Clone 17A2, BioLegend), CD4 (AF700, Clone RM4-5, BD Biosciences), and CD8 (FITC, Clone 53-6.7, BioLegend). Subsequently, the stained cells were fixed and permeabilized in permeabilizing buffer (BD Biosciences), followed by staining with antibodies to anti-IFN-γ (PE, Clone XMG1.2, BD Biosciences), anti-IL-2 (APC, Clone JES6-5H4, BioLegend), or anti-TNF-α (BV605, Clone MP6-XT22, BioLegend). Data were collected using BD FACSAria III flow cytometer (BD Biosciences) and analyzed using FlowJo 10.

Virus-neutralization measurement

Virus-neutralization antibody titers were determined with the fluorescent-antibody virus-neutralization (FAVN) assay as previously described (31). Briefly, 3-fold serial dilutions of standard serum (0.5 IU/ml) and test serum samples (four replicates per sample) were prepared in 96-well plates and mixed with 100 $TCID_{50}$ of CVS-11 (50 μl/well). They were then incubated at 37°C for 1 h in a 5% CO_2 incubator. Next, 50 μl of suspension containing 210^4 BHK-21 cells was added to the mixture and continued to incubate at 37°C for 48 h. Cells were first fixed with 80% acetone for 30 min at 4°C and then stained with FITC-labeled RABV-N antibody (Veterinary Research Institute, Changchun, China). Fluorescence was observed under ultraviolet microscopy, and the VNA titers were determined and normalized compared with the value of the standard serum.

Viral RNA extraction and RT-PCR

According to the manufacturer's guide, total RNA was extracted from the brains of infected mice with the RNA isolation kit (Direct-zol RNA Miniprep Plus kit, Zymo Research). First, the rabies virus was detected using the Reverse Transcription System (Promega) and then SYBR green-based real-time PCR (GoTaq qPCR Master Mix; Promega) through a Bioer real-time PCR system with the N protein-specific primers. The oligo primers used were:

F: 5'-AATGCGACGGTTATTGCTGC-3'; R: 5'-TGCCACGTCGGTCTTTGTTA-3'.

The steps of real-time RT-PCR were carried out as follows: 42°C for 15 min and 95°C for 2 min, 40 cycles of amplification at 95°C for 15 s and 60°C for 30 s.

Histopathology and RNA *in Situ* hybridization

Histopathological lesions in the brains were detected through hematoxylin and eosin staining. Brains were first fixed in 4% (v/v) paraformaldehyde and then prepared into paraffin sections (4–5 μm). For analyzing viral RNA expression in brain sections by RNAscope *in situ* hybridization (ISH), the viral nucleoprotein (NP) RNA was used as the target RNA for its high conservation. The NP-specific RNAscope probe was V-RABV-gp4 (220268) from ACDBio. The RNA ISH assay was performed with the previously described RNAscope Multiplex Fluorescent Reagent Kit V2 kit (Advanced Cell Diagnostics, 323100) (32).

Ethics statement

All animal experiments in this study were approved by the Institutional Animal Care and Use Committee (IACUC) of the Shanghai Public Health Clinical Center. All the animal studies were strictly conducted following the animal ethics guidelines.

Statistical analysis

For all the analyses, *p* values were obtained from the Mann-Whitney test or One-way ANOVA followed by Tukey's multiple comparisons test through the GraphPad Prism. If $p<0.05$, data were determined statistically significant (*$p< 0.05$; **$p< 0.01$; ***$p< 0.001$; ****$p< 0.0001$; ns, not significant). All of the graphs were generated with GraphPad Prism Version 9.4 software.

Results

Design and characterization of RABV-G mRNA vaccine

To test our conventional optimized non-amplifying mRNA platform, we designed an mRNA vaccine that encodes the codon-optimized glycoprotein of the Rabies virus Pitman-Moore (PM) strain (Figure 1A). The synthesized RABV-G mRNA *in vitro* includes the modified nucleoside N1-methylpseudouridine to suppress innate immune sensing and enhance mRNA translation (21). Then we examined the RABV-G mRNA expression by transfecting HEK293T cells or Hela cells. Western blot demonstrated that RABV-G protein could be expressed effectively and with the right size (67 kDa) in transfected cells (Figure 1B). To improve the mRNA expression *in vivo*, we encapsulated the RABV-G mRNA in lipid nanoparticles (LNPs). The LNPs had a ratio of 50:10:38:2 for the four lipids, Dlin-MC3-DMA, DSPC, cholesterol, and PEG2000-DMG (Figure 1C). Furthermore, dynamic light scattering analysis showed that the average particle size of LNPs in PBS was 114 nm, with a PDI of 0.089 (Figure 1D). Then a Zeta potential measurement showed a potential of −8.86 mV in PBS (Figure 1D).

Immunogenicity evaluation of various doses of nucleoside-modified RABV-G mRNA vaccine

The immune responses induced by our RABV-G mRNA vaccine were analyzed in BALB/c mice. First, we assessed the effects of different vaccination dosages on the immunogenicity of vaccines. Female BALB/c mice were divided into five groups (n = 5) and intramuscularly injected with 0.3 μg, 1 μg, 3 μg, and 10 μg RABV-G

10.3389/fimmu.2022.1099991

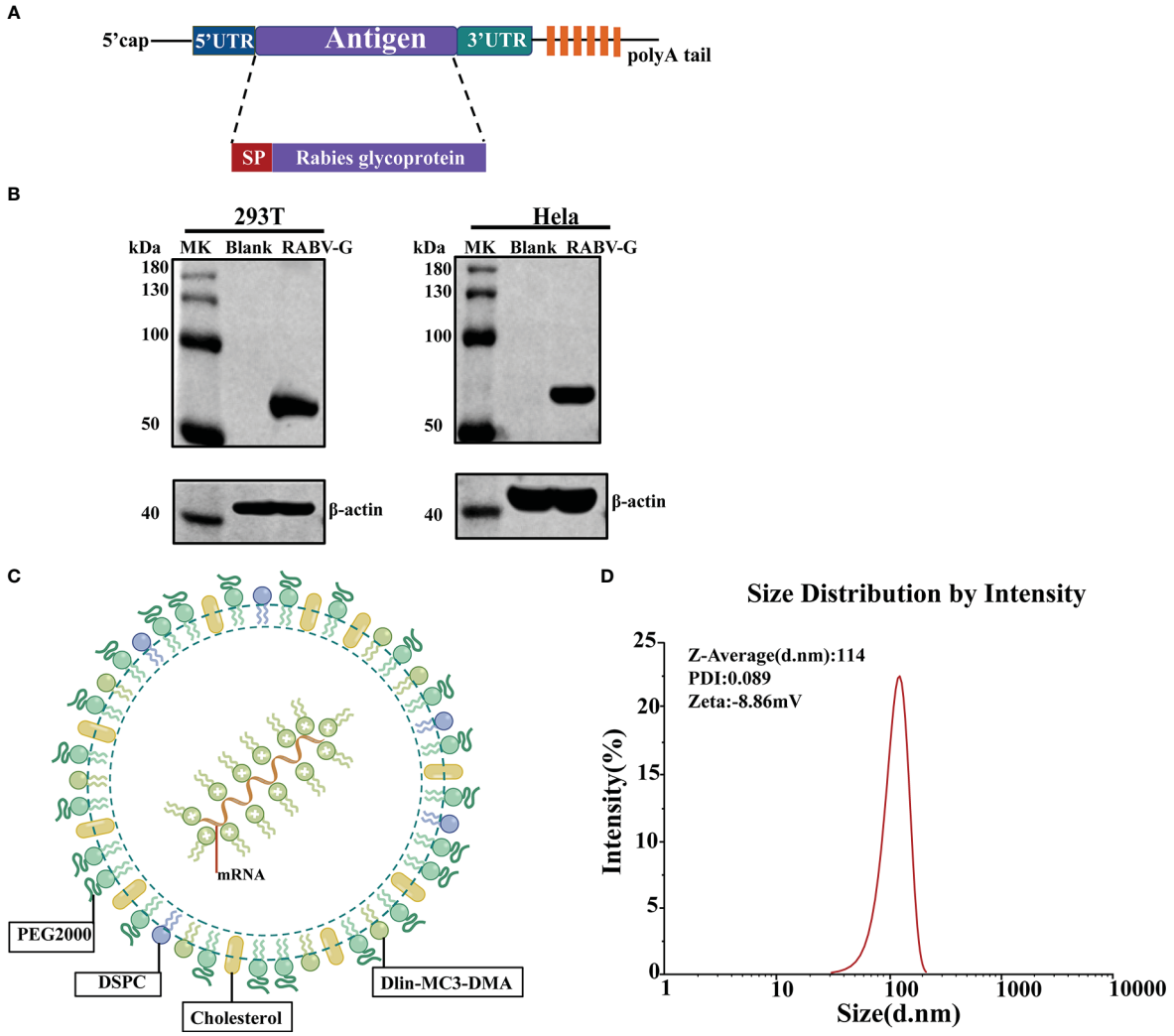

FIGURE 1
Design and Characterization of RABV-G mRNA Vaccine. **(A)** Schematic of RABV-G mRNA construct comprising a 5'cap, a 5'UTR, a signal peptide, an antigen (RABV-G from strain Pitman-Moore), a 3'UTR, and a 250 poly **(A)** tail. **(B)** RABV-G mRNA was transfected into HEK293T or Hela cells. RABV-G expression in the cell lysate at 24 h was analyzed by western blotting. **(C)** Schematic representation of the RABV-G mRNA packaged into LNPs. **(D)** Particle size graph of LNPs by dynamic light scattering.

mRNA or the equivalent amount of empty-LNP without mRNA as a negative control, with a prime-boost regimen at 3-week intervals (Figure 2A). Serum samples were harvested on days 21 and 35 to measure RABV-G-specific IgG and virus-neutralizing titers. The virus-neutralization antibody titers (VNTs) in different weeks post-immunization were determined by the FAVN method as shown in the method. Mice receiving 1 μg, 3 μg, or 10 μg doses of the RABV-G mRNA produced high endpoint binding titers on day 21 after the initial vaccination, whereas 0.3 μg of RABV-G mRNA induced the lowest antibody titers or VNTs in all immunized groups (Figures 2B, 2C $p< 0.05$, $p< 0.01$). Two weeks after the second immunization, all four separate doses (0.3 μg, 1 μg, 3 μg, and 10 μg) successfully induced the RABV-G binding antibody titers, with a geometric mean titer (GMT) of 470507, 409600, 654324, and 547615, respectively, and no statistically significant differences across any of the dosages (Figure 2B). Notably, all inoculated mice in each group developed VNTs above 0.5 IU/ml, whether 21 days after the initial immunization or two weeks after the boost (Figure 2C). Moreover, a dose-dependent increase in neutralization titer was observed; the VNTs at 21 days post-vaccination ranged from 1.75 to 18.3 IU/ml (Figure 2C, $p< 0.05$), while the VNTs increased by 100-fold or more following a second injection, with an average of 642, 979, 1689, and 1221 IU/ml (as in 0.3 μg, 1 μg, 3 μg, and 10 μg groups; Figure 2C, $p<0.01$). Interestingly, it showed that the 3 μg group, rather than the 10 μg one, produced the highest VNTs among these doses.

A single RABV-G mRNA vaccination elicits high and Th-1 biased humoral immune response in mice

Having demonstrated that each dosage could induce a viral neutralization titer (VNT) higher than 0.5 IU/ml, considered to be protective in humans, dogs, and cats, we determined the immune responses of a single vaccination with various doses. Groups of mice (n = 6) were immunized I.M. once with a low dose of 0.3 μg, a

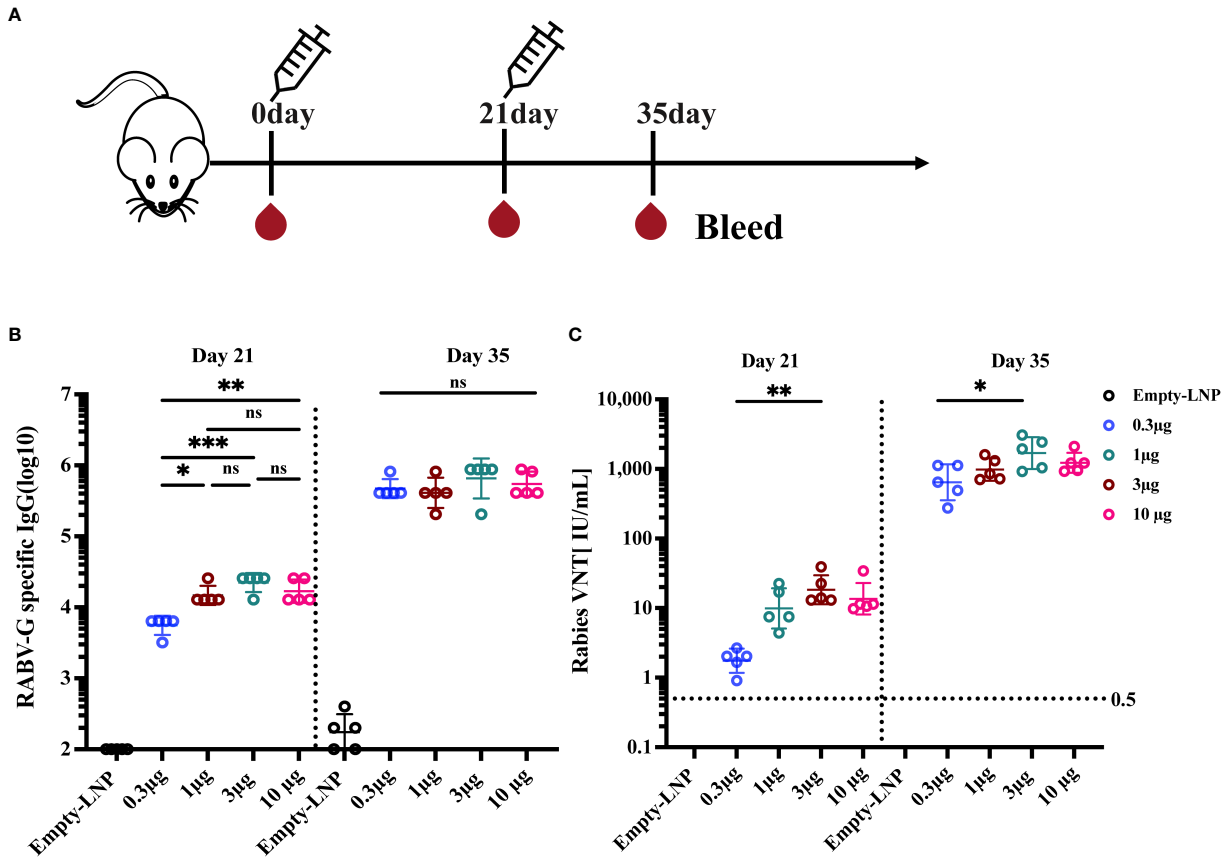

FIGURE 2
Immunogenicity evaluation of various doses of RABV-G mRNA Vaccine. Female BALB/c mice (n=5) were immunized with 0.3 μg, 1 μg, 3 μg, and 10 μg RABV-G mRNA or empty-LNP as a negative control with a prime-boost regimen at a 3-week interval **(A)**. Serum was collected on days 21 and 35 for analysis. RABV-G-specific IgG and virus-neutralizing antibody titers were measured as shown in **(B)** and **(C)**, respectively. The dashed line at 0.5 IU/ml represents a protective titer for Rabies VNTS. Each point represents an individual mouse. Titer data were GMT + geometric standard deviation (GSD). Comparisons among experimental groups were determined using One-way ANOVA followed by Tukey's multiple comparisons tests (*p< 0.05; **p< 0.01; ***p< 0.001; ns, not significant).

moderate dose of 1 μg, a high dose of 3 μg, or an empty-LNP (Figure 3A). As a positive control, a licensed inactivated vaccine group was injected I.M. three times on days 0, 7, and 21 with 100 μl (0.1 human dose; according to the immunization procedure of the donated inactivated vaccine; Figure 3A). By ELISA, serum samples obtained 2, 3, and 4 weeks post-vaccination were evaluated for RABV-G-specific IgG and IgG subtypes. All three dosages induced potent RABV-G-specific antibody and VNA responses after a single immunization. Binding affinity for the RABV-G and virus-neutralizing titers became detectable two weeks after immunization and continued to rise between 2 and 4 weeks. As a result, at week 2, the geometric mean endpoint titers of RABV-G-specific IgG in mice immunized with the high dose rose to 16127. They were significantly higher than those observed in mice immunized with the low dose (5701.5; Figure 3B, p<0.001, Supplementary Figure 1A). By week four after immunization, compared to the inactivated vaccine group (57470.1), the high-dose group had an average binding endpoint titer of 40637.5. In contrast, those moderate-dose and low-dose animals had respective values of 22807 and 9050.97 (Figure 3B, Supplementary Figure 1A). The high-dose group elicited the highest VNTs of 20.3 IU/mL for virus-neutralizing activity at week 4. They were 10-, 1.7-, and 5-fold higher than those observed in the low-dose group (p<0.0001), moderate-dose one (p>0.05), and the inactivated vaccine group (p<0.001), respectively (Figure 3C, Supplementary Figure 1B). These results indicate that the three doses are all immunogenic, but the high-dose group (3 μg) was superior in inducing binding and neutralizing antibody responses in BALB/c mice. Additionally, all three doses elicited IgG2a and IgG1 subclass RABV-G-specific antibodies in sera collected at week four post-prime (Figure 3D). The assessment revealed an average IgG2a/IgG1 ratio above one across all groups, indicating a Th1-biased response (Figure 3E).

RABV-G mRNA vaccines effectively elicit an antigen-specific T-cell immune response

To evaluate the cellular responses induced by RABV-G mRNA with various doses (0.3 μg, 1 μg, 3 μg) or the licensed inactivated vaccine as a positive control, enzyme-linked immunospot (ELISPOT) and intracellular cytokine staining (ICS) assays were carried out at ten days or 30 days post-immunization. The splenocytes isolated from vaccinated mice (n = 4) were re-stimulated with a pooled library of RABV-G peptides *in vitro*. Ten days post-vaccination, ELISPOT assays

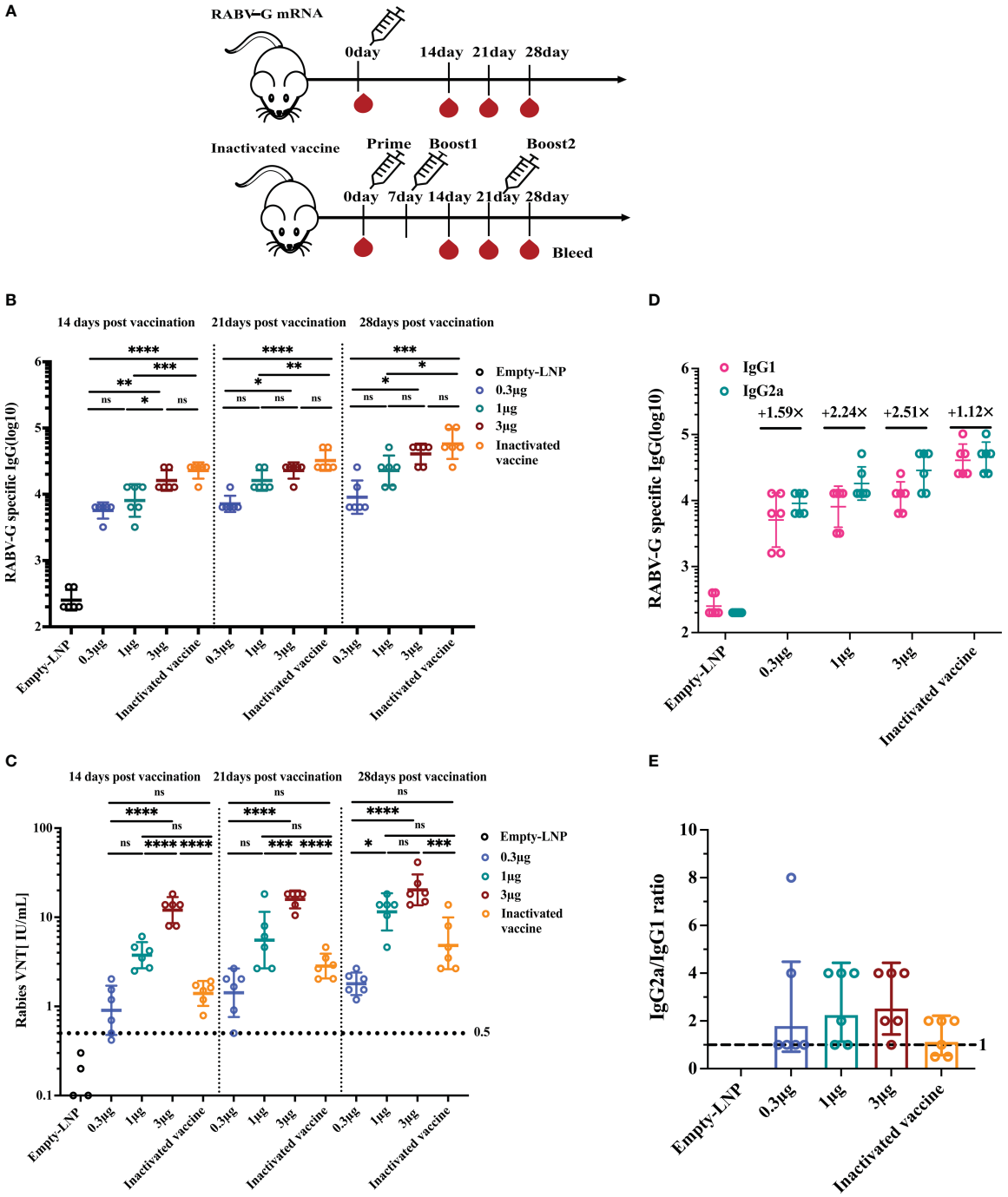

FIGURE 3
Humoral immune response upon single vaccination with escalating doses of RABV-G mRNA compared to three injections of inactivated vaccine. Female BALB/c mice (n = 6) were inoculated with a single intramuscular injection of RABV-G mRNA at various doses (0.3g, 1g, and 3g) or an empty-LNP **(A)**. As a positive control, a licensed inactivated vaccine group (n = 6) was injected three times on days 0, 7, and 21 with 100l (0.1 human dose) *via* the intramuscularly (I.M.) route. Serum was collected on days 14, 21, and 28 to detect specific antibody responses **(B)** and virus-neutralizing antibody titers **(C)**. Serum levels of IgG1 and IgG2a antibodies specific for RABV-G **(D)** and IgG2a/IgG1 ratios **(E)** were evaluated by ELISA. Comparisons among experimental groups were determined using One-way ANOVA followed by Tukey's multiple comparisons tests (*p< 0.05; **p< 0.01; ***p< 0.001; ****p< 0.0001; ns, not significant).

demonstrated that T cells secreting gamma interferon (IFN-γ) from immunized mice of the high dose group (3 μg; Mean = 1844) were significantly more numerous than those from the inactivated vaccine group (the group received two injections at day 10; Mean = 641; Figure 4A, p<0.0001), while the specific T cells of mice in the low dose (0.3 μg; Mean = 564) or the moderate dose (1 μg; Mean = 1175) group were comparable to the mice receiving the licensed inactivated vaccine (Figure 4A). Moreover, flow cytometric analysis also showed that RABV-G-specific polyfunctional CD4+ and CD8+T cells secreting interferon γ (IFN-γ) and interleukin-2 (IL-2) were significantly elevated in RABV-G mRNA immunized mice (especially the high dose group) compared to inactivated vaccine-treated animals (mean of

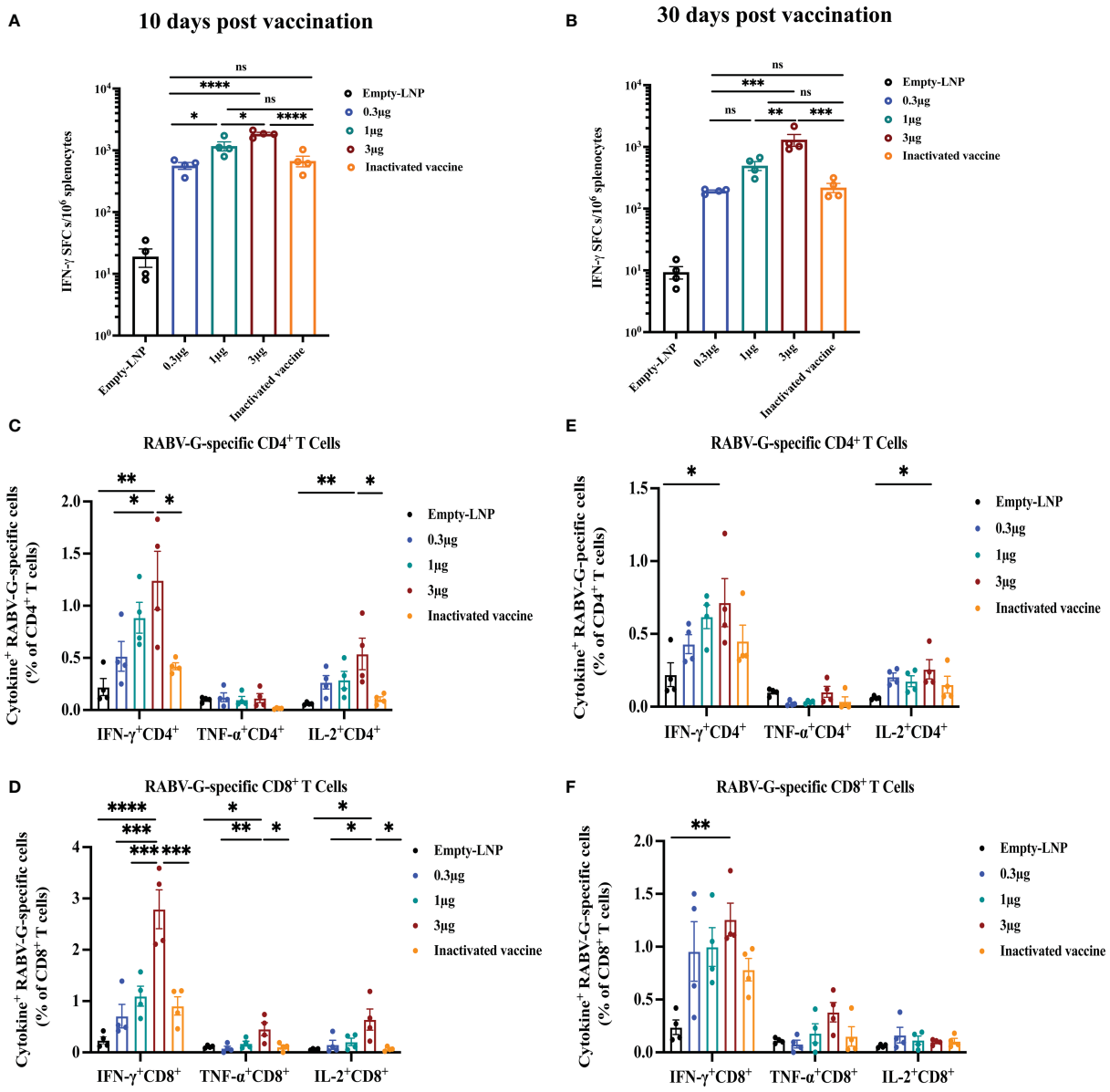

FIGURE 4
T-cell immune responses in vaccinated mice. An ELISPOT experiment was conducted to determine the ability of splenocytes to release IFN- after re-stimulation with RABV-G peptide pools at ten days **(A)** or 30 days post-vaccination **(B)**. Then RABV-G-specific CD4+ and CD8+ T cells producing IFN-γ, TNF-α, and IL-2 were measured by flow cytometry at ten days **(C, D)** or 30 days **(E, F)**. The data are shown as the number of IFNγ spot forming cells (SFC)/10^6 splenocytes. ELISpot counts were represented as mean + SEM (standard error of the mean). Comparisons among experimental groups were determined using one-way ANOVA followed by Tukey's multiple comparisons tests (*p< 0.05; **p< 0.01; ***p< 0.001; ****p< 0.0001; ns, not significant).

1.2% for IFN-γ expressing CD4+ T cells after the high dose RABV-G mRNA and 0.42% after inactivated vaccine immunization) (Figure 4C, Supplementary Figure 2). In contrast, frequencies of antigen-specific tumor necrosis factor-alpha (TNF-α) were low across the groups (Figures 4C, D, Supplementary Figure 2).

Additionally, we further examined RABV-G mRNA induced cellular immune at 30 days post-vaccination. Compared to the inactivated vaccine-treated group (the one that received three injections on day 30), the stimulated splenocytes in the high-dose group produced a higher population of CD4+ and CD8+ cytokine IFN-γ- and TNF-α- expressing cells (Figures 4E, F). The frequencies of antigen-specific polyfunctional CD4+ and CD8+T cells were similar in the other two groups (the moderate and low doses; Figures 4E, F). ELISPOT analysis also revealed significant induction of IFN-γ in the splenocytes of RABV-G mRNA vaccinated mice in the high dose group (Mean = 1307) than in the inactivated vaccine one (Mean = 220) (Figure 4B, p<0.001). Our results demonstrated that the RABV-G mRNA vaccine could effectively activate RABV-G-specific antigen T-cell responses in addition to humoral immune responses, the frequencies of antigen-specific T-cells were dose-dependent, and better induction of T cells by our RABV-G mRNA vaccine compared to the inactivated vaccine.

10.3389/fimmu.2022.1099991

RABV-G mRNA vaccines confer complete protection against the rabies virus

To explore the *in vivo* protection efficacy of the RABV-G mRNA vaccine against lethal rabies virus challenge, BALB/c mice (n = 13) received one immunization with three dosages 0.3 μg, 1 μg, and 3 μg) of RABV-G mRNA or empty-LNP *via* I.M. route, and positive control mice (n = 13) were vaccinated three times intramuscularly with a 0.1 human dose of the inactivated vaccine (Figure 5A). All mice were challenged with 20-fold MLD_{50} of rabies virus CVS-11 (challenge virus standard-11) *via* the I.M. route on day 30 (Figure 5A). We monitored the body weight of each mouse daily for 15 days post-infection. We found that body weight dropped at 1 dpi compared to the empty-LNP group but increased more rapidly during the

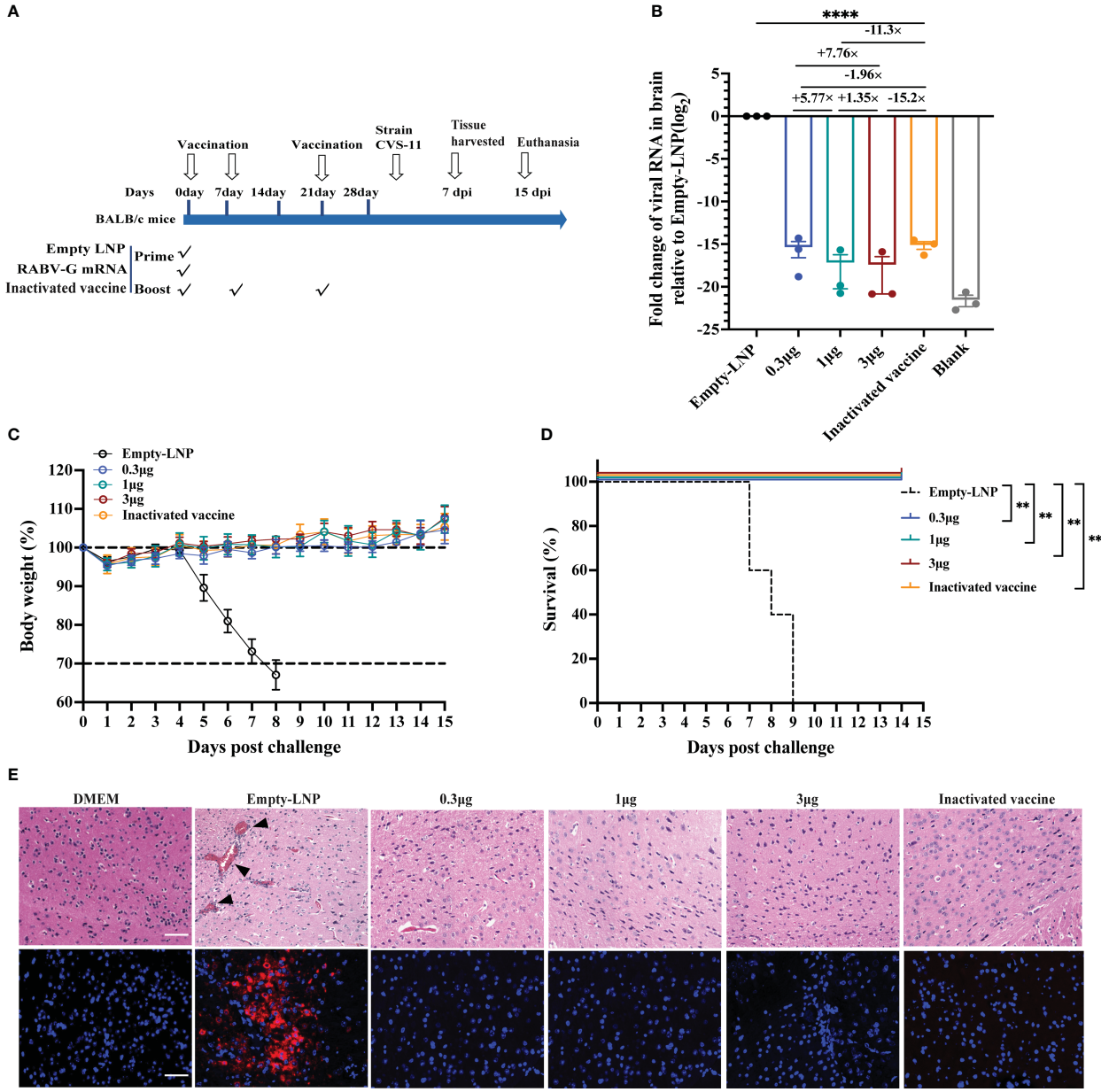

FIGURE 5
Protection of RABV-G mRNA in BALB/c mice against rabies virus challenge. Groups of female BALB/c mice (n = 13) received a single dose of RABV-G mRNA or three doses of inactivated vaccine or empty-LNP via the I.M. route. Four weeks post initial vaccination, mice were I.M. challenged with 20MLD50 of CVS-11 virus in a total volume of 50μl. **(A)** Mice immunization and challenge schedule. The black hollow arrows indicate the time of vaccination and the virus challenge. **(B)** Relative messenger RNA (mRNA) expression of viral N protein (log2 fold change from Empty-LNP group) on day seven post-infection.Comparations among experimental groups were determined using one-way ANOVA followed by Tukey's multiple comparisons tests (****p< 0.0001). **(C)** The body weight of challenged mice was monitored daily and is shown as the mean + SEM (n = 5). As soon as animals lost 25% of their initial body weight (dotted line), they were sacrificed. **(D)** A Kaplan-Meyer analysis illustrates the survival curves during a 15-day observation period. Bars represent the mean and SEM (n = 5/group, **p <0.01). **(E)** H&E staining and RNAscope in situ hybridization (ISH) assay of Brain tissues from DMEM group mice or infected mice (n = 3/group). At 7 d.p.i., sagittal sections of the mouse brain were cut and stained with H&E, histopathological analysis was performed, and the representative histological changes (scale bars, 50 μm) are presented. Black triangles indicate pathological changes, including inflammatory cuffs of blood vessels (perivascular cuffing) and/or intravascular coagulations. Representative images of ISH showed virus NP expression in the brain. Each red dot represents a single NP RNA molecule, with nuclei counterstained by DAPI.

following days (Figure 5C). There were no significant differences in body weight among each vaccinated group (Figure 5C). Moreover, all vaccination groups survived post-infection (Figure 5D). Three mice of each group were euthanized at 7 dpi, brain tissues of infected mice were collected for viral RNA loads and histopathology, and RNAscope analyzed the viral expression *in situ* hybridization (ISH; Figure 5E down). Half of the brain was tested for rabies virus replication by quantitative RT-PCR of RNA encoding the rabies nucleoprotein (N protein). As expected, all mice in the empty-LNP group had abundant rabies virus RNAs (Figure 5B). In contrast, most animals in the vaccination groups had extremely low but detectable levels (Figure 5B). Compared to the positive control animals, the average brain viral RNA levels for high-dose, moderate-dose, and low-dose groups were approximately 15.2-fold, 11.3-fold, and 1.96-fold lower, respectively. There were significantly ($p < 0.0001$) lower rabies virus RNA levels in the brain of all four immunized groups compared with the empty-LNP group (Figure 5B). Histopathological analyses revealed intravascular coagulation and perivascular cuffing in the empty-LNP group (Figure 5E top). In contrast, no lesion changes were observed in the high-dose, moderate-dose, or positive control groups, and only a few intravascular coagulations in the brain of the low-dose group (Figure 5E). Similarly, dot signals of viral RNAs were detected in the brains of empty-LNP mice using RNAScope but not in the vaccinated groups (Figure 5E). These results showed that even at a low dose, single immunization with our nucleoside-modified RABV-G mRNA vaccine afforded complete protection against the lethal challenge of rabies virus in mice.

Immune response kinetics following vaccination of RABV-G mRNA

Prophylactic immunization must produce long-lasting protection. First, we assessed the endurance of the humoral immune response following a single vaccination. The remaining BALB/c mice (n = 5) of each group were bled from the time of immunization until 25 weeks

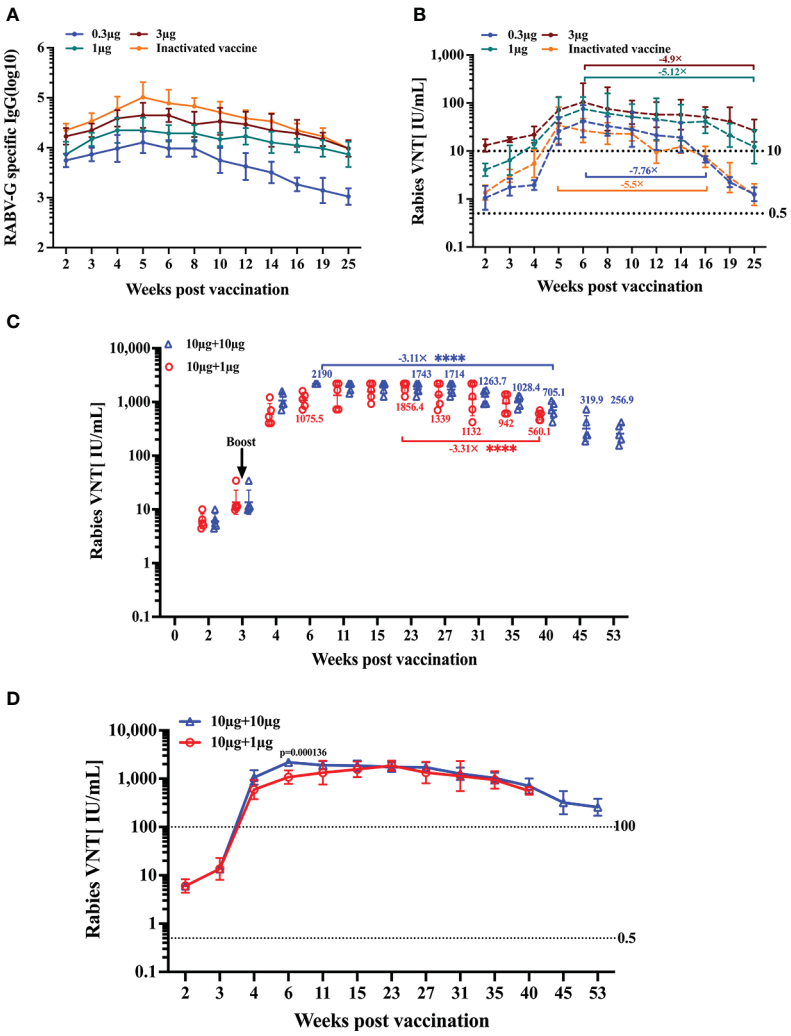

FIGURE 6
Duration of immune response induced by RABV-G mRNA. The durability of the antibody response was analyzed using **(A)** ELISA of total IgG and **(B)** virus-neutralizing antibody titers up to 25 weeks after a single-dose immunization or three injections of inactivated vaccine. Kinetic of virus-neutralizing antibody from two I.M. immunizations with different dosages in 3-week intervals; the initial vaccination was 10 μg, and the booster was 10 μg or 1 μg **(C, D)**. Titer data are shown as GMT + GSD. Comparisons among experimental groups were determined using one-way ANOVA followed by Tukey's multiple comparisons tests ****$p < 0.0001$.

after that. We found that the peak RABV-G-specific antibody level in the inactivated vaccine group was higher than in other groups (Figure 6A). However, the peak neutralizing antibody titers in the high-dose group (3 μg) were at average higher than those in the positive control group. (Figure 6B). (Figure 6B). Notably, the VNTs of the RABV-G mRNA groups peaked six weeks after immunization and remained stable during the 6–14 week period (Figure 6B). Furthermore, we observed a dramatic fall in VNTs to 6.8 and 8.5 IU/mL in both the low dosage and positive groups at week 16, with a decrease of 7.76-fold and 5.5-fold compared to their peak VNTs (Figure 6B). At week 25, the VNA titers in the moderate and high dose groups decreased by 5.12-fold and 4.9-fold from their peak VNTs, but remained higher than 10 IU/mL, whereas the other groups' levels dropped to 1.3 IU/mL, a decrease of nearly 40-fold.

Following a single dose of vaccination, effective neutralizing antibody responses persisted for at least 25 weeks; we wondered whether a second booster immunization would help the VNA response sustain at higher titers for longer. Thus, we evaluated the kinetics of induced humoral response following two vaccinations. Mice (n = 5) received two I.M. immunizations with different dosages at 3-week intervals. The initial vaccination was 10 μg, and the booster was 10 μg or 1 μg, respectively. Monitoring the antibody titers for 53 weeks in a group receiving two I.M. immunizations of 10 μg, we could demonstrate that neutralizing titers stabilized at a level of about 1000–2000 IU/ml for 4–35 weeks. In contrast, at week 40 post-initial immunization, the VNT decreased by 3.11-fold from their peak of 2190 IU/mL (Figures 6C, D). While in the 1 μg boost group, neutralizing titers rose to 594.8 IU/mL at week 4, peaked at 23 weeks, then, at week 40, dropped to 560.1 IU/mL, a decrease of 3.31-fold from the peak VNTs (Figures 6C, D).

These data suggest that a single immunization with RABV-G mRNA (even a low dose) through the I.M. route can induce a strong and durable antibody response for at least half a year. Furthermore, we observed that pronounced boosting effects were achieved through a second immunization regardless of whether it was a high or low-dose booster. High-neutralizing antibodies could be maintained for one year or much longer.

Discussion

Rabies is an infectious mortality disease that occurs worldwide. Current commercial inactivated vaccines have relatively poor immunogenicity and require repeated injections. In recent years, numerous studies have been carried out to develop novel, safe, and effective rabies vaccines, such as recombinant virus-vector vaccines (33–38), DNA and RNA-based vaccines (15, 16, 27, 28), live attenuated rabies vaccines (39), and protein vaccines (40). In this study, we mainly demonstrated that a single immunization of nucleoside-modified RABV-G mRNA vaccine induced a more potent immunogenic response than commercial inactivated rabies vaccines, providing complete protection against lethal rabies virus challenge, and induced durable NAb responses in BALB/c mice.

We first found that the RABV-G mRNA vaccine with a dose of 0.3 μg could elicit strong humoral immune responses following a two-dose immunization regimen, with neutralizing antibody titers of 642 IU/ml. In comparison, in a previous study, a dose of 0.5 μg LNP formulated nucleoside-unmodified RABV-G mRNA induced a median VNT of 650 IU/ml after two injections in murine models (16). Furthermore, a dose-dependent increase in neutralization titer was observed with a prime-boost regimen. We further probed the immune response of a single vaccination. We demonstrated that a single administration of RABV-G mRNA at doses of 0.3 μg, 1 μg, and 3 μg elicited VNTs of 1.8, 11.5, and 20.3 IU/ml, respectively, at four weeks post-vaccination. Consistent with the VNTs, our results showed that the single dose of RABV-G mRNA-LNP conferred complete protection against the rabies virus of CVS-11 infection *in vivo*, even at a low dose of 0.3 μg in mice. Then the VNTs were monitored for the following 25 weeks, and it was apparent that RABV-G mRNA peaked six weeks after immunization and remained at high levels in the ensuing period. The inactivated vaccine group dropped to 1.3 IU/mL at week 25, but the VNTs in the moderate and high dose groups remained higher than 10 IU/mL. Surprisingly, we found that the inactivated vaccine has the highest IgG-specific levels but the lowest VNTs. One possible reason may be the disruption of the heterogeneous structure of RABV-G on the virion surface of the inactivated vaccine. This structural heterogeneity may have an impact on the production of neutralizing antibodies that frequently target quaternary epitopes and may result in the short duration of the postvaccination immunological response (41).

It has been shown that T-cell immunity responses—particularly the Th1 immune response—are essential for eliminating RABV viruses from the central nervous system (42, 43). In our study, the single RABV-G mRNA vaccination strongly elicited Th1-biased responses in BALB/c mice. In addition, it effectively activated obvious RABV-G antigen-specific CD4+ and CD8+ T-cell responses, in line with the findings of previous mRNA vaccines (44, 45). Thus, the help of RABV-G antigen-specific T-cell responses may be one of the possible explanations for the sustained VNTs after a single RABV-G mRNA vaccination.

Recently, the recombinant virus-vector vaccine, like ChAd155-RG, has reported that a single vaccination elicited protective efficacy against rabies challenges in animal models (34). Compared to the single immunization of ChAd155-RG, which induced a peak VNT of 30 IU/mL (at a high dose of 10^8 VP) in outbred mice, our single high-dose group produced a higher peak VNT of 100 IU/mL in BALB/c mice. It was comparable with ChAdOx1 or ChAdOx2 adenovirus-vectored rabies vaccines (at a high dose of 1×10^8 IU) (36) (both peak VNTs around 100 IU/mL).

The rabies virus is usually transmitted through dog bites in developing countries, like Asia and Africa, and children are at high risk of exposure. Therefore, the rabies vaccine should be included in childhood immunization programs. The previous research demonstrated that using rabies vaccines for vaccination programs in children could produce recall responses rapidly (46). In this study, we also observed the kinetics of induction of VNA by RABV-G mRNA-LNP following two inoculations in mice; the durability of the serum VNA response after two vaccinations remained stable with a high VNT of 1,000 IU/ml up to almost one year. Therefore, the RABV-G mRNA may be one of the candidates for Children's vaccination programs. Moreover, it also could be combined with adenovirus-vectored vaccines in a prime-boost regimen to circumvent the problem of pre-existing anti-vector antibodies.

According to the phase 1 clinical trials conducted by CureVac AG, CV7201 generated virus-neutralizing antibodies above the 0.5 IU/mL threshold in up to 83% of volunteers and needed repeated injections to meet the threshold (15). Then CV7202 could induce modest protective

virus-neutralizing antibodies with two immunizations, whereas a single dose failed to elicit VNTs over 0.5 IU/mL. Likewise, the high doses were not well tolerated, and the trial had to be temporarily stopped (28). Similar disappointing results were also demonstrated in their non-nucleoside-modified SARS-CoV-2 mRNA vaccines (47). Nevertheless, the nucleoside-modified SARS-CoV mRNA vaccine exhibited good tolerance at higher dosages and superior immunogenicity (25, 26). In our study, we employed the powerful nucleoside-modified mRNA-LNP vaccine platform, which has produced effective clinical vaccine candidates against SARS-CoV-2 (25). Therefore, we hypothesized that our mRNA vaccine candidate RABV-G could produce excellent immune protective efficacy *in vivo* only with a single dosage due to the adoption of different vaccine platforms.

There were also several limitations in our study that warrant future investigation. Firstly, we have not had a chance to compare our vaccine with mRNA vaccines generated from unmodified nucleotides, which would allow us to determine the potential benefits associated with switching from unmodified to modified nucleotides. However, the advantage of unmodified nucleotides has been clearly demonstrated by previous studies, and it is tempting to speculate that such an advantage is also applicable to the Rabies mRNA vaccine, underlying the ability of RABV-G mRNA-LNP to induce robust neutralizing titers with a single low dose. Secondly, it is worth notifying there exists uncertainty about the translation of vaccination success in mouse study to human use. Further investigation of vaccine efficacy in a more clinically relevant animal model, like non-human primates, is necessary for deriving the vaccination regimen optimal for human use in terms of both safety and protective efficiency. Nevertheless, our results provide proof-of-concept evidence supporting the feasibility of developing a nucleoside-modified Rabies mRNA vaccine capable of affording safe, effective, and durable protection with a single dose.

Data availability statement

The datasets presented in this study can be found in online repositories. The names of the repository/repositories and accession number(s) can be found in the article/Supplementary Material.

Author contributions

SB and TY performed experiments and analyzed data. CZ, MF, LZ, ZZ, XW, RY, and XP conducted the mice sample collection, Elisa, or Virus-neutralization measurement. SB wrote the manuscript. XZ, JX, and CZ organized the study, guided experiments, and revised the manuscript. All authors contributed to the article and approved the submitted version.

Funding

This work was supported by the National Natural Science Foundation of China (No. 82071788), and the technology Service Platform for Detecting High level Biological Safety Pathogenic Microorganism Supported by Shanghai Science and Technology Commission (21DZ2291300).

Acknowledgments

We thank Rongan Biological Co., Ltd for kindly donating the freeze-dried purified Vero cell culture vaccine. We thank Wuxi Xin Lianxin Biotech co. LTD (Wuxi, China) for kindly donating the CVS-11 rabies challenge virus.

Conflict of interest

The authors declare that the research was conducted in the absence of any commercial or financial relationships that could be construed as a potential conflict of interest.

Publisher's note

All claims expressed in this article are solely those of the authors and do not necessarily represent those of their affiliated organizations, or those of the publisher, the editors and the reviewers. Any product that may be evaluated in this article, or claim that may be made by its manufacturer, is not guaranteed or endorsed by the publisher.

Supplementary material

The Supplementary Material for this article can be found online at: https://www.frontiersin.org/articles/10.3389/fimmu.2022.1099991/full#supplementary-material

References

1. Hampson K, Coudeville L, Lembo T, Sambo M, Kieffer A, Attlan M, et al. Estimating the global burden of endemic canine rabies. *PLoS Negl Trop Dis* (2015) 9(4):e0003709. doi: 10.1371/journal.pntd.0003709

2. Davis BM, Rall GF, Schnell MJ. Everything you always wanted to know about rabies virus (But were afraid to ask). *Annu Rev Virol* (2015) 2(1):451–71. doi: 10.1146/annurev-virology-100114-055157

3. Anilionis A, Wunner WH, Curtis PJ. Structure of the glycoprotein gene in rabies virus. *Nature* (1981) 294:275–8. doi: 10.1038/294275a0

4. Evans JS, Selden D, Wu G, Wright E, Horton DL, Fooks AR, et al. Antigenic site changes in the rabies virus glycoprotein dictates functionality and neutralizing capability against divergent lyssaviruses. *J Gen Virol* (2018) 99(2):169–80. doi: 10.1099/jgv.0.000998

5. Hankins DG, Rosekrans JA. Overview, prevention, and treatment of rabies. *Mayo Clin Proc* (2004) 79(5):671–6. doi: 10.4065/79.5.671

6. Brunker K, Mollentze N. Rabies virus. *Trends Microbiol* (2018) 26(10):886–7. doi: 10.1016/j.tim.2018.07.001

7. Dodet B, Durrheim DN, Rees H. Rabies: underused vaccines, unnecessary deaths. *Vaccine* (2014) 32(18):2017–9. doi: 10.1016/j.vaccine.2013.12.031

8. Pichon S, Guinet-Morlot F, Minutello M, Donazzolo Y, Rouzier R, Chassard D, et al. A serum-free, purified vero cell rabies vaccine is safe and as immunogenic as the reference vaccine verorab for pre-exposure use in healthy adults: results from a randomized controlled phase-II trial. *Vaccine* (2013) 31(18):2295–301. doi: 10.1016/j.vaccine.2013.02.058

9. World Health O. Rabies vaccines: WHO position paper, April 2018–Recommendations. *Vaccine* (2018) 36(37):5500–3. doi: 10.1016/j.vaccine.2018.06.061

10. Rao AK, Briggs D, Moore SM, et al. Use of a Modified Preexposure Prophylaxis Vaccination Schedule to Prevent Human Rabies: Recommendations of the Advisory Committee on Immunization Practices — United States, 2022. *MMWR Morb Mortal Wkly Rep* (2022) 71:619–27. doi: 10.15585/mmwr.mm7118a2

11. WHO. Rabies vaccines: WHO position paper–recommendations. *Vaccine* (2010) 28(44):7140–2. doi: 10.1016/j.vaccine.2010.08.082

12. Kariko K, Buckstein M, Ni H, Weissman D. Suppression of RNA recognition by toll-like receptors: The impact of nucleoside modification and the evolutionary origin of RNA. *Immunity* (2005) 23(2):165–75. doi: 10.1016/j.immuni.2005.06.008

13. Kariko K, Muramatsu H, Welsh FA, Ludwig J, Kato H, Akira S, et al. Incorporation of pseudouridine into mRNA yields superior nonimmunogenic vector with increased translational capacity and biological stability. *Mol Ther* (2008) 16(11):1833–40. doi: 10.1038/mt.2008.200

14. Thess A, Grund S, Mui BL, Hope MJ, Baumhof P, Fotin-Mleczek M, et al. Sequence-engineered mRNA without chemical nucleoside modifications enables an effective protein therapy in Large animals. *Mol Ther* (2015) 23(9):1456–64. doi: 10.1038/mt.2015.103

15. Alberer M, Gnad-Vogt U, Hong HS, Mehr KT, Backert L, Finak G, et al. Safety and immunogenicity of a mRNA rabies vaccine in healthy adults: An open-label, non-randomised, prospective, first-in-human phase 1 clinical trial. *Lancet* (2017) 390 (10101):1511–20. doi: 10.1016/S0140-6736(17)31665-3

16. Lutz J, Lazzaro S, Habbeddine M, Schmidt KE, Baumhof P, Mui BL, et al. Unmodified mRNA in LNPs constitutes a competitive technology for prophylactic vaccines. *NPJ Vaccines* (2017) 2:29. doi: 10.1038/s41541-017-0032-6

17. Kariko K, Muramatsu H, Ludwig J, Weissman D. Generating the optimal mRNA for therapy: HPLC purification eliminates immune activation and improves translation of nucleoside-modified, protein-encoding mRNA. *Nucleic Acids Res* (2011) 39(21):e142. doi: 10.1093/nar/gkr695

18. Sahin U, Kariko K, Tureci O. mRNA-based therapeutics–developing a new class of drugs. *Nat Rev Drug Discovery* (2014) 13(10):759–80. doi: 10.1038/nrd4278

19. Sita Awasthi LMH, Pardi N, Wang F, Myles A, Cancro MP, Cohen GH, et al. Nucleoside-modified mRNA encoding HSV-2 glycoproteins C, D, and E prevents clinical and subclinical genital herpes. *Sci Immunol* (2019) 4(39):1–15. doi: 10.1126/sciimmunol.aaw7083

20. Espeseth AS, Cejas PJ, Citron MP, Wang D, DiStefano DJ, Callahan C, et al. Modified mRNA/lipid nanoparticle-based vaccines expressing respiratory syncytial virus f protein variants are immunogenic and protective in rodent models of RSV infection. *NPJ Vaccines* (2020) 5(1):16. doi: 10.1038/s41541-020-0163-z

21. Freyn AW, Ramos da Silva J, Rosado VC, Bliss CM, Pine M, Mui BL, et al. A multi-targeting, nucleoside-modified mRNA influenza virus vaccine provides broad protection in mice. *Mol Ther* (2020) 28(7):1569–84. doi: 10.1016/j.ymthe.2020.04.018

22. Meyer M, Huang E, Yuzhakov O, Ramanathan P, Ciaramella G, Bukreyev A. Modified mRNA-based vaccines elicit robust immune responses and protect Guinea pigs from Ebola virus disease. *J Infect Dis* (2018) 217(3):451–5. doi: 10.1093/infdis/jix592

23. Pardi N, Hogan MJ, Pelc RS, Muramatsu H, Andersen H, DeMaso CR, et al. Zika virus protection by a single low-dose nucleoside-modified mRNA vaccination. *Nature* (2017) 543(7644):248–51. doi: 10.1038/nature21428

24. Richner JM, Himansu S, Dowd KA, Butler SL, Salazar V, Fox JM, et al. Modified mRNA vaccines protect against zika virus infection. *Cell* (2017) 168(6):1114–1125.e10. doi: 10.1016/j.cell.2017.02.017

25. Baden LR, El Sahly HM, Essink B, Kotloff K, Frey S, Novak R, et al. Efficacy and safety of the mRNA-1273 SARS-CoV-2 vaccine. *N Engl J Med* (2021) 384(5):403–16. doi: 10.1056/NEJMoa2035389

26. Skowronski DM, De Serres G. Safety and efficacy of the BNT162b2 mRNA covid-19 vaccine. *New Engl J Med* (2021) 384(16)::1576–7. doi: 10.1056/NEJMc2036242

27. Schnee M, Vogel AB, Voss D, Petsch B, Baumhof P, Kramps T, et al. An mRNA vaccine encoding rabies virus glycoprotein induces protection against lethal infection in mice and correlates of protection in adult and newborn pigs. *PLoS Negl Trop Dis* (2016) 10 (6):e0004746. doi: 10.1371/journal.pntd.0004746

28. Aldrich C, Leroux-Roels I, Huang KB, Bica MA, Loeliger E, Schoenborn-Kellenberger O, et al. Proof-of-concept of a low-dose unmodified mRNA-based rabies vaccine formulated with lipid nanoparticles in human volunteers: A phase 1 trial. *Vaccine* (2021) 39(8):1310–8. doi: 10.1016/j.vaccine.2020.12.070

29. Yu P, Lv X, Shen X, Tang Q, Liang G. Establishment and preliminary application of a rapid fluorescent focus inhibition test (RFFIT) for rabies virus. *Virol Sin* (2013) 28 (4):223–7. doi: 10.1007/s12250-013-3321-x

30. Kangli Cao XW, Peng H, Ding L, Wang X, Hu Y, Dong L, et al. A single vaccine protects against SARS-CoV-2 and influenza virus in mice. *J Virol* (2022) 96(4):1–13. doi: 10.1128/jvi.01578-21

31. Cliquet MA F, Sagne L. Development of a fluorescent antibody virus neutralisation test (FAVN test) for the quantitation of rabies-neutralising antibody. *J Immunol Methods* (1998) 212(1):79–87. doi: 10.1016/S0022-1759(97)00212-3

32. He F, Fu W, Cao K, He Q, Ding X, Chen J, et al. IFN-k suppresses the replication of influenza a viruses through the IFNAR-MAPK-Fos-CHD6 axis. *Sci Signal* (2020) 13(626): eaaz3381. doi: 10.1126/scisignal.aaz3381

33. Liang M, Wang Z, Wu C, Xiong S, Zhao L, Dong C. A single dose of recombinant VSV-RABVG vaccine provides full protection against RABV challenge. *Virol Sin* (2022) 37(3):455–8. doi: 10.1016/j.virs.2022.02.008

34. Napolitano F, Merone R, Abbate A, Ammendola V, Horncastle E, Lanzaro F, et al. A next generation vaccine against human rabies based on a single dose of a chimpanzee adenovirus vector serotype C. *PLoS Negl Trop Dis* (2020) 14(7):e0008459. doi: 10.1371/journal.pntd.0008459

35. Shi C, Tian L, Zheng W, Zhu Y, Sun P, Liu L, et al. Recombinant adeno-associated virus serotype 9 AAV-RABVG expressing a rabies virus G protein confers long-lasting immune responses in mice and non-human primates. *Emerg Microbes Infect* (2022) 11 (1):1439–51. doi: 10.1080/22221751.2022.2078226

36. Wang C, Dulal P, Zhou X, Xiang Z, Goharriz H, Banyard A, et al. A simian-adenovirus-vectored rabies vaccine suitable for thermostabilisation and clinical development for low-cost single-dose pre-exposure prophylaxis. *PLoS Negl Trop Dis* (2018) 12(10):e0006870. doi: 10.1371/journal.pntd.0006870

37. Yan L, Zhao Z, Xue X, Zheng W, Xu T, Liu L, et al. A bivalent human adenovirus type 5 vaccine expressing the rabies virus glycoprotein and canine distemper virus hemagglutinin protein confers protective immunity in mice and foxes. *Front Microbiol* (2020) 11:1070. doi: 10.3389/fmicb.2020.01070

38. Zhang YN, Chen C, Deng CL, Zhang CG, Li N, Wang Z, et al. A novel rabies vaccine based on infectious propagating particles derived from hybrid VEEV-rabies replicon. *EBioMedicine* (2020) 56:102819. doi: 10.1016/j.ebiom.2020.102819

39. Li J, Ertel A, Portocarrero C, Barkhouse DA, Dietzschold B, Hooper DC, et al. Postexposure treatment with the live-attenuated rabies virus (RV) vaccine TriGAS triggers the clearance of wild-type RV from the central nervous system (CNS) through the rapid induction of genes relevant to adaptive immunity in CNS tissues. *J Virol* (2012) 86(6):3200–10. doi: 10.1128/JVI.06699-11

40. Koraka P, Bosch BJ, Cox M, Chubet R, Amerongen G, Lovgren-Bengtsson K, et al. A recombinant rabies vaccine expressing the trimeric form of the glycoprotein confers enhanced immunogenicity and protection in outbred mice. *Vaccine* (2014) 32(36):4644–50. doi: 10.1016/j.vaccine.2014.06.058

41. Callaway HM, Zyla D, Larrous F, Melo GDde, Hastie KM, Avalos RD, et al. Structure ofthe rabies virus glycoprotein trimer bound to a prefusion-specific neutralizing antibody. *Sci Adv* (2022) 8(24):eabp9151. doi: 10.1126/sciadv.abp9151

42. Lebrun A, Portocarrero C, Kean RB, Barkhouse DA, Faber M, Hooper DC. T-Bet is required for the rapid clearance of attenuated rabies virus from central nervous system tissue. *J Immunol* (2015) 195(9):4358–68. doi: 10.4049/jimmunol.1501274

43. Hooper DC, Roy A, Barkhouse DA, Li J, Kean RB. Rabies virus clearance from the central nervous system. *Adv Virus Res* (2011) 79:55–71. doi: 10.1016/B978-0-12-387040-7.00004-4

44. Sahin U, Muik A, Derhovanessian E, Vogler I, Kranz LM, Vormehr M, et al. COVID-19 vaccine BNT162b1 elicits human antibody and TH1 T cell responses. *Nature* (2020) 586(7830):594–9. doi: 10.1038/s41586-020-2814-7

45. Zhang NN, Li XF, Deng YQ, Zhao H, Huang YJ, Yang G, et al. A thermostable mRNA vaccine against COVID-19. *Cell* (2020) 182(5):1271–1283 e1216. doi: 10.1016/j.cell.2020.07.024

46. Malerczyk C, Briggs DJ, Dreesen DW, Banzhoff A. Duration of immunity: an anamnestic response 14 years after rabies vaccination with purified chick embryo cell rabies vaccine. *J Travel Med* (2007) 14(1):63–4. doi: 10.1111/j.1708-8305.2006.00097.x

47. Kremsner PG, Ahuad Guerrero RA, Arana-Arri E, Aroca Martinez GJ, Bonten M, Chandler R, et al. Efficacy and safety of the CVnCoV SARS-CoV-2 mRNA vaccine candidate in ten countries in Europe and Latin America (HERALD): A randomised, observer-blinded, placebo-controlled, phase 2b/3 trial. *Lancet Infect Dis* (2022) 22(3):329–40. doi: 10.1016/S1473-3099(21)00677-0

frontiers | Frontiers in Immunology

TYPE Review
PUBLISHED 17 January 2023
DOI 10.3389/fimmu.2022.1093607

OPEN ACCESS

EDITED BY
Gang Zhou,
Augusta University, United States

REVIEWED BY
Andrea Nicolini,
University of Pisa, Italy
Jin Xie,
University of Georgia, United States
Jinxing Wei,
Department of Hepatobiliary Surgery,
Sun Yat-sen University, China

*CORRESPONDENCE
Zhifang Xi
xzf198007@163.com
Zhaogang Yang
zhaogangyang@jlu.edu.cn

†These authors have contributed equally to this work

SPECIALTY SECTION
This article was submitted to Cancer Immunity and Immunotherapy, a section of the journal Frontiers in Immunology

RECEIVED 10 November 2022
ACCEPTED 23 December 2022
PUBLISHED 17 January 2023

CITATION
Zhang H, Wang S, Sun M, Cui Y, Xing J, Teng L, Xi Z and Yang Z (2023) Exosomes as smart drug delivery vehicles for cancer immunotherapy. *Front. Immunol.* 13:1093607. doi: 10.3389/fimmu.2022.1093607

Exosomes as smart drug delivery vehicles for cancer immunotherapy

Huan Zhang[1†], Simiao Wang[1†], Man Sun[1], Yaxin Cui[1], Jianming Xing[1], Lesheng Teng[1], Zhifang Xi[2*] and Zhaogang Yang[1*]

[1]School of Life Sciences, Jilin University, Changchun, China, [2]School of Horticulture and Food, Guangdong Eco-Engineering Polytechnic, Guangzhou, China

Exosomes (Exos) as drug delivery vehicles have been widely used for cancer immunotherapy owing to their good biocompatibility, low toxicity, and low immunogenicity. Some Exos-based cancer immunotherapy strategies such as tuning of immunosuppressive tumor microenvironment, immune checkpoint blockades, and cancer vaccines have also been investigated in recent years, which all showed excellent therapeutic effects for malignant tumor. Furthermore, some Exos-based drug delivery systems (DDSs) for cancer immunotherapy have also undergone clinic trails, indicating that Exos are a promising drug delivery carrier. In this review, in order to promote the development of Exos-based DDSs in cancer immunotherapy, the biogenesis and composition of Exos, and Exos as drug delivery vehicles for cancer immunotherapy are summarized. Meanwhile, their clinical translation and challenges are also discussed. We hope this review will provide a good guidance for Exos as drug delivery vehicles for cancer immunotherapy.

KEYWORDS

exosomes, immunotherapy, drug delivery system, immune checkpoint blockade, tumor immune microenvironment

1 Introduction

Cancer has become a major cause of death worldwide. According to the latest statistiscs, there will be a total of more than 1.9 million new cancer patients and 600 thousand cancer deaths in the United States in 2022, suggesting that cancer has seriously threatened human health (1, 2). Although traditional therapeutics, including radiation, chemotherapy and surgery, have shown a certain tumoricidal ability, there are still some limitations (3, 4). These therapeutics often kill both cancer and normal cells, leading to severe side effects and drugs resistance (5). Therefore, it is critical to find an effective therapeutic approach with low or no side effects (6).

10.3389/fimmu.2022.1093607

Cancer immunotherapy is a novel therapeutic approach that exploits the body's own immune system to recognize and eradicate tumor cells (3, 7). In order to achieve sustained antitumor immune response, the cancer immunity cycle must be repeatedly initiated and expanded (3), as shown in Figure 1. Firstly, tumor cells release some tumor-specific immunogenic antigens, and then, antigen-presenting cells (APCs) including dendritic cells (DCs) and macrophages present antigens for the activation of certain lymphocytes *via* major histocompatibility complex I (MHC-I). After that, these antigens can be further recognized by T cells including $CD4^+$ T cells and $CD8^+$ T cells inside the lymph nodes, and thus resulting in specific immune responses to the cancer cells. In this case, cancer immunotherapy can specifically kill cancer cells with minimal effect to normal cells, and induce immunological memory to trigger long-term protection against tumor recurrence (5, 8). Therefore, cancer immunotherapy has attracted widespread attentions in the field of cancer therapy.

Nowadays, a series of cancer immunotherapy approaches including nonspecific immune stimulation (9), immune checkpoint blockades (ICB) (10), and cancer vaccines (11, 12) have been evaluated to modulate immune responses. Moreover, some cancer immunotherapy drugs including cytotoxic T-lymphocyte-associated protein 4 (CTLA-4) inhibitors (10), programmed cell death 1 (PD-1) inhibitors and programmed cell death 1 ligand 1 (PD-L1) inhibitors have been authorized by the United States Food and Drug Administration (FDA) for clinical use (13, 14). Although these inhibitors have shown exciting outcomes, some shortcomings still exist. For instance, many malignant tumors have the ability of releasing different immunosuppressive molecules into the tumor microenvironment (TME), promoting their immune escape or suppressing immune reactions (15). Furthermore, their therapeutic effect is often diminished by off-targeting delivery, the induction of immune tolerance and evasion, and all these limit their applications (13, 16). In order to overcome these shortcomings, many researchers

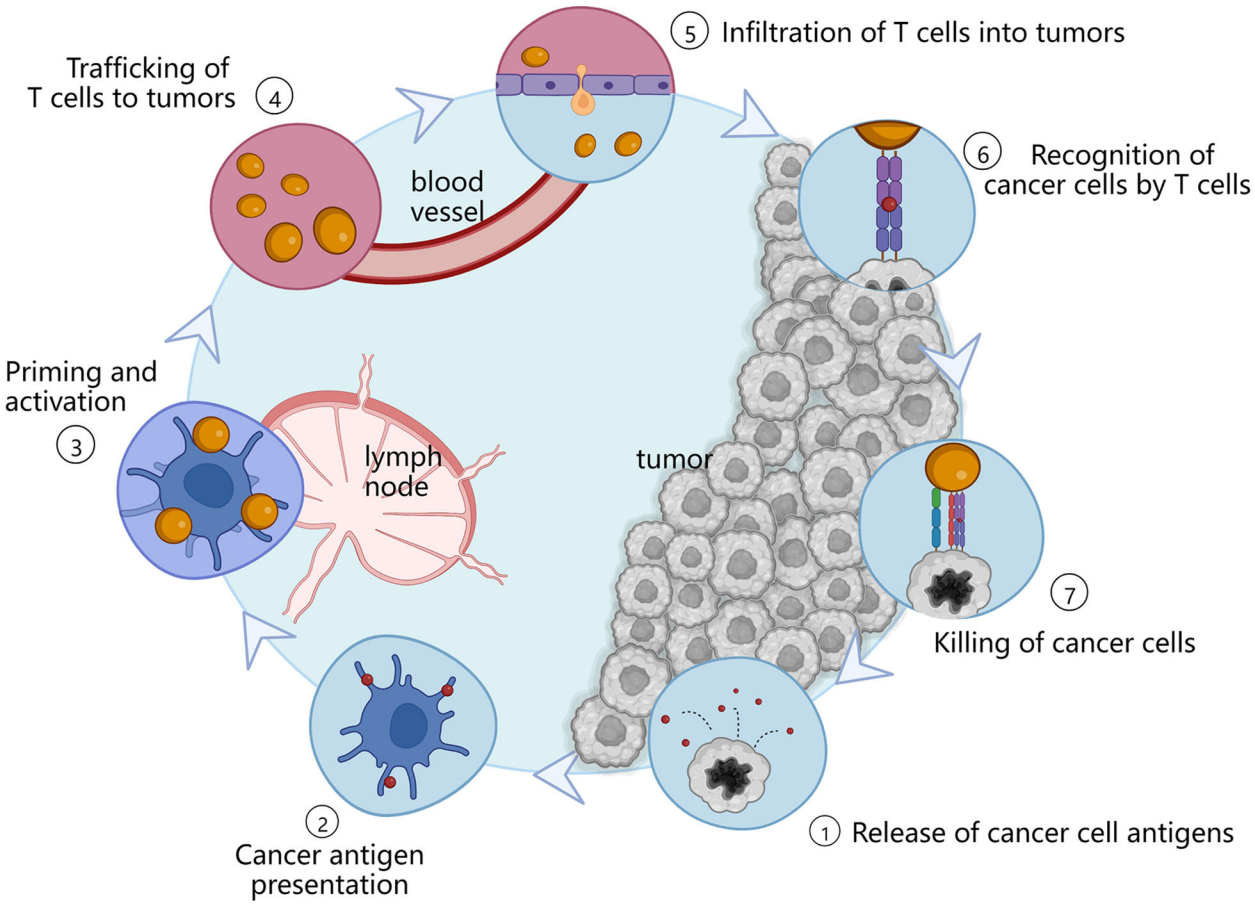

FIGURE 1
Immune actions in the cancer immunity cycle. APCs present antigens which are released by tumor cells to lymphocytes. And then, these antigens can be subsequently recognized by T cells located in the lymph nodes, thereby activating specific immune responses to the tumor sites.

focus on the application of drug delivery systems (DDSs). DDSs can deliver payloads including immune checkpoint inhibitors (ICIs) and immunosuppressive regulatory molecules to the desired site and realize the sustained release of the drugs, thereby improving the efficiency of cancer immunotherapy. Currently, various DDSs, such as exosomes (Exos), liposomes, and nanoparticles, have been extensively studied and hold great promise in cancer immunotherapy.

Exos, one of drug delivery carriers, are 40–160 nm sized extracellular vesicles secreted by live cells and can be found in different types of biological fluids (e.g., serum, saliva, and urine) (17). They possess many advantages such as small size, good biocompatibility, low toxicity, and low immunogenicity (18). Meanwhile, Exos can protect cancer immunotherapeutic agents from degradation, thus increasing their circulation time and targeting ability (19). Unlike liposomes and other synthetic drug nanoparticle carriers, Exos are able to inherit the properties of parent cells and obtain some components of parent cells such as proteins, lipids and nucleic acids, which may endow them homing effect and the ability to activate immune responses (20). Moreover, Exos contain transmembrane and membrane anchored proteins, which may enhance target cells' endocytosis and promote the delivery of their internal content (16). In addition, Exos could be easily engineered to improve drug-loading capacity and tissue-specific targeting (21). Therefore, Exos are recognized as a promising drug carrier.

In order to promote the development of Exos in cancer immunotherapy, in this review, we comprehensively summarized the application of Exos as smart drug delivery vehicles for cancer immunotherapy. First, the biogenesis and composition of Exos are introduced. Then, Exos as drug carrier for cancer immunotherapy are discussed. Finally, the clinical translation and challenges of Exos as drug delivery vehicles are presented.

2 Exosomes

The name "exosome" (Exo) first appeared in 1981. At that time, Trams et al. (22) extracted plasma membrane-derived vesicles with 5'-nucleotidase activity, and referred the vesicles as Exos. Exos are the important subset of extracellular vesicles, possessing 40–160 nm particle size (23). A large number of researches have proven that Exos can be actively secreted by most, if not all, organisms including bacteria (24) and almost all cell types (e.g., red blood cells (25), platelets (26), immune cells (27), fibroblasts (28), endothelial cells (29), epithelial cells (30) and tumor cells (31). Their secretion mechanism is simple, and the scheme is shown in Figure 2. It is generally recognized that the generation of Exos involves three major steps: invagination, multivesicular bodies generation, and secretion (32, 33). The generation of Exos begins with the inward budding of the plasma membrane and generates several endocytic vesicles which encapsulate proteins both on the surface of the plasma membrane and in the extracellular matrix (32). And then, early sorting endosomes (ESEs) are formed under the effect of the endocytic sorting complex and the proteins required for transport. After that, ESEs mature into late sorting endosomes, and continue inward invagination to form multivesicular bodies (MVBs). Finally, MVBs, which contain many intraluminal vesicles (ILVs), can either fuse with the cytoplasmic membrane to release Exos into the extracellular environment or fuse with lysosomes or autophagosomes to be degraded.

It is generally believed that the biogenesis of Exos is a tightly controlled process. In brief, two potential mechanisms are involved in this process: endosomal sorting complexes required for transport (ESCRT) dependent mechanism and ESCRT-independent mechanism (34). Of which, ESCRT provides a crucial mechanism for the formation and sorting of the ILVs (35). ESCRT consists of a five-part protein complex with different roles including ESCRT-0, -I, -II, -III and the AAA ATPase Vps4. Specifically, ubiquitin-binding ESCRT-0 binds directly to specific structural domains of the endosomal membrane through the action of hepatocyte growth factor-regulated tyrosine kinase substrate (HRS) with endosomal-specific phosphatidylinositol 3-phosphate (PtdIns-3-P) (36). Then, ESCRT-I and ESCRT-II are recruited by the interaction between HRS and the ESCRT-I subunit TSG101 (37), and the complexes further recruit ESCRT-III which consists of various soluble coiled-coil-containing proteins Vps2, Vps20, Vps24, and Snf7 to form a protein complex which is involved in promoting the inward budding processes (38). The ESCRT-III complex drives vesicle division and is dissociated and recovered from the MVB membrane through the mediation of the AAA ATPase Vps4 (39). An increasing number of studies demonstrated that several ESCRT-related proteins can affect the secretion of Exos (40, 41). For example, the experimental results of twenty-three components of the ESCRT machinery in Exos biogenesis and related proteins in MHC II-expressing HeLa cells by RNA interference (RNAi) have shown that silencing of HRS, STAM1 and TSG101 can reduce secretion of Exos and decrease the expression of MHC II and CD63 proteins (40, 41). Meanwhile, silencing of VPS4B increased secretion of exosome marker proteins (CD63, MHC II, HSC70), and depletion of ALIX enhanced MHC II-expression on Exos and secreting cells (40). Another research also showed that ESCRT-III-associated protein ALIX interacts with cytoplasmic adaptor syntenin, thus promoting the intraluminal budding of endosomal membrane and Exos' secretion (42). Likewise, the depletion of ESCRT-III and its associated proteins, including CHMP4C, VTA1, increased Exos' secretion (42).

Exos are regarded as small "progeny" of parental cells, because it contains components of parental cells. They contain thousands of proteins, lipids and nucleic acids, and the scheme is presented in Figure 2. Typically, Exos contain a variety of non-specific proteins, including heat shock proteins (HSP70, HSP90), membrane transport proteins (such as annexins and flotillin),

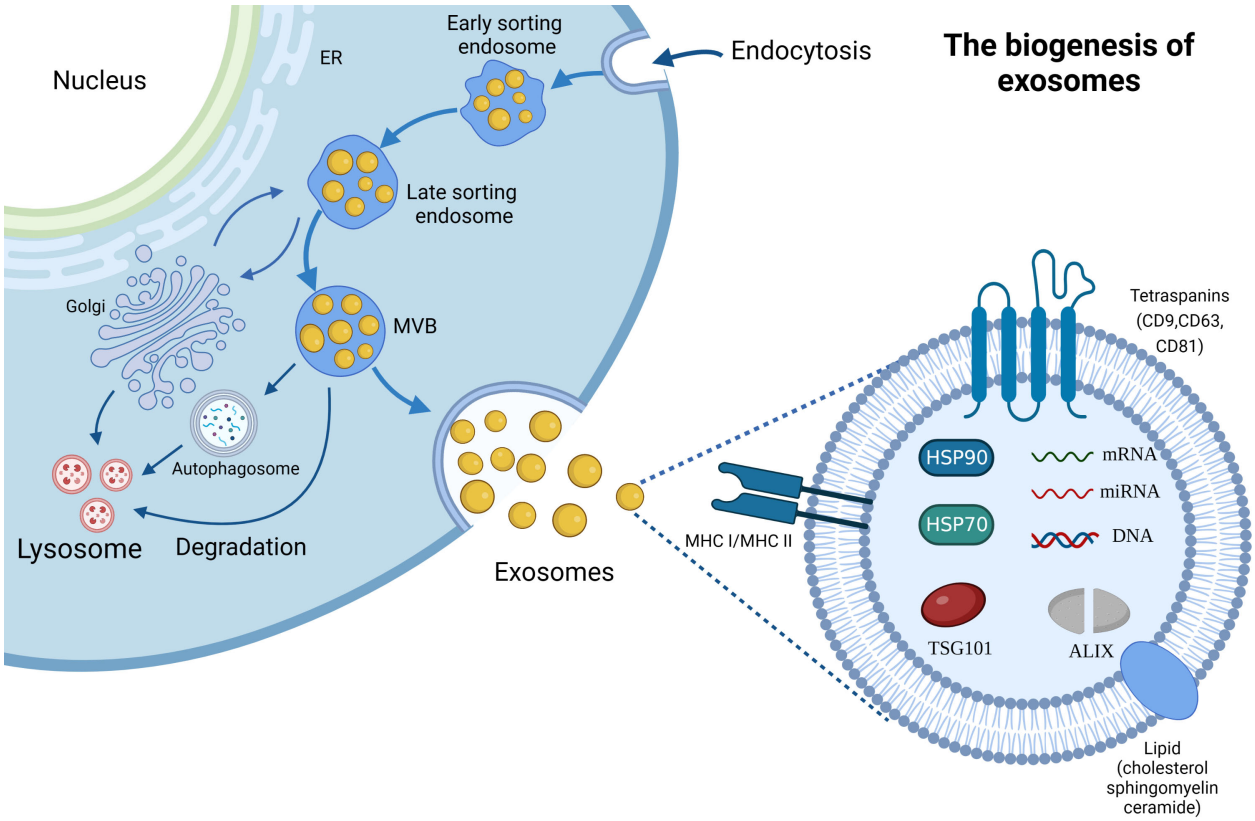

FIGURE 2
The biogenesis and composition of Exos. ER; Endoplasmic reticulum, MVB; Multivesicular Body.

cytoskeletal proteins (myosin, actin and tubulin), MHC proteins (MHC I and MHC II) (43), adhesion molecules (CD11b and CD54) (44), and tetraspanins protein superfamily (CD9, CD63 and CD81) which is considered as the marker protein of Exos (45). Moreover, ALIX and TSG101 proteins aforementioned are also the important components of Exos. Cell type-specific proteins have also been discovered in Exos, such as the A33 protein secreted by the human colon tumor cell line LIM1215 (46), further suggesting that their composition is related to the type and physiological condition of the source cells. In addition, Exos also possess extensive lipids, cholesterol, sphingomyelin, glycosphingolipids and different patterns of RNAs including mRNAs and non-coding RNAs (e.g., miRNAs, circRNAs, lncRNAs, ribosomal RNAs (rRNAs) and transfer RNAs (tRNAs)) (47, 48). Of which, bioactive lipids play an important role in the stability and structural rigidity of Exos, cholesterol can regulate Exos' secretion, and sphingomyelin triggers calcium influx (47). Meanwhile, exosomal miRNAs, such as miR-214, miR-29a, miR-1, miR-126, and miR-320, participate in angiogenesis, hematopoiesis, exocytosis, and tumorigenesis (48). Moreover, exosomal lncRNAs as an intercellular signaling are also involved in the development of oncogenesis and regulation of the TME.

3 Exos as drug delivery carrier for cancer immunotherapy

3.1 The source of Exos

Exos, especially these secreted from tumor cells and immune cells, may influence the phenotype and immune function of target cells (49). In order to better understand the source of Exos as drug delivery carrier, in this section, we summarized the characteristics of immune cell-derived and tumor cell-derived Exos (TEXs).

3.1.1 Immune cells-derived Exos

Immune cells mainly include DCs, macrophage, B lymphocytes, T lymphocyte cells, etc. Phagocytes (e.g., macrophages and neutrophils) and natural killer (NK) cells act as the first line of defense against pathogens, rapidly activating the innate immune response and killing pathogens; T cells, B cells and related cytokines can activate specialized humoral and cellular immune responses, respectively (50). However, Exos produced by immune cells are able to inherit the properties of parent cells and participate in the innate and adaptive immune

responses (20). Therefore, a large number of researches have used immune cells-derived Exos as drug carriers for cancer immunotherapy.

DCs are classical APCs that stimulate specific antigenic immune responses (23). DCs-derived Exos (DEXs), which mainly contain MHC-I, MHC-II, costimulatory molecules (CD80 and CD86), heat shock proteins (HSP70 and HSP90) and adhesion molecules (ICAM-1) (51), are the most widely used immune cells-derived drug carrier. They can activate T cells to kill cancer cells through directly binding of MHC-peptide complex and costimulatory molecules to T cell receptors (TCR) (51). Moreover, DEXs also can present the MHC-peptide complex to another DCs which is possibly an inactivated DC, thereby increasing the expression of the MHC-peptide complex, and subsequently leading to large-scale activation of T cells (52). In fact, DEXs have the same therapeutic effect as the parent DCs. For example, genetically modified DEXs contain Th2 cytokines (e.g., IL-4 and IL-10) and apoptotic proteins (e.g., FASL) to inhibit inflammation and ameliorate the extent of collagen-induced arthritis (53). In contrast, NK cells derived Exos contain NK markers like CD56, NKG2D, CD94, CD40L and killer proteins (e.g., FASL and perforin) (54). NK cells-derived Exos can induce tumor cells apoptosis by significant activation of caspase death pathways *via* perforin and FASL (55, 56). In addition to killer proteins, NK cell-derived Exos may also carry tumor suppressor miRNAs such as miR-186, and thus inhibiting tumor growth and TGFβ1-dependent immune escape, and all of which exhibited the therapeutic potential of NK cell-derived Exos (57).

Macrophage-derived Exos, another immune cells-derived Exos, exhibit pro-inflammatory and pro-tumor functions, which mainly depend on the phenotype of macrophages (M1 and M2 subtypes) (58, 59). For instance, M1 phenotype macrophages-derived Exos (M1-Exos) can activate NLRP3 inflammasomes to enhance the cytotoxicity of T cells and NK cells and thus inhibiting the growth of tumor (20). Moreover, they can also upregulate the expression of miRNAs (e.g., miR-146a, miR-146b and miR-21-3p) and resolve inflammation by inhibiting NF-κB and TLR signaling pathways (60, 61). Meanwhile, a study has proven that M1-Exos can repolarize M2 tumor associated macrophages (TAMs) to M1 macrophages, resulting in pro-inflammatory cytokines releasing and synergistic effects of anti-PD-L1 in tumor immunotherapy (62). In contrast, M2 phenotype macrophages derived Exos showed the ability to suppress T-cell function and participate in tumor proliferation, migration, angiogenesis, and facilitate tumor immune escape (63).

In addition, B lymphocytes and T lymphocyte cells are also immune cells used for Exos generation. B lymphocytes derived –Exos contain CD19, B cell-specific markers, and the immunogenic molecules (e.g., MHC-I, MHC-II, CD40, CD54 and CD86), which stimulate T lymphocytes proliferation, activation and T(H)2-like cytokine production (64–66). Meanwhile, T cell-derived Exos express TCR, adhesion factors and various markers including CD2, CD3, CD4, CD8, CD11c, CD25, CD69, LFA-1, CXCR4, FASL, GITR (67). In general, T lymphocyte cells are classified into two phenotypes: $CD4^+$ T cells and $CD8^+$ T cells (68). Depending on their functions and the expression of antigens, $CD4^+$ T cells are further classified as regulatory T cells (Tregs), Th cells and follicular helper T cells (Tfhs) (67). The Exos secreted by different phenotypes T cells have distinct regulatory effects on immune cells and non-immune cells (67). For example, Exos purified from $CD8^+$ T cells generate proliferation in autologous resting cells and produce a higher proportion of $CD8^+$ T cells (69). $CD8^+$ cytotoxic T lymphocyte (CTL)-derived Exos have a potent benefit when used as DDSs for tumor immunotherapy since the inherited CTL properties. Exos derived from IL-12-stimulated CTLs could directly activate naive $CD8^+$ T cells in the absence of antigen, producing IFN-γ and granzyme B, and eliminating tumor cells (70, 71). Conversely, Treg-derived Exos contain specific molecular cargo (let-7b, let-7d, miRNA-155 and iNOS) and cooperate with cytokines (IL-10 and TGF-β) to perform immunosuppressive functions (72).

Furthermore, other immune cell-derived Exos as drug delivery carrier, including neutrophil-derived Exos (73), mast cell-derived Exos (74), eosinophils-derived Exos (75) and myeloid-derived suppressor cell-derived Exos (76), also showed an essential role in the immune microenvironment, participating in immune regulation, inflammatory responses, intercellular communication, etc. (77, 78).

3.1.2 Tumor-derived Exos

In general, TEXs are rarely used as drug carriers for cancer immunotherapy, which mainly because they accurately reproduce the content of parent tumor cells (79–82), and transfer oncogenic signals including activated oncoproteins, transcripts, oncogenic DNA sequences and oncogenic micro-RNAs (83–85) to surrounding immune cells, stromal cells and other tumor cells, and induce various functional changes in the cells (86–89). However, TEXs also contain some immunostimulatory molecules, such as CD80, CD86, MHC complexes (90, 91). They can act as adjuvants and participate in antigen presentation, and thus stimulating the activation of immune response (92). For example, TEXs serve as effective carriers of the chemotherapeutic drug methotrexate and simultaneously act as immunomodulators, stimulating the recruitment of large quantity of neutrophils to the cholangiocarcinoma tumor region and activating the neutrophil anti-tumor response to alleviate obstructive extrahepatic cholangiocarcinoma (93). TEXs are also important mediators in intercellular communication and immune regulation, and the ability of TEXs to protect internal proteins or nucleic acids from degradation makes TEXs the most promising choice as diagnostic and prognostic biomarkers (94).

Currently, TEXs are widely used as diagnostic biomarkers for non-small cell lung cancer (95), pancreatic cancer (96), colorectal cancer (97), and gastric cancer (98).

3.2 Drug-loading strategy

Various studies have suggested that exosome is a potential drug delivery carrier due to its high biocompatibility, low toxicity, low immunogenicity and the ability of crossing natural barriers (99). Various drug-loading strategies have been designed and developed, including incubation (100), physical loading techniques (e.g., electroporation, ultrasound and extrusion) (101, 102), and cell engineering techniques (103), etc. Their pros and cons are presented in Table 1.

Incubation is the simplest drug-loading method, where the drug diffuses into the exosome membrane or cell membrane according to a concentration gradient (99). Up to now, three incubation strategies have been developed: direct incubation, transfection reagent-mediated incubation, and source cell-mediated incubation (118). They present multiple advantages such as simple operation, no special equipment requirement, preservation of exosome integrity and with minimum damage to Exos and drugs, and these drug-loading strategies have been applied to load different types of drugs. For example, study showed that $Exo^{Ce6+R848}$ was constructed by simple co-incubation of HEK 293T cell-derived Exos with Chlorin e6 (Ce6) and immune adjuvant R848 to reprogram immunosuppressive M2-like phenotypic macrophages and restore the immune microenvironment (119).

Although some payloads cannot be loaded by co-incubation, commercial reagents with better transfection efficacy (e.g., lipofectamine and dharmaFECT3) have been applied to load drugs into Exos (120, 121). For instance, PD-L1 siRNA can be entrapped by Lipofectamine® 2000, and then, adding Exos inside can decrease its cytotoxicity and improve its targeting (120). In addition, source cell-mediated incubation was also utilized to obtain DDSs (122). Specifically, donor cells were co-incubated with drugs, causing the secretion of Exos loaded with active drug components (123). Although incubation presents many advantages, the variety of encapsulated drugs is limited and the drug-loading efficiency is relatively low (124).

Physical loading methods including electroporation, ultrasound and extrusion have also been widely applied to load drugs (125). Electroporation is a strategy that drugs are instantaneously loaded into Exos under an electrical impulse (126). In this situation, when the transmembrane potential reaches a certain threshold, a hydrophilic channel is formed in the membrane allowing small molecules hydrophilic nucleic acids to be rapidly loaded by the electric field, followed by self-healing of membranes, which can improve the drug-loading efficiency (127). In view of this, bone marrow mesenchymal stem cell (BM-MSC) Exos were loaded with galectin-9 siRNA by electroporation and modified with oxaliplatin (OXA) prodrug as an immunogenic cell death trigger to disrupt tumor immunosuppression by M2 TAMs and recruit cytotoxic T lymphocytes, achieving significant therapeutic efficacy in the immunotherapy of pancreatic ductal adenocarcinoma (128). In another study, it was indicated that the loading efficiency of electroporation was three times higher than that of normal incubation (129). Although electroporation showed high drug-loading efficiency, it may damage the intact structure of the Exos and cause cargo aggregation. Therefore, in order to solve these shortcomings, various innovative electroporation strategies were developed to load cargo into Exos (130, 131). Chang et al. (130) batch-produced a 3D NEP chip with a uniform and parallel nanochannel array. The results indicated that this chip showed a significant higher efficiency and transfection uniformity. In addition, our groups (131) developed a cellular nanoporation (CNP) biochip with 500 nm nanochannels, and the scheme is presented in Figure 3. In this work, pores were produced in the cell membrane under transient electrical pulses, and DNA plasmids were shuttled from the buffer into cells. The experimental results indicated that this approach causes less cellular damage and produces more than 50-fold Exos than that of conventional strategies. Moreover, more than 1000-fold mRNA transcripts were loaded inside compared to control. Different from this, the ultrasound method allows the drug to enter the Exos *via* disrupting the Exos membrane by mechanical shear (132). However, ultrasound can result in a degree of membrane damage (106). Extrusion is a technology that breaks the exosome membrane by external force, allowing the mixture of Exos and drugs to recombine into a new exosome (110). Though physical loading methods have been widely used, they also exist some limitations, such as damage the stability and integrity of Exos, specialized equipment requirement and limitation of production scale (118).

In addition to above-mentioned approaches, cell engineering technology is also a drug-loading method. It is a technology that modify the donor cells through gene editing technology or other methods to secrete Exos with target proteins on the cell surface. This approach is the most well-established and complex method, and has been extensively applied to load cargo into Exos (133, 134). Yong et al. (117) developed Exosome-sheathed doxorubicin-loaded PSiNPs (DOX@E-PSiNPs) generated by exocytosis of the tumor cells after treatment with DOX-loaded porous silicon nanoparticles (PSiNPs), penetrating deep into the tumor and exhibiting significant tumor toxicity. In spite of the wide range of applications and greater scope for manipulation of cellular engineering modifications, there are still limitations, such as complicated operations and uncertainty about the cargo of Exos and the amount of cargo (135).

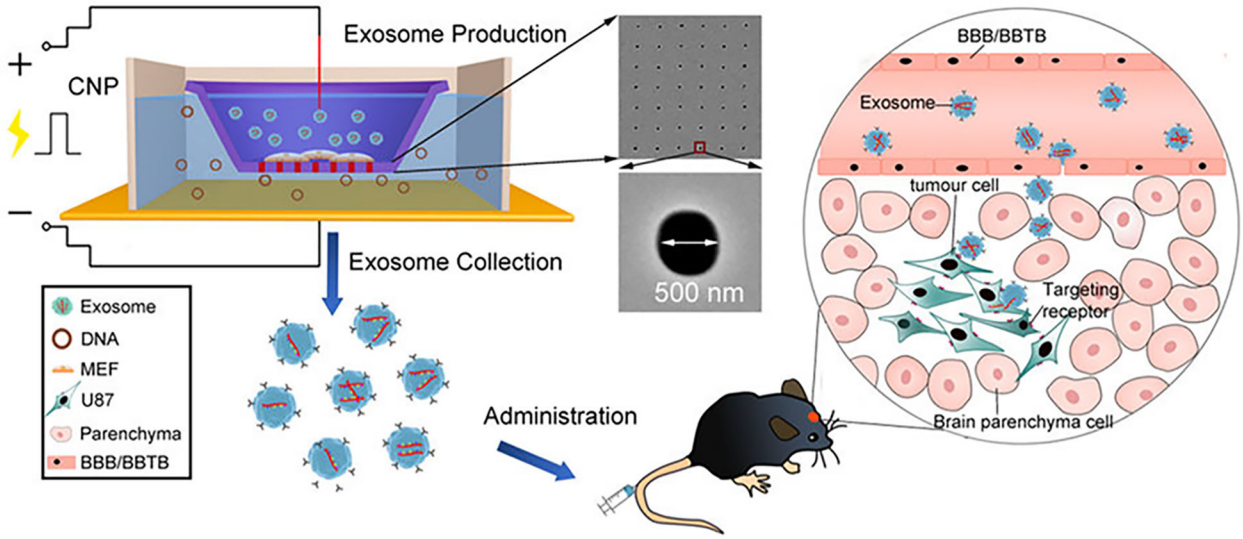

FIGURE 3
Schematic representation of CNP-generated EVs for targeted nucleic acid delivery (Reprinted with the permission from Ref. 131). Abbreviation: CNP: Cellular Nanoporation; BBB: Blood Brain Barrier; BBTB: Blood Brain Tumor Barrier.

3.3 Exos-based cancer immunotherapy strategies

Exos as a promising drug carrier show the advantage of good biocompatibility, low toxicity, and low immunogenicity. Exos-based cancer immunotherapy strategies including tuning of immunosuppressive tumor microenvironment (ITME), ICB, and cancer vaccines have been widely applied, as shown in Table 2. In order to better understand these strategies, their research status was summarized below.

3.3.1 Tuning of immunosuppressive tumor microenvironment

As is known to us, TME is very complex and comprised of multiple components including cytokines, inflammatory cytokines, extracellular matrix and blood vessels, etc. (3). It plays an important role in the recruitment of immune cells and tumor progression (143). However, some cancer cells may evade immune systems due to the downregulation of tumor associated antigens, high infiltration of multiple immunosuppressive cells such as TAMs, and low expression of antitumor cytokines (144). In addition, both the physicochemical properties of cancer cells (e.g., hypoxia and weak acidity) and the abnormal metabolic activities can also promote the immune escape of tumors, resulting in an ITME, which becomes one of the major obstacles in cancer immunotherapy (136). Therefore, tuning of ITME can efficiently enhance cancer immunotherapeutic effects.

TAMs, essential elements of the immune responses in TME, play a critical role in inhibiting tumor growth and metastasis (6). TAMs were divided into two phenotypes: tumor-suppressing M1 macrophages and tumor-promoting M2 macrophages. In

TABLE 1 The pros and cons of exosomes-based drug-loading strategies.

Drug-loading strategies	Pros	Cons	Ref
Incubation	Simple operation; No special equipment required; Preservation of exosome integrity; Little damage to exosomes and drugs	Low drug loading efficiency; Cause cytotoxicity	(99, 100, 104, 105)
Ultrasound	High drug loading efficiency	Exosome membrane damage	(106–109)
Extrusion	High drug loading efficiency; Uniform exosome particle size	After reintegrating exosome integrity damage	(110–113)
Electroporation	High drug loading efficiency	Exosome aggregation; Require process optimization; Damage to exosome integrity	(101, 102, 107, 114)
Cell Engineering Techniques	Well-established operating strategy; Toxicity reduction	Complicated operation; Uncertainty of exosomal contents and the amount of cargo	(103, 115–117)

TABLE 2 The samples of Exos-based DDSs for cancer immunotherapy.

DDSs	Exos source	Disease	Kind of study	Immunotherapy strategy	Immunotherapy efficacy	Ref
PTX-M1-Exos	M1-polarized macrophages	Breast cancer	*In vivo;* breast xenograft tumors model	Tuning of ITME	High anti-tumor effects	(109)
Exo@DOX–EPT1	Milk	Oral squamous cell carcinomas	*In vivo;* oral squamous cell carcinoma xenograft tumors model	pH targeting and tuning of ITME	High effectively treat oral squamous cell carcinomas	(136)
cGAMP@dual-antiExos	Melanoma cell	Melanoma	*In vitro*; B16F10 cells	ICB	Effectively activating immune response and inhibiting of immune escape	(137)
Exos encapsulated with sonosensitizers Ce6 and immune adjuvant R848	HEK293T cells	Prostate cancer	*In vivo;* mouse brain inflammatory model	Tuning of ITME	Activating effector T cells and reverting the immunosuppressive microenvironment	(119)
Engineered multifunctional immune-modulating Exos	Expi293F cell	Triple negative breast cancer	*In vivo*, NOD.Cg-Prkdcscid Il2rgtm1Wjl/SzJ (NSG) mice model	ICB	Activating T cells and eliciting robust anticancer immunity, and thus killing cancer cells	(138)
CpG-SAV-exo	Tumor cell	Murine melanoma	*In vivo*, B16BL6 tumor-bearing mice model	Antigen presentation and T-cell activation	Presenting stronger *in vivo* antitumor effects in B16BL6 tumor-bearing mice	(9)
Exos loaded CD62L and OX40L	HEK293T cells	Metastatic breast cancer	*In vitro*; 4T1 syngeneic mouse model	Tuning of ITME	Activating effector T cells and inhibiting Treg induction, and inhibiting tumor development	(139)
iEXO-OXA	Bone marrow mesenchymal stem cell	Pancreatic cancer	*In vivo*, Rthotopic PANC-02/luci tumor-bearing mice model	Tuning of ITME	Achieving significant therapeutic efficacy in cancer treatment	(128)
Exos with MART-1 peptide and CCL22 siRNA	Immunogenically dying tumor cells	Bladder cancer	*In vivo*; bladder cancer mice model	Cancer vaccines	High anti-tumor effects	(140)
Exos	CAR-T cell	Triple-negative breast cancer	*In vivo*; triple-negative breast cancer model	T-cell activation	Showing a highly effective tumor inhibition rate	(141)
SMART-Exos	Expi293 cells	Breast Cancer	*In vitro*; breast cancer cells (HCC 1954 cells)	T-cell activation	Showing a highly effective tumor inhibition rate	(142)

PTX-M1-Exos; M1-exosomes loading paclitaxel, ITME; Immunosuppressive tumor microenvironment, Exo@DOX–EPT1; Exosome-doxorubicin-anthracene endoperoxide derivative, ICB; Immune checkpoint blockades, Ce6; Chlorin e6, CpG-SAV-exo; CpG-SAV-exosomes, iEXO-OXA; Exosomes losding oxaliplatin; Exos, Exosomes.

general, TME promotes the functionality of TAMs into M2 phenotypes, and M2 macrophages produce immunosuppressive cytokines to facilitate tumor progression (145). In contrast, M1 macrophages are activated by pro-inflammatory cytokines, resulting in tumor suppression (146). Thus, regulation of macrophage polarization from M2 phenotypes to M1 phenotypes can efficiently inhibit cancer progression. In order to reactivate TME and enhance the efficiency of breast cancer therapy, Zhao et al. (6) designed and established exosome delivery system derived from M1 macrophage (DTX-M1-Exo). The results indicated that DTX-M1-Exo can promote the development of naïve macrophages into M1 phenotype. Meanwhile, M1 macrophages was long-term maintained by modulating mitochondrial function. DTX-M1-Exo showed a great antitumor therapeutic efficacy. Similarly, Zhou et al. (128) designed and developed a pancreatic-targeting Exos-based dual delivery biosystem (iEXO-OXA) for pancreatic immunotherapy, and the scheme is shown in Figure 4A). In their work, Exos were secreted from bone marrow mesenchymal stem cell. Galectin-9 siRNA was loaded inside Exos by electroporation method, and OXA was modified on the surface to trigger immunogenic cell death. The results indicated that iEXO-OXA promoted the polarization of M2 phenotype to M1 phenotype upon disrupting the combination of galectin-9 and dectin 1, and TME was reprogrammed, increasing anti-tumor immunity for pancreatic cancer. Moreover, researches showed

10.3389/fimmu.2022.1093607

that high molecular-weight folic acid could suppresses M1 macrophage polarization and enhance M2 polarization, resulting in immunosuppression (15). In order to modulate TME, Feng et al. (15) designed and fabricated folic acid modified exos with expressing of human hyaluronidase (PH20) drug delivery platform (Exos-PH20-FA) for cancer therapy. The results indicated that Exos-PH20-FA can degrade high molecular-weight folic acid to low-molecular-weight folic acid and polarize macrophages to the M1 type, thereby improving the efficiency of cancer therapy. Meanwhile, Exos-PH20-FA also reduced tumor cell metastasis, which provides a promising treatment for cancer.

Persistent inflammation is also another characteristic of TME (146). It can induce stromal destruction and normal

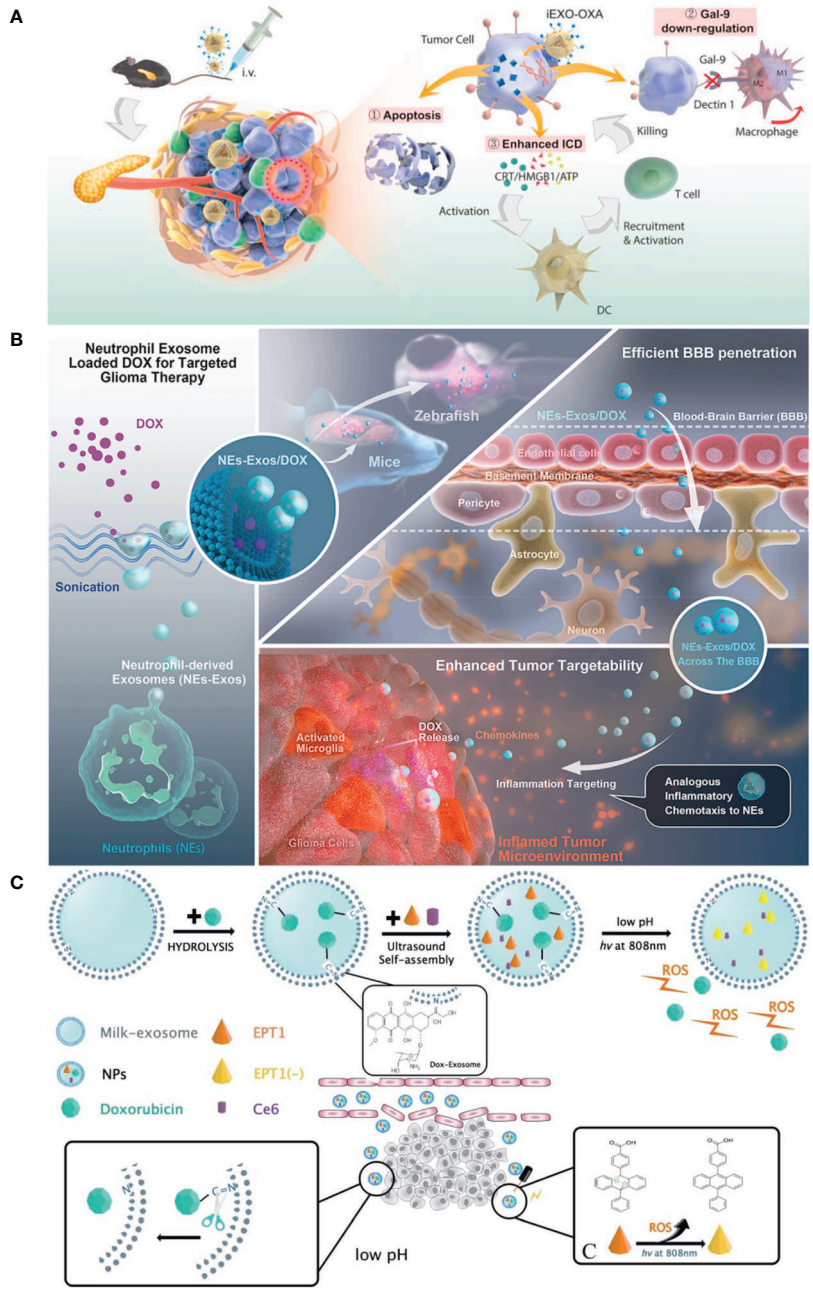

FIGURE 4
(A) Pancreatic-targeting exosomes-based dual delivery biosystem for pancreatic immunotherapy and reprogramming tumor microenvironment (Reprinted with the permission from Ref. 128); **(B)** The Scheme of NEs-Exos system for glioma immunotherapy (Reprinted with the permission from Ref. 147); **(C)** The preparation scheme and therapeutic process of Exo@DOX–EPT1 for oral squamous cell carcinoma (Reprinted with the permission from Ref. 136). iEXO-OXA, Exosomes losding oxaliplatin; ICD, immunogenic cell death; EPT1, Endoperoxide derivative; NPs, Nanoparticles; DOX, Doxorubicin; ROS, reactive oxygen; Ce6, Chlorin e6.

tumor vasculature, and thus inhibiting tumor growth. Researches showed that the secretion of pro-inflammatory cytokines, such as TNF-α, can trigger the apoptosis of cancer cells in tumor site (148). Wang et al. (109) established DDSs based on M1-EXOs. The results indicated that the expression level of caspase-3 and pro-inflammatory cytokines were elevated when M1-Exos were exposed around macrophages. Macrophages were polarized to M1 phenotype, and thus enhancing antitumor activity. In addition, in recent years, inflammatory TME targeting has been recognized as a promising and attractive therapeutic strategy. Encouraged by these, Wang et al. (147) designed and developed a neutrophil-Exos (NEs-Exos) system to deliver DOX for glioma immunotherapy, and the scheme is shown in Figure 4B). First, they isolated Exos from neutrophil by ultracentrifugation technique. And then, DOX was loaded inside Exos by sonication. The cellular uptake and the effect of NEs-Exos *in vitro* were investigated. In addition, the tumor-targetability and anti-glioma effect of NEs-Exos were also examined *in vivo*. The results indicated that NEs-Exos not only present the ability of crossing blood brain barrier, but can also respond to inflammatory stimuli and move to inflamed glioma site.

In addition, owing to high glycolysis rate and increased production of lactate, weak acidity becomes another distinct hallmark of ITME, and it can induce irreversible tumor metastasis and promote the tumor growth (149). Therefore, many researchers were devoted to develop pH-responsive DDSs to target tumors and improve tumor therapy efficiency. Kim et al. (149) fabricated a pH-responsive DDSs based on i-motif-modified Exos (Exo-i-motif) to delivery DOX for anti-proliferation activity. The results indicated that Exo-i-motif showed significant anti-proliferation effect in MCF-7/MDR cells. Meanwhile, hypoxia is another feature of ITME and it can promote the tumor growth (149). In this situation, the reactive oxygen (ROS) secreted could correct hypoxia in TME and suppress cancer cells. Therefore, targeting acidic TME and correcting the hypoxic TME is also a promising approach for cancer therapy. Based on these, Zhang et al. (136) established a novel pH/light sensitive drug delivery platform using milk-Exos (Exo@DOX–EPT1) in squamous cell carcinoma therapy, and the scheme is shown in Figure 4C). In their work, DOX was conjugated to the membrane of Exos by a pH-cleavable bond which can target acidic microenvironment. Endoperoxides and Ce6 were both incorporated inside the Exos. The results indicated that Exo@DOX–EPT1 can be efficiently accumulated in tumor site and DOX was specifically released by acid environment stimulation. Ce6 could produce plasmonic heat upon NIR irradiating and ROS was effectively released to kill cancer cells.

3.3.2 Immune checkpoint blockade

ICB as an emerging cancer immunotherapy can block the regulatory receptors which are expressed on immune cells or tumor cells, and thus activating antitumor cytotoxic T-cell responses and improving cancer therapy efficiency (110, 150). In the past years, PD-1 and CTLA-4 inhibitory receptors were extensively studied and undergone clinic success (151). Despite ICB showed excellent cancer therapy effects, and some inhibitors including anti-CTLA-4 and PD-L1 monoclonal antibodies have been approved by FDA, however, some limitations still exist such as high off-target, low objective response rate and the risk of immune-related side effects (152). Therefore, in order to solve aforementioned drawbacks, many researchers focus on ICB inhibitors DDSs. For instance, Fan et al. (137) developed an Exos-based DDSs (named as cGAMP@dual-anti-Exos) in which anti-PD-L1 and anti-CD40 were all engineered on the surface of Exos for cancer immunotherapy, and the scheme is shown in Figure 5A). Firstly, lipophilic DSPE-PEG-anti-CD40 and DSPE-PEG-PLGVA-anti-PD-L1 were synthesized and applied to donor cells. Meanwhile, immune drug (2'-3'-cyclic guanosine monophosphate-adenosine monophosphate (cGAMP)) was also incubated with donor cells. And then, cGAMP@dual-anti-Exos was generated with these molecules loaded inside. The results indicated that cGAMP@dual-anti-Exos presented excellent targeting and anti-tumor effects, since PLGVA peptides could be cut off by the matrix metalloproteinase enzyme (MMP-2) inside the TME, and anti-PD-L1 was separated from Exos to achieve ICB (137). Similarly, Zhou et al. (153) designed and fabricated exosome-mimetic nanovesicles co-loading CD73 inhibitor (AB680) and PD-L1 antibodies (AB680@EMVs-aPDL1) to target bladder cancer, and the scheme is presented in Figure 5B). In this work, macrophage cell line (RAW264.7 cells) was chosen to secret exosome-mimetic nanovesicles and AB680 was loaded inside by coextrusion method. After that, PD-L1 antibodies was conjugated to the surface of the exosome-mimetic nanovesicles for ICB. The results suggested that AB680@EMVs-aPDL1 was conducive to drive the transition of $CD8^+$ T-cells into effector cells owing to the existence of CD73 molecules. Moreover, a more efficient antitumor effect to PD-1 inhibition and better tumor regression were presented owing to a higher $CD8^+/CD4^+$ ratio in bladder cancer. In addition, the toxicity and biosafety *in vivo* were also evaluated, indicating that AB680@EMVs-aPDL1 was safe and had low toxicity. This work also provides a new and useful strategy for bladder cancer immunotherapy.

CTLA-4, which belongs to the CD28 receptor family, is overexpressed on the activated T cells and Tregs (10). It interacts with CD80/CD86 molecules expressed on the APCs and impedes T-cell activation and downregulates immune responses (21). Therefore, blocking the interaction between CTLA-4 and CD80/CD86 molecules on the APCs can activate T cells and enhance tumor immunotherapeutic efficacy. Recently, many researchers focus on this therapeutic strategy. For example, Phung et al. (10) constructed an exosome-based drug delivery platform (EXO-OVA-mAb) in which Exos were secreted from DCs and anti-CTLA-4 antibody was modified on their surface. EXO-OVA-mAb presented stronger ability of

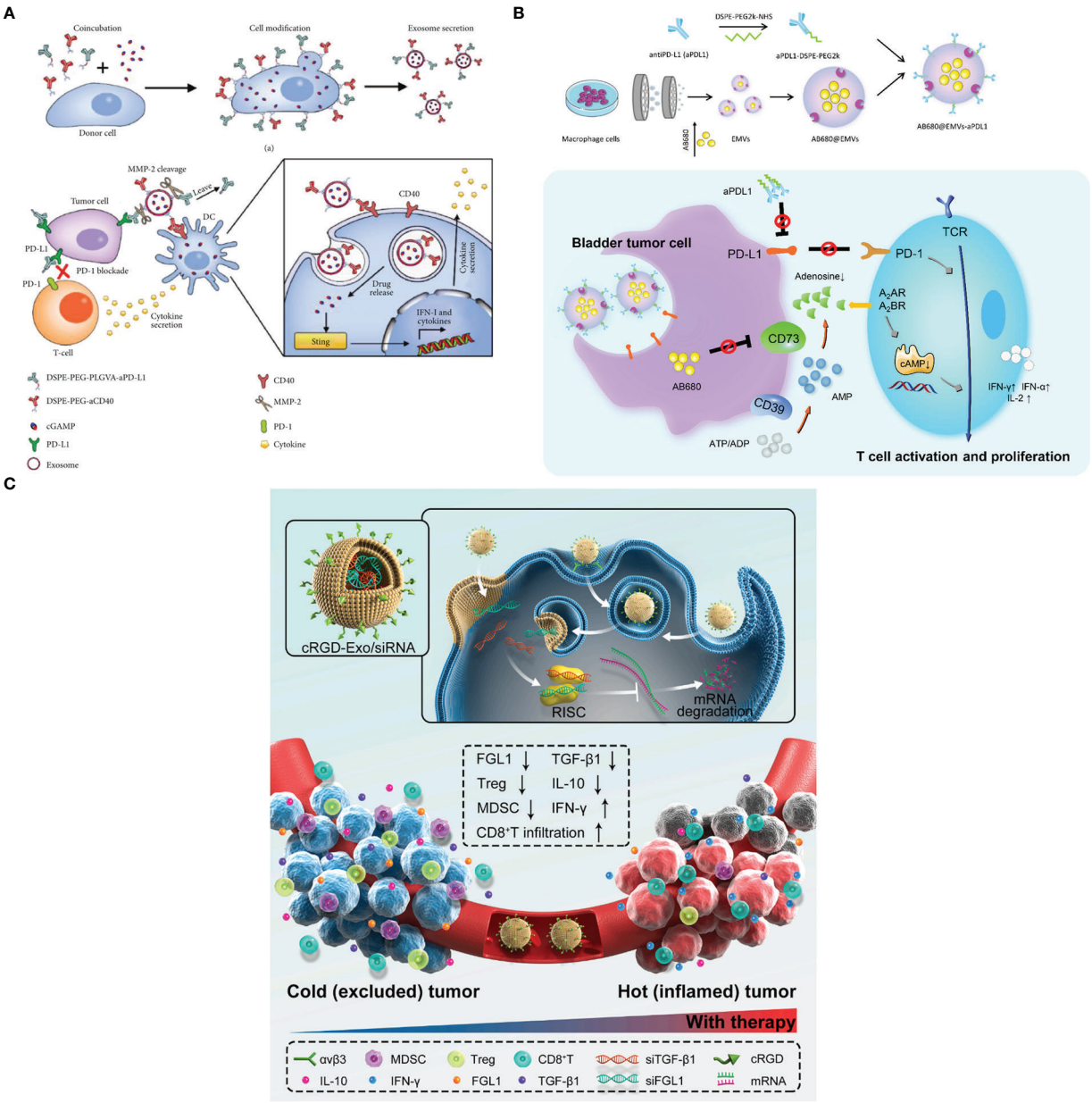

FIGURE 5
(A) The fabricated scheme of cGAMP@dual-anti-Exos and the process of cancer immunotherapy (Reprinted with the permission from Ref. 137). **(B)** The scheme of AB680@EMVs-aPDL1 for bladder cancer therapy (Reprinted with the permission from Ref. 153). **(C)** The mechanism of cRGD-Exo/siMix for colorectal cancer immunotherapy *in vivo* (Reprinted with the permission from Ref. 154). PD-1; Programmed cell death protein 1, PD-L1; Programmed cell death ligand; MMP-2; Matrix metalloproteinase enzyme; cGAMP; 2′-3′-cyclic guanosine monophosphate–adenosine monophosphate; AB680; CD73 inhibitor, EMVs; Exosome-mimetic nanovesicles, aPDL1; Monoclonal antibody targeting programmed cell death ligand 1; cRGD-Exo/siMix; a cyclic RGD peptide (cRGD)-modified exosome delivery system that simultaneously delivered FGL1 and TGFβ1 siRNAs.

activating T cells than others and increased the CTLs/Treg ratio within the tumor site, and this phenomenon may be attributed to the crucial role of anti-CTLA-4 antibody. Moreover, EXO-OVA-mAb also increased the level of IFN-γ and TNF-α in both serum and tumors, and thus enhancing cancer therapeutic effect.

CD47 as another immune checkpoint is also overexpressed on the most tumor cells, and it often interacts with signal regulatory protein α (SIRPα) on phagocytic cells, which activates "don't eat me signal" of CD47 and leads tumor cells to escape from immune monitoring (16). Therefore, blocking the interaction between CD47 and SIRPα can enhance tumor therapeutic efficacy. Based on this strategy, Koh et al. (155) designed and developed SIRPα-Exos for interfering CD47-SIRPa interaction to enhance cancer immunotherapy. In their

work, plasmid DNA encoding SIRPa variant was firstly constructed and cocultured with HEK293T cells. And then, engineered Exos with SIRPα proteins were obtained by ultracentrifuged method. Finally, the anti-tumor effect was evaluated in mouse model. The results indicated that SIRPα-Exos presented higher CD47 affinity than control Exos, and enhanced tumor cell phagocytosis *in vitro* and *in vivo*. In addition, the existence of SIRPα-Exos also improved the infiltration of $CD8^+$ T cell, suggesting that SIRPα-Exos could efficiently induce tumor phagocytosis and lead to anti-tumor T cell response.

In addition, silencing the expression of tumor immune checkpoint is also another strategy for cancer immunotherapy. Pei et al. (154) established a cyclic RGD peptide (cRGD)-modified exosome co-loaded with siFGL1 and siTGF-β1 (cRGD-Exo/siMix) for colorectal cancer immunotherapy by ICB, and the scheme is shown in Figure 5C). cRGD-Exo/siMix can efficiently deliver siFGL1 to silence the expression of tumor immune checkpoint ligand FGL1, and T cells were significantly activated.

3.3.3 Exosomes-based therapeutic cancer vaccines

It is well known that cancer immunotherapy is largely dependent on the functions of APCs and T cell, because the cancer immunity cycle must be repeatedly initiated and expanded to achieve sustained cancer immune response. In view of this, many researchers focus on cancer immunotherapy *via* Exos-based therapeutic cancer vaccines.

DEXs have been widely used in therapeutic vaccines as an effective alternative to tumor antigens and have tremendous potential for cancer immunotherapy due to their features of long validity period and easily being engineered (156). DEXs express peptide/MHC-I and peptide/MHC-II complexes (pMHC I and pMHC II), heat-shock proteins (HSP), costimulatory molecules (CD80, CD86) and adhesion molecules, and they are involved in antigen uptake and presentation, and also activation of the antitumor response in $CD4^+$ and $CD8^+$ T cells (157), and the interaction mechanism is shown in Figure 6. Research found that Exos secreted from α-fetoprotein (AFP)-expressing DCs (DEX_{AFP}) stimulated $CD8^+$ T lymphocytes to express IFN-γ and secrete IL-2, which leaded to the reduced $CD25^+Foxp3^+$ Treg, IL-10 and TGF-β in the tumor microenvironment (158). DEX_{AFP} elicited potent antigen-specific immune responses and was proved to be a cell-free vaccine for immunotherapy. Furthermore, a novel EXO-T vaccine was developed which converted the exhausted T cells into tumor-specific effector CTL *via* the CD40L signaling pathway of $CD4^+$ T cells to stimulate a more massive CTL anti-tumor response (159). Moreover, HER2-specific exosome (EXO)-T vaccine was also developed to trigger the activation of immune responses and assist in the treatment against HER2-positive breast cancer (160).

In general, TEXs can also interfere with the immune system by delivering tumor antigens to DCs. However, because TEXs have the dual role of immunosuppressive and immune activating effects, there is a concern that TEXs will block antigen processing and presentation in DCs (161–164). Study showed that TEXs could be used for vaccine with immunostimulatory effects because they have the same rejection antigens as tumor cells (165). Recently, TEXs containing tumor-specific antigens were extracted from autologous tumor tissue to regulate the Th1 immune response in melanoma, and they blocked tumor growth and metastasis (166). However, the immune response elicited by TEXs is relatively weak which results in the unsatisfactory antitumor effect, so efforts have been made to generate vaccine systems, such as artificially modified TEXs and TEXs-loaded DC, with higher immunogenicity, (167). Common strategies for TEXs modifications include genetic modification (168), external stimulation of donor cells (169), and incorporation of fusion proteins (170). CIITA (Class II transactivator) gene was transduced into B16F1 murine melanoma cell line (B16F1-CIITA) by genetic engineering, and the secreted Exos (CIITA-Exo) expressed high level of MHC-II as well as the tumor antigen TRP2. CIITA-Exo enhanced the splenocyte proliferation and IL-2 secretion, and induced inflammatory cytokines (such as TNF-α and IL-12) mRNA production, so that CIITA-Exo had a more potent anti-tumor immune response compared to control Exos (168). In addition, Morishita et al. (9) chose TEXs as tumor antigen carrier to establish a tumor antigens-adjuvant co-delivery system. In their work, firstly, murine melanoma B16BL6 tumor cells were engineered to produce Exos expressing SAV-LA, and then immunostimulatory CpG DNA was modified on the surface of Exos by SAV-biotin interaction (CpG-SAV-Exo), and the scheme is shown in Figure 7A). The results indicated that CpG-SAV-Exo could efficiently deliver CpG DNA to APC, showing a high antigens-presenting capacity. Meanwhile, CpG-SAV-Exo can efficiently activate T cells and present an excellent antitumor efficacy. Apart from genetic modification, to enrich Exos with more HSP70, external heat stimulation was applied to tumor cells, and the HSP70-enriched Exos (HS Exo) was shown to increase the expression of MHC-II and achieve higher productions of IgG2a and IFN-γ, resulting in strong Th1 immune responses and eliminating cancer cells (169). In addition, the incorporation of viral fusion proteins (such as the G protein of vesicular stomatitis virus (VSV-G)) into TEXs enhances their uptake, induces the maturation of DCs, and improves immunogenicity (172). Co-expression of antigen OVA and VSV-G on TEXs induced a specific CTL immune response *in vivo*, as exhibited with increased IgG2a antibody responses and amplification of antigen-specific $CD8^+$ T cells (170). In addition, another strategy to enhance TEXs vaccine activity is the application of TEXs-loaded DCs, which is due to the advantage of efficient antigen processing and MHC I loading of DCs after co-incubation with TAA-TEXs. Therefore, *in vitro* activation and loading of TEXs into DCs initiate an effective antitumor response, which overcomes the immunosuppressive

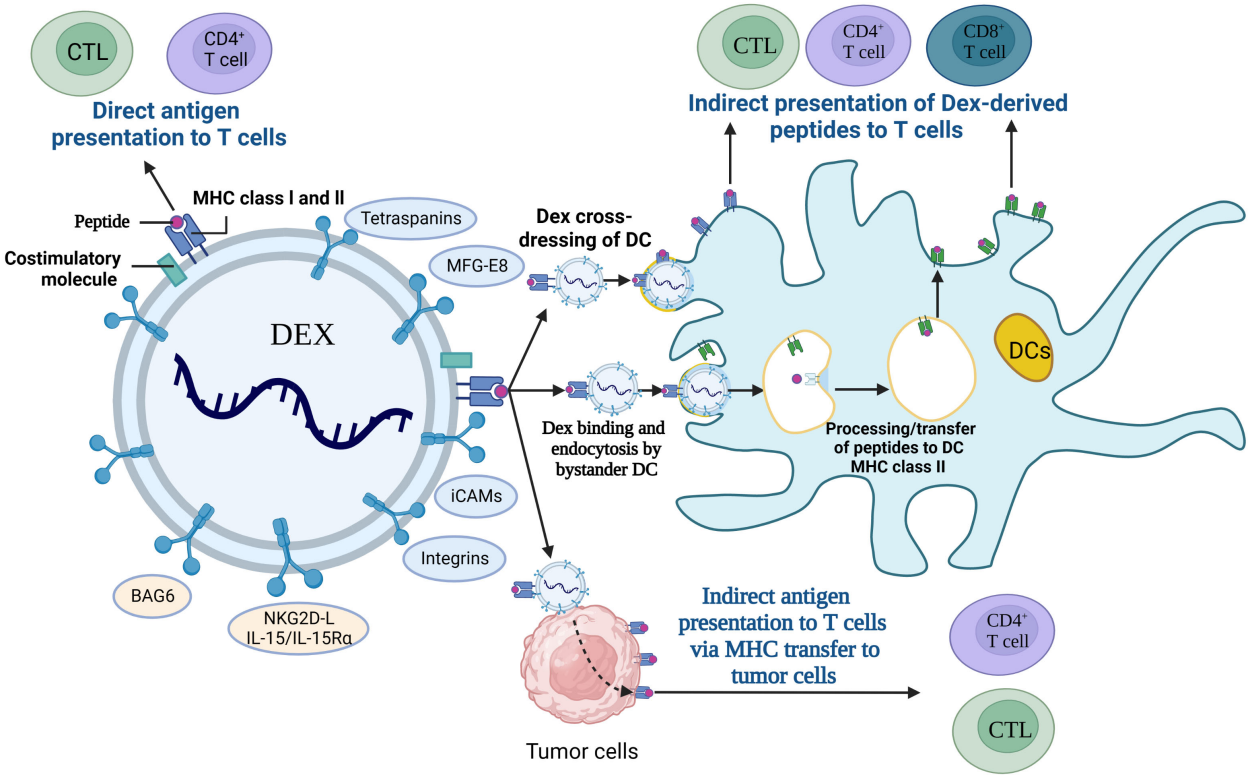

FIGURE 6
Interaction of DEXs with immune cells. CTL; cytotoxic T lymphocyte, DCs; Dendritic cells, MFG-E8; milk fat globule EGF factor 8, iCAMs; intercellular cell adhesion molecules, BAG6; Bcl-2-associated athanogen-6, NKG2D-L; natural killer group 2, member D receptor ligands, Dex; DC-derived exosomes, MHC; major histocompatibility complex.

limitations of TEXs alone (165). TEXs-loaded DCs activate T lymphocytes to develop into antigen-specific CTLs and trigger specific CTL immune responses with strongly cytotoxicity to autologous tumor cells (173). In a similar study, DCs that loaded with Exos from the supernatant of HeLa cells (HeLa-TEXs) enhanced the proliferation and cytotoxic activity of CTLs, whereas HeLa-TEXs alone showed no effect (174). Before TEXs-loaded DCs were developed, DCs were also used to load tumor lysates, but there is no disputing that TEXs are a better source of TAA due to the better antigen processing and presentation (175). In a comparative study, TEXs-loaded DCs (DC-TEXs) was significantly superior to lysate-loaded DCs in vaccination efficacy. TEX is more effective than tumor lysates in inducing an appropriate anti-tumor immune response, avoiding potentially fatalities in inoculated mice, and providing more persistent antigen presentation and priority antigen processing (176). Overall, immunogenic Exos could serve as adjuvants for therapeutic cancer vaccines in the future.

In addition, a novel strategy for directly activating T cells was also introduced in recently years. Zhao et al. (171) designed and developed a microfluidic device to produce antigenic Exos modified with peptide complex (e.g., gp-100, MART-1, and MAGE-A3) on demand. They also designed magnetic-nanoparticles with functionalized photo-cleavable and peptide affinity probe for capturing antigenic Exos *via* a light trigger. Meanwhile, the antitumor capability of antigenic Exos was also evaluated *in vitro* and *in vivo*, and the scheme is shown in Figure 7B). The results indicated that Exos which were modified with melanoma tumor peptides including gp-100, MART-1 and MAGE-A3 enhanced the ability of antigen presentation and T cell activation. This is because MHC-I and tumor peptides can form MHC-I/peptide binding complex which can be presented to cytotoxic T cells and thus triggering an immediate response from the immune system (3, 171). Moreover, conjugating cytokine-loaded Exos to T cells surfaces is also another strategy that can enhance adaptive T cell therapy. This approach is simple and can minimize systemic side effects of adjuvant drugs (21).

3.3.4 Combination therapy

The development of immunotherapy has yielded remarkable results in recent years. Currently, various ICIs have been approved by FDA as single agents for cancer treatment, however, the response rate for ICIs is only 10-35% (177–179). The effectiveness of immunotherapy is directly dependent on the state of the tumor microenvironment, while TME mostly presents an

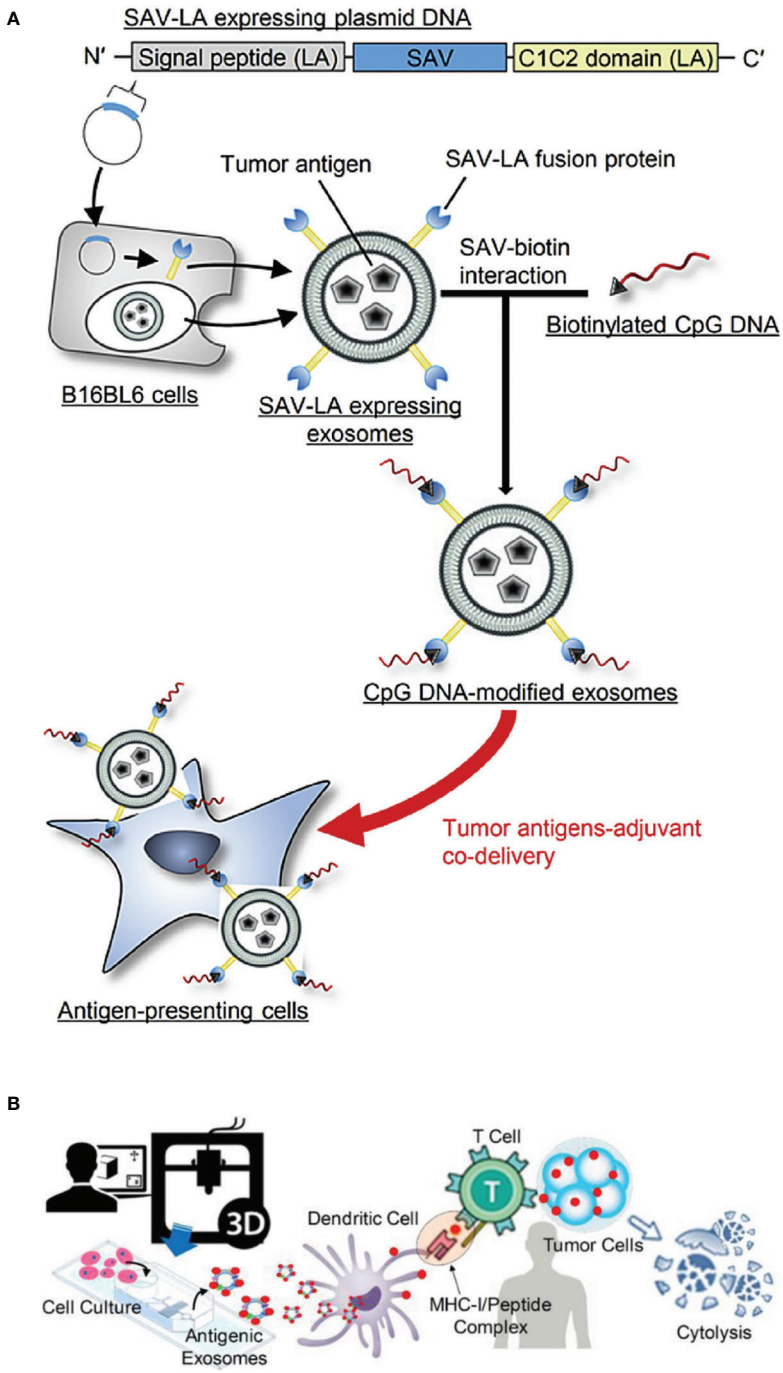

FIGURE 7
(A) The scheme of CpG-SAV-exo to deliver APCs (Reprinted with the permission from Ref. 9); **(B)** The scheme of MHC-I positive exosomes for activating anti-tumor responses (Reprinted with the permission from Ref. 171). SAV; Streptavidin, SAV-LA; N-terminal secretion signal of lactadherin (LA) and C1C2 domain of LA.

immunosuppressed condition with lack of T-cell infiltration or dysfunction, poor immunogenicity. Moreover, multiple mechanisms of drug resistance also contribute to the low efficiency in immunotherapy (180). Therefore, new alternative treatment strategies are being explored, and combination therapy containing two or three anti-tumor approaches (including chemotherapy, radiotherapy, photodynamic therapy, targeted therapy, vaccines, oncolytic viruses, ICB, ACT etc.) to achieve

higher efficacy is under evaluation (181, 182). Chemotherapeutic agents [such as anthracyclines, cyclophosphamide, oxaliplatin and paclitaxel (183)] are highly cytotoxic. However, chemotherapeutic drugs can trigger immunogenic cell death to act as adjuvants for immunotherapy by releasing damage-associated molecular patterns and activating apoptosis which make tumors more sensitive to immunotherapy (184). TEX-loaded DC vaccine in combination with chemotherapy could effectively suppress tumor-infiltrating MDSCs, inhibite tumor cell migration and promote greater T-cell activation, resulting in a longer survival time compared to DCs-TEX vaccinated only mice (185). Likewise, radiotherapy can enhance the antitumor effects of immunotherapy by increasing tumor antigenicity through multiple approaches. Radiation has an abscopal effect allowing for systemic tumor control (186) and can trigger the cGAS/STING pathway and stimulate innate and adaptive immune responses through DNA damage and ROS production (187). Short-burst radiation treatment significantly enhanced the delivery efficiency of PD-L1siRNA-loaded targeted Exos, altered the immune environment, sensitized poorly immunogenic glioblastomas to ICB, inhibited tumor growth, and prolonged the survival of tumor-bearing mice (188, 189). Otherwise, photodynamic therapy in synergy with immunotherapy has become a focus of research to overcome the low efficacy of immunotherapy for primary tumors and to monitor the drug delivery status at the target site (190). TEXs loaded with the photosensitizer Ce6 have been used as vehicles for photoacoustic-guided photodynamic therapy and as tumor antigens to stimulate the immune system to activate anti-tumor responses (191), and the scheme is illustrated in Figure 8A. The lack of tumor infiltration in ICB can also be addressed by oncolytic viruses, which provide a critical switch for the immune system. Oncolytic viruses invade tumor cells and replicate extensively inside, leading to tumor cell lysis (194), and on the other hand recruiting TILs into the damaged tumor, initiating the release of tumor antigens and pro-inflammatory cytokines and promoting the activation of the immune system (195). The scheme is shown in Figure 8B, and it was demonstrated that VSVΔ51 oncolytic viruses loaded with artificial amiRNA-4, when co-targeted with Exos carrying amiRNA-4 and PD-L1 shRNA cargoes, upregulated PD-L1 expression, sensitized tumors to CTLA4 and PD-1 immune checkpoint inhibition, enhanced death of tumor cells, and prolonged overall survival in mice (192). Chimeric antigen receptor T (CAR T) cell therapy has achieved remarkable results in hematologic malignancies, but the results in solid tumors have been less than satisfactory. TDC-Exo, a DC-secreted exosome stimulated by tumor antigen carrying MHC-antigen complexes and CD86, was developed as the "CAR" portion of CAR-T, activating T cells and cooperating with anti-CD3 and anti-EGFR

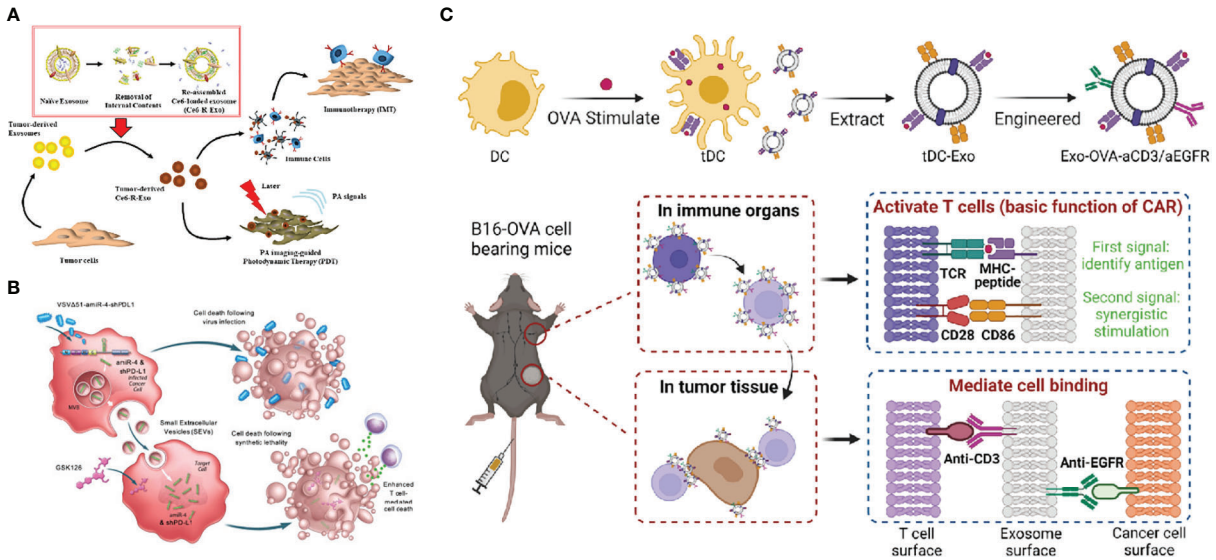

FIGURE 8
(A) Schematic diagram of photoacoustic imaging-guided combined photodynamic and immunotherapy for Ce6-R-Exo treatment (Reprinted with the permission from Ref. 191) **(B)** Schematic illustration of VSVΔ51-amiR-4-shPD-L1 exerting enhanced T cell-mediated cancer cell death (Reprinted with the permission from Ref. 192) **(C)** The above diagram is a schematic view of the construction of the engineered tDC-Exo (Exo-OVA-aCD3/aEGFR) with anti-CD3 and anti-EGFR antibodies. The bottom diagram shows the simulated CAR-T treatment process (Reprinted with the permission from Ref. 193). R-Exo; re-assembled exosome, Ce6-R-Exo; chlorin e6-loaded R-Exo, IMT; immunotherapy, PDT; photodynamic therapy, PA; photoacoustic, VSVΔ51-amiR-4-shPD-L1; VSVΔ51 oncolytic viruses- artificial microRNA-4- shPD-L1, MVB; multivesicular bodies, SEVs; small extracellular vesicles, DC; dendritic cells, tDC-Exo;tumor antigen-stimulated dendritic cell-derived exosomes, aEGFR; anti-epidermal growth factor receptors antibodies, OVA; ovalbumin, CAR; chimeric antigen receptor, TCR; T cell receptor, MHC; major histocompatibility complex.

and immune checkpoint inhibitory antibodies anti-PD-L1, further enhancing the efficacy of the CAR-T cell therapy mimetic platform for solid tumor treatment (193). The scheme is demonstrated in Figure 8C.

4 Clinical translation and challenges of Exos as DDSs

Currently, several cancers therapeutic strategies-based Exos DDSs have undergone clinic trials, and the relevant data which was obtained from https://clinicaltrials.gov/ are present in Table 3. As shown in Table 3, only few of Exos-based DDSs for cancer therapy have entered into clinical trials. Moreover, all of them are in the early clinical stage, suggesting that they still face many challenges.

Firstly, the stable mass production of Exos is the primary challenge. As is known to all, the selection and culture of donor cells are one of significantly important factors. In recent years, mesenchymal stromal cells and cardiac progenitor cells have been proved to provide stable Exos production during scale-up culture. Moreover, cell culture technologies have also been improved and up to 20,000 L of cells can also be cultured *via* stainless-steel bioreactors. In spite of this, the clinical translation of Exos is still difficult. The main reason is that the scaling-up process is relatively expensive. Furthermore, the conditions of cell culture also need to be meticulous, because improper operation may cause cell contamination, which can result in cell subtypes and variation. Therefore, strictly controlling and maintaining the genetic stability of donor cells are difficult.

Secondly, the isolation and purification of Exos are another challenge. Currently, the extraction technologies including ultracentrifugation, tangential flow fractionation, exclusion chromatography and commercial extraction kits have been extensively employed to isolate Exos. Of which, tangential flow fractionation is often used in the mass production of Exos in the clinical trials. However, the purity of Exos obtained by this separation method is low, thereby limiting its application. Although high purity of Exos can be obtained by ultracentrifugation, its features of low throughput and high cost limit the mass production of Exos. Currently, there is no standard procedures for large-scale Exos separation. Therefore, it is urgent to develop an advanced technique with high efficiency, high quality and low cost to separate Exos for DDSs.

Furthermore, the surface modification of Exos is also one of important factors because it affects the targeting functions and biological effects of DDSs. In general, two methods including chemical modification and genetic engineering can be used for the surface modification of Exos. Genetic engineering is highly effective for surface modification by fusing the gene sequence of targeting protein with exosomal membrane protein. However, this approach is limited to genetically encoded targeting motifs. Chemical modification often affects the structure and function of Exos, and thus limiting their application. Meanwhile, there is no standard strategies for loading drugs. Recently, many drug-loading strategies including incubation, electroporation, ultrasound, and cell engineering techniques have been applied. They all have their limitations to some extent. For instance, incubation is the simplest drug-loading method. It does not require special equipment, and the structure of Exos is rarely damaged. However, low drug-loading efficiency was presented in this loading method. Although ultrasound and electroporation can improve drug-loading efficiency, the membrane of exosome maybe damaged and aggregation of Exos may be caused by these methods. Meanwhile, the operation of cell engineering techniques is too complicated though it is considered as well-established operating strategy.

In addition to these limitations mentioned above, the storage conditions of purified Exos also play critical role in clinical translation of Exos. An increasing number of researches suggested that Exos derived from different sources require different storage conditions, because the storage temperature and storage solution (e.g., saline, PBS, cell culture media, etc.) all affected the particle size and protein content of Exos. Therefore, further researches should take the influences of storge conditions into consideration for Exos as drug delivery carriers.

5 Conclusions

In this review, some relevant knowledges including the biogenesis and composition of Exos, the source of Exos for DDSs, drug-loading strategies, cancer immunotherapy strategies, and their clinical translation and challenges were discussed. Exos are mainly divided into immune cell-derived and tumor cell-derived Exos. They can inherit the properties of donor cells and participate in the innate and adaptive immune

TABLE 3 The current clinical trials of Exos as drug delivery vehicles.

DDSs	Exos source	Disease	NTC number	Clinic phase
Curcumin Exos	Plant	Colon cancer	NCT01294072	Phase 1
A vaccination with tumor antigen-loaded Exos	Dendritic cell	Non-small cell lung cancer	NCT01159288	Phase 2
Exos with KRAS G12D siRNA (iExos)	Mesenchymal stromal cells	Pancreatic cancer	NCT03608631	Phase 1
The data is obtained from https://clinicaltrials.gov/.				

responses, thus promoting extensive applications of immune cells-derived Exos as drug delivery carrier. Meanwhile, various drug-loading strategies of Exos-based DDSs including incubation, physical loading techniques (e.g., electroporation, ultrasound and extrusion), and cell engineering techniques have been designed and developed. In addition, Exos-based cancer immunotherapy strategies (e.g., tuning of ITME, ICB, cancer vaccines, etc.) have been extensively applied, they all presented excellent therapeutic effects.

To our delight, nowadays, several cancers immunotherapeutic strategies-based Exos DDSs have undergone clinic trials. In spite of this, they still face many challenges including their stable mass production, their isolation and purification, their surface modification, and their storage conditions. Therefore, cell culture technologies should be further improved and related bioreactors should also be designed and developed to scale up the Exos production in the future. In addition, it is urgent to develop an advanced technique with high efficiency, high quality and low cost to separate and purify Exos which can be used in DDSs. Meanwhile, the storage conditions of purified Exos from different cell sources should be further explored. Overall, although Exos as drug delivery vesicles still exist some challenges, they provide an excellent platform for cancer immunotherapy.

Author contributions

All authors listed have made a substantial, direct, and intellectual contribution to the work and approved it for publication.

Funding

This review paper was supported by the projects of National Natural Science Foundation of China (82073784(LT) and 21HAA01203(ZY)), and Forestry Science and Technology Innovation Project of Guangdong Province (No. 2021KJCX010(ZX))

Acknowledgments

We acknowledged the support of BioRender, Figure 1, Figure 2 and Figure 6 were created with BioRender.com.

Conflict of interest

The authors declare that the research was conducted in the absence of any commercial or financial relationships that could be construed as a potential conflict of interest.

Publisher's note

All claims expressed in this article are solely those of the authors and do not necessarily represent those of their affiliated organizations, or those of the publisher, the editors and the reviewers. Any product that may be evaluated in this article, or claim that may be made by its manufacturer, is not guaranteed or endorsed by the publisher.

References

1. Siegel RL, Miller KD, Fuchs HE, Jemal A. Cancer statistics 2022. *CA Cancer J Clin* (2022) 72:7–33. doi: 10.3322/caac.21708

2. Wang X, Zhao YR, Dong SY, Lee RJ, Yang DS, Zhang H, et al. Cell-penetrating peptide and transferrin co-modified liposomes for targeted therapy of glioma. *Molecules* (2019) 24:3540. doi: 10.3390/molecules24193540

3. Yang Z, Ma Y, Zhao H, Yuan Y, Kim BYS. Nanotechnology platforms for cancer immunotherapy. *Wiley Interdiscip Rev Nanomed Nanobiotechnol* (2020) 12: e1590. doi: 10.1002/wnan.1590

4. Cai GS, Wang SM, Zhao L, Sun YT, Yang DS, Lee RJ, et al. Thiophene derivatives as anticancer agents and their delivery to tumor cells using albumin nanoparticles. *Molecules* (2019) 24:192. doi: 10.3390/molecules24010192

5. Thakur A, Parra DC, Motallebnejad P, Brocchi M, Chen HJ. Exosomes: Small vesicles with big roles in cancer, vaccine development, and therapeutics. *Bioactive Mater* (2022) 10:281–94. doi: 10.1016/j.bioactmat.2021.08.029

6. Zhao Y, Zheng Y, Zhu Y, Li H, Zhu H, Liu T. Docetaxel-loaded M1 macrophage-derived exosomes for a safe and efficient chemoimmunotherapy of breast cancer. *J Nanobiotechnol* (2022) 20:359. doi: 10.1186/s12951-022-01526-2

7. Tan M, Chen Y, Guo Y, Yang C, Liu M, Guo D, et al. A low-intensity focused ultrasound-assisted nanocomposite for advanced triple cancer therapy: Local chemotherapy, therapeutic extracellular vesicles and combined immunotherapy. *Biomater Sci* (2020) 8:6703–17. doi: 10.1039/d0bm00804d

8. Ma XB, Yang SC, Zhang T, Wang S, Yang QC, Xiao Y, et al. Bioresponsive immune-booster-based prodrug nanogel for cancer immunotherapy. *Acta Pharm Sin B* (2022) 12:451–66. doi: 10.1016/j.apsb.2021.05.0162211-3835

9. Morishita M, Takahashi Y, Matsumoto A, Nishikawa M, Takakura Y. Exosome-based tumor antigens-adjuvant co-delivery utilizing genetically engineered tumor cell-derived exosomes with immunostimulatory CpG DNA. *Biomaterials* (2016) 111:55–65. doi: 10.1016/j.biomaterials.2016.09.031

10. Phung CD, Pham TT, Nguyen HT, Nguyen TT, Ou W, Jeong JH, et al. Anti-CTLA-4 antibody-functionalized dendritic cell-derived exosomes targeting tumor-draining lymph nodes for effective induction of antitumor T-cell responses. *Acta Biomater* (2020) 115:371–82. doi: 10.1016/j.actbio.2020.08.008

11. Rasihashemi SZ, Sahrai H, Rezazadeh-Gavgani E, Yazdani Y, Khalaji A, Lotfinejad P. Exosomes carrying immune checkpoints, a promising therapeutic approach in cancer treatment. *Med Oncol* (2022) 39:183. doi: 10.1007/s12032-022-01781-1

12. Tran TH, Mattheolabakis G, Aldawsari H, Amiji M. Exosomes as nanocarriers for immunotherapy of cancer and inflammatory diseases. *Clin Immunol* (2015) 160:46–58. doi: 10.1016/j.clim.2015.03.021

13. Francis DM, Thomas SN. Progress and opportunities for enhancing the delivery and efficacy of checkpoint inhibitors for cancer immunotherapy. *Adv Drug Delivery Rev* (2017) 114:33–42. doi: 10.1016/j.addr.2017.04.011

14. Choi JU, Park IK, Lee YK, Hwang SR. The biological function and therapeutic potential of exosomes in cancer: Exosomes as efficient nanocommunicators for cancer therapy. *Int J Mol Sci* (2020) 21:7363. doi: 10.3390/ijms21197363

15. Feng C, Xiong Z, Wang C, Xiao W, Xiao H, Xie K, et al. Folic acid-modified exosome-PH20 enhances the efficiency of therapy *via* modulation of the tumor microenvironment and directly inhibits tumor cell metastasis. *Bioactive Mater* (2021) 6:963–74. doi: 10.1016/j.bioactmat.2020.09.014

16. Kamerkar S, LeBleu VS, Sugimoto H, Yang S, Ruivo CF, Melo SA, et al. Exosomes facilitate therapeutic targeting of oncogenic KRAS in pancreatic cancer. *Nature* (2017) 546:498–503. doi: 10.1038/nature22341

17. Fang Z, Ding Y, Xue Z, Li P, Li J, Li F. Roles of exosomes as drug delivery systems in cancer immunotherapy: a mini-review. *Discovery Oncol* (2022) 13:74. doi: 10.1007/s12672-022-00539-5

18. Chen R, Xu X, Qian Z, Zhang C, Niu Y, Wang Z, et al. The biological functions and clinical applications of exosomes in lung cancer. *Cell Mol Life Sci* (2019) 76:4613–33. doi: 10.1007/s00018-019-03233-y

19. Bell BM, Kirk ID, Hiltbrunner S, Gabrielsson S, Bultema JJ. Designer exosomes as next-generation cancer immunotherapy. *Nanomedicine* (2016) 12:163–9. doi: 10.1016/j.nano.2015.09.011

20. Hazrati A, Soudi S, Malekpour K, Mahmoudi M, Rahimi A, Hashemi SM, et al. Immune cells-derived exosomes function as a double-edged sword: role in disease progression and their therapeutic applications. *biomark Res* (2022) 10:30. doi: 10.1186/s40364-022-00374-4

21. Jo SD, Nam G-H, Kwak G, Yang Y, Kwon IC. Harnessing designed nanoparticles: Current strategies and future perspectives in cancer immunotherapy. *Nano Today* (2017) 17:23–37. doi: 10.1016/j.nantod.2017.10.008

22. Trams EG, Lauter CJ, Salem NJr., Heine U. Exfoliation of membrane ecto-enzymes in the form of micro-vesicles. *Biochim Biophys Acta* (1981) 645:63–70. doi: 10.1016/0005-2736(81)90512-5

23. Marar C, Starich B, Wirtz D. Extracellular vesicles in immunomodulation and tumor progression. *Nat Immunol* (2021) 22:560–70. doi: 10.1038/s41590-021-00899-0

24. Guo S, Zhao L, Tao S, Zhang C. Research progress on the role of extracellular vesicles in bacterial pathogenesis. *Zhongguo Xiu Fu Chong Jian Wai Ke Za Zhi* (2018) 32:1597–604. doi: 10.7507/1002-1892.201805075

25. Danesh A, Inglis HC, Jackman RP, Wu S, Deng X, Muench MO, et al. Exosomes from red blood cell units bind to monocytes and induce proinflammatory cytokines, boosting T-cell responses *in vitro*. *Blood* (2014) 123:687–96. doi: 10.1182/blood-2013-10-530469

26. Aatonen MT, Ohman T, Nyman TA, Laitinen S, Grönholm M, Siljander PR. Isolation and characterization of platelet-derived extracellular vesicles. *J Extracell Vesicles* (2014) 3:24692. doi: 10.3402/jev.v3.24692

27. Yu X, Huang C, Song B, Xiao Y, Fang M, Feng J, et al. $CD4^+CD25^+$ regulatory T cells-derived exosomes prolonged kidney allograft survival in a rat model. *Cell Immunol* (2013) 285:62–8. doi: 10.1016/j.cellimm.2013.06.010

28. Luga V, Wrana JL. Tumor-stroma interaction: Revealing fibroblast-secreted exosomes as potent regulators of wnt-planar cell polarity signaling in cancer metastasis. *Cancer Res* (2013) 73:6843–7. doi: 10.1158/0008-5472.Can-13-1791

29. Ju R, Zhuang ZW, Zhang J, Lanahan AA, Kyriakides T, Sessa WC, et al. Angiopoietin-2 secretion by endothelial cell exosomes: regulation by the phosphatidylinositol 3-kinase (PI3K)/Akt/endothelial nitric oxide synthase (eNOS) and syndecan-4/syntenin pathways. *J Biol Chem* (2014) 289:510–9. doi: 10.1074/jbc.M113.506899

30. Riches A, Campbell E, Borger E, Powis S. Regulation of exosome release from mammary epithelial and breast cancer cells-a new regulatory pathway. *Eur J Cancer* (2014) 50:1025–34. doi: 10.1016/j.ejca.2013.12.019

31. Kim SM, Yang Y, Oh SJ, Hong Y, Seo M, Jang M. Cancer-derived exosomes as a delivery platform of CRISPR/Cas9 confer cancer cell tropism-dependent targeting. *J Control Release* (2017) 266:8–16. doi: 10.1016/j.jconrel.2017.09.013

32. Kalluri R, LeBleu VS. The biology, function, and biomedical applications of exosomes. *Science* (2020) 367:640. doi: 10.1126/science.aau6977

33. Johnstone RM, Adam M, Hammond JR, Orr L, Turbide C. Vesicle formation during reticulocyte maturation. association of plasma membrane activities with released vesicles (exosomes). *J Biol Chem* (1987) 262:9412–20. doi: 10.1016/S0021-9258(18)48095-7

34. Katzmann DJ, Babst M, Emr SD. Ubiquitin-dependent sorting into the multivesicular body pathway requires the function of a conserved endosomal protein sorting complex, ESCRT-I. *Cell* (2001) 106:145–55. doi: 10.1016/s0092-8674(01)00434-2

35. Saksena S, Emr SD. ESCRTs and human disease. *Biochem Soc Trans* (2009) 37:167–72. doi: 10.1042/bst0370167

36. Raiborg C, Bremnes B, Mehlum A, Gillooly DJ, D'Arrigo A, Stang E, et al. FYVE and coiled-coil domains determine the specific localisation of hrs to early endosomes. *J Cell Sci* (2001) 114:2255–63. doi: 10.1242/jcs.114.12.2255

37. Lu Q, Hope LW, Brasch M, Reinhard C, Cohen SN. TSG101 interaction with HRS mediates endosomal trafficking and receptor down-regulation. *Proc Natl Acad Sci U.S.A.* (2003) 100:7626–31. doi: 10.1073/pnas.0932599100

38. Babst M, Katzmann DJ, Estepa-Sabal EJ, Meerloo T, Emr SD. Escrt-III: An endosome-associated heterooligomeric protein complex required for mvb sorting. *Dev Cell* (2002) 3:271–82. doi: 10.1016/s1534-5807(02)00220-4

39. Babst M, Wendland B, Estepa EJ, Emr SD. The Vps4p AAA ATPase regulates membrane association of a vps protein complex required for normal endosome function. *EMBO J* (1998) 17:2982–93. doi: 10.1093/emboj/17.11.2982

40. Colombo M, Moita C, van Niel G, Kowal J, Vigneron J, Benaroch P, et al. Analysis of ESCRT functions in exosome biogenesis, composition and secretion highlights the heterogeneity of extracellular vesicles. *J Cell Sci* (2013) 126:5553–65. doi: 10.1242/jcs.128868

41. Tamai K, Tanaka N, Nakano T, Kakazu E, Kondo Y, Inoue J, et al. Exosome secretion of dendritic cells is regulated by hrs, an ESCRT-0 protein. *Biochem Biophys Res Commun* (2010) 399:384–90. doi: 10.1016/j.bbrc.2010.07.083

42. Baietti MF, Zhang Z, Mortier E, Melchior A, Degeest G, Geeraerts A, et al. Syndecan-syntenin-ALIX regulates the biogenesis of exosomes. *Nat Cell Biol* (2012) 14:677–85. doi: 10.1038/ncb2502

43. McAndrews KM, Kalluri R. Mechanisms associated with biogenesis of exosomes in cancer. *Mol Cancer* (2019) 18:52. doi: 10.1186/s12943-019-0963-9

44. Cho JA, Yeo DJ, Son HY, Kim HW, Jung DS, Ko JK, et al. Exosomes: a new delivery system for tumor antigens in cancer immunotherapy. *Int J Cancer* (2005) 114:613–22. doi: 10.1002/ijc.20757

45. Zhang Y, Liu Y, Liu H, Tang WH. Exosomes: biogenesis, biologic function and clinical potential. *Cell Biosci* (2019) 9:19. doi: 10.1186/s13578-019-0282-2

46. Mathivanan S, Lim JW, Tauro BJ, Ji H, Moritz RL, Simpson RJ. Proteomics analysis of A33 immunoaffinity-purified exosomes released from the human colon tumor cell line LIM1215 reveals a tissue-specific protein signature. *Mol Cell Proteomics* (2010) 9:197–208. doi: 10.1074/mcp.M900152-MCP200

47. Skotland T, Sandvig K, Llorente A. Lipids in exosomes: current knowledge and the way forward. *Prog Lipid Res* (2017) 66:30–41. doi: 10.1016/j.plipres.2017.03.001

48. Xie Y, Dang W, Zhang S, Yue W, Yang L, Zhai X, et al. The role of exosomal noncoding RNAs in cancer. *Mol Cancer* (2019) 18:37. doi: 10.1186/s12943-019-0984-4

49. Valcz G, Újvári B, Buzás EI, Krenács T, Spisák S, Kittel Á., et al. Small extracellular vesicle DNA-mediated horizontal gene transfer as a driving force for tumor evolution: Facts and riddles. *Front Oncol* (2022) 12:945376. doi: 10.3389/fonc.2022.945376

50. Xu M, Yang Q, Sun X, Wang Y. Recent advancements in the loading and modification of therapeutic exosomes. *Front Bioeng Biotechnol* (2020) 8:586130. doi: 10.3389/fbioe.2020.586130

51. Viaud S, Théry C, Ploix S, Tursz T, Lapierre V, Lantz O, et al. Dendritic cell-derived exosomes for cancer immunotherapy: What's next? *Cancer Res* (2010) 70:1281–5. doi: 10.1158/0008-5472.Can-09-3276

52. Théry C, Duban L, Segura E, Véron P, Lantz O, Amigorena S. Indirect activation of naïve $CD4^+$ T cells by dendritic cell-derived exosomes. *Nat Immunol* (2002) 3:1156–62. doi: 10.1038/ni854

53. Bianco NR, Kim SH, Morelli AE, Robbins PD. Modulation of the immune response using dendritic cell-derived exosomes. *Methods Mol Biol* (2007) 380:443–55. doi: 10.1007/978-1-59745-395-0_28

54. Shoae-Hassani A, Hamidieh AA, Behfar M, Mohseni R, Mortazavi-Tabatabaei SA, Asgharzadeh S. NK cell-derived exosomes from NK cells previously exposed to neuroblastoma cells augment the antitumor activity of cytokine-activated NK cells. *J Immunother* (2017) 40:265–76. doi: 10.1097/cji.0000000000000179

55. Federici C, Shahaj E, Cecchetti S, Camerini S, Casella M, Iessi E, et al. Natural-killer-derived extracellular vesicles: immune sensors and interactors. *Front Immunol* (2020) 11:262. doi: 10.3389/fimmu.2020.00262

56. Fais S. NK cell-released exosomes: Natural nanobullets against tumors. *Oncoimmunology* (2013) 2:e22337. doi: 10.4161/onci.22337

57. Neviani P, Wise PM, Murtadha M, Liu CW, Wu CH, Jong AY, et al. Natural killer-derived exosomal miR-186 inhibits neuroblastoma growth and immune escape mechanisms. *Cancer Res* (2019) 79:1151–64. doi: 10.1158/0008-5472.Can-18-0779

58. McDonald MK, Tian Y, Qureshi RA, Gormley M, Ertel A, Gao R, et al. Functional significance of macrophage-derived exosomes in inflammation and pain. *Pain* (2014) 155:1527–39. doi: 10.1016/j.pain.2014.04.029

59. Cheng L, Wang Y, Huang L. Exosomes from M1-polarized macrophages potentiate the cancer vaccine by creating a pro-inflammatory microenvironment in the lymph node. *Mol Ther* (2017) 25:1665–75. doi: 10.1016/j.ymthe.2017.02.007

60. Taganov KD, Boldin MP, Chang KJ, Baltimore D. NF-kappaB-dependent induction of microRNA miR-146, an inhibitor targeted to signaling proteins of innate immune responses. *Proc Natl Acad Sci U.S.A.* (2006) 103:12481–6. doi: 10.1073/pnas.0605298103

61. Wang G, Jin S, Ling X, Li Y, Hu Y, Zhang Y, et al. Proteomic profiling of LPS-induced macrophage-derived exosomes indicates their involvement in acute liver injury. *Proteomics* (2019) 19:e1800274. doi: 10.1002/pmic.201800274

62. Choo YW, Kang M, Kim HY, Han J, Kang S, Lee JR, et al. M1 macrophage-derived nanovesicles potentiate the anticancer efficacy of immune checkpoint inhibitors. *ACS Nano* (2018) 12:8977–93. doi: 10.1021/acsnano.8b02446

63. Arteaga-Blanco LA, Mojoli A, Monteiro RQ, Sandim V, Menna-Barreto RFS, Pereira-Dutra FS, et al. Characterization and internalization of small

extracellular vesicles released by human primary macrophages derived from circulating monocytes. *PloS One* (2020) 15:e0237795. doi: 10.1371/journal.pone.0237795

64. Admyre C, Bohle B, Johansson SM, Focke-Tejkl M, Valenta R, Scheynius A, et al. B cell-derived exosomes can present allergen peptides and activate allergen-specific T cells to proliferate and produce TH2-like cytokines. *J Allergy Clin Immunol* (2007) 120:1418–24. doi: 10.1016/j.jaci.2007.06.040

65. Klinker MW, Lizzio V, Reed TJ, Fox DA, Lundy SK. Human b cell-derived lymphoblastoid cell lines constitutively produce fas ligand and secrete MHCII(+) FasL(+) killer exosomes. *Front Immunol* (2014) 5:144. doi: 10.3389/fimmu.2014.00144

66. Wubbolts R, Leckie RS, Veenhuizen PT, Schwarzmann G, Möbius W, Hoernschemeyer J, et al. Proteomic and biochemical analyses of human b cell-derived exosomes. potential implications for their function and multivesicular body formation. *J Biol Chem* (2003) 278:10963–72. doi: 10.1074/jbc.M207550200

67. Lu J, Wu J, Tian J, Wang S. Role of T cell-derived exosomes in immunoregulation. *Immunol Res* (2018) 66:313–22. doi: 10.1007/s12026-018-9000-0

68. Geltink RIK, Kyle RL, Pearce EL. Unraveling the complex interplay between t cell metabolism and function. *Annu Rev Immunol* (2018) 36:461–88. doi: 10.1146/annurev-immunol-042617-053019

69. Wahlgren J, Karlson Tde L, Glader P, Telemo E, Valadi H. Activated human T cells secrete exosomes that participate in IL-2 mediated immune response signaling. *PloS One* (2012) 7:e49723. doi: 10.1371/journal.pone.0049723

70. Li L, Jay SM, Wang Y, Wu SW, Xiao Z. IL-12 stimulates CTLs to secrete exosomes capable of activating bystander CD8(+) T cells. *Sci Rep* (2017) 7:13365. doi: 10.1038/s41598-017-14000-z

71. Mittelbrunn M, Gutiérrez-Vázquez C, Villarroya-Beltri C, González S, Sánchez-Cabo F, González M, et al. Unidirectional transfer of microRNA-loaded exosomes from T cells to antigen-presenting cells. *Nat Commun* (2011) 2:282. doi: 10.1038/ncomms1285

72. Okoye IS, Coomes SM, Pelly VS, Czieso S, Papayannopoulos V, Tolmachova T, et al. MicroRNA-containing T-regulatory-cell-derived exosomes suppress pathogenic T helper 1 cells. *Immunity* (2014) 41:503. doi: 10.1016/j.immuni.2014.08.008

73. Allen ER, Lempke SL, Miller MM, Bush DM, Braswell BG, Estes CL, et al. Effect of extracellular vesicles from s. aureus-challenged human neutrophils on macrophages. *J Leukoc Biol* (2020) 108:1841–50. doi: 10.1002/jlb.3ab0320-156r

74. Li F, Wang Y, Lin L, Wang J, Xiao H, Li J, et al. Mast cell-derived exosomes promote Th2 cell differentiation *via* OX40L-OX40 ligation. *J Immunol Res* (2016) 2016:3623898. doi: 10.1155/2016/3623898

75. Cañas JA, Sastre B, Mazzeo C, Fernández-Nieto M, Rodrigo-Muñoz JM, González-Guerra A, et al. Exosomes from eosinophils autoregulate and promote eosinophil functions. *J Leukoc Biol* (2017) 101:1191–9. doi: 10.1189/jlb.3AB0516-233RR

76. Zöller M. Janus-faced myeloid-derived suppressor cell exosomes for the good and the bad in cancer and autoimmune disease. *Front Immunol* (2018) 9:137. doi: 10.3389/fimmu.2018.00137

77. Zhu D, Tian J, Wu X, Li M, Tang X, Rui K, et al. G-MDSC-derived exosomes attenuate collagen-induced arthritis by impairing Th1 and Th17 cell responses. *Biochim Biophys Acta Mol Basis Dis* (2019) 1865:165540. doi: 10.1016/j.bbadis.2019.165540

78. Skokos D, Botros HG, Demeure C, Morin J, Peronet R, Birkenmeier G, et al. Mast cell-derived exosomes induce phenotypic and functional maturation of dendritic cells and elicit specific immune responses *in vivo*. *J Immunol* (2003) 170:3037–45. doi: 10.4049/jimmunol.170.6.3037

79. Wieckowski EU, Visus C, Szajnik M, Szczepanski MJ, Storkus WJ, Whiteside TL. Tumor-derived microvesicles promote regulatory T cell expansion and induce apoptosis in tumor-reactive activated CD8+ T lymphocytes. *J Immunol* (2009) 183:3720–30. doi: 10.4049/jimmunol.0900970

80. Whiteside TL. The effect of tumor-derived exosomes on immune regulation and cancer immunotherapy. *Future Oncol* (2017) 13:2583–92. doi: 10.2217/fon-2017-0343

81. Ren W, Zhang X, Li W, Feng Q, Feng H, Tong Y, et al. Exosomal miRNA-107 induces myeloid-derived suppressor cell expansion in gastric cancer. *Cancer Manag Res* (2019) 11:4023–40. doi: 10.2147/cmar.S198886

82. Choi D, Spinelli C, Montermini L, Rak J. Oncogenic regulation of extracellular vesicle proteome and heterogeneity. *Proteomics* (2019) 19:e1800169. doi: 10.1002/pmic.201800169

83. Zhang Y, Pfannenstiel LW, Bolesta E, Montes CL, Zhang X, Chapoval AI, et al. Interleukin-7 inhibits tumor-induced CD27-CD28- suppressor T cells: implications for cancer immunotherapy. *Clin Cancer Res* (2011) 17:4975–86. doi: 10.1158/1078-0432.Ccr-10-3328

84. Tauro BJ, Mathias RA, Greening DW, Gopal SK, Ji H, Kapp EA, et al. Oncogenic h-ras reprograms madin-Darby canine kidney (MDCK) cell-derived exosomal proteins following epithelial-mesenchymal transition. *Mol Cell Proteomics* (2013) 12:2148–59. doi: 10.1074/mcp.M112.027086

85. Whiteside TL. Exosomes and tumor-mediated immune suppression. *J Clin Invest* (2016) 126:1216–23. doi: 10.1172/jci81136

86. Groh V, Wu J, Yee C, Spies T. Tumour-derived soluble MIC ligands impair expression of NKG2D and T-cell activation. *Nature* (2002) 419:734–8. doi: 10.1038/nature01112

87. Qu JL, Qu XJ, Zhao MF, Teng YE, Zhang Y, Hou KZ, et al. Gastric cancer exosomes promote tumour cell proliferation through PI3K/Akt and MAPK/ERK activation. *Dig Liver Dis* (2009) 41:875–80. doi: 10.1016/j.dld.2009.04.006

88. Melo SA, Sugimoto H, O'Connell JT, Kato N, Villanueva A, Vidal A, et al. Cancer exosomes perform cell-independent microRNA biogenesis and promote tumorigenesis. *Cancer Cell* (2014) 26:707–21. doi: 10.1016/j.ccell.2014.09.005

89. de la Torre Gomez C, Goreham RV, Bech Serra JJ, Nann T, Kussmann M. "Exosomics"-a review of biophysics, biology and biochemistry of exosomes with a focus on human breast milk. *Front Genet* (2018) 9:92. doi: 10.3389/fgene.2018.00092

90. Whiteside TL. Tumor-derived exosomes and their role in cancer progression. *Adv Clin Chem* (2016) 74:103–41. doi: 10.1016/bs.acc.2015.12.005

91. Whiteside TL. The potential of tumor-derived exosomes for noninvasive cancer monitoring: an update. *Expert Rev Mol Diagn* (2018) 18:1029–40. doi: 10.1080/14737159.2018.1544494

92. Zhao H, Yang L, Baddour J, Achreja A, Bernard V, Moss T, et al. Tumor microenvironment derived exosomes pleiotropically modulate cancer cell metabolism. *Elife* (2016) 5:e10250. doi: 10.7554/eLife.10250

93. Gao Y, Zhang H, Zhou N, Xu P, Wang J, Gao Y, et al. Methotrexate-loaded tumour-cell-derived microvesicles can relieve biliary obstruction in patients with extrahepatic cholangiocarcinoma. *Nat BioMed Eng* (2020) 4:743–53. doi: 10.1038/s41551-020-0583-0

94. Nedaeinia R, Manian M, Jazayeri MH, Ranjbar M, Salehi R, Sharifi M, et al. Circulating exosomes and exosomal microRNAs as biomarkers in gastrointestinal cancer. *Cancer Gene Ther* (2017) 24:48–56. doi: 10.1038/cgt.2016.77

95. Jakobsen KR, Paulsen BS, Bæk R, Varming K, Sorensen BS, Jørgensen MM. Exosomal proteins as potential diagnostic markers in advanced non-small cell lung carcinoma. *J Extracell Vesicles* (2015) 4:26659. doi: 10.3402/jev.v4.26659

96. An M, Lohse I, Tan Z, Zhu J, Wu J, Kurapati H, et al. Quantitative proteomic analysis of serum exosomes from patients with locally advanced pancreatic cancer undergoing chemoradiotherapy. *J Proteome Res* (2017) 16:1763–72. doi: 10.1021/acs.jproteome.7b00024

97. Jia S, Zhang R, Li Z, Li J. Clinical and biological significance of circulating tumor cells, circulating tumor DNA, and exosomes as biomarkers in colorectal cancer. *Oncotarget* (2017) 8:55632–45. doi: 10.18632/oncotarget.17184

98. Fu H, Yang H, Zhang X, Wang B, Mao J, Li X, et al. Exosomal TRIM3 is a novel marker and therapy target for gastric cancer. *J Exp Clin Cancer Res* (2018) 37:162. doi: 10.1186/s13046-018-0825-0

99. Didiot MC, Hall LM, Coles AH, Haraszti RA, Godinho BM, Chase K, et al. Exosome-mediated delivery of hydrophobically modified siRNA for huntingtin mRNA silencing. *Mol Ther* (2016) 24:1836–47. doi: 10.1038/mt.2016.126

100. Zhuang X, Xiang X, Grizzle W, Sun D, Zhang S, Axtell RC, et al. Treatment of brain inflammatory diseases by delivering exosome encapsulated anti-inflammatory drugs from the nasal region to the brain. *Mol Ther* (2011) 19:1769–79. doi: 10.1038/mt.2011.164

101. Alvarez-Erviti L, Seow Y, Yin H, Betts C, Lakhal S, Wood MJ. Delivery of siRNA to the mouse brain by systemic injection of targeted exosomes. *Nat Biotechnol* (2011) 29:341–5. doi: 10.1038/nbt.1807

102. Kobayashi M, Sawada K, Miyamoto M, Shimizu A, Yamamoto M, Kinose Y, et al. Exploring the potential of engineered exosomes as delivery systems for tumor-suppressor microRNA replacement therapy in ovarian cancer. *Biochem Biophys Res Commun* (2020) 527:153–61. doi: 10.1016/j.bbrc.2020.04.076

103. Pascucci L, Coccè V, Bonomi A, Ami D, Ceccarelli P, Ciusani E, et al. Paclitaxel is incorporated by mesenchymal stromal cells and released in exosomes that inhibit *in vitro* tumor growth: a new approach for drug delivery. *J Control Release* (2014) 192:262–70. doi: 10.1016/j.jconrel.2014.07.042

104. Haney MJ, Klyachko NL, Zhao Y, Gupta R, Plotnikova EG, He Z, et al. Exosomes as drug delivery vehicles for parkinson's disease therapy. *J Control Release* (2015) 207:18–30. doi: 10.1016/j.jconrel.2015.03.033

105. Lin Y, Wu J, Gu W, Huang Y, Tong Z, Huang L, et al. Exosome-liposome hybrid nanoparticles deliver CRISPR/Cas9 system in MSCs. *Adv Sci (Weinh)* (2018) 5:1700611. doi: 10.1002/advs.201700611

106. Salarpour S, Forootanfar H, Pournamdari M, Ahmadi-Zeidabadi M, Esmaeeli M, Pardakhty A. Paclitaxel incorporated exosomes derived from glioblastoma cells: Comparative study of two loading techniques. *Daru* (2019) 27:533–9. doi: 10.1007/s40199-019-00280-5

107. Kim MS, Haney MJ, Zhao Y, Mahajan V, Deygen I, Klyachko NL, et al. Development of exosome-encapsulated paclitaxel to overcome MDR in cancer cells. *Nanomedicine* (2016) 12:655–64. doi: 10.1016/j.nano.2015.10.012

108. Li X, Li X, Lin J, Sun X, Ding Q. Exosomes derived from low-intensity pulsed ultrasound-treated dendritic cells suppress tumor necrosis factor-induced endothelial inflammation. *J Ultrasound Med* (2019) 38:2081–91. doi: 10.1002/jum.14898

109. Wang P, Wang H, Huang Q, Peng C, Yao L, Chen H, et al. Exosomes from M1-polarized macrophages enhance paclitaxel antitumor activity by activating macrophages-mediated inflammation. *Theranostics* (2019) 9:1714–27. doi: 10.7150/thno.30716

110. Yang Z, Xie J, Zhu J, Kang C, Chiang C, Wang X, et al. Functional exosome-mimic for delivery of siRNA to cancer: *In vitro* and *in vivo* evaluation. *J Control Release* (2016) 243:160–71. doi: 10.1016/j.jconrel.2016.10.008

111. Sun L, Fan M, Huang D, Li B, Xu R, Gao F, et al. Clodronate-loaded liposomal and fibroblast-derived exosomal hybrid system for enhanced drug delivery to pulmonary fibrosis. *Biomaterials* (2021) 271:120761. doi: 10.1016/j.biomaterials.2021.120761

112. Zhou W, Chen X, Zhou Y, Shi S, Liang C, Yu X, et al. Exosomes derived from immunogenically dying tumor cells as a versatile tool for vaccination against pancreatic cancer. *Biomaterials* (2022) 280:121306. doi: 10.1016/j.biomaterials.2021.121306

113. Li L, He D, Guo Q, Zhang Z, Ru D, Wang L, et al. Exosome-liposome hybrid nanoparticle codelivery of TP and miR497 conspicuously overcomes chemoresistant ovarian cancer. *J Nanobiotechnol* (2022) 20:50. doi: 10.1186/s12951-022-01264-5

114. Jia G, Han Y, An Y, Ding Y, He C, Wang X, et al. NRP-1 targeted and cargo-loaded exosomes facilitate simultaneous imaging and therapy of glioma *in vitro* and *in vivo*. *Biomaterials* (2018) 178:302–16. doi: 10.1016/j.biomaterials.2018.06.029

115. Suetsugu A, Honma K, Saji S, Moriwaki H, Ochiya T, Hoffman RM. Imaging exosome transfer from breast cancer cells to stroma at metastatic sites in orthotopic nude-mouse models. *Adv Drug Delivery Rev* (2013) 65:383–90. doi: 10.1016/j.addr.2012.08.007

116. Tian Y, Li S, Song J, Ji T, Zhu M, Anderson GJ, et al. A doxorubicin delivery platform using engineered natural membrane vesicle exosomes for targeted tumor therapy. *Biomaterials* (2014) 35:2383–90. doi: 10.1016/j.biomaterials.2013.11.083

117. Yong T, Zhang X, Bie N, Zhang H, Zhang X, Li F, et al. Tumor exosome-based nanoparticles are efficient drug carriers for chemotherapy. *Nat Commun* (2019) 10:3838. doi: 10.1038/s41467-019-11718-4

118. Mehryab F, Rabbani S, Shahhosseini S, Shekari F, Fatahi Y, Baharvand H, et al. Exosomes as a next-generation drug delivery system: An update on drug loading approaches, characterization, and clinical application challenges. *Acta Biomater* (2020) 113:42–62. doi: 10.1016/j.actbio.2020.06.036

119. Wang D, Wan Z, Yang Q, Chen J, Liu Y, Lu F, et al. Sonodynamical reversion of immunosuppressive microenvironment in prostate cancer *via* engineered exosomes. *Drug Delivery* (2022) 29:702–13. doi: 10.1080/10717544.2022.2044937

120. Lv H, Wang T, Ma F, Zhang K, Gao T, Pei R, et al. Aptamer-functionalized targeted siRNA delivery system for tumor immunotherapy. *BioMed Mater* (2022) 17:024108. doi: 10.1088/1748-605X/ac5415

121. Dong SXM, Caballero R, Ali H, Roy DLF, Cassol E, Kumar A. Transfection of hard-to-transfect primary human macrophages with bax siRNA to reverse resveratrol-induced apoptosis. *RNA Biol* (2020) 17:755–64. doi: 10.1080/15476286.2020.1730081

122. Fu W, Li T, Chen H, Zhu S, Zhou C. Research progress in exosome-based nanoscale drug carriers in tumor therapies. *Front Oncol* (2022) 12:919279. doi: 10.3389/fonc.2022.919279

123. Wang J, Yeung BZ, Cui M, Peer CJ, Lu Z, Figg WD, et al. Exosome is a mechanism of intercellular drug transfer: Application of quantitative pharmacology. *J Control Release* (2017) 268:147–58. doi: 10.1016/j.jconrel.2017.10.020

124. Agrawal AK, Aqil F, Jeyabalan J, Spencer WA, Beck J, Gachuki BW, et al. Milk-derived exosomes for oral delivery of paclitaxel. *Nanomedicine* (2017) 13:1627–36. doi: 10.1016/j.nano.2017.03.001

125. Lee J, Lee JH, Chakraborty K, Hwang J, Lee YK. Exosome-based drug delivery systems and their therapeutic applications. *RSC Adv* (2022) 12:18475–92. doi: 10.1039/d2ra02351b

126. Familtseva A, Jeremic N, Tyagi SC. Exosomes: cell-created drug delivery systems. *Mol Cell Biochem* (2019) 459:1–6. doi: 10.1007/s11010-019-03545-4

127. Shi J, Ma Y, Zhu J, Chen Y, Sun Y, Yao Y, et al. A review on electroporation-based intracellular delivery. *Molecules* (2018) 23:3044. doi: 10.3390/molecules23113044

128. Zhou W, Zhou Y, Chen X, Ning T, Chen H, Guo Q, et al. Pancreatic cancer-targeting exosomes for enhancing immunotherapy and reprogramming tumor microenvironment. *Biomaterials* (2021) 268:120546. doi: 10.1016/j.biomaterials.2020.120546

129. Toffoli G, Hadla M, Corona G, Caligiuri I, Palazzolo S, Semeraro S, et al. Exosomal doxorubicin reduces the cardiac toxicity of doxorubicin. *Nanomed (Lond)* (2015) 10:2963–71. doi: 10.2217/nnm.15.118

130. Chang L, Bertani P, Gallego-Perez D, Yang Z, Chen F, Chiang C, et al. 3D nanochannel electroporation for high-throughput cell transfection with high uniformity and dosage control. *Nanoscale* (2016) 8:243–52. doi: 10.1039/c5nr03187g

131. Yang Z, Shi J, Xie J, Wang Y, Sun J, Liu T, et al. Large-Scale generation of functional mRNA-encapsulating exosomes *via* cellular nanoporation. *Nat BioMed Eng* (2020) 4:69–83. doi: 10.1038/s41551-019-0485-1

132. Liao W, Du Y, Zhang C, Pan F, Yao Y, Zhang T, et al. Exosomes: The next generation of endogenous nanomaterials for advanced drug delivery and therapy. *Acta Biomater* (2019) 86:1–14. doi: 10.1016/j.actbio.2018.12.045

133. Armstrong JP, Holme MN, Stevens MM. Re-engineering extracellular vesicles as smart nanoscale therapeutics. *ACS Nano* (2017) 11:69–83. doi: 10.1021/acsnano.6b07607

134. Liang Y, Xu X, Li X, Xiong J, Li B, Duan L, et al. Chondrocyte-targeted MicroRNA delivery by engineered exosomes toward a cell-free osteoarthritis therapy. *ACS Appl Mater Interfaces* (2020) 12:36938–47. doi: 10.1021/acsami.0c10458

135. Xu Z, Zeng S, Gong Z, Yan Y. Exosome-based immunotherapy: a promising approach for cancer treatment. *Mol Cancer* (2020) 19:160. doi: 10.1186/s12943-020-01278-3

136. Zhang Q, Xiao Q, Yin H, Xia C, Pu Y, He Z, et al. Milk-exosome based pH/light sensitive drug system to enhance anticancer activity against oral squamous cell carcinoma. *RSC Adv* (2020) 10:28314–23. doi: 10.1039/d0ra05630h

137. Fan Y, Zhou Y, Lu M, Si H, Li L, Tang B. Responsive dual-targeting exosome as a drug carrier for combination cancer immunotherapy. *Res (Wash D C)* (2021) 2021:9862876. doi: 10.34133/2021/9862876

138. Cheng Q, Dai Z, Smbatyan G, Epstein AL, Lenz HJ, Zhang Y. Eliciting anti-cancer immunity by genetically engineered multifunctional exosomes. *Mol Ther* (2022) 30:3066–77. doi: 10.1016/j.ymthe.2022.06.013

139. Ji P, Yang Z, Li H, Wei M, Yang G, Xing H, et al. Smart exosomes with lymph node homing and immune-amplifying capacities for enhanced immunotherapy of metastatic breast cancer. *Mol Ther Nucleic Acids* (2021) 26:987–96. doi: 10.1016/j.omtn.2021.10.009

140. Zhou X, Miao Y, Wang Y, He S, Guo L, Mao J, et al. Tumour-derived extracellular vesicle membrane hybrid lipid nanovesicles enhance siRNA delivery by tumour-homing and intracellular freeway transportation. *J Extracell Vesicles* (2022) 11:e12198. doi: 10.1002/jev2.12198

141. Yang P, Cao X, Cai H, Feng P, Chen X, Zhu Y, et al. The exosomes derived from CAR-T cell efficiently target mesothelin and reduce triple-negative breast cancer growth. *Cell Immunol* (2021) 360:104262. doi: 10.1016/j.cellimm.2020.104262

142. Shi X, Cheng Q, Hou T, Han M, Smbatyan G, Lang JE, et al. Genetically engineered cell-derived nanoparticles for targeted breast cancer immunotherapy. *Mol Ther* (2020) 28:536–47. doi: 10.1016/j.ymthe.2019.11.020

143. Chen JM, Fei XF, Wang JL, Cai ZJ. Tumor-derived extracellular vesicles: Regulators of tumor microenvironment and the enlightenment in tumor therapy. *Pharmacol Res* (2020) 159:105041. doi: 10.1016/j.phrs.2020.105041

144. Taghikhani A, Farzaneh F, Sharifzad F, Mardpour S, Ebrahimi M, Hassan ZM. Engineered tumor-derived extracellular vesicles: potentials in cancer immunotherapy. *Front Immunol* (2020) 11:221. doi: 10.3389/fimmu.2020.00221

145. Donoso-Meneses D, Figueroa-Valdes AI, Georges N, Tobar HE, Alcayaga-Miranda F. Turning adversity into opportunity: Small extracellular vesicles as nanocarriers for tumor-associated macrophages re-education. *Bioeng Trans Med* (2022) e10349. doi: 10.1002/btm2.10349

146. Rezaie J, Ahmadi M, Ravanbakhsh R, Mojarad B, Mahbubfam S, Shaban SA, et al. Tumor-derived extracellular vesicles: The metastatic organotropism drivers. *Life Sci* (2022) 289:120216. doi: 10.1016/j.lfs.2021.120216

147. Wang J, Tang W, Yang M, Yin Y, Li H, Hu F, et al. Inflammatory tumor microenvironment responsive neutrophil exosomes-based drug delivery system for targeted glioma therapy. *Biomaterials* (2021) 273:120784. doi: 10.1016/j.biomaterials.2021.120784

148. Rincon-Riveros A, Lopez L, Villegas EV, Rodriguez JA. Regulation of antitumor immune responses by exosomes derived from tumor and immune cells. *Cancers* (2021) 13:847. doi: 10.3390/cancers13040847

149. Kim JY, Song J, Jung H, Mok H. I-Motif-coated exosomes as a pH-sensitive carrier for anticancer drugs. *Appl Biol Chem* (2018) 61:599–606. doi: 10.1007/s13765-018-0394-0

150. Yong TY, Wei ZH, Gan L, Yang XL. Extracellular-vesicle-based drug delivery systems for enhanced antitumor therapies through modulating the cancer-immunity cycle. *Adv Mater* (2022) doi. doi: 10.1002/adma.202201054

151. Nam GH, Choi Y, Kim GB, Kim S, Kim SA, Kim IS. Emerging prospects of exosomes for cancer treatment: From conventional therapy to immunotherapy. *Advanced Mater* (2020) 32:2002440. doi: 10.1002/adma.202002440

152. Zocchi MR, Tosetti F, Benelli R, Poggi A. Cancer nanomedicine special issue review anticancer drug delivery with nanoparticles: Extracellular vesicles or synthetic nanobeads as therapeutic tools for conventional treatment or immunotherapy. *Cancers* (2020) 12:1886. doi: 10.3390/cancers12071886

153. Zhou Q, Ding W, Qian Z, Zhu Q, Sun C, Yu Q, et al. Immunotherapy strategy targeting programmed cell death ligand 1 and CD73 with macrophage-derived mimetic nanovesicles to treat bladder cancer. *Mol Pharm* (2021) 18:4015–28. doi: 10.1021/acs.molpharmaceut.1c00448

154. Pei X, Zhang X, Zhang L, Yuan M, Sun L, Yu F, et al. Targeted exosomes for co-delivery of siFGL1 and siTGF-β1 trigger combined cancer immunotherapy by remodeling immunosuppressive tumor microenvironment. *Chem Eng J* (2021) 421:129774. doi: 10.1016/j.cej.2021.129774

155. Koh E, Lee EJ, Nam GH, Hong Y, Cho E, Yang Y, et al. Exosome-SIRPα, a CD47 blockade increases cancer cell phagocytosis. *Biomaterials* (2017) 121:121–9. doi: 10.1016/j.biomaterials.2017.01.004

156. Pitt JM, André F, Amigorena S, Soria JC, Eggermont A, Kroemer G, et al. Dendritic cell-derived exosomes for cancer therapy. *J Clin Invest* (2016) 126:1224–32. doi: 10.1172/jci81137

157. Lindenbergh MFS, Stoorvogel W. Antigen presentation by extracellular vesicles from professional antigen-presenting cells. *Annu Rev Immunol* (2018) 36:435–59. doi: 10.1146/annurev-immunol-041015-055700

158. Lu Z, Zuo B, Jing R, Gao X, Rao Q, Liu Z, et al. Dendritic cell-derived exosomes elicit tumor regression in autochthonous hepatocellular carcinoma mouse models. *J Hepatol* (2017) 67:739–48. doi: 10.1016/j.jhep.2017.05.019

159. Wang R, Xu A, Zhang X, Wu J, Freywald A, Xu J, et al. Novel exosome-targeted T-cell-based vaccine counteracts T-cell anergy and converts CTL exhaustion in chronic infection *via* CD40L signaling through the mTORC1 pathway. *Cell Mol Immunol* (2017) 14:529–45. doi: 10.1038/cmi.2016.23

160. Li R, Chibbar R, Xiang J. Novel EXO-T vaccine using polyclonal CD4(+) T cells armed with HER2-specific exosomes for HER2-positive breast cancer. *Onco Targets Ther* (2018) 11:7089–93. doi: 10.2147/ott.S184898

161. Morse MA, Garst J, Osada T, Khan S, Hobeika A, Clay TM, et al. A phase I study of dexosome immunotherapy in patients with advanced non-small cell lung cancer. *J Transl Med* (2005) 3:9. doi: 10.1186/1479-5876-3-9

162. Escudier B, Dorval T, Chaput N, André F, Caby MP, Novault S, et al. Vaccination of metastatic melanoma patients with autologous dendritic cell (DC) derived-exosomes: results of thefirst phase I clinical trial. *J Transl Med* (2005) 3:10. doi: 10.1186/1479-5876-3-10

163. Dai S, Wei D, Wu Z, Zhou X, Wei X, Huang H, et al. Phase I clinical trial of autologous ascites-derived exosomes combined with GM-CSF for colorectal cancer. *Mol Ther* (2008) 16:782–90. doi: 10.1038/mt.2008.1

164. Dunand-Sauthier I, Santiago-Raber ML, Capponi L, Vejnar CE, Schaad O, Irla M, et al. Silencing of c-fos expression by microRNA-155 is critical for dendritic cell maturation and function. *Blood* (2011) 117:4490–500. doi: 10.1182/blood-2010-09-308064

165. Wolfers J, Lozier A, Raposo G, Regnault A, Théry C, Masurier C, et al. Tumor-derived exosomes are a source of shared tumor rejection antigens for CTL cross-priming. *Nat Med* (2001) 7:297–303. doi: 10.1038/85438

166. Lee EY, Park KS, Yoon YJ, Lee J, Moon HG, Jang SC, et al. Therapeutic effects of autologous tumor-derived nanovesicles on melanoma growth and metastasis. *PloS One* (2012) 7:e33330. doi: 10.1371/journal.pone.0033330

167. Liu Y, Gu Y, Cao X. The exosomes in tumor immunity. *Oncoimmunology* (2015) 4:e1027472. doi: 10.1080/2162402x.2015.1027472

168. Lee YS, Kim SH, Cho JA, Kim CW. Introduction of the CIITA gene into tumor cells produces exosomes with enhanced anti-tumor effects. *Exp Mol Med* (2011) 43:281–90. doi: 10.3858/emm.2011.43.5.029

169. Cho JA, Lee YS, Kim SH, Ko JK, Kim CW. MHC independent anti-tumor immune responses induced by Hsp70-enriched exosomes generate tumor regression in murine models. *Cancer Lett* (2009) 275:256–65. doi: 10.1016/j.canlet.2008.10.021

170. Temchura VV, Tenbusch M, Nchinda G, Nabi G, Tippler B, Zelenyuk M, et al. Enhancement of immunostimulatory properties of exosomal vaccines by incorporation of fusion-competent G protein of vesicular stomatitis virus. *Vaccine* (2008) 26:3662–72. doi: 10.1016/j.vaccine.2008.04.069

171. Zhao Z, McGill J, Gamero-Kubota P, He M. Microfluidic on-demand engineering of exosomes towards cancer immunotherapy. *Lab Chip* (2019) 19:1877–86. doi: 10.1039/c8lc01279b

172. Marsac D, Loirat D, Petit C, Schwartz O, Michel ML. Enhanced presentation of major histocompatibility complex class I-restricted human immunodeficiency virus type 1 (HIV-1) gag-specific epitopes after DNA immunization with vectors coding for vesicular stomatitis virus glycoprotein-pseudotyped HIV-1 gag particles. *J Virol* (2002) 76:7544–53. doi: 10.1128/jvi.76.15.7544-7553.2002

173. Bu N, Wu H, Sun B, Zhang G, Zhan S, Zhang R, et al. Exosome-loaded dendritic cells elicit tumor-specific $CD8^+$ cytotoxic T cells in patients with glioma. *J Neurooncol* (2011) 104:659–67. doi: 10.1007/s11060-011-0537-1

174. Ren G, Wang Y, Yuan S, Wang B. Dendritic cells loaded with HeLa-derived exosomes simulate an antitumor immune response. *Oncol Lett* (2018) 15:6636–40. doi: 10.3892/ol.2018.8126

175. Mahaweni NM, Kaijen-Lambers ME, Dekkers J, Aerts JG, Hegmans JP. Tumour-derived exosomes as antigen delivery carriers in dendritic cell-based immunotherapy for malignant mesothelioma. *J Extracell Vesicles* (2013) 2:22492. doi: 10.3402/jev.v2i0.22492

176. Gu X, Erb U, Büchler MW, Zöller M. Improved vaccine efficacy of tumor exosome compared to tumor lysate loaded dendritic cells in mice. *Int J Cancer* (2015) 136:E74–84. doi: 10.1002/ijc.29100

177. Ungefroren H. Blockade of TGF-β signaling: a potential target for cancer immunotherapy? *Expert Opin Ther Targets* (2019a) 23:679–93. doi: 10.1080/14728222.2019.1636034

178. Ungefroren H. TGF-β signaling in cancer: control by negative regulators and crosstalk with proinflammatory and fibrogenic pathways. *Cancers (Basel)* (2019b) 11:384. doi: 10.3390/cancers11030384

179. Hellmann MD, Friedman CF, Wolchok JD. Combinatorial cancer immunotherapies. *Adv Immunol* (2016) 130:251–77. doi: 10.1016/bs.ai.2015.12.005

180. Zhu S, Zhang T, Zheng L, Liu H, Song W, Liu D, et al. Combination strategies to maximize the benefits of cancer immunotherapy. *J Hematol Oncol* (2021) 14:156. doi: 10.1186/s13045-021-01164-5

181. Griffith JW, Sokol CL, Luster AD. Chemokines and chemokine receptors: positioning cells for host defense and immunity. *Annu Rev Immunol* (2014) 32:659–702. doi: 10.1146/annurev-immunol-032713-120145

182. Klein C, Waldhauer I, Nicolini VG, Freimoser-Grundschober A, Nayak T, Vugts DJ, et al. Cergutuzumab amunaleukin (CEA-IL2v), a CEA-targeted IL-2 variant-based immunocytokine for combination cancer immunotherapy: Overcoming limitations of aldesleukin and conventional IL-2-based immunocytokines. *Oncoimmunology* (2017) 6:e1277306. doi: 10.1080/2162402x.2016.1277306

183. Galon J, Bruni D. Approaches to treat immune hot, altered and cold tumours with combination immunotherapies. *Nat Rev Drug Discovery* (2019) 18:197–218. doi: 10.1038/s41573-018-0007-y

184. Garg AD, Galluzzi L, Apetoh L, Baert T, Birge RB, Bravo-San Pedro JM, et al. Molecular and translational classifications of DAMPs in immunogenic cell death. *Front Immunol* (2015) 6:588. doi: 10.3389/fimmu.2015.00588

185. Xiao L, Erb U, Zhao K, Hackert T, Zöller M. Efficacy of vaccination with tumor-exosome loaded dendritic cells combined with cytotoxic drug treatment in pancreatic cancer. *Oncoimmunology* (2017) 6:e1319044. doi: 10.1080/2162402x.2017.1319044

186. Whiteside TL, Demaria S, Rodriguez-Ruiz ME, Zarour HM, Melero I. Emerging opportunities and challenges in cancer immunotherapy. *Clin Cancer Res* (2016) 22:1845–55. doi: 10.1158/1078-0432.Ccr-16-0049

187. Woo SR, Fuertes MB, Corrales L, Spranger S, Furdyna MJ, Leung MY, et al. STING-dependent cytosolic DNA sensing mediates innate immune recognition of immunogenic tumors. *Immunity* (2014) 41:830–42. doi: 10.1016/j.immuni.2014.10.017

188. Colak S, Ten Dijke P. Targeting TGF-β signaling in cancer. *Trends Cancer* (2017) 3:56–71. doi: 10.1016/j.trecan.2016.11.008

189. Tian T, Liang R, Erel-Akbaba G, Saad L, Obeid PJ, Gao J, et al. Immune checkpoint inhibition in GBM primed with radiation by engineered extracellular vesicles. *ACS Nano* (2022) 16:1940–53. doi: 10.1021/acsnano.1c05505

190. Lee H, Han J, Shin H, Han H, Na K, Kim H. Combination of chemotherapy and photodynamic therapy for cancer treatment with sonoporation effects. *J Control Release* (2018) 283:190–9. doi: 10.1016/j.jconrel.2018.06.008

191. Jang Y, Kim H, Yoon S, Lee H, Hwang J, Jung J, et al. Exosome-based photoacoustic imaging guided photodynamic and immunotherapy for the treatment of pancreatic cancer. *J Control Release* (2021) 330:293–304. doi: 10.1016/j.jconrel.2020.12.039

192. Wedge ME, Jennings VA, Crupi MJF, Poutou J, Jamieson T, Pelin A, et al. Virally programmed extracellular vesicles sensitize cancer cells to oncolytic virus and small molecule therapy. *Nat Commun* (2022) 13:1898. doi: 10.1038/s41467-022-29526-8

193. Fan M, Liu H, Yan H, Che R, Jin Y, Yang X, et al. A CAR T-inspiring platform based on antibody-engineered exosomes from antigen-feeding dendritic cells for precise solid tumor therapy. *Biomaterials* (2022) 282:121424. doi: 10.1016/j.biomaterials.2022.121424

194. Zamarin D, Holmgaard RB, Subudhi SK, Park JS, Mansour M, Palese P, et al. Localized oncolytic virotherapy overcomes systemic tumor resistance to immune checkpoint blockade immunotherapy. *Sci Transl Med* (2014) 6:226ra232. doi: 10.1126/scitranslmed.3008095

195. Bommareddy PK, Shettigar M, Kaufman HL. Integrating oncolytic viruses in combination cancer immunotherapy. *Nat Rev Immunol* (2018) 18:498–513. doi: 10.1038/s41577-018-0014-6

frontiers | Frontiers in Immunology

TYPE Review
PUBLISHED 31 January 2023
DOI 10.3389/fimmu.2023.1053550

OPEN ACCESS

EDITED BY
Brian J. Ferguson,
University of Cambridge, United Kingdom

REVIEWED BY
Rossella Sartorius,
National Research Council (CNR), Italy
Zongmin Zhao,
University of Illinois at Chicago,
United States

*CORRESPONDENCE
Kirill A. Afonin
kafonin@uncc.edu

SPECIALTY SECTION
This article was submitted to Molecular Innate Immunity, a section of the journal Frontiers in Immunology

RECEIVED 25 September 2022
ACCEPTED 18 January 2023
PUBLISHED 31 January 2023

CITATION
Panigaj M, Skelly E, Beasock D, Marriott I, Johnson MB, Salotti J and Afonin KA (2023) Therapeutic immunomodulation by rationally designed nucleic acids and nucleic acid nanoparticles.
Front. Immunol. 14:1053550.
doi: 10.3389/fimmu.2023.1053550

Therapeutic immunomodulation by rationally designed nucleic acids and nucleic acid nanoparticles

Martin Panigaj[1,2], Elizabeth Skelly[1], Damian Beasock[1], Ian Marriott[3], M. Brittany Johnson[3], Jacqueline Salotti[4] and Kirill A. Afonin[1*]

[1]Nanoscale Science Program, Department of Chemistry, The University of North Carolina at Charlotte, Charlotte, NC, United States, [2]Institute of Biology & Ecology, Faculty of Science, Pavol Jozef Safarik University in Kosice, Kosice, Slovakia, [3]Department of Biological Sciences, University of North Carolina at Charlotte, Charlotte, NC, United States, [4]Mouse Cancer Genetics Program, Center for Cancer Research, National Cancer Institute, Frederick, MD, United States

The immune system has evolved to defend organisms against exogenous threats such as viruses, bacteria, fungi, and parasites by distinguishing between "self" and "non-self". In addition, it guards us against other diseases, such as cancer, by detecting and responding to transformed and senescent cells. However, for survival and propagation, the altered cells and invading pathogens often employ a wide range of mechanisms to avoid, inhibit, or manipulate the immunorecognition. As such, the development of new modes of therapeutic intervention to augment protective and prevent harmful immune responses is desirable. Nucleic acids are biopolymers essential for all forms of life and, therefore, delineating the complex defensive mechanisms developed against non-self nucleic acids can offer an exciting avenue for future biomedicine. Nucleic acid technologies have already established numerous approaches in therapy and biotechnology; recently, rationally designed nucleic acids nanoparticles (NANPs) with regulated physiochemical properties and biological activities has expanded our repertoire of therapeutic options. When compared to conventional therapeutic nucleic acids (TNAs), NANP technologies can be rendered more beneficial for synchronized delivery of multiple TNAs with defined stabilities, immunological profiles, and therapeutic functions. This review highlights several recent advances and possible future directions of TNA and NANP technologies that are under development for controlled immunomodulation.

KEYWORDS

PRR, PAMP, DAMP, NANPs, immunomodulation, innate immune system, therapy

Immunorecognition of nucleic acids

From prokaryotes to eukaryotes, all cellular forms of life possess a variety of conserved defense mechanisms against pathogens. Bacteria and archaea have evolved multiple intracellular immune systems to protect against viral phage infections, including restricted-modification (R-M), prokaryotic Argonaute proteins (pAgo), clustered regularly interspaced palindromic repeats (CRISPR) and CRISPR associated (Cas) proteins, abortive infection (Abi) and the more recently discovered antiviral STAND NTPase (Avs) homolog proteins (1, 2).

Conceptually parallel to eukaryotic organisms, prokaryotes have both innate (e.g., R-M and pAgo) and adaptive (e.g., CRISPR/Cas) systems; most of which target invading nucleic acids (1, 3). The R-M and similar systems are based on the endonuclease-mediated cleavage of any DNA that lacks specific epigenetic modifications. CRISPR/Cas-mediated immunological memory consists of the insertion of short DNA sequences from intruding DNA into CRISPR arrays in the host genome, ultimately providing sequence-specific cleavage/degradation of foreign nucleic acids after a second encounter (4, 5).

In eukaryotes, defense against pathogenic infection involves multiple cellular and molecular strategies. One example of protection against pathogenic nucleic acids is RNA interference (RNAi), which is conserved from unicellular eukaryotes to mammals. RNAi machinery has many functions, including the recognition of "non-self" double-stranded RNAs originated from viruses and retrotransposons triggering silencing of the target RNA (6). Small silencing RNAs include small interfering RNAs (siRNAs), microRNAs (miRNAs), and PIWI-interacting RNAs (piRNAs) that regulate not only antimicrobial immunity but also "self" gene expression. In cases of viral infection, Dicer-dependent production of virus-derived small interfering RNAs (vsiRNAs) or Dicer-independent production of virus-derived piRNAs (vpiRNAs) can guide specific virus elimination (7).

Metazoan somatic cells have evolved cell-autonomous self-defense mechanisms that synergize with specialized innate immune cells. In addition to innate immunity, vertebrates have developed adaptive immunity (8). While innate immunity provides the first line of defense against infections or damaged cells, adaptive immunity develops at a later stage and requires the activation of lymphocytes. The innate immune system recognizes molecular structures (non-self) that are absent on the host but produced by foreign pathogens. Known as pathogen-associated molecular patterns (PAMPs), these are structures that are distinctive for the particular pathogen and include proteins, lipids, carbohydrates, and nucleic acids that are unique to the viral or microbial pathogens. Examples of nucleic acid PAMPs include single-stranded (ss) or double-stranded (ds) RNAs present in replicating viruses and unmethylated CpG DNA typical for viruses, bacteria, and fungi (9, 10). PAMPs are recognized through their interactions with a diverse set of pattern recognition receptors (PRRs) expressed by host cells. In addition to PAMPs, PRRs can recognize so called damage-associated molecular patterns (DAMPs) of endogenous origin, which are molecules released from damaged or dying cells (11). PRRs are present in most cell types, but their expression is highly abundant in certain myeloid sentinel cells such as macrophages and dendritic cells. Examples of PRRs recognizing foreign nucleic acids include: (i) cytosolic RIG-I-like receptors (RLRs), which recognize foreign RNA; (ii) Toll-like receptors (TLRs), which are transmembrane proteins in the plasma and endosomal membranes that identify "non-self" RNA and unmethylated CpG DNA; (iii) the nucleotide oligomerization domain containing (NOD)-like receptor (NLR) family pyrin domain containing 1 (NLRP1) receptor, which forms part of a macromolecular inflammasome complex; and (iv) cytosolic DNA sensors (CDSs), which detect bacterial and viral DNA (7). These pathways (briefly described below) are not mutually exclusive and can be activated simultaneously and even synergistically within the same cell.

Within the endosome, TLR3, TLR7, TLR8, and TLR9 detect foreign nucleic acids. TLR3 is responsible for detecting dsRNA and induces downstream activation of NF-κB (12, 13). DsRNA is produced by most viruses during their replication process (14). TLR7 is responsible for the detection of ssRNA. This is required by the immune system for detection of RNA viruses, especially influenza, which sequesters its double stranded RNA (15). TLR7 recognizes ssRNA sequences containing successive uridines relative to sequences with single uridines (16). TLR8 is phylogenetically and structurally similar to TLR7 and is also responsible for the detection of ssRNA. However, the localization and cytokine induction profiles for TLR7 and TLR8 differ slightly. TLR7 is predominantly expressed in the lungs, spleen, and placenta and induces IFNα and IFN-regulated cytokine production. In contrast, TLR8 is expressed in lungs and monocytes and induces predominantly TNF production (17–19). TLR9 detects non-methylated CpG-motifs found in bacterial or viral DNA (20). All nucleic acid specific TLRs, activate the adapter protein, MyD88 (21, 22), except for TLR3 that activates TRIF (23). RIG-I, MDA5, and LGP2 are categorized as RIG-I-like receptors. These receptors are involved in the sensing of RNA viruses and initiate/modulate the immune response upon virus detection (24). ()A critical component of innate cellular defense, located predominantly in cytoplasm, is RIG-I, which can differentiate foreign RNAs from native forms. The prevailing opinion is that the triphosphate on the 5'- blunt end (5'-ppp) of RNA duplexes that are at least 10 nucleotides long is required for effective recognition by RIG-I, but apparently single ssRNAs with 5'-ppp may also lead to RIG-I mediated responses as shown by its activation during influenza A virus infections (25, 26). Also, it has been demonstrated that the RNA aptamer Cl9, that is specific to RIG-I, can trigger downstream signaling in a 5'-ppp independent manner (27). The stimulation of RIG-I downstream signaling subsequently leads to production of type I IFNs and IFN-stimulated genes (ISGs) that are important for the induction of adaptive immune responses.

Importantly, the cytosolic presence of 5'-ppp dsRNA is not limited to RNA virus infection but can arise following infection with several DNA viruses and intracellular bacteria due to the transcriptional activity of DNA-dependent RNA polymerase III (RNA Pol III) (28, 29). Cytosolic RNA Pol III therefore represents an important component in host defenses against disparate intracellular pathogens. In contrast, nuclear RNA Pol III, which can transcribe a plethora of ncRNAs with diverse roles including the control of immune functions (as extensively reviewed elsewhere (30, 31), synthesizes nucleus-specific ncRNAs containing 5'-ppp that are not recognized by RIG-I under normal physiological conditions. In this case, the presence of the nuclear envelope appears to help to

isolate the RNA Pol III transcripts from cytosolic RIG-I until these ncRNAs are processed further and become immunoquiescent. The largest pool of such RNA Pol III transcripts are tRNAs that are dephosphorylated by dual-specificity phosphatase 11 (DUSP11). Another strategy to avoid RIG-I recognition is to shield the 5'-ppp by binding to a protein. An example of this is the binding of the RNA component of the signal recognition particle 7SL1 (RN7SL1) with the protein signal recognition particle (SRP) (32).

RLRs and TLR3 recognition of foreign nucleic acids converge on pathways that activate the transcription factors, interferon (IFN)-regulatory factor (IRF) 3 and IRF7, and NF-κB. IRF3/7 stimulate production of type I IFNs, whereas NF-κB induces the expression of proinflammatory cytokines, chemokines, and adhesion and costimulatory molecules that induce acute inflammation and initiate adaptive immune responses. Furthermore, crosstalk occurs between these receptors and their signaling components resulting in complex immune responses to particular viral and nonviral nucleic acids (33–36) (Figure 1).

The cyclic guanosine monophosphate–adenosine monophosphate synthase (cGAS) -stimulator of IFN genes (STING) pathway is an important mechanism underlying cytosolic dsDNA-induced type I IFN responses. Activated cGAS generates the signaling molecule cyclic GMP-AMP (cGAMP), which binds to STING and triggers its translocation from the endoplasmic reticulum to the Golgi apparatus. STING then activates the TBK1 kinase that, in turn, activates IRF3, leading to type I IFN gene expression. STING also responds to other cytosolic DNA including DNA-dependent activator of IFN-regulatory factors (DAI; also known as Z-DNA binding protein 1 (ZBP1)) and IFN inducible protein 16 (IFI16) (37). In addition to inducing IFN production, STING also stimulates autophagy that serves both an innate immune function by delivering cytosolic microbes to the lysosome for elimination (38), and a role in adaptive immunity as a mechanism whereby microbial antigenic epitopes are generated in the lysosomes for presentation to lymphocytes (39).

In summary, activation of PRRs in addition to other pathways, such as global inhibition of protein synthesis mediated by protein kinase R (PKR) and oligoadenylate synthases (OASes) described elsewhere, elicit multiple cellular responses including immediate host responses such as inflammation and more specific subsequent adaptive immunity that are capable of pathogen clearance and long-term protection against reinfection (40).

Therapeutic nucleic acids and PRR agonists as immunomodulators

The presence of an intricate array of PRRs for non-self or abnormal RNA and DNA raises the safety concerns for broader applications of therapeutic nucleic acids (TNAs). Accordingly, the development of nanoparticle-carrier formulations that are immunoquiescent has obvious benefits for the translation of this highly promising biotechnology to the clinic, as severe complications, including severe inflammatory reactions that include cytokine storms

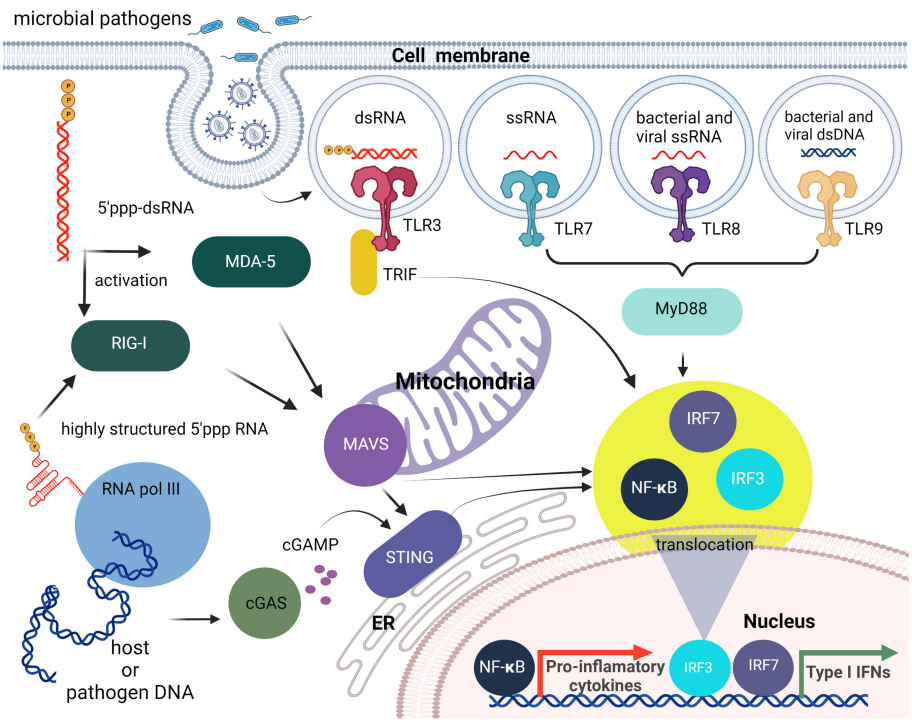

FIGURE 1
Brief overview of cellular innate immunity with an emphasis on nucleic acid recognition. The first line of nucleic acid PRRs consists of TLRs that can sense different PAMPs specific for non-self nucleic acids. Then cytosolic pathogen-associated nucleic acids can be sensed by members of the RLR family (RIG-I, MDA5). The endogenous and viral DNAs can also lead to RIG-I activation following their transcription by cytosolic RNA pol III, or can be detected directly as dsDNAs *via* cytosolic DNA sensing systems such as the cGAS-cGAMP-STING pathway. All of these pathways initiate the translocation of transcription factors including IRF3/7 and NF-κB to the nucleus and the subsequent induction type I IFN and pro-inflammatory cytokine production.

and complement activation-related pseudoallergies (CARPA), are circumvented.

As recently discussed at length, the presence of an array of cytosolic and endosomal nucleic acid sensors by most mammalian cells represents a highly attractive target to bolster beneficial host immune responses to infectious agents or to augment vaccine efficacy (41). This is illustrated by the promise of nucleic acid sensor agonists such as the TLR7 agonist, imiquimod, that has been approved for the treatment of genital warts (HPV), and the recent "shock and kill" strategies aimed at eradicating latent HIV viral reservoirs using TLR7 and TLR9 ligands, such as GS-9620 (vesatolimod) and MGN1703 (lefitolimod), respectively, to initiate viral reactivation and promote immune-mediated killing of infected cells (42–44).

Efficacious vaccines require the use of adjuvants that target pattern recognition receptors on antigen presenting cells to promote their ability to deliver antigen to B and T cells, and to provide essential co-stimulation, to achieve potent and long-lasting antigen-specific humoral and cellular immune responses. Currently, there are only a handful of vaccine adjuvants that are approved for human use and most of these have limitations, such as the inability of alum to promote cellular immune responses (45). As discussed previously (41, 46), nucleic acid sensors, including TLRs, RLRs and the cGAS-STING pathway, have been an attractive target for adjuvant development. The well-known adjuvant alum is now recognized to function through the induction of endogenous DAMPs, including DNA-based TNAs, that activate nucleic acid sensing pathways (47, 48). Similarly, more recent preclinical studies have showed that modified CpG-based adjuvants or combination adjuvants, such as AS15 and K3 CpG + cGAMP, are potent inducers of both humoral and cellular immune responses, and agonists of TLR3 and MDA5, such as synthetic dsRNA TNAs including poly-IC, the RNase-resistant derivative poly-ICLC (Hiltonol), and poly-IC12U (Ampligen), have been explored for clinical use (46, 49, 50). Furthermore, the TLR7 and TLR8 agonist 3M-052, formulated in a lipid-based nanoparticle (3M-052-AF), is being evaluated as an adjuvant for a preventive HIV vaccine, while a liposome formulated cyclic dinucleotide-based adjuvant has been shown to protect against a range of influenza strains (51, 52). As such, the array of nucleic acid sensors expressed by mammalian cells, as well as the identification of natural and synthetic ligands for these receptors, represents tremendous potential for the development of novel and effective adjuvants

Endogenous noncoding RNAs as immunomodulators

RNA provides diverse functions; classically, RNA allows for the flow of genetic information from DNA to proteins by mRNA translation, where tRNA and rRNA are prominent in facilitating expression with the help of post-transcriptional regulation *via* RNAi. The other noncoding (nc) RNAs participate in splicing and, thus, finalize the functional mRNA sequence. Besides this, a diverse cornucopia of short or long ncRNAs are involved in physiological as well as pathological processes, often described with little detailed mechanistic understanding. Most interactions are carried out in association with proteins and all processes are spatially and temporally controlled, which allows sensing of potentially pathogenic conditions and the alerting of host defensive systems (53). Hence, a better understanding of these processes and the ncRNAs involved may identify new targets for therapeutic intervention.

While a detailed understanding of the exact physiological roles of endogenous ncRNAs in innate system are only now emerging, it has become clear that dysregulation of their transcription, processing, and trafficking can have serious impact on RIG-I activation. Similarly, the participation of endogenous ncRNAs is open for therapeutic exploitation, either as a target or an effector, and their potential has recently been explored for some RNA Pol III transcripts (32).

The development and use of immune checkpoint inhibitors that disrupt co-inhibitory T-cell signaling has revolutionized cancer therapy. Upon relieving such blockade, the most efficient T-cell anti-tumor responses occur in an inflammatory microenvironment where there is an increased expression of type I IFNs, ISGs, pro-apoptotic molecules, and T-cell attracting chemokines. Many therapeutic strategies have focused on inducing inflammation within tumors and an attractive emerging strategy has been to exploit cellular nucleic acid PRRs (54).

Furthermore, the controlled stimulation of RIG-I in cancer cells using ligands that mimic an infection represents a new adjunctive therapeutic approach by increasing the susceptibility of tumor cells to conventional treatments. Such a possibility is supported by the observation that patients with intact RIG-I signaling are responsive to radio- and chemotherapy, while those with RIG-I suppression show tumor resistance (55). In addition, RIG-I activation renders cultured cancer cells susceptible to natural killer cell-mediated killing and promoted phagocytosis of tumor cells *in vivo* (56, 57). The intrinsic molecular heterogeneity of tumor cells within each patient generally requires a combinatorial approach. For example, the simultaneous suppression of tumor cell survival by targeting factors such as Bcl-2 or TGF-ß using RNAi approaches while simultaneously increasing the immunogenicity of tumor cells by activating RIG-I with 5'-ppp RNAs can decrease tumor viability. In summary, the combination of traditional approaches with emerging immunostimulatory treatments holds the promise of improving clinical outcomes (58–62).

Contrary to this, many tumors express high levels of ISGs in response to DAMPs and inflammation at the tumor site is often associated with cancer progression and treatment resistance. It is likely that, under various stress conditions induced by cancer treatment, endogenous RNAs can serve as DAMPs *via* as yet poorly understood mechanisms. Under physiological conditions, epithelial cells are typically not in contact with fibroblasts, but they may interact at wound sites or at sites of tumor invasion. Such tumor-stromal cell interactions may then lead to damage signal release that could prove crucial for tumor invasiveness and resistance to therapy (63). Emerging evidence suggests that ISG activation in responsive tumor cells (e.g., breast cancer) by specific ncRNAs from stromal cells promotes survival and progression of cancer (32). Exosomes that deliver RN7SL1 ncRNA generated by RNA Pol III were identified as the pivotal link between activated stromal cells and RIG-I dependent activation of ISG signaling in breast cancer cells. While RN7SL1 is shielded by SRP9 and SRP14 to avoid detection by RIG-I under normal circumstances, naked RN7SL1 is transferred to stromal exosomes following contact between fibroblasts and ISG-R breast cancer cells. The unshielding of RN7SL1 and its loading into

exosomes is a consequence of a disrupted stoichiometry between RNA Pol III-driven transcription and unchanged SRP expression. This imbalance is induced by stromal NOTCH1-MYC signaling which, in turn, is enhanced by contact-dependent signaling by breast cancer cells. As a result, RN7SL1 delivered by exosomes to breast cancer cells activates RIG-I signaling (Figure 2) (32).

The immune recognition of RN7SL1 ncRNA has been employed in a follow up study where it was used to enhance the function of chimeric antigen receptor T-cells (CAR-T cells) (64). CAR therapy has recently emerged as a major advance in cancer immunotherapy with six different CAR-T cell products having been approved by the US Food and Drug Administration thus far. This treatment is based on T-cells isolated from the patient's body and customized to their needs by genetic engineering to express recombinant chimeric antigen receptor (CAR) proteins on their membranes. CAR-T cells are then expanded ex vivo and introduced into the patient where they continue to divide and, using the engineered receptor, identify and eliminate cancer cells displaying the specific antigen. CAR-T therapy has shown remarkable efficiency in some hematologic cancers, but application of this treatment to solid tumors has remained challenging. Poor infiltration of CAR-T cells into the tumor microenvironment, immunosuppressive conditions at the tumor site, and poor expansion of CAR-T cells, are some of the issues that may be responsible for these problems

To improve the performance of CAR-T cells in such solid tumors, a plasmid encoding ncRNA RN7SL1 was used as a key component in an experimental treatment. RN7SL1 ncRNA was overexpressed in CAR-T cells and was found to activate IFN production in murine and human immune cells. A construct expressing two clinically relevant CARs, the M5BBz CAR targeting human mesothelin (MSLN) and the 19BBz CAR against human CD19, and RN7SL1 driven by the U6 promoter was then developed and tested. It was found that most of the expanded CAR-T cell population that expressed RN7SL1 RNA showed a memory T-cell phenotype and persisted longer in both the tumor and the bloodstream than RN7SL negative CAR-T cells, which were quickly exhausted. RN7SL overexpression resulted in its translocation to exosomes and its predominant export to immune cells residing in the tumor microenvironment, but not cancer cells, leading to IFN signaling. This, therefore, prevented the immunosuppression and tumor progression previously observed in another study (Figure 3) (64). Since RN7SL1 ncRNA was transcribed from an engineered construct here, it raises the intriguing question of whether natural and synthetic 5'-ppp ncRNAs provide similar immunostimulatory activity in such a system.

Interestingly, a role for a long ncRNA (lncRNA) in RIG-I regulation has been observed in a murine virus infection model. The endogenous lncRNA, lnc-Lsm3b, is normally present in the cytoplasm at low copy numbers, but such expression was increased tenfold after infection with Sendai virus or vesicular stomatitis virus (VSV). This upregulation was shown to be induced by a high concentrations of type I IFNs in a time dependent manner. Surprisingly, lnc-Lsm3b transcription silencing during infection resulted in higher type-I IFN production, which suggests that lnc-Lsm3b may suppress RIG-I activation at late stages of infection (65). While the therapeutic potential of lnc-Lsm3b binding motifs as RIG-I decoys is obvious, it remains unclear whether such treatments would be similarly effective in decreasing of RIG-I activity in human subjects.

Aptamers as extracellular immunomodulators

Aptamers are single-stranded nucleic acids (RNA, DNA, or chemical analogs) selected to adopt a conformation that allows for the highest binding affinity and specificity to its pre-defined target.

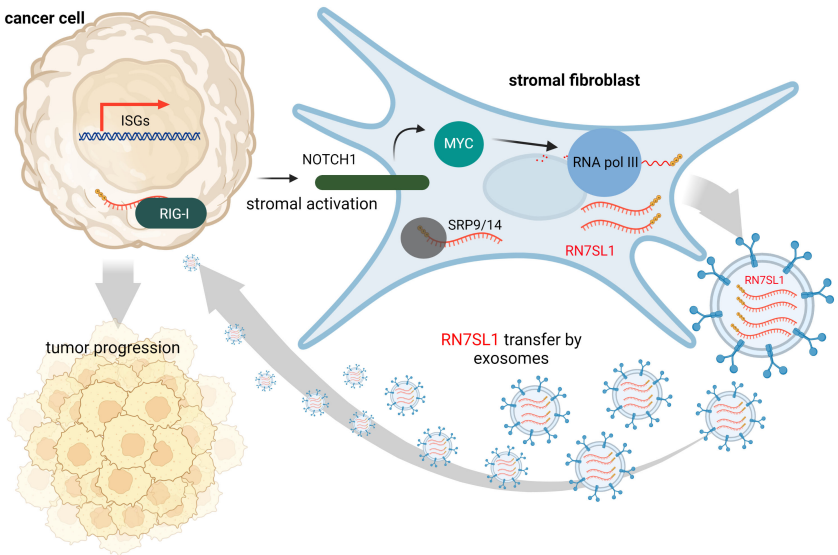

FIGURE 2
During contact with stromal fibroblasts, breast cancer cells activate NOTCH1/MYC signaling that leads to higher transcription of ncRNA RN7SL1 carrying 5'-ppp. These transcripts then remain unshielded since levels of their protein-binding partner (SRP9/14) remain constant. Naked RN7SL1 is loaded to exosomes and, upon interaction with breast cancer cells, can activate RIG-I signaling leading to an inflammatory tumor microenvironment that can promote tumor progression and poor clinical outcomes.

10.3389/fimmu.2023.1053550

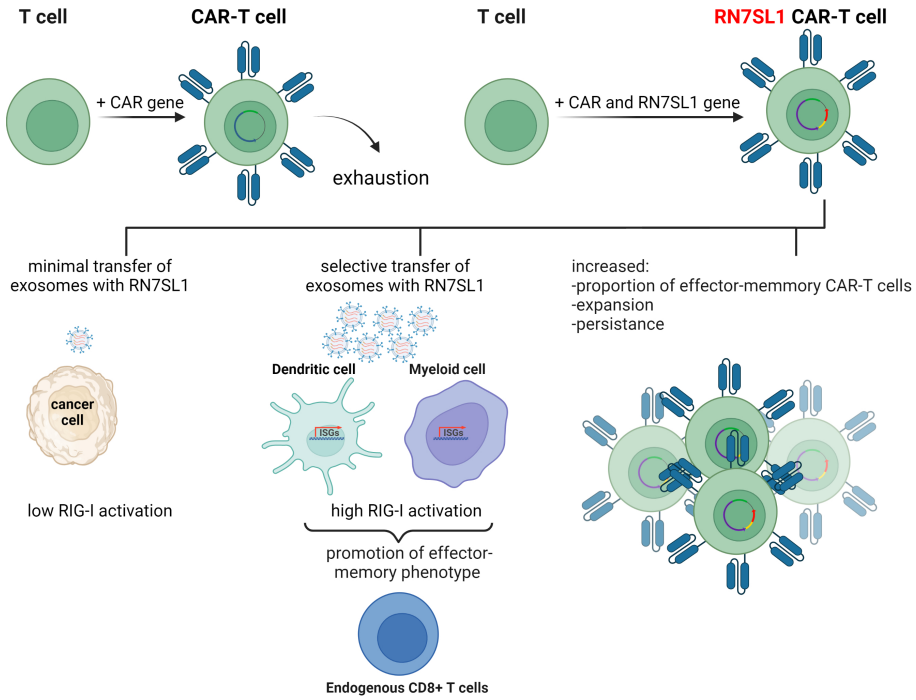

FIGURE 3
The use of endogenous RN7SL1 ncRNA to improve CAR-T cell therapy efficacy. Engineered CAR-T cells transcribe transgenic RN7SL1 ncRNA together with a chimeric antigen receptor. The resulting cell-autonomous effect prevents T-cell exhaustion and increases cell expansion. In addition, excreted exosomes transport RN7SL1 to intratumor myeloid cells, such as dendritic cells, rather than cancer cells, thereby avoiding inflammation triggered by tumor cells.

The correct aptamer sequences are identified during a process called SELEX (systematic evolution of ligands by exponential enrichment), where the library of ~10^{12} different oligonucleotides is presented to the target molecule and subjected to several rounds of selection (66). Due to their known sequence and batch-to-batch consistency, aptamers selected against certain receptors can be used similarly to their monoclonal antibody (mAbs) analogs to either prevent receptor interactions with its natural ligand or inhibit/activate receptor downstream signaling. However, compared to mAbs, aptamers have a greater shelf life, and their storage and transportation does not require cold chain maintenance. Also, aptamers have additional benefits as they are synthetic and can be manufactured in significantly less time than mAbs, as the chemical synthesis of aptamers does not require living systems. Furthermore, aptamers are amenable to chemical modifications and precise conjugation to other drugs and imaging agents.

Cell-to-cell interactions between cancer and immune cells represent a crucial interplay for tumor survival. One aspect of this communication is represented by immune checkpoints, receptor-ligand pairs expressed on the cell surface that control the strength of T-cell activation under physiological conditions. When T-cells recognize checkpoint proteins on tumor cells that are often overexpressed, it sends an inhibitory signal that prevents T-cell attack. Therefore, aptamers with proteins involved in the inactivation of co-immunostimulatory pathways on the one side and activators of signaling that lead to immune quiescence on the other represent potent prospective therapeutic agents. Given that the concept of immune checkpoint inhibitors has revolutionized cancer immunotherapy, it is not surprisingly that several monoclonal antibodies targeting such interactions have already been approved and many clinical trials are ongoing (67). Furthermore, it is fully appreciated that the use of antibody combinations against multiple targets can exert synergistic effects.

The application of extracellular immunomodulating aptamers has contributed to this therapeutic approach with several original concepts, as extensively reviewed by Thomas et al. (68). Due to the programmability of nucleic acids, aptamers can be rationally designed to assemble into higher order structures that enhance or even alter their original functionality. Such a relatively simple approach cannot be achieved with mAbs. The multivalent, and usually bispecific, aptamers can be designed and synthesized as a single continuous sequence, hybridized, or circularized (Figure 4A). The combinatorial potential of linking aptamers together offers not only the possibility of creating multivalent aptamers targeting the same or different epitopes of the same target molecule, but also the assembly of aptamers targeting diverse proteins. This presents an opportunity to promote specific cell-to-cell interactions, where the immune cell can anchor to the tumor cell and provide co-stimulatory signals more efficiently (Figure 4B) (68–71).

Alternatively, before T-cell interactions with cancer cells, the co-stimulatory signal on T-cells could be triggered by a bispecific aptamer targeted to abundant protein, such as VEGF that is secreted to the tumor stroma and linked to an agonistic aptamer specific for an inducible costimulatory receptor, such as 4-1BB. This approach has been tested in a murine model and was found to outperform the administration of an agonistic 4-1BB Ab or 4-1BB aptamer alone (Figure 4C) (72).

One of the first studies to explore the binding of antagonist RNA aptamers to T-cells expressing the negative co-stimulatory molecule

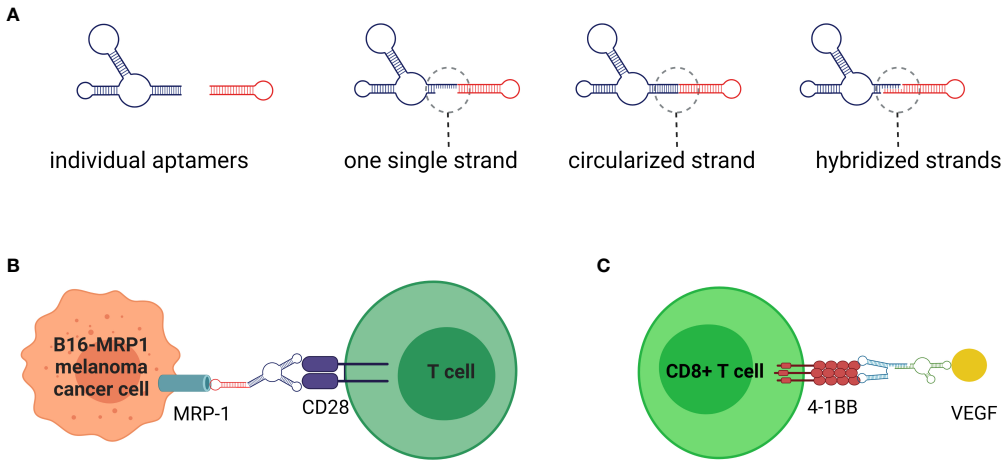

FIGURE 4
Aptamers are nucleic acids selected to specifically bind the molecules of interest in a similar manner to monoclonal antibodies. **(A)** Nanotechnology offers significant advantages in fusing individual aptamers to multivalent or bispecific molecules. Thus, by linking together the same or different aptamers, the increased binding affinity and/or ability to crosslink target cell receptors can be achieved. **(B)** Bispecific aptamers can promote cell-to-cell interactions with potential immunomodulatory applications. For example, a single stranded bispecific aptamer targeting CD28 on T cells and Multidrug-Resistant-associated Protein 1 (MRP1), involved in chemotherapy on B16 melanoma cancer cells, has been used to provide the necessary co-stimulatory signal for T cell activation. **(C)** Instead of cell membrane receptors that may be quickly internalized, an alternative strategy could be to target co-stimulatory signals to proteins (e.g., VEGF) overexpressed on tumor stroma.

CTLA-4 showed that integration of four individual aptamers into a tetravalent structure increased its bioactivity in a murine model (73). Similarly, linking two RNA aptamers targeting the co-stimulatory aptamer, exerted co-stimulatory activity on cytotoxic CD8+ T cells *in vitro* and promoted tumor rejection *in vivo* (74). An interesting functional change was described in two 2'-F modified RNA aptamers specific for the CD28 receptor for B7. Binding of one aptamer prevented co-stimulation *via* CD28, while binding of a second aptamer did not have a functional outcome. However, when both aptamers were linked together, either by double-strand linker or fusion into a single-strand molecule, their binding led to CD28-mediated activation (75). Gain of function upon assembly of aptamers on the scaffold was also observed in the T cell costimulatory receptor of T cells, which, in the monomer state, does not stimulate OX40. However, the annealing of two RNA aptamers to two separate complementary DNA oligonucleotides, linked by a polyethylene spacer, led to dimerization of OX40 and subsequent activation of downstream signaling (76). Indeed, the linking of individual aptamers in one complex represents a potentially versatile combinatorial therapeutic tool.

Although the principle of agonistic or antagonistic aptamers in immunomodulation is relatively straightforward, many technological and biological challenges remain. The engagement of aptamers with cell surface molecules implies their delivery in a naked form, which exposes them to degradation by serum nucleases. Traditionally, replacing natural nucleotides with chemical analogs, either during the SELEX process or post-selection, increases nucleic acid resistance to nucleases (77). After therapeutic application, aptamers, due to their small size, have a high chance of penetrating the tumor microenvironment. However, their small size negatively affects the rate of clearance, which is a contributor to half-life in the blood. To overcome their shorter half-life *in vivo*, a higher dose of aptamers might be required to increase their duration in the blood and allow for delivery to target tissues and cells.

The choice of target also determines the functional output. To prevent side effects, the selected target receptor molecule should ideally be as tumor cell specific as possible. Furthermore, receptor turnover rate is an important factor that affects the effectiveness of bispecific aptamers mediating cell-cell interactions. Rapid internalization with bound aptamer decreases the chance of establishing physical interactions between the cells. In other words, the receptor has to be displayed on the surface for sufficient time to allow the creation of a synapse between the immune and tumor cells.

Nucleic acid nanoparticles as intracellular modulators

NANPs are innovative scaffolds composed of rationally designed oligonucleotides or oligonucleotide chemical analogs. Because of their biocompatibility, functional versatility of nucleic acids, and tunability of their physicochemical and biological properties, NANPs have demonstrated strong potential for the development of future nanomedicine. Both RNA and DNA can form intra- or intermolecular hydrogen bonds *via* canonical base pairing, allowing for design and assembly of an almost limitless library of architecturally diverse nanoscaffolds with high batch to batch consistency (78, 79). The presence of a 2'-OH group in RNA ribose sugars enables RNA to adopt more sophisticated geometric optimization which expands the repertoire of possible hydrogen bonds classified in 12 geometric families (79–81). This is why RNA molecules naturally present a plethora of structural and long-range interacting motifs that can be engineered into NANPs with precisely controlled shapes (*e.g.*, 3D vs 2D vs 1D), sizes (10-100 nm), and compositions (RNA *vs* DNA *vs* chemical analogs); various functionalities and bioactive properties can be encoded in the NANPs' architectures (82–85) (Figures 5A, B). Functionalization of NANPs can be achieved *via* self-assembly of different TNAs, either

using toeholds or by incorporating TNAs directly into the sequences of nanoscaffolds. Both approaches allow the same NANP scaffolds to be formulated with different TNAs and other functionalities. For example, hexameric RNA rings have been designed to carry multiple aptamers (*e.g.*, specific for human epidermal growth factor receptor), siRNAs targeting various genes, and fluorophores for NANPs' visualization in cells and *in vivo* (82).

The psychochemical properties of NANPs are favorable for the pharmaceutical industry. Depending on the overall design principles and composition, various NANPs can be assembled under several simple protocols (Figure 5C). Assembled NANPs can be subsequently stored and transported in solution on ice or can be dehydrated and handled at ambient temperatures. In a recent study, several novel protocols for drying NANPs were compared with traditional lyophilization methods (86). It was discovered that while the light assisted drying (LAD) approach was fine-tunable and more reproducible in retention of NANP structures upon rehydration, this approach only allowed for processing a relatively small volume of NANPs solution, and processing of only one sample at the time. Lyophilization permits high throughput processing while also preserving structural stability of NANPs, but the retention of biological functionality becomes questionable. Addition of cryoprotectants such as trehalose seemed to aid in reducing the potential structural damage, but more investigation is necessary to reveal biological and immunomodulatory potential of trehalose preserved NANPs in clinical settings.

The physiochemical properties of nucleic acids also affect their immunostimulatory properties. Unsurprisingly, the immunorecognition of NANPs is dependent on nucleic acid composition, size, and dimensionality as PRRs recognize distinct ligand motifs (87–89). Using these parameters as predictive indicators of immunostimulatory properties, NANPs can be designed to either be immunoquiescent or enhance desired immunological responses. For example, the NANPs composed of DNA are consistently immunoquiescent when transfected into human immune cells but this was not the case for their RNA analogs (88). The proportion of DNA and RNA can be specified during construction of DNA/RNA hybrid NANPs for the desired immune response or lack thereof. Similarly, the vast library of planar and globular NANP shapes allows for further optimization of this immunomodulator scaffold. Globular 3D NANPs made of RNA induce the strongest immunorecognition while the fibrous 1D NANPs are the least immunostimulatory (90). Furthermore, incorporation of modified nucleic acids can be utilized to avoid certain recognitions *via* specific PRRs. For example, incorporation of 2'-fluoro modified pyrimidines in NANP strands abrogate TLR7-dependent immune responses (91).

NANPs complexed with TNAs display great promise as immune response modulators. Importantly, the NANP scaffold allows for

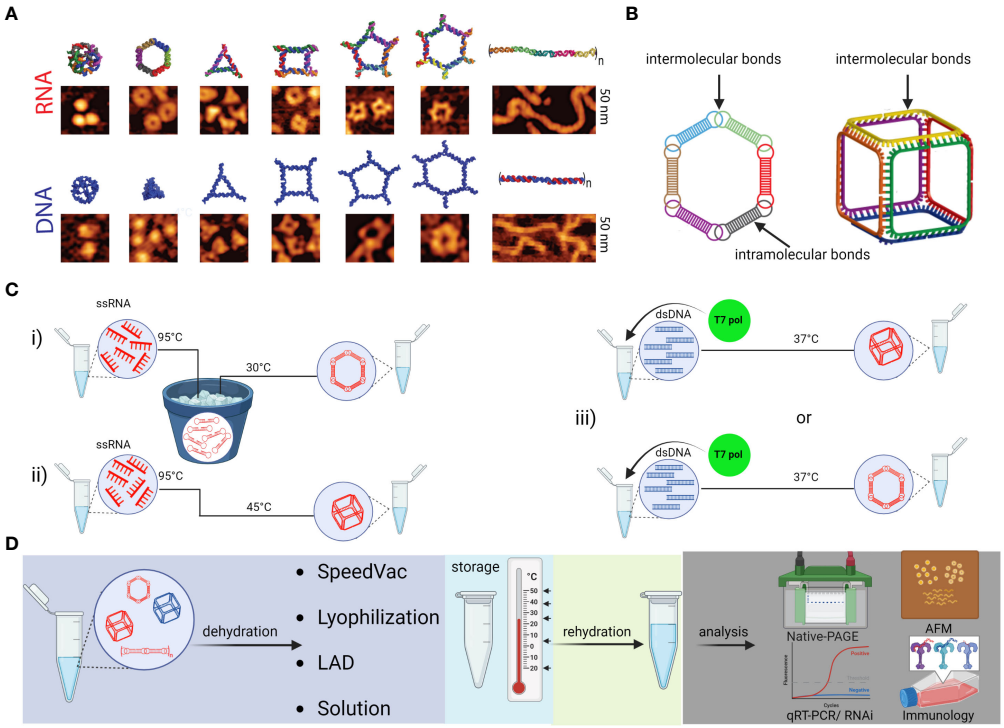

FIGURE 5
Schematic depiction of various NANPs, their production, characterization, storage, and handling. **(A)** Computational 3D visualization of individual NANPs with corresponding representative AFM images. **(B)** Two orthogonal NANPs design strategies are based either on the presence of both intra- and intermolecular or only intermolecular bonds, which also determine the assembly protocol of corresponding NANPs. **(C)** Several protocols for efficient one-pot NANPs self-assembly. Protocol (i) promotes secondary structure formation of individual monomers needed for NANPs assembly *via* long-range interacting motifs. For this assembly protocol, the individual ssRNAs are first denatured by heating at 95°C and then snap cooled on ice to form intramolecular Watson-Crick (W-C) bonds. The following incubation at 30°C in the presence of Mg^{2+} ions allows intermolecular bindings of monomers and assembly of NANPs. In (ii)> protocol, monomers form only intermolecular canonical Watson-Crick base pairs, thus no pre-folding is needed, and any intramolecular interactions should be avoided by design. The (iii) protocol allows for co-transcriptional assembly of different types of NANPs formed as their RNA strands are transcribed from dsDNA templates. **(D)** Assembled NANPs can be stored and transported in anhydrous forms at ambient temperatures. The impact on structure stability, immunorecognition, and functionality depends of dehydration protocol and needs to be checked after rehydration for each type of NANP.

controlled and coordinated delivery of multiple functional groups to the same cell (92). For example, the individual strands of NANPs functionalized with a combination of different TNAs and TNA-functionalized RNA ring nanoscaffolds that target all four variants of lysophosphatidylcholine acyltransferases (LPCATs) significantly increased susceptibility of melanoma cells to radiation treatment (93). Notably, recent evidence indicates that the orientation of added TNAs can additionally contribute to the immunostimulatory properties of NANPs. Accessibility of NANP components to PRR binding may contribute to the observed difference in their immunostimulation. For example, despite the number of 5'-ppp remaining constant for functional and non-functional NANPs, RIG-I was specifically activated in response to transfected NANPs that carried TNAs. The response for some orientations of TNAs was stronger than for others. This data indicates that the cytosolic sensor, RIG-I, can distinguish between non-functional and functional NANPs and the extent of functionalization (94).

Functional group delivery can be further controlled through the intracellular reassociation of RNA/DNA hybrid NANPs. In this scenario, a pair of complementary RNA/DNA hybrids are engineered to be non-functional by carrying various split RNA functionalities such as RNAi inducers and aptamers (95–98). When interdependent RNA/DNA hybrids are both present in the cytosol, there is complementary base-pairing at toehold regions that drive branch migrations and the release of functional groups (89, 95, 96). This system has been used to effectively deliver dicRNAi inducers for the knockdown of gene expression of HIV-1 and relevant oncogenes *in vitro* (83). Additionally, RNA/DNA fibers have been optimized to deliver and activate both RNAi inducers and DNA decoys, targeting NF-κB, a transcription factor that induces production of proinflammatory cytokines (Figure 6) (99). These NF-κB targeting NANPs display great promise for reducing inflammatory immune response, as the decoys function to prevent translocation of activated NF-κB to the nucleus. In addition, the RNAi inducers may serve to reduce overall NF-κB expression.

In summary, the immune responses elicited by functionalized NANPs depend on their shape. This has been previously shown where all RNA-made NANPs, when functionalized with TNAs on each monomer, induced high levels of type I (IFNα, IFNβ, and IFNω) and type III (IFNλ) IFN responses. IFN responses to RNA cubes, rings, and fibers where every monomer was functionalized were comparable to ODN2216, a CpG oligonucleotide, a known IFN inducer. However, when the fibers were only functionalized on every other monomer, IFN response were significantly decreased, indicating that the spacing between the functionalization groups plays an important role in PRR activation. This decrease in IFN responses was mirrored by decreases in the proinflammatory responses evoked by the NANPs with the same amount of siRNA delivered (83).

Combinations of different carriers and NANPs as intracellular modulators

In the absence of a carrier, the negative charge of all of our NANPs prevented penetration through biological membranes (88, 100). As such, a variety of carriers, including cationic lipids, liposomes, polymers, magnetic nanoparticles, mesoporous silica-based nanoparticles, and exosomes, most be employed as agents to protect against nuclease degradation and to facilitate delivery (91, 100–103). Furthermore, in the absence of a carrier, NANPs are essentially invisible to cells and so are immunoquiescent (104–106). This makes them perfect candidates for extracellular use (107). Cationic lipids and liposomes have been extensively explored as carriers for TNAs and can also serve as viable carrier options for NANPs. The transfection reagents lipofectamine and DOTAP have been previously employed to deliver NANPs to non-immune and immune cells (106, 108, 109). However, the use of Lipofectamine 2000 as a carrier is limited to *in vitro* cell delivery. Alternatively, cationic bolaamphiplies form highly stable delivery vesicles that can be utilized *in vitro* and *in vivo* due to low toxicity. Notably, bolaamphiplies are a promising carrier as previous studies indicate that they deliver siRNAs across biological barriers, including the blood brain barrier (110, 111). Similar to lipid-based carriers, polymers, such as polyethylenimine (PEI), poly(β-amino esters), polyamidoamine (PAMAM) dendrimers, and branched PEI, can be employed to deliver TNAs (100, 101, 112). The cationic, amphiphilic co-polymer, poly(lactide-co-glycolide)-grafted-polyethylenimine (PgP) is a micelle forming co-polymer that can deliver both TNAs and TNA functionalized NANPs to multiple cell types *in vitro* (100) (95). Recent data also indicates that PgP effectively delivers functional NANPs following retro-orbital administration in mice models. Similar to PgP, due to electrostatic interactions, NANPs can be complexed with cationic PAMAM dendrimers (101). These dendrimers facilitate NANP uptake to adherent cell lines and PBMCs. Finally, exosomes, 30 – 150 nm vesicles released upon fusion of multivesicular bodies with the cell membrane, mirror the characteristics of the parent cell. Exosomes facilitate cellular communication as cargo is delivered to neighboring cells by either receptor-mediated endocytosis, micropinocytosis, or membrane fusion. Exosomes have been documented to effectively deliver TNAs and functional NANPs *in vitro* and in murine *in vivo* models to target cells and/or tissues (113, 114). Exosomes also defend against nuclease degradation and efficiently deliver NANPs of differing three dimensional conformations functionalized with siRNA.

Importantly, carrier selection affects NANP immunostimulatory properties. First, the carriers discussed above can have immunostimulatory properties independent of the NANPs. Additionally, carrier selection determines both the efficiency of NANP delivery to specific cell types and the cellular route of NANP entry (91). NANPs complexed with lipid-based carriers have been demonstrated to first traffic through an endosomal compartment prior to delivery to the cytosol (88, 91). RNA cubes, rings, and fibers stimulate varying degrees of proinflammatory and IFN responses in part due to recognition *via* endosomal TLRs. In contrast to lipofectamine delivery, using a cationic amphiphilic co-polymer carrier stimulates reduced inflammatory cytokine production and no IFN production (100) Likewise, NANPs delivered with dendrimers are largely immunoquiescent (101).

Due to highly cell type specific expression and subcellular localization of PRRs, carrier selection can also impact nucleic acid sensor detection of NANPs thereby altering the subsequent immune responses. Previous studies using human peripheral blood mononuclear cells have indicated that plasmacytoid dendritic cells are the primary producers of IFNs following delivery of NANPs

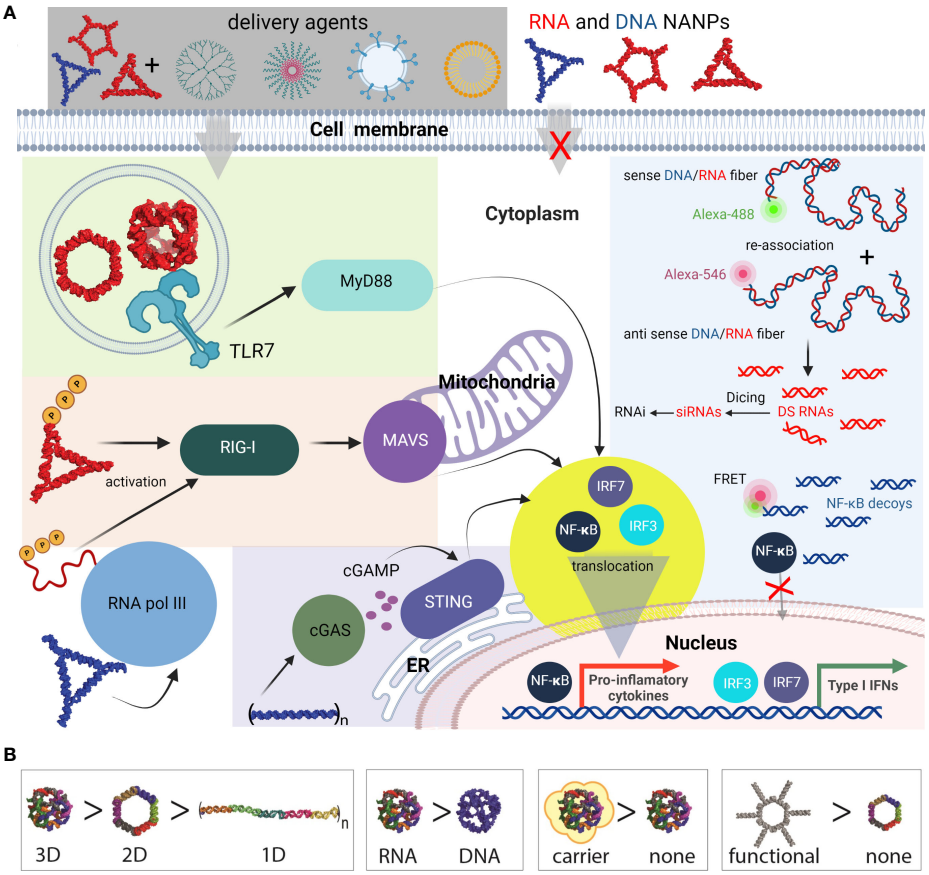

FIGURE 6
Most common innate pathways shown to be activated upon NANPs internalization. **(A)** Intracellular delivery of NANPs requires carriers; naked NANPs are immunoquiescent due to their ineffective crossing of biological membranes. Delivery of RNA rings and cubes trigger the immune system through TLR7. By-passing of TLR sensing can be compensated by RIG-I that can detect RNA NANPs bearing 5′ triphosphates. DNA containing NANPs can be sensed after promoter independent transcription of NANPs strands by RNA pol III. DNA fibers stimulate cellular immunity through cGAS-cGAMP-STING pathway. Additionally, interdependent DNA/RNA fiber NANPs can be rationally designed to release of RNAi inducers and NF-κB decoys upon their intracellular re-association. This results in gene specific silencing while simultaneously blocking NF-kB translocation to nucleus thus lowering the proinflammatory immune responses. **(B)** Some of the architectural and compositional parameters that define immunorecognition of NANPs.

complexed with a lipid-based carrier (88, 91, 106). Notably, this observation supports results in reporter cell-lines indicating that RNA cubes and rings activate TLR7 and TLR9 as plasmacytoid dendritic cells are known to express the endosomal Toll-like receptors, TLR7 and TLR9.

NANPs can be designed to have switchable, tunable, and programable properties for a number of applications. As noted above, RNA cubes are the most immunostimulatory. While similar in shape, DNA and RNA cubes have different immune responses for the same carriers; RNA cubes induce significant amounts of IFNα and IFNω, while DNA cubes only produce IFNβ and IFNλ. RNA- and DNA-based rings have been found to be more immunostimulatory than their fiber counterparts (88). NANPs have been designed to interact with the immune system *via* their structure (88) and used to address specific biochemical problems (99, 115, 116). This includes the use of NANPs as scaffolds to carry TNAs with controlled and tunable immunostimulants (113) and the use of functionalized NANPs to silence specific genes to inhibit virus production (82). This has been achieved through the application of our knowledge of the structure and function of natural and artificial classes of nucleic acids to NANP structure. Furthermore, known therapeutics and targeting agents can be attached to NANPs, and used for drug delivery, biosensing, and as molecular devices (89, 95, 115, 117–119).

Together, these studies indicate that cellular responses to NANPs is dependent on their structure, composition, and functionalization, in addition to type of carrier employed for intracellular delivery. Previous work has shown trends in the degree of immune response based on the previously mentioned design features (106) (101). Differences in dimensionality (1D, 2D, and 3D), composition (DNA or RNA), and connectivity (intramolecular, intermolecular, or both) evoke varying immune responses and enable NANPs to be customized based on the intended therapeutic effect (107). The field of therapeutic nucleic acids continues to advance and holds the promise of the development of versatile new means to manipulate host cell machinery to achieve a desired therapeutic effect in the absence of detrimental recipient responses (120, 121).

Translation of immunomodulatory nucleic acid therapeutics to the clinic

The immunomodulatory nucleic acids can be divided to two groups. In the first group, nucleic acids deliver genetic information that translates to immunogenic/immunomodulatory proteins such as chimeric antigen (CAR-T therapy) or nucleic acid-based vaccines (mRNA vaccines and adenovirus delivered vaccines). The second group contains noncoding nucleic acids that directly interact with proteins involved in immune pathways.

Noncoding nucleic acid-based therapeutics are only slowly entering medical use. Since 1998, when first oligonucleotide drug, Vitravene (also known as Fomivirsen) was approved by the FDA, only 15 non-coding oligonucleotides have been approved for clinical use. This group contains nine antisense oligonucleotides (ASOs), four siRNAs, one aptamer, and one natural oligonucleotide product made by depolymerization of porcine intestinal mucosal DNA (122–124) (Figure 7A). Six of these formulations are administered subcutaneously, another six are administered intravenously, two intravitreally, and one intrathecally (Figure 7B). However, none of the approved oligonucleotides are intended to be immunostimulatory. Recently, several clinical trials of a short synthetic RNA ligand that is selective for RIG-I, RGT100, have been conducted. One of these studies employing such a ligand (MK-4621) has been terminated due to business concerns (125), but this agent was found to activate RIG-I and contribute to modest antitumor activity, albeit with no substantial improvement over current treatments (125). In addition to antitumor activity, RIG-I agonists have been examined in preclinical trials as antiviral agents (126). Specifically, short hairpin RNA SLR14 complexed with polyethyleneimine was found to protect against SARS-CoV-2 infection in human angiotensin-converting enzyme 2 transgenic mice (126).

Rintatolimod is a dsRNA composed of inosinic and cytidylic acid residues that stimulates TLR3 but not cytosolic helicases. In addition, it activates 2′-5′ adenylate synthetase. First identified in the 1970s, rintatolimod has been tested clinically for the treatment of various conditions including breast and ovarian cancers and HIV infections. However, to date, the FDA has only granted it an orphan drug designation status for patients with pancreatic cancer in 2020 and the treatment of Ebola virus infection in 2022 (127). It is currently in Phase II and III double-blinded, randomized, placebo-controlled clinical trials for the treatment of chronic fatigue syndrome/myalgic encephalomyelitis (CFS/ME), and has shown promising results (128, 129).

Another group of noncoding immunomodulatory RNAs that are being tested in clinical trials include two spiegelmers, the L-stereoisomer RNA acid aptamers (130). PEGylated NOX-E36 binds the chemokine CCL2 thereby preventing the infiltration of CCR2-dependent tumor associated macrophages that initiate tumor-supporting angiogenesis (131, 132). In contrast, the NOX-A12 spiegelmer's target is CXCL12 that is implicated in the exclusion of T cells from the tumor microenvironment, and so blocking the actions of this chemokine should lead to increased protective T-cell infiltration. Excitingly, NOX-A12 has recently been studied in patients with advance stage colorectal and pancreatic cancer where it has been shown positive synergistic effects when combined with the PD1 immune checkpoint inhibitor, Pembrolizumab (133, 134).

Summary

Innate immunity is an evolutionary conserved network that provides immediate protection and precipitates specific and long-term adaptive immunity. In addition to providing defense against infectious organisms, the innate immune system can recognize danger signals that originate from cell stress and/or tissue injury. The integration of a wide range of signaling pathways initiated by exogenous and endogenous stimuli culminates in the expression of genes that underlie responses that include inflammation. The existence of certain types of nucleic acids and their cellular location is closely monitored by PRRs. These molecules play an important role in distinguishing foreign or altered self-nucleic acids, or their presence in appropriate locations, that can be manifestations of viral and bacterial infection or cellular damage/transformation. Due to their physicochemical properties, biocompatibility, and easy synthesis, nucleic acids may represent an ideal tool to manipulate the immune system. Immunogenic motifs from virus transcripts or RNA genomes can be derived and synthetically selected sequences or

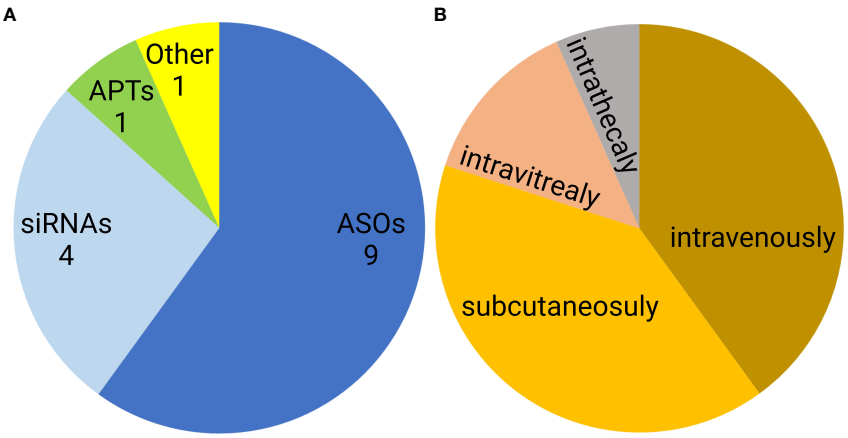

FIGURE 7
Distribution of FDA approved noncoding nucleic acid therapeutics according to type **(A)** and route of administration **(B)**. ASO- antisense oligonucleotides, siRNAs- small interfering RNAs, APTs- aptamers.

cellular ncRNAs can be employed. However, the potency of individual immunogenic ncRNAs is currently unknown and their activity is likely to differ based upon the particular application. However, the use of NANP nanotechnology alone has already identified many of the properties, such as composition, architectural parameters, dimensionality, size, and chemical stability, that define the immunogenicity of such structures (135). The complications experienced in translating simple TNAs to clinical therapies are also important considerations for complex NANPs, but it should be noted that the properties of NANPs are more than the sum of their constitutive parts (120). While resistance to nucleases and renal clearance can be solved relatively easily, other safety and efficacy concerns remain challenging. Targeted delivery, barrier penetration, and toxicity, remain the principal obstacles for nucleic acid therapeutics. This problem is compounded by the current nonexistence of FDA guidance documents for such agents, in contrast to other strategies including gene therapy. Another issue is the scalability of NANP synthesis for mass production and the present lack of simple and unified assembly protocols.

Despite these issues, it is clear that NANP technology holds great promise and has high therapeutic potential. Over the last decade, we and others have explored the possibility of multifunctional NANPs that carry diverse functional moieties (aptamers, siRNAs, ASOs, decoys, etc.). It now remains to combine immunostimulatory ncRNAs with NANP scaffolds to create new multi-tasking NANPs that permit conditional activation as the next generation of nucleic acid-based theranostics.

Author contributions

All authors listed have made a substantial, direct, and intellectual contribution to the work and approved it for publication.

Funding

Research reported in this publication was supported by the National Institute of General Medical Sciences of the National Institutes of Health under Award Number R35GM139587 (to KA). The content is solely the responsibility of the authors and does not necessarily represent the official views of the National Institutes of Health. MP's work on the subject was partially supported by the VEGA grant 1/0869/21.

Acknowledgments

All figures were made with BioRender (www.biorender.com).

Conflict of interest

The authors declare that the research was conducted in the absence of any commercial or financial relationships that could be construed as a potential conflict of interest.

Publisher's note

All claims expressed in this article are solely those of the authors and do not necessarily represent those of their affiliated organizations, or those of the publisher, the editors and the reviewers. Any product that may be evaluated in this article, or claim that may be made by its manufacturer, is not guaranteed or endorsed by the publisher.

References

1. Bernheim A, Sorek R. The pan-immune system of bacteria: Antiviral defence as a community resource. *Nat Rev Microbiol* (2020) 18(2):113–9. doi: 10.1038/s41579-019-0278-2

2. Gao LA, Wilkinson ME, Strecker J, Makarova KS, Macrae RK, Koonin EV, et al. Prokaryotic innate immunity through pattern recognition of conserved viral proteins. *Science* (2022) 377(6607):eabm4096. doi: 10.1126/science.abm4096

3. Dimitriu T, Szczelkun MD, Westra ER. Evolutionary ecology and interplay of prokaryotic innate and adaptive immune systems. *Curr Biol* (2020) 30(19):R1189–R202. doi: 10.1016/j.cub.2020.08.028

4. Marraffini LA. CRISPR-cas immunity in prokaryotes. *Nature* (2015) 526(7571):55–61. doi: 10.1038/nature15386

5. Hille F, Richter H, Wong SP, Bratovic M, Ressel S, Charpentier E. The biology of CRISPR-cas: Backward and forward. *Cell* (2018) 172(6):1239–59. doi: 10.1016/j.cell.2017.11.032

6. Li H, Li WX, Ding SW. Induction and suppression of RNA silencing by an animal virus. *Science* (2002) 296(5571):1319–21. doi: 10.1126/science.1070948

7. Guo Z, Li Y, Ding SW. Small RNA-based antimicrobial immunity. *Nat Rev Immunol* (2019) 19(1):31–44. doi: 10.1038/s41577-018-0071-x

8. Randow F, MacMicking JD, James LC. Cellular self-defense: How cell-autonomous immunity protects against pathogens. *Science* (2013) 340(6133):701–6. doi: 10.1126/science.1233028

9. Tan X, Sun L, Chen J, Chen ZJ. Detection of microbial infections through innate immune sensing of nucleic acids. *Annu Rev Microbiol* (2018) 72:447–78. doi: 10.1146/annurev-micro-102215-095605

10. Figueiredo RT, Carneiro LA, Bozza MT. Fungal surface and innate immune recognition of filamentous fungi. *Front Microbiol* (2011) 2:248. doi: 10.3389/fmicb.2011.00248

11. Roh JS, Sohn DH. Damage-associated molecular patterns in inflammatory diseases. *Immune Netw* (2018) 18(4):e27. doi: 10.4110/in.2018.18.e27

12. Alexopoulou L, Holt AC, Medzhitov R, Flavell RA. Recognition of double-stranded RNA and activation of NF-kB by toll-like receptor 3. *Nature* (2001) 413(6857):732–8. doi: 10.1038/35099560

13. Ranjith-Kumar CT, Miller W, Xiong J, Russell WK, Lamb R, Santos J, et al. Biochemical and functional analyses of the human toll-like receptor 3 ectodomain. *J Biol Chem* (2007) 282(10):7668–78. doi: 10.1074/jbc.m610946200

14. Jacobs BL, Langland JO. When two strands are better than one: The mediators and modulators of the cellular responses to double-stranded RNA. *Virology* (1996) 219 (2):339–49. doi: 10.1006/viro.1996.0259

15. Diebold SS, Montoya M, Unger H, Alexopoulou L, Roy P, Haswell LE, et al. Viral infection switches non-plasmacytoid dendritic cells into high interferon producers. *Nature* (2003) 424(6946):324–8. doi: 10.1038/nature01783

16. Zhang Z, Ohto U, Shibata T, Taoka M, Yamauchi Y, Sato R, et al. Structural analyses of toll-like receptor 7 reveal detailed RNA sequence specificity and recognition mechanism of agonistic ligands. *Cell Rep* (2018) 25(12):3371–81.e5. doi: 10.1016/j.celrep.2018.11.081

17. Gorden KB, Gorski KS, Gibson SJ, Kedl RM, Kieper WC, Qiu X, et al. Synthetic TLR agonists reveal functional differences between human TLR7 and TLR8. *J Immunol* (2005) 174(3):1259–68. doi: 10.4049/jimmunol.174.3.1259

18. De Marcken M, Dhaliwal K, Danielsen AC, Gautron AS, Dominguez-Villar M. TLR7 and TLR8 activate distinct pathways in monocytes during RNA virus infection. *Sci Signaling* (2019) 12(605):eaaw1347. doi: 10.1126/scisignal.aaw1347

19. Heil F. Species-specific recognition of single-stranded RNA *Via* toll-like receptor 7 and 8. *Science* (2004) 303(5663):1526–9. doi: 10.1126/science.1093620

20. Latz E, Visintin A, Espevik T, Golenbock DT. Mechanisms of TLR9 activation. *J Endotoxin Res* (2004) 10(6):406–12. doi: 10.1179/096805104225006525

21. Akira S. Toll-like receptors and innate immunity. *Adv Immunol* (2001) 78:1–56. doi: 10.1016/s0065-2776(01)78001-7

22. Zheng C, Chen J, Chu F, Zhu J, Jin T. Inflammatory role of TLR-MyD88 signaling in multiple sclerosis. *Front Mol Neurosci* (2019) 12:314. doi: 10.3389/fnmol.2019.00314

23. Ullah MO, Sweet MJ, Mansell A, Kellie S, Kobe B. TRIF-dependent TLR signaling, its functions in host defense and inflammation, and its potential as a therapeutic target. *J Leukocyte Biol* (2016) 100(1):27–45. doi: 10.1189/jlb.2RI1115-531R

24. Loo Y-M, Gale M. Immune signaling by RIG-I-Like receptors. *Immunity* (2011) 34 (5):680–92. doi: 10.1016/j.immuni.2011.05.003

25. Thoresen D, Wang W, Galls D, Guo R, Xu L, Pyle AM. The molecular mechanism of RIG-I activation and signaling. *Immunol Rev* (2021) 304(1):154–68. doi: 10.1111/imr.13022

26. Pichlmair A, Schulz O, Tan CP, Naslund TI, Liljestrom P, Weber F, et al. RIG-I-Mediated antiviral responses to single-stranded RNA bearing 5'-phosphates. *Science* (2006) 314(5801):997–1001. doi: 10.1126/science.1132998

27. Hwang S-Y, Sun H-Y, Lee K-H, Oh B-H, Cha YJ, Kim BH, et al. 5'-Triphosphate-RNA-Independent activation of RIG-I *Via* RNA aptamer with enhanced antiviral activity. *Nucleic Acids Res* (2012) 40(6):2724–33. doi: 10.1093/nar/gkr1098

28. Chiu YH, Macmillan JB, Chen ZJ. RNA Polymerase III detects cytosolic DNA and induces type I interferons through the RIG-I pathway. *Cell* (2009) 138(3):576–91. doi: 10.1016/j.cell.2009.06.015

29. Zhang Y, Dittmer DP, Mieczkowski PA, Host KM, Fusco WG, Duncan JA, et al. RIG-I detects kaposi's sarcoma-associated herpesvirus transcripts in a RNA polymerase III-independent manner. *Mbio* (2018) 9(4). doi: 10.1128/mBio.00823-18

30. Kessler AC, Maraia RJ. The nuclear and cytoplasmic activities of RNA polymerase III, and an evolving transcriptome for surveillance. *Nucleic Acids Res* (2021) 49 (21):12017–34. doi: 10.1093/nar/gkab1145

31. Graczyk D, White RJ, Ryan KM. Involvement of RNA polymerase III in immune responses. *Mol Cell Biol* (2015) 35(10):1848–59. doi: 10.1128/MCB.00990-14

32. Nabet BY, Qiu Y, Shabason JE, Wu TJ, Yoon T, Kim BC, et al. Exosome RNA unshielding couples stromal activation to pattern recognition receptor signaling in cancer. *Cell* (2017) 170(2):352–66e13. doi: 10.1016/j.cell.2017.06.031

33. Zevini A, Olagnier D, Hiscott J. Crosstalk between cytoplasmic RIG-I and sting sensing pathways. *Trends Immunol* (2017) 38(3):194–205. doi: 10.1016/j.it.2016.12.004

34. Tan RS, Ho B, Leung BP, Ding JL. TLR cross-talk confers specificity to innate immunity. *Int Rev Immunol* (2014) 33(6):443–53. doi: 10.3109/08830185.2014.921164

35. Palazzo M, Gariboldi S, Zanobbio L, Dusio GF, Selleri S, Bedoni M, et al. Cross-talk among toll-like receptors and their ligands. *Int Immunol* (2008) 20(5):709–18. doi: 10.1093/intimm/dxn027

36. Kawai T, Akira S. Toll-like receptors and their crosstalk with other innate receptors in infection and immunity. *Immunity* (2011) 34(5):637–50. doi: 10.1016/j.immuni.2011.05.006

37. Hopfner KP, Hornung V. Molecular mechanisms and cellular functions of cGAS-STING signalling. *Nat Rev Mol Cell Biol* (2020) 21(9):501–21. doi: 10.1038/s41580-020-0244-x

38. Gui X, Yang H, Li T, Tan X, Shi P, Li M, et al. Autophagy induction *Via* sting trafficking is a primordial function of the cGAS pathway. *Nature* (2019) 567(7747):262–6. doi: 10.1038/s41586-019-1006-9

39. Munz C. Antigen processing for MHC class II presentation *Via* autophagy. *Front Immunol* (2012) 3:9. doi: 10.3389/fimmu.2012.00009

40. Sadler AJ, Williams BRG. Interferon-inducible antiviral effectors. *Nat Rev Immunol* (2008) 8(7):559–68. doi: 10.1038/nri2314

41. McWhirter SM, Jefferies CA. Nucleic acid sensors as therapeutic targets for human disease. *Immunity* (2020) 53(1):78–97. doi: 10.1016/j.immuni.2020.04.004

42. Macedo AB, Novis CL, De Assis CM, Sorensen ES, Moszczynski P, Huang SH, et al. Dual TLR2 and TLR7 agonists as HIV latency-reversing agents. *JCI Insight* (2018) 3 (19). doi: 10.1172/jci.insight.122673

43. Lim SY, Osuna CE, Hraber PT, Hesselgesser J, Gerold JM, Barnes TL, et al. TLR7 agonists induce transient viremia and reduce the viral reservoir in SIV-infected rhesus macaques on antiretroviral therapy. *Sci Transl Med* (2018) 10(439). doi: 10.1126/scitranslmed.aao4521

44. Vibholm LK, Konrad CV, Schleimann MH, Frattari G, Winckelmann A, Klastrup V, et al. Effects of 24-week toll-like receptor 9 agonist treatment in HIV type 1+ individuals. *AIDS* (2019) 33(8):1315–25. doi: 10.1097/QAD.0000000000002213

45. Hogenesch H. Mechanism of immunopotentiation and safety of aluminum adjuvants. *Front Immunol* (2012) 3:406. doi: 10.3389/fimmu.2012.00406

46. Temizoz B, Kuroda E, Ishii KJ. Combination and inducible adjuvants targeting nucleic acid sensors. *Curr Opin Pharmacol* (2018) 41:104–13. doi: 10.1016/j.coph.2018.05.003

47. Desmet CJ, Ishii KJ. Nucleic acid sensing at the interface between innate and adaptive immunity in vaccination. *Nat Rev Immunol* (2012) 12(7):479–91. doi: 10.1038/nri3247

48. Junt T, Barchet W. Translating nucleic acid-sensing pathways into therapies. *Nat Rev Immunol* (2015) 15(9):529–44. doi: 10.1038/nri3875

49. Martins KA, Bavari S, Salazar AM. Vaccine adjuvant uses of poly-IC and derivatives. *Expert Rev Vaccines* (2015) 14(3):447–59. doi: 10.1586/14760584.2015.966085

50. Longhi MP, Trumpfheller C, Idoyaga J, Caskey M, Matos I, Kluger C, et al. Dendritic cells require a systemic type I interferon response to mature and induce CD4+ Th1 immunity with poly IC as adjuvant. *J Exp Med* (2009) 206(7):1589–602. doi: 10.1084/jem.20090247

51. Fox CB, Orr MT, Van Hoeven N, Parker SC, Mikasa TJ, Phan T, et al. Adsorption of a synthetic TLR7/8 ligand to aluminum oxyhydroxide for enhanced vaccine adjuvant activity: A formulation approach. *J Control Release* (2016) 244(Pt A):98–107. doi: 10.1016/j.jconrel.2016.11.011

52. Wang J, Li P, Yu Y, Fu Y, Jiang H, Lu M, et al. Pulmonary surfactant-biomimetic nanoparticles potentiate heterosubtypic influenza immunity. *Science* (2020) 367(6480). doi: 10.1126/science.aau0810

53. Cech T, Steitz JA, Atkins JF. *RNA Worlds : New tools for deep exploration. 2nd ed*. Cold Spring Harbor, New York: Cold Spring Harbor Laboratory Press (2019).

54. Iurescia S, Fioretti D, Rinaldi M. Nucleic acid sensing machinery: Targeting innate immune system for cancer therapy. *Recent Pat Anticancer Drug Discovery* (2018) 13(1):2–17. doi: 10.2174/1574892812666171030163804

55. Ranoa DRE, Parekh AD, Pitroda SP, Huang X, Darga T, Wong AC, et al. Cancer therapies activate RIG-i-like receptor pathway through endogenous non-coding RNAs. *Oncotarget* (2016) 7(18):26496–515. doi: 10.18632/oncotarget.8420

56. Ellermeier J, Wei J, Duewell P, Hoves S, Stieg MR, Adunka T, et al. Therapeutic efficacy of bifunctional siRNA combining TGF-β1 silencing with RIG-I activation in pancreatic cancer. *Cancer Res* (2013) 73(6):1709–20. doi: 10.1158/0008-5472.CAN-11-3850

57. Duewell P, Steger A, Lohr H, Bourhis H, Hoelz H, Kirchleitner SV, et al. RIG-i-like helicases induce immunogenic cell death of pancreatic cancer cells and sensitize tumors toward killing by CD8(+) T cells. *Cell Death Differ* (2014) 21(12):1825–37. doi: 10.1038/cdd.2014.96

58. Demaria O, Cornen S, Daeron M, Morel Y, Medzhitov R, Vivier E. Harnessing innate immunity in cancer therapy. *Nature* (2019) 574(7776):45–56. doi: 10.1038/s41586-019-1593-5

59. Elion DL, Cook RS. Harnessing RIG-I and intrinsic immunity in the tumor microenvironment for therapeutic cancer treatment. *Oncotarget* (2018) 9(48):29007–17. doi: 10.18632/oncotarget.25626

60. Elion DL, Jacobson ME, Hicks DJ, Rahman B, Sanchez V, Gonzales-Ericsson PI, et al. Therapeutically active RIG-I agonist induces immunogenic tumor cell killing in breast cancers. *Cancer Res* (2018) 78(21):6183–95. doi: 10.1158/0008-5472.CAN-18-0730

61. Heidegger S, Kreppel D, Bscheider M, Stritzke F, Nedelko T, Wintges A, et al. RIG-I activating immunostimulatory RNA boosts the efficacy of anticancer vaccines and synergizes with immune checkpoint blockade. *EBioMedicine* (2019) 41:146–55. doi: 10.1016/j.ebiom.2019.02.056

62. Poeck H, Besch R, Maihoefer C, Renn M, Tormo D, Morskaya SS, et al. 5'-Triphosphate-siRNA: Turning gene silencing and RIG-I activation against melanoma. *Nat Med* (2008) 14(11):1256–63. doi: 10.1038/nm.1887

63. Kalluri R. The biology and function of fibroblasts in cancer. *Nat Rev Cancer* (2016) 16(9):582–98. doi: 10.1038/nrc.2016.73

64. Johnson LR, Lee DY, Eacret JS, Ye D, June CH, Minn AJ. The immunostimulatory RNA RN7SL1 enables CAR-T cells to enhance autonomous and endogenous immune function. *Cell* (2021) 184(19):4981–95.e14. doi: 10.1016/j.cell.2021.08.004

65. Jiang M, Zhang S, Yang Z, Lin H, Zhu J, Liu L, et al. Self-recognition of an inducible host lncRNA by RIG-I feedback restricts innate immune response. *Cell* (2018) 173 (4):906–19.e13. doi: 10.1016/j.cell.2018.03.064

66. Sola M, Menon AP, Moreno B, Meraviglia-Crivelli D, Soldevilla MM, Carton-Garcia F, et al. Aptamers against live targets: Is in vivo SELEX finally coming to the edge? *Mol Ther Nucleic Acids* (2020) 21:192–204. doi: 10.1016/j.omtn.2020.05.025

67. Lentz RW, Colton MD, Mitra SS, Messersmith WA. Innate immune checkpoint inhibitors: The next breakthrough in medical oncology? *Mol Cancer Ther* (2021) 20 (6):961–74. doi: 10.1158/1535-7163.MCT-21-0041

68. Thomas BJ, Porciani D, Burke DH. Cancer immunomodulation using bispecific aptamers. *Mol Ther Nucleic Acids* (2022) 27:894–915. doi: 10.1016/j.omtn.2022.01.008

69. Liu X, Yan H, Liu Y, Chang Y. Targeted cell-cell interactions by DNA nanoscaffold-templated multivalent bispecific aptamers. *Small* (2011) 7(12):1673–82. doi: 10.1002/smll.201002292

70. Soldevilla MM, Villanueva H, Casares N, Lasarte JJ, Bendandi M, Inoges S, et al. MRP1-CD28 bi-specific oligonucleotide aptamers: Target costimulation to drug-resistant melanoma cancer stem cells. *Oncotarget* (2016) 7(17):23182–96. doi: 10.18632/oncotarget.8095

71. Pastor F, Kolonias D, McNamara JO, Gilboa E. Targeting 4-1BB costimulation to disseminated tumor lesions with bi-specific oligonucleotide aptamers. *Mol Ther* (2011) 19 (10):1878–86. doi: 10.1038/mt.2011.145

72. Schrand B, Berezhnoy A, Brenneman R, Williams A, Levay A, Kong L-Y, et al. Targeting 4-1BB costimulation to the tumor stroma with bispecific aptamer conjugates enhances the therapeutic index of tumor immunotherapy. *Cancer Immunol Res* (2014) 2 (9):867–77. doi: 10.1158/2326-6066.CIR-14-0007

73. Santulli-Marotto S, Nair SK, Rusconi C, Sullenger B, Gilboa E. Multivalent RNA aptamers that inhibit CTLA-4 and enhance tumor immunity. *Cancer Res* (2003) 63 (21):7483–9.

74. McNamara JO, Kolonias D, Pastor F, Mittler RS, Chen L, Giangrande PH, et al. Multivalent 4-1BB binding aptamers costimulate CD8+ T cells and inhibit tumor growth in mice. *Crit Rev Microbiol* (2008) 118(1):376–86. doi: 10.1172/JCI33365

75. Soldevilla MM, Villanueva H, Bendandi M, Inoges S, López-Díaz de Cerio A, Pastor F. 2-Fluoro-RNA oligonucleotide CD40 targeted aptamers for the control of b

lymphoma and bone-marrow aplasia. *Biomaterials* (2015) 67:274–85. doi: 10.1016/j.biomaterials.2015.07.020

76. Dollins CM, Nair S, Boczkowski D, Lee J, Layzer JM, Gilboa E, et al. Assembling OX40 aptamers on a molecular scaffold to create a receptor-activating aptamer. *Chem Biol* (2008) 15(7):675–82. doi: 10.1016/j.chembiol.2008.05.016

77. Agnello L, Camorani S, Fedele M, Cerchia L. Aptamers and antibodies: Rivals or allies in cancer targeted therapy? *Explor Target Antitumor Ther* (2021) 2(1):107–21. doi: 10.37349/etat.2021.00035

78. Nagaswamy U, Voss N, Zhang Z, Fox GE. Database of non-canonical base pairs found in known RNA structures. *Nucleic Acids Res* (2000) 28(1):375–6. doi: 10.1093/nar/28.1.375

79. Bhattacharyya D, Mitra A. Canonical and non-canonical base pairs in DNA or RNA: Structure, function and dynamics . Available at: https://osf.io/suhpw/download.

80. Velema WA, Kool ET. The chemistry and applications of RNA 2′-OH acylation. *Nat Rev Chem* (2020) 4(1):22–37. doi: 10.1038/s41570-019-0147-6

81. Leontis NB, Westhof E. Geometric nomenclature and classification of RNA base pairs. *RNA* (2001) 7(4):499–512. doi: 10.1017/s1355838201002515

82. Afonin KA, Viard M, Koyfman AY, Martins AN, Kasprzak WK, Panigaj M, et al. Multifunctional RNA nanoparticles. *Nano Lett* (2014) 14(10):5662–71. doi: 10.1021/nl502385k

83. Rackley L, Stewart JM, Salotti J, Krokhotin A, Shah A, Halman JR, et al. RNA Fibers as optimized nanoscaffolds for siRNA coordination and reduced immunological recognition. *Adv Funct Mater* (2018) 28(48). doi: 10.1002/adfm.201805959

84. Afonin KA, Kasprzak WK, Bindewald E, Kireeva M, Viard M, Kashlev M, et al. In silico design and enzymatic synthesis of functional RNA nanoparticles. *Acc Chem Res* (2014) 47(6):1731–41. doi: 10.1021/ar400329z

85. Afonin KA, Bindewald E, Yaghoubian AJ, Voss N, Jacovetty E, Shapiro BA, et al. *In vitro* assembly of cubic RNA-based scaffolds designed in silico. *Nat Nanotechnol* (2010) 5(9):676–82. doi: 10.1038/nnano.2010.160

86. Tran AN, Chandler M, Halman J, Beasock D, Fessler A, McKeough RQ, et al. Anhydrous nucleic acid nanoparticles for storage and handling at broad range of temperatures. *Small* (2022) 18(13):e2104814. doi: 10.1002/smll.202104814

87. Johnson MB, Halman JR, Satterwhite E, Zakharov AV, Bui MN, Benkato K, et al. Programmable nucleic acid based polygons with controlled neuroimmunomodulatory properties for predictive QSAR modeling. *Small* (2017) 13(42). doi: 10.1002/smll.201701255

88. Hong E, Halman JR, Shah AB, Khisamutdinov EF, Dobrovolskaia MA, Afonin KA. Structure and composition define immunorecognition of nucleic acid nanoparticles. *Nano Lett* (2018) 18(7):4309–21. doi: 10.1021/acs.nanolett.8b01283

89. Halman JR, Satterwhite E, Roark B, Chandler M, Viard M, Ivanina A, et al. Functionally-interdependent shape-switching nanoparticles with controllable properties. *Nucleic Acids Res* (2017) 45(4):2210–20. doi: 10.1093/nar/gkx008

90. Chandler M, Afonin KA. Smart-responsive nucleic acid nanoparticles (NANPs) with the potential to modulate immune behavior. *Nanomaterials (Basel)* (2019) 9(4). doi: 10.3390/nano9040611

91. Johnson MB, Halman JR, Miller DK, Cooper JS, Khisamutdinov EF, Marriott I, et al. The immunorecognition, subcellular compartmentalization, and physicochemical properties of nucleic acid nanoparticles can be controlled by composition modification. *Nucleic Acids Res* (2020) 48(20):11785–98. doi: 10.1093/nar/gkaa908

92. Stewart JM, Viard M, Subramanian HK, Roark BK, Afonin KA, Franco E. Programmable RNA microstructures for coordinated delivery of siRNAs. *Nanoscale* (2016) 8(40):17542–50. doi: 10.1039/c6nr05085a

93. Saito RF, Rangel MC, Halman JR, Chandler M, de Sousa Andrade LN, Odete-Bustos S, et al. Simultaneous silencing of lysophosphatidylcholine acyltransferases 1-4 by nucleic acid nanoparticles (NANPs) improves radiation response of melanoma cells. *Nanomedicine* (2021) 36:102418. doi: 10.1016/j.nano.2021.102418

94. Chandler M, Rolband L, Johnson MB, Shi D, Avila YI, Cedrone E, et al. Expanding structural space for immunomodulatory nucleic acid nanoparticles (NANPs) via spatial arrangement of their therapeutic moieties. *Adv Funct Mater* (2022) 32. doi: 10.1002/adfm.202205581

95. Afonin KA, Viard M, Martins AN, Lockett SJ, Maciag AE, Freed EO, et al. Activation of different split functionalities on re-association of RNA-DNA hybrids. *Nat Nanotechnol* (2013) 8(4):296–304. doi: 10.1038/nnano.2013.44

96. Afonin KA, Desai R, Viard M, Kireeva ML, Bindewald E, Case CL, et al. Co-Transcriptional production of RNA-DNA hybrids for simultaneous release of multiple split functionalities. *Nucleic Acids Res* (2014) 42(3):2085–97. doi: 10.1093/nar/gkt1001

97. Afonin KA, Viard M, Tedbury P, Bindewald E, Parlea L, Howington M, et al. The use of minimal RNA toeholds to trigger the activation of multiple functionalities. *Nano Lett* (2016) 16(3):1746–53. doi: 10.1021/acs.nanolett.5b04676

98. Martins AN, Ke W, Jawahar V, Striplin M, Striplin C, Freed EO, et al. Intracellular reassociation of RNA-DNA hybrids that activates RNAi in HIV-infected cells. *Methods Mol Biol* (2017) 1632:269–83. doi: 10.1007/978-1-4939-7138-1_18

99. Ke W, Hong E, Saito RF, Rangel MC, Wang J, Viard M, et al. RNA-DNA Fibers and polygons with controlled immunorecognition activate RNAi, FRET and transcriptional regulation of NF-kB in human cells. *Nucleic Acids Res* (2019) 47(3):1350–61. doi: 10.1093/nar/gky1215

100. Halman JR, Kim KT, Gwak SJ, Pace R, Johnson MB, Chandler MR, et al. A cationic amphiphilic Co-polymer as a carrier of nucleic acid nanoparticles (NANPs) for controlled gene silencing, immunostimulation, and biodistribution. *Nanomedicine* (2020) 23:102094. doi: 10.1016/j.nano.2019.102094

101. Avila YI, Chandler M, Cedrone E, Newton HS, Richardson M, Xu J, et al. Induction of cytokines by nucleic acid nanoparticles (NANPs) depends on the type of delivery carrier. *Molecules* (2021) 26(3). doi: 10.3390/molecules26030652

102. Cruz-Acuna M, Halman JR, Afonin KA, Dobson J, Rinaldi C. Magnetic nanoparticles loaded with functional RNA nanoparticles. *Nanoscale* (2018) 10(37):17761–70. doi: 10.1039/c8nr04254c

103. Juneja R, Vadarevu H, Halman J, Tarannum M, Rackley L, Dobbs J, et al. Combination of nucleic acid and mesoporous silica nanoparticles: Optimization and therapeutic performance. *In Vitro ACS Appl Mater Interfaces* (2020) 12(35):38873–86. doi: 10.1021/acsami.0c07106

104. Afonin KA, Dobrovolskaia MA, Church G, Bathe M. Opportunities, barriers, and a strategy for overcoming translational challenges to therapeutic nucleic acid nanotechnology. *ACS Nano* (2020) 14(8):9221–7. doi: 10.1021/acsnano.0c04753

105. Dobrovolskaia MA, Afonin KA. Use of human peripheral blood mononuclear cells to define immunological properties of nucleic acid nanoparticles. *Nat Protoc* (2020) 15(11):3678–98. doi: 10.1038/s41596-020-0393-6

106. Hong E, Halman JR, Shah A, Cedrone E, Truong N, Afonin KA, et al. Toll-like receptor-mediated recognition of nucleic acid nanoparticles (NANPs) in human primary blood cells. *Molecules* (2019) 24(6). doi: 10.3390/molecules24061094

107. Ke W, Chandler M, Cedrone E, Saito RF, Rangel MC, de Souza Junqueira M, et al. Locking and unlocking thrombin function using immunoquiescent nucleic acid nanoparticles with regulated retention in vivo. *Nano Lett* (2022) 22(14):5961–72. doi: 10.1021/acs.nanolett.2c02019

108. Bila D, Radwan Y, Dobrovolskaia MA, Panigaj M, Afonin KA. The recognition of and reactions to nucleic acid nanoparticles by human immune cells. *Molecules* (2021) 26(14). doi: 10.3390/molecules26144231

109. Johnson MB, Halman JR, Burmeister AR, Currin S, Khisamutdinov EF, Afonin KA, et al. Retinoic acid inducible gene-I mediated detection of bacterial nucleic acids in human microglial cells. *J Neuroinflamm* (2020) 17(1):139. doi: 10.1186/s12974-020-01817-1

110. Gupta K, Afonin KA, Viard M, Herrero V, Kasprzak W, Kagiampakis I, et al. Bolaamphiphiles as carriers for siRNA delivery: From chemical syntheses to practical applications. *J Controlled Release* (2015) 213:142–51. doi: 10.1016/j.jconrel.2015.06.041

111. Kim T, Viard M, Afonin KA, Gupta K, Popov M, Salotti J, et al. Characterization of cationic bolaamphiphile vesicles for siRNA delivery into tumors and brain. *Mol Ther Nucleic Acids* (2020) 20:359–72. doi: 10.1016/j.omtn.2020.02.011

112. Shi D, Beasock D, Fessler A, Szebeni J, Ljubimova JY, Afonin KA, et al. To pegylate or not to pegylate: Immunological properties of nanomedicine's most popular component, polyethylene glycol and its alternatives. *Adv Drug Delivery Rev* (2022) 180:114079. doi: 10.1016/j.addr.2021.114079

113. Ke W, Afonin KA. Exosomes as natural delivery carriers for programmable therapeutic nucleic acid nanoparticles (NANPs). *Adv Drug Delivery Rev* (2021) 176:113835. doi: 10.1016/j.addr.2021.113835

114. Nordmeier S, Ke W, Afonin KA, Portnoy V. Exosome mediated delivery of functional nucleic acid nanoparticles (NANPs). *Nanomedicine* (2020) 30:102285. doi: 10.1016/j.nano.2020.102285

115. Chandler M, Lyalina T, Halman J, Rackley L, Lee L, Dang D, et al. Broccoli fluorets: Split aptamers as a user-friendly fluorescent toolkit for dynamic RNA nanotechnology. *Molecules* (2018) 23(12). doi: 10.3390/molecules23123178

116. Johnson MB, Chandler M, Afonin KA. Nucleic acid nanoparticles (NANPs) as molecular tools to direct desirable and avoid undesirable immunological effects. *Adv Drug Delivery Rev* (2021) 173:427–38. doi: 10.1016/j.addr.2021.04.011

117. Yokobayashi Y. Aptamer-based and aptazyme-based riboswitches in mammalian cells. *Curr Opin Chem Biol* (2019) 52:72–8. doi: 10.1016/j.cbpa.2019.05.018

118. Panigaj M, Johnson MB, Ke W, McMillan J, Goncharova EA, Chandler M, et al. Aptamers as modular components of therapeutic nucleic acid nanotechnology. *ACS Nano* (2019) 13(11):12301–21. doi: 10.1021/acsnano.9b06522

119. Sajja S, Chandler M, Striplin C, Afonin KA. Activation of split RNA aptamers: Experiments demonstrating the enzymatic synthesis of short RNAs and their assembly as observed by fluorescent response. *J Chem Educ* (2018) 95:1861-1866. doi: 10.1021/acs.jchemed.7b00759

120. Afonin KA, Dobrovolskaia MA, Ke W, Grodzinski P, Bathe M. Critical review of nucleic acid nanotechnology to identify gaps and inform a strategy for accelerated clinical translation. *Adv Drug Delivery Rev* (2022) 181:114081. doi: 10.1016/j.addr.2021.114081

121. Chandler M, Johnson B, Khisamutdinov E, Dobrovolskaia MA, Sztuba-Solinska J, Salem AK, et al. The international society of RNA nanotechnology and nanomedicine (ISRNN): The present and future of the burgeoning field. *ACS Nano* (2021) 15:16957-16973. doi: 10.1021/acsnano.0c10240

122. Stein CA, Castanotto D. FDA-Approved oligonucleotide therapies in 2017. *Mol Ther* (2017) 25(5):1069–75. doi: 10.1016/j.ymthe.2017.03.023

123. Igarashi J, Niwa Y, Sugiyama D. Research and development of oligonucleotide therapeutics in Japan for rare diseases. *Future Rare Dis* (2022) 2(1):FRD19. doi: 10.2217/frd-2021-0008

124. Kulkarni JA, Witzigmann D, Thomson SB, Chen S, Leavitt BR, Cullis PR, et al. The current landscape of nucleic acid therapeutics. *Nat Nanotechnol* (2021) 16(6):630–43. doi: 10.1038/s41565-021-00898-0

125. ClinicalTrials.gov. *Intratumoral/Intralesional administration of MK-4621/ JetPEI™ with or without pembrolizumab in participants with Advanced/Metastatic or recurrent solid tumors (MK-4621-002).* https://clinicaltrials.gov/ct2/show/NCT03739138

126. Mao T, Israelow B, Lucas C, Vogels CBF, Gomez-Calvo ML, Fedorova O, et al. A stem-loop RNA RIG-I agonist protects against acute and chronic SARS-CoV-2 infection in mice. *J Exp Med* (2022) 219(1). doi: 10.1084/jem.20211818

127. . *Orphan drug designations and approvals*. https://www.accessdata.fda.gov/scripts/opdlisting/oopd/detailedIndex.cfm?cfgridkey=907922

128. Mitchell WM. Efficacy of rintatolimod in the treatment of chronic fatigue Syndrome/Myalgic encephalomyelitis (CFS/ME). *Expert Rev Clin Pharmacol* (2016) 9 (6):755–70. doi: 10.1586/17512433.2016.1172960

129. Strayer DR, Young D, Mitchell WM. Effect of disease duration in a randomized phase III trial of rintatolimod, an immune modulator for myalgic Encephalomyelitis/ Chronic fatigue syndrome. *PloS One* (2020) 15(10):e0240403. doi: 10.1371/ journal.pone.0240403

130. Eulberg D, Klussmann S. Spiegelmers: Biostable aptamers. *ChemBioChem* (2003) 4(10):979–83. doi: 10.1002/cbic.200300663

131. Ehling J, Bartneck M, Wei X, Gremse F, Fech V, Mockel D, et al. CCL2-dependent infiltrating macrophages promote angiogenesis in progressive liver fibrosis. *Gut* (2014) 63 (12):1960–71. doi: 10.1136/gutjnl-2013-306294

132. Bartneck M, Schrammen PL, Mockel D, Govaere O, Liepelt A, Krenkel O, et al. The CCR2(+) macrophage subset promotes pathogenic angiogenesis for tumor vascularization in fibrotic livers. *Cell Mol Gastroenterol Hepatol* (2019) 7(2):371–90. doi: 10.1016/j.jcmgh.2018.10.007

133. Zboralski D, Hoehlig K, Eulberg D, Fromming A, Vater A. Increasing tumor-infiltrating T cells through inhibition of CXCL12 with NOX-A12 synergizes with PD-1 blockade. *Cancer Immunol Res* (2017) 5(11):950–6. doi: 10.1158/2326-6066.CIR-16-0303

134. Suarez-Carmona M, Williams A, Schreiber J, Hohmann N, Pruefer U, Krauss J, et al. Combined inhibition of CXCL12 and PD-1 in MSS colorectal and pancreatic cancer: Modulation of the microenvironment and clinical effects. *J Immunother Cancer* (2021) 9 (10). doi: 10.1136/jitc-2021-002505

135. Chandler M, Johnson M, Panigaj M, Afonin K. Innate immune responses triggered by nucleic acids inspire the design of immunomodulatory nucleic acid nanoparticles (NANPs). *Curr Opin Biotechnol* (2020) 63:8–15. doi: 10.1016/j.copbio.2019.10.011

frontiers | Frontiers in Immunology

TYPE Review
PUBLISHED 27 February 2023
DOI 10.3389/fimmu.2023.1129296

OPEN ACCESS

EDITED BY
Kirill Afonin,
University of North Carolina at Charlotte,
United States

REVIEWED BY
Paolo Macor,
University of Trieste, Italy
Borislav Angelov,
Institute of Physics (ASCR), Czechia

*CORRESPONDENCE
Victor Puntes
victor.puntes@icn2.cat

SPECIALTY SECTION
This article was submitted to Molecular Innate Immunity, a section of the journal Frontiers in Immunology

RECEIVED 21 December 2022
ACCEPTED 14 February 2023
PUBLISHED 27 February 2023

CITATION
González-Rioja R, Salazar VA, Bastús NG and Puntes V (2023) The development of highly dense highly protected surfactant ionizable lipid RNA loaded nanoparticles. *Front. Immunol.* 14:1129296. doi: 10.3389/fimmu.2023.1129296

The development of highly dense highly protected surfactant ionizable lipid RNA loaded nanoparticles

Ramon González-Rioja[1], Vivian A. Salazar[1], Neus G. Bastús[1,2] and Victor Puntes[1,2,3,4]*

[1]Institut Català de Nanociència i Nanotecnologia (ICN2), Consejo Superior de Investigaciones Científicas (CSIC), The Barcelona Institute of Science and Technology (BIST), Universitat Autònoma de Barcelona (UAB), Barcelona, Spain, [2]Centro de Investigación Biomédica en Red (CIBER) en Bioingeniería, Biomateriales y Nanomedicina, Centro de Investigación Biomédica en Red en Bioingeniería Biomateriales y Nanomedicina (CIBER-BBN), Madrid, Spain, [3]Malalties Infeccioses, Nanopartícules farmacocinétiques, Vall d'Hebron Institut de Recerca, Barcelona, Spain, [4]Institució Catalana de Recerca i Estudis Avançats (ICREA), Barcelona, Spain

The long quest for efficient drug administration has been looking for a universal carrier that can precisely transport traditional drugs, new genomic and proteic therapeutic agents. Today, researchers have found conditions to overcome the two main drug delivery dilemmas. On the one side, the versatility of the vehicle to efficiently load, protect and transport the drug and then release it at the target place. On the other hand, the questions related to the degree of PEGylation which are needed to avoid nanoparticle (NP) aggregation and opsonization while preventing cellular uptake. The development of different kinds of lipidic drug delivery vehicles and particles has resulted in the development of ionizable lipid nanoparticles (iLNPs), which can overcome most of the typical drug delivery problems. Proof of their success is the late approval and massive administration as the prophylactic vaccine for SARS-CoV-2. These ILNPs are built by electrostatic aggregation of surfactants, the therapeutic agent, and lipids that self-segregate from an aqueous solution, forming nanoparticles stabilized with lipid polymers, such as PEG. These vehicles overcome previous limitations such as low loading and high toxicity, likely thanks to low charge at the working pH and reduced size, and their entry into the cells *via* endocytosis rather than membrane perforation or fusion, always associated with higher toxicity. We herein revise their primary features, synthetic methods to prepare and characterize them, pharmacokinetic (administration, distribution, metabolization and excretion) aspects, and biodistribution and fate. Owing to their advantages, iLNPs are potential drug delivery systems to improve the management of various diseases and widely available for clinical use.

KEYWORDS

ionizable lipid nanoparticles, RNA-loading, drug delivery carriers, pharmacokinetics, biodistribution and clearance

Introduction

The modern concept of drug delivery probably started with German Nobel laureate Paul Erlich's "magic bullet" in 1907, a bullet that cannot miss its target (1, 2) and became common with penicillin in the early 20th century (3, 4). The initial idea was to kill prokaryotes leaving eukaryotes unharmed, thus reducing damage to the body associated with uncontrolled biodistribution. Soon it was also developed to improve dosing and, with it, therapeutic effects. More recently, the concept was actualized for chemotherapy due to its severe side effects, and thus, the firsts Drug Delivery Systems (DDS) were developed to improve the transport of antitumoral drugs such as doxorubicin (5). Before, excipients allowed the drug to solubilize and properly reach their target, but their capacity was limited to solubility issues, with poor capabilities in directing and protecting the drugs during the journey to the target. Similarly, if the development of DDS was initially intended for solubilizing common drugs, it rapidly opened the possibility of loading other substances, such as genetic material or proteins – antibodies, enzymes, etc.-. These substances cannot be administered in a free form since they are highly immunogenic and rapidly biodegraded. Therefore, the full development of DDS will not only optimize the pharmacology of current drugs but also dramatically expand the pharmacopoeia we have available for the cure, which will have a clear impact on population health.

It is important to note that therapeutic effectiveness strongly depends on pharmacokinetic aspects, on how drugs travel and interact through the body, reach their target, perform their intended effect, are modified (metabolized), and excreted. Up to now, pharmacokinetic principles were based on small drug properties, where balanced hydrophobicity and hydrophilicity allow it to reach all corners of the body (6) so that reaching the target was assured at the expense of undesirable side effects. For example, after cisplatin injection, a common chemotherapeutic agent, 60% goes to the kidney causing nephrotoxicity, 36% irreversibly binds to albumin losing its activity, and only a small fraction of the remaining 4% reaches the tumor cell's DNA and performs its therapeutic action (7). In this scenario, protecting the drug and carrying it to the region of interest is a natural evolution of pharmacology.

Together with the quest for efficient drug administration, chemists and nanochemists have searched for a universal carrier that can accommodate many different substances. In addition, the carrier has to be safe, more than its loading. DDSs have to be so safe that repeated administrations across one person's life should not be a problem. Also, for practical reasons, they have to be easy to produce and easy to store.

As expected, DDS have been developed and exploited to enhance the delivery of drugs in treating several diseases showing potential benefits in terms of pharmaceutical flexibility, selectivity, dose reduction and minimization of adverse effects (8). In these platforms, different drugs, ligands and biomolecules can be combined by absorption (9), loading (10), coordination bonding (11), and entrapment (12) to perform different tasks. While DDS popularization started in the 80s and developed as a full academic and technological discipline, nanotechnology irrupted in the 2000s offering unprecedented control of mater structured at the nanoscale, allowing for the rapid and widespread development of new, more precise and more functional DDS. Interestingly, the initial vehicles were called microspheres and then renamed nanocarriers, even if some nanocarriers were bigger than some microspheres.

Among DDS, polymeric nanoparticles (NPs) were the first to be employed, showing significant therapeutic benefits but accompanied by polymeric toxicity, high cost, and lack of feasibility for scaling up. Besides, liposomes have traditionally been the more developed and implemented DDS. Lipid-based NPs made of lipids and surfactants (amphipathic molecules) are simple and safe, but there is typically a low degree of loading and structural fragility. They have become an up-and-coming delivery platform for hydrophobic and hydrophilic substances or a combination of both (13, 14). These carriers can penetrate abnormal tissue, remain for a long time and release their cargo drugs, increasing drug efficacy. For example, *in-vitro* studies by Wang et al. (15, 16) have shown the successful target delivery of resveratrol, a poor aqueous solubility drug and curcumin hydrophobic polyphenol in breast cancer. Recently developed lipid-based formulations included micro and nanoemulsions, self-emulsifying formulations, liposomes, lipid NPs and lipid-drug conjugates. Among the extensive range of lipid formulations, the solid lipid nanoparticles (SLNs) (17–19), the nanostructured lipid carried (NLCs) (14, 20), and the lipid-based nucleic acid therapeutics (21, 22) have probably centered the majority of the attention due to their successful activities toward multiples disease models. Other alternatives have been protein aggregates for unsoluble chemotherapeutic agents such as paclitaxel in Abraxane® (23) or made of biological molecules such as polylactic-co-glycolic acid (PGLA) NPs, which has been considered one of the first universal nanocarrier platforms (24, 25).

In this work, we refer to those NPs made of a mixture of lipids, ionizable surfactants, and nucleic acids, which spontaneously form NPs by the electrostatic and hydrophobic collapse in water. These lead to highly dense and highly protective NPs, which can be singularized as ionizable lipid nanoparticles, iLNPs. These NPs can overcome the main biological barriers to cell transfection, including protection from endonucleases, and RNases, and selective targeting, when targeting moieties such as antibodies or aptamers are included, to improve the contact with the targeted tissues or cells (26), cell internalization, and intracellular release. Herein we focus on RNA-ionizable lipid NPs. RNA is not only a major player in genetic medicine that needs to be transported, but it is also a model of macromolecule that has to be protected until delivered inside the cells.

From a historical perspective, ionizable lipids evolved from years of working with permanently charged cationic lipids for transfection. The mechanism by which these cationic lipids capture nucleic acids is through complexing them by ionic interaction between the negatively charged phosphate groups on the nucleic acid molecules and a positively charged group on the lipid head, forming nucleotides-lipid complexes-, probably starting in 1987 with DOTMA, the first bi-layer forming cationic lipid, specifically designed and used for DNA transfection (27). However, due to its net positive charge, it presented unacceptable levels of

toxicity at the doses necessary to produce therapeutically relevant levels of transgene expression, especially *in vivo* animal models, making its transition into clinical praxis impossible (28–30). In addition, the positive net charge induces plasma protein adsorption and rapid clearance by the immune system, negatively affecting transfection efficiency (31). They commonly present hemodynamic toxicities, such as the activation of the complement system and an increase in blood coagulation time (32–34). Ionizable lipids entered the field as an answer to this problem. These lipids are a pivotal element of the iLNP systems (35) and are characterized by having an ionizable functional group in their polar head with an acid-dissociation constant (pKa) below 7.0 (36). Their pH-tunable charge allows them to be neutral at physiological pH, minimizing their cationic burden and toxicity but be protonated at a lower pH at the maturing, acidified endosome. Their cationic nature inside the endosome will help its break and escape by enabling the interaction with the anionic membrane lipids (and subsequent formation of non-by-layer phases), allowing cytosolic delivery. Indeed, the ability to activate and deactivate the ionizable lipid cationicity, when necessary, enables it to adapt to the needs of the synthesis (charge on), distribution within the body (charge off) and escape from the endosome (charge on). These positively charged vesicles present the advantages of a liposome-mediated transfection (e.g., fusion with the cell membrane, protection from degradation, digestion, opsonization, etc.) and of a cationic-mediated transfection (e.g., complex formation with nucleic acids, association with the negatively charged cell surface).

Today, iLNPs have proven to be an efficient vehicle for effectively delivering RNA inside the cells, opening the doors to gene therapy. Their rapid implantation in several medicines already approved for human use is an unprecedented success within the community of nanomedicine, drug delivery and gene therapy. Though, to date, only three different systems of RNA delivery are approved by the FDA: antitumoral Patisiran and two RNA COVID-19 vaccines (Pfizer/BionTech and Moderna) (37), and many others are under clinical trial. Encouraged by the successful application of the SarCov2 mRNA-lipid vaccines produced by Moderna and Pfizer companies, the high biocompatibility of the lipid nanocarriers is being explored to treat many other diseases. Thus, in a continuous effort to cure other viral diseases, other mRNA vaccines are developing to fight against etiological agents such as Cytomegalovirus, Syncytial respiratory, or influenza viruses (Trial number: NCT05085366, NCT05127434, NCT04956575). In the field of cancer disease, the pharmaceutical companies Moderna and BioNTech are advancing in the commercialization of a potent therapy based on mRNA vaccines for melanoma; their clinical trials are in phases 1 and 2, respectively (Trial number: NCT0389788, NCT04526899). The multifunctional characteristics of the iLNPs also have been advancing in treating solid tumors. In a lack of successful results compared to the CART cell therapy in liquid tumors, the BioNTech company has developed an RNA-based CAR-T cell therapy to counter the accelerated growth in the Gastric, Pancreatic, Ovarian, and Biliary Tract Tumors (Trial number: NCT04503278) (38).

Ionizable lipid nanoparticles: Structure, composition and characterization

Ionizable Lipid NPs consist of nanometrically sized particles (39) could be understood as a dense condensation of surfactants, lipids and genetic material. These NPs can be synthesized quickly and efficiently to encapsulate genetic material with high efficiency (high density) and have sufficient stability and robustness to travel through the body to their destination without being degraded or opsonized, protecting their cargo, and able to carry out an efficient cytoplasmic delivery of the genetic material. Their standard composition consists of 5 different compounds: i) the genetic material which has to be delivered, ii) an ionizable cationic lipid to interact with the genetic material and render it hydrophobic, iii) a helper amphipathic molecule, usually a phospholipid such as DSPC, iv) a helper sterol lipid, in the majority of cases Cholesterol, to making the structure more robust, and v) a PEG-lipid at the particle surface for surface stabilization and to avoid NP aggregation and opsonization. The ratio between these components varies among different formulations, but typically it can be around: ionizable lipid 50%mol (60%mass), phospholipid 10%mol (15%mass), Cholesterol 38%mol (15%mass), PEG-lipid 1,5%mol (8%mass).

These components interact and spontaneously structure themselves through a self-assembly process based on the ethanol injection method, which consists of rapid mixing of an ethanol phase, where the lipids are dissolved, into an aqueous phase, where the nucleic acids are dissolved in an acidic buffer. This rapid mixing induces the sudden supersaturation of the lipidic molecules, which leads to burst nucleation and their assembly into NPs, trapping the surfactants and genetic material (36). The process by which the genetic material is encapsulated in the lipid structure takes place in the first steps of the synthesis process when the ethanolic phase is mixed with the aqueous phase and self-assembly of lipids occurs. The first force that drives this self-assembly is an electrostatic interaction between the polar head of the positively-charged ionizable lipids at acidic pH and the negative charges of the nucleic acid chains at the working pH (typically around 4), and the second is the increase in polarity of the lipidic solvent by the addition of water, expulsing lipidic material from the liquid phase into the NPs. Thus, as the polarity of the solvent progressively increases, inverted micelle-like structures coalesce, interacting with the rest of the lipids and surfactants, which at the NP surface closes the particle in a spherical form making the NPs soluble in water.

The PEG-lipid anchors to the NP surface's lipidic domains while extending its water-soluble part away from the NP, forming a hydrophilic steric barrier that provides colloidal stability and prevents NP aggregation and opsonization (40). The whole phase mixing and complexation of the nucleic acid is done at pH<<pKa of the ionizable lipid so that it is cationic-charged nature, and the entrapment efficiency of the nucleic acid is maximized. Afterwards, once the synthesis is complete, the pH can be adjusted to physiological value since the nucleic acid is already complexed and integrated inside the NP. In this way, a neutral charge of the

vehicle is achieved and significantly minimizes the cationic burden and its related toxicity that the particles would experiment with once they are administered (Figure 1).

An essential part of this process is how efficient and fast the mixing between these two phases is, since it determines size, and size plays a decisive role in NP biodistribution, delivery efficiency, and transfection potency (41). As shown by Belliveau et al.in 2012 (42) when investigating the influence of the flow rate on the iLNP particle size, the NP size decreased as the flow rate of the injection of the ethanolic phase into the aqueous phase increased. Indeed, there is an universal tendency for NPs to decrease surface energy (surface-to-volume ratio) by growth. Because of that, the PEG-lipid is employed to reduce the surface energy and stabilize the NPs. Multiple studies have shown that increasing the molar ratio of the PEG-lipid, by stabilizing NPs against aggregation yields significantly smaller iLNPs, independent of other lipid components (41–43). This indicates that without PEG, or other similar biocompatible polymers, the NPs would continuously aggregate and grow until complete phase separation.

Besides size, as discussed in the previous section, a determining functional parameter is the charge, a fundamental aspect of iLNPs, which should be positively charged during iLNPs formation to allow nucleic acid complexation, neutral at physiological pH for its administration, and positively charged at the acidified, maturing endosome for membrane disruption. The pKa value of the ionizable lipid will be the factor that determines the charge on the iLNP under the different pH conditions, which has to find a balance between (44, 45) i) being acidic during RNA trapping, ii) being neutral at physiological pH, to minimize toxicity and avoid rapid immune-clearance, iii) being as positively charged as possible at late endosome stage to maximize the interaction with the endosome's membrane and its disruption. Also important to consider the effect produced by absorbing protons during endosome acidification, inducing proton sponge effects.

The pKa value in which this balance is optimal is not a universal value for all lipids and depends on the iLNPs formulation and the nucleic acid sequences they carry. However, several studies demonstrated that a pKas between 5,5 and 6,5 tend to show maximal potency *in vivo* (21, 46–48). Regarding their chemical structure, as a rule of thumb, one can say that small head groups of the ionizable lipid, such as dimethylamino-based, show higher transfection efficiencies compared to higher substituted moieties, which increase their steric hindrance as well as affecting the pKa (49–51). So it is the case of DLin-MC3-DMA, the ionizable lipid part of the patisiran (Onpattro®) formulation. It is important in the history of the development of ionizable lipids and corresponding NPs since, when first synthesized, it exhibited an improvement in the potency of more than two orders of magnitude compared to the previous benchmark formulation (DLinDMA), which allowed the TTR02 (later known as patisiran) formulation to transition into clinical development (45). Notably, the structure and formulation of DLin-MC3-DMA laid the groundwork for further iLNPs development. Currently, the search for new biodegradable, ionizable lipids with more potency or different properties is at the center of research to advance iLNPs, and this effort is yielding a large array of diverse and exciting types of iLNPs to adapt them to organs and diseases (52). The structures and pKas of the ionizable lipids present in the approved iLNP formulations appear in Figure 2.

They share branched (bulky) lipophilic moieties and hydrophilic amino terminations. This geometry allows for a cone-like conformation of the amphipathic molecules and of the cationic-anionic lipid pair that occurs once the ionizable lipid interacts with the lipids of the endosomal membrane. This non-by-layer, cone-like conformation of the amphipathic molecules favors high surface curvature and is responsible for iLNP disruption. Once the endosome and the iLNP have been disrupted, the pH goes back to 7, and the iLNP release its cargo so that free mRNA can enter ribosomes for expression. This disintegration is probably simultaneous with the endosomal disruption and mediated by the many (negatively) charged and detergent-like (amphipathic) compounds inside the cell –indeed, all proteins have hydrophilic and hydrophobic domains- interfering with the amphipathic molecules of the iLNPs.

Due to their reduced size and complex and unstable (dynamic) nature, their characterization can be a serious challenge, especially in the biological matrix (Figure 3). The standard parameters to evaluate include particle size, surface charge (ζ-potential), drug content and surface state (composition and conformation). Particle size, polydispersity index and charge analysis can be measured by dynamic light scattering (DLS) and associated ζ-potential with the main advantage of not being time-consuming. Besides, electron microscopy allows for high-resolution observation of these NPs.

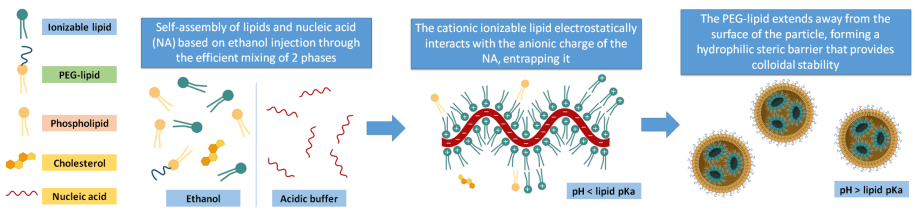

FIGURE 1
Main components of the iLNPs. The lipid components are dissolved in an ethanolic phase, and the nucleic acid is in an acidic buffer. When these two phases are efficiently mixed, the ionizable lipid gets protonated and electrostatically interacts with the anionic charges of the nucleic acids while the rest of the lipids self-assemble to form the iLNP structure. When the formation is complete, the pH of the batch can be brought to a value higher than the ionizable lipid pKa.

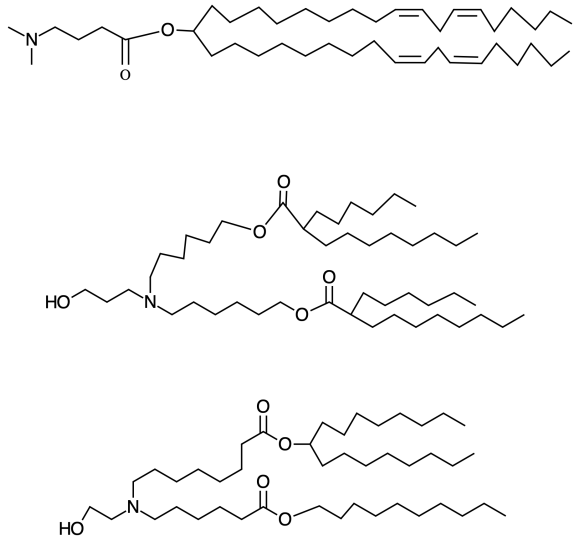

FIGURE 2
Structure of the approved Ionizable lipids. From up to down DLin-MC3-DMA, Alc-0315 and SM-102, the ionizable lipids present in Onpattro, Comirnaty (BioNTech/Pifizer) and Spikevax (Moderna), respectively, with the pKas: 6.44, 6.09, 6.75, respectively. The number of hydrophobic tails has geometrical consequences in the structure of the iLNPs contributing to the determination of size and robustness.

However, they are frail in high vacuum and under the electron beam, and therefore cryo-TEM is often employed, providing 2D images of stable frozen-hydrated particles. Alternatively, low electron beam energy and staining also allow observation of the iLNPs morphology (53). These iLNPs can also be fluorescently-labelled for their visualization and quantification in fluorescence microscopy and spectroscopy techniques (54). Concentration and composition are also studied using thermogravimetry and differential scanning calorimetric analysis (55).

Information about the internal structure of the systems can be obtained through X-ray (SAXS) and neutron (SANS) small angle scattering (55). In the past decade, SAXS has been shown to be very useful at providing information about the fine structure in self-assembled soft matter materials, like iLNPs (56–59). Still, the full understanding of the nanoscale organization of the lipids and genetic material in the interior of the particle remains yet to be achieved (60). It has been observed that depending on operational factors or compositional changes, the synthesis yields different arrangements

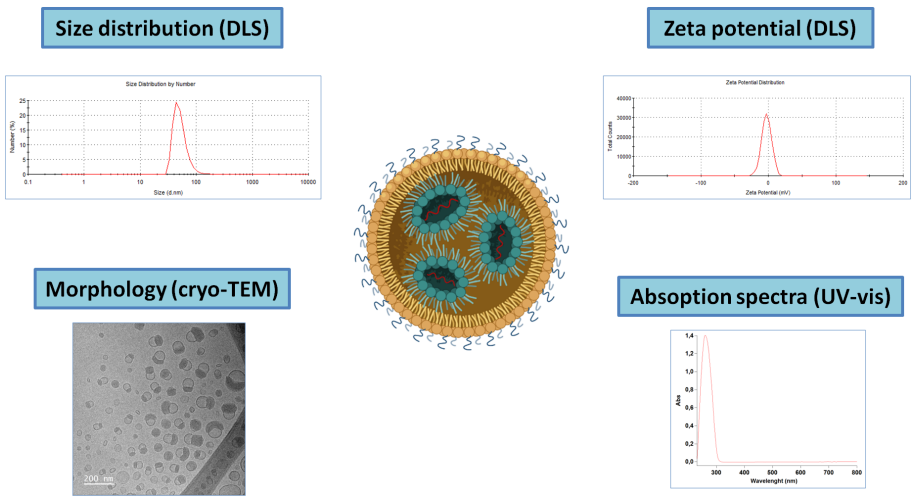

FIGURE 3
Schematic representation of the main techniques for iLNPs characterization. Note that for the UV-vis absorption spectra, the signal corresponding to the nucleic acids present in the sample will account for the majority part of the signal.

of iLNPs, such as multilamellar structures (61), Ia3d and Pm3n cubic phases (62), and other types of non-lamellar structures where the RNA molecules are inside aqueous cylinders (63).

Ionizable lipid nanoparticles: Pharmacokinetics

It is well accepted that the potential use of iLNPs in medicine is determined by the pharmacokinetic (administration, distribution, metabolization and excretion) aspects that govern iLNP behavior, which is different from previous drugs. Pharmacokinetics describes what the body does to the drug rather than what the drug does to the body; the latter would be pharmacodynamics. The field of pharmacokinetics has developed with the implantation of small-molecule drugs as principal therapeutic agents. This is because small molecule drugs can distribute across the body and enter inside the cells. However, everything changes when we pretend to employ large and structured substances such as proteins, genetic material or nanoparticles. Because of that, new pharmacokinetic models, which describe the behavior of these materials once injected until they are excreted, have to be developed for the proper implementation of new medical substances and materials into the clinic practice, taking into account that the biochemical composition of NPs and its entrance route into the human body, determines the final activity of these NPs (64). We focus on the existing clinical trials and *in-vivo* experimental models using RNA-lipid carrier systems. Many DDS enter the body *via* inhalation, oral ingestion, topical (cutaneous and ocular) application, and parenteral administration.

Herein, we first analyze the different transformations iLNPs may suffer, such as aggregation, interactions with proteins and disintegration/dissolution, and then comment on their biodistribution and excretion since the latter strongly depends on the formers. These alterations significantly impact their behavior and must be considered for their intended use in medicine. Therefore, research on iLNPs effects should strive to correlate with how they interact, evolve and are transformed during their exposure to the human body. That is, during their Administration, Distribution, Metabolization and Excretion (ADME) phases.

Transformations and metabolization

Regarding nanosized objects in general, due to interactions between NPs and components from the biological medium, NPs are known to suffer different alterations when applied. Indeed, NPs are intrinsically out of equilibrium, and transformations such as Ostwald ripening, NPs collapse, and over-grow always tend to occur. When administered, the NP's environment radically changes from low electrolytic NP concentrated media to a media full of cells, proteins and electrolytes. The main alteration they may suffer is the loose of colloidal stability and consequent aggregation. This loss of colloidal stability and subsequent aggregation and expulsion from the media has a dramatic effect on the abilities of NPs to travel through the body and to be well dispersed in organs and tissues, provoking, in too many cases, the lack of -or unexpected- biological results (65, 66). Note that the final size of NP, which will reach the cells, is also determined by the interaction with the biological matrix, ultimately determining the distribution and kinetics of delivery.

Several factors cause the aggregation of colloidal NPs; for instance, the initial concentration of NPs, their chemical nature and the ionic strength of the medium (67). The most widely employed strategy to passivate the surface of nanosized objects, in general, has been modifying the NP surface with hydrophilic polymers as polyethyleneglycol (PEG), which acts as a steric barrier that minimizes interactions at the NP surface, indispensable to stabilize the surface and allow NPs to exist isolated in solution. This steric barrier "closes" the surface of the NP, provides colloidal stability and facilitates the small and narrow size distribution. However, the PEGylation of the NP surface dramatically difficult the interaction with cellular membranes, reducing the necessary close contact required for endocytosis. This double effect has been called the "PEG-dilemma" (68–71). Although alternative strategies are proposed, like cleavage of a PEG moiety (72), this problem is majorly addressed by a strategy based on "reversible PEGylation", where a lipid-containing PEG slowly detaches from the NP surface once administered. This allows to take advantage of the disposing of the high PEG concentration needed for small and monodisperse synthesis and distribution, and the lower PEG concentration needed to have a good cellular uptake at the moment when the NP reaches the target organ. Note that an increase in the concentration of PEG also influences its conformation and protective effects, increasing the circulation time of the iLNPs (71). Indeed, a completely PEG-covered iLNP surface will dramatically inhibit the interaction with cells and serum proteins, modifying circulation time and biodistribution (68, 71). Such PEG-lipids remain integrated into the LNP structure during formation and under storage conditions, but in the presence of a lipid sink like in plasma, these PEG-lipids are stripped off the particle and into de medium, leaving the surface of the iLNP gradually unshielded (45). These PEG-lipids have short alkyl chains -which act as "hydrophobic anchors"-allowing a reasonable desorption rate once they enter blood circulation (71). The proper balance between a fully protected surface for iLNP synthesis and distribution, and a relatively unshielded surface for interactions with cell membranes, is achieved by finding a compromise between alkyl chain length and PEG-lipid surface concentration.

Special mention deserves the interaction of NPs with proteins, adjusted by the size and concentration of PEG at the NP surface. When NPs are administrated into the body, they first interact with biological fluids. Depending on the administration site, the biomolecules that will interact with the NPs can vary: from lung surfactants when inhaled to the interstitial fluid when locally injected into blood plasma following intravenous administration (73). Proteins, which are the most important of these biomolecules, will adsorb -to some extent- on the NP surface, especially as PEG is removed, coating the surface with a new layer that will define the biological identity of the NP, the so-called "biomolecular corona", or "protein corona" (74, 75) which can dramatically alter the surface

properties of nanosized particles and determine their *in vivo* fate (76). Already in 2004, it was reported that the presence of proteins in physiological media affects the entry and intracellular localization of NPs in cells, thus modulating their potential biological effects and toxicity. Later on, the formation of a protein corona on top of the NP surface was observed to control biodistribution, uptake and biological response, transforming them from innocuous to toxic or vice versa. This surface coating can be formed by hundreds of biomolecules, including albumin, apolipoproteins, immunoglobulins, coagulation factors, and many others (77). Some of these biomolecules might associate almost irreversibly with the iLNP surface, in either their native or denatured form, affecting, de facto, all subsequent interactions. It has been proposed that the corona is comprised of both these tightly bound proteins ("hard" corona), which presumably bind directly to the iLNP surface with high affinity, and also a looser, more dynamic layer ("soft" corona) which constantly exchanges with proteins in the environment (78). The hard and soft corona are both considered relevant in determining iLNP interactions with cells (73).

Traditionally, for biomedical applications, this corona has only been conceived as a disruptive effect that hinders the functionality of nanoparticles, provoking underestimated side effects like loss of colloidal stability, aggregation, sedimentation or rapid clearance by the immune system. But the protein corona also plays an active role in deciding the destination organ for delivery and accumulation of the particles. For iLNPs, it has been shown that in Onpattro, there is a close relationship between the protein corona and the target organ of delivery, mediated through the adsorption of Alipoprotein E onto the iLNP surface. Authors proposed that binding to ApoE will act as a highly effective targeting ligand by binding to lipoprotein receptors on the surface of hepatocytes, triggering the uptake by hepatocytes (45, 79). This relationship between the protein corona and the biodistribution of NPs could allow the fate of the particles to be actively altered. Indeed, the multifunctional physicochemical properties of lipids can be designed to target different body tissues. Min Qiu et al. (80) have achieved a lung-selective delivery in mice with the use of a series of ionizable lipids containing an amide bond in the tail which changes the interactions between plasma proteins in contrast with other types of lipids, like the ones with an ester bond in the PEG lipidic tail (as those present in the approved formulations), which easily accumulate in the liver (81). These are exciting and promising results for improving the delivery of iLNP beyond these organs, and other relationships between lipid composition and biodistribution should be carried out in the future. Active targeting by grafting a specific moiety, that is, the ligand of an over-expressed receptor onto the NP surface, is a very appealing strategy that, to this day, fails to impact the biodistribution drastically. However, once the NPs have reached the organs, their uptake can be influenced by targeting moieties (75)

Degradation and disintegration of iLNPs

It is well-known that NPs can dissolve in certain dispersing media (82–84). The extent of their dissolution depends not only on their intrinsic properties, such as size and shape, but also on characteristics of the surrounding media, including pH and ionic strength, as well as the presence of organic matter (85, 86). Thus, while small NPs can be preserved in solution in the appropriate (as–synthesized) conditions for a long time, they may also be prone to rapid degradation in physiological media. This is why iLNPs can be kept for a long time in storage conditions while in hours disintegrates once in the body. Indeed, it has been reported that it is below c.a. 30 nm in diameter (87), where NPs cannot support the high surface energy anymore and tends to dissolve. The driving force behind dissolution strongly depends on the solubility of the constituent ions in a given environment and their concentration gradients in the solution. This phenomenon, enhanced at the nanoscale, is referred to as the Gibbs-Thomson effect, and in NPs manifests as Ostwald ripening, where NPs in solution spontaneously dissolve or grow due to concentration gradients, becoming progressively larger and more polydisperse. Controlled release of matter from an NP is illustrated in the Noyes-Whitney equation, which relates the rate of dissolution to the properties of the components and the dissolution medium. If the released components are removed from the equilibrium because, for example, are used in competitive reactions or simple diluted in the body, the system is moved away from the saturation point, reaches sink conditions, and the NP tends towards complete dissolution. For a given mass, the kinetics of dissolution will be proportional to the specific surface area and the coordination of the constituents at that surface (which decreases with size). NPs have to release their cargo at the appropriate rate and quantity: larger NPs may release them too slowly and too much, while the smaller ones may release them too fast and an insufficient amount of it. Thus, the reactivity of the NP has to be adjusted to persist more or less inside the different parts of the body.

Biodistribution and fate of iLNPs

The primary purpose of using these iLNPs is to cross natural barriers, interact with the target cell, and deliver the treatment efficiently. The first natural barrier the iLNPs need to cross is the biological fluids, blood or lymph, sweat or tear, and the corresponding extracellular matrix, consisting of macromolecules and minerals that change in different tissues, compartments, and health status (88). To overcome these barriers, some iLNPs can interact with particular matrix components that facilitate the interaction with the target cell and the entrance by endocytosis (87). The second natural barrier is the mononuclear phagocyte system, capable of recognizing foreign substances and commensal organisms when entering the body, labelling them with opsonins and enhancing uptake by phagocytic cells, such as kupffer cells in the liver. Basically, if NPs are recognized as a foreign substance, the innate immune response reduces their plasma half-life, decreasing the drug delivery efficiency to the target cell. However, the size range of NPs is that of recognition of the immune system which is supramolecular structures and molecular patters of few tens of nm, mainly found is viruses and bacteria, in such a way that the immune response to NPs can be complex from tolerance, to pro-inflammation to immunomodulation (89). As mentioned above, the

lipid nanoparticle-surface functionalization with PEG minimizes opsonization and therefore the immune response and increases blood circulation time (90). Nonetheless, the activation of the immune system has been found against some of the iLNPs components as PEG. It has been reported that some patients can develop anti-PEG antibodies after a first dose of a PEGylated drug (anti-PEG immunoglobulin M (IgM)) (91), leading to rapid NPs clearance in the liver and spleen, removing the drug from circulation (92). Fortunately, PEG immunogenicity is not so prevalent and not so aggressive, while the rest of the approved iLNPs components are safe.

The precise behavior of these materials during their full-life cycle inside the body is still relatively unknown, with controversy about disparities between the *in vitro* and *in vivo* results. Additionally, subtle modifications of their nature -composition, size, shape and surface state- may have or not have a strong influence on their behavior, affecting their interaction with proteins (93), aggregation state (94), chemical transformation and degradation (95), and consequently biological responses (96). Once they are stable and do not aggregate when administered, their behavior is very different from small molecules, and they are subordinated to the many-body barriers to protect integrity. In addition to immunogenicity, which is somewhat tolerant to small molecules, the body is full of physical barriers. Considering intravenous administration, it is essential to note that the main blood vessels and capillaries in the body have a continuous lining of endothelial cells with pores of 6 nm. Besides, the fenestrated capillaries found in the intestine and some endocrine and exocrine glands may have pores up to 50–60 nm, while discontinuous capillaries, as those found in the liver, spleen and the bone marrow, have pores between 100–1000 nm, which is where typically NPs are found (97). Special attention deserves the tight junctions, including the blood-brain barrier, placenta and testis barrier, where pores smaller than 1 nm have been reported, where the hydrophobic nature of LNPs seems to favor translocation (98). In such conditions, small molecules can diffuse in-and-out from the blood vessels into the lymph, while the passive transport of large objects, like proteins and NPs, through these porous is negligible, and they tend to accumulate in organs of the mononuclear phagocytic system, such as the liver and spleen, which are the two usual places of NPs fate and accumulation (97, 99).

It is worth noting here that blood vessel and tissue permeability is altered during the course of diseases, allowing for the passive accumulation of NPs in those areas. Indeed, this passive accumulation can increase one order of magnitude the concentration of the drug in tissue (11). For example, in solid tumors, their rapid growth results in leaky vessels with large pores resulting from a defective angiogenic process, which facilitates NP accumulation in the absence of a functional lymphatic drain. This phenomenon, known as the Enhanced Permeability and Retention effect (100), is widely reported in the literature and has been exploited to accumulate nanocarriers in tumors (101) passively. Note that protein aggregates and cell debris are naturally found in solid tumors due to the EPR effect. Thus, by increasing NP circulation times, this passive accumulation has been employed to deliver therapeutic doses of drugs. It is the case of Doxil (liposomal doxorubicin), where the inclusion of PEG-1,2-distearoyl-sn-glycero-3-phosphorylethanolamine (PEG-DSPE) extended circulation time over 4- to a 16-fold enhancement of drug level (101). With this increased circulation time, the Doxil liposome formulation could accumulate more at the tumor site (101), achieving a more significant therapeutic effect (102, 103). Besides, blood and tissue porosity increases during inflammation, which allows NPs to accumulate in those sites (104).

Once the NPs reach their target cells, they must enter and deliver the cargo. The cytoplasmatic membrane is very robust and impermeable; things naturally enter either transported, typically ions and small molecules, or endocytosed, for proteins and larger objects. Endocytosis can be divided into pinocytosis (cell "drinking") and phagocytosis (cell "eating"). Pinocytosis, commonly termed endocytosis, is when a fraction of the membrane is invaginated, and whatever is on its surface or around it is trapped. Endocytosis can be receptor-mediated or receptor-independent when the cell membrane recycles (105). Alternatively, substances like cationic detergents can permeate through the membrane, and large liposomes can fuse with the membrane. Both pathways often show toxicity, especially membrane permeation, being endocytosis the most benign way to introduce substances inside the cell. For the case of iLNP the successful endocytosis process is determined by their size, surface composition, and target cells (99). Once the iLNP reaches the target cell and is up-taken by endocytosis (45), the cargo must be released and reach the cytoplasm. It is important to note that the relationship between cellular uptake of NPs and transfection efficiency is not trivial since this is determined by the ability to escape from the endosome. Once engulfed into the cell by the endocytic process, the early endosomes mature into late endosomes and fuse with lysosomes decreasing pH and digesting its content for recycling (106). When the pH becomes smaller than the ionizable lipid pKa, it becomes positively charged again, enabling an electrostatic interaction between the iLNP and the negatively charged lipids of the cell membranes, as cationic lipids do.

This interaction can have disruptive effects, first on the NP structure and integrity, and second, on the endosome membrane, leading to its disruption (49, 107–109), promoting endosomal escape and cytoplasmatic release of the nucleic acid cargo (107). As the electrostatic interactions between ionizable lipid and RNA increase as pH decreases, it is difficult to imagine the liberation of the cationic surfactant associated with the RNA from the NP, indicating the presence of an excess of ionizable lipids in the iLNP formulation. It has been proposed that endosome disruption is achieved by forming non-bi-layer phases due to the electrostatic interaction between the lipids. Of particular interest is the HII inverted hexagonal structure since it's been shown that this phase is not compatible with bilayers, and, as lipids tend to adopt it once they are mixed, membrane fusion and membrane disruption events are more likely to occur (35, 49, 107, 109). Regarding endosomal disruption, another possible factor playing a significant role in endosomal disruption would be the proton sponge effect. The proton sponge effect happens when during the maturation of endosomes, HCl influxes to decrease pH for digestion. The amine groups of the cationic lipid become

protonated, capturing protons from the media that resist acidification. As a result, more protons are pumped into the endosomes, followed by passive entry of more chloride ions by osmosis, the consequent increase in ionic concentration, leading to osmotic water influx and swelling, and up to rupture of the endosomes -and endolysosomes-, releasing their contents into the cytosol (110). Likely, membrane disruption and proton sponge effects happen in parallel: while the excess of ionizable lipids perturbs the membrane, RNA-bonded ionizable lipids scavenge H^+ intended for acidification. Once the cargo is delivered, pH returns to 7, quenching the cationic charge and leaving the genetic material ready for action. Finally, it is also important to note the clear difference that exists typically in cellular uptake between an *in vitro* system and an *in vivo* system, since *in vitro* conditions, the limitation of a low charge at physiological pH is much more relaxed, allowing the use of ionizable lipids with higher pKa, which can give a higher efficiency than *in vivo* (3). The endosomal escape mechanism mediated by the iLNPs, is illustrated in Figure 4.

Excretion of iLNPs

Once the NP disintegrates, its components have to be processed and excreted from the body. DSPC and Cholesterol are both part of cell membranes; therefore, degradation and metabolism of these products will occur integrated within the natural processes of the cell. Nucleases metabolize the delivered genetic material to nucleotides of various lengths. In the case of the ionizable lipids, the three (DLin-MC3-DMA, SM-102 and ALC-0315) present in the approved formulations have ester bonds, which are degraded by hydrolysis, allowing their degradation into different metabolites that are more easily excreted or harmless. The introduction of ester bonds, stable at physiological pH, which are hydrolyzed by enzymes once inside the cell or tissues, is a widely used strategy to increase the biodegradability of these lipids, reducing their accumulation and possible consequent side effects (52). DLin-MC3-DMA is primarily metabolized by hydrolysis to 4-dimethylaminobutyric acid (DMBA) and excreted from the body through the urine (ONPATRO Assessment report EMA/554262/2018). On the other hand, PEG2000-C-DMG seems not to be extensively metabolized and is suggested to be eliminated unchanged through the hepatobiliary tract to the feces (ONPATRO Assessment report EMA/554262/2018). In the case of ALC-0159, the PEG-lipid present in Comirnaty, the BioNtech Pfizer vaccine, the primary route of metabolism appears to be related to amide bond hydrolysis, yielding N,Nditetradecylamine (COMIRNATY Assessment report EMA/707383/2020).

Current challenges for ionizable lipid nanoparticles to be used in medicine

Regarding DDS, a common limitation is dosing. In systemic delivery, taking into account that there is a limitation of volume that can be injected in a single shot into the body (e.g. 10 mL/Kg for intravenous injection in mammals), the therapeutic dose might not be reached unless iLNPs have been previously concentrated because, during synthesis and storage, high concentrations lead to larger and polydisperse particles. Besides, *in vitro* simple tests, as those assessed in monolayer cell cultures, do not consider important

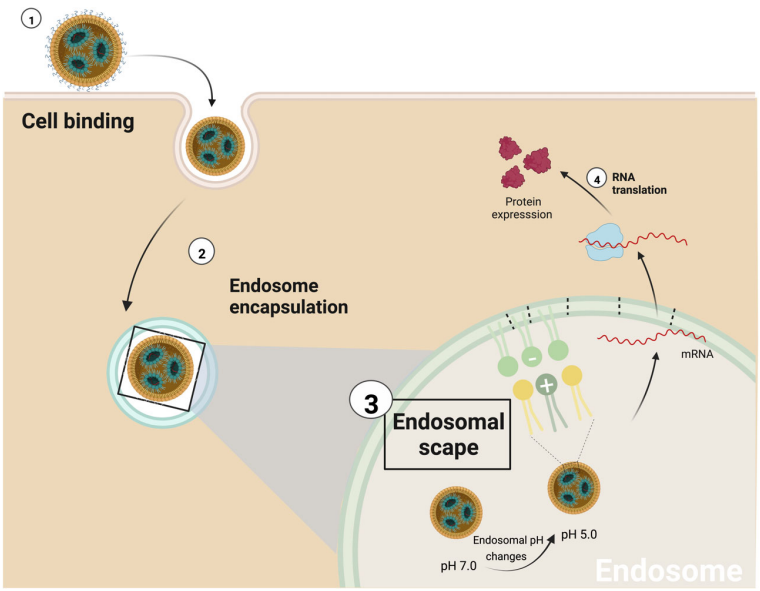

FIGURE 4
Schematic representation of endosomal scape mediated by iLNPs. 1) The first interaction between iLNPs and the target cell activates the endocytosis process, and 2) subsequently, the nanocarrier is encapsulated by the endosome. 3) As proton pumps reduce the pH of the endosome, the ionizable cationic lipid becomes progressively protonated (positively charged). As a result, it can interact with the endosome's membrane anionic lipids to produce non-bilayer structures, disrupting the endosomal membrane and the iLNP structure and 4) releasing the mRNA into the cell cytoplasm.

factors such as organ vascularity, organ penetration and other differential properties given by the organ microenvironment (111), something that is not so critical for small molecule drugs but that is determinant for NP biodistribution and effects. Similarly, different *in vivo* models show variations between them, such as the different sizes of pores in vessels or different immunological responses, which may result in different efficacy for the same NPs depending on the model being used. Also, to be able to work with animals with implanted tumors, SCID (Severe Compromised Immunodeficiency) models are often used, which lack a fully functional immune system, significantly when its size ranges between virus and bacteria. In this context, 3D cell cultures have been proposed as suitable models to study the behavior of iLNPs in a particular environment due to the possibility of mimicking a controlled extracellular matrix and different organ regions (112).

Regarding the penetration and distribution inside organs, it is known that macromolecular carriers fail to penetrate deep into organs and tumors and are generally accumulated just some micrometers away from the vessels that transported them (113–115). Furthermore, solid tumor penetration is also challenging for small molecules (111). Finally, as carriers, they could carry the substance to the wrong place with high precision, producing unexpected side effects. Also, regarding safety, as the vehicle aims at universality, it will be applied repeatedly to the individual across their life, which may end up triggering pro-inflammatory immune responses towards the iLNPs or some of their components, for example, PEG (116, 117). Beyond parenteral application, in the following, we list some of the current iLNPs developments showing the universality of the vehicle's ability to transport different sequences through different organs and portals of entry:

Oral ingestion

The most preferred administration route for medical treatments is oral delivery. Several studies suggest that the lipid nanoparticle composition enchases their biodisponibility in the gastrointestinal mucosae following the natural entrance in the digestion process (118). Additionally, studies on the siRNA- lipid nanoparticle stability showed that the LPNs remained potent and stable after exposure to solutions with pH values as low as 1.2. However, future research needs to increase cargo delivery and improve the effectiveness once mucin is present in the intestines (119). Interestingly, new research conducted by Sung et al. (120), demonstrates the efficiency deliver of IL-22 mRNA -loaded iLPS administrated by oral route in a mouse model of acute colitis. The results showed a high level of expression of interleukin 22, the recovery of body weight, and an accelerated healing process in the colon tissues.

Ocular applications

The main medicaments designed for ocular applications act in the anterior part of the eye. However, some degenerative processes, such as age-related macular degeneration, retinitis pigmentosa, and diabetic retinopathy, occur at the retina level in the posterior part of the eye. Here iLNPs provide sustained gene expression that could overcome these limitations (121). Recently, Wang and co-workers employed an iLNP to generate a cell-specific gene delivery system with sustained gene expression in the eye tissue (122).

Cutaneous application

As an external barrier, skin homeostasis is a complex process. Therefore, a broad spectrum of topical medication treats diverse cutaneous diseases. Herein, iLNPs are a promissory agent to improve drug penetration through the stratum corneum. Although to date, no iLNP has been reported for commercial cutaneous applications, the efficient encapsulation of distinct cosmetic agents such as oils, vitamins, and antimycotic and anti-age compounds are the most common pharmaceutical approximations (123). As an approach to treating a chronic wound, Gainza and co-workers loaded the recombinant human epidermal growth factor (rhEGF) into an iLNP showing an essential recovery in healing grade and wound maturity (124).

Conclusions and future perspectives

The iLNPs are a promissory concept to explore the efficient drug delivery of a broad range of substances, including genetic material, proteins and other NPs, decreasing collateral effects in healthy tissues and cells. However, despite the current knowledge on the subject being scattered and too heterogeneous, many recent discoveries and advances preclude the inevitable success of iLNPs. Indeed it has been predicted that Nanoparticulate DDS will be the most innovative and crucial cornerstones in pharmaceutical research, with a tremendous economic impact, where the possibility to adjust their physicochemical characteristics and increase the interaction with the target cell, and control the escape from the endosomal compartment allow for precision medicine. Thus, novel iLNPs will be developed with growing interest and improved pharmacokinetic profiles compared to standard drug delivery.

They are simple to produce, can load hydrophobic and hydrophilic substances, and are easily functionalizable with target moieties to ensure better precise delivery once an organ is reached. Indeed, encapsulating the genetic material into iLNPs is one of the fastest currently developing pharmaceutical technology. This success is the result of its clever design, which, in a biomimetic way, adapts to the different barriers and biological difficulties encountered along the way. All in all, in the near future, iLNPs may result in a quantum leap in medicine history.

Author contributions

RG-R, VS, NB, and VP contributed to the design and implementation of the bibliographic research, the analysis and

discussion of the literature and the writing of the manuscript. All authors contributed to the article and approved the submitted version.

Acknowledgments

We acknowledge financial support from the Spanish Ministerio de Ciencia, Innovación y Universidades (MCIU) (RTI2018-099965-B-I00, AEI/FEDER,UE) proyectos de I+D+i de programación conjunta internacional MCIN/AEI (CONCORD, PCI2019-103436) cofunded by the European Union and Generalitat de Catalunya (2017-SGR-1431). ICN2 is supported by the Severo Ochoa program from Spanish MINECO (SEV-2017-0706) and is funded by the CERCA Programme/Generalitat de Catalunya.

Conflict of interest

The authors declare that the research was conducted in the absence of any commercial or financial relationships that could be construed as a potential conflict of interest.

Publisher's note

All claims expressed in this article are solely those of the authors and do not necessarily represent those of their affiliated organizations, or those of the publisher, the editors and the reviewers. Any product that may be evaluated in this article, or claim that may be made by its manufacturer, is not guaranteed or endorsed by the publisher.

References

1. Ehrlich P. Experimental researches on specific therapy. In: *The collected papers of Paul Ehrlich* (1960) (Elsevier Science). p. 106–17.

2. Zipfel PF, Skerka C. From magic bullets to modern therapeutics: Paul Ehrlich, the German immunobiologist and physician coined the term 'complement'. *Mol Immunol* (2022) 150:90–8. doi: 10.1016/j.molimm.2022.08.002

3. Park K. Controlled drug delivery systems: Past forward and future back. *J Control Release* (2014) 190:3–8. doi: 10.1016/j.jconrel.2014.03.054

4. Gaynes R. The discovery of penicillin–new insights after more than 75 years of clinical use. *Emerging Infect Dis* (2017) 23(5):849–53. doi: 10.3201/eid2305.161556

5. Zhao N, Woodle MC, Mixson AJ. Advances in delivery systems for doxorubicin. *J Nanomed Nanotechnol* (2018) 9(5), 1000519. doi: 10.4172/2157-7439.1000519

6. Lipinski CA, Lombardo F, Dominy BW, Feeney PJ. Experimental and computational approaches to estimate solubility and permeability in drug discovery and development settings. *Adv Drug Delivery Rev* (2001) 46(1-3):3–26. doi: 10.1016/S0169-409X(00)00129-0

7. Das S, Jagan L, Isiah R, Rajesh B., Backianathan S., Subhashini J., et al. Nanotechnology in oncology: Characterization and in vitro release kinetics of cisplatin-loaded albumin nanoparticles: Implications in anticancer drug delivery. *Indian J Pharmacol* (2011) 43(4):409–13. doi: 10.4103/0253-7613.83111

8. Pelaz B, Alexiou C, Alvarez-Puebla RA, Alves F., Andrews A. M., Ashraf S., et al. Diverse applications of nanomedicine. *ACS Nano* (2017) 11(3):2313–81. doi: 10.1021/acsnano.6b06040

9. Jain PK, Huang X, El-Sayed IH, El-Sayed MA. Noble metals on the nanoscale: Optical and photothermal properties and some applications in imaging, sensing, biology, and medicine. *Acc. Chem Res* (2008) 41(12):1578–86. doi: 10.1021/ar7002804

10. Xia Y, Li W, Cobley CM, Chen J., Xia X., Zhang Q., et al. Gold nanocages: from synthesis to theranostic applications. *Acc Chem Res* (2011) 44(10):914–24. doi: 10.1021/ar200061q

11. Comenge J, Sotelo C, Romero F, Gallego O., Barnadas A., Parada T. G., et al. Detoxifying antitumoral drugs via nanoconjugation: The case of gold nanoparticles and cisplatin. *PloS One* (2012) 7(10):e47562. doi: 10.1371/journal.pone.0047562

12. Puntes VF, Comenge J. The role of PEG conformation in mixed layers: From protein corona substrate to steric stabilization avoiding protein adsorption. *ScienceOpen Res* (2015). doi: 10.14293/S2199-1006.1.SOR-MATSCI.A0Z6OM.v1

13. Daraee H, Etemadi A, Kouhi M, Alimirzalu S, Akbarzadeh A. Application of liposomes in medicine and drug delivery. *Artif Cells Nanomed Biotechnol* (2016) 44 (1):381–91. doi: 10.3109/21691401.2014.953633

14. Garg J, Pathania K, Sah SP, Pawar SV. Nanostructured lipid carriers: a promising drug carrier for targeting brain tumours. *Future J Pharm Sci* (2022) 8(1), 1. doi: 10.1186/s43094-022-00414-8

15. Wang W, Zhang L, Chen T, Guo W., Bao X., Wang D., et al. Anticancer effects of resveratrol-loaded solid lipid nanoparticles on human breast cancer cells. *Molecules* (2017) 22(11):1814. doi: 10.3390/molecules22111814

16. Wang W, Chen T, Xu H, Ren B., Cheng X., Qi R., et al. Curcumin-loaded solid lipid nanoparticles enhanced anticancer efficiency in breast cancer. *Molecules* (2018) 23 (7):1578. doi: 10.3390/molecules23071578

17. Mk D, Karthikeyan M, Ad A, Pc S., Sd O., Rc S., et al. Comprehensive review on solid lipid nanoparticles. *Ann Pharmacol Pharmaceutics* (2020) 5(4):1–6. doi: 10.47583/ijpsrr.2021.v67i01.027

18. Scioli Montoto S, Muraca G , Ruiz ME. Solid lipid nanoparticles for drug delivery: Pharmacological and biopharmaceutical aspects. *Front Mol Biosci* (2020) 7:587997. doi: 10.3389/fmolb.2020.587997

19. Mishra V, Bansal KK, Verma A, Yadav N., Thakur S., Sudhakar K., et al. Solid lipid nanoparticles: Emerging colloidal nano drug delivery systems. *Pharmaceutics* (2018) 10(4):191. doi: 10.3390/pharmaceutics10040191

20. Khosa A, Reddi S, Saha RN. Nanostructured lipid carriers for site-specific drug delivery. *BioMed Pharmacother* (2018) 103:598–613. doi: 10.1016/j.biopha.2018.04.055

21. Buck J, Grossen P, Cullis PR, Huwyler J, Witzigmann D. Lipid-based DNA therapeutics: Hallmarks of non-viral gene delivery. *ACS Nano* (2019) 13(4):3754–82. doi: 10.1021/acsnano.8b07858

22. Zhang C, Ma Y, Zhang J, Kuo J. C., Zhang Z., Xie H., et al. Modification of lipid-based nanoparticles: An efficient delivery system for nucleic acid-based immunotherapy. *Molecules* (2022) 27(6):943. doi: 10.3390/molecules27061943

23. Miele E, Spinelli GP, Miele E, Tomao F, Tomao S. Albumin-bound formulation of paclitaxel (Abraxane ABI-007) in the treatment of breast cancer. *Int J Nanomedicine* (2009) 4(1):99–105. doi: 10.2147/ijn.s3061

24. Shi J, Votruba AR, Farokhzad OC, Langer R. Nanotechnology in drug delivery and tissue engineering: from discovery to applications. *Nano Lett* (2010) 10(9):3223–30. doi: 10.1021/nl102184c

25. Hernandez-Giottonini KY, Rodriguez-Cordova RJ, Gutierrez-Valenzuela CA, Penunuri-Miranda O., Zavala-Rivera P., Guerrero-German P., et al. PLGA nanoparticle preparations by emulsification and nanoprecipitation techniques: effects of formulation parameters. *RSC Adv* (2020) 10(8):4218–31. doi: 10.1039/C9RA10857B

26. Zu H, Gao D. Non-viral vectors in gene therapy: Recent development, challenges, and prospects. *AAPS J* (2021) 23(4):78. doi: 10.1208/s12248-021-00608-7

27. Felgner PL, Gadek TR, Holm M, Roman R., Chan H. W., Wenz M., et al. Lipofection: a highly efficient, lipid-mediated DNA-transfection procedure. *Proc Natl Acad Sci U.S.A.* (1987) 84(21):7413–7. doi: 10.1073/pnas.84.21.7413

28. Tam YK, Madden TD, Hope MJ. Pieter cullis' quest for a lipid-based, fusogenic delivery system for nucleic acid therapeutics: success with siRNA so what about mRNA? *J Drug Target* (2016) 24(9):774–9. doi: 10.1080/1061186X.2016.1221955

29. Tan Y, Huang L. Overcoming the inflammatory toxicity of cationic gene vectors. *J Drug Target* (2002) 10(2):153–60. doi: 10.1080/10611860290016757

30. Zhang JS, Liu F, Huang L. Implications of pharmacokinetic behavior of lipoplex for its inflammatory toxicity. *Advanced Drug Delivery Rev* (2005) 57:689–98. doi: 10.1016/j.addr.2004.12.004

31. Semple SC, Klimuk SK, Harasym TO, Dos Santos N., Ansell S. M., Wong K. F., et al. Efficient encapsulation of antisense oligonucleotides in lipid vesicles using ionizable aminolipids: Formation of novel small multilamellar vesicle structures. *Biochim Biophys Acta* (2001) 1510(1-2):152–66. doi: 10.1016/S0005-2736(00)00343-6

32. Plank C, Mechtler K, Szoka FCJr., Wagner E. Activation of the complement system by synthetic DNA complexes: a potential barrier for intravenous gene delivery. *Hum Gene Ther* (1996) 7(12):1437–46. doi: 10.1089/hum.1996.7.12-1437

33. Devine DV, Wong K, Serrano K, Chonn A, Cullis PR. Liposome-complement interactions in rat serum: Implications for liposome survival studies. *Biochim Biophys Acta* (1994) 1191(1):43–51. doi: 10.1016/0005-2736(94)90231-3

34. Marjan J, Xie Z, Devine DV. Liposome-induced activation of the classical complement pathway does not require immunoglobulin. *Biochim Biophys Acta* (1994) 1192(1):35–44. doi: 10.1016/0005-2736(94)90140-6

35. Fenton OS, Kauffman KJ, McClellan RL, Appel E. A., Dorkin J. R., Tibbitt M. W., et al. Bioinspired alkenyl amino alcohol ionizable lipid materials for highly potent in vivo mRNA delivery. *Adv Mater* (2016) 28(15):2939–43. doi: 10.1002/adma.201505822

36. Evers MJW, Kulkarni JA, van der Meel R, Cullis P. R., Vader P., Schiffelers R. M., et al. State-of-the-Art design and rapid-mixing production techniques of lipid nanoparticles for nucleic acid delivery. *Small Methods* (2018) 2(9):1700375. doi: 10.1002/smtd.201700375

37. Suzuki Y, Ishihara H. Difference in the lipid nanoparticle technology employed in three approved siRNA (Patisiran) and mRNA (COVID-19 vaccine) drugs. *Drug Metab Pharmacokinet* (2021) 41:100424. doi: 10.1016/j.dmpk.2021.100424

38. Guevara ML, Persano F , Persano S. Advances in lipid nanoparticles for mRNA-based cancer immunotherapy. *Front Chem* (2020) 8:589959. doi: 10.3389/fchem.2020.589959

39. Gomez-Aguado I, Rodriguez-Castejon J, Vicente-Pascual M, Rodriguez-Gascon A., Pozo-Rodriguez A. D., Solinis Aspiazu M. A., et al. Nucleic acid delivery by solid lipid nanoparticles containing switchable lipids: Plasmid DNA vs. messenger RNA. *Molecules* (2020) 25(24):5995. doi: 10.3390/molecules25245995

40. Hald Albertsen C, Kulkarni JA, Witzigmann D, Lind M., Petersson K., Simonsen J. B., et al. The role of lipid components in lipid nanoparticles for vaccines and gene therapy. *Adv Drug Delivery Rev* (2022) 188:114416. doi: 10.1016/j.addr.2022.114416

41. Kulkarni JA, Witzigmann D, Leung J, Tam YYC, Cullis PR. On the role of helper lipids in lipid nanoparticle formulations of siRNA. *Nanoscale* (2019) 11(45):21733–9. doi: 10.1039/C9NR09347H

42. Belliveau NM, Huft J, Lin PJ, Chen S., Leung A. K., Leaver T. J., et al. Microfluidic synthesis of highly potent limit-size lipid nanoparticles for in vivo delivery of siRNA. *Mol Ther Nucleic Acids* (2012) 1(8):e37. doi: 10.1038/mtna.2012.28

43. Kauffman KJ, Dorkin JR, Yang JH, Heartlein M. W., DeRosa F., Mir F. F., et al. Optimization of lipid nanoparticle formulations for mRNA delivery in vivo with fractional factorial and definitive screening designs. *Nano Lett* (2015) 15(11):7300–6. doi: 10.1021/acs.nanolett.5b02497

44. Jayaraman M, Ansell SM, Mui BL, Tam Y. K., Chen J., Du X., et al. Maximizing the potency of siRNA lipid nanoparticles for hepatic gene silencing in vivo. *Angew Chem Int Ed Engl* (2012) 51(34):8529–33. doi: 10.1002/anie.201203263

45. Akinc A, Maier MA, Manoharan M, Fitzgerald K., Jayaraman M., Barros S., et al. The onpattro story and the clinical translation of nanomedicines containing nucleic acid-based drugs. *Nat Nanotechnol* (2019) 14(12):1084–7. doi: 10.1038/s41565-019-0591-y

46. Maier MA, Jayaraman M, Matsuda S, Liu J., Barros S., Querbes W., et al. Biodegradable lipids enabling rapidly eliminated lipid nanoparticles for systemic delivery of RNAi therapeutics. *Mol Ther* (2013) 21(8):1570–8. doi: 10.1038/mt.2013.124

47. Whitehead KA, Dorkin JR, Vegas AJ, Chang P. H., Veiseh O., Matthews J., et al. Degradable lipid nanoparticles with predictable in vivo siRNA delivery activity. *Nat Commun* (2014) 5(1):4277. doi: 10.1038/ncomms5277

48. Hao J, Kos P, Zhou K, Miller J. B., Xue L., Yan Y., et al. Rapid synthesis of a lipocationic polyester library via ring-opening polymerization of functional valerolactones for efficacious siRNA delivery. *J Am Chem Soc* (2015) 137(29):9206–9. doi: 10.1021/jacs.5b03429

49. Semple SC, Akinc A, Chen J, Sandhu A. P., Mui B. L., Cho C. K., et al. Rational design of cationic lipids for siRNA delivery. *Nat Biotechnol* (2010) 28(2):172–6. doi: 10.1038/nbt.1602

50. Li AV, Moon JJ, Abraham W, Suh H., Elkhader J., Seidman M. A., et al. Generation of effector memory T cell-based mucosal and systemic immunity with pulmonary nanoparticle vaccination. *Sci Transl Med* (2013) 5(204):204ra130. doi: 10.1126/scitranslmed.3006516

51. Miller JB, Kos P, Tieu V, Zhou K, Siegwart DJ. Development of cationic quaternary ammonium sulfonamide amino lipids for nucleic acid delivery. *ACS Appl Mater Interfaces* (2018) 10(3):2302–11. doi: 10.1021/acsami.7b15982

52. Han X, Zhang H, Butowska K, Swingle K. L., Alameh M. G., Weissman D., et al. An ionizable lipid toolbox for RNA delivery. *Nat Commun* (2021) 12(1):7233. doi: 10.1038/s41467-021-27493-0

53. Crawford R, Dogdas B, Keough E, Haas R. M., Wepukhulu W., Krotzer S., et al. Analysis of lipid nanoparticles by cryo-EM for characterizing siRNA delivery vehicles. *Int J Pharm* (2011) 403(1-2):237–44. doi: 10.1016/j.ijpharm.2010.10.025

54. Chen C, Chen C, Li Y, Gu R, Yan X. Characterization of lipid-based nanomedicines at the single-particle level. *Fundam Res* (2022). doi: 10.1016/j.fmre.2022.09.011

55. Bunjes H, Unruh T. Characterization of lipid nanoparticles by differential scanning calorimetry, X-ray and neutron scattering. *Advanced Drug Delivery Rev* (2007) 59:379–402. doi: 10.1016/j.addr.2007.04.013

56. Schilt Y, Berman T, Wei X, Barenholz Y, Raviv U. Using solution X-ray scattering to determine the high-resolution structure and morphology of PEGylated liposomal doxorubicin nanodrugs. *Biochim Biophys Acta* (2016) 1860(1 Pt A):108–19. doi: 10.1016/j.bbagen.2015.09.012

57. Dong YD, Boyd BJ. Applications of X-ray scattering in pharmaceutical science. *Int J Pharm* (2011) 417(1-2):101–11. doi: 10.1016/j.ijpharm.2011.01.022

58. Pabst G, Kucerka N, Nieh MP, Rheinstadter MC, Katsaras J. Applications of neutron and X-ray scattering to the study of biologically relevant model membranes. *Chem Phys Lipids* (2010) 163(6):460–79. doi: 10.1016/j.chemphyslip.2010.03.010

59. Di Cola E, Grillo I, Ristori S. Small angle X-ray and neutron scattering: Powerful tools for studying the structure of drug-loaded liposomes. *Pharmaceutics* (2016) 8(2):10. doi: 10.3390/pharmaceutics8020010

60. Cui L, Renzi S, Quagliarini E, Digiacomo L., Amenitsch H., Masuelli L., et al. Efficient delivery of DNA using lipid nanoparticles. *Pharmaceutics* (2022) 14(8):1698. doi: 10.3390/pharmaceutics14081698

61. Viger-Gravel J, Schantz A, Pinon AC, Rossini A. J., Schantz S., Emsley L., et al. Structure of lipid nanoparticles containing siRNA or mRNA by dynamic nuclear polarization-enhanced NMR spectroscopy. *J Phys Chem B* (2018) 122(7):2073–81. doi: 10.1021/acs.jpcb.7b10795

62. Martinez-Negro M, Kumar K, Barran-Berdon AL, Datta S., Kondaiah P., Junquera E., et al. Efficient cellular knockdown mediated by siRNA nanovectors of Gemini cationic lipids having delocalizable headgroups and oligo-oxyethylene spacers. *ACS Appl Mater Interfaces* (2016) 8(34):22113–26. doi: 10.1021/acsami.6b08823

63. Yanez Arteta M, Kjellman T, Bartesaghi S, Wallin S., Wu X., Kvist A. J., et al. Successful reprogramming of cellular protein production through mRNA delivered by functionalized lipid nanoparticles. *Proc Natl Acad Sci U.S.A.* (2018) 115(15):E3351–60. doi: 10.1073/pnas.1720542115

64. Zak MM, Zangi L. Lipid nanoparticles for organ-specific mRNA therapeutic delivery. *Pharmaceutics* (2021) 13(10):1675. doi: 10.3390/pharmaceutics13101675

65. Cho EC, Zhang Q, Xia Y. The effect of sedimentation and diffusion on cellular uptake of gold nanoparticles. *Nat Nanotechnol* (2011) 6(6):385–91. doi: 10.1038/nnano.2011.58

66. Krug HF. Nanosafety research–are we on the right track? *Angew Chem Int Ed Engl* (2014) 53(46):12304–19. doi: 10.1002/anie.201403367

67. Bian SW, Mudunkotuwa IA, Rupasinghe T, Grassian VH. Aggregation and dissolution of 4 nm ZnO nanoparticles in aqueous environments: influence of pH, ionic strength, size, and adsorption of humic acid. *Langmuir* (2011) 27(10):6059–68. doi: 10.1021/la200570n

68. Xia Y, Tian J, Chen X. Effect of surface properties on liposomal siRNA delivery. *Biomaterials* (2016) 79:56–68. doi: 10.1016/j.biomaterials.2015.11.056

69. Harvie P, Wong FMP, Bally MB. Use of poly(ethylene glycol)-lipid conjugates to regulate the surface attributes and transfection activity of lipid-DNA particles. *J Pharm Sci* (2000) 89:652–63. doi: 10.1002/(SICI)1520-6017(200005)89:5<652::AID-JPS11>3.0.CO;2-H

70. Song L. Y., Ahkong Q. F., Rong Q., Wang Z., Ansell S., Hope M. J., et al. Characterization of the inhibitory effect of PEG-lipid conjugates on the intracellular delivery of plasmid and antisense DNA mediated by cationic lipid liposomes. *Biochim Biophys Acta* (2002) 1558(1):1–13. doi: 10.1016/S0005-2736(01)00399-6

71. Mui BL, Tam YK, Jayaraman M, Ansell S. M., Du X., Tam Y. Y., et al. Influence of polyethylene glycol lipid desorption rates on pharmacokinetics and pharmacodynamics of siRNA lipid nanoparticles. *Mol Ther Nucleic Acids* (2013) 2(12):e139. doi: 10.1038/mtna.2013.66

72. Hashiba K, Sato Y, Harashima H. pH-labile PEGylation of siRNA-loaded lipid nanoparticle improves active targeting and gene silencing activity in hepatocytes. *J Control Release* (2017) 262:239–46. doi: 10.1016/j.jconrel.2017.07.046

73. Francia V, Schiffelers RM, Cullis PR, Witzigmann D. The biomolecular corona of lipid nanoparticles for gene therapy. *Bioconjug Chem* (2020) 31(9):2046–59. doi: 10.1021/acs.bioconjchem.0c00366

74. Walczyk D, Bombelli FB, Monopoli MP, Lynch I, Dawson KA. What the cell "sees" in bionanoscience. *J Am Chem Soc* (2010) 132(16):5761–8. doi: 10.1021/ja910675v

75. Monopoli MP, Aberg C, Salvati A, Dawson KA. Biomolecular coronas provide the biological identity of nanosized materials. *Nat Nanotechnol* (2012) 7(12):779–86. doi: 10.1038/nnano.2012.207

76. Cai R, Chen C. The crown and the scepter: Roles of the protein corona in nanomedicine. *Adv Mater* (2019) 31(45):e1805740. doi: 10.1002/adma.201805740

77. Nguyen VH, Lee BJ. Protein corona: A new approach for nanomedicine design. *Int J Nanomedicine* (2017) 12:3137–51. doi: 10.2147/IJN.S129300

78. Casals E, Pfaller T, Duschl A, Oostingh GJ, Puntes V. Time evolution of the nanoparticle protein corona. *ACS Nano* (2010) 4(7):3623–32. doi: 10.1021/nn901372t

79. Akinc A, Querbes W, De S, Qin J., Frank-Kamenetsky M., Jayaprakash K. N., et al. Targeted delivery of RNAi therapeutics with endogenous and exogenous ligand-based mechanisms. *Mol Ther* (2010) 18(7):1357–64. doi: 10.1038/mt.2010.85

80. Qiu M, Tang Y, Chen J, Muriph R., Ye Z., Huang C., et al. Lung-selective mRNA delivery of synthetic lipid nanoparticles for the treatment of pulmonary lymphangioleiomyomatosis. *Proc Natl Acad Sci U.S.A.* (2022) 119(8):e2116271119. doi: 10.1073/pnas.2116271119

81. Rejman J, Oberle V, Zuhorn IS, Hoekstra D. Size-dependent internalization of particles via the pathways of clathrin- and caveolae-mediated endocytosis. *Biochem J* (2004) 377(Pt 1):159–69. doi: 10.1042/bj20031253

82. Geranio L, Heuberger M, Nowack B. The behavior of silver nanotextiles during washing. *Environ Sci Technol* (2009) 43(21):8113–8. doi: 10.1021/es9018332

83. Elzey S, Grassian VH. Agglomeration, isolation and dissolution of commercially manufactured silver nanoparticles in aqueous environments. *J Nanoparticle Res* (2009) 12(5):1945–58. doi: 10.1007/s11051-009-9783-y

84. Li X, Lenhart JJ, Walker HW. Aggregation kinetics and dissolution of coated silver nanoparticles. *Langmuir* (2012) 28(2):1095–104. doi: 10.1021/la202328n

85. Li X, Lenhart JJ, Walker HW. Dissolution-accompanied aggregation kinetics of silver nanoparticles. *Langmuir* (2010) 26(22):16690–8. doi: 10.1021/la101768n

86. Liu J, Hurt RH. Ion release kinetics and particle persistence in aqueous nano-silver colloids. *Environ Sci Technol* (2010) 44(6):2169–75. doi: 10.1021/es9035557

87. Hwang J, Sullivan MO, Kiick KL. Targeted drug delivery via the use of ECM-mimetic materials. *Front Bioeng Biotechnol* (2020) 8:69. doi: 10.3389/fbioe.2020.00069

88. Henke E, Nandigama R, Ergün S. Extracellular matrix in the tumor microenvironment and its impact on cancer therapy. *Front Mol Biosci* (2020) 6. doi: 10.3389/fmolb.2019.00160

89. Ernst LM, Casals E, Italiani P, Boraschi D, Puntes V. The interactions between nanoparticles and the innate immune system from a nanotechnologist perspective. *Nanomaterials (Basel)* (2021) 11(11):2991. doi: 10.3390/nano11112991

90. Arana L, Bayon-Cordero L, Sarasola LI, Berasategi M., Ruiz S., Alkorta I., et al. Solid lipid nanoparticles surface modification modulates cell internalization and improves chemotoxic treatment in an oral carcinoma cell line. *Nanomaterials (Basel)* (2019) 9(3):464. doi: 10.3390/nano9030464

91. Sebak AA. Limitations of pegylated nanocarriers: Unfavourable physicochemical properties, biodistribution patterns and cellular and subcellular fates. *Int J Appl Pharmaceutics* (2018) 10(5):6–12. doi: 10.22159/ijap.2018v10i5.27568

92. Hoang Thi TT, Pilkington EH, Nguyen DH, Lee J. S., Park K. D., Truong N. P., et al. The importance of poly(ethylene glycol) alternatives for overcoming PEG immunogenicity in drug delivery and bioconjugation. *Polymers (Basel)* (2020) 12 (2):298. doi: 10.3390/polym12020298

93. Goy-Lopez S, Juarez J, Alatorre-Meda M, Casals E., Puntes V. F., Taboada P., et al. Physicochemical characteristics of proteina-NP bioconjugates: the role of particle curvature and solution conditions on human serum albumin conformation and fibrillogenesis inhibition. *Langmuir* (2012) 28(24):9113–26. doi: 10.1021/la300402w

94. Ojea-Jimenez I, Puntes V. Instability of cationic gold nanoparticle bioconjugates: the role of citrate ions. *J Am Chem Soc* (2009) 131(37):13320–7. doi: 10.1021/ja902894s

95. Casals E, Barrena R, Garcia A, Gonzalez E., Delgado L., Busquets-Fite M., et al. Programmed iron oxide nanoparticles disintegration in anaerobic digesters boosts biogas production. *Small* (2014) 10(14):2801–8, 2741. doi: 10.1002/smll.201303703

96. Bastus NG, Casals E, Vázquez-Campos S, Puntes V. Reactivity of engineered inorganic nanoparticles and carbon nanostructures in biological media. *Nanotoxicology* (2008) 2(3):99–112. doi: 10.1080/17435390802217830

97. Barua S, Mitragotri S. Challenges associated with penetration of nanoparticles across cell and tissue barriers: A review of current status and future prospects. *Nano Today* (2014) 9(2):223–43. doi: 10.1016/j.nantod.2014.04.008

98. Dal Magro R, Ornaghi F, Cambianica I, Beretta S., Re F., Musicanti C., et al. ApoE-modified solid lipid nanoparticles: A feasible strategy to cross the blood-brain barrier. *J Control Release* (2017) 249:103–10. doi: 10.1016/j.jconrel.2017.01.039

99. Carlander U, Li D, Jolliet O, Emond C, Johanson G. Toward a general physiologically-based pharmacokinetic model for intravenously injected nanoparticles. *Int J Nanomedicine* (2016) 11:625–40. doi: 10.2147/IJN.S94370

100. Maeda H, Wu J, Sawa T, Matsumura Y, Hori K. Tumor vascular permeability and the EPR effect in macromolecular therapeutics: a review. *J Control Release* (2000) 65(1-2):271–84. doi: 10.1016/S0168-3659(99)00248-5

101. Martin F, Huang A, Uziely B, Kaufman B., Safra T., Gabizon A., et al. Prolonged circulation time and enhanced accumulation in malignant exudates of doxorubicin encapsulated in polyethylene-glycol coated liposomes. *Cancer Researc* (1994) 54(4):987–92.

102. Safra T, Muggia F, Jeffers S, Tsao-Wei D. D., Groshen S., Lyass O., et al. Pegylated liposomal doxorubicin (doxil): Reduced clinical cardiotoxicity in patients reaching or exceeding cumulative doses of 500 mg/m2. *Ann Oncol* (2000) 11(8):1029–33. doi: 10.1023/A:1008365716693

103. Gabizon A, Shmeeda H, Barenholz Y. Pharmacokinetics of pegylated liposomal doxorubicin: Review of animal and human studies. *Clin Pharmacokinet* (2003) 42 (5):419–36. doi: 10.2165/00003088-200342050-00002

104. Brusini R, Varna M, Couvreur P. Advanced nanomedicines for the treatment of inflammatory diseases. *Adv Drug Delivery Rev* (2020) 157:161–78. doi: 10.1016/j.addr.2020.07.010

105. Rennick JJ, Johnston APR, Parton RG. Key principles and methods for studying the endocytosis of biological and nanoparticle therapeutics. *Nat Nanotechnol* (2021) 16(3):266–76. doi: 10.1038/s41565-021-00858-8

106. Herrera M, Kim J, Eygeris Y, Jozic A, Sahay G. Illuminating endosomal escape of polymorphic lipid nanoparticles that boost mRNA delivery. *Biomater Sci* (2021) 9 (12):4289–300. doi: 10.1039/D0BM01947J

107. Hafez IM, Maurer N, Cullis PR. On the mechanism whereby cationic lipids promote intracellular delivery of polynucleic acids. *Gene Ther* (2001) 8(15):1188–96. doi: 10.1038/sj.gt.3301506

108. Miao L, Lin J, Huang Y, Li L., Delcassian D., Ge Y., et al. Synergistic lipid compositions for albumin receptor mediated delivery of mRNA to the liver. *Nat Commun* (2020) 11(1):2424. doi: 10.1038/s41467-020-16248-y

109. Cullis PR, Hope MJ. Lipid nanoparticle systems for enabling gene therapies. *Mol Ther* (2017) 25(7):1467–75. doi: 10.1016/j.ymthe.2017.03.013

110. Behr J-P. The proton sponge: A trick to enter cells the viruses did not exploit. *Chimia* (1997) 51(1-2):34. doi: 10.2533/chimia.1997.34

111. Tredan O, Galmarini CM, Patel K, Tannock IF. Drug resistance and the solid tumor microenvironment. *J Natl Cancer Inst* (2007) 99(19):1441–54. doi: 10.1093/jnci/djm135

112. Papi M, Pozzi D, Palmieri V, Caracciolo G. Principles for optimization and validation of mRNA lipid nanoparticle vaccines against COVID-19 using 3D bioprinting. *Nano Today* (2022) 43:101403. doi: 10.1016/j.nantod.2022.101403

113. Ruenraroengsak P, Cook JM, Florence AT. Nanosystem drug targeting: Facing up to complex realities. *J Control Release* (2010) 141(3):265–76. doi: 10.1016/j.jconrel.2009.10.032

114. Perrault SD, Walkey C, Jennings T, Fischer HC, Chan WC. Mediating tumor targeting efficiency of nanoparticles through design. *Nano Lett* (2009) 9(5):1909–15. doi: 10.1021/nl900031y

115. Minchinton AI, Tannock IF. Drug penetration in solid tumours. *Nat Rev Cancer* (2006) 6(8):583–92. doi: 10.1038/nrc1893

116. Chen BM, Cheng TL, Roffler SR. Polyethylene glycol immunogenicity: Theoretical, clinical, and practical aspects of anti-polyethylene glycol antibodies. *ACS Nano* (2021) 15(9):14022–48. doi: 10.1021/acsnano.1c05922

117. Kong YW , Dreaden EC. PEG: Will it come back to you? polyethelyne glycol immunogenicity, COVID vaccines, and the case for new PEG derivatives and alternatives. *Front Bioeng Biotechnol* (2022) 10:879988. doi: 10.3389/fbioe.2022.879988

118. Talegaonkar S, Bhattacharyya A. Potential of lipid nanoparticles (SLNs and NLCs) in enhancing oral bioavailability of drugs with poor intestinal permeability. *AAPS PharmSciTech* (2019) 20(3):121. doi: 10.1208/s12249-019-1337-8

119. Ball RL, Bajaj P, Whitehead KA. Oral delivery of siRNA lipid nanoparticles: Fate in the GI tract. *Sci Rep* (2018) 8(1):2178. doi: 10.1038/s41598-018-20632-6

120. Sung J, Alghoul Z, Long D, Yang C, Merlin D. Oral delivery of IL-22 mRNA-loaded lipid nanoparticles targeting the injured intestinal mucosa: A novel therapeutic solution to treat ulcerative colitis. *Biomaterials* (2022) 288(August):121707. doi: 10.1016/j.biomaterials.2022.121707

121. Wang Y, Rajala A, Rajala RV. Lipid nanoparticles for ocular gene delivery. *J Funct Biomater* (2015) 6(2):379–94. doi: 10.3390/jfb6020379

122. Toualbi L, Toms M, Moosajee M. The landscape of non-viral gene augmentation strategies for inherited retinal diseases. *Int J Mol Sci* (2021) 22(5):1–14. doi: 10.3390/ijms22052318

123. Garces A, Amaral MH, Sousa Lobo JM, Silva AC. Formulations based on solid lipid nanoparticles (SLN) and nanostructured lipid carriers (NLC) for cutaneous use: A review. *Eur J Pharm Sci* (2018) 112(September 2017):159–67. doi: 10.1016/j.ejps.2017.11.023

124. Gainza G, Bonafonte DC, Moreno B, Aguirre J. J., Gutierrez F. B., Villullas S., et al. The topical administration of rhEGF-loaded nanostructured lipid carriers (rhEGF-NLC) improves healing in a porcine full-thickness excisional wound model. *J Control Release* (2015) 197:41–7. doi: 10.1016/j.jconrel.2014.10.033

frontiers | Frontiers in Immunology

TYPE Original Research
PUBLISHED 09 May 2023
DOI 10.3389/fimmu.2023.1128582

OPEN ACCESS

EDITED BY
Kirill Afonin,
University of North Carolina at Charlotte,
United States

REVIEWED BY
Rong Hai,
University of California, Riverside,
United States
Massimo Masserini,
University of Milano-Bicocca, Italy

*CORRESPONDENCE
Neus G. Bastús
neus.bastus@icn2.cat
Víctor Puntes
victor.puntes@icn2.cat

RECEIVED 20 December 2022
ACCEPTED 21 April 2023
PUBLISHED 09 May 2023

CITATION
Gustà MF, Edel MJ, Salazar VA, Alvarez-Palomo B, Juan M, Broggini M, Damia G, Bigini P, Corbelli A, Fiordaliso F, Barbul A, Korenstein R, Bastús NG and Puntes V (2023) Exploiting endocytosis for transfection of mRNA for cytoplasmatic delivery using cationic gold nanoparticles. *Front. Immunol.* 14:1128582. doi: 10.3389/fimmu.2023.1128582

Exploiting endocytosis for transfection of mRNA for cytoplasmatic delivery using cationic gold nanoparticles

Muriel F. Gustà[1,2,3], Michael J. Edel[4,5,6], Vivian A. Salazar[1], Belén Alvarez-Palomo[7], Manel Juan[4], Massimo Broggini[8], Giovanna Damia[8], Paolo Bigini[8], Alessandro Corbelli[8], Fabio Fiordaliso[8], Alexander Barbul[9], Rafi Korenstein[9], Neus G. Bastús[1,3]* and Víctor Puntes[1,2,3,10]*

[1]Institut Català de Nanociència i Nanotecnologia (ICN2), Consejo Superior de Investigaciones Científicas (CSIC), The Barcelona Institute of Science and Technology (BIST), Barcelona, Spain, [2]Vall d'Hebron Institut de Recerca (VHIR), Barcelona, Spain, [3]Biomedical Research Networking Center in Bioengineering, Biomaterials and Nanomedicine (CIBER-BBN), Madrid, Spain, [4]Hospital Clínic de Barcelona, Servei Immunologia-IDIBAPS, Barcelona, Spain, [5]Unit of Anatomy and Embryology, Universitat Autònoma de Barcelona, Faculty of Medicine, Barcelona, Spain, [6]University of Western Australia, Faculty of Medicine, Discipline of Medical Sciences and Genetics, School of Biomedical Sciences, Perth, WA, Australia, [7]Banc de Sang i Teixits, Cell Therapy Service, Barcelona, Spain, [8]IRCCS-Istituto di Ricerche Farmacologiche Mario Negri, Milano, Italy, [9]Tel Aviv University, Sackler School of Medicine, Tel Aviv-Yafo, Israel, [10]Institució Catalana de Recerca i Estudis Avançats (ICREA), Barcelona, Spain

Introduction: Gene therapy holds promise to cure various diseases at the fundamental level. For that, efficient carriers are needed for successful gene delivery. Synthetic 'non-viral' vectors, as cationic polymers, are quickly gaining popularity as efficient vectors for transmitting genes. However, they suffer from high toxicity associated with the permeation and poration of the cell membrane. This toxic aspect can be eliminated by nanoconjugation. Still, results suggest that optimising the oligonucleotide complexation, ultimately determined by the size and charge of the nanovector, is not the only barrier to efficient gene delivery.

Methods: We herein develop a comprehensive nanovector catalogue comprising different sizes of Au NPs functionalized with two different cationic molecules and further loaded with mRNA for its delivery inside the cell.

Results and Discussion: Tested nanovectors showed safe and sustained transfection efficiencies over 7 days, where 50 nm Au NPs displayed the highest transfection rates. Remarkably, protein expression was increased when nanovector transfection was performed combined with chloroquine. Cytotoxicity and risk assessment demonstrated that nanovectors are safe, ascribed to lesser cellular damage due to their internalization and delivery via endocytosis. Obtained results may pave the way to design advanced and efficient gene therapies for safely transferring oligonucleotides.

KEYWORDS

gold nanoparticles, cationic, transfection, gene therapeutics, safety

Introduction

Developing efficient gene therapies depends on the means for transferring oligonucleotides (DNA or RNA) into the cell. The most common vectors used are replication-defective vector systems based on two types of viruses: retroviruses and adenoviruses. These vectors have been engineered to drastically reduce the transcriptional activity of the virus, virtually eliminating the possibility of viral reactivation. However, uncontrolled integration into the genome can potentially lead to insertional mutagenesis if the integration of vector DNA into host cells is placed near an oncogene, posing serious concerns in their clinical application (1). Additionally, their production is complex, and their production under Good Manufacturing Practices is burdened with strict regulations. Last but not least, DNA-insertion therapies in the context of CAR-T cell therapy, where ex-vivo transfection reprograms T cells to destroy B cells in the case of leukaemia, deplete patients of B cells for life with the corresponding health and societal burden. As an alternative, the idea of mRNA transfection will lead to transient cell therapy, dramatically reducing genetic therapy side effects. In addition, the transfection with mRNA has to be performed in the cytoplasm, opening the venue for non-viral transfection vectors.

Unlike viral vectors, nonviral ones rely on forming noncovalent assemblies between mRNA (a polyanion), cationic polymers, and lipidic moieties. Although a leading class of synthetic gene-delivery vehicles, cationic polymers suffer from high toxicity, and their efficiency does not compare to viral systems (2). To overcome these limitations, the delivery of oligonucleotides using nanovectors, a nanoparticle-based transfection vector, is attracting increasing attention (3–6). This includes lipidic and polymeric NPs composed of biocompatible units that self-assemble encapsulating nucleic acids. Also, inorganic NPs which can be functionalized with DNA or mRNA and can be used for *in vitro* transfection applications. Among the candidates, Au nanoparticles (NPs) are remarkably interesting due to their small size and monodispersity, low cytotoxicity, low immunogenicity, biocompatibility, straightforward synthesis and easy functionalization (7). Indeed, the chemical functionalization of Au NPs with cationic molecules (5, 8–12), especially polyethylenimine (PEI) molecules (13, 14), favours efficient oligonucleotide adsorption by high-affinity electrostatic interactions, ultimately enabling transfection. In any case, the interactions between the innate immune system and nanoparticles and derived objects can be especially immunogenic. Thus, purity, solubility, and surface state has to be precisely controlled (15).

The efficient loading of the nanovectors is ultimately determined by its size and charge. By adjusting its size, its loading capacity is modified (16). Thus, the load vs carrier ratio increases as the vector becomes smaller. Similarly, the loading depends on the charge of the nanovector. Cationic polymers possess many positive charges providing strong interactions with oligonucleotides, which are negatively charged. As simple as that, results suggest that optimising the oligonucleotide complexation is not the only barrier to gene delivery (8, 9, 13, 14, 17). A higher grafting density of PEI does not always result in more compact and smaller complexes with mRNA, intended to prevent degradation and facilitate cytosolic mobility. Besides, approaches that work for one cell line might not perform well for others, suggesting that the mechanisms that NPs use for cell entry and cell trafficking are essential factors to consider when designing efficient transfection nanovectors (18).

The second aspect is the cellular uptake of the nanovector. Endocytosis is the primary mechanism for the uptake of nanovector- oligonucleotide complexes (19). During this process, the loaded nanovector is engulfed by the cell membrane and delivered into the cell within a vesicle. The internalization process depends on nanovector size and charge. The highest cellular internalization is observed for NPs in the size ranges of 25–50 nm (20). Alternatives for cell entry other than endocytosis are membrane permeation and membrane fusion, which often result in high toxicity, especially permeation (21, 22). Similarly, surface charge determines cellular uptake. The negatively charged cell membrane enhances the uptake of positively charged NPs. However, the uptake of positively charged NPs may disrupt the integrity of the cell membrane and lead to an increase in toxicity (23) unless size and structure are provided.

The third aspect is the endosomal escape of the nanovector. Once inside the cell, the nanovector complex is trapped within a vesicle. Several mechanisms have been identified to escape the endosome into the cytosol, the most popularly known as the "proton sponge mechanism" (24). The proton sponge mechanism relies on the fact that present amines are not protonated under physiological conditions. These basic moieties can buffer the decreasing pH within the endosome. As more protons are pumped, more counter ions (mainly chloride) influx into the endosome for electroneutrality. This fact increases the osmotic pressure and, ultimately, the passive diffusion of water into the endosome. Consequently, the endosome continues to swell until the increasing membrane stress leads to membrane rupture and a release of the contents.

In this context, the study's main objective is to design and develop transfection nanovectors for releasing nucleic acids as messenger RNA (mRNA) inside the cell ready for transfection. The introduction of mRNA by nonviral transfection vectors allows the gene's transient expression, which presents several medical advantages. For instance, note that people treated with DNA CAR-T cell immunotherapy get deprived of B cells for life (25, 26). The nanovector consists of a cationic Au NP where mRNA is adsorbed for further delivery into the cytosol. There are two critical points in the development of the nanovector: i) the tight absorption of enough mRNA and ii) the efficient cytoplasmic release of the mRNA following the "proton sponge" effect. The number of mRNA molecules adsorbed onto the nanovector is expected to depend on the size of the nanovector and the density of amino groups present at their surface, and this density will also determine the efficiency of the cytoplasmic release. In addition, the absorption of the mRNA onto the NP, as occur with other molecules as proteins, protects them from degradation.

Thus, a nanovector catalogue has been developed comprising different sizes of Au NP cores, later functionalized with two different cationic molecules. These nanovectors were further

loaded with mRNA for their application as nonviral transfection vectors. Cationic molecules have already been used as transfection agents, but with significant toxicity concerns (27–30). However, its absorption to the NP's surface promotes the loss of flexibility and the membrane pore formation ability. Instead, PEI-derived NPs (nanovectors) attach to the cell membrane, not crossing it but inducing endocytosis. Consequently, its toxic aspect is eliminated thanks to nanoconjugation. Indeed, detoxification by nanoconjugation has been observed before in different systems (31). Thus, the monolayer coverage of Au NPs allows for tuning the charge and structure to maximize transfection efficiency while reducing associated toxicity.

Results and discussion

Synthesis, cationic functionalization and mRNA loading of citrate-stabilized Au NPs

The first critical point in the design of the nanovector is the efficient adsorption of mRNA for their further delivery into the cytosol. The number of molecules adsorbed onto the nanovector depends on the size and density of amino groups at their surface. Therefore, a nanovector catalogue comprising different sizes of Au NPs functionalized with two different cationic molecules and further loaded with mRNA was developed. By adjusting the size of the Au NPs and the nature of the cationic molecule, their loading capacity was modified. Characterization by UV-Vis spectroscopy, DLS and Z-Potential was performed at each step and summarized in Table 1. The sizes of choice were 5, 20 and 50 nm as this size regime favours NP's endocytosis (32–35) and presents proven stability in physiological media (36, 37). As synthesized Au NPs were further functionalized with either 11-amino-1-undecanethiol acid (AUT) or polyethyleneimine 2kDa (PEI). Both cationic molecules contain amine terminal groups providing a positive charge to the Au NPs at physiological pH while differing in their molecular structure and density of amino groups. While AUT consists of an 11-carbon chain with a terminal amine and a thiol group in the opposite site that pseudo-covalently binds to gold. The employed PEI is a branched polymer that binds electrostatically to the NP. Linear PEI was also tested but increased toxicity without increasing efficacy (data not shown).

Citrate-stabilized Au NPs were produced using a well-established seeded growth approach based on the citrate reduction of $HAuCl_4$ (38, 39). Citrate is a good capping agent because it only binds loosely at the Au NP surface, being easily replaced by other ligands such as thiol- or amine-containing ligands, which have higher binding affinities for Au surfaces (~ 45 Kcal/mol (40) and ~ 6 Kcal/mol (41), respectively). Representative transmission electron microscopy (TEM) images of 5 nm, 20 nm and 50 nm Au NPs are shown in Figure 1, revealing their high monodispersity and quasi-spherical morphology. Citrate-stabilized Au NPs are stable in aqueous media and display a well-defined surface plasmon resonance (SPR) peak that red-shifts and increases in intensity as NPs increases in size.

As synthesized citrate-stabilized Au NPs were functionalized with AUT and PEI by incubating them with an excess of the cationic molecule at pH 2.5 for 24 hours. Remarkably, under these extremely acidic conditions, the stability of citrate-capped Au NPs is compromised due to loss of electrostatic repulsion, and aggregation is only prevented by the effective conjugation of the selected molecules. Citrate has three pKa points which are 6.3, 4.7, and 3.1. Therefore, below pH~ 3, all the hydroxyl residues become protonated, losing their negative charge, and, in turn, NPs lose the electrostatic repulsion provided by the citrate capping. The presence of a self-assembled AUT monolayer provides colloidal stability to

TABLE 1 Characterization of the nanovector catalogue.

	NPs	NPs-AUT	NPs-AUT+RNA	NPs-PEI	NPs-PEI+RNA
Au 5 nm					
SPR (nm)	510	521	533	516	519
DLS (nm)	6.1 ± 1.2	11.6 ± 3.6	62.7 ± 25.5	15.6 ± 4.9	15.1 ± 3.6
Z-Pot (mV)	-59.7	+5.8	-10.3	+26.2	+9.3
Au 20 nm					
SPR (nm)	522	526	531	523	524
DLS (nm)	30.4 ± 10.6	37.0 ± 13.3	54.6 ± 22.9	38.9 ± 15.3	44.9 ± 19.6
Z-Pot (mV)	-44.4	+18.6	-28.6	+34.4	+21.7
Au 50 nm					
SPR (nm)	531	533	540	531	534
DLS (nm)	49.6 ± 14.5	58.8 ± 25.9	75.0 ± 35.7	67.5 ± 30.2	72.8 ± 26.4
Z-Pot (mV)	-41.2	+31.2	-25.7	+44.3	+34.9

Summary of sizes, optical properties and surface charge of citrate-capped Au NPs of 5, 20 and 50 nm, cationic functionalized Au NPs with AUT of PEI, and loaded with mRNA. Note that the pH at which ζ-Potential of the citrate-capped NPs was measured (pH~8.6) is different from the other measurements, where NPs were dispersed in MES buffer (pH~5). This fact fundamentally impacts the surface charge of the NP.

10.3389/fimmu.2023.1128582

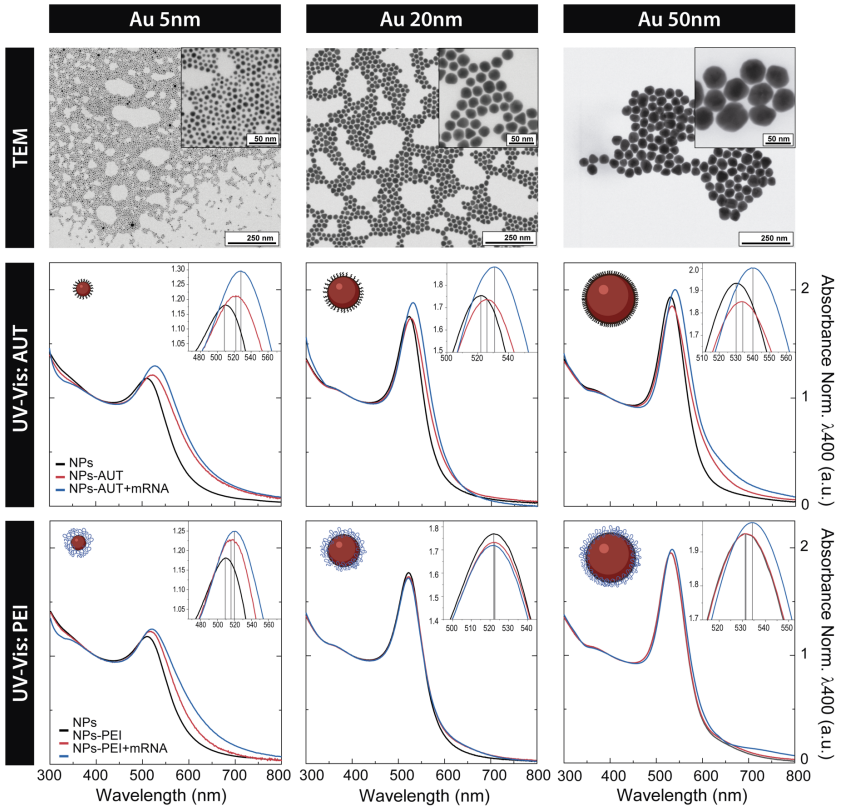

FIGURE 1
Nanovector Catalogue. Representative transmission electron microscopy images of highly monodisperse citrate-stabilized Au NPs of ~5 nm, ~20 nm, and ~50 nm. UV-Vis spectra of citrate-capped Au NPs of 5, 20 and 50 nm, cationic functionalized Au NPs with AUT of PEI, and loaded with mRNA. Absorbance is normalized to λ400 nm for a better comparison.

NPs through the positively charged amine-terminal residue that avoids aggregation by electrostatic repulsion. Therefore, appropriate conjugation conditions are critical to retaining NP stability during the coating process (see Figure S1, Figure S2).

Characterization by UV-Vis spectroscopy indicates the effective conjugation of Au NPs to cationic molecules. The absorption spectrum is sensitive to the Au NP environment, and an observable red-shift of the SPR band of about 6-10 nm can be seen once the Au NPs are functionalized with the cationic molecules (42, 43). The shift occurs within a few minutes and then remains unaltered, suggesting that the conjugation process is quick and that NPs are stable for long periods. The extent of the redshift depends on the Au NPs size, the structure of the cationic molecule and the nature of the anchoring group (42). Thus, smaller Au NPs functionalized with AUT molecules bond *via* thiol groups exhibit the largest SPR shift. Although PEI is relatively big, it interacts electrostatically with NP's surface by the positively charged amine residues, not forming covalent bonds, ultimately leading to smaller SPR shifts.

The functionalization process was further assessed by dynamic light scattering (DLS). An apparent increase in the hydrodynamic size of the NPs is observed after conjugation. Remarkably, monomodal distribution profiles were obtained in all cases, indicating that cationic Au NPs are colloidally stable. Measurement of NP surface charge, performed by ζ-potential measurements, revealed that cationic functionalization leads to highly positively charged Au NPs. Independently of their size, an increased surface charge is observed for PEI than AUT conjugates, explained by the higher amine density of the PEI coating due to its branched polymeric nature (44).

Functionalized NPs were purified and redispersed in MES buffer (pH ~ 5.5) for their later loading with oligonucleotides. Based on our previous expertise (36, 37, 45), we added the cationic NPs to the oligonucleotide solution to maximize NPs surface coverage while avoiding uncontrolled aggregation during the mixture of both solutions (46). The ratio of oligonucleotide molecules to NP was optimized for each NP's size tested to achieve the maximum loading while avoiding NP aggregation (**see** Figure S3). The incubation was performed at 4 °C for 24 hours to minimize the risk of nucleic acid degradation while ensuring surface saturation (Figure S4 shows complete kinetics of the loading process). Samples were purified before characterization analysis.

As seen in Figure 1, at any given NP size and cationic coating, a red shift in the SPR peak position of about 1-2 nm can be observed, confirming the effective oligonucleotide loading. Accordingly, their hydrodynamic diameter increased, and their ζ-potential dropped due to the presence of the negatively charged mRNA molecules at the acidic pH of work (47). Yet, the increase in the hydrodynamic diameter is larger for PEI than for AUT-functionalized Au NPs. These results, coupled with the fact that the surface charge doesn't

invert to negative values in the case of PEI-functionalized Au NPs, point out that significant differences attributed to the disposition of the cationic coating at the NP's surface could exist. As previously mentioned, AUT forms a regular self-assembled monolayer, whereas PEI, with a branched polymeric nature and high molecular weight, is most likely in a mushroom configuration. The fact that PEI-functionalized Au NPs remain positive after oligonucleotide loading has a significant impact on the interaction of the nanovectors with the cell surface and has a critical role in their transfection efficiency. Finally, aiming to calculate the loading of oligonucleotides to cationic Au NPs, quantification was performed by Nanodrop. For this, after the loading process, Au NPs were purified, and the supernatant was analyzed. Spectrophotometric results reveal a loading of 48% (9.3 ng/µl) for NPs-AUT and 45% (8.7 ng/µl) for NPs-PEI for 50 nm Au NPs. All in all, the presented results, along with the nanovector stability (Figure S5) and release studies (Figure S6), provided a deep understanding of the nanovectors properties and proved the high stability of the nanovector-oligonucleotide complex.

Nanovector cytotoxicity studies

A key point in the success of nanovectors as nonviral transfection vehicles must be their low cytotoxicity. Other standard transfection methods, such as TransIT® or Lipofectamine®, show good transfection rates but have very low cell viability. It is claimed that their internalization pathway is through membrane disruption, which ultimately causes their toxicity (48). In contrast, nanovectors internalize *via* endocytosis, significantly reducing the associated toxicity. To evaluate the safety of nanovectors in HEK293 cells, we first measured the cell viability by Resazurin reduction using Prestoblue and then Annexin V/PI staining was performed to analyze cell viability. (Figure 2).

Some previous studies reported that Au NPs cytotoxicity is mediated by their size, which inhibited the proliferation and triggered cell cycle arrest (49–51). However, the present results suggest no toxic effect related to NP size, at last in the studied range. Yet, cationic functionalization of the Au NPs did compromise cell viability and membrane integrity in some cases. A slight decrease in cell viability in HEK293 cells was determined with an exposition of 5 nm Au NPs coated with PEI and PEI-RNA at the maximum concentration of 3.3x10 (13) NP/mL. On the contrary, AUT-coated 5nm Au NP do not show any cytotoxic effect. Regarding 20 nm and 50 nm Au NPs, non-significant variation in the cell viability between Au-treated and non-treated cells was quantified even when exposing the cells to the highest concentration, corresponding to $2.7x10^{12}$ NP/mL and $3x10^{11}$ NP/mL, respectively.

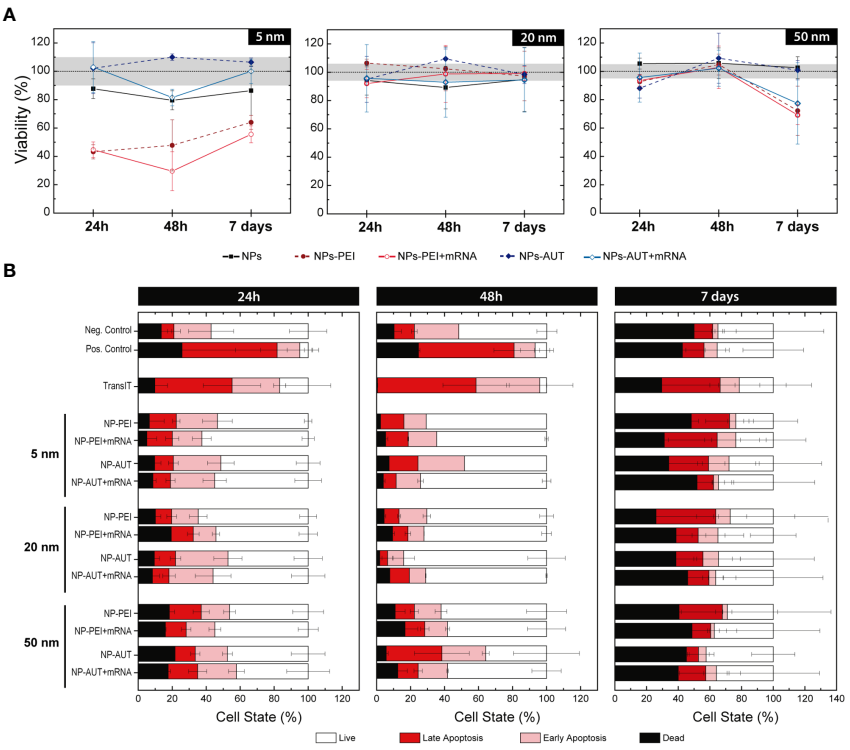

FIGURE 2
Nanovector Cytotoxicity Studies. The action of Au NP coated with PEI and AUT, and loaded with oligonucleotides was tested at different concentrations. **(A)** The percentage of resazurin reduction is shown at the maximum Au NP's concentration. The dashed-black line corresponds to control values for reference, and the grey area overlaid to its relative standard deviation. **(B)** After 24h, 48h, or 7 days of HEK293 cells exposition to cationic NPs, alone or loaded with mRNA, Annexin V/PI staining was performed to analyze cell viability. Cell state was classified as live, in early or late apoptosis, or dead according to the relative intensity of each marker.

To gain further insight into transfection-associated toxicity, HEK293 cells were exposed to nanovectors and sorted based on their viability state. Annexin V/PI staining was used to categorize cell populations as live, in early or late apoptosis, and dead. Viability controls were also included, cells without any treatment for the negative control and lethal H_2O_2 doses for positive cell death control. In this experiment, TransIT® was also included to compare its toxicity with the NP-based nanovectors carrying similar amounts of oligonucleotides. Results show an evident difference in the viability profile of TransIT® compared to nanovectors at short times. Cationic NPs, either loaded with mRNA or not, present a cell population distribution similar to the negative control. However, for TransIT® exposed cells, the proportion of cells in a pro-apoptotic state is much higher, comparable with those treated with H_2O_2. The percentage of early and late apoptosis was maintained at 48 h. Accordingly, the dead cell proportion increased at each incubation time. In contrast, cells transfected with the nanovectors preserved their viability, and the apoptosis entrance was delayed. At 7 days post-exposure, viability values stabilized. Only a non-significant slight increase in the pro-apoptotic populations can be observed for TransIT® and 5 nm Au NPs-PEI. These results confirm that NP-based formulations are safe for their use as delivery vectors. Cationic AuNPs non-loaded with DNA rapidly absorb negatively charged proteins from the medium losing their cationic charge and may cause uncontrolled aggregation (Figure S5, Table S1).

Endosomal escape

Reaching the cytoplasmic space is critical for the delivery of mRNA into the cytosol, where the ribosomes that will translate it into the coded protein are located. NPs with sizes ranging 5-100 nm enter the intracellular space *via* endocytosis, but the subcellular fate of the NPs will depend on their properties (32, 52). Upon vesicle formation, they enter into the endocytic pathway, where pH progressively decreases with the vesicle maturation process for digestion. However, NPs with pH buffering capacity can inhibit this process, disrupt the endosomal membrane, and escape from the endosome by the so-called proton sponge effect (53–55). Two parallel studies were performed to investigate the ability of the nanovectors to escape from the endosome (Figure 3).

First, the proton buffering capacity was tested *in vitro* by monitoring a solution's acidification in cationic Au NPs. The

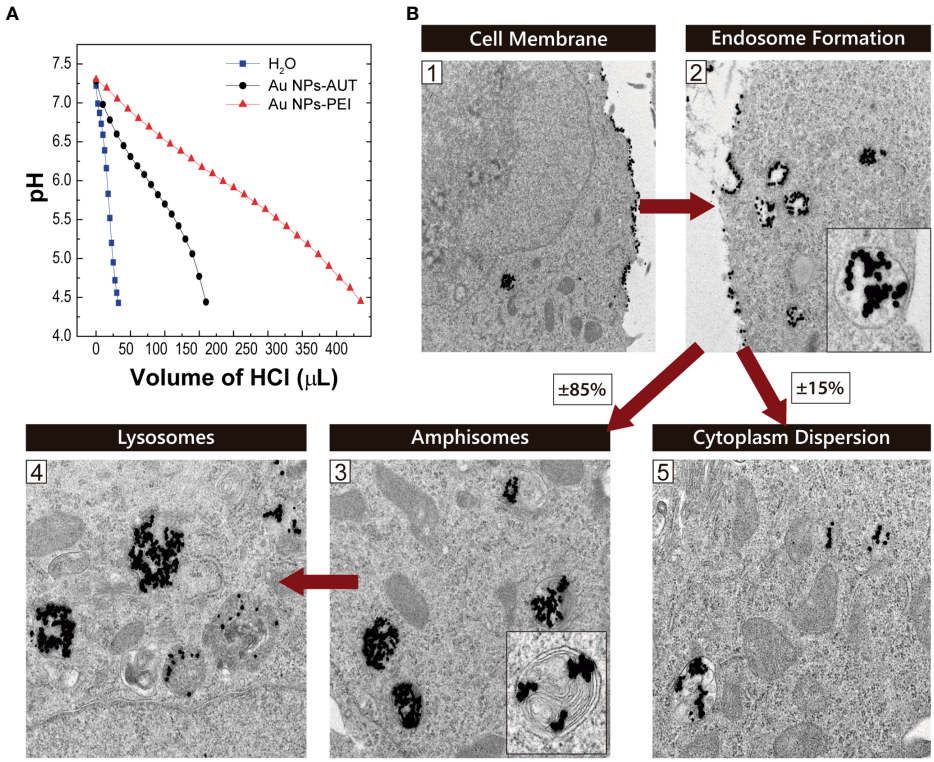

FIGURE 3
Endosomal Escape. **(A)** The proton buffer capacity of the cationic-coated Au NPs was analyzed by measuring the decrease in pH as a function of HCl volume added to the solution. **(B)** Au NP-PEI Intracellular Trafficking on HEK293 cells. Representative transmission electron microscopy images from HEK293 cells exposed to PEI-coated 20 nm Au NPs. The proposed internalization pathway is schematically represented at the different stages: (1) membrane attachment, (2) internalization in endosomes, maturation to (3) amphisomes and later (4) lysosomes. (5) Shows NPs dispersed in the cytoplasmic space after escaping from the endosomes. Red arrows indicate time evolution.

proton sponge efficiency of the NPs was evaluated as a function of the HCl added; thus, H^+ needed to reach the same pH value. As observed, PEI and AUT-coated NP solutions present a delay in the pH drop compared to the aqueous solution used as a reference. In detail, the Au NPs-PEI show a much greater ability to capture protons than NPs-AUT. This correlates with the amine concentration of the PEI-coated NPs being higher. These results were correlated with the findings from the NP intracellular trafficking study. The observation of cells exposed to cationic NP by TEM reveals that NPs follow an internalization pathway *via* endocytosis. After NPs-PEI stuck to the cell membrane, they were internalized in endocytic vesicles. In a typical endocytosis process, the maturation of these vesicles has several steps, from early and late endosomes to amphisomes, to finally reach the active lysosome stage, where the proteases digest the cargo. In this case, it could be observed that close to 85% of the internalized NPs-PEI were found either in amphisomes or in lysosomes. However, the 15% remaining were located dispersed in the cytoplasmic space. This fact entails that NPs-PEI escaped from the endocytic pathway at some point.

As discussed before, the coating of Au NPs with PEI confers proton sponge capacities allowing for an endosomal escape, as results suggest. However, the loading of cationic NP with oligonucleotides and their interfacing with biological media may impact on their interation with cells. In fact, the interaction with components from biological fluids -as the potential formation of a protein corona- could influence nanovectors cell internalization, distribution and fate (56). In our case, cells are transfected in serum free medium avoiding interaction with proteins in the cell culture.

Transfection: GFP expression

The effectiveness of Au transfection in HEK293 cells was assayed using 5, 20 and 50 nm Au NP coated with PEI and AUT, loaded with green fluorescence protein, *GFP* mRNA. The GFP expression was analyzed at short (24 and 48 h) and long (7 days) times post-transfection, by flow cytometry and fluorescence microscopy. The observation of the transfected cells by fluorescence microscopy allowed for a first visual inspection of the samples to evaluate cell morphology and GFP expression qualitatively. In addition, the transfection efficiency from the total cell population was measured by flow cytometry.

Figures 4A, B shows the transient expression of GFP. While all the Au NP-PEI could transfect the HEK293 cells, the transfection performed with the AUT-coated nanovectors was unsuccessful since no GFP expression was observed because the NPs did not reach the cytosol, either because they did not release the mRNA. Interestingly, the expression of the GFP protein was preserved for 7 days which could be adscribed to a slow mRNA from the nanovector (Figure S6). Some morphological and adherence changes were observed, especially after exposition to 5nm NPs-PEI and the commercial reagent TransIT®, consistent with necrosis as reported in the cytotoxicity studies. Additionally, to evaluate ribosomal occupancy and saturation different concentrations of mRNA were tested, which allowed to standardize the transfection protocol with nanovectors (Figure S7). It was observed that the transfected population increased with the amount of mRNA indicating that despite the high amounts of mRNA, the ribosomes were far from saturation, probably due to the slow and sustained release of mRNA in the cytosol.

Cellular viability was evaluated by flow cytometry using Annexin/PI combined staining to study apoptosis phenomena in those expressing GFP cells to gain further insights into the transfection events. Thus, GFP-positive cells were sorted into live, early or late apoptosis, or dead depending on the relative intensity of both viability markers. Figure 4B shows the expression in live cells at 24h, 48h and 7 days. HEK293 cells transfected with TransIT® show the highest GFP fluorescence signal but with relatively high-intensity variability within the same population. Regarding the PEI-nanovectors, 50 nm NP show the highest efficiency on all time points, and GFP expressions are maintained for 7 days, while that from TransIT® has started decreasing.

Interestingly, when GFP expression is reviewed as the proportion of live to total transfected cells (Figure 4C), differences between TransIT® and nanovectors dramatically change. These results reveal a high and prolonged transfection efficiency of HEK293 cells by PEI-nanovectors, coupled with low cytotoxicity, since the apoptosis cell ratio is not enhanced. It can be seen that the amount of healthy transfected cells is similar in both cases, TransIT® and AuNPs, but while there is a large population of transfected apoptotic cells with the former, they are almost none in the latter, especially at short times. Additionally, the observation of the samples under the CLSM enabled the image of the Au NPs simultaneously by reflectance mode (57–59) (Figure S8). These findings, coupled with the TEM observations of the NPs intracellular trafficking, may indicate that despite most of the cells having internalized nanovectors, they are not yet dispersed in the cytoplasmic space. Therefore, endosomal escape may happen later for these nanovectors, delaying the mRNA delivery and expression, which also agrees with the sustained GFP expression observed by flow cytometry. Additionally, variability in GFP expression could be ascribed to differences in the cell cycle stage between the HEK293 population (60).

Aiming to test the versatility of the developed nanovectors, different cells lines were also trasnfected with GFP mRNA loaded on 5, 20 and 50 nm Au NP-PEI. The transfection efficiency of the nanovectors on Jurkat cells, an immortalized line of human T lymphocyte cells that are used to study acute T cell leukaemia and RAW264.7 as a model of macrophage has been tested. Immune cells, and particularly T cells morphology is specially challenging for cytoplasmatic delivery since the majority of the cell volume is occupied by the cell nucleous. Obtained results demonstrate the capacity of the nanovectors to deliver mRNA to different cell lines (Figure S9).

Transfection: Cloroqiuine Effect

Here, the combined use of nanovectors with chloroquine is explored to enhance the transfection efficiency (Figure 5).

10.3389/fimmu.2023.1128582

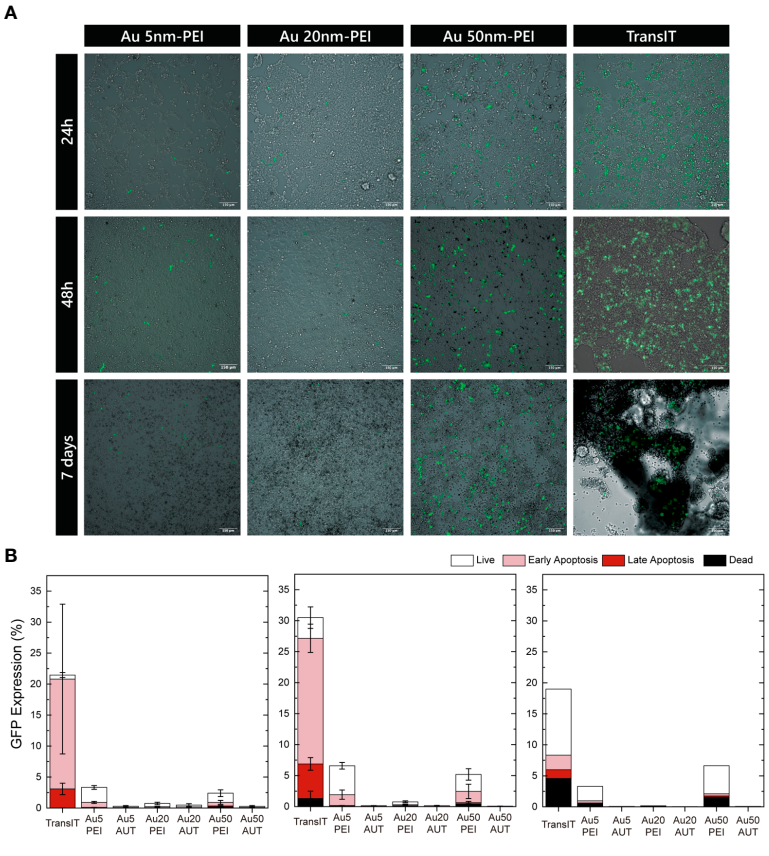

C

Time	AUT			PEI			TransIT
	5nm	20nm	50nm	5nm	20nm	50nm	
24h	69.2	62.3	68.9	72.7	70.7	61.9	3.0
48h	8.0	5.4	10.9	70.8	59.0	52.8	10.9
7 days	12.1	21.7	6.5	70.4	53.7	68.4	56.1

FIGURE 4
GFP Expression. **(A)** Wide-Field fluorescence overlaid onto Bright-Field images of transfected HEK293 cells at 24h, 48h, and 7 days. Scale bar = 150 µm. **(B)** Quantifying the nanovectors transfection based on the mean GFP expression at 24h, 48h, and 7 days. Cell viability was analyzed by Annexin V/PI iodine staining, and the cell state was classified as live, in early or late apoptosis, or dead. **(C)** Summary of the GFP-expressing live cells relative to the total GFP-expressing cells.

Chloroquine, as largely reported in the literature, is a common compound used to halt endosomal maturation, which in turn acts to boost NP endosomal escape by enhancing the proton sponge effect (61, 62). So, HEK293 cells were treated with chloroquine for 4 hours prior to transfection with PEI-nanovectors and GFP expression at 24h was visualized by wide-field fluorescence microscopy.

The statistical analysis from the GFP expression quantification shows a significant fluorescence signal increase for 5nm and 50nm PEI-nanovectors, and higher but not so significant for 20nm. Conversely, no enhancement effect was observed in cells transfected with AUT-coated nanovectors (data not shown). Accordingly, these results support the hypothesis that Au NPs-PEI reaches the cytoplasmic space *via* endosomal escape by the proton sponge mechanism. Further, this study provides new insights into the characterization of nanovectors that ensure suitable mRNA delivery into the cells without a cytotoxic effect.

Conclusions

In this work role of cationic functionalized Au NPs as transfection vectors has been explored. Au NPs of 5 nm, 20 nm and 50 nm were synthesized with high monodispersity following a previously reported seeded-growth method. NPs were successfully coated with either AUT or PEI to provide cationic surface charge and then loaded with mRNA, which constitutes the nanovector construct. We studied stability in biological media and the ability to release the previously loaded mRNA over time. Nanovectors also displayed proton sponge capacity, and further microscopy studies suggested their delivery into the cytosol *via* endosomal escape. The use of PEI-coated Au NPs as mRNA delivery vectors showed a relatively low transfection efficiency but sustained GFP protein expression over 7 days, where 50 nm Au NPs displayed the highest

10.3389/fimmu.2023.1128582

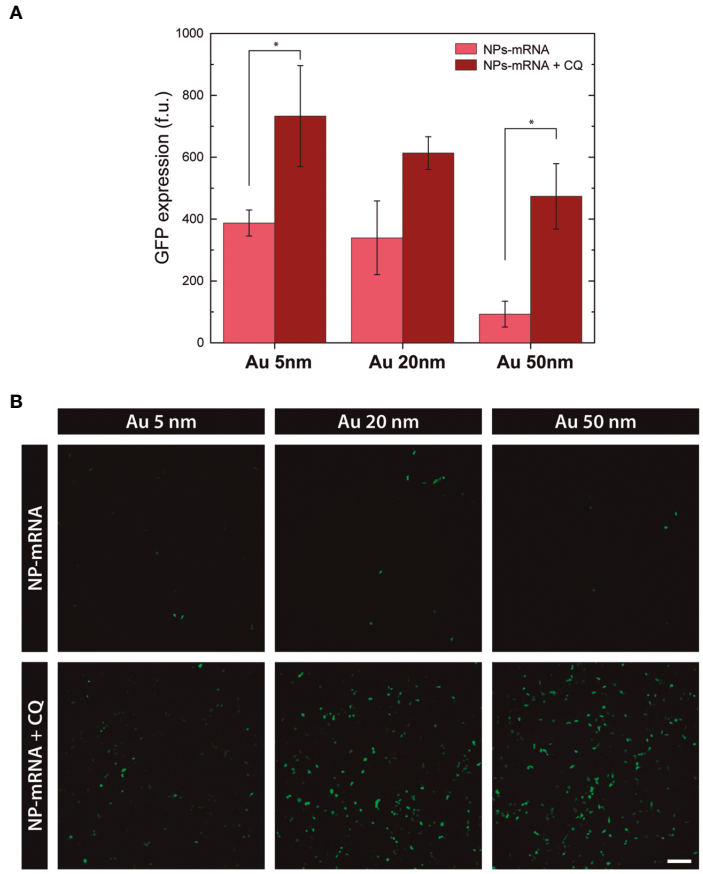

FIGURE 5
Effect of Chloroquine in transfection. **(A)** Transfection efficiency based on the mean GFP expression at 24h. (* p>0.05) **(B)** Wide-field Fluorescence images of HEK293 cells transfected with PEI-coated nanovectors, alone or in combination with chloroquine, at 24h. Scale bar = 150 µm.

transfection rates. Cytotoxicity and risk assessment performed by Prestoblue and Annexin V/PI assays demonstrated are safe and didn't induce significant cell damage, except for 5 nm Au-PEI NPs that showed higher toxicity, similar to TransIT transfection control. Protein expression was increased when nanovector-mRNA transfection was performed combined with chloroquine. The mRNA transfection with NPs induced less cellular damage and mortality due to their internalization and delivery *via* endocytosis. All in all, cationic Au NPs were proven to be safe, nonviral vectors for mRNA delivery into cells, with a wide margin for improvement.

In conclusion, the introduction of mRNA into the cells for protein overexpression is an alternative to viral vectors that includes several advantages: no threat of mutagenic insertion, no threat of viral particle reactivation, accessible to dose control, and synthetic animal product-free production, which altogether makes it an attractive approach for clinical use since they allow for a transient expression of the desired gene. Not only that, but non-viral vectors have gained importance in recent years because of their safety in handling and ease of application compared with viral vectors. In contrast, they are customizable, non-pathogenic, relatively safe, and easily produced and scaled-up.

Materials and methods

Chemicals

Gold(III) chloride trihydrate ($HAuCl_4{\cdot}3H_2O$), trisodium citrate ($Na_3C_6H_5O_7$), tannic acid ($C_{76}H_{52}O_{46}$), potassium carbonate (K_2CO_3), amino-undecanethiol (AUT), poly-ethyleneimine branched Mn2000 (PEI), 2-(N-morpholino)ethanesulfonic acid buffer solution (MES), sodium hydroxide (NaOH), hydrogen chloride (HCl), oligonucleotide model 600-800 bases (D1626), Sodium Phosphate Dibasic (Na_2HPO_4), Sodium phosphate monobasic (NaH_2PO_4), poly-L-lysine, Paraformaldehyde (PFA), Triton-X, Bovine Serum Albumin (BSA), Sodium Chloride (NaCl), and Calcium Chloride ($CaCl_2$) were purchased from Sigma-Aldrich. Dulbecco's Modified Eagle Medium (DMEM), Foetal Bovine Serum (FBS), Hoechst 3342 (H1399), Prolong antifade mounting medium (11559306), Optimem Medium, Pacific Blue-Annexin V, Propidium iodide (PI), accutase, 4-(2-hydroxyethyl)-1-piperazineethanesulfonic acid buffer (HEPES), and Prestoblue were purchased from Thermo Fisher. Phalloidin Alexa Fluor 647 (ab176759) was purchased from Abcam. Clean CAP eGFP mRNA (5 moU) was purchased from Tebu-Bio. TransIT®-LT1 Transfection Reagent was purchased from

MirusBio. All chemicals were used as received without further purification. Distilled water passed through a Millipore system (ρ = 18.2 MΩ) was used in all experiments. All glassware was first rinsed with acetone and then with Millipore water before use.

Gold nanoparticle synthesis

5 nm citrate-stabilized Au NPs were producted following Piella et al. In detail, a 150 mL of freshly prepared reducing solution of sodium citrate (SC, 2.2 mM) containing 0.1 mL of tannic acid (TA, 2.5 mM) and 1 mL of potassium carbonate (K_2CO_3, 150 mM) was heated with a heating mantle in a 250 mL three-necked round-bottom flask under vigorous stirring. When the temperature reached 70°C, 1 mL of tetrachloroauric acid ($HAuCl_4$, 25 mM) was injected. The colour of the solution changed rapidly to black-grey (less than 10 s) and then to orange-red in the following 1–2 min. The solution was kept at 70°C for 5 min more to ensure complete reaction of the gold precursor. Immediately after the synthesis and in the reaction same vessel, the sample was diluted by extracting 55 mL and adding 55 mL of SC (2.2 mM). When the temperature reached again 70°C, two injections of 0.5 mL of $HAuCl_4$ (25 mM) on a time interval of 10 min were done. This growing step comprising sample dilution plus 2 injections of $HAuCl_4$ was repeated until the particles reached the desired size.

20nm and 50nm citrate-stabilized Au NPs were produced following Bastus et al. In detail, a solution of 2.2 mM sodium citrate (SC) in Milli-Q water (150 mL) was heated with a heating mantle in a 250 mL three-necked round-bottomed flask for 15 min under vigorous stirring. A condenser was utilized to prevent the evaporation of the solvent. After boiling had commenced, 1 mL of $HAuCl_4$ (25 mM) was injected. The colour of the solution changed from yellow to bluish grey and then to soft pink in 10 min. Immediately after the synthesis of the Au seeds and in the same reaction vessel, the reaction was cooled until the temperature of the solution reached 90°C. Then, 1 mL of a $HAuCl_4$ solution (25 mM) was injected. After 30 min, the reaction was finished. This process was repeated twice. After that, the sample was diluted by extracting 55 mL of sample and adding 53 mL of Mili-Q water and 2 mL of 60 mM sodium citrate. This solution was then used as a seed solution, and the process was repeated again until the particles reached the desired size.

Functionalization of nanoparticles

Functionalization of Gold Nanoparticles with AUT. First parameter explored for a stable functionalization of Au NPs was the concentration of AUT. For this, 20nm Au NPs were concentrated 10-fold relative to the synthesis concentration by centrifugation (conditions were set according the Stokes law for each particle size). Next, AUT solutions with concentrations ranging between 50-400 μM were prepared in HCl 10 mM (pH<3). NPs (10% to final volume) were rapidly added into the AUT solution under vigorous stirring. After 1h, samples were characterized by UV-Vis. Note that at pH values above 3, NPs aggregate and precipitate upon dispersion in the AUT solution. The positive charges of the amine residues of AUT interact with the negatively charged hydroxyl residues of citrate and crosslink triggering NPs aggregation. The conjugation time was analyzed by monitoring the NPs by UV-Vis from 5 min to 1 month. Finally, the purification process of the AUT-coated NPs was studied. The conjugated NPs were precipitated by centrifugation twice, and resuspended to the initial volume, first with HCl 2 mM and then with MES 10 mM.

Functionalization of Gold Nanoparticles with PEI. The optimal PEI concentration and pH were studied for Au NPs PEI-coating. On the first case, 50nm Au NPs were concentrated 10-fold relative to the synthesis concentration by centrifugation. Next, PEI solutions with concentrations ranging between 50-200 μM were prepared in HCl 34mM (pH~7). NPs (10% to final volume) were rapidly added into the PEI solution under vigorous stirring. After 1h, samples were characterized by UV-Vis. 10-fold concentrated 50nm Au NPs were conjugated to PEI (200 μM) at different pH conditions ranging from 2 to 7. NPs (10% to final volume) were rapidly added into the PEI solution under vigorous stirring. After 24h, samples were characterized by UV-Vis. The conjugated NPs were precipitated by centrifugation, resuspended to the initial volume with water and characterized again by UV-Vis.

Loading of cationic gold nanoparticles with oligonucleotides

Optimization of the NP : RNA ratio

50 nm (at $3x10^{11}$) NP/mL) Au NPs coated with AUT were used, previously purified and dispersed in MES 10 mM. Single-stranded DNA (ssDNA) with a molecular weight similar to an average mRNA construct was used as an oligonucleotide model. For ssDNA loading, first 900 μl of 2-fold serial dilutions in MES 10mM were prepared, ranging from 53-0.41 μg/mL. Next, 100 μl of NPs were rapidly added onto the ssDNA and the mixture was gently homogenized. Thus, the final relative ssDNA : NP ratios ranged from [39-5000]. Samples were incubated for 24 h at 4°C under stirring. Next day, samples were characterized by UV-Vis spectroscopy, DLS and Z-Pot before and after purification. For purification, NPs were precipitated by centrifugation, supernatant was discarded and pellets were resuspended in MES 10 mM to the initial volume.

Loading kinetics

50 nm Au NPs coated with AUT were loaded with ssDNA. Briefly, 900μl of NPs dispersed in MES 10 mM were added onto 100 μl of ssDNA to a final ratio DNA : NP=300. Samples were kept at 4 ° C under stirring. At each time point, 1 mL of sample was taken for characterization. For purification, NPs were precipitated by centrifugation, supernatant was stored for ssDNA quantification and pellets were resuspended in MES 10 mM to the initial volume. Conjugates were analyzed by UV-Vis spectroscopy, DLS and additionally Z-Potential was measured after purification. The quantification of the ssDNA loaded on the NPs was extrapolated from the measurement of the supernatants at 24h by Nanodrop (Nanodrop 2000 Spectrophotometer, ThermoFisher).

Stability of nanovectors

To study the stability of nanovectors, 50 nm Au NPs coated with AUT and PEI, alone or loaded with ssDNA, were used. For this, NP solution was diluted 1:10 in the media of study and incubated for 24h at 4 °C. Different biologically relevant media were tested: Optimem (pH 7.4) and Phosphate Buffer (PB) 10mM (pH 7.4). NPs dispersed in MES 10 mM (pH 5) were used as a control. NP stability was studied by UV-Vis and DLS. After 24 h samples were characterized. Au NPs were precipitated by centrifugation, the pellets were redispersed in the media of study and Z-Potential was measured.

In vitro experiments

Cells culture

HEK293 cell culture was maintained in culture in 75 cm^2 tissue culture flask using DMEM with heat- inactivated foetal bovine serum (FBS) at 10% at 37 °C and humidified 5% CO_2.

TEM imaging of cultured cells exposed to NPs

HEK293 cells were seeded on a 10 cm petri dish at 100.000 cell/cm^2 and incubated overnight. 20 nm Au NPs coated with PEI were added dropwise onto cell cultures and gently homogenized. At 24 h cells were fixed with 2.5% glutaraldehyde in 0.1 M PB. Next, samples were embedded in paraffin following a standard protocol. For observation, paraffin-embedded samples were sectioned using a ultra-microtome and transferred carbon-coated copper TEM grid.

Proton sponge efficiency of cationic gold nanoparticles

First, the pH of a cationic Au NPs solution was adjusted to 7.3 with NaOH. Then, pH was monitored continuously as a known volume of HCl (10 mM) was added dropwise on the Au NPs solution under stirring, until pH 4 was reached. A solution of Mili Q water was used as a control. The proton sponge efficiency of the cationic NPs was calculated based on the HCl volume added, normalized to Au surface (nm^2).

Cytotoxicity

Cytotoxicity assessment of nanovectors

The action of Au NPs in the viability of the HEK-293 cells was evaluated by PrestoBlue and Annexin V/Propidium Iodide assay, according to the manufacturer's recommendations.

Prestoblue

HEK293 cells were seeded to $1x10^5$ cell/mL in 96-well plate during 24 hours before to Au NPs exposition. Serial dilutions of nanoparticles were added at final concentration ranging from $3.3x10^{13}$ - $1.2x10^{11}$ for Au 5nm NPs/mL, $2.7x10^{12}$) - $1.0x10^{10}$ for Au 20 nm NPs/mL and $3x10^{11}$ - $1.1x10^9$ for Au 50nm NPs/mL. To assay the ratio oligonucleotide:NPs cytotoxicity the PEI/AUT nanoparticles were loaded with oligonucleotide. After 24 h, 48 h and 7 days cell viability was measured. For this, 10 µL of PrestoBlue was added to each well, plates were incubated for 2h and fluorescence was measured (λ_{ex}531nm, λ_{em}572nm) by Varioskan LUX (Thermo Fisher Scientific). All experiments were carried out in triplicate, and data was treated and calculated with OriginLab software.

Annexin V/propidium iodide

To determinate the cell viability, HEK293 cells were stained with Pacific Blue- Annexin V/propidium iodide (PI) in accord with the manufacturer's recommendations to determine cell viability. Briefly, HEK293 cells were collected by cell detachment using accutase and washed with PBS. After centrifugation cells were resuspended in 100 µL of Annexin binding buffer (10 mM HEPES, 140 mM NaCl and 2.5 mM $CaCl_2$). 5 µL of Annexin V and PI (1 mg/mL) were added and incubated at room temperature for 15 minutes. After the incubation period, additional 400 µL of the binding buffer was added. Acquisition was configured to stop after recording 10,000 events within the HEK293 cell population.

Transfection efficiency

Transfection of mRNA with nanovectors

To evaluate the transfection capacity of gold nanoparticles coated with PEI and AUT, HEK- 293 cells were cultured in DMEM with FBS 10% in 24-well plate at 50.000 cells/mL. The transfection was performed with 60-70% confluence and final mRNA concentration of 1000 ng. After 2h the incubation at 37°C the DMEM medium was removed and replaced for 900 µL of Optimem medium. Next, specific colloidal ratios [mRNA : NP] were added (100 µL) for each nanoparticle size for 5 nm Au NPs [5:1], 20 nm [50:1] and 50 nm [300:1]. The next day 100µL of FBS were added to each well and left for 48h and 7 days after transfection process. The transfection and cell viability percentages were evaluated by confocal microscopy and flow cytometry.

Chloroquine effect

To further inside to the proton sponge mechanism the transfected HEK-cells were treated with chloroquine at 20 µM for 4 hours before nanovector transfection, performed as described above. At 24h cells were visualized by Wide-Field fluorescence microscopy and GFP signal intensity quantified. Statistical analysis was performed by the 2-way ANOVA test, using the GraphPad Prism software. For significance, $p>0.005$ was considered.

Flow cytometry

The percentage of Green Fluorescence Protein (GFP) expression after transfection was analyzed with BD LSRFortessa™ Cell Analyzer. Forward and side-scatter areas (FSC-A, SSC-A) in a linear scale were used to gate HEK293 population, and GFP expression was detected by excitation through 480-500nm. To determinate the cell viability, HEK293 cells were stained with Pacific Blue- Annexin V/propidium iodide (PI) in accord with the

manufacturer's recommendations. Briefly, HEK293 cells were collected by cell detachment using accutase and washed with PBS. After centrifugation cells were resuspended in 100 µL of Annexin binding buffer (10mM HEPES, 140mM NaCl and 2.5mM $CaCl_2$). 5 µL of Annexin V and PI (1mg/mL) were added and incubated at room temperature for 15 minutes. After the incubation period, additional 400 µL of the binding buffer was added. Acquisition was configured to stop after recording 10,000 events within the HEK293 cell population.

Wide-field fluorescence microscopy

Au nanoparticles transfection efficiency in HEK293 cells was calculated by GFP expression analyzed by Wide-Field microscopy. To this end, HEK293 cells were visualized in Thunder Wide-Field Fluorescence Microscope (Leica). For GFP imaging, a 475 nm LED was used for excitation while the emission channel was set to 506-532 nm. For deconvolution of each image, we utilized the algorithm Small Volume Computational Clearing (SVCC).

Data availability statement

The raw data supporting the conclusions of this article will be made available by the authors, without undue reservation.

Author contributions

MB, GD, PB, RK, ME, MJ, NB, VP conceived of the presented idea MG, ME, VS, AA-P, AB, AC, and FF designed and performed the experiments. All authors contributed to the article and approved the submitted version.

Funding

We acknowledge financial support from the Spanish Ministerio de Ciencia, Innovación y Universidades (MCIU) (RTI2018-099965-B-I00, AEI/FEDER,UE) proyectos de I+D+i de programación conjunta internacional MCIN/AEI (CONCORD, PCI2019-103436) cofunded by the European Union and Generalitat de Catalunya (2017-SGR-1431). ICN2 is supported by the Severo Ochoa program from Spanish MINECO (SEV-2017-0706) and is funded by the CERCA Programme/Generalitat de Catalunya.

Conflict of interest

The authors declare that the research was conducted in the absence of any commercial or financial relationships that could be construed as a potential conflict of interest.

Publisher's note

All claims expressed in this article are solely those of the authors and do not necessarily represent those of their affiliated organizations, or those of the publisher, the editors and the reviewers. Any product that may be evaluated in this article, or claim that may be made by its manufacturer, is not guaranteed or endorsed by the publisher.

Supplementary material

The Supplementary Material for this article can be found online at: https://www.frontiersin.org/articles/10.3389/fimmu.2023.1128582/full#supplementary-material

References

1. Marshall E. Gene therapy death prompts review of adenovirus vector. *Science* (1999) 286(5448):2244–5. doi: 10.1126/science.286.5448.2244

2. Phillips AJ. The challenge of gene therapy and DNA delivery. *J Pharm Pharmacol* (2001) 53(9):1169–74. doi: 10.1211/0022357011776603

3. Gemeinhart RA, Luo D, Saltzman WM. Cellular fate of a modular DNA delivery system mediated by silica nanoparticles. *Biotechnol Prog* (2005) 21(2):532–7. doi: 10.1021/bp049648w

4. Kneuer C, Sameti M, Bakowsky U, Schiestel T, Schirra H, Schmidt H, et al. A nonviral DNA delivery system based on surface modified silica-nanoparticles can efficiently transfect cells. *vitro. Bioconjugate Chem* (2000) 11(6):926–32. doi: 10.1021/bc0000637

5. Xiang JJ, Tang JQ, Zhu SG, Nie XM, Lu HB, Shen SR, et al. IONP-PLL: a novel non-viral vector for efficient gene delivery. *J Gene Med* (2003) 5(9):803–17. doi: 10.1002/jgm.419

6. Ojea-Jimenez I, Comenge J, Garcia-Fernandez L, Megson ZA, Casals E, Puntes VF. Engineered inorganic nanoparticles for drug delivery applications. *Curr Drug Metab* (2013) 14(5):518–30. doi: 10.2174/13892002113149990008

7. Shukla R, Bansal V, Chaudhary M, Basu A, Bhonde RR, Sastry M. Biocompatibility of gold nanoparticles and their endocytotic fate inside the cellular compartment: a microscopic overview. *Langmuir* (2005) 21(23):10644–54. doi: 10.1021/la0513712

8. Noh SM, Kim WK, Kim SJ, Kim JM, Baek KH, Oh YK. Enhanced cellular delivery and transfection efficiency of plasmid DNA using positively charged biocompatible colloidal gold nanoparticles. *Biochim Biophys Acta* (2007) 1770(5):747–52. doi: 10.1016/j.bbagen.2007.01.012

9. Niidome T, Nakashima K, Takahashi H, Niidome Y. Preparation of primary amine-modified gold nanoparticles and their transfection ability into cultivated cells. *Chem Commun (Camb)* (2004) 17):1978–9. doi: 10.1039/b406189f

10. Ghosh PS, Kim CK, Han G, Forbes NS, Rotello VM. Efficient gene delivery vectors by tuning the surface charge density of amino acid-functionalized gold nanoparticles. *ACS Nano* (2008) 2(11):2213–8. doi: 10.1021/nn800507t

11. Li P, Li D, Zhang L, Li G, Wang E. Cationic lipid bilayer coated gold nanoparticles-mediated transfection of mammalian cells. *Biomaterials* (2008) 29 (26):3617–24. doi: 10.1016/j.biomaterials.2008.05.020

12. Pujals S, Bastús NG, Pereiro E, López-Iglesias C, Puntes VF, Kogan MJ, et al. Shuttling gold nanoparticles into tumoral cells with an amphipathic proline-rich peptide. *ChemBioChem* (2009) 10(6):1025–31. doi: 10.1002/cbic.200800843

13. Thomas M, Klibanov AM. Conjugation to gold nanoparticles enhances polyethylenimine's transfer of plasmid DNA into mammalian cells. *Proc Natl Acad Sci* (2003) 100(16):9138–43. doi: 10.1073/pnas.1233634100

14. Cebrian V, Martin-Saavedra F, Yague C, Arruebo M, Santamaria J, Vilaboa N. Size-dependent transfection efficiency of PEI-coated gold nanoparticles. *Acta Biomater* (2011) 7(10):3645–55. doi: 10.1016/j.actbio.2011.06.018

15. Ernst LM, Casals E, Italiani P, Boraschi D, Puntes V. The interactions between nanoparticles and the innate immune system from a nanotechnologist perspective. *Nanomaterials* (2021) 11(11):20. doi: 10.3390/nano11112991

16. Hill HD, Millstone JE, Banholzer MJ, Mirkin CA. The role radius of curvature plays in thiolated oligonucleotide loading on gold nanoparticles. *ACS Nano* (2009) 3 (2):418–24. doi: 10.1021/nn800726e

17. Sandhu KK, McIntosh CM, Simard JM, Smith SW, Rotello VM. Gold nanoparticle-mediated transfection of mammalian cells. *Bioconjug Chem* (2002) 13 (1):3–6. doi: 10.1021/bc015545c

18. Gigante A, Li M, Junghänel S, Hirschhäuser C, Knauer S, Schmuck C. Non-viral transfection vectors: are hybrid materials the way forward? *Medchemcomm* (2019) 10 (10):1692–718. doi: 10.1039/C9MD00275H

19. Conner SD, Schmid SL. Regulated portals of entry into the cell. *Nature* (2003) 422(6927):37–44. doi: 10.1038/nature01451

20. Zhang S, Li J, Lykotrafitis G, Bao G, Suresh S. Size-dependent endocytosis of nanoparticles. *Adv Mater* (2009) 21(4):419–24. doi: 10.1002/adma.200801393

21. Meng Z, O'Keeffe-Ahern J, Lyu J, Pierucci L, Zhou D, Wang W. A new developing class of gene delivery: messenger RNA-based therapeutics. *Biomaterials Sci* (2017) 5(12):2381–92. doi: 10.1039/C7BM00712D

22. Grabbe S, Haas H, Diken M, Kranz LM, Langguth P, Sahin U. Translating nanoparticulate-personalized cancer vaccines into clinical applications: case study with RNA-lipoplexes for the treatment of melanoma. *Nanomedicine (Lond)* (2016) 11 (20):2723–34. doi: 10.2217/nnm-2016-0275

23. Foroozandeh P, Aziz AA. Insight into cellular uptake and intracellular trafficking of nanoparticles. *Nanoscale Res Lett* (2018) 13(1):339. doi: 10.1186/s11671-018-2728-6

24. Boussif O, Lezoualc'h F, Zanta MA, Mergny MD, Scherman D, Demeneix B, et al. A versatile vector for gene and oligonucleotide transfer into cells in culture and in vivo: polyethylenimine. *Proc Natl Acad Sci* (1995) 92(16):7297–301. doi: 10.1073/pnas.92.16.7297

25. Namuduri M, Brentjens RJ. Medical management of side effects related to CAR T cell therapy in hematologic malignancies. *Expert Rev Hematol* (2016) 9(6):511–3. doi: 10.1080/17474086.2016.1183479

26. Jackson HJ, Rafiq S, Brentjens RJ. Driving CAR T-cells forward. *Nat Rev Clin Oncol* (2016) 13(6):370–83. doi: 10.1038/nrclinonc.2016.36

27. Wang T, Larcher L, Ma L, Veedu R. Systematic screening of commonly used commercial transfection reagents towards efficient transfection of single-stranded oligonucleotides. *Molecules* (2018) 23(10):2564. doi: 10.3390/molecules23102564

28. Kulkarni JA, Myhre JL, Chen S, Tam YYC, Danescu A, Richman JM, et al. Design of lipid nanoparticles for in vitro and *in vivo* delivery of plasmid DNA. *Nanomedicine-Nanotechnology Biol Med* (2017) 13(4):1377–87. doi: 10.1016/j.nano.2016.12.014

29. Khare P, Dave KM, Kamte YS, Manoharan MA, O'Donnell LA, Manickam DS. Development of lipidoid nanoparticles for siRNA delivery to neural cells. *AAPS J* (2022) 24(1). doi: 10.1208/s12248-021-00653-2

30. Kumar Y, Kuche K, Swami R, Katiyar SS, Chaudhari D, Katare PB, et al. Exploring the potential of novel pH sensitive lipoplexes for tumor targeted gene delivery with reduced toxicity. *Int J Pharm* (2020) 573:12. doi: 10.1016/j.ijpharm.2019.118889

31. Comenge J, Sotelo C, Romero F, Gallego O, Barnadas A, Parada TG, et al. Detoxifying antitumoral drugs via nanoconjugation: the case of gold nanoparticles and cisplatin. *PloS One* (2012) 7(10):e47562. doi: 10.1371/journal.pone.0047562

32. Shan Y, Ma S, Nie L, Shang X, Hao X, Tang Z, et al. Size-dependent endocytosis of single gold nanoparticles. *Chem Commun (Camb)* (2011) 47(28):8091–3. doi: 10.1039/c1cc11453k

33. Lesniak A, Salvati A, Santos-Martinez MJ, Radomski MW, Dawson KA, Aberg C. Nanoparticle adhesion to the cell membrane and its effect on nanoparticle uptake efficiency. *J Am Chem Soc* (2013) 135(4):1438–44. doi: 10.1021/ja309812z

34. Cheng X, Tian X, Wu A, Li J, Tian J, Chong Y, et al. Protein corona influences cellular uptake of gold nanoparticles by phagocytic and nonphagocytic cells in a size-dependent manner. *ACS Appl Mater Interfaces* (2015) 7(37):20568–75. doi: 10.1021/acsami.5b04290

35. Liu X, Huang N, Li H, Jin Q, Ji J. Surface and size effects on cell interaction of gold nanoparticles with both phagocytic and nonphagocytic cells. *Langmuir* (2013) 29 (29):9138–48. doi: 10.1021/la401556k

36. Casals E, Pfaller T, Duschl A, Oostingh GJ, Puntes V. Time evolution of the nanoparticle protein corona. *ACS Nano* (2010) 4(7):3623–32. doi: 10.1021/nn901372t

37. Casals E, Pfaller T, Duschl A, Oostingh GJ, Puntes VF. Hardening of the nanoparticle-protein corona in metal (Au, Ag) and oxide (Fe3O4, CoO, and CeO2) nanoparticles. *Small* (2011) 7(24):3479–86. doi: 10.1002/smll.201101511

38. Bastus NG, Comenge J, Puntes V. Kinetically controlled seeded growth synthesis of citrate-stabilized gold nanoparticles of up to 200 nm: size focusing versus ostwald ripening. *Langmuir* (2011) 27(17):11098–105. doi: 10.1021/la201938u

39. Piella J, Bastús NG, Puntes V. Size-controlled synthesis of Sub-10-nanometer citrate-stabilized gold nanoparticles and related optical properties. *Chem Mater* (2016) 28(4):1066–75. doi: 10.1021/acs.chemmater.5b04406

40. Sellers H, Ulman A, Shnidman Y, Eilers JE. Structure and binding of alkanethiolates on gold and silver surfaces: implications for self-assembled monolayers. *J Am Chem Soc* (2002) 115(21):9389–401. doi: 10.1021/ja00074a004

41. Di Felice R, Selloni A. Adsorption modes of cysteine on Au(111): thiolate, amino-thiolate, disulfide. *J Chem Phys* (2004) 120(10):4906–14. doi: 10.1063/1.1645789

42. Bastus NG, Piella J, Puntes V. Quantifying the sensitivity of multipolar (Dipolar, quadrupolar, and octapolar) surface plasmon resonances in silver nanoparticles: the effect of size, composition, and surface coating. *Langmuir* (2016) 32(1):290–300. doi: 10.1021/acs.langmuir.5b03859

43. Schulz F, Vossmeyer T, Bastus NG, Weller H. Effect of the spacer structure on the stability of gold nanoparticles functionalized with monodentate thiolated poly (ethylene glycol) ligands. *Langmuir* (2013) 29(31):9897–908. doi: 10.1021/la401956c

44. Hill RJ. Hydrodynamics and electrokinetics of spherical liposomes with coatings of terminally anchored poly(ethylene glycol): numerically exact electrokinetics with self-consistent mean-field polymer. *Phys review. E Statistical nonlinear soft matter Phys* (2004) 70(5 Pt 1):051406. doi: 10.1103/PhysRevE.70.051406

45. Vitali M, Casals E, Canals F, Colome N, Puntes V. Simple spectroscopic determination of the hard protein corona composition in AuNPs: albumin at 75. *Nanoscale* (2020) 12(29):15832–44. doi: 10.1039/D0NR02379E

46. Piella J, Bastus NG, Puntes V. Size-dependent protein-nanoparticle interactions in citrate-stabilized gold nanoparticles: the emergence of the protein corona. *Bioconjug Chem* (2017) 28(1):88–97. doi: 10.1021/acs.bioconjchem.6b00575

47. Sherbet GV, Lakshmi MS, Cajone F. Isoelectric characteristics and the secondary structure of some nucleic acids. *Biophysics structure Mech* (1983) 10(3):121–8. doi: 10.1007/BF00537554

48. Meng Z, O'Keeffe-Ahern J, Lyu J, Pierucci L, Zhou D, Wang W. A new developing class of gene delivery: messenger RNA-based therapeutics. *Biomater Sci* (2017) 5(12):2381–92. doi: 10.1039/C7BM00712D

49. Vales G, Suhonen S, Siivola KM, Savolainen KM, Catalan J, Norppa H. Genotoxicity and Cytotoxicity of Gold Nanoparticles In Vitro: Role of Surface Functionalization and Particle Size. *Nanomaterials* (2020) 10(2):271. doi: 10.3390/nano10020271

50. Sani A, Cao C, Cui D. Toxicity of gold nanoparticles (AuNPs): a review. *Biochem biophysics Rep* (2021) 26:100991. doi: 10.1016/j.bbrep.2021.100991

51. Jawaid P, Rehman MU, Zhao QL, Misawa M, Ishikawa K, Hori M, et al. Small size gold nanoparticles enhance apoptosis-induced by cold atmospheric plasma via depletion of intracellular GSH and modification of oxidative stress. . *Cell Death Discovery* (2020) 6(1):83. doi: 10.1038/s41420-020-00314-x

52. Saha K, Rahimi M, Yazdani M, Kim ST, Moyano DF, Hou S, et al. Regulation of macrophage recognition through the interplay of nanoparticle surface functionality and protein corona. *ACS Nano* (2016) 10(4):4421–30. doi: 10.1021/acsnano.6b00053

53. Wanling L, Jenny KWL. Endosomal escape pathways for non-viral nucleic acid delivery systems. In: Brian C, editor. *Molecular regulation of endocytosis*. IntechOpen: Rijeka (2012). p. p Ch. 17.

54. Behr J-P. The proton sponge: a trick to enter cells the viruses did not exploit. *Chimia* (1997) 51(1-2):34. doi: 10.2533/chimia.1997.34

55. Smith SA, Selby LI, Johnston APR, Such GK. The endosomal escape of nanoparticles: toward more efficient cellular delivery. *Bioconjug Chem* (2019) 30 (2):263–72. doi: 10.1021/acs.bioconjchem.8b00732

56. Cox A, Andreozzi P, Dal Magro R, Fiordaliso F, Corbelli A, Talamini L, et al. Evolution of nanoparticle protein corona across the blood–brain barrier. *ACS Nano* (2018) 12(7):7292–300. doi: 10.1021/acsnano.8b03500

57. Gibbs-Flournoy EA, Bromberg PA, Hofer TP, Samet JM, Zucker RM. Darkfield-confocal microscopy detection of nanoscale particle internalization by human lung cells. *Part Fibre Toxicol* (2011) 8(1):2. doi: 10.1186/1743-8977-8-2

58. Wang F, Chen B, Yan B, Yin Y, Hu L, Liang Y, et al. Scattered light imaging enables real-time monitoring of label-free nanoparticles and fluorescent biomolecules in live cells. *J Am Chem Soc* (2019) 141(36):14043–7. doi: 10.1021/jacs.9b05894

59. Garcia-Fernandez L, Garcia-Pardo J, Tort O, Prior I, Brust M, Casals E, et al. Conserved effects and altered trafficking of cetuximab antibodies conjugated to gold nanoparticles with precise control of their number and orientation. *Nanoscale* (2017) 9 (18):6111–21. doi: 10.1039/C7NR00947J

60. Yu JN, Ma SF, Miao DQ, Tan XW, Liu XY, Lu JH, et al. Effects of cell cycle status on the efficiency of liposome-mediated gene transfection in mouse fetal fibroblasts. *J Reprod Dev* (2006) 52(3):373–82. doi: 10.1262/jrd.17097

61. Fredericksen BL, Wei BL, Yao J, Luo T, Garcia JV. Inhibition of endosomal/lysosomal degradation increases the infectivity of human immunodeficiency virus. *J Virol* (2002) 76(22):11440–6. doi: 10.1128/JVI.76.22.11440-11446.2002

62. Heath N, Osteikoetxea X, de Oliveria TM, Lazaro-Ibanez E, Shatnyeva O, Schindler C, et al. Endosomal escape enhancing compounds facilitate functional delivery of extracellular vesicle cargo. *Nanomedicine (Lond)* (2019) 14(21):2799–814. doi: 10.2217/nnm-2019-0061

Frontiers in Immunology

Explores novel approaches and diagnoses to treat immune disorders.

The official journal of the International Union of Immunological Societies (IUIS) and the most cited in its field, leading the way for research across basic, translational and clinical immunology.

Discover the latest Research Topics

See more →

Frontiers

Avenue du Tribunal-Fédéral 34
1005 Lausanne, Switzerland
frontiersin.org

Contact us

+41 (0)21 510 17 00
frontiersin.org/about/contact